SYNTHESIS AND ANTI-TUBERCULAR ACTIVITY OF HETEROCYCLIC AND SPIRO COMPOUNDS

A THESIS SUBMITTED TO

NATIONAL INSTITUTE OF TECHNOLOGY WARANGAL

FOR THE DEGREE OF

DOCTOR OF PHILOSOPHY

IN

CHEMISTRY

BY

ALLAKA BHARGAVA SAI

(Roll No. 701641)

DEPARTMENT OF CHEMISTRY

NATIONAL INSTITUTE OF TECHNOLOGY WARANGAL

HANAMKONDA-506 004, TELANGANA, INDIA

JANUARY, 2022

Dedicated to

…My parents and guide

Dr. B. Srinivas
Assistant Professor
Department of Chemistry
National Institute of Technology Warangal
Hanamkonda - 506 004
Telangana, India

Mobile: +91-9703351571
Email: basavojusrinivas@nitw.ac.in

CERTIFICATE

This is to certify that the research work presented in this thesis entitled **"Synthesis and anti-tubercular activity of heterocyclic and spiro compounds"** submitted by **Mr. Allaka Bhargava Sai** for the degree of Doctor of Philosophy in Chemistry, National Institute of Technology Warangal (Telangana), under my supervision and that the same has not been submitted elsewhere for a degree.

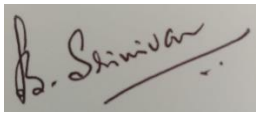

Date: 13.01.2022
Place: NIT Warangal

Dr. B. Srinivas
Thesis Supervisor

DECLARATION

I hereby declare that the work embodied in this thesis entitled **"Synthesis and anti-tubercular activity of heterocyclic and spiro compounds"** is based entirely on the results of the investigations and research work carried out by me under the supervision of **Dr. B. Srinivas**, Department of Chemistry, National Institute of Technology Warangal. I declare that this work is original and has not been submitted in part or full, for any degree or diploma to this or any other University.

Date: 13.01.2022 **(Allaka Bhargava Sai)**

Place: NIT Warangal

ACKNOWLEDGEMENTS

The work presented in this thesis would not have been possible without my close association with many people. I take this opportunity to extend my sincere gratitude and appreciation to all those who made this Ph.D. thesis possible.

It gives me an immense pleasure and delight to express my deep sense of gratitude to my research supervisor ***Dr. B. Srinivas*****,** Assistant Professor, Department of Chemistry, National Institute of Technology Warangal for his inspiring and valuable guidance. His unfailing attention, unmitigated encouragement and co-operation have helped me in attaining my goal. It would have been impossible to achieve this goal without his able support and valuable advice. I consider myself fortunate that he has given me a decisive tune, a significant acceleration to my career. I will be thankful to him throughout my lifetime.

I am greatly indebted to ***Prof. N. V. Ramana Rao*****,** Director, National Institute of Technology Warangal for allowing me to submit my research work in the form of a thesis. I express my gratitude to ***Prof. G. R. C. Reddy*****,** former Director, National Institute of Technology Warangal for giving me the opportunity to carry out the research work.

My special words of thanks to ***Dr. Vishnu Shanker,*** Head, Department of Chemistry and ***Prof. P. V. Srilakshmi, Prof. K. V. Gobi,*** former Heads, Department of Chemistry, National Institute of Technology Warangal for their valuable advice, help and support.

I express my sincere thanks to the Doctoral Scrutiny Committee (DSC) members, ***Prof. V. Rajeswar Rao*****,** ***Dr. K. Hari Prasad,*** Department of Chemistry and ***Prof. N. Narasaiah,*** Department of Materials & Metallurgical Engineering for their support and valuable suggestions.

I take this opportunity to express thanks to ***Prof. B. Venkata Appa Rao (Retd), Prof. P. Nageswara Rao (Retd), Prof. A. Ramachandraiah (Retd), Prof. K. Laxma Reddy, Dr. D. Kashinath, Dr. Venkatathri Narayanan, Dr. Raghu Chitta, Dr. S. Nagarajan, Dr. M. Raghasudha, Dr. C. Jugun Prakash, Dr. Ravinder Pawar, Dr. Mukul Pradhan, Dr. Rajeshkhanna Gaddam, Dr. V. Rajeshkumar*** for their suggestions and encouragement.

Financial assistance from the Government of India, University Grants Commission ***(UGC)*** in the form of fellowship is gratefully acknowledged.

My sincere thanks to ***Prof. Dharmarajan Sriram***, Birla Institute of Technology & Science-Pilani, Hyderabad Campus, ***Dr. Vagolu Siva Krishna,*** Postdoctoral Researcher, University of Oslo, Norway for evaluating the anti-TB, cytotoxicity and ***Dr. Ramakrishna Gamidi*** (Ramanujan fellow) NCL-Pune for providing the single crystal X-ray diffraction data.

My special thanks to ***Dr. K. Hari Prasad,*** Assistant Professor, faculty incharge (Bruker-400 MHz NMR instrument) for rendering un-interrupted services to run the instrument.

I am very delighted to work with my colleagues ***Dr. Vinay Pogaku, B. Sravanthi, K. Madhu and V Rukya Naik*** for their support and encouragement during my Ph.D. and this thesis would not have come to a successful completion without the help of these labmates.

It gives me a great pleasure to express my gratitude to my colleagues ***T. Dhananjay Rao, A. Naveen Kumar, G. Sivaparwathi, G. Srinath, B. Prashanth, Dr. G. Ramesh, Dr. K. Vimal Kumar, P. Soumya, Dr. T. Sanjeeva, Dr. Ch. Suman, Dr. V. Sunil Kumar, Dr. M. Venkanna, Dr. K. Sujatha, Dr. J. parameswara chary, Dr. M. Srikanth, Dr. P. Babji, K. Vijendar reddy, A. Ramesh, N. Satyanarayana, Dr. K. Sathish, Dr. K. Shekar, Ch. Raju, Dr. S. Suresh, R. Venkatesh, M. Shireesha, G. Sripal reddy, P. Venkatesham, K. Sampath, T. Shirisha, R. Vara Prasad, B. Anjaiah, R. Arun, S. Akanksha, J. Swathi, B. Srikanth, Pooja, Anindya Roy, Khushboo Agarwala, Tohira Banoo, M. Sasi Sree, Akash Kumar, Avinash Sharma, B. Apurba, M. Subir, M. Faizan, M. Arokiaraj, M. Vijay and all the research scholars from physics and various departments*** for their good compensation and creating a nice atmosphere in and outside the laboratory and their encouragement and help during my research period.

I express my gratitude to my friends ***A. Govind, Ch. P. N. Murthy, D. Bola Shanker, A. Ramya, P. J. V. Surya, G. Krishna and E. Madhu Rekha*** for their encouragement and support.

Also, my thanks to ***Konda Venkanna*** (NMR instrument operator) for his support in recording the NMR spectra.

It would be an understatement to say that I would not be the person I am today without my family. I am extremely grateful to my beloved father ***Sri. Sathibabu*** for his moral support and inspiration to never give up. My heartfelt thanks to my beloved mother ***Smt. Veera Raghava*** for her best wishes and blessings for my success. I would never forget the motivational, inspiring, enthusiastic

behavior of my Sister and Brother-in-law: ***Kusuma*** *and* ***Sandeep***; Brother and Sister-in-law: ***Vasu*** *and* ***Lakshmi***; Grandfather: ***K. Marideswararao***; Grandmothers: ***A. Subbalakshmi*** *and* ***K. Lakshmi***; Uncles and Aunties: ***N. Chandrasekhar*** and ***Ganga Bhavani***; ***B. Rama Krishna*** and ***Gowri***; ***B. Venkateswarulu*** and ***Tharangani***; ***A. Veera Bhadrarao*** and ***Rani***; ***K. Ganesh*** and ***Anusha***; Nephew and Niece: ***Kushal*** *and* ***Thanusree***; for their constant support, cooperation, encouragement, inspiration, love and affection whose blessings made the journey worth effort. I owe everything to them.

(Allaka Bhargava Sai)

ABBREVIATIONS

AChE	:	Acetylcholinesterase enzyme
ACN	:	Acetonitrile (CH_3CN)
AcOH	:	Acetic acid
ADME	:	Absorption, distribution, metabolism and excretion
ADT	:	AutoDock tool
AgOTf	:	Silver trifluoromethanesulfonate
ALA	:	Alanine
Ar	:	Aryl
ARG	:	Arginine
ASN	:	Asparagine
ASP	:	Aspartic acid
a.u.	:	Arbitrary units
$BF_3.Et_2O$	:	Boron trifluoride etherate
Boc	:	*tert*-Butyloxycarbonyl
CCDC	:	Cambridge crystallographic data centre
$CDCl_3$	:	Deuterated chloroform
CFL	:	Compact fluorescent lamp
CH_3CN	:	Acetonitrile
Conc.	:	Concentrated
$CuSO_4$	:	Copper(II) sulphate
CNS	:	Central nervous system
CTAB	:	Cetyltrimethylammonium bromide
Cs_2CO_3	:	Cesium carbonate
$Cu(OAc)_2$	:	Copper(II) acetate
CuI	:	Cupper iodide
CuOTf	:	Copper(I) trifluoromethanesulfonate
d	:	Doublet
dd	:	Doublet of doublet
DABCO	:	1,4-Diazabicyclo[2.2.2]octane
DBH	:	Dibenzoylhydrazine

DBU	:	1,8-Diazabicyclo[5.4.0]undec-7-ene
DCE	:	1,2-Dichloroethane
DCM	:	Dichloromethane
DDQ	:	2,3-Dichloro-5,6-dicyano-1,4-benzoquinone
DEA	:	Diethyl amine
DEAD	:	Diethyl azodicarboxylate
DEPT	:	Distortionless enhancement by polarization transfer
DFT	:	Density functional theory
DHFR	:	Dihydrofolate reductase
DIPEA	:	*N*,*N*-Diisopropylethylamine
DMSO-d_6	:	Deuterated dimethyl sulfoxide
DMF	:	*N*,*N*-Dimethylformamide
DMSO	:	Dimethyl sulfoxide
DNA	:	Deoxyribonucleic acid
D_2O	:	Deuterium oxide
DPPH	:	2,2-diphenyl-1-picrylhydrazyl/1,1-diphenyl-2-picrylhydrazyl
EDX	:	Energy-dispersive X-ray
EGFR	:	Epidermal growth factor receptor
EtOH	:	Ethanol
Et_3N	:	Triethylamine
ESI	:	Electrospray ionization
EtOAc	:	Ethyl acetate
Equiv	:	Equivalents
FT-IR	:	Fourier transform infrared
$FeCl_3$	:	Iron(III) chloride
$Fe(NO_3)_3$	:	Iron(III) nitrate
$Fe(OTs)_3$	:	Iron(III) tosylate
GLN	:	Glutamine
GLU	:	Glutamic acid
GLY	:	Glycine

h	:	Hours
HCT116	:	Human colorectal carcinoma cell line
HepG2	:	Liver hepatocellular carcinoma
H_2O	:	Water
H_2O_2	:	Hydrogen peroxide
HRMS	:	High resolution mass spectrometry
HIV	:	Human immunodeficiency virus
H_Z	:	Hertz
IC_{50}	:	Half maximal inhibitory concentration
ILE	:	Isoleucine
$InCl_3$	:	Indium chloride
InhA	:	Enoyl acyl carrier protein
IR	:	Infrared
J	:	Coupling constant
KBr	:	Potassium bromide
K_2CO_3	:	Potassium carbonate
KOAc	:	Potassium acetate
KO*t*-Bu	:	Potassium *tert*-butoxide
LEU	:	Leucine
LiO*t*-Bu	:	Lithium *tert*-butoxide
LYS	:	Lysine
m	:	Multiplet
m-CPBA	:	*meta*-Chloroperoxybenzoic acid
MCF-7	:	Michigan cancer foundation-7
MCR	:	Multicomponent reaction
MDA-MB 231	:	M.D. anderson - Metastatic breast 231
MDM2	:	Murine double minute 2
MeOH	:	Methanol
$Mg(OTf)_2$	:	Magnesium triflate
MS	:	Molecular sieves
MS/MS	:	Tandem mass spectrometry

MET	:	Methionine
mg	:	Milligram
MHz	:	Megahertz
min	:	Minutes
MIC	:	Minimum inhibitory concentration
mL	:	Millilitre
mmol	:	Milli mole
mp	:	Melting point
MTT	:	3-(4,5-dimethylthiazol-2-yl)-2,5-diphenyltetrazolium Bromide
MTB	:	Mycobacterium tuberculosis
MsOH	:	Methanesulfonic acid
MW	:	Microwave irradiation
NADP	:	Nicotinamide adenine dinucleotide phosphate
NADPH	:	Reduced form of nicotinamide adenine dinucleotide phosphate
$NaHCO_3$	:	Sodium bicarbonate
NaN_3	:	Sodium azide
NaOAc	:	Sodium acetate
NaOH	:	Sodium hydroxide
ND	:	Not determined
$(NH_4)_2CO_3$	:	Ammonium carbonate
NH_4OAc	:	Ammonium acetate
NMR	:	Nuclear magnetic resonance
NSAID	:	Non-steroidal anti-inflammatory drugs
ORTEP	:	Oak ridge thermal ellipsoid plot
PC-3	:	Prostate cancer stem cells
PDB	:	Protein data bank
Pd/C	:	Palladium on carbon
$PdCl_2$	:	Palladium(II) chloride
$Pd(PPh_3)_4$	:	Tetrakis(triphenylphosphine)palladium(0)

$Pd(OAc)_2$	:	Palladium(II)acetate
PEG	:	Polyethylene glycol
Ph	:	Phenyl
PHE	:	Phenylalanine
$PhI(OAc)_2$	:	(Diacetoxyiodo)benzene
PivOH	:	Pivalic acid
PLK4	:	Polo-like kinase 4
$P(NMe_2)_3$	:	Tris(dimethylamino)phosphine
ppm	:	Parts per million
PRO	:	Proline
q	:	quartet
$Rh_2(OAc)_4$	:	Rhodium(II) acetate dimer
RT	:	Room temperature
s	:	Singlet
SAR	:	Structure activity relationship
SD	:	Standard deviation
SER	:	Serine
SiO_2	:	Silicon dioxide
SKOV-3	:	Ovarian cancer cell line
SOI	:	Secondary orbital interaction
Sm	:	Samarium
$SnCl_2$	:	Tin(II) chloride
SXRD	:	Single crystal X-ray diffraction
t	:	Triplet
TB	:	Tuberculosis
TBHP	:	*tert*-Butyl hydroperoxide
TBP	:	Tributyl phosphate
TBPB	:	*tert*-Butyl peroxybenzoate
^tBuOH	:	*tert*-Butyl alcohol
TEMPO	:	(2,2,6,6-Tetramethylpiperidin-1-yl)oxyl
TFA	:	Trifluoroacetic acid

TFE	:	Trifluoroethanol
TfOH	:	Triflic acid
THF	:	Tetrahydrofuran
THR	:	Threonine
$TiCl_4$	:	Titanium tetrachloride
TLC	:	Thin layer chromatography
TMS	:	Tetramethylsilane
TMSCN	:	Trimethylsilyl cyanide
TPP	:	Thiamine pyrophosphate
Ts	:	Toluenesulfonyl
UV-Vis	:	Ultraviolet-visible
$VOSO_4$	:	Vanadium(IV) oxysulfate
W	:	Watts
ZSM-5	:	Zeolite socony mobil-5
μg/mL	:	Microgram/millilitre
μM	:	Micro molar
)))))	:	Ultrasonication
Δ	:	Thermal
δ	:	Chemical shift
hν	:	Photochemical

Table of Contents

CHAPTER-I

INTRODUCTION

1.1. Introduction

Heterocyclic compounds are cyclic organic compounds which contain one or more hetero atoms (N, O, S etc.) in their ring system. These are building blocks for various pharmaceutical drugs such as captopril, metronidazole, isoniazid, azidothymidine, chlorpromazine, chloroquine, sitagliptin, diazepam, ozanimod and methotrexate. They have been found to be useful in wide range of applications like medicinal chemistry which exhibits anti-cancer, anti-inflammatory, anti-microbial, anti-tubercular, anti-viral, anti-diabetic, anti-malarial activities, pharmaceuticals, agrochemicals and materials chemistry. Among these, spiro heterocyclic compounds are the unique class of heterocyclic compounds [1-5].

In 1900, Adolf von Baeyer first described the nomenclature of the spiran. Spiro compounds are the compounds in which the two rings are connected by a single atom [6]. In the past few decades, a plethora of efficient methods has been established for the construction of spiro heterocyclic compounds and novel methods are still emerging due to their unique structural features and biological applications [7,8] (Figure 1.1).

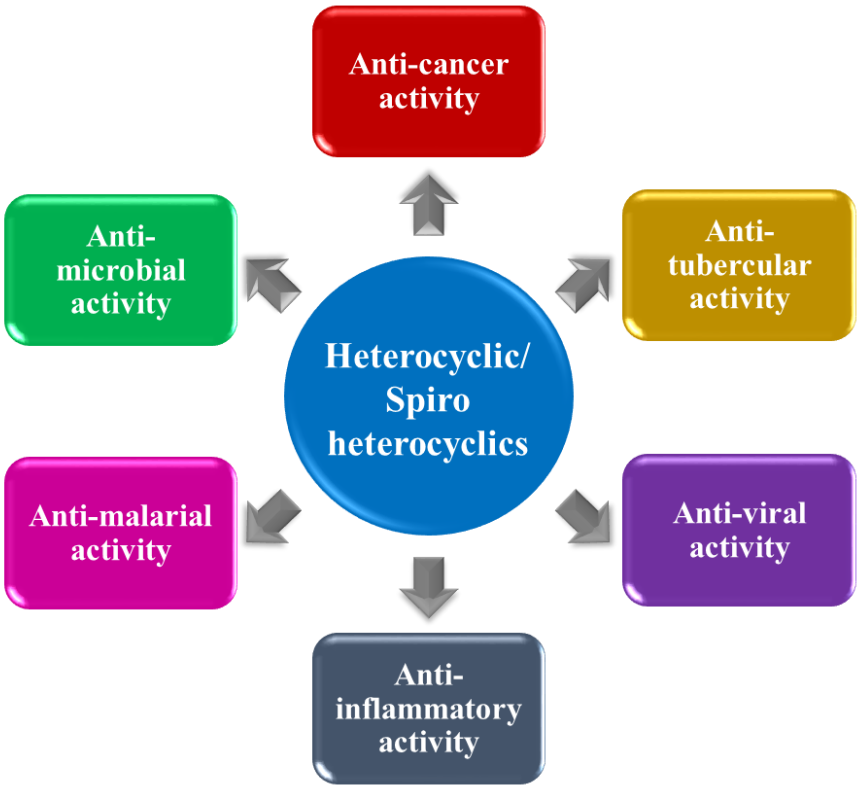

Figure 1.1. Various pharmacological activities of the heterocyclic/spiro heterocyclic compounds.

Several spiro heterocyclic compounds have been used as drugs and some are under clinical trials. For example, spironolactone, griseofulvin, fluspirilene, irbesartan and rifabutin are the spiro cyclic drugs used for the treatment of various diseases [9] (Figure 1.2).

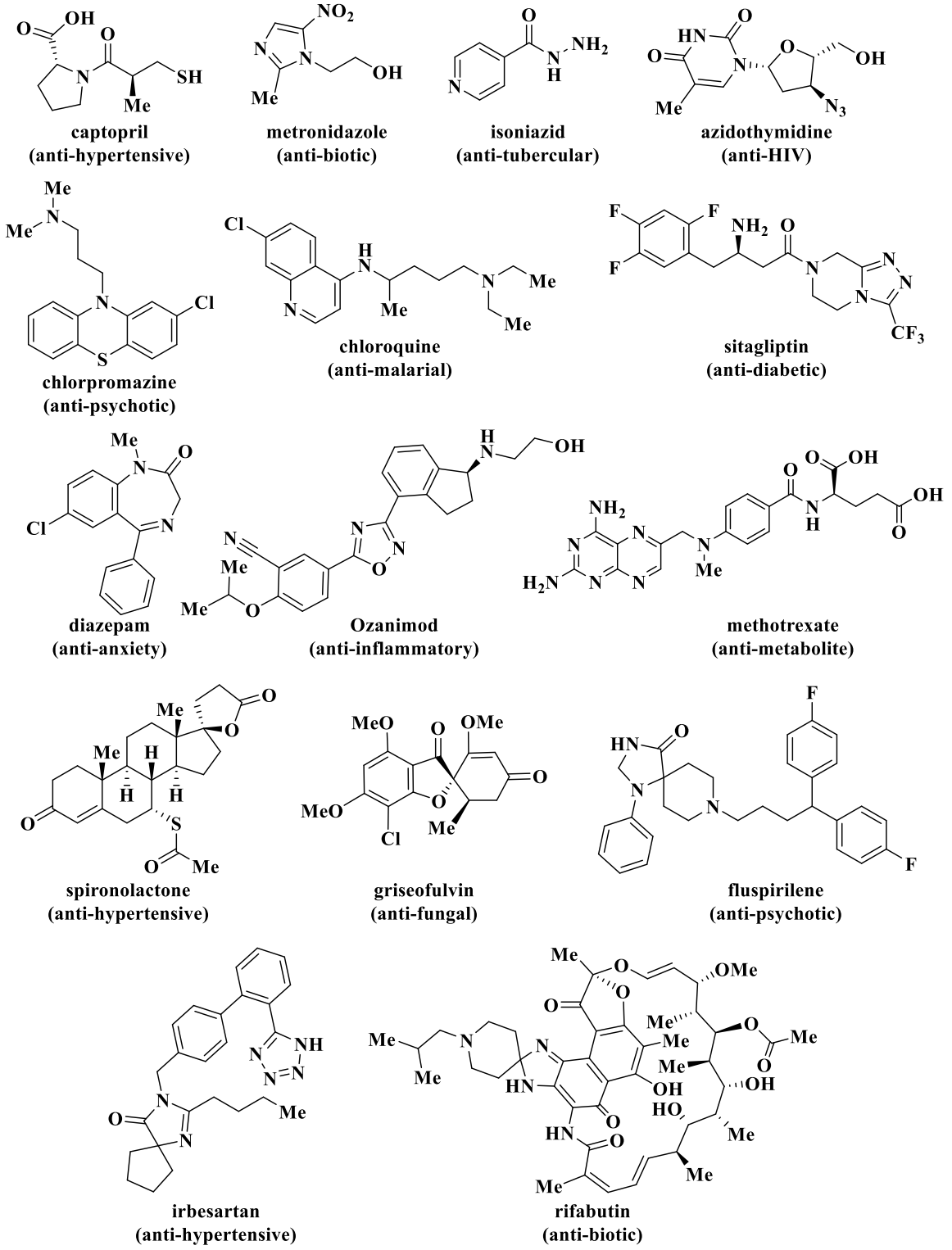

Figure 1.2. Some of the important pharmaceuticals containing heterocyclic and spiro heterocyclic moieties.

On the other hand, nitrogen containing heterocycles have been displayed a prominent role in designing a new class of structural entities for medicinal applications [10]. In particular pyrrole, pyrazole and triazoles are attracted frame works for the discovery and development of wide range of biologically active compounds for the treatment of various diseases [11,12].

1.2. Pyrroles

Pyrrole is a nitrogen containing simple heterocycle that can be found in a wide range of natural products and drug molecules [13]. Pyrrole unit has diverse applications in therapeutically active molecules including anti-fungal, anti-biotic, anti-inflammatory drugs, cholesterol reducing agents, anti-tumor agents [14-16]. Moreover, they are also precursors of polymers, indigoid dyes and of larger aromatic rings [17]. The marketed drugs having a pyrrole ring system are known to have many biological properties. For instance, tolmetin is a nonsteroidal anti-inflammatory drug consisting of pyrrole moiety marketed as tolectin [18]. Whereas, amtolmetin is a non-acidic prodrug of tolmetin, having nonsteroidal anti-inflammatory properties with additional analgesic, anti-pyretic, and gastro protective properties [19]. The drug sudoterb is under phase-III clinical trials for the treatment of tuberculosis [20]. A natural marine alkaloid, polycitone A was isolated from the marine ascidian polycitor africanus [21], used for the treatment of cancer (Figure 1.3).

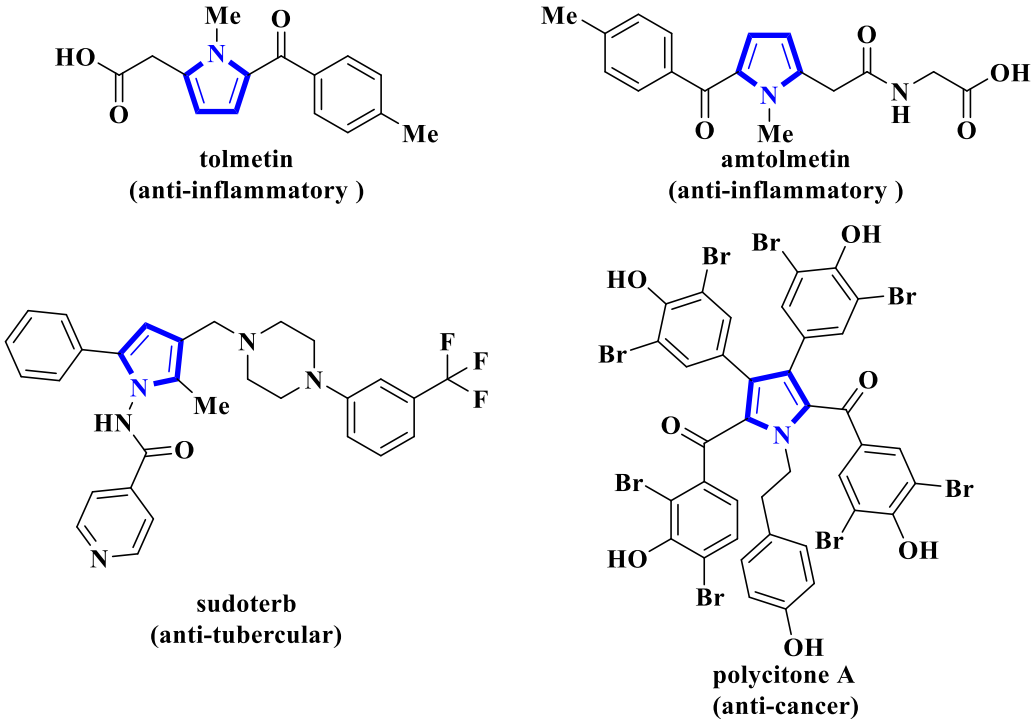

Figure 1.3. Commercially available pharmaceuticals having pyrrole moiety.

1.2.1. Synthesis and biological activities of the pyrrole derivatives

Dyson et al. synthesized the analogues of natural product oroidin and screened their biological activity against twelve cancer cell lines (Figure 1.4). Out of all the compounds seven compounds exhibit potent activity against colon cancer cell line HT29 [22].

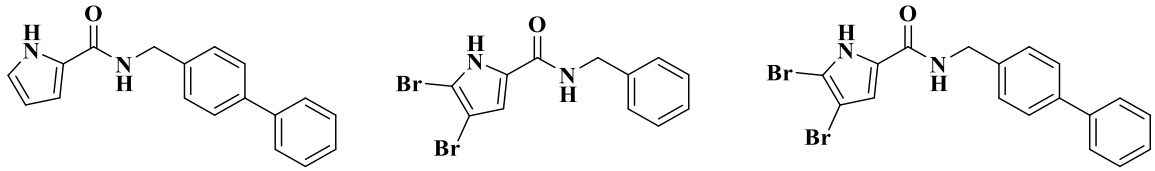

Figure 1.4

Biava and co-workers design and synthesized 1,5-diaryl-2-methyl pyrrole derivatives as anti-tubercular agents (Figure 1.5). Among all the synthesized compounds the best active compound showed a good biological profile towards both mycobacterium tuberculosis (MTB) H37Rv and MTB rifampicin-resistant strains [23].

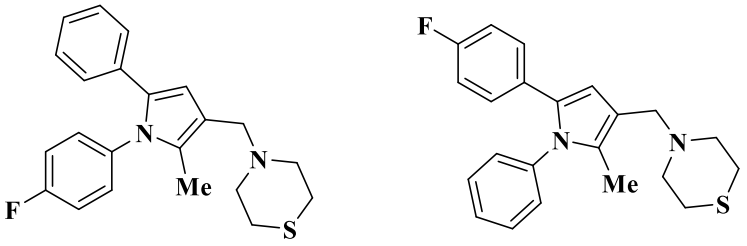

Figure 1.5

Romagnoli and co-workers reported the palladium mediated coupling approach for the synthesis of pyrrole moiety interposed between two aryl rings and evaluated for *in vitro* anti-proliferative activity (Figure 1.6). Further, cytotoxicity studies and *in vivo* activity were also evaluated for the potent molecules [24].

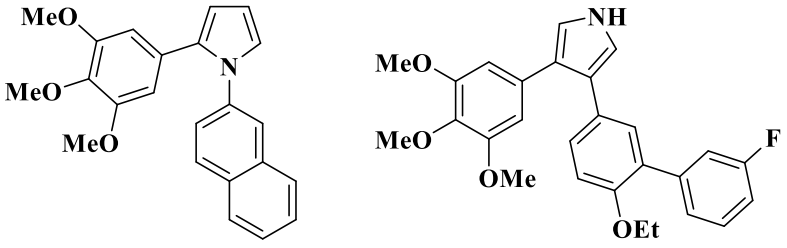

Figure 1.6

Luo et al. demonstrated highly chemo and regioselective synthesis of multi-substituted pyrroles *via* AgOTf catalyzed [4+1] cascade reaction of enaminones with donor/acceptor or donor/donor carbenes (Scheme 1.1). This protocol was used for the formal synthesis of natural product lamellarin L [25].

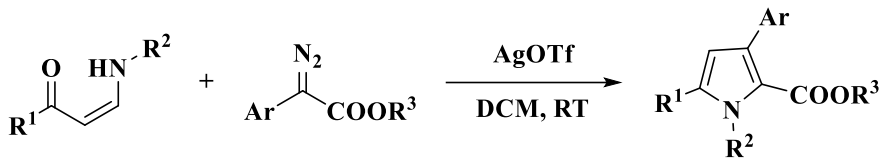

Scheme 1.1

Dou et al. described the titanium catalyzed highly regioselective synthesis of polysubstituted pyrroles through three component reaction of 1,3-diketones, aldehydes and amines (Scheme 1.2). High regioselectivity, shorter reaction times, high yields and commercially available starting materials were the main feature of this methodology [26].

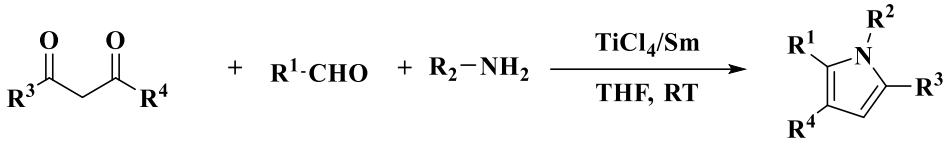

Scheme 1.2

Hong et al. developed an efficient approach for the construction of polysubstituted pyrroles *via* a copper catalyzed three component reaction of α-diazoketones, nitroalkenes and amines under aerobic conditions (Scheme 1.3). This cascade approach involves an N-H insertion of carbene, oxidative dehydrogenation of amine and [3+2] cycloaddition of azomethine ylide [27].

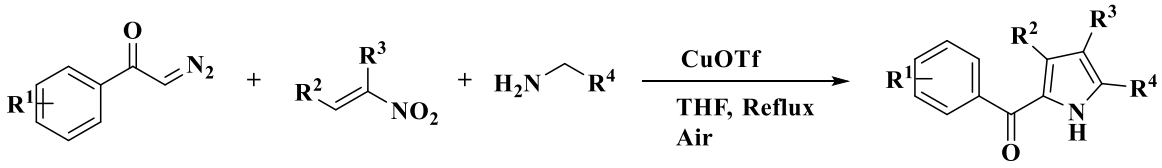

Scheme 1.3

1.3. Pyrazoles

Pyrazole is a five membered heterocycle composed of three carbon atoms and two nitrogen atoms present at adjacent position. Pyrazole scaffolds are attractive and having a wide range of applications in various fields like medicinal chemistry, pharmaceuticals, agrochemicals, catalysis, pesticides and materials chemistry [28-31]. Various pyrazole containing heterocyclic compounds are also gain significant attention because of their utility as synthetic reagents in multicomponent reactions, chiral auxiliaries, semiconductors, liquid crystals, organic light emitting diodes and brightening agents [32,33]. Pyrazoles exhibit various biological activities such as anti-bacterial, anti-viral, anti-cancer, anti-inflammatory, anti-convulsant, anti-tuberculosis, anti-parasitic, anti-neoplastic [34,35] etc. Several pyrazole linked heterocyclic derivatives have been found as

drugs for the treatment of various diseases. For example, bixafen is a pyrazole based insecticide which is used as fungicide on cereals [36]. Fezolamine is a drug which was investigated by Sterling Drug as an anti-depressant [37]. Whereas, sedaxane is a pyrazole amide chemical moiety used as fungicide in the European union [38]. Crizotinib used for the treatment of cancer [39], which was sold under the brand name xalkori and the compound lonazolac is a pyrazole carboxylic acid based nonsteroidal anti-inflammatory drug used for the treatment of painful inflammatory rheumatic diseases of the joints and spine [40] (Figure 1.7).

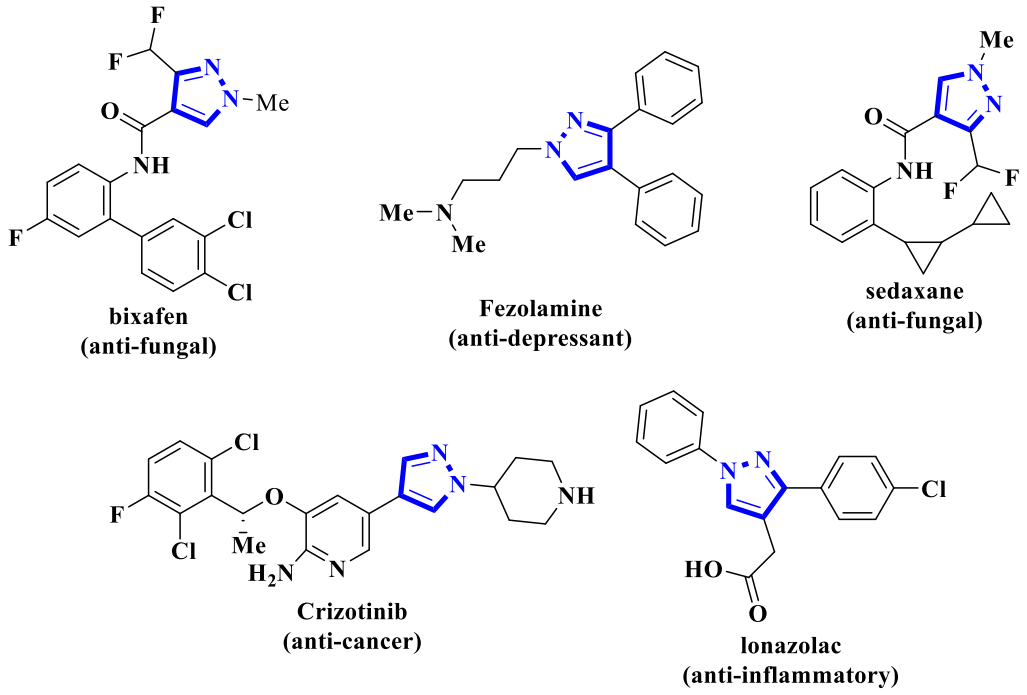

Figure 1.7. Commercially available pyrazole based pharmaceuticals.

1.3.1. Synthesis and biological activities of the pyrazole derivatives

Ramesh et al. repurposed the rimonabant scaffold towards the development of potent anti-tubercular agents (Figure 1.8). The *in vitro* anti-tubercular activity was evaluated against Mtb H37Rv using alamar blue assay method. In addition, cytotoxicity studies and ADME prediction were also performed to the most active compounds [41].

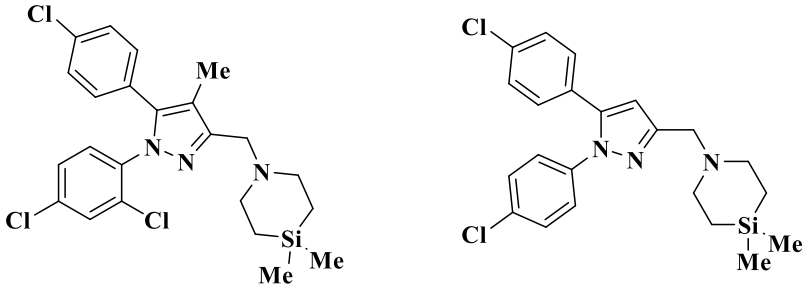

Figure 1.8

Kalaria and co-workers presented L-proline promoted regioselective synthesis of pyrazole based trifluoromethyl fused thiazolopyran scaffolds (Figure 1.9). All the synthesized compounds were tested for *in vitro* anti-bacterial activity against gram positive bacteria B. subtilis, C. tetani and *in vitro* anti-tubercular activity against mycobacterium tuberculosis H37Rv. Majority of the synthesized compounds showed potent inhibitory against bacterial strains and exhibited good anti-tuberculosis activities [42].

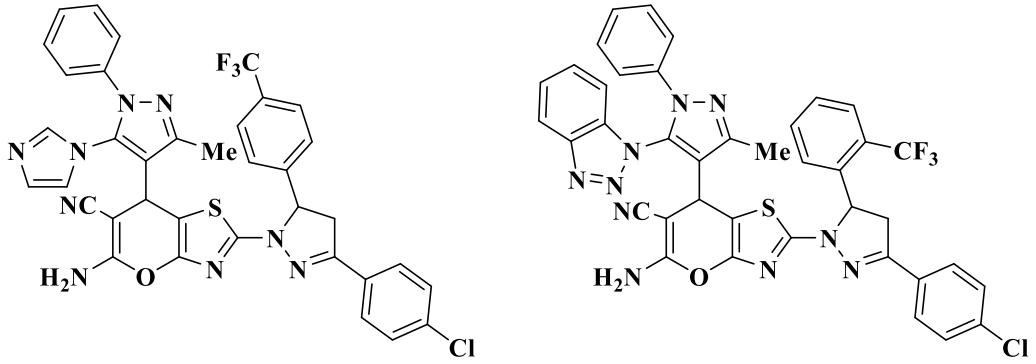

Figure 1.9

Kumar et al. disclosed chromenylpyrazolecarboxylates as novel anti-cancer agents. The title compounds were synthesized by [3+2] cycloaddition of chromenophenylhydrazones with diethyl acetylenedicarboxylates (Figure 1.10). All the synthesized compounds were screened for *in vitro* anti-cancer activity against three human cancer cell lines such as prostate (DU-145), lung adenocarcinoma (A549), and cervical (HeLa) by standard MTT assay method [43].

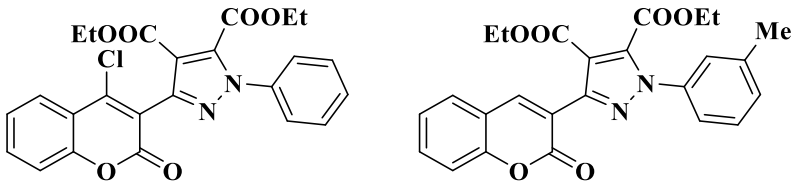

Figure 1.10

Panda and co-workers developed an iron catalyzed one-pot regioselective synthesis of 1,3-disubstituted pyrazoles from diarylhydrazones and vicinal diols (Scheme 1.4). Various electron donating and electron withdrawing substituents on aromatic ring were well tolerated in this reaction [44].

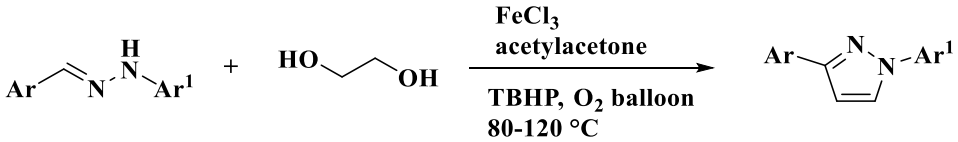

Scheme 1.4

Zhang and co-workers employed a simple and straight forward one-pot reaction of vinyl azides, aldehydes and tosylhydrazine for the construction of polysubstituted pyrazoles (Scheme 1.5). The reaction proceeded regioselectively in the presence of base and afforded a wide range of substituted pyrazoles in moderate to excellent yields [45].

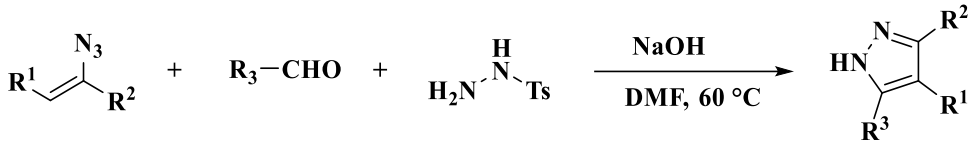

Scheme 1.5

Senadi et al. described the I_2-TBHP catalyzed oxidative cross-coupling reaction of *N*-sulfonyl hydrazones with isocyanides for the generation of 5-aminopyrazoles *via* [4+1] annulation (Scheme 1.6). Metal free strategy, atom economy, shorter reaction times, broad functional group tolerance and good reaction yields were the main features of this protocol [46].

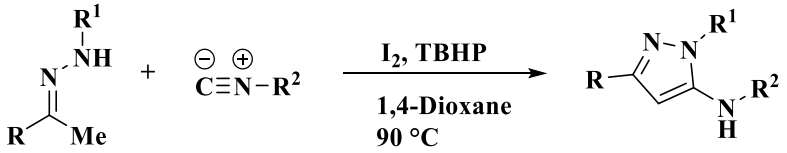

Scheme 1.6

1.4. Triazoles

Triazoles constitute a prominent role in chemical community because of their various applications in pharmaceuticals, agrochemicals and materials sciences [47-49]. In particular, 1,2,3-triazoles show a broad spectrum of biological activities such as anti-cancer, anti-tubercular, analgesic, anti-viral, anti-fungal, anti-bacterial, anti-inflammatory etc [50-52]. Currently, several 1,2,3-triazole based heterocyclic compounds are used as drugs and some of the compounds are under clinical trials for the treatment of various diseases. For instance, mubritinib is a protein kinase inhibitor and commercially available as TAK-165 used for the treatment of cancer [53]. I-A09 is a triazole linked noncompetitive mycobacterial protein tyrosine phosphatases A and B (mPTPB) inhibitor, which is under clinical trials for the treatment of tuberculosis [54]. Whereas, the compound 4-carboxy-5-(1-pentyl) hexylsulfanyl-1,2,3-triazole (DB04374) is under clinical trials as anti-bacterial drug [55] (Figure 1.11).

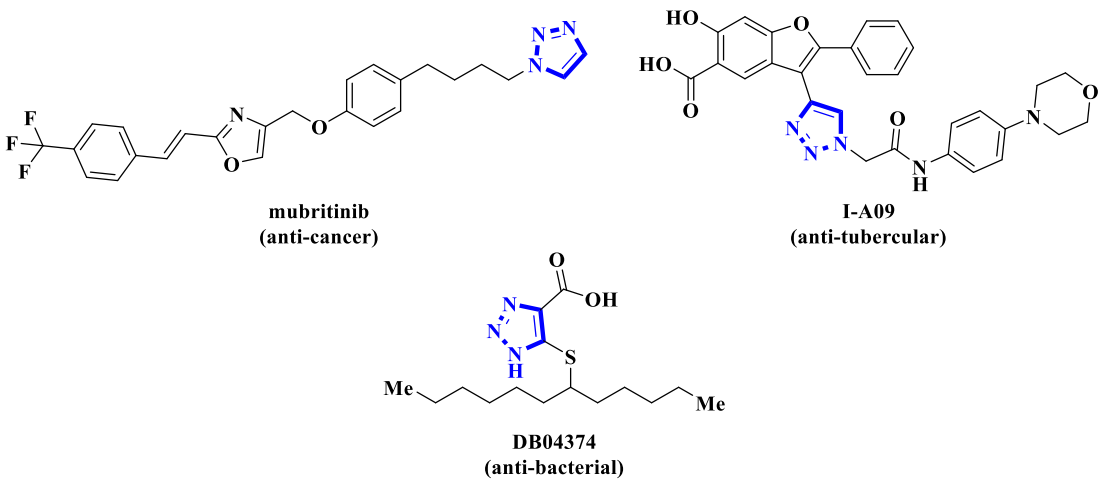

Figure 1.11. Some of the biologically active triazole derivatives.

1.4.1. Synthesis and biological activities of the triazoles

Chui and co-workers design and synthesized triazole linked 1,3,5-triazanes as selective mycobacterium tuberculosis dihydrofolate reductase (DHFR) inhibitors (Figure 1.12). All the synthesized compounds showed good anti-tubercular activity on M. tuberculosis H37Rv, in addition the potent compounds exhibited low cytotoxicity and hemolytic activity [56].

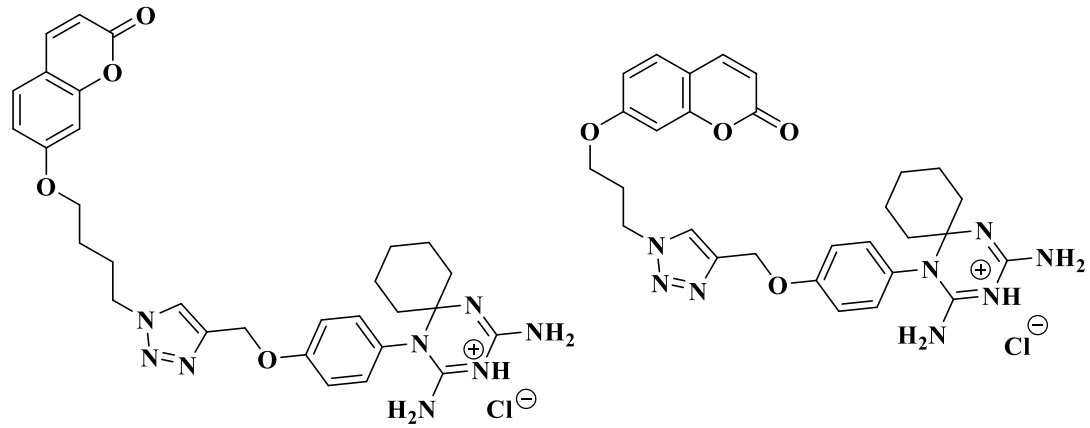

Figure 1.12

Hou et al. established a concise and efficient approach to generate 1,2,3-triazole-tethered dehydroabietic acids (Figure 1.13). Further, *in vitro* anti-proliferative activity was evaluated on four different human cancer cell lines, including ovary (SKOV-3), prostate (PC-3) and breast (MDA-MB-231 and MCF-7). The results showed that most of the synthesized compounds exhibited potent anti-proliferative activities [57].

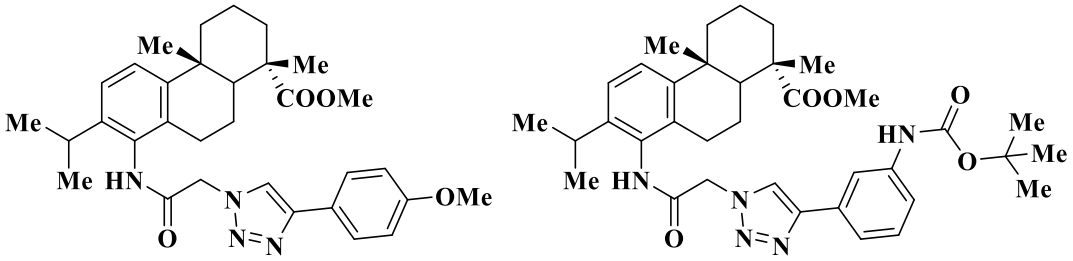

Figure 1.13

Stevaert et al. described the discovery of 1,2,3-triazolo-fused betulonic acid derivatives as a class of human coronavirus (HCoV) nsp15 inhibitors (Figure 1.14). The structure activity relationship analysis, resistance data and molecular docking studies provided a strong evidence that the synthesized compounds showed good anti-viral activity [58].

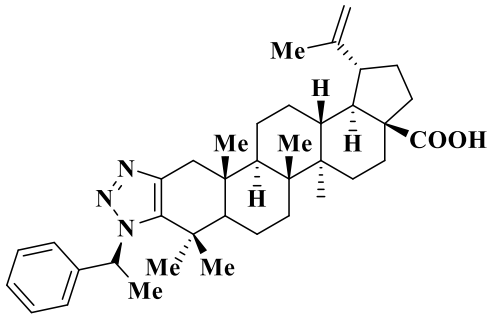

Figure 1.14

Shu and co-workers reported a molecular iodine promoted [4+1] cyclization reaction for the generation of 4-aryl-*NH*-1,2,3-triazoles from *N*-tosylhydrazones and sodium azide (Scheme 1.7). In this protocol various 1,2,3-triazoles were produced under metal free approach through sequential C–N and N–N bond formation in a single step [59].

Scheme 1.7

Qiu et al. disclosed the potassium *tert*-butoxide promoted intermolecular cycloaddition of *N*-tosylhydrazones with nitriles for the construction of 4,5-diaryl-2*H*-1,2,3-triazoles (Scheme 1.8). In this transformation, a variety of triazoles were prepared in good yields under azide and transition metal free approach [60].

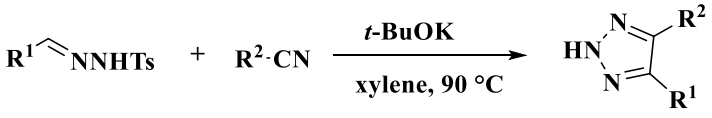

Scheme 1.8

Chen et al. described a new general approach for the preparation of polysubstituted triazoles from anilines and *N*-tosylhydrazones through copper mediated reaction (Scheme 1.9). Low cost of reagents, broad substrate scope and convenient operating conditions were the main features of this protocol [61].

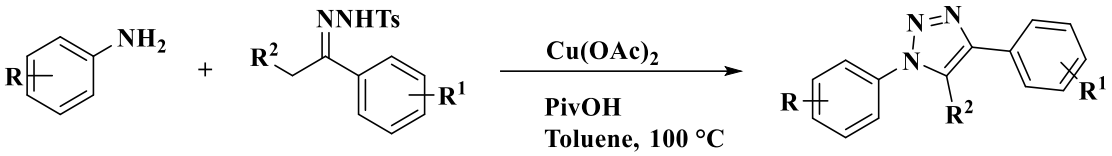

Scheme 1.9

1.5. Spirooxindoles

Spirocyclic scaffolds are playing an important role in the drug discovery and medicinal chemistry because of their privileged biological properties [62]. The three dimensional structure of spirocyclic moiety allows more easily binding interactions with three dimensional binding sites of various biological targets when compared to the planar (hetero) aromatic systems as ligands [63]. Subsequently, a large number of spirocyclic scaffolds are frequently exist in natural biologically active products [64]. Among them, spirooxindolo-pyrrolidine hybrid frameworks (oxindoles attached with pyrrolidines *via* a spiro carbon) are present in several alkaloids and pharmacologically active compounds [65,66]. These derivatives have been reported their wide range of biological activities such as anti-cancer, anti-tuberculosis, anti-microbial, anti-malarial, anti-HIV, anti-inflammatory, analgesic, local anesthetic and AChE inhibitors [67-69]. These are also used as pharmacophores for the treatment of various diseases. For example, some of the natural products such as spirotryprostatin B (anti-cancer) [70], strychnofoline (anti-cancer) [71], elacomine (anti-analgesic) [72], uncarine F (anti-cancer) [73], speciophylline (anti-neoplastic) [74], cipargamin (anti-malarial) [75] were reported their promising activities and synthetic molecules MI-888 and MI-219 are under clinical studies for the treatment of cancer [76]. Some of the biologically active spirooxindoles were shown in Figure 1.15.

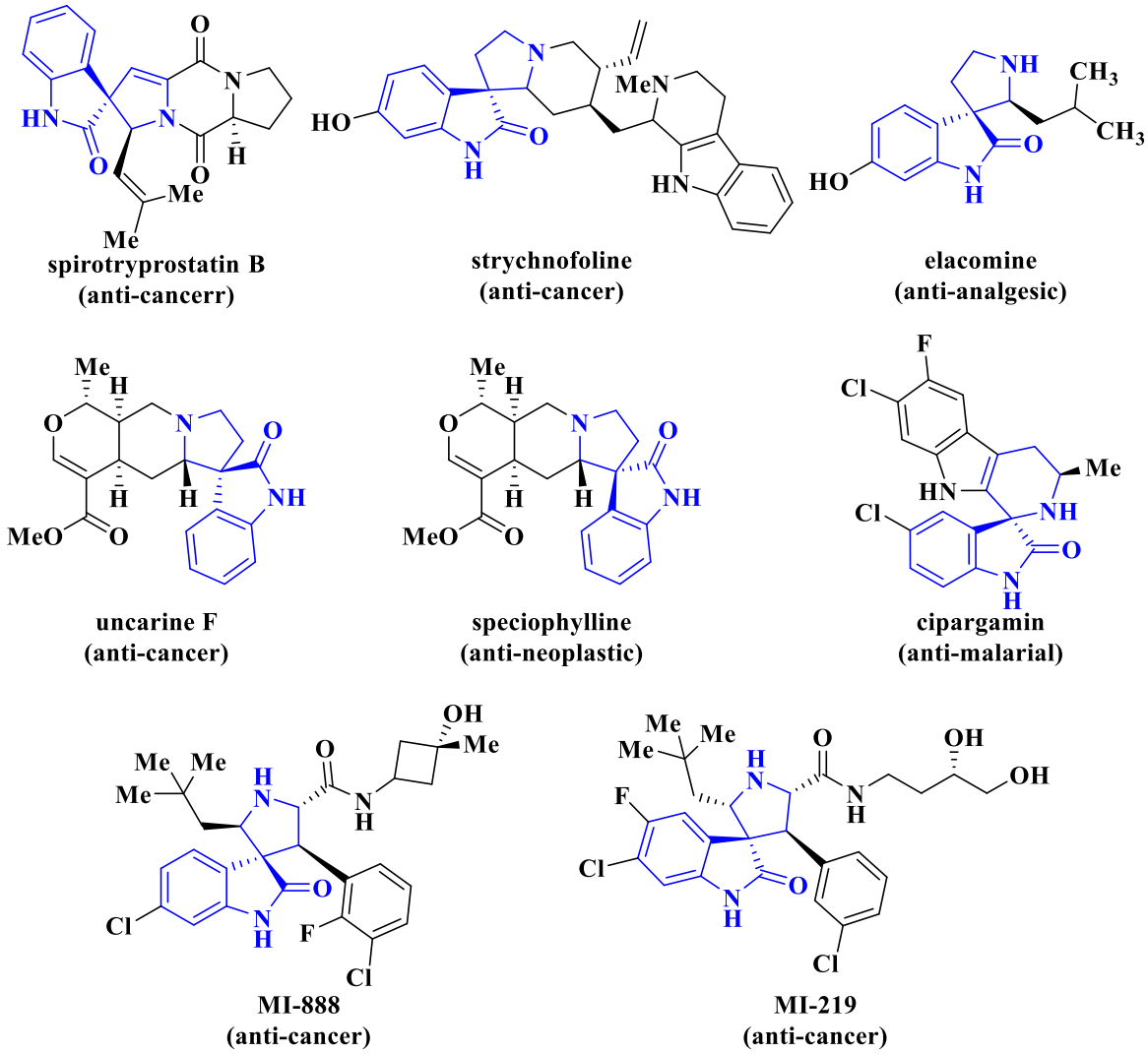

Figure 1.15. Some of the biologically active spirooxindoles.

1.5.1. Reported methods for the synthesis and biological activities of spirooxindoles

Rodriguez et al. reported a combined scaffold directed synthesis for the generation of bis-spirooxindolo-cyclopropanes (Figure 1.16). The synthesized compounds were evaluated for cancer cell proliferation through disruption of ribosomal function and the findings reported that they have showed good anti-cancer activity [77].

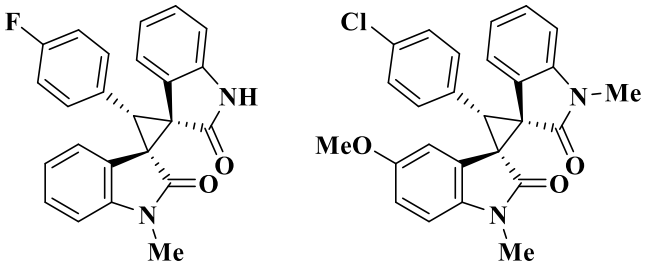

Figure 1.16

Li and co-workers design and synthesized (3-aryl-1*H*-indazolyl)spirocyclopropane-indolinones as potent PLK4 inhibitors with oral anti-cancer efficacy (Figure 1.17). Subsequently, *in vivo* anti-cancer activity of the highly active compounds were evaluated on mouse xenograft studies using the MDA-MB-468 human breast cancer cell line [78].

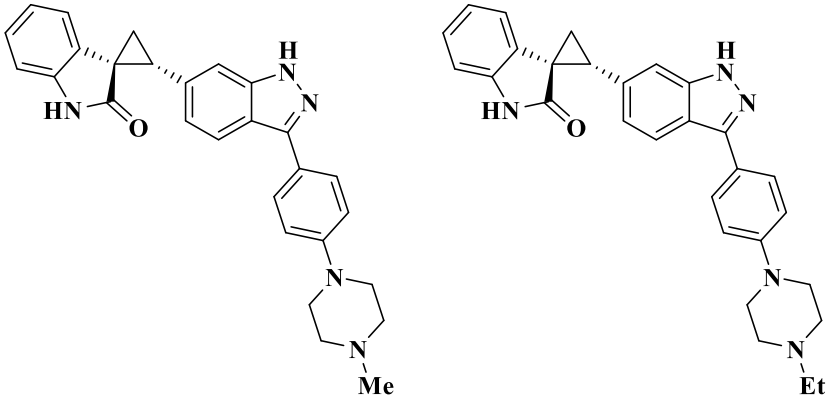

Figure 1.17

Ding et al. described the structure based strategy for the synthesis of non-peptide small molecule spirooxindolo-pyrrolidines as anti-cancer agents (Figure 1.18). The synthesized compounds act as MDM2 inhibitors to target the p53-MDM2 interaction for the treatment of cancer [79].

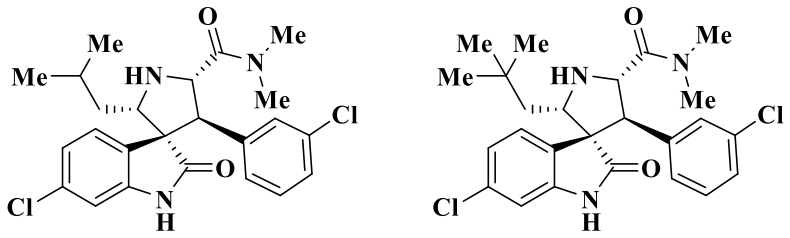

Figure 1.18

Arumugam et al. accomplished a facile and one-pot synthesis of novel spiropyrrolidines with β-lactum substituent through 1,3-dipolar cycloaddition (Figure 1.19). Further, the synthesized compounds were evaluated for anti-microbial activity against four human bacterial pathogens and found to exhibit good anti-microbial activity at lower concentration [80].

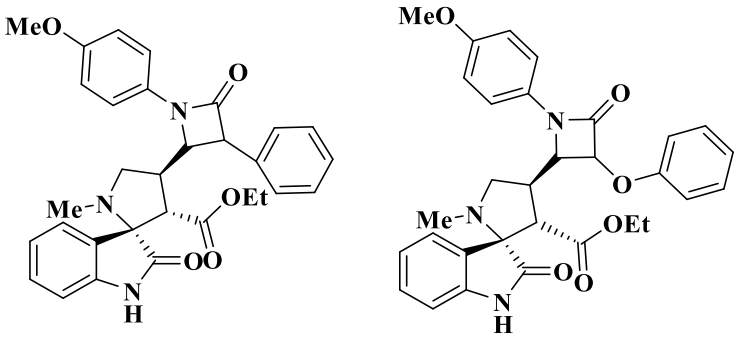

Figure 1.19

Osman and co-workers discovered the novel piperidine grafted spirooxindolo-pyrrolizines as potent cholinesterase inhibitors (Figure 1.20). In addition, molecular modeling stimulation for the binding interaction of the most active compounds were evaluated and found that the docking results were in well agreement with their cholinesterase assay [81].

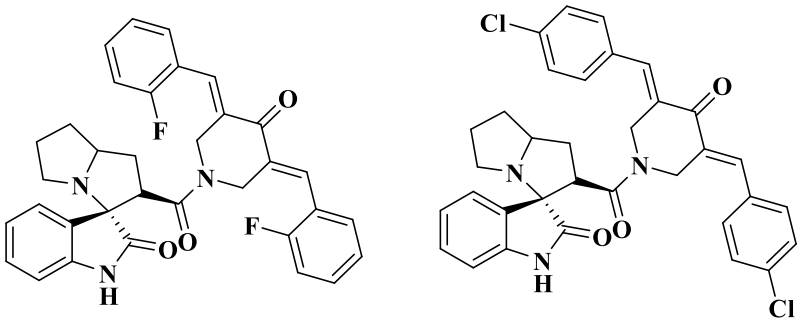

Figure 1.20

Perumal and co-workers synthesized dispirooxindolo-pyrrolidine derivatives through 1,3-dipolar cycloaddition reaction (Figure 1.21). Further, the synthesized compounds were evaluated for anti-microbial activity against both gram positive and gram negative bacteria and also anti-cancer activity against A549 human lung adenocarcinoma cancer cell lines [82].

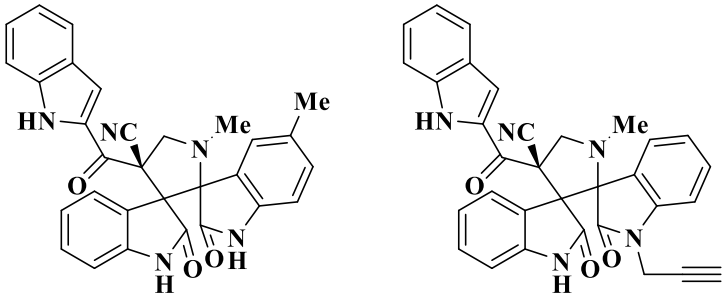

Figure 1.21

Lin et al. developed a diversity oriented one-pot multicomponent synthesis of pyrrolizidinyl-dispirooxindoles *via* multicomponent [3+2] cycloaddition reaction (Figure 1.22). Further, all the synthesized compounds were evaluated their anti-cancer activity on human cancer cell lines and the potent molecules were also screened for cytotoxicity on normal cell lines [83].

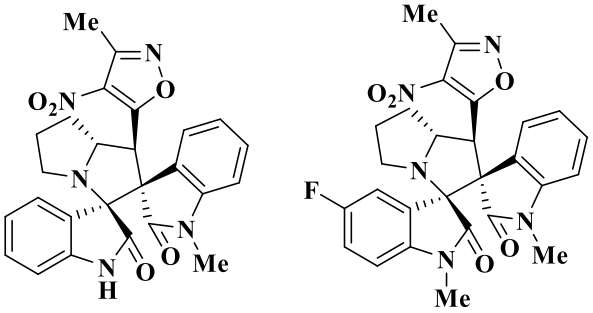

Figure 1.22

Lu and co-workers employed an asymmetric cyclopropanation of oxindoles for the generation of highly diastereo divergent spirocyclopropyloxindoles (Scheme 1.10). In this reaction oxindoles were utilized as C_1 synthons and bromonitroolefins as C_2 synthons [84].

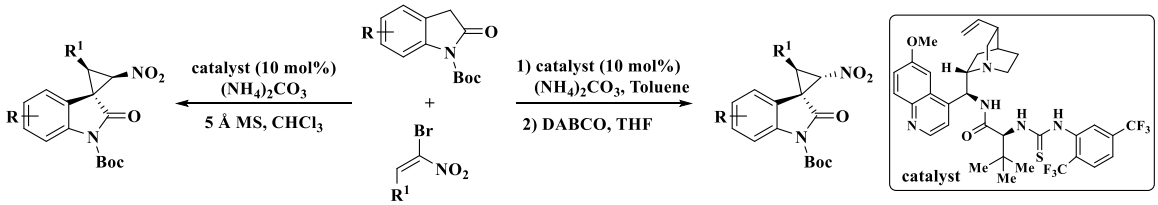

Scheme 1.10

Zhou and co-workers reported a deoxygenative [4+1] annulation for the efficient synthesis of tri-substituted spirooxadiazoles using *N*-acyldiazenes and isatins (Scheme 1.11). Mild reaction conditions, commercially available starting materials and broad substrate scope were the main features of this protocol [85].

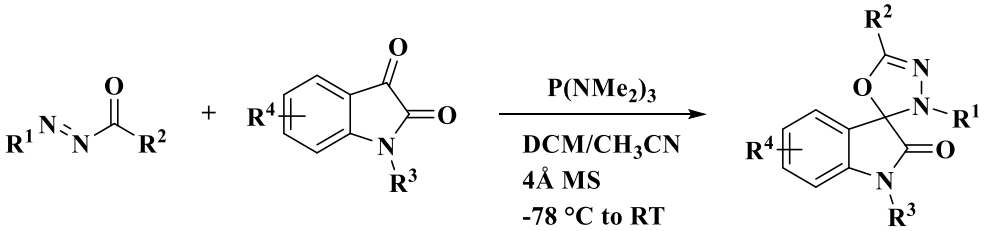

Scheme 1.11

Gong and co-workers established an efficient protocol for the construction of biologically prominent spiro-pyrrolidin-oxindole scaffolds with contiguous quaternary stereogenic

centers using an organocatalytic [3+2] cycloaddition of isatin based azomethine ylide (Scheme 1.12). Further, preliminary cytotoxicity assay was evaluated for the synthesized compounds and showed moderate cytotoxicity to SW116 cells [86].

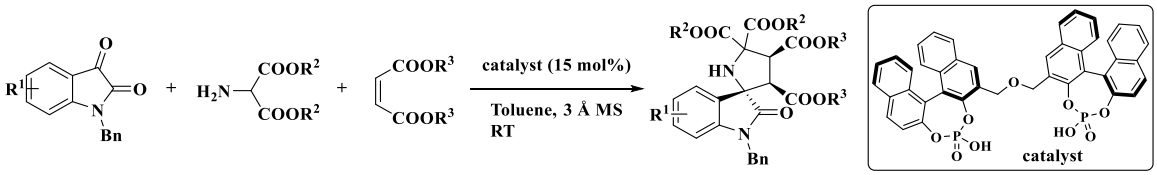

Scheme 1.12

Singh and co-workers synthesized a series of benzimidazo[2,1-*b*]thiazolidinone based dispirooxindolo-pyrrolidines *via* 1,3-dipolar cycloaddition reaction under an efficient and eco-friendly reaction parameters (Scheme 1.13). Shorter reaction times, high yields and utilization of trifluoroethanol (TFE) as an efficient reaction medium were the main features of this protocol [87].

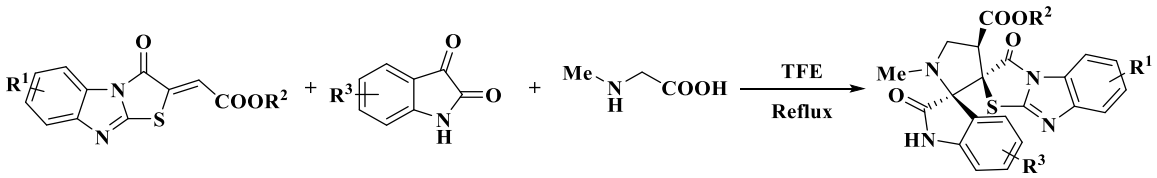

Scheme 1.13

1.6. Quinolines

Quinoline is one of the prominent moiety for the construction of large number of heterocyclic scaffolds. They play a vital role in medicinal chemistry due to their wide occurrence in natural products and broad spectrum of biological activities [88]. The incorporation of quinoline or its derivatives with other compounds could increase their biological activity or create new medicinal properties like anti-tumor activity, anti-tubercular activity, cytotoxic toward the leukemia P388 cells [89,90] etc. Camptothecin is a quinoline having natural product, which is used as traditional Chinese medicine for the treatment of cancer [91]. Topotecan is a quinoline containing synthetic drug sold under brand name hycamtin for the treatment of cancer [92]. The drug TMC207 is under clinical trials for the treatment of tuberculosis [93]. Whereas, the drug mefloquine sold under brand name lariam, is a medication used to prevent malaria [94] (Figure 1.23).

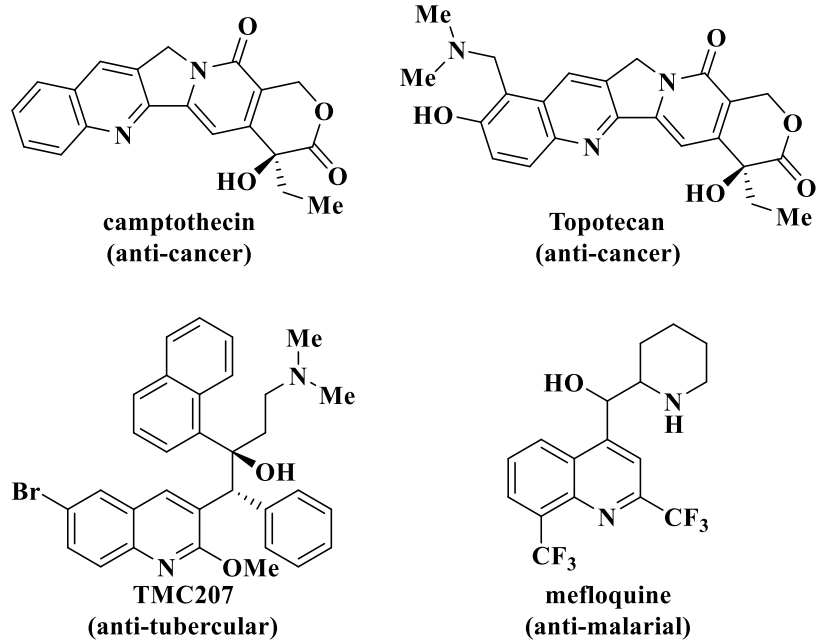

Figure 1.23. Some of the biologically active quinoline scaffolds.

Khunt and co-workers synthesized substituted 2-chloroquinoline derivatives as anti-tubercular agents against mycobacterium tuberculosis H37Rv (Figure 1.24). Further, comparative molecular field analysis (CoMFA) and comparative molecular similarity indices analysis (CoMSIA) were performed on potent compounds [95].

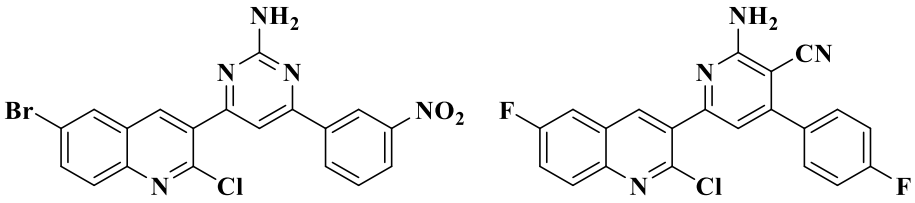

Figure 1.24

Kumar et al. disclosed a novel series of substituted quinolines as anti-cancer agents and selective EGFR blocker (Figure 1.25). All the synthesized compounds were evaluated for anti-cancer activity against MCF-7 (human breast), HepG2 (human liver), HCT116 (human colorectal) and PC-3 (human prostate) cancer cell lines with MTT assay. In addition, molecular docking studies and ADME prediction were also evaluated for the active compounds [96].

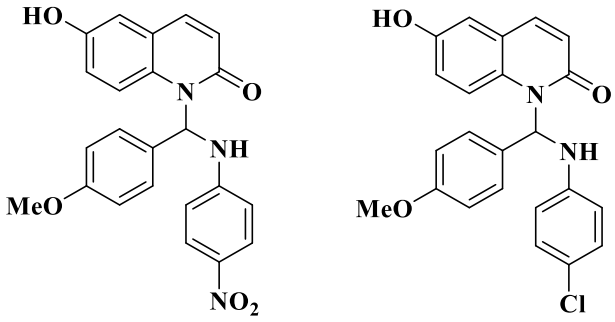

Figure 1.25

1.7. Quinazolinones

Quinazolinone is the medicinally important nitrogen containing fused heterocycle, displaying diverse biological activities including anti-cancer, anti-microbial, anti-convulsant, anti-bacterial, anti-malarial, anti-inflammatory, anti-hypertensive, anti-diabetic, anti-tubercular, kinase inhibitory activities [97-100]. There are many synthetic and natural product-based drugs, having quinazolinone moiety, which are used clinically for treatment of various diseases. For instant, quinethazone is a quinazolinone having synthetic drug, used for the treatment of hypertension [101]. Febrifugine is a quinazolinone based alkaloid isolated from the dichroa febrifuga, which is used as anti-malarial drug [102]. Whereas, metolazone is a thiazide linked quinazolinone drug marketed under the brand name zytanix, used to treat congestive heart failure (anti-cardiovascular) [103]. Some of the biologically active quinazolinone based drugs were shown in Figure 1.26.

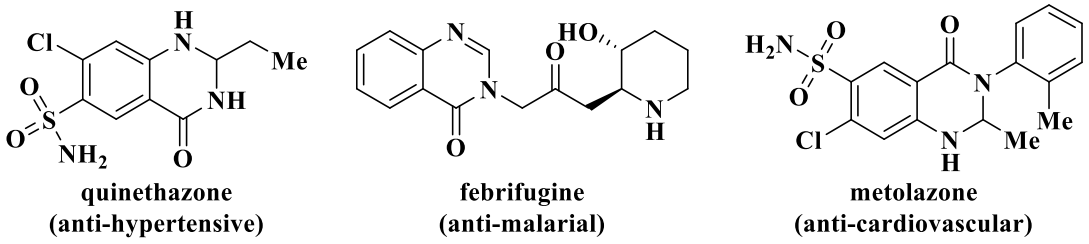

Figure 1.26. some of the commercially available quinazolinone drugs.

Lu et al. design and synthesized substituted quinazolinone benzoates as novel anti-tubercular agents targeting acetohydroxyacid synthase (Figure 1.27). The anti-tubercular activity has evaluated *in vitro* against standard MTB strain H37Rv and the results indicated that most of the compounds displayed potent activity [104].

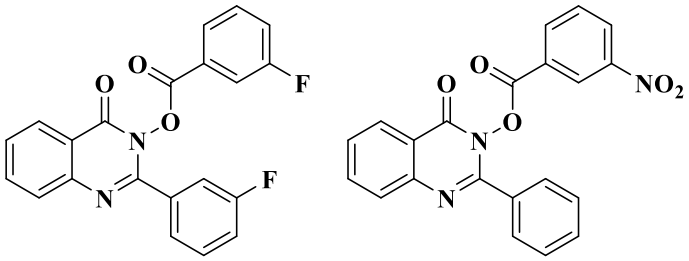

Figure 1.27

Dohle et al. described quinazolinone based sulfamates as potent anti-cancer agents (Figure 1.28). In this study, *in vitro* anti-cancer activity was evaluated against human breast and prostate tumor cell lines and also the potent molecules were screened *in vivo* against myeloma xenograft model for oral availability [105].

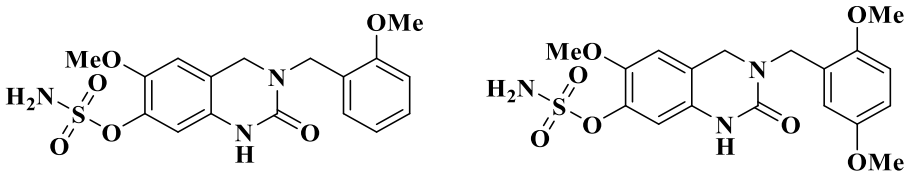

Figure 1.28

From the afore mentioned literature reports and biological significance of spirooxindoles, quinoline and quinazolinone moieties prompted us to synthesize new chemical entities bearing these moieties in a single frame through efficient methodologies in this thesis.

1.8. Multicomponent reactions (MCRs)

Multicomponent reactions (MCRs) are convergent reactions in which three or more readily available or commercially available starting materials react to form a final product through the construction of several covalent bonds without isolating any intermediates [106,107]. Depending on their reactivity and reaction parameters, MCRs are classified into three types. The domino-type MCRs involve all the reactants from the beginning of the reaction process. The sequential MCRs are the subsequent addition of reactants in a well-defined order without altering the reaction parameters. The consecutive MCRs are similar to the sequential MCRs but the reaction parameters are changing from step to step [108]. MCRs show synthetic advantages over conventional methods in regard to simplicity, selectivity, efficiency, convergence and atom economy [109]. MCRs have been recognized by the synthetic community in industry and academia as a preferred method to design and synthesize biologically active compounds due to their rapid and easy access to pharmacological relevant compounds, as well as their scaffold diversity [110]. In the year

1838, Gerhard and Laurent established the first multicomponent reaction for the generation of cyanohydrin imines. Later, a number of multicomponent reactions were developed such as Strecker synthesis, Hantzsch reaction, Biginelli reaction, Mannich reaction, Passerini reaction, Ugi reaction etc [111].

1.9. Ultrasound irradiation

Over the past few decades, ultrasound irradiation has been extensively used in organic synthesis [112]. It is a relatively new approach for the interaction of matter with energy which promotes chemical and physical changes. The primary mechanism of ultrasonic irradiation is cavitational collapse, in which ultrasonic irradiation produces a large number of cavitation bubbles that grow rapidly and undergoes collapses, that can generate high cavitational energy, heat transfer between reactants and significant mixing effect in reaction leads to accelerate the reactions [113]. Under ultrasonic irradiation, organic transformations occur in high yield, short reaction times, convenient and easily controlled reaction conditions compared to conventional methods [114]. Based on energy conservation and minimal waste generation in the reaction, ultrasound technique is extensively considered as a green chemistry approach [115].

Ultrasonication reactions in this thesis were performed on PCi-Analytics-6.5L200H1DTC ultrasonic cleaner whose frequency is 25 kHz, input voltage range of 170–270 VAC at 50 Hz and output power is 250 W (Mumbai, India).

1.10. Molecular docking studies

The major application of the molecular docking studies is to design the compounds *in silico* and target against proteins (macromolecules), the binding modes of these compounds (ligands) with the active site of a target protein. Thus the compounds which are strongly bound to a protein were treated as lead molecules. In *in vitro* experiments, drugs are discovered by a chance in a trial-and-error method by using high-throughput screening of a large number of compounds against a given target. This process is time consuming and highly expensive. Whereas, if the 3D structure of the compound is known, then the molecular docking is a useful tool in the identification of drug candidates by virtual screening of compound database. The energetically more favorable ligand conformation is suitable for the docking [116]. In general, low energy scores represent better protein-ligand bindings. The molecular docking studies in the thesis work were carried out by using AutoDock Tools (ADT) version 1.5.6 and AutoDock version 4.2.5.1 docking program and the visualization of the final compounds were carried out on discovery tools software [117].

AutoDock is a suite of free open–source software (http://autodock.scripps.edu) for the computational docking and virtual screening of designed molecules to macromolecular receptors and has been widely used in research and drug discovery [118]. AutoDock is a computational docking program based on an empirical free energy force field and rapid Lamarckian genetic algorithm search method. AutoDock Tools is an interactive graphical tool for coordinate preparation, docking and analysis [119].

1.11. Mycobacterium tuberculosis protein

Dihydrofolate reductase (DHFR) enzyme catalyzes the NADPH-dependent reduction of dihydrofolate to tetrahydrofolate and is essential for the synthesis of thymidylate, purines and several amino acids. The enzyme has been studied extensively as a drug target for mycobacterial, protozoal and fungal infections. In this thesis, we have used docking approaches to study the binding orientations and predict binding affinities of target compounds by using co-crystallized mycobacterium tuberculosis DHFR protein PDB code: 1DF7 and enoyl reductase proteins PDB code: 1P44 and 4TZK [120].

1.12. ADME prediction

At each stage of drug candidate screening, evaluation of absorption, distribution, metabolism and excretion (ADME) properties are necessary and responsible approach in drug discovery and design, which aided to lower the risk of compounds failing in clinical trials [121]. The main role of *in silico* ADME modelling is to predict the *in vivo* affinity behavior of the drug candidates in the human body [122].

In order to evaluate the drug like properties of the synthesized compounds in the thesis, we have used online ADME servers ADMETlab 2.0 and pkCSM to estimate *in silico* ADME properties (https://admetmesh.scbdd.com/service/evaluation/cal) [123,124].

1.13. General information

All the starting materials for the synthesis of final compounds in this thesis were purchased from Merck/Spectrochem. All melting points were checked by using Stuart SMP30 melting point apparatus (Bibby Scientific Ltd. United Kingdom) and were uncorrected. The reaction progress was checked with TLC plates (E. Merck, Mumbai, India). IR spectra were recorded on KBr disc by using Perkin-Elmer 100S spectrophotometer (Perkin-Elmer Ltd. United Kingdom) from 4000-400 cm^{-1}. ^{1}H and ^{13}C NMR spectra were recorded on Avance-III Bruker-400 and -500 MHz spectrometers (Bruker Corporation Ltd., Germany) using $CDCl_3$, DMSO-d_6 as solvents and TMS as an

internal standard and chemical shifts were expressed as *ppm*. HRMS and ESI-MS/MS spectra were recorded on Agilent Q-TOF 6230 spectrometer. Powder X-ray Diffraction patterns of the synthesized materials were recorded on a Ni filtered Cu-Kα (λ = 1.5406 Å) PAN analytical advanced X-ray diffractometer in the scan range 2θ between 6° and 90°. Morphological characteristics and existence of elements were investigated on a Field-emission scanning electron microscopy (FE-SEM, FEI-Apreo LoVac) combined with an energy dispersive X-ray spectrometry (EDX), model VEGA 3 TESCAN, USA. The SXRD data of the synthesized compounds were collected and solved by using Bruker Kappa Apex II CCD diffractometer and ShelXT software.

1.14. References

[1] V. Zhdankin, A. R. K. Christopher, A. R. John, A. J. Viktor, *Handbook of Heterocyclic Chemistry*, Elsevier, **2010**.

[2] K. M. John A. Joule, *Heterocyclic Chemistry, 5th Edition*, Wiley, **2010**.

[3] F. Salehian, H. Nadri, L. Jalili-Baleh, L. Youseftabar-Miri, S. N. Abbas Bukhari, A. Foroumadi, T. Tüylü Küçükkilinç, M. Sharifzadeh, M. Khoobi, *Eur. J. Med. Chem.* **2021**, *212*, 113034–113072.

[4] E. Vitaku, D. T. Smith, J. T. Njardarson, *J. Med. Chem.* **2014**, *57*, 10257–10274.

[5] C. T. Walsh, *Tetrahedron Lett.* **2015**, *56*, 3075–3081.

[6] G. S. Singh, Z. Y. Desta, *Chem. Rev.* **2012**, *112*, 6104–6155.

[7] A. C. Murphy, S. R. A. Devenish, A. C. M. Taylor, J. W. Blunt, M. H. G. Munro, *Org. Biomol. Chem.* **2008**, *6*, 3854–3862.

[8] S.-J. Liu, Q. Zhao, C. Peng, Q. Mao, F. Wu, F.-H. Zhang, Q.-S. Feng, G. He, B. Han, *Eur. J. Med. Chem.* **2021**, *217*, 113359–113375.

[9] K. A. Quiroga, C. R. Peña, L. S. Nerio, M. Gutiérrez, E. P. Cuadrado, *RSC Adv.* **2021**, *11*, 21926–21954.

[10] G. Li Petri, V. Spanò, R. Spatola, R. Holl, M. V. Raimondi, P. Barraja, A. Montalbano, *Eur. J. Med. Chem.* **2020**, *208*, 112783–112795.

[11] F. E. Bennani, L. Doudach, Y. Cherrah, Y. Ramli, K. Karrouchi, M. Ansar, M. E. A. Faouzi, *Bioorg. Chem.* **2020**, *97*, 103470–103531.

[12] Z. Xu, S. J. Zhao, Y. Liu, *Eur. J. Med. Chem.* **2019**, *183*, 111700–111736.

[13] N. Singh, S. Singh, S. Kohli, A. Singh, H. Asiki, G. Rathee, R. Chandra, E. A. Anderson, *Org. Chem. Front.* **2021**, *8*, 5550–5573.

[14] M. da C. A. D. Bianco, D. I. L. F. Marinho, L. V. B. Hoelz, M. M. Bastos, N. Boechat, *Pharmaceuticals* **2021**, *14*, 893–910.

[15] S. Ahmad, O. Alam, M. J. Naim, M. Shaquiquzzaman, M. M. Alam, M. Iqbal, *Pyrrole: An Insight into Recent Pharmacological Advances with Structure Activity Relationship*, Elsevier Masson SAS, **2018**.

[16] S. S. Gholap, *Eur. J. Med. Chem.* **2016**, *110*, 13–31.

[17] A. N. Bismillah, I. Aprahamian, *Chem. Soc. Rev.* **2021**, *50*, 5631–5649.

[18] J. M. Grindel, *Drug Metab. Rev.* **1981**, *12*, 363–377.

[19] D. F. Teixeira, A. M. Santos, A. M. S. Oliveira, J. A. C. Nascimento Júnior, L. A. Frank, M. T. De Santana Souza, E. A. Camargo, M. R. Serafini, *Expert Rev. Clin. Pharmacol.* **2021**, *14*, 677–686.

[20] A. M. Ginsberg, *Drugs* **2010**, *70*, 2201–2214.

[21] A. Rudi, T. Evan, M. Aknin, Y. Kashman, *J. Nat. Prod.* **2000**, *63*, 832–833.

[22] L. Dyson, A. D. Wright, K. A. Young, J. A. Sakoff, A. McCluskey, *Bioorg. Med. Chem.* **2014**, *22*, 1690–1699.

[23] M. Biava, G. C. Porretta, G. Poce, A. De Logu, R. Meleddu, E. De Rossi, F. Manetti, M. Botta, *Eur. J. Med. Chem.* **2009**, *44*, 4734–4738.

[24] R. Romagnoli, P. Oliva, M. K. Salvador, S. Manfredini, C. Padroni, A. Brancale, S. Ferla, E. Hamel, R. Ronca, F. Maccarinelli, F. Rruga, E. Mariotto, G. Viola, R. Bortolozzi, *Eur. J. Med. Chem.* **2021**, *214*, 113229–113248.

[25] K. Luo, S. Mao, K. He, X. Yu, J. Pan, J. Lin, Z. Shao, Y. Jin, *ACS Catal.* **2020**, *10*, 3733–3740.

[26] G. Dou, C. Shi, D. Shi, *J. Comb. Chem.* **2008**, *10*, 810–813.

[27] D. Hong, Y. Zhu, Y. Li, X. Lin, P. Lu, Y. Wang, *Org. Lett.* **2011**, *13*, 4668–4671.

[28] M. F. Khan, M. M. Alam, G. Verma, W. Akhtar, M. Akhter, M. Shaquiquzzaman, *Eur. J. Med. Chem.* **2016**, *120*, 170–201.

[29] V. Kumar, K. Kaur, G. K. Gupta, A. K. Sharma, *Eur. J. Med. Chem.* **2013**, *69*, 735–753.

[30] Z. Q. Long, L. L. Yang, J. R. Zhang, S. T. Liu, Jiao Xie, P. Y. Wang, J. J. Zhu, W. Bin Shao, L. W. Liu, S. Yang, *J. Agric. Food Chem.* **2021**, *69*, 8380–8393.

[31] S. Zhu, W. Yang, Q. Gan, C. Feng, *J. Phys. Chem. A* **2021**, *125*, 10340–10350.

[32] K. M. Pandya, S. Battula, P. J. Naik, *Tetrahedron Lett.* **2021**, *81*, 153353–153358.

[33] Y. Grell, X. Xie, S. I. Ivlev, E. Meggers, *ACS Catal.* **2021**, *11*, 11396–11406.

[34] M. J. Alam, O. Alam, P. Alam, M. J. Naim, *Int. J. Pharma Sci. Res.* **2015**, *6*, 1433–1442.

[35] G. S. Masaret, *ChemistrySelect* **2021**, *6*, 974–982.

[36] P. Xiao, W. Li, J. Lu, Y. Liu, Q. Luo, H. Zhang, *Ecotoxicol. Environ. Saf.* **2021**, *228*, 113007–113014.

[37] S. Zisook, J. Mendels, D. Janowsky, J. Feighner, J. C. M. Lee, A. Fritz, *Neuropsychobiology* **1987**, *17*, 133–138.

[38] C. Dal Cortivo, G. B. Conselvan, P. Carletti, G. Barion, L. Sella, T. Vamerali, *Front. Plant Sci.* **2017**, *8*, 1–11.

[39] I. Dagogo-Jack, A. T. Shaw, *Ann. Oncol.* **2016**, *27*, 42–50.

[40] M. A. H. Ismail, J. Lehmann, D. A. Abou El Ella, A. Albohy, K. A. M. Abouzid, *Med. Chem. Res.* **2009**, *18*, 725–744.

[41] R. Ramesh, R. D. Shingare, V. Kumar, A. Anand, S. B, S. Veeraraghavan, S. Viswanadha, R. Ummanni, R. Gokhale, D. Srinivasa Reddy, *Eur. J. Med. Chem.* **2016**, *122*, 723–730.

[42] P. N. Kalaria, S. P. Satasia, D. K. Raval, *RSC Adv.* **2014**, *4*, 32353–32362.

[43] J. A. Kumar, G. Saidachary, G. Mallesham, B. Sridhar, N. Jain, S. V. Kalivendi, V. J. Rao, B. C. Raju, *Eur. J. Med. Chem.* **2013**, *65*, 389–402.

[44] N. Panda, A. K. Jena, *J. Org. Chem.* **2012**, *77*, 9401–9406.

[45] G. Zhang, H. Ni, W. Chen, J. Shao, H. Liu, B. Chen, Y. Yu, *Org. Lett.* **2013**, *15*, 5967–5969.

[46] G. C. Senadi, W. P. Hu, T. Y. Lu, A. M. Garkhedkar, J. K. Vandavasi, J. J. Wang, *Org. Lett.* **2015**, *17*, 1521–1524.

[47] J. Krzywik, A. Nasulewicz-Goldeman, W. Mozga, J. Wietrzyk, A. Huczyński, *ACS Omega* **2021**, *6*, 26583–26600.

[48] X. Huang, H. W. Liu, Z. Q. Long, Z. X. Li, J. J. Zhu, P. Y. Wang, P. Y. Qi, L. W. Liu, S. Yang, *J. Agric. Food Chem.* **2021**, *69*, 4615–4627.

[49] F. Ahmed, H. Xiong, *Dye. Pigment.* **2021**, *185*, 108905–108943.

[50] A. Oubella, A. E. El Mansouri, M. Fawzi, A. Bimoussa, Y. Laamari, A. Auhmani, H. Morjani, A. Robert, A. Riahi, M. Youssef Ait Itto, *Bioorg. Chem.* **2021**, *115*, 105184–105196.

[51] S. Zhang, Z. Xu, C. Gao, Q. C. Ren, L. Chang, Z. S. Lv, L. S. Feng, *Eur. J. Med. Chem.* **2017**, *138*, 501–513.

[52] Y. Qin, L. Xu, Y. Teng, Y. Yang, Y. Wang, P. Ma, *Bioorg. Med. Chem. Lett.* **2021**, *49*, 128330–128335.

[53] R. Wang, M. Cui, Q. Yang, C. Kuang, *Synthesis* **2021**, *53*, 978–982.

[54] D. Addla, A. Jallapally, D. Gurram, P. Yogeeswari, D. Sriram, S. Kantevari, *Bioorg. Med. Chem. Lett.* **2014**, *24*, 233–236.

[55] C. Knox, V. Law, T. Jewison, P. Liu, S. Ly, A. Frolkis, A. Pon, K. Banco, C. Mak, V. Neveu, Y. Djoumbou, R. Eisner, A. C. Guo, D. S. Wishart, *Nucleic Acids Res.* **2011**, *39*, 1035–1041.

[56] X. Yang, W. Wedajo, Y. Yamada, S. L. Dahlroth, J. J. L. Neo, T. Dick, W. K. Chui, *Eur. J. Med. Chem.* **2018**, *144*, 262–276.

[57] W. Hou, Z. Luo, G. Zhang, D. Cao, D. Li, H. Ruan, B. H. Ruan, L. Su, H. Xu, *Eur. J. Med. Chem.* **2017**, *138*, 1042–1052.

[58] A. Stevaert, B. Krasniqi, B. Van Loy, T. Nguyen, J. Thomas, J. Vandeput, D.

Jochmans, V. Thiel, R. Dijkman, W. Dehaen, A. Voet, L. Naesens, *J. Med. Chem.* **2021**, *64*, 5632–5644.

[59] W. M. Shu, X. F. Zhang, X. X. Zhang, M. Li, A. J. Wang, A. X. Wu, *J. Org. Chem.* **2019**, *84*, 14919–14925.

[60] S. Qiu, Y. Chen, X. Song, L. Liu, X. Liu, L. Wu, *Synlett* **2021**, *32*, 86–90.

[61] Z. Chen, Q. Yan, Z. Liu, Y. Xu, Y. Zhang, *Angew. Chemie - Int. Ed.* **2013**, *52*, 13324–13328.

[62] Y. J. Zheng, C. M. Tice, *Expert Opin. Drug Discov.* **2016**, *11*, 831–834.

[63] R. Rios, *Chem. Soc. Rev.* **2012**, *41*, 1060–1074.

[64] H. M. Hügel, N. H. de Silva, A. Siddiqui, E. Blanch, A. Lingham, *Bioorg. Med. Chem.* **2021**, *43*, 116270–116283.

[65] C. Marti, E. M. Carreira, *Eur. J. Org. Chem.* **2003**, *2003*, 2209–2219.

[66] S. S. Panda, R. A. Jones, P. Bachawala, P. P. Mohapatra, *Mini-Reviews Med. Chem.* **2017**, *17*, 1515–1536.

[67] D. Bora, A. Kaushal, N. Shankaraiah, *Eur. J. Med. Chem.* **2021**, *215*, 113263–113301.

[68] P. Saraswat, G. Jeyabalan, M. Z. Hassan, M. U. Rahman, N. K. Nyola, *Synth. Commun.* **2016**, *46*, 1643–1664.

[69] S. B. Korrapati, P. Yedla, G. G. Pillai, F. Mohammad, V. R. R. Ch., P. Bhamidipati, R. Amanchy, R. Syed, A. Kamal, *Biomed. Pharmacother.* **2021**, *134*, 111132–111142.

[70] P. R. Sebahar, R. M. Williams, *J. Am. Chem. Soc.* **2000**, *122*, 5666–5667.

[71] A. Lerchner, E. M. Carreira, *J. Am. Chem. Soc.* **2002**, *124*, 14826–14827.

[72] F. Y. Miyake, K. Yakushijin, D. A. Horne, *Org. Lett.* **2004**, *6*, 711–713.

[73] R. Paniagua-Pérez, E. Madrigal-Bujaidar, D. Molina-Jasso, S. Reyes-Cadena, I. Álvarez-González, L. Sánchez-Chapul, J. Pérez-Gallaga, *Basic Clin. Pharmacol. Toxicol.* **2009**, *104*, 222–227.

[74] D. Pierrot, V. Sinou, S. S. Bun, D. Parzy, N. Taudon, J. Rodriguez, E. Ollivier, D. Bonne, *Drug Dev. Res.* **2019**, *80*, 133–137.

[75] G. Ndayisaba, A. Yeka, K. P. Asante, M. P. Grobusch, E. Karita, H. Mugerwa, S. Asiimwe, A. Oduro, B. Fofana, S. Doumbia, J. P. Jain, S. Barsainya, G. A. Kullak-Ublick, G. Su, E. K. Schmitt, K. Csermak, P. Gandhi, D. Hughes, *Malar. J.* **2021**, *20*, 478–487.

[76] X. Cui, G. Pan, Y. Chen, X. Guo, T. Liu, J. Zhang, X. Yang, M. Cheng, H. Gao, F. Jiang, *Pharmacol. Res.* **2021**, *169*, 105683–105693.

[77] K. X. Rodriguez, E. N. Howe, E. P. Bacher, M. Burnette, J. L. Meloche, J. Meisel, P. Schnepp, X. Tan, M. Chang, J. Zartman, S. Zhang, B. L. Ashfeld, *ChemMedChem* **2019**, *14*, 1653–1661.

[78] S. W. Li, Y. Liu, P. B. Sampson, N. K. Patel, B. T. Forrest, L. Edwards, R. Laufer, M. Feher, F. Ban, D. E. Awrey, R. Hodgson, I. Beletskaya, G. Mao, J. M. Mason, X. Wei, X. Luo, R. Kiarash, E. Green, T. W. Mak, G. Pan, H. W. Pauls, *Bioorg. Med. Chem. Lett.* **2016**, *26*, 4625–4630.

[79] K. Ding, Y. Lu, Z. Nikolovska-Coleska, S. Qiu, Y. Ding, W. Gao, J. Stuckey, K. Krajewski, P. P. Roller, Y. Tomita, D. A. Parrish, J. R. Deschamps, S. Wang, *J. Am. Chem. Soc.* **2005**, *127*, 10130–10131.

[80] N. Arumugam, G. Periyasami, R. Raghunathan, S. Kamalraj, J. Muthumary, *Eur. J. Med. Chem.* **2011**, *46*, 600–607.

[81] Y. Kia, H. Osman, R. S. Kumar, V. Murugaiyah, A. Basiri, S. Perumal, H. A. Wahab, C. S. Bing, *Bioorg. Med. Chem.* **2013**, *21*, 1696–1707.

[82] Y. Arun, G. Bhaskar, C. Balachandran, S. Ignacimuthu, P. T. Perumal, *Bioorg. Med. Chem. Lett.* **2013**, *23*, 1839–1845.

[83] B. Lin, W. H. Zhang, D. D. Wang, Y. Gong, Q. Di Wei, X. L. Liu, T. T. Feng, Y. Zhou, W. C. Yuan, *Tetrahedron* **2017**, *73*, 5176–5188.

[84] X. Dou, Y. Lu, *Chem. - A Eur. J.* **2012**, *18*, 8315–8319.

[85] R. Zhou, L. Han, H. Zhang, R. Liu, R. Li, *Adv. Synth. Catal.* **2017**, *359*, 3977–3982.

[86] F. Shi, Z.-L. Tao, S.-W. Luo, S.-J. Tu, L.-Z. Gong, *Chem. - A Eur. J.* **2012**, *18*, 6885–6894.

[87] D. Bhardwaj, R. Singh, *Tetrahedron Lett.* **2021**, *85*, 153491–153496.

[88] B. S. Matada, R. Pattanashettar, N. G. Yernale, *Bioorg. Med. Chem.* **2021**, *32*, 115973–115999.

[89] A. Lauria, G. La Monica, A. Bono, A. Martorana, *Eur. J. Med. Chem.* **2021**, *220*, 113555–113587.

[90] A. Uddin, M. Chawla, I. Irfan, S. Mahajan, S. Singh, M. Abid, *RSC Med. Chem.* **2021**, *12*, 24–42.

[91] C. J. Thomas, N. J. Rahier, S. M. Hecht, *Bioorg. Med. Chem.* **2004**, *12*, 1585–1604.

[92] D. C. Drummond, C. O. Noble, Z. Guo, M. E. Hayes, C. Connolly-Ingram, B. S. Gabriel, B. Hann, B. Liu, J. W. Park, K. Hong, C. C. Benz, J. D. Marks, D. B. Kirpotin, *J. Control. Release* **2010**, *141*, 13–21.

[93] A. Matteelli, A. C. C. Carvalho, K. E. Dooley, A. Kritski, *Future Microbiol.* **2010**, *5*, 849–858.

[94] F. Nosten, M. Van Vugt, R. Price, C. Luxemburger, K. L. Thway, A. Brockman, R. McGready, F. Ter Kuile, S. Looareesuwan, N. J. White, *Lancet* **2000**, *356*, 297–302.

[95] R. C. Khunt, V. M. Khedkar, E. C. Coutinho, *Chem. Biol. Drug Des.* **2013**, *82*, 669–684.

[96] C. B. P. Kumar, M. S. Raghu, B. S. Prathibha, M. K. Prashanth, G. Kanthimathi, K. Y. Kumar, L. Parashuram, F. A. Alharthi, *Bioorg. Med. Chem. Lett.* **2021**, *44*, 128118–128126.

[97] F. Plescia, B. Maggio, G. Daidone, D. Raffa, *Eur. J. Med. Chem.* **2021**, *213*, 113070–113093.

[98] U. A. Kshirsagar, *Org. Biomol. Chem.* **2015**, *13*, 9336–9352.

[99] I. Khan, A. Ibrar, N. Abbas, A. Saeed, *Eur. J. Med. Chem.* **2014**, *76*, 193–244.

[100] Z. Haghighijoo, L. Zamani, F. Moosavi, S. Emami, *Eur. J. Med. Chem.* **2022**, *227*,

113949–113982.

[101] C. Temperini, A. Cecchi, A. Scozzafava, C. T. Supuran, *Bioorg. Med. Chem. Lett.* **2008**, *18*, 2567–2573.

[102] S. Jiang, Q. Zeng, M. Gettayacamin, A. Tungtaeng, S. Wannaying, A. Lim, P. Hansukjariya, C. O. Okunji, S. Zhu, D. Fang, *Antimicrob. Agents Chemother.* **2005**, *49*, 1169–1176.

[103] D. A. Sica, *Congest. Hear. Fail.* **2003**, *9*, 100–105.

[104] W. Lu, I. A. Baig, H. J. Sun, C. J. Cui, R. Guo, I. P. Jung, D. Wang, M. Dong, M. Y. Yoon, J. G. Wang, *Eur. J. Med. Chem.* **2015**, *94*, 298–305.

[105] W. Dohle, F. L. Jourdan, G. Menchon, A. E. Prota, P. A. Foster, P. Mannion, E. Hamel, M. P. Thomas, P. G. Kasprzyk, E. Ferrandis, M. O. Steinmetz, M. P. Leese, B. V. L. Potter, *J. Med. Chem.* **2018**, *61*, 1031–1044.

[106] B. H. Rotstein, S. Zaretsky, V. Rai, A. K. Yudin, *Chem. Rev.* **2014**, *114*, 8323–8359.

[107] Preeti, K. N. Singh, *Org. Biomol. Chem.* **2021**, *19*, 2622–2657.

[108] L. Levi, T. J. J. Müller, *Chem. Soc. Rev.* **2016**, *45*, 2825–2846.

[109] Q. Tang, X. Yin, R. R. Kuchukulla, Q. Zeng, *Chem. Rec.* **2021**, *21*, 893–905.

[110] E. Ruijter, R. V. A. Orru, *Drug Discov. Today Technol.* **2013**, *10*, 1–6.

[111] J. Li, C. G. Daniliuc, G. Kehr, G. Erker, *Org. Biomol. Chem.* **2021**, *19*, 5551–5554.

[112] N. Pokhrel, P. K. Vabbina, N. Pala, *Ultrason. Sonochem.* **2016**, *29*, 104–128.

[113] M. V. Rao, A. S. Sengar, S. C K, A. Rawson, *Trends Food Sci. Technol.* **2021**, *116*, 975–991.

[114] S. V. Sancheti, P. R. Gogate, *Ultrason. Sonochem.* **2017**, *36*, 527–543.

[115] G. Chatel, *Ultrason. Sonochem.* **2018**, *40*, 117–122.

[116] R. Thomsen, M. H. Christensen, *J. Med. Chem.* **2006**, *49*, 3315–3321.

[117] L. Ravi, K. Krishnan, *Innovare J. Med. Sci.* **2016**, *4*, 1–6.

[118] S. Forli, R. Huey, M. E. Pique, M. F. Sanner, D. S. Goodsell, A. J. Olson, *Nat.*

Protoc. **2016**, *11*, 905–919.

[119] G. M. Morris, R. Huey, W. Lindstrom, M. F. Sanner, R. K. Belew, D. S. Goodsell, A. J. Olson, *J. Comput. Chem.* **2009**, *30*, 2785–2791.

[120] R. Li, R. Sirawaraporn, P. Chitnumsub, W. Sirawaraporn, J. Wooden, F. Athappilly, S. Turley, W. G. J. Hol, *J. Mol. Biol.* **2000**, *295*, 307–323.

[121] D. Z. Huang, J. C. Baber, S. S. Bahmanyar, *Expert Opin. Drug Discov.* **2021**, *16*, 1045–1056.

[122] H. G. Vogel, J. Maas, F. J. Hock, D. Mayer, *Drug Discovery and Evaluation: Safety and Pharmacokinetic Assays, Second Edition*, **2013**.

[123] G. Xiong, Z. Wu, J. Yi, L. Fu, Z. Yang, C. Hsieh, M. Yin, X. Zeng, C. Wu, A. Lu, X. Chen, T. Hou, D. Cao, *Nucleic Acids Res.* **2021**, *49*, 5–14.

[124] D. E. V. Pires, T. L. Blundell, D. B. Ascher, *J. Med. Chem.* **2015**, *58*, 4066–4072.

CHAPTER-II
Section-A

A green catalyst $Fe(OTs)_3/SiO_2$ for the synthesis of 4-pyrrolo-12-oxoquinazolines

2A.1. Introduction

Nowadays, the development of innovative sustainable approaches is of great interest towards the environmental and scientific communities [1]. To attain these, solvent free protocols without using harmful organic solvents gaining significance in the development of green chemistry [2]. In particular, solvent free grinding technique is a powerful green synthetic route compared to traditional methods [3]. The reactions are not only interesting from economical point of view, but they also provide significant benefits in terms of yield [4], selectivity [5], easy handling with high atom efficiency [6].

On the other hand, iron catalyzed reactions have acquired significant attention in recent years due to its numerous advantages such as low cost, limited toxicity and natural abundance [7]. A large variety of iron based heterogeneous catalysts are developing for the increasing demand for green and sustainable chemistry [8]. Iron based heterogeneous acid catalysts have been focused in the organic synthesis in view of their excellent catalytic performance, including ease of separation, recyclability and reusability [9-11]. A variety of heterogeneous catalysts have been efficiently employed in various multicomponent reactions [12,13]. In this regard, $Fe(OTs)_3/SiO_2$ is considered as one of the most important acid catalysts and has been utilized as an effective catalyst in organic transformations due to their high strength of acidity, non-toxicity, high activity at low temperatures and reusability [14].

Most of the natural and synthetic drugs, agrochemicals and other biologically prominent molecules are heterocyclic compounds, predominantly nitrogen heterocycles [15]. In particular, pyrrole is one of the simplest nitrogen heterocycle found in various biologically active compounds [16]. A large number of pyrrole derivatives aided as potential drugs for many diseases [17]. They are known to comprise with noteworthy biological activities including anti-cancer [18], anti-HIV [19], anti-bacterial [20], anti-oxidant [21] etc.

Several pyrrole containing drugs are available in the market for the treatment of various diseases and some are under clinical trials [22]. For example, sunitinib is a multi targeted receptor tyrosine kinase (RTK) inhibitor used for the treatment of cancer [23]. Atorvastatin is a stain medication used to prevent cardiovascular disease (anti-inflammatory) [24]. Whereas, elopiprazole is an anti-psychotic drug [25]. Zomepirac is an orally effective anti-inflammatory drug [26]. The drug prodigiosin exhibits wide range of biological applications, including anti-malarial, anti-fungal, anti-biotic and anti-cancer [27]

and the drug BM 212 is under final stage clinical trials for the treatment of tuberculosis [28] (Figure 2A.1).

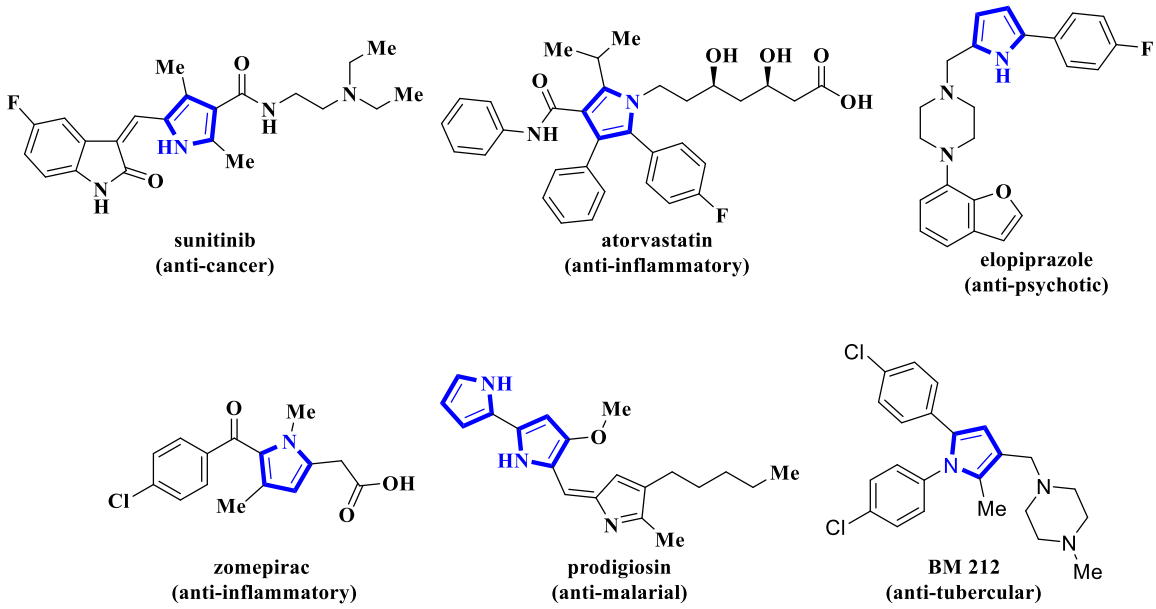

Figure 2A.1. Biologically important drugs containing pyrrole ring moiety.

Pyrroles also play a vital key role as various building blocks in organic synthesis and in material science [29]. Because of their diverse applications, various methodologies have been proposed to construct the pyrrole moieties [30].

2A.1.1. Reported methods for the preparation of pyrroles

Wang and co-workers described one pot multicomponent synthesis of polysubstituted pyrroles from amines, alkyne esters and chalcones under solvent free ball milling conditions (Scheme 2A.1). This protocol features mild reaction conditions, high efficiency and feasibility for large scale synthesis [31].

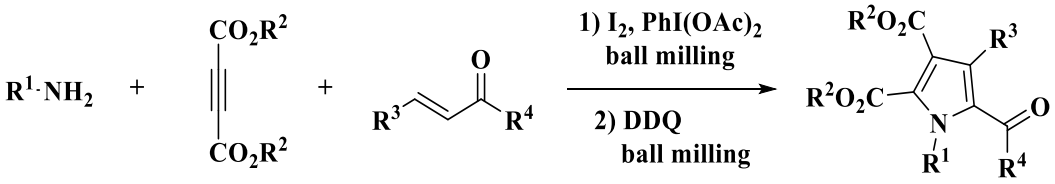

Scheme 2A.1

Paciorek et al. employed a vanadium catalyzed straightforward synthesis of fully substituted pyrroles through one pot reaction of 3-oxoanilides with benzoylhydrazines (Scheme 2A.2). An efficient and ecofriendly method is provided by this protocol under mild reaction conditions in the presence of air [32].

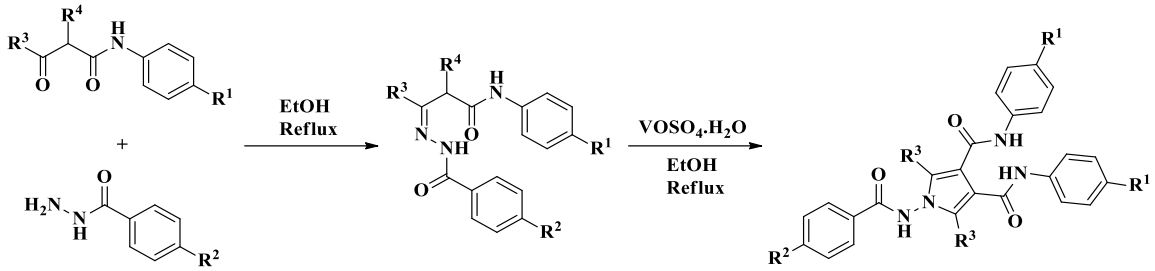

Scheme 2A.2

Gui et al. reported ultrasound assisted multicomponent tandem synthesis of tetra-substituted pyrroles from readily available alkenes, TMSCN and *N*,*N*-disubstituted formamides under metal- and solvent-free conditions (Scheme 2A.3). In this reaction molecular iodine plays dual role as catalyst and oxidant [33].

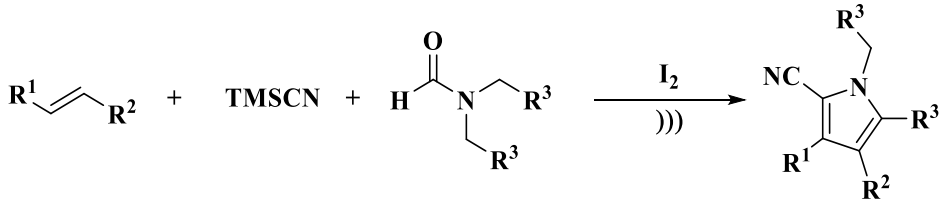

Scheme 2A.3

Ma and co-workers introduced double decarboxylative transannulation reaction for the synthesis of highly functionalized pyrroles using potassium acetate as a catalyst (Scheme 2A.4). This transformation represents a novel approach to skeletal remodeling by utilizing the CO_2 moiety as traceless activating and directing groups for the divergent synthesis of pyrrole pharmacophore atorvastatin [34].

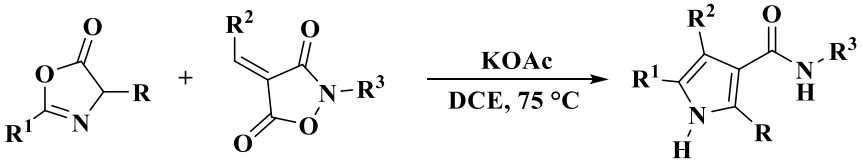

Scheme 2A.4

Zuben et al. developed a visible light driven metal-free synthesis for the generation of highly substituted pyrroles through C–H functionalization (Scheme 2A.5). The reaction utilizes readily available benzophenone as an accessible photocatalyst under solvent free conditions [35].

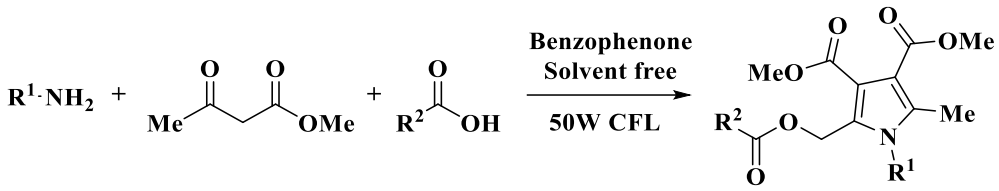

Scheme 2A.5

Zhang et al. demonstrated an efficient synthesis of 2,3,4-trisubstituted pyrroles through base catalyzed [3+2] cyclization between isocyanides and 4-(arylidene)-2-substituted oxazol-5(4*H*)-ones (Scheme 2A.6). This reaction occurs at room temperature without requiring any metal catalysts [36].

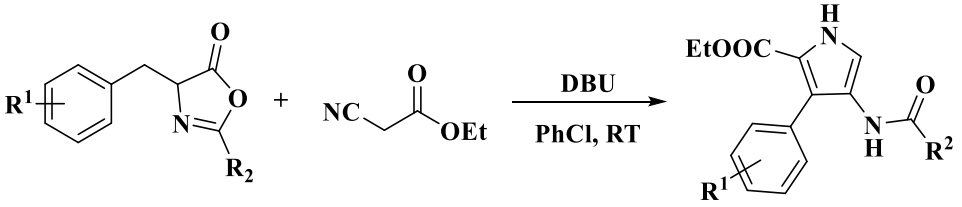

Scheme 2A.6

Chen et al. reported an efficient and ecofriendly synthesis of substituted 1*H*-pyrrole-carbonitriles using commercially available HZSM-5 and Pd/C as recyclable heterogeneous catalysts (Scheme 2A.7). The conspicuous feature of this method is to successful synthesis of pyrrole pharmacophore vonoprazan [37].

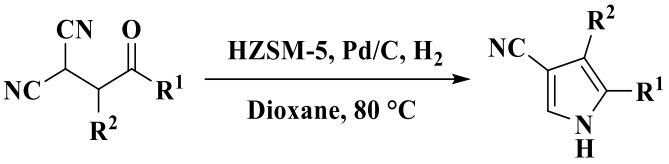

Scheme 2A.7

Algul and co-workers described a one-pot four component reaction of commercially available primary amines, 1,3-dicarbonyl compounds, benzaldehyde and nitromethane for the production of highly substituted pyrroles (Scheme 2A.8). In this transformation lactic acid was used as a bio-based green solvent and catalyst [38].

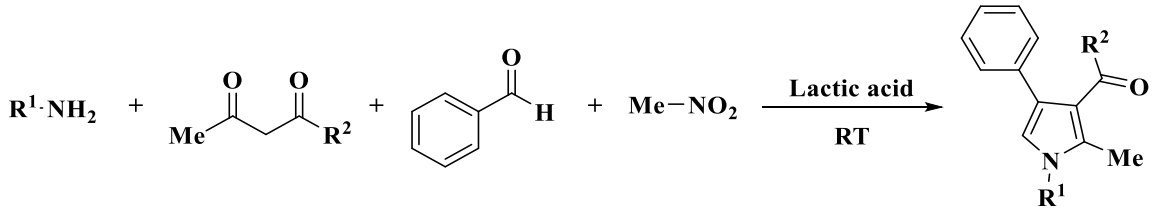

Scheme 2A.8

Zheng et al. demonstrated a novel Pd(II)-catalyzed oxidative arylative cyclization of *N*-homoallylic amines with arylboronic acids for the construction of polysubstituted pyrroles (Scheme 2A.9). This transformation proceeded through C–C and C–N bonds formation by aza-Wacker cyclization reaction [39].

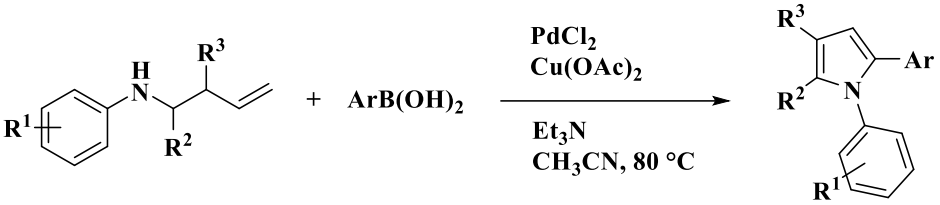

Scheme 2A.9

2A.2. Present work

In light of above mentioned literature and considering the importance of pyrrole moiety, we have developed a novel method using $Fe(OTs)_3/SiO_2$ as a reusable catalyst under one pot solvent free grinding conditions for the generation of poly substituted pyrroles.

2A.2.1. Synthesis of quinazolinyl chalcone 1

The reaction of indolo[2,1-*b*]quinazoline-6,12-dione **A** (1.0 mmol) with acetophenone **B** (1.0 mmol) in methanol (3 mL) and 10% aq. NaOH at room temperature affords 6-hydroxy-6-(2-oxo-2-phenylethyl)indolo[2,1-*b*]quinazolin-12(6*H*)-one (**1'**) (Scheme 2A.10). The obtained intermediate **1'** was treated with 20 mol% $BF_3.Et_2O$ in acetic acid at 60 °C gives the chalcone **1** in 88% yield (Scheme 2A.10) [40].

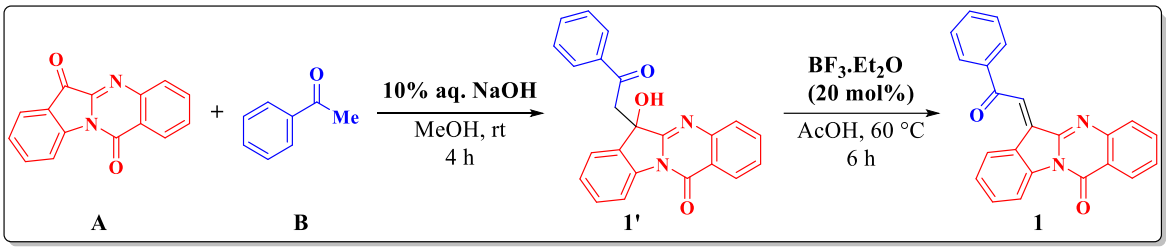

Scheme 2A.10

2A.2.2. Synthesis of heterogeneous catalyst $Fe(OTs)_3/SiO_2$

The catalyst $Fe(OTs)_3/SiO_2$ was synthesized from the reaction of $Fe(OTs)_3$ with silica gel in ethanol at 100 °C and confirmed by comparing with Energy-dispersive X-ray spectrum (EDX) (Figure 2A.3) and powder X-ray diffraction pattern (PXRD) (Figure 2A.4) of the literature report [14]. EDX spectrum of the catalyst showed the presence of the peaks for Fe, S, Si and O elements which confirms the formation $Fe(OTs)_3/SiO_2$.

The target compounds **4a-s** were synthesized by taking quinazolinyl chalcones **1a-j**, 1,3-dicarbonyl compounds **2a-b** and ammonium acetate **3** in the presence of $Fe(OTs)_3/SiO_2$ as a catalyst under solvent free grinding conditions (Scheme 2A.11). All the synthesized compounds were tested for the *in vitro* anti-tubercular activity, *in silico* molecular docking and ADME prediction.

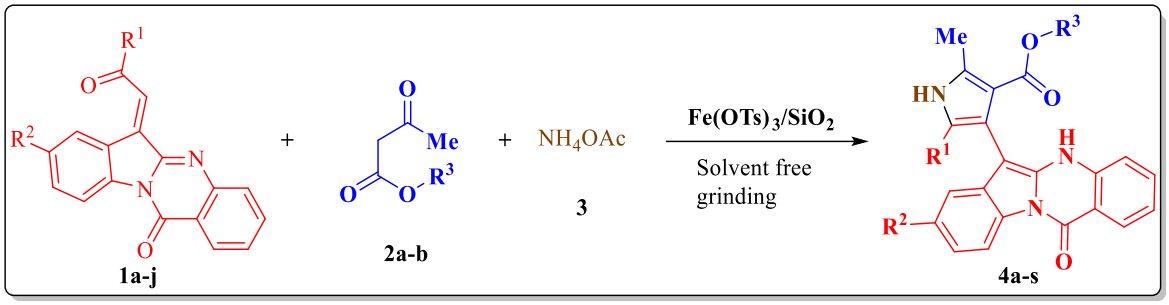

Scheme 2A.11. Synthesis of highly substituted pyrroles **4a-s**.

2A.2.3. Results and discussion

An ecofriendly green protocol was developed for the synthesis of novel 4-pyrrolo-12-oxoquinazolines **4a-s** with high yields and in lesser reaction times in the presence of heterogeneous catalyst $Fe(OTs)_3/SiO_2$ under solvent free grinding conditions. The chalcone 6-(2-oxo-2-phenylethylidene)indolo[2,1-*b*]quinazolin-12(6*H*)-one **1a,** 1,3-dicarbonyl compound **2a** and ammonium acetate (NH_4OAc) **3** were taken as trial reactants to investigate the parameters of reaction for the synthesis of the target compounds **4a-s.** The screened reaction conditions were presented in Table 2A.1.

Initially a pilot experiment was carried out in refluxing methanol without using any catalyst for 8 h and rendered the target compound **4a** with 48% yield (Table 2A.1, entry 1). Further, the same reaction was performed in different solvents such as ethanol, acetonitrile and 1,4-dioxane under reflux conditions resulting the target compound **4a** with moderate yields (Table 2A.1, entries 2-4). In order to improve the yields and reaction times, various Lewis acid catalysts including $SnCl_2.H_2O$, $FeCl_3$, $Fe(OTs)_3$, SiO_2 and $Fe(OTs)_3/SiO_2$ were employed (Table 2A.1, entries 5-22). When $SnCl_2.H_2O$ and $FeCl_3$ were used as catalysts, moderate yields were obtained (Table 2A.1, entries 5, 6). Then an attempt was made by taking 20 mol% and 100 mg of $Fe(OTs)_3$ as a catalyst leading to the desired product **4a** with the yield 70% in both the cases (Table 2A.1, entries 7, 8). Since the yields were still not satisfactory, the reaction was screened in the presence of heterogeneous $Fe(OTs)_3/SiO_2$ catalyst with 100 mg at different temperatures (Reflux and RT) under the conventional method (Table 2A.1, entries 9, 10). It was noticed that the catalyst $Fe(OTs)_3/SiO_2$ yielded

4a with 78% under reflux where as 75% at RT. The reaction was also executed separately with SiO_2 to evaluate the role of $Fe(OTs)_3$ but obtained a moderate yield (Table 2A.1, entry 11).

As a general practice in our laboratory towards green methodologies, the same reaction was carried out by using environmentally benign grinding method using mortar and pestle under solvent free condition with $Fe(OTs)_3/SiO_2$ catalyst. Gratifyingly, the target compound **4a** was achieved with 95% yield in 10 min (Table 2A.1, entry 12). Again this solvent free grinding methodology was tested in order to check the yields with $Fe(OTs)_3$ and SiO_2 separately which leads inferior results (Table 2A.1, entries 13, 14). Subsequently, the potential effect of the catalyst loading in the reaction was evaluated. However, it was observed that no improvement in the yield of **4a** at higher the amount of catalyst loading (Table 2A.1, entry 15), moreover, a slight decrease in the yield was occurred with lower amount of catalyst even after 20 min (Table 2A.1, entry 16). On the other hand, the reaction was carried out by just mixing the contents at RT for 75 min without grinding leading to 75% of **4a** (Table 2A.1, entry 17) which shows the significance of grinding.

Table 2A.1. Optimization of the reaction conditions[a]

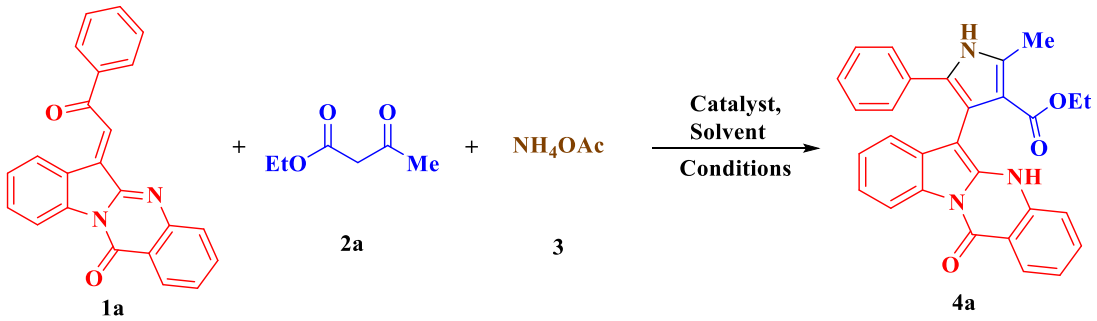

Entry	Catalyst	Solvent	Method	Time	Yield (%)[b]
1	None	Methanol	Reflux	8 h	48
2	None	Ethanol	Reflux	8 h	54
3	None	Acetonitrile	Reflux	12 h	45
4	None	1,4-Dioxane	Reflux	12 h	40
5	$SnCl_2.H_2O$ (20 mol%)	Ethanol	Reflux	8 h	58
6	$FeCl_3$ (20 mol%)	Ethanol	Reflux	6 h	60
7	$Fe(OTs)_3$ (20 mol%)	Ethanol	Reflux	6 h	70
8	$Fe(OTs)_3$ (100 mg)	Ethanol	Reflux	6 h	70
9	$Fe(OTs)_3/SiO_2$ (100 mg)	Ethanol	Reflux	4 h	78

10	$Fe(OTs)_3/SiO_2$ (100 mg)	Ethanol	RT	3 h	75
11	SiO_2 (100 mg)	Ethanol	Reflux	8 h	68
12	**$Fe(OTs)_3/SiO_2$ (100 mg)**	**Solvent free**	**Grinding**	**10 min**	**95**
13	$Fe(OTs)_3$ (100 mg)	Solvent free	Grinding	40 min	70
14	SiO_2 (100 mg)	Solvent free	Grinding	60 min	70
15	$Fe(OTs)_3/SiO_2$ (150 mg)	Solvent free	Grinding	10 min	95
16	$Fe(OTs)_3/SiO_2$ (50 mg)	Solvent free	Grinding	20 min	85
17	$Fe(OTs)_3/SiO_2$ (100 mg)	Solvent free	RT (physical mixture)	75 min	75
18	$Fe(OTs)_3/SiO_2$ (100 mg)	Ethanol	Grinding	10 min	95
19	$Fe(OTs)_3/SiO_2$ (100 mg)	Water	Grinding	10 min	93
20	$Fe(OTs)_3/SiO_2$ (100 mg)	Methanol	Grinding	15 min	90
21	$Fe(OTs)_3/SiO_2$ (100 mg)	Acetonitrile	Grinding	15 min	86
22	$Fe(OTs)_3/SiO_2$ (100 mg)	1,4-Dioxane	Grinding	20 min	81
23	None	Solvent free	Grinding	60 min	-[c]
24	None	Water	Grinding	60 min	-[c]

[a]Reaction condition: compound **1a** (1.0 mmol), Ethyl acetoacetate **2a** (1.0 mmol) and Ammonium acetate **3** (2.5 mmol). [b]Isolated yields. [c]No reaction. RT: room temperature.

In addition, in order to highlight the solvent free protocol, we have also carried out liquid assisted grinding (LAG) by adding few drops of ethanol, water, methanol, acetonitrile and 1,4-dioxane in presence of $Fe(OTs)_3/SiO_2$ catalyst and found ethanol and water are better solvents in LAG (Table 2A.1, entries 18-22). Furthermore, two more reactions were carried out without the catalyst under solvent free and in the presence of few drops of water leading to no product formation (Table 2A.1, entries 23, 24) which shows the importance of the $Fe(OTs)_3/SiO_2$ catalyst. Also, it is worth mentioning that there was no effect of fast grinding or slow grinding to affect the reaction kinetics. Thus, $Fe(OTs)_3/SiO_2$ with 100 mg under solvent free grinding condition (Table 2A.1, entry 12) was considered as the best optimized condition for the synthesis of 4-pyrrolo-12-oxoquinazolines. From these results, it is noteworthy that the $Fe(OTs)_3/SiO_2$ is important and essential catalyst for the efficient synthesis of the target compounds **4a-s**.

Table 2A.2. Synthesis of novel 4-pyrrolo-12-oxoquinazolines **4a-s**[a,b]

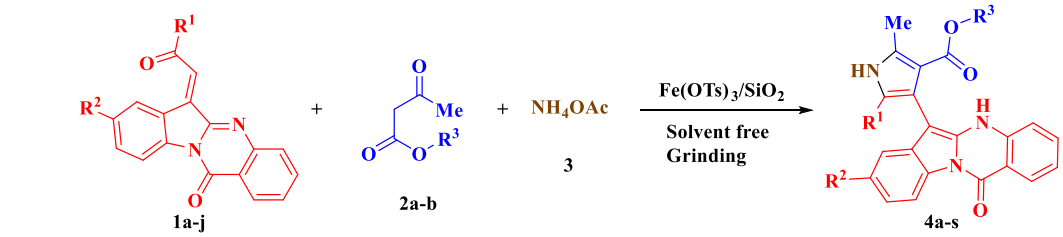

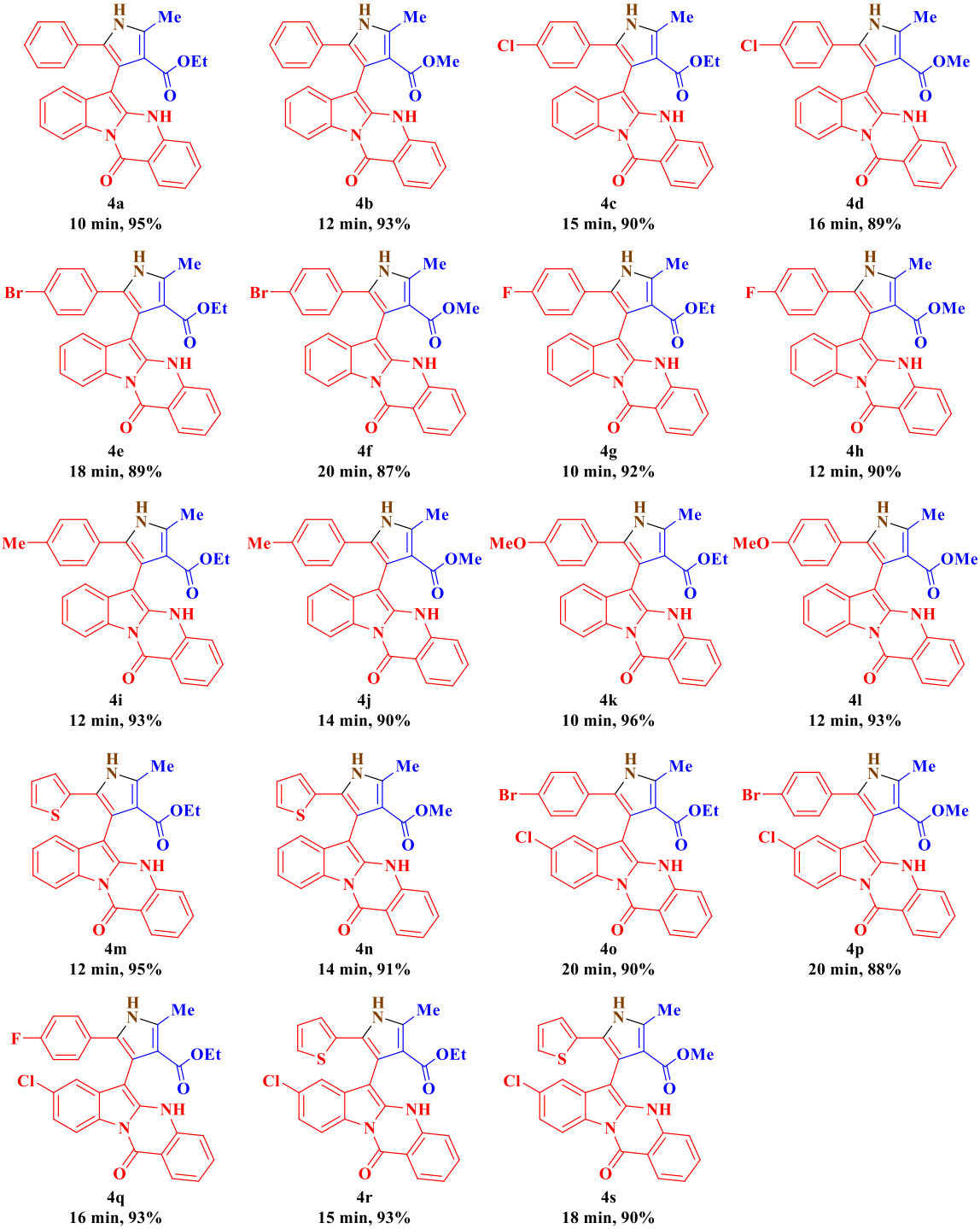

[a]Reaction condition: quinazolinyl chalcones **1a-j** (1.0 mmol), 1,3-dicarbonyl compounds **2a-b** (1.0 mmol), ammonium acetate **3** (2.5 mmol) and $Fe(OTs)_3/SiO_2$ (100 mg) under solvent free grinding. [b]Isolated yields.

Further, the substrate tolerance of this catalyst for the synthesis of 4-pyrrolo-12-oxoquinazolines was tested using different varieties of chalcones **1a-j** and active methylene compounds **2a-b** under optimized conditions. The results depicted in Table 2A.2 shows that quinazoline chalcones **1a-j** bearing electron donating (–Me, –OMe) and halogen (–F, –Cl, –Br) groups had no substantial impact on the efficiency of the reaction and also hetero aromatic groups reacted smoothly with active methylene compounds to produce target compounds **4a-s** in good to excellent yields.

To check the feasibility of our process on a preparative scale, we conducted the synthesis of 4-pyrrolo-12-oxoquinazoline **4a** on a gram scale (1g of **1a**). With 500 mg of $Fe(OTs)_3/SiO_2$, the reaction between chalcone **1a**, ethyl acetoacetate **2a** and ammonium acetate **3** furnished 1.18g (90% yield) of the desired product **4a** within 10 min of grinding in both solvent free and liquid assisted (EtOH) grinding (LAG).

The reusability of $Fe(OTs)_3/SiO_2$ catalyst was also investigated using the reaction between 6-(2-oxo-2-phenylethylidene)indolo[2,1-*b*]quinazolin-12(6*H*)-one **1a**, ethyl acetoacetate **2a** and ammonium acetate **3** as a model system to obtain compound **4a**. After completion of the reaction as monitored by TLC, ethyl acetate was added to the reaction mixture. The catalyst was recovered by filtration, washed with ethanol and reused for next cycles. It was found that after five cycles the catalytic activity had a low decrease (Figure 2A.2) suggesting the good recyclability of this catalyst for 4-pyrrolo-12-oxoquinazolines synthesis. These experiments were also supported by EDX, PXRD and scanning electron microscopy (SEM) of catalyst at initial and after five cycles (Figure 2A.3, Figure 2A.4 and Figure 2A.5). The PXRD and SEM images have shown no significant changes in the morphology corroborating substantial possession of the catalytic activity and its stability during its reuse.

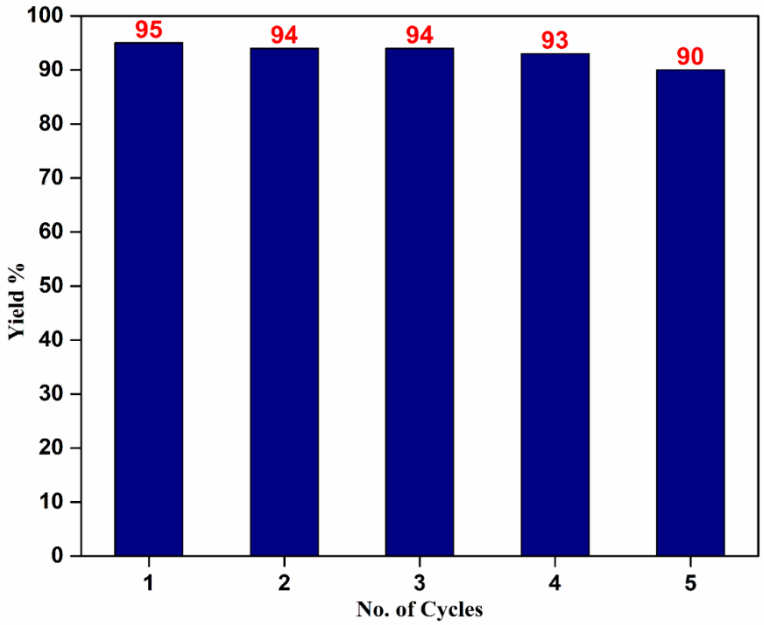

Figure 2A.2. Recyclability and reusability of $Fe(OTs)_3/SiO_2$.

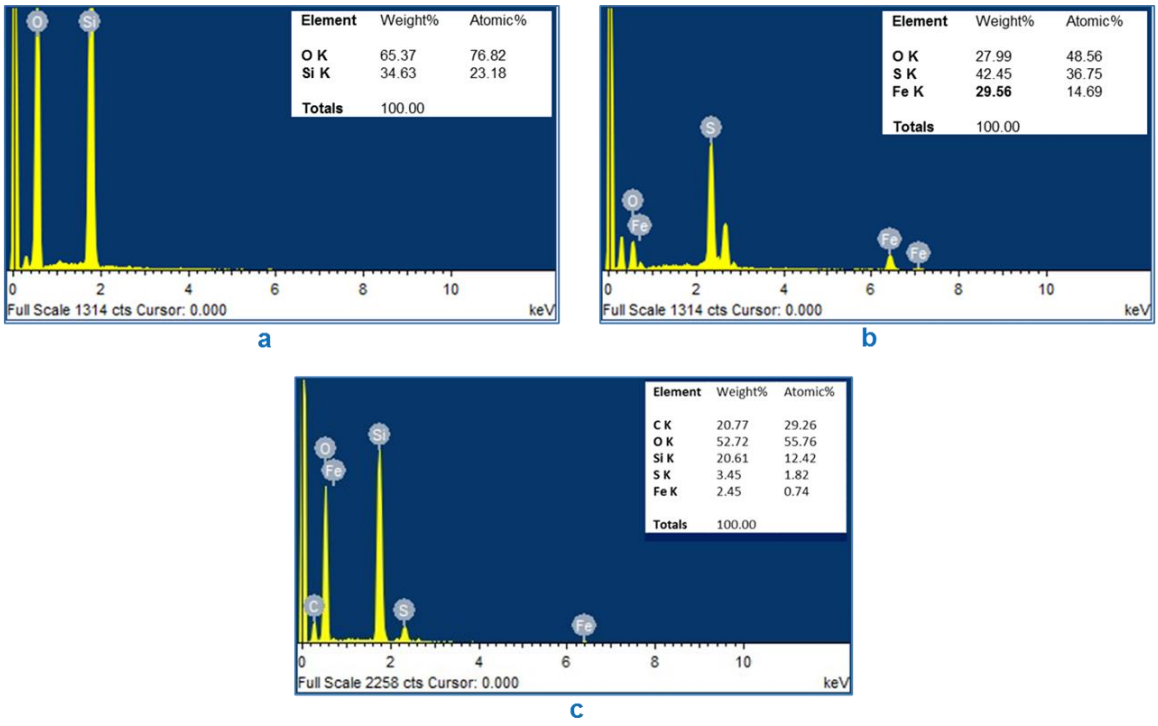

Figure 2A.3. EDX spectrum of (a) SiO_2 (b) $Fe(OTs)_3$ (c) $Fe(OTs)_3/SiO_2$.

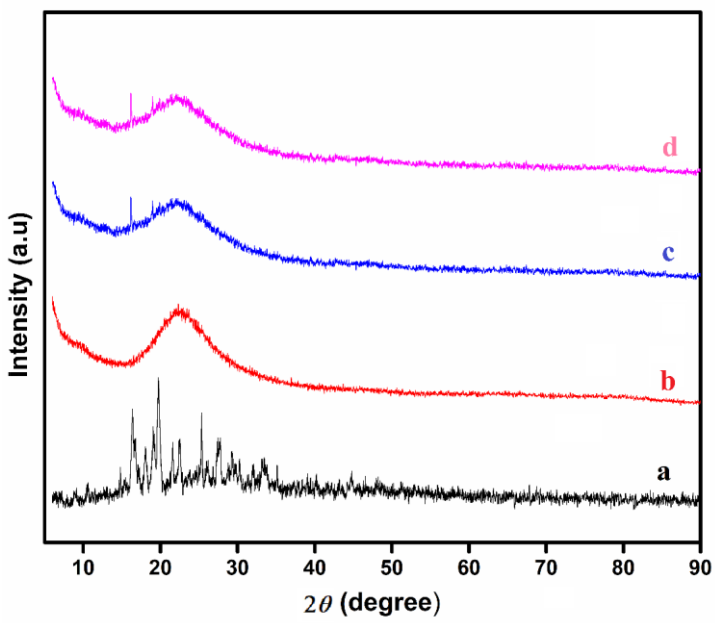

Figure 2A.4. PXRD pattern of (a) $Fe(OTs)_3$; (b) SiO_2; (c) freshly prepared $Fe(OTs)_3/SiO_2$; (d) $Fe(OTs)_3/SiO_2$ after five cycles.

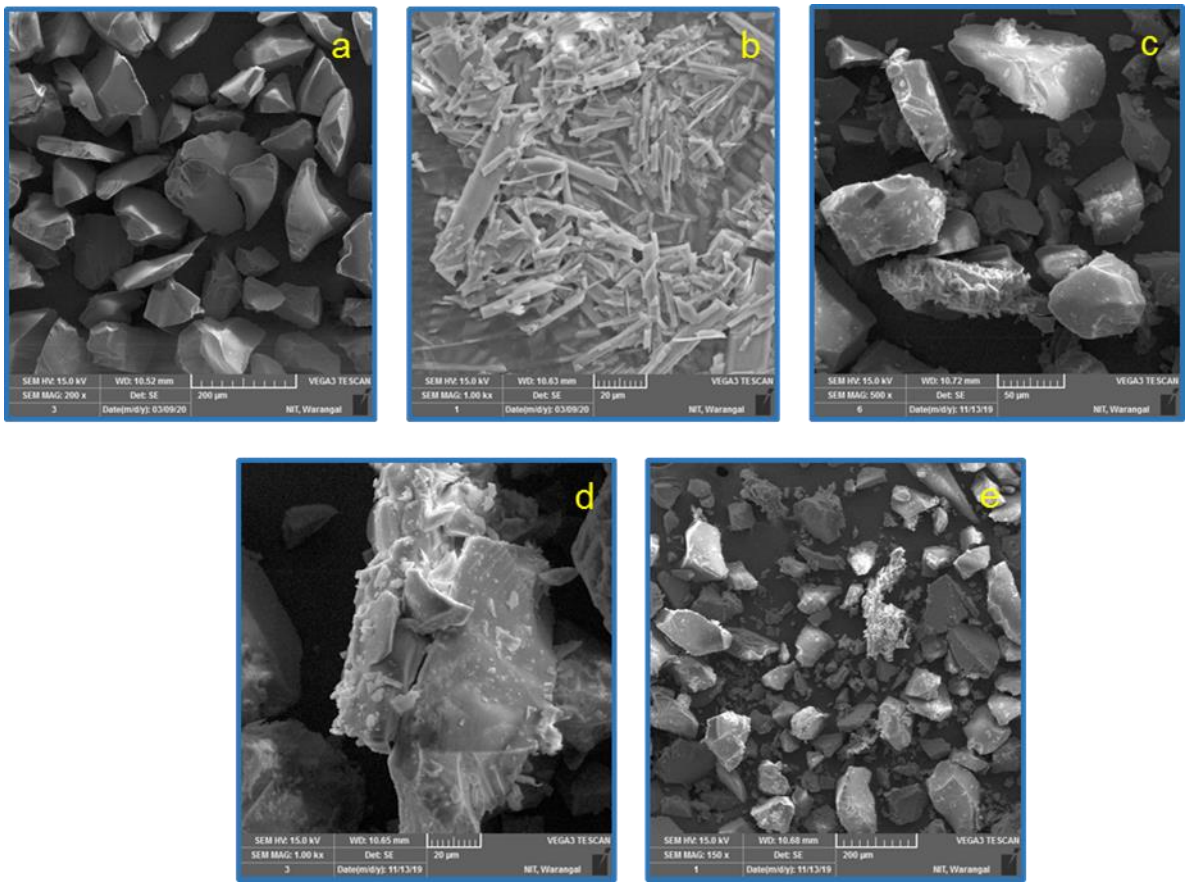

Figure 2A.5. SEM images of (a) SiO_2; (b) $Fe(OTs)_3$; (c & d) freshly synthesized $Fe(OTs)_3/SiO_2$ at different magnifications; (e) morphology after five catalytic cycles of $Fe(OTs)_3/SiO_2$ catalyst.

The plausible reaction mechanism for the formation of the title compounds **4a-s** was shown in scheme 2A.12. It was assumed that, initially, the $Fe(OTs)_3/SiO_2$ coordinates with carbonyl oxygen and imine nitrogen of chalcone **1** facilitating to react with enol **5** of 1,3-carbonyl compound ensuing the intermediate **6** *via* attacking the enol on α-carbon atom of the chalcone. While $Fe(OTs)_3/SiO_2$ also coordinates with two carbonyl oxygens of intermediate **6**, this interaction makes the carbonyl carbons more reactive and undergoes Paal-Knorr condensation with ammonium acetate to afford the product **4a**. The literature shows that due to good dispersion of $Fe(OTs)_3$ on the surface of the silica gel, the catalyst is effective in terms of reaction time and product yield [14]. This might be leading to metal (Fe) more electrophilic to be attacked by the lone pairs of the carbonyl oxygen making the carbonyl as more electrophilic center.

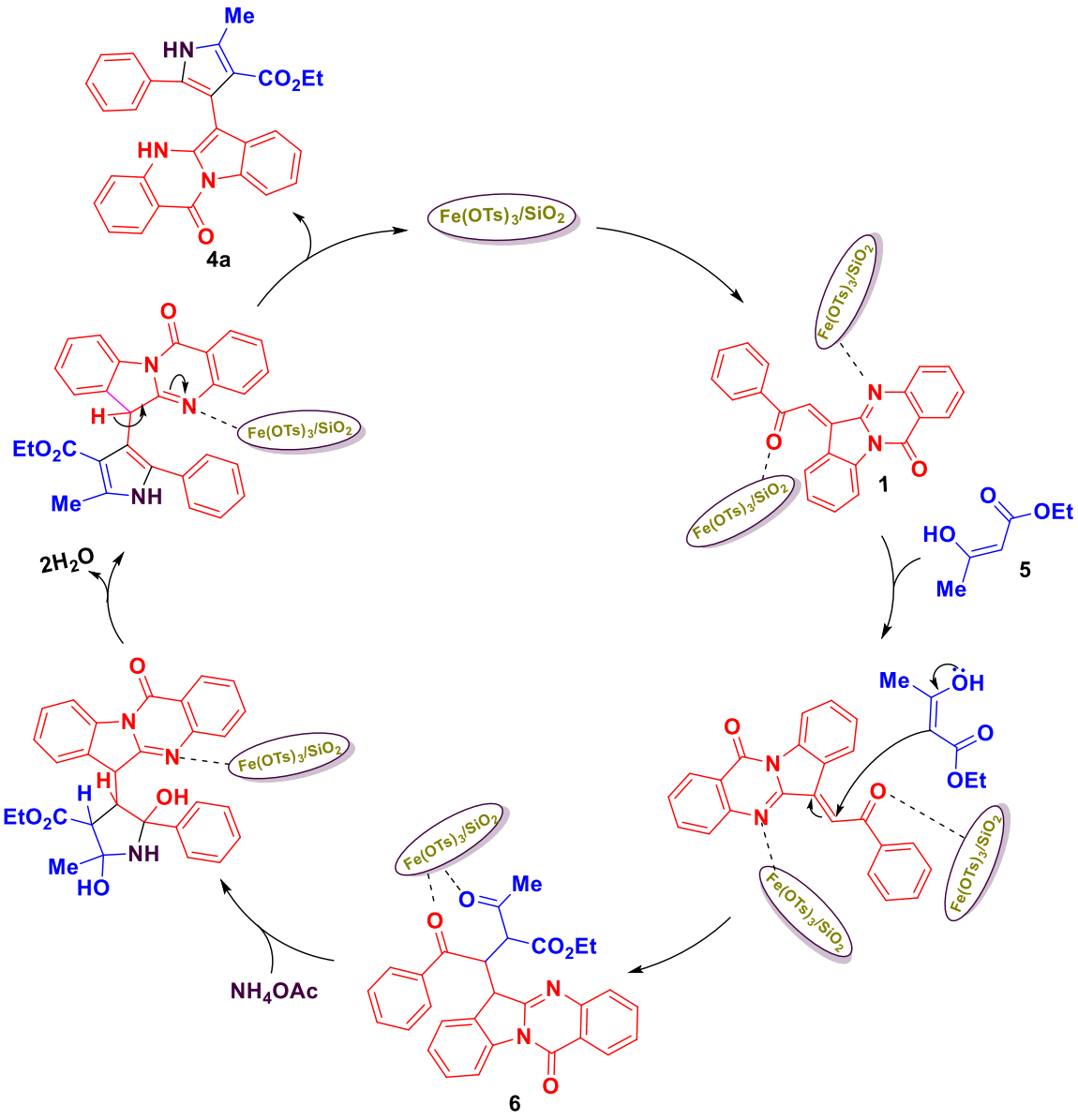

Scheme 2A.12. Plausible reaction mechanism for the formation of title compounds **4a-s**.

The synthesized compounds **4a-s** were well characterized by analyzing the IR, ^{1}H NMR, ^{13}C NMR and mass spectral data. For instance, the IR spectrum of compound **4a** shows the absorption bands at 3307 cm^{-1} and 3246 cm^{-1} represent the N–H groups of pyrrole ring and quinazoline ring. The bands at 1666 cm^{-1} and 1643 cm^{-1} represent the ester carbonyl and quinazoline ring carbonyl groups respectively [41, 42]. The peaks in the ^{1}H NMR spectrum at δ 11.79 and δ 11.00 corresponds to the two N–H protons of pyrrole and quinazoline moieties respectively [43, 44], the singlet at δ 2.63 corresponds $–CH_3$ protons which are attached to the pyrrole group. In all the ethyl ester ($–COOCH_2CH_3$) derivatives, two multiplets from δ 3.86 to δ 3.69 correspond to $–CH_2$ protons. These multiplets are found to be two quartet of doublets (qd) as the $–CH_2$ protons are diastereotopic due to atropisomerism in these molecules. The ^{13}C NMR spectrum showed peaks at δ 165.04 and δ 159.46 correspond to the carbonyl carbons of ester and quinazoline amide groups. The peak appeared at δ 90.04 represents the C=C carbon of quinazoline ring attached to the pyrrole ring. The compounds **4g**, **4h** and **4q** showed hetero nuclear coupling (C–F) in ^{13}C NMR spectrum with coupling constant values around *J*(*ipso*) = 240.0 Hz, *J*(*ortho*) = 30.0 Hz, *J*(*meta*) = 8.0 Hz and *J*(*para*) = 3.0 Hz. The high resolution mass spectrum (HRMS) of the compound **4a** showed the molecular ion peak at *m/z* 462.1821 $[M+H]^+$ determines the molecular weight of the compound **4a**. Further, fragmentation pathway of the compound **4a** was supported by the MS/MS spectrum analysis (Scheme 2A.13).

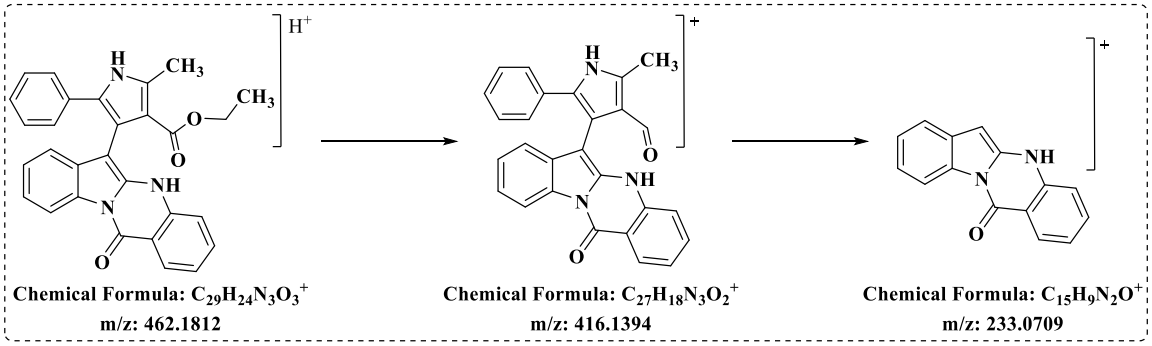

Scheme 2A.13. Fragmentation pathway of the compound **4a**.

2A.2.4. Biological activity

2A.2.4.1. Anti-tubercular activity (anti-TB)

The anti-tubercular activity of the synthesized 4-pyrrolo-12-oxoquinazolines **4a-s** were examined using the Microplate Alamar Blue Assay (MABA) method against *Mycobacterium tuberculosis* H37Rv (ATCC27294) strain and ethambutol as a standard

drug [45]. The experiments were conducted in duplicates and the MIC values (µg/mL) were listed in Table 2A.3.

The results of anti-TB activity indicate that all the screened compounds exhibited significant to poor activity with the MIC values ranging from 6.25 µg/mL to >25.00 µg/mL. Among these, two compounds **4o** and **4r** exhibited good activity with MIC value 6.25 µg/mL when compared to the standard drug ethambutol (MIC: 1.56 µg/mL). On the other hand, three compounds **4b**, **4i** and **4q** displayed moderate anti-TB activity with the MIC value 12.5 µg/mL. The remaining derivatives showed poor anti-TB activity.

Table 2A.3. *In vitro* anti-tubercular activity of title compounds **4a-s**

Entry	Compound	MIC (µg/mL)	% of Inhibition @25µM[a]
1	4a	25	ND[b]
2	4b	12.5	ND
3	4c	>25	ND
4	4d	25	ND
5	4e	>25	ND
6	4f	25	ND
7	4g	25	ND
8	4h	>25	ND
9	4i	12.5	ND
10	4j	25	ND
11	4k	>25	ND
12	4l	>25	ND
13	4m	>25	ND
14	4n	25	ND
15	**4o**	**6.25**	**21.87**
16	4p	>25	ND
17	4q	12.5	ND
18	**4r**	**6.25**	**22.05**
19	4s	>25	ND
20	**Ethambutol**	**1.56**	ND

[a]% inhibition was examined using RAW 264.7 cell line, [b]ND = not determined.

2A.2.4.2. Cytotoxicity studies

The promising anti-TB active compounds (**4o** and **4r**) have been screened for their safety profile by the evaluation of cytotoxicity on normal RAW 264.7 cells at 25 µg/mL [46] and the results were depicted in Table 2A.3. In this study, the compounds **4o** and **4r** showed lower percentage of inhibition *i.e.*, 21.87 and 22.05% respectively on the normal RAW 264.7 cell line.

2A.2.4.3. Structure activity relationship studies

In the structure activity relationship (SAR) studies, diverse donar and acceptor abilities of the substituted groups on phenyl ring are crucial in their anti-tubercular activity of the synthesized compounds. SAR studies reveal that the presence of halogen (-Br) on the phenyl ring and hetero aryl (thiophene) substitution significantly enhances the anti-tubercular activity.

2A.3. Molecular docking studies

All the synthesized compounds were successfully docked against *Mycobacterium tuberculosis* protein and the outcome of the results revealed that all the synthesized compounds **4a-s** were efficiently fit into the active sites of the protein (PDB ID: 1DF7) [47]. The results of the molecular docking study were presented in Table 2A.4. Among all, the compounds **4c**, **4d**, **4e**, **4f**, **4o**, **4p** and **4r** show good binding energies with -11.10, -11.04, -11.35, -11.09, -11.59, -11.34 and -11.22 kcal/mol respectively. Among these, the compound **4o** exhibited more negative binding energy -11.59 kcal/mol, forms two hydrogen bonds with the amino acid residues ASP27 (2.21 Å) and SER49 (1.78 Å) and also forms nine hydrophobic interactions (π···π and π···alkyl) with the amino acids ALA7 (4.48 and 4.65Å), ILE14 (5.09 Å), ILE20 (3.14, 3.37 and 3.40 Å), TRP22 (4.34 Å), PHE31 (3.88 Å) and LEU50 (5.45 Å). Whereas, the compound **4r** displayed binding energy -11.22 kcal/mol and forms three hydrogen bonds with the amino acid residues ASP27 (1.95 Å), GLN28 (2.56 Å) and PRO51 (3.38 Å). Also, exhibit seven hydrophobic interactions (π···alkyl) with the amino acids ALA7 (5.28 Å), ILE20 (4.16, 4.74, 5.27 and 5.50 Å), PRO51 (5.21 Å) and VAL54 (5.46 Å). The ligand interactions of the compounds **4o** and **4r** with 1DF7 protein were presented in Figure 2A.6 and Figure 2A.7.

Table 2A.4. Docking results of the compounds **4a-s** against 1DF7

Ent-ry	Compound	Binding energy (kcal/mol)	No. of hydrogen bonds	Residues involved in the hydrogen bonding	Hydrogen bond length (Å)
1	**4a**	-10.38	3	ALA7, GLN28, TYR100	1.77, 2.47, 2.77
2	**4b**	-10.44	3	ALA7, GLN28, TYR100	1.81, 2.43, 2.74
3	**4c**	-11.10	2	SER49, PRO51	1.92, 3.27
4	**4d**	-11.04	2	ASP27, SER49	1.87, 2.01
5	**4e**	-11.35	2	SER49, PRO51	1.91, 3.26
6	**4f**	-11.09	2	SER49, PRO51	1.92, 3.26
7	**4g**	-10.79	6	ALA7, TRP22, LEU24, GLN28, ILE94, TYR100	1.84, 2.40, 2.50, 2.70, 2.92, 3.04

8	**4h**	-10.41	6	ALA7, TRP22, LEU24, GLN28, ILE94, TYR100	1.86, 2.45, 2.51, 2.72, 2.83, 3.00
9	**4i**	-10.89	2	SER49, PRO51	1.91, 3.25
10	**4j**	-10.94	4	ALA7, GLN28, ILE94, TYR100	1.82, 2.42, 2.64, 3.17
11	**4k**	-10.63	4	ASP27, SER49, PRO51	1.86, 3.20, 3.30, 3.43
12	**4l**	-10.63	4	ASP27, SER49, PRO51	1.93, 3.08, 3.13, 3.22
13	**4m**	-10.20	4	GLN28, SER49, TYR100	2.41, 2.77, 3.20, 3.45
14	**4n**	-10.15	3	ALA7, GLN28, TYR100	1.85, 2.39, 2.68
15	**4o**	**-11.59**	2	ASP27, SER49	2.21, 1.78
16	**4p**	-11.34	3	TRP6, ASP27, SER49	1.82, 2.02, 3.70
17	**4q**	-10.62	3	LEU24, ASP27, SER49	1.89, 1.95, 2.69
18	**4r**	**-11.22**	3	ASP27, GLN28, PRO51	1.95, 2.56, 3.38
19	**4s**	-10.33	2	ASP27, SER49	1.83, 2.04

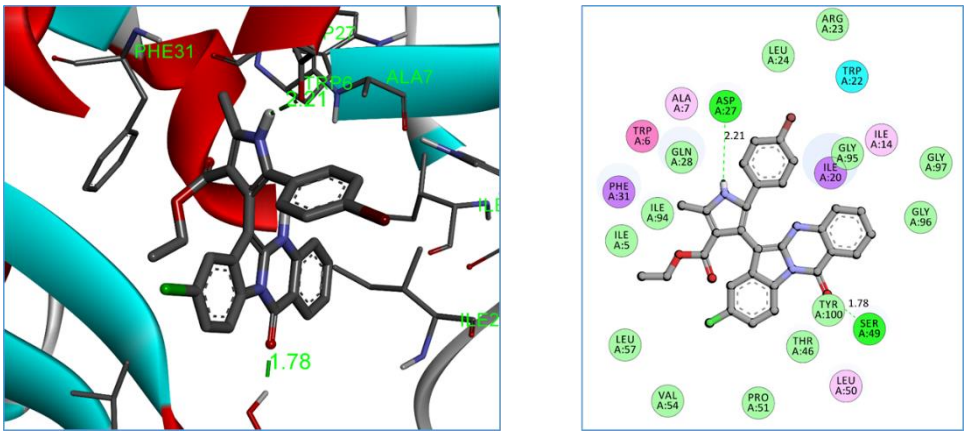

Figure 2A.6. Binding interactions between compound **4o** with active site of 1DF7. The hydrogen atoms (except N–H) of **4o** were removed for clarity.

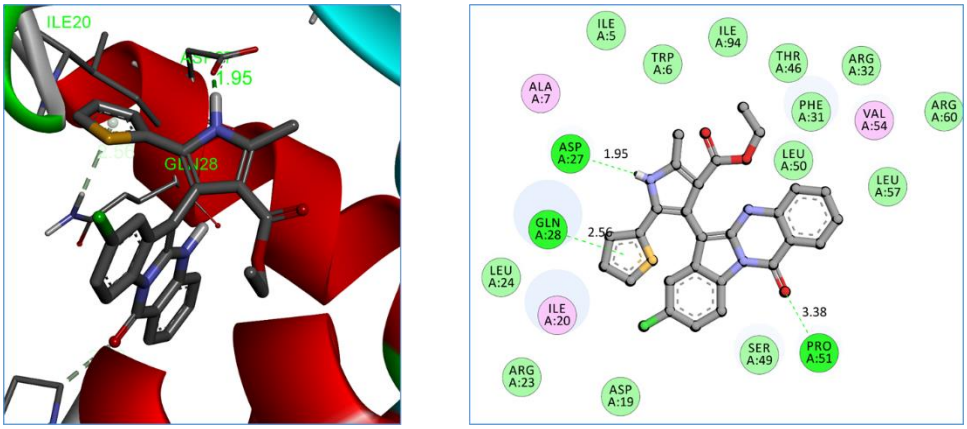

Figure 2A.7. Binding interactions between compound **4r** with active site of 1DF7. The hydrogen atoms (except N–H) of **4r** were removed for clarity.

2A.4. ADME prediction

The measurement of absorption, distribution, metabolism and excretion (ADME) makes it easier to identify molecules at the therapeutic dose with a high safety profile. Moreover, *in silico* prediction of pharmacokinetic parameters reduces the risk of failure of drug during the final stages of a clinical trial. ADME prediction results of the synthesized compounds were presented in Table 2A.5.

Estimation of octanol/water partition coefficient (lipophilicity) is examined by LogP. The predicted lipophilicity values are in the ranging from 5.007 to 6.59, and these values revealed that moderate lipophilicity of the compounds. The anticipated aqueous solubility (LogS) values for the synthesized compounds varied from -7.041 to -8.05, which indicates their moderate solubility in aqueous media due to presence of lipophilic groups. However, the topological polar surface area (TPSA) values (≤140 Å) reveal that the compounds have good oral bioavailability. The results from logarithm of the apparent permeability co-efficient (logPapp) suggests that all the compounds have moderate Caco-2 permeability in the range of 0.68 x 10^{-6} to 0.83 x 10^{-6}. Remarkably, all the synthesized compounds have high human intestinal absorption (HIA: 93.115–97.52%). Blood-brain partition co-efficient (logBB) values of all the compounds were in considerable range to cross the blood-brain barrier (BBB). The reported drug like properties and *in silico* ADME prediction suggests that the synthesized compounds **4a-s** exhibit acceptable pharmacokinetic parameters and can be considered as lead molecules for the development of new drugs.

Table 2A.5. *In silico* drug likeness and ADME prediction of the compounds **4a-s**

Entry	Mol. Wt	H-donor	H-acceptor	No. of rotatable bonds	LogP	LogS	TPSA (Å)	Caco-2 Permeability (logPapp in 10^{-6} cm/s)	HIA (% absorbed)	BBB permeability (log BB)
	≤500	**≤5**	**≤10**	**≤10**	**≤5**	**<0.5**	**≤140**	**>8x10^{-6}**	**70 - 100%**	**-3.0 - 1.2**
4a	461.17	2	6	5	5.460	-7.168	79.36	0.725	96.033	-1.211
4b	447.16	2	6	4	5.108	-7.041	79.36	0.763	96.499	-1.160
4c	495.13	2	6	5	6.056	-7.566	79.36	0.746	94.641	-1.396
4d	481.12	2	6	4	5.746	-7.466	79.36	0.785	95.108	-1.345
4e	539.08	2	6	5	6.156	-7.675	79.36	0.738	94.574	-1.417
4f	525.07	2	6	4	5.866	-7.594	79.36	0.776	95.041	-1.365
4g	479.16	2	6	5	5.569	-7.351	79.36	0.747	95.645	-1.360
4h	465.15	2	6	4	5.219	-7.230	79.36	0.785	96.112	-1.309
4i	475.19	2	6	5	5.881	-7.416	79.36	0.796	96.1	-1.243
4j	461.17	2	6	4	5.548	-7.327	79.36	0.834	96.566	-1.191

4k	491.18	2	7	6	5.493	-7.429	88.59	0.779	97.054	-1.342
4l	477.17	2	7	5	5.138	-7.325	88.59	0.818	97.520	-1.291
4m	467.13	2	6	5	5.367	-7.199	79.36	0.681	94.284	-1.357
4n	453.11	2	6	4	5.007	-7.064	79.36	0.720	94.751	-1.306
4o	573.05	2	6	5	6.594	-8.058	79.36	0.754	93.405	-1.586
4p	559.03	2	6	4	6.347	-7.971	79.36	0.792	93.871	-1.534
4q	513.13	2	6	5	6.123	-7.760	79.36	0.763	94.476	-1.529
4r	501.09	2	6	5	5.955	-7.610	79.36	0.697	93.115	-1.526
4s	487.08	2	6	4	5.637	-7.519	79.36	0.736	93.582	-1.475

Mol. Wt: molecular weight; **H-donor**: number of hydrogen bond donors; **H-acceptor**: number of hydrogen bond acceptors; **LogP**: octanol/water partition coefficient; **LogS**: aqua solubility parameter; **TPSA**: topological polar surface area; **Caco-2**: cell permeability; **HIA**: human intestinal absorption; **LogBB**: blood/brain partition co-efficient.

2A.5. Conclusion

This chapter describes the utilization of $Fe(OTs)_3/SiO_2$ for the first time as a green and sustainable catalyst in a three component domino synthetic protocol. This methodology is the first report on the diversity oriented synthetic protocol involving the reaction of chalcones, 1,3-diketone and ammonium acetate with the help of the catalyst $Fe(OTs)_3/SiO_2$ in grinding method. The reactions were performed under mild conditions and provided the products in good to excellent yields with special features of the synthetic protocol like high atom economy, operational simplicity, environmentally benign synthesis, short reaction time and excellent yields. The efficiency of the catalyst was studied by its recyclability reactions. In addition, *in vitro* anti-TB activity of the synthesized compounds were tested against *Mycobacterium tuberculosis* H37Rv. Among them, two compounds **4o** and **4r** displayed significant activity with MIC value 6.25 µg/mL when compared to the standard drug ethambutol (MIC: 1.56 µg/mL) and they were also shown relatively low levels of cytotoxicity against RAW 264.7 cell line. Moreover, *in silico* molecular docking studies and ADME prediction of the title compounds suggest that these moieties can serve as lead molecules in future research.

2A.6. Experimental Section

2A.6.1. Typical procedure for the synthesis of 6-(2-oxo-2-phenylethylidene)indolo quinazolinones (1a-j)

To a mixture of tryptanthrin **A** (1.0 mmol), corresponding acetophenones **B** (1.0 mmol) and 10% aq. NaOH (1 mL) in methanol (3 mL) at room temperature was stirred for 6 h. After completion of reaction (monitored by TLC), solid was collected by filtration and washed with methanol to furnish the intermediates (**1'a-j**). Then, to a solution of **1'** (1.0

mmol) in acetic acid (3 mL), BF_3Et_2O (20 mol%) was added, the mixture was kept at 60 °C for appropriate time. After completion of reaction, the reaction mixture was cooled to room temperature and the obtained products (**1a-j**) were filtered and recrystallized from methanol.

2A.6.2. Typical procedure for the synthesis of 4-pyrrolo-12-oxoquinazolines (4a-s)

A mixture of chalcones **1** (1.0 mmol), 1,3-diketone **2** (1.0 mmol), ammonium acetate **3** (2.5 mmol) and 100 mg of $Fe(OTs)_3/SiO_2$ was thoroughly grinded in an agate mortar with a pestle manually until completion of the reaction (monitored by TLC). After that ethyl acetate (5 mL) was added to this reaction mixture. The catalyst was recovered by filtration, washed with ethanol (3 x 5 mL) and reused for next cycles. The filtrate was concentrated to furnish the desired products (**4a-s**) which were further purified by recrystallization from ethanol.

2A.6.3. Protocol for the anti-TB screening

The MIC of the synthesized compounds was tested using *in vitro* Microplate Alamar Blue Assay using the reported protocol [48]. The *Mycobacterium tuberculosis* H37Rv strain (ATCC27294) was used for the screening. The inoculum was prepared from fresh LJ medium re-suspended in 7H9-S medium (7H9 broth, 0.1% casitone, 0.5% glycerol, supplemented oleic acid, albumin, dextrose, and catalase [OADC]), adjusted to a OD_{590} 1.0, and diluted 1:20; 100 µL was used as inoculum. Each drug stock solution was thawed and diluted in 7H9-S at four-fold the final highest concentration tested. Serial two-fold dilutions of each drug were prepared directly in a sterile 96-well microtiter plate using 100 µL 7H9-S. A growth control containing no antibiotic and a sterile control were also prepared on each plate. Sterile water was added to all perimeter wells to avoid evaporation during the incubation. The plate was covered, sealed in plastic bags and incubated at 37 ^oC in normal atmosphere. After 7 days incubation, 30 µL of alamar blue solution was added to each well, and the plate was re-incubated overnight. A change in colour from blue (oxidised state) to pink (reduced) indicated the growth of bacteria, and the MIC was defined as the lowest concentration of drug that prevented this change in colour.

2A.6.4. *In vitro* cytotoxicity screening

The *in vitro* cytotoxicity of the privileged anti-tubercular active analogues with lower MIC value were assessed by 3-(4,5-dimethylthiazol-2-yl)-2,5-diphenyltetrazolium bromide (MTT) assay against growth inhibition of RAW 264.7 cells at 25 µg/mL

concentration [49]. Cell lines were maintained at 37 °C in a humidified 5% CO_2 incubator (Thermo scientific). Detached the adhered cells and followed by centrifugation to get cell pellet. Fresh media was added to the pellet to make a cell count using haemocytometer and plate 100 µL of media with cells ranging from 5,000 - 6,000 per well in a 96-well plate. The plate was incubated overnight in CO_2 incubator for the cells to adhere and regain its shape. After 24 h cells were treated with the test compounds at 25 µg/mL diluted using the media to deduce the percentage inhibition on normal cells. The cells were incubated for 48 h to assay the effect of the test compounds on different cell lines. Zero hour reading was noted down with untreated cells and also control with 1% DMSO to subtract further from the 48 h reading. After 48 h incubation, cells were treated by MTT (4,5-dimethylthiazol-2-yl)-2,5-diphenyltetrazolium bromide) dissolved in PBS (5 mg/mL) and incubated for 3-4 h at 37 °C. The formazan crystals thus formed were dissolved in 100 µL of DMSO and the viability was measured at 540 nm on a multimode reader (Spectra max). The values were further calculated for percentage inhibition which in turn helps us to know the cytotoxicity of the test compounds.

2A.6.5. Molecular docking protocol

The docking studies are predominating tools for the assessment of the binding affinity to the ligand-protein receptor. All the synthesized compounds were subjected to *in silico* molecular docking studies by using the AutoDockTools (ADT) version 1.5.6 and AutoDock version 4.2.5.1 docking program [50]. The 3D-structures of all the synthesized compounds were prepared by using chem3D pro 12.0 software. The optimized 3D structures were saved in pdb format. The structure of the dihydrofolate reductase of *Mycobacterium tuberculosis* (PDB code: 1DF7) protein was extracted from the protein data bank (http://www.rcsb.org/pdb). The bound ligand and water molecules in protein were removed by using Discovery Studio Visualizer version 4.0 to prepare the protein. Non polar hydrogens were merged and gasteiger charges were added to the protein. The grid file was saved in gpf format. The three dimensional grid box having dimensions 60 x 60 x 60 $Å^3$ was created around the protein with spacing 0.3750 Å. The genetic algorithm was carried out with the population size and the maximum number of evaluations were 150 and 25,00,000 respectively. The docking output file was saved as Lamarckian Ga (4.2) in dpf format. The ligand-protein complex binding sites were visualized by Discovery Studio Visualizer version 4.0.

2A.6.6. ADME prediction

In silico ADME prediction of the synthesized compounds were calculated by using the online servers ADMETlab 2.0 and pkCSM [51]. The ADMET properties, human intestinal absorption (HIA), Caco-2 cell permeability, plasma protein binding and blood brain barrier penetration (BBB) were predicted using this program.

2A.7. Spectral data of synthesized compounds 4a-s

ethyl 2-methyl-4-(12-oxo-5,12-dihydroindolo[2,1-*b*]quinazolin-6-yl)-5-phenyl-1*H*-pyrrole-3-carboxylate (**4a**)

Yellow solid. mp: 284-286 °C. IR (KBr, cm^{-1}): 3307, 3246, 1666, 1643, 1536, 1488, 1430. ^{1}H NMR (400 MHz, DMSO-d_6) δ: 11.79 (s, 1H), 11.00 (s, 1H), 8.63 (d, J = 7.2 Hz, 1H), 8.18 (d, J = 7.6 Hz, 1H), 7.88 (d, J = 7.2 Hz, 1H), 7.63 (t, J = 7.6 Hz, 1H), 7.53-7.46 (m, 1H), 7.43 (d, J = 8.0 Hz, 1H), 7.36 (d, J = 7.2 Hz, 1H), 7.15 (d, J = 5.6 Hz, 4H), 7.04 (t, J = 7.2 Hz, 1H), 6.97 (d, J = 6.8 Hz, 1H), 3.88-3.80 (m, 1H), 3.78-3.71 (m, 1H), 2.63 (s, 3H), 0.64 (t, J = 7.2 Hz, 3H). ^{13}C NMR (125 MHz, DMSO-d_6) δ: 165.04, 159.46, 141.32, 137.22, 135.13, 134.83, 132.92, 131.68, 129.63, 129.21, 128.74, 127.81, 126.53, 125.97, 124.30, 120.31, 119.83, 117.33, 115.88, 115.62, 113.18, 111.54, 110.42, 90.04, 58.57, 14.03, 13.96. MS/MS m/z: 462.1771 $[M+H]^+$, 416.1359 $[M\text{-}OC_2H_5]^+$, 233.0637 $[M\text{-}OC_2H_5\text{-}CH_3\text{-}CO\text{-}C_4HN\text{-}C_6H_5]^+$. HRMS (ESI, m/z): $[M+H]^+$ calcd. for $C_{29}H_{24}N_3O_3$: 462.1818; found: 462.1821.

methyl 2-methyl-4-(12-oxo-5,12-dihydroindolo[2,1-*b*]quinazolin-6-yl)-5-phenyl-1*H*-pyrrole-3-carboxylate (**4b**)

Yellow solid. mp: 304-306 °C. IR (KBr, cm^{-1}): 3303, 3057, 2944, 1672, 1637, 1617, 1580, 1450. ^{1}H NMR (400 MHz, DMSO-d_6) δ: 11.80 (s, 1H), 10.96 (s, 1H), 8.64 (d, J = 6.8 Hz, 1H), 8.18 (d, J = 7.6 Hz, 1H), 7.63 (t, J = 8.0 Hz, 1H), 7.41 (d, J = 8.0 Hz, 1H), 7.33 (d, J = 7.6 Hz, 2H), 7.15-7.11 (m, 5H), 7.03 (t, J = 7.2 Hz, 1H), 6.96 (d, J = 8.0 Hz, 1H), 3.40 (s, 3H), 2.63 (s, 3H). ^{13}C NMR (100 MHz, DMSO-d_6 + $CDCl_3$) δ: 165.28, 159.47, 141.31, 136.94, 135.10, 134.80, 132.89, 131.55, 129.75, 129.25, 128.71, 127.81, 126.56, 126.04, 124.30, 120.31, 119.83, 117.36, 115.89, 115.66, 112.95, 111.58, 110.70, 89.77, 50.55, 14.23. HRMS (ESI, m/z): $[M+H]^+$ calcd. for $C_{28}H_{22}N_3O_3$: 448.1661; found: 448.1665.

ethyl 5-(4-chlorophenyl)-2-methyl-4-(12-oxo-5,12-dihydroindolo[2,1-*b*]quinazolin-6-yl)-1*H*-pyrrole-3-carboxylate (**4c**)

Yellow solid. mp: 359-361 °C. IR (KBr, cm^{-1}): 3278, 3166, 1667, 1639, 1617, 1579, 1471. ^{1}H NMR (400 MHz, DMSO-d_6) δ: 11.85 (s, 1H), 11.00 (s, 1H), 8.63 (dd, J = 6.8, 2.4 Hz,

1H), 8.17 (d, *J* = 6.8 Hz, 1H), 7.63 (t, *J* = 8.4 Hz, 1H), 7.41 (d, *J* = 8.0 Hz, 1H), 7.35 (d, *J* = 8.8 Hz, 2H), 7.20 (d, *J* = 8.4 Hz, 2H), 7.16 – 7.11 (m, 3H), 6.93 (dd, *J* = 6.8, 2.4 Hz, 1H), 3.87-3.79 (m, 1H), 3.77-3.69 (m, 1H), 2.61 (s, 3H), 0.63 (t, *J* = 7.2 Hz, 3H). ^{13}C NMR (100 MHz, DMSO-d_6) δ: 164.97, 159.48, 141.29, 137.63, 135.18, 134.92, 131.76, 131.40, 130.91, 129.28, 128.80, 128.36, 127.82, 127.51, 124.38, 120.42, 119.94, 117.22, 115.88, 115.69, 113.34, 111.61, 111.09, 89.60, 58.66, 14.02, 13.94. HRMS (ESI, m/z): $[M+H]^+$ calcd. for $C_{29}H_{23}ClN_3O_3$: 496.1428; found: 496.1428.

methyl 5-(4-chlorophenyl)-2-methyl-4-(12-oxo-5,12-dihydroindolo[2,1-*b*]quinazolin-6-yl)-1*H*-pyrrole-3-carboxylate (**4d**)

Yellow solid. mp: 337-339 °C. IR (KBr, cm^{-1}): 3317, 3066, 2947, 1671, 1638, 1599, 1536, 1449. ^{1}H NMR (400 MHz, DMSO-d_6) δ: 11.85 (s, 1H), 10.96 (s, 1H), 8.63 (d, *J* = 8.0 Hz, 1H), 8.17 (d, *J* = 7.6 Hz, 1H), 7.63 (t, *J* = 8.0 Hz, 1H), 7.40 (d, *J* = 8.4 Hz, 1H), 7.31 (d, *J* = 8.4 Hz, 2H), 7.19 (d, *J* = 8.4 Hz, 2H), 7.15-7.11 (m, 3H), 6.93 (dd, *J* = 6.4, 2.4 Hz, 1H), 3.38 (s, 3H), 2.61 (s, 3H). ^{13}C NMR (100 MHz, DMSO-d_6) δ: 165.18, 159.47, 141.28, 137.34, 135.16, 134.90, 131.73, 131.25, 130.95, 129.31, 128.78, 128.46, 127.83, 127.57, 124.37, 120.41, 119.94, 117.24, 115.90, 115.73, 113.11, 111.65, 111.36, 89.33, 50.61, 14.24. HRMS (ESI, m/z): $[M+H]^+$ calcd. for $C_{28}H_{21}ClN_3O_3$: 482.1271; found: 482.1270.

ethyl 5-(4-bromophenyl)-2-methyl-4-(12-oxo-5,12-dihydroindolo[2,1-*b*]quinazolin-6-yl)-1*H*-pyrrole-3-carboxylate (**4e**)

Yellow solid. mp: 358-360 °C. IR (KBr, cm^{-1}): 3274, 3063, 1664, 1639, 1617, 1578, 1433. ^{1}H NMR (400 MHz, DMSO-d_6) δ: 11.87 (s, 1H), 11.02 (s, 1H), 8.64 (d, *J* = 8.0 Hz, 1H), 8.18 (d, *J* = 7.6 Hz, 1H), 7.64 (t, *J* = 7.2 Hz, 1H), 7.42 (d, *J* = 8.4 Hz, 1H), 7.32 (dd, *J* = 10.4, 8.8 Hz, 4H), 7.19 – 7.12 (m, 3H), 6.94 (d, *J* = 6.4 Hz, 1H), 3.88 – 3.80 (m, 1H), 3.78 – 3.70 (m, 1H), 2.62 (s, 3H), 0.63 (t, *J* = 7.2 Hz, 3H). ^{13}C NMR (100 MHz, DMSO-d_6) δ: 164.94, 159.47, 141.29, 137.68, 135.17, 134.92, 132.11, 131.70, 131.37, 129.29, 128.36, 127.80, 124.37, 120.41, 119.94, 119.43, 117.21, 115.88, 115.69, 113.39, 111.62, 111.16, 89.59, 58.66, 14.03, 13.94. HRMS (ESI, m/z): $[M+H]^+$ calcd. for $C_{29}H_{23}BrN_3O_3$: 540.0923; found: 540.0920.

methyl 5-(4-bromophenyl)-2-methyl-4-(12-oxo-5,12-dihydroindolo[2,1-*b*]quinazolin-6-yl)-1*H*-pyrrole-3-carboxylate (**4f**)

Yellow solid. mp: 331-333 °C. IR (KBr, cm^{-1}): 3322, 3066, 2945, 1667, 1644, 1620, 1578, 1448. ^{1}H NMR (400 MHz, DMSO-d_6) δ: 11.88 (s, 1H), 10.99 (s, 1H), 8.64 (d, *J* = 7.6 Hz,

1H), 8.19 (d, *J* = 8.0 Hz, 1H), 7.87 (d, *J* = 8.0 Hz, 1H), 7.64 (t, *J* = 7.6 Hz, 1H), 7.41 (d, *J* = 8.4 Hz, 1H), 7.34 (d, *J* = 8.0 Hz, 2H), 7.27 (d, *J* = 8.4 Hz, 2H), 7.16 – 7.13 (m, 2H), 6.94 (d, *J* = 6.4 Hz, 1H), 3.40 (s, 3H), 2.62 (s, 3H). ^{13}C NMR (100 MHz, DMSO-d_6) δ: 165.18, 159.48, 141.28, 137.40, 135.17, 134.90, 133.32, 132.07, 131.68, 131.21, 129.31, 128.47, 127.86, 124.39, 120.43, 119.95, 119.48, 117.22, 115.89, 115.74, 113.14, 111.65, 111.42, 89.32, 50.62, 14.23. HRMS (ESI, m/z): $[M+H]^+$ calcd. for $C_{28}H_{21}BrN_3O_3$: 526.0766; found: 526.0768.

ethyl 5-(4-fluorophenyl)-2-methyl-4-(12-oxo-5,12-dihydroindolo[2,1-*b*]quinazolin-6-yl)-1*H*-pyrrole-3-carboxylate (**4g**)

Yellow solid. mp: 335-337 °C. IR (KBr, cm^{-1}): 3299, 3062, 2970, 1664, 1641, 1616, 1585, 1458. ^{1}H NMR (400 MHz, DMSO-d_6) δ: 11.82 (s, 1H), 11.00 (s, 1H), 8.64 (d, *J* = 6.4 Hz, 1H), 8.18 (d, *J* = 7.2 Hz, 1H), 7.64 (t, *J* = 6.8 Hz, 1H), 7.43 (d, *J* = 8.0 Hz, 1H), 7.37 (bs, 2H), 7.15 (d, *J* = 6.0 Hz, 3H), 7.03 – 6.95 (m, 3H), 3.88-3.82 (m, 1H), 3.77-3.71 (m, 1H), 2.63 (s, 3H), 0.65 (s, 3H). ^{13}C NMR (100 MHz, DMSO-d_6) δ: 165.04, 159.48, 141.31, 137.18 (d, *J* = 231.6 Hz), 135.16, 134.92, 131.58, 129.48 (d, *J* = 23.8 Hz), 128.78, 128.03 (d, *J* = 8.8 Hz), 127.81, 124.34, 120.38, 119.90, 117.28, 115.87, 115.76 (d, *J* = 3.2 Hz), 115.66, 115.55, 113.11, 111.58, 110.32, 89.77, 58.62, 14.02, 13.97. HRMS (ESI, m/z): $[M+H]^+$ calcd. for $C_{29}H_{23}FN_3O_3$: 480.1723; found: 480.1720.

methyl 5-(4-fluorophenyl)-2-methyl-4-(12-oxo-5,12-dihydroindolo[2,1-*b*]quinazolin-6-yl)-1*H*-pyrrole-3-carboxylate (**4h**)

Yellow solid. mp: 330-332 °C. IR (KBr, cm^{-1}): 3313, 3280, 1668, 1642, 1599, 1578, 1446. ^{1}H NMR (400 MHz, DMSO-d_6) δ: 11.81 (s, 1H), 10.96 (s, 1H), 8.64 (d, *J* = 7.2 Hz, 1H), 8.18 (d, *J* = 7.6 Hz, 1H), 7.64 (t, *J* = 7.2 Hz, 1H), 7.41 (d, *J* = 8.0 Hz, 1H), 7.34 (t, *J* = 6.4 Hz, 2H), 7.15-7.12 (m, 3H), 6.98 (q, *J* = 9.6 Hz, 3H), 3.40 (s, 3H), 2.62 (s, 3H). ^{13}C NMR (125 MHz, DMSO-d_6) δ: 165.25, 161.99 (d, *J* = 242.2 Hz), 159.46, 141.28, 136.89, 135.13 (d, *J* = 33.2 Hz), 131.40, 129.44 (d, *J* = 2.4 Hz), 129.26, 128.87, 128.08 (d, *J* = 7.6 Hz), 127.81, 124.33, 120.36, 119.88, 117.28, 115.87 (d, *J* = 20.6 Hz), 115.54, 112.85, 111.59, 110.58, 89.48, 50.57, 14.21. HRMS (ESI, m/z): $[M+H]^+$ calcd. for $C_{28}H_{21}FN_3O_3$: 466.1567; found: 466.1565.

ethyl 2-methyl-4-(12-oxo-5,12-dihydroindolo[2,1-*b*]quinazolin-6-yl)-5-(*p*-tolyl)-1*H*-pyrrole-3-carboxylate (**4i**)

Yellow solid. mp: 330-332 °C. IR (KBr, cm^{-1}): 3280, 3063, 2975, 1668, 1638, 1617, 1581, 1457. ^{1}H NMR (400 MHz, DMSO-d_6) δ: 11.73 (s, 1H), 11.00 (s, 1H), 8.62 (d, *J* = 7.2 Hz,

1H), 8.17 (d, *J* = 8.0 Hz, 1H), 7.63 (t, *J* = 7.6 Hz, 1H), 7.43 (d, *J* = 8.0 Hz, 1H), 7.24 (d, *J* = 7.6 Hz, 2H), 7.17 – 7.10 (m, 3H), 6.94 (d, *J* = 7.6 Hz, 3H), 3.87-3.79 (m, 1H), 3.77-3.68 (m, 1H), 2.61 (s, 3H), 2.13 (s, 3H), 0.63 (t, *J* = 6.8 Hz, 3H). ^{13}C NMR (125 MHz, DMSO-d_6) δ: 165.07, 159.46, 141.33, 136.92, 135.67, 135.12, 134.81, 131.73, 130.14, 129.75, 129.33, 129.19, 127.81, 125.90, 124.29, 120.29, 119.79, 117.35, 115.89, 115.60, 113.05, 111.53, 109.83, 90.17, 58.52, 21.04, 14.01, 13.96. HRMS (ESI, m/z): $[M+H]^+$ calcd. for $C_{30}H_{26}N_3O_3$: 476.1974; found: 476.1978.

methyl 2-methyl-4-(12-oxo-5,12-dihydroindolo[2,1-*b*]quinazolin-6-yl)-5-(*p*-tolyl)-1*H*-pyrrole-3-carboxylate (**4j**)

Yellow solid. mp: 303-305 °C. IR (KBr, cm^{-1}): 3289, 3063, 2945, 1672, 1642, 1615, 1580, 1448. ^{1}H NMR (400 MHz, DMSO-d_6) δ: 11.74 (s, 1H), 10.97 (s, 1H), 8.65 (d, *J* = 3.2 Hz, 1H), 8.19 (d, *J* = 4.8 Hz, 1H), 7.64 (s, 1H), 7.44 (d, *J* = 4.0 Hz, 1H), 7.23 (s, 2H), 7.15 (s, 3H), 6.96 (s, 3H), 3.40 (s, 3H), 2.63 (s, 3H), 2.15 (s, 3H). ^{13}C NMR (100 MHz, DMSO-d_6) δ: 165.31, 159.48, 141.34, 136.66, 135.73, 135.12, 134.80, 131.60, 130.11, 129.88, 129.32, 127.83, 125.96, 124.31, 120.32, 119.82, 117.38, 115.91, 115.65, 112.83, 111.57, 110.11, 89.91, 50.53, 21.05, 14.23. HRMS (ESI, m/z): $[M+H]^+$ calcd. for $C_{29}H_{24}N_3O_3$: 462.1818; found: 462.1817.

ethyl 5-(4-methoxyphenyl)-2-methyl-4-(12-oxo-5,12-dihydroindolo[2,1-*b*]quinazolin-6-yl)-1*H*-pyrrole-3-carboxylate (**4k**)

Yellow solid. mp: 296-298 °C. IR (KBr, cm^{-1}): 3279, 2986, 1666, 1637, 1618, 1536, 1439. ^{1}H NMR (400 MHz, DMSO-d_6) δ: 11.67 (s, 1H), 10.98 (s, 1H), 8.63 (d, *J* = 7.2 Hz, 1H), 8.17 (d, *J* = 9.2 Hz, 1H), 7.64 (t, *J* = 7.2 Hz, 1H), 7.43 (d, *J* = 8.0 Hz, 1H), 7.28 (d, *J* = 9.2 Hz, 2H), 7.19 – 7.11 (m, 3H), 6.97 (d, *J* = 5.2 Hz, 1H), 6.73 (d, *J* = 8.8 Hz, 2H), 3.86-3.80 (m, 1H), 3.77 – 3.70 (m, 1H), 3.61 (s, 3H), 2.61 (s, 3H), 0.63 (t, *J* = 7.2 Hz, 3H). ^{13}C NMR (100 MHz, DMSO-d_6) δ: 165.11, 159.48, 158.09, 141.34, 136.60, 135.13, 134.83, 131.85, 129.73, 129.18, 127.81, 127.35, 125.56, 124.31, 121.75, 120.29, 119.80, 117.37, 115.89, 115.61, 114.22, 112.91, 111.52, 109.11, 90.24, 58.50, 55.36, 14.00, 13.97. HRMS (ESI, m/z): $[M+H]^+$ calcd. for $C_{30}H_{26}N_3O_4$: 492.1923; found: 492.1928.

methyl 5-(4-methoxyphenyl)-2-methyl-4-(12-oxo-5,12-dihydroindolo[2,1-*b*] quinazolin-6-yl)-1*H*-pyrrole-3-carboxylate (**4l**)

Yellow solid. mp: 280-282 °C. IR (KBr, cm^{-1}): 3313, 3070, 2946,1671, 1638, 1614, 1582, 1449. ^{1}H NMR (400 MHz, DMSO-d_6) δ: 11.67 (s, 1H), 10.93 (s, 1H), 8.61 (d, *J* = 7.2 Hz,

1H), 8.17 (d, *J* = 8.8 Hz, 1H), 7.62 (t, *J* = 9.6 Hz, 1H), 7.41 (d, *J* = 8.4 Hz, 1H), 7.24 (d, *J* = 7.2 Hz, 2H), 7.14 – 7.10 (m, 3H), 6.95 (d, *J* = 6.8 Hz, 1H), 6.71 (d, *J* = 8.4 Hz, 2H), 3.60 (s, 3H), 3.37 (s, 3H), 2.59 (s, 3H). ^{13}C NMR (75 MHz, DMSO-d_6) δ: 164.60, 158.97, 157.69, 140.90, 135.98, 134.51, 134.32, 131.49, 129.31, 128.77, 127.29, 126.91, 125.18, 123.72, 119.72, 119.26, 116.89, 115.38, 115.09, 113.75, 112.57, 111.14, 108.72, 89.88, 57.94, 54.91, 13.45. HRMS (ESI, m/z): $[M+H]^+$ calcd. for $C_{29}H_{24}N_3O_4$:478.1767; found: 478.1772.

ethyl 2-methyl-4-(12-oxo-5,12-dihydroindolo[2,1-*b*]quinazolin-6-yl)-5-(thiophen-2-yl)-1*H*-pyrrole-3-carboxylate (**4m**)

Yellow solid. mp: 324-326 °C. IR (KBr, cm^{-1}): 3289, 3060, 2969, 1661, 1640, 1615, 1582, 1473. ^{1}H NMR (400 MHz, DMSO-d_6) δ: 11.88 (s, 1H), 11.00 (s, 1H), 8.65 (d, *J* = 7.6 Hz, 1H), 8.18 (d, *J* = 7.6 Hz, 1H), 7.63 (t, *J* = 7.6 Hz, 1H), 7.41 (d, *J* = 8.4 Hz, 1H), 7.29 (s, 1H), 7.22-7.12 (m, 3H), 7.04 – 7.00 (m, 2H), 6.89 (s, 1H), 3.83 – 3.75 (m, 2H), 2.62 (s, 3H), 0.64 (t, *J* = 6.8 Hz, 3H). ^{13}C NMR (100 MHz, DMSO-d_6) δ: 164.87, 159.46, 141.22, 137.14, 135.21, 135.14, 134.52, 131.74, 129.48, 125.59, 113.04, 111.56, 110.31, 89.37, 58.63, 13.99, 13.91. HRMS (ESI, m/z): $[M+H]^+$ calcd. for $C_{27}H_{22}N_3O_3S$: 468.1382; found: 468.1382.

methyl 2-methyl-4-(12-oxo-5,12-dihydroindolo[2,1-*b*]quinazolin-6-yl)-5-(thiophen-2-yl)-1*H*-pyrrole-3-carboxylate (**4n**)

Yellow solid. mp: 318-320 °C. IR (KBr, cm^{-1}): 3305, 3069, 2943, 1671, 1638, 1616, 1583, 1446. ^{1}H NMR (400 MHz, DMSO-d_6) δ: 11.89 (s, 1H), 10.99 (s, 1H), 8.65 (d, *J* = 7.2 Hz, 1H), 8.19 (d, *J* = 7.2 Hz, 1H), 7.63 (t, *J* = 7.6 Hz, 1H), 7.39 (d, *J* = 7.6 Hz, 1H), 7.29 (s, 1H), 7.20-7.12 (m, 3H), 7.04-7.00 (m, 2H), 6.89 (s, 1H), 3.40 (s, 3H), 2.62 (s, 3H). ^{13}C NMR (100 MHz, DMSO-d_6) δ: 165.17, 159.48, 141.20, 136.96, 135.22, 135.15, 134.39, 131.61, 129.51, 125.68, 112.84, 111.58, 110.51, 89.11, 50.63, 14.20. HRMS (ESI, m/z): $[M+H]^+$ calcd. for $C_{26}H_{20}N_3O_3S$: 454.1225; found: 454.1227.

ethyl 5-(4-bromophenyl)-4-(8-chloro-12-oxo-5,12-dihydroindolo[2,1-*b*]quinazolin-6-yl)-2-methyl-1*H*-pyrrole-3-carboxylate (**4o**)

Yellow solid. mp: 364-366 °C. IR (KBr, cm^{-1}): 3301, 3069, 2981, 1670, 1640, 1577, 1535, 1444. ^{1}H NMR (400 MHz, DMSO-d_6) δ: 11.85 (s, 1H), 11.00 (s, 1H), 8.63 (d, *J* = 6.8 Hz, 1H), 8.17 (d, *J* = 7.6 Hz, 1H), 7.63 (t, *J* = 8.4 Hz, 1H), 7.41 (d, *J* = 8.4 Hz, 1H), 7.31 (q, *J* = 8.8 Hz, 4H), 7.17 – 7.11 (m, 2H), 6.93 (d, *J* = 8.4 Hz, 1H), 3.87-3.79 (m, 1H), 3.77 – 3.69

(m, 1H), 2.61 (s, 3H), 0.62 (t, *J* = 7.2 Hz, 3H). ^{13}C NMR (100 MHz, DMSO-d_6) δ: 164.85, 159.28, 141.16, 137.83, 136.33, 135.40, 131.92, 131.78, 128.95, 128.59, 127.86, 120.87, 119.62, 117.00, 116.23, 116.06, 113.26, 111.67, 110.30, 89.29, 58.71, 14.00, 13.96. HRMS (ESI, m/z): $[M+H+2]^+$ calcd. for $C_{29}H_{22}BrClN_3O_3$: 576.0533; found: 576.0538.

methyl 5-(4-bromophenyl)-4-(8-chloro-12-oxo-5,12-dihydroindolo[2,1-*b*]quinazolin-6-yl)-2-methyl-1*H*-pyrrole-3-carboxylate (**4p**)

Yellow solid. mp: 346-348 °C. IR (KBr, cm^{-1}): 3305, 3069, 2949, 1672, 1637, 1624, 1577, 1446. ^{1}H NMR (400 MHz, DMSO-d_6) δ: 11.91 (s, 1H), 11.16 (s, 1H), 8.61 (d, *J* = 8.4 Hz, 1H), 8.06 (d, *J* = 7.2 Hz, 1H), 7.67 (t, *J* = 7.2 Hz, 1H), 7.43 (d, *J* = 8.0 Hz, 1H), 7.36 (d, *J* = 8.0 Hz, 2H), 7.27 (d, *J* = 7.6 Hz, 2H), 7.19-7.13 (m, 2H), 6.86 (s, 1H), 3.42 (s, 3H), 2.62 (s, 3H). ^{13}C NMR (100 MHz, DMSO-d_6) δ: 164.23, 158.42, 140.27, 135.60, 134.67, 134.06, 129.05, 128.82, 128.26, 126.77, 124.89, 123.25, 119.26, 118.76, 116.32, 114.85, 114.59, 111.76, 109.05, 88.85, 49.47, 13.17. HRMS (ESI, m/z): $[M+H]^+$ calcd. for $C_{28}H_{20}BrClN_3O_3$: 560.0377; found: 560.0389.

ethyl 4-(8-chloro-12-oxo-5,12-dihydroindolo[2,1-b]quinazolin-6-yl)-5-(4-fluoro phenyl)-2-methyl-1*H*-pyrrole-3-carboxylate (4q)

Yellow solid. mp: 352-354 °C. IR (KBr, cm^{-1}): 3307, 3070, 1664, 1641, 1617, 1576, 1451. ^{1}H NMR (400 MHz, DMSO-d_6) δ: 11.86 (s, 1H), 11.18 (s, 1H), 8.60 (d, *J* = 8.8 Hz, 1H), 8.18 (d, *J* = 8.0 Hz, 1H), 7.67 (t, *J* = 8.0 Hz, 1H), 7.44 (d, *J* = 8.4 Hz, 1H), 7.36 (dd, *J* = 8.0, 6.0 Hz, 2H), 7.19-7.13 (m, 2H), 7.03 (t, *J* = 8.8 Hz, 2H), 6.88 (s, 1H), 3.88 – 3.74 (m, 2H), 2.62 (s, 3H), 0.66 (t, *J* = 7.2 Hz, 3H). ^{13}C NMR (100 MHz, DMSO-d_6) δ: 164.95, 162.33 (d, *J* = 242.6 Hz), 159.90, 159.28, 141.16, 137.36, 136.34, 135.41, 133.23, 129.30, (d, *J* = 3.0 Hz), 129.00, 128.93, 128.13 (d, *J* = 8.0 Hz), 127.81, 127.68, 120.86, 119.50, 116.30, (d, *J* = 24.2 Hz), 115.85, 115.64, 112.95, 111.61, 109.50, 89.46, 58.68, 13.98. HRMS (ESI, m/z): $[M+H]^+$ calcd. for $C_{29}H_{22}ClFN_3O_3$: 514.1334; found: 514.1334.

ethyl 4-(8-chloro-12-oxo-5,12-dihydroindolo[2,1-*b*]quinazolin-6-yl)-2-methyl-5-(thiophen-2-yl)-1*H*-pyrrole-3-carboxylate (**4r**)

Yellow solid. mp: 370-372 °C. IR (KBr, cm^{-1}):3289, 3066, 2976, 1662, 1639, 1618, 1579, 1439. ^{1}H NMR (400 MHz, DMSO-d_6) δ: 11.93 (s, 1H), 11.20 (s, 1H), 8.63 (d, *J* = 8.8 Hz, 1H), 8.19 (d, *J* = 7.6 Hz, 1H), 7.66 (t, *J* = 7.2 Hz, 1H), 7.42 (d, *J* = 8.0 Hz, 1H), 7.32 (s, 1H), 7.17 (d, *J* = 7.6 Hz, 2H), 7.07 (s, 1H), 6.93 (s, 2H), 3.82 (d, *J* = 6.4 Hz, 2H), 2.62 (s, 3H), 0.67 (t, *J* = 6.4 Hz, 3H). ^{13}C NMR (100 MHz, DMSO-d_6) δ: 164.78, 159.26, 141.09,

137.34, 136.57, 135.48, 134.29, 133.44, 128.99, 127.93, 125.73, 112.91, 111.58, 109.42, 89.05, 58.70, 14.04, 13.95. MS/MS m/z: 502.0954 $[M+H]^+$, 456.0520 $[M-OC_2H_5]^+$, 421.0851 $[M-OC_2H_5-Cl]^+$, 380.1662 $[M-OC_2H_5-Cl-CO-CH_3]^+$. HRMS (ESI, m/z): $[M+H]^+$ calcd. for $C_{27}H_{21}ClN_3O_3S$: 502.0992; found: 502.0994.

methyl 4-(8-chloro-12-oxo-5,12-dihydroindolo[2,1-*b*]quinazolin-6-yl)-2-methyl-5-(thiophen-2-yl)-1*H*-pyrrole-3-carboxylate (**4s**)

Yellow solid. mp: 361-363 °C. IR (KBr, cm^{-1}): 3298, 3067, 2924, 1665, 1639, 1617, 1579, 1446. ^1H NMR (400 MHz, DMSO-d_6) δ: 11.94 (s, 1H), 11.19 (s, 1H), 8.63 (d, J = 8.8 Hz, 1H), 8.20 (d, J = 8.0 Hz, 1H), 7.66 (t, J = 8.4 Hz, 1H), 7.41 (d, J = 7.6 Hz, 1H), 7.32 (s, 1H), 7.17 (d, J = 7.6 Hz, 2H), 7.07 (s, 1H), 6.92 (d, J = 7.2 Hz, 2H), 3.43 (s, 3H), 2.62 (s, 3H). ^{13}C NMR (75 MHz, DMSO-d_6) δ: 164.58, 158.77, 140.66, 136.55, 136.13, 134.85, 133.77, 132.93, 128.54, 127.54, 127.34, 126.39, 125.34, 124.36, 122.05, 120.41, 119.11, 116.48, 115.88, 115.59, 112.41, 111.24, 109.29, 88.43, 50.08, 13.50. HRMS (ESI, m/z): $[M+H]^+$ calcd. for $C_{26}H_{19}ClN_3O_3S$: 488.0836; found: 488.0834.

2A.8. References

[1] A. Sarkar, S. Santra, S. K. Kundu, A. Hajra, G. V. Zyryanov, O. N. Chupakhin, V. N. Charushin, A. Majee, *Green Chem.* **2016**, *18*, 4475–4525.

[2] G. Zhao, R. Tong, *Green Chem.* **2019**, *21*, 64–68.

[3] M. Leonardi, M. Villacampa, J. C. Menéndez, *Chem. Sci.* **2018**, *9*, 2042–2064.

[4] A. Kumar, S. Sharma, *Green Chem.* **2011**, *13*, 2017–2020.

[5] R. Thorwirth, F. Bernhardt, A. Stolle, B. Ondruschka, J. Asghari, *Chem. - A Eur. J.* **2010**, *16*, 13236–13242.

[6] G. Brahmachari, I. Karmakar, P. Karmakar, *Green Chem.* **2021**, *23*, 4762–4770.

[7] S. Khan, B. Baire, *Chem. Rec.* **2021**, *21*, 1–13.

[8] Y. Ding, J. Kuang, X. Xiao, L. Wang, Y. Ma, *J. Org. Chem.* **2021**, *86*, 12257–12266.

[9] K. Ghasemi, M. Darroudi, M. Rahimi, H. Rouh, A. R. Gupta, C. Cheng, A. Amini, *New J. Chem.* **2021**, *45*, 16119–16130.

[10] A. Yadav, P. Patil, D. Chandam, S. Jadhav, A. Ghule, S. Hangirgekar, S. Sankpal,

J. Mol. Struct. **2021**, *1245*, 130960–130968.

[11] M. Deepa, U. Selvarasu, K. Kalaivani, K. Parasuraman, *J. Organomet. Chem.* **2021**, *954*, 122073–122078.

[12] R. Mondal, G. Chakraborty, A. K. Guin, S. Sarkar, N. D. Paul, *J. Org. Chem.* **2021**, *86*, 13186–13197.

[13] J. Aboonajmi, F. Panahi, H. Sharghi, *ACS Omega* **2021**, *6*, 22395–22399.

[14] S. Tarannum, Z. N. Siddiqui, *RSC Adv.* **2015**, *5*, 74242–74250.

[15] M. M. Heravi, V. Zadsirjan, *RSC Adv.* **2020**, *10*, 44247–44311.

[16] M. K. Hunjan, S. Panday, A. Gupta, J. Bhaumik, P. Das, J. K. Laha, *Chem. Rec.* **2021**, *21*, 715–780.

[17] G. Li Petri, V. Spanò, R. Spatola, R. Holl, M. V. Raimondi, P. Barraja, A. Montalbano, *Eur. J. Med. Chem.* **2020**, *208*, 112783–112796.

[18] H. Zeynali, H. Keypour, L. Hosseinzadeh, R. W. Gable, *J. Mol. Struct.* **2021**, *1244*, 130956–130964.

[19] A. M. Jassem, A. M. Dhumad, *ChemistrySelect* **2021**, *6*, 2641–2647.

[20] S. N. Adamovich, E. K. Sadykov, I. A. Ushakov, E. N. Oborina, L. A. Belovezhets, *Mendeleev Commun.* **2021**, *31*, 204–206.

[21] T. Kundu, A. Pramanik, *Bioorg. Chem.* **2020**, *98*, 103734–103743.

[22] P. D. MacLean, E. E. Chapman, S. L. Dobrowolski, A. Thompson, L. R. C. Barclay, *J. Org. Chem.* **2008**, *73*, 6623–6635.

[23] S. Faivre, G. Demetri, W. Sargent, E. Raymond, *Nat. Rev. Drug Discov.* **2007**, *6*, 734–745.

[24] H. Lennernas, *Clin. Pharmacokinet.* **2003**, *42*, 1141–1160.

[25] I. Van Wijngaarden, C. G. Kruse, J. A. M. van der Heyden, M. T. M. Tulp, *J. Med. Chem.* **1988**, *31*, 1934–1940.

[26] M. Wang, M. D. Gorrell, G. W. McCaughan, R. G. Dickinson, *Life Sci.* **2001**, *68*, 785–797.

[27] A. Fürstner, *Angew. Chemie - Int. Ed.* **2003**, *42*, 3582–3603.

[28] M. Biava, *Curr. Med. Chem.* **2002**, *9*, 1859–1869.

[29] S. Alvi, R. Ali, *Org. Biomol. Chem.* **2021**, DOI 10.1039/D1OB01618K.

[30] I. Azad, F. Hassan, M. Saquib, N. Ahmad, A. R. Khan, A. G. Al-Sehemi, M. Nasibullah, *Orient. J. Chem.* **2018**, *34*, 1670–1700.

[31] H. Xu, H. W. Liu, K. Chen, G. W. Wang, *J. Org. Chem.* **2018**, *83*, 6035–6049.

[32] P. Paciorek, J. Szklarzewicz, B. Trzewik, D. Cież, W. Nitek, M. Hodorowicz, A. Jurowska, *J. Org. Chem.* **2021**, *86*, 1649–1658.

[33] Q. W. Gui, F. Teng, S. N. Ying, Y. Liu, T. Guo, J. X. Tang, J. Y. Chen, Z. Cao, W. M. He, *Chinese Chem. Lett.* **2020**, *31*, 3241–3244.

[34] J. K. Li, B. Zhou, Y. C. Tian, C. Jia, X. S. Xue, F. G. Zhang, J. A. Ma, *Org. Lett.* **2020**, *22*, 9585–9590.

[35] T. W. Von Zuben, G. Cariello Silva, A. G. Salles, *Green Chem.* **2021**, *23*, 6361–6365.

[36] J. Zhang, M. Liu, C. Li, Y. J. Xu, L. Dong, *Org. Chem. Front.* **2020**, *7*, 420–424.

[37] J. Chen, C. Li, Y. Zhou, C. Sun, T. Sun, *ChemCatChem* **2019**, *11*, 1943–1948.

[38] D. Akbaslar, E. S. Giray, O. Algul, *Mol. Divers.* **2021**, *25*, 2321–2338.

[39] J. Zheng, L. Huang, C. Huang, W. Wu, H. Jiang, *J. Org. Chem.* **2015**, *80*, 1235–1242.

[40] A. M. Tucker, P. Grundt, *Arkivoc* **2012**, *2012*, 546–569.

[41] G. Shanthi, P. T. Perumal, *Tetrahedron Lett.* **2009**, *50*, 3959–3962.

[42] A. Kamal, B. V. S. Reddy, B. Sridevi, A. Ravikumar, A. Venkateswarlu, G. Sravanthi, J. P. Sridevi, P. Yogeeswari, D. Sriram, *Bioorg. Med. Chem. Lett.* **2015**, *25*, 3867–3872.

[43] A. S. Al-Bogami, A. S. El-Ahl, *Synth. Commun.* **2015**, *45*, 2462–2472.

[44] T. Abe, K. Yamada, *Org. Lett.* **2016**, *18*, 6504–6507.

[45] R. Cordeiro, M. Kachroo, *Bioorg. Med. Chem. Lett.* **2020**, *30*, 127655–127661.

[46] T. M. Dhameliya, K. I. Patel, R. Tiwari, S. K. Vagolu, D. Panda, D. Sriram, A. K. Chakraborti, *Bioorg. Chem.* **2021**, *107*, 104538–104549.

[47] R. Li, R. Sirawaraporn, P. Chitnumsub, W. Sirawaraporn, J. Wooden, F. Athappilly, S. Turley, W. G. J. Hol, *J. Mol. Biol.* **2000**, *295*, 307–323.

[48] R. Tiwari, P. A. Miller, L. R. Chiarelli, G. Mori, M. Šarkan, I. Centárová, S. Cho, K. Mikušová, S. G. Franzblau, A. G. Oliver, M. J. Miller, *ACS Med. Chem. Lett.* **2016**, *7*, 266–270.

[49] J. Scheel, S. Weimans, A. Thiemann, E. Heisler, M. Hermann, *Toxicol. Vitr.* **2009**, *23*, 531–538.

[50] G. M. Morris, R. Huey, W. Lindstrom, M. F. Sanner, R. K. Belew, D. S. Goodsell, A. J. Olson, *J. Comput. Chem.* **2009**, *30*, 2785–2791.

[51] G. Xiong, Z. Wu, J. Yi, L. Fu, Z. Yang, C. Hsieh, M. Yin, X. Zeng, C. Wu, A. Lu, X. Chen, T. Hou, D. Cao, *Nucleic Acids Res.* **2021**, *49*, 5–14.

2A.9. Selected IR, NMR (^{1}H and ^{13}C) and Mass spectra

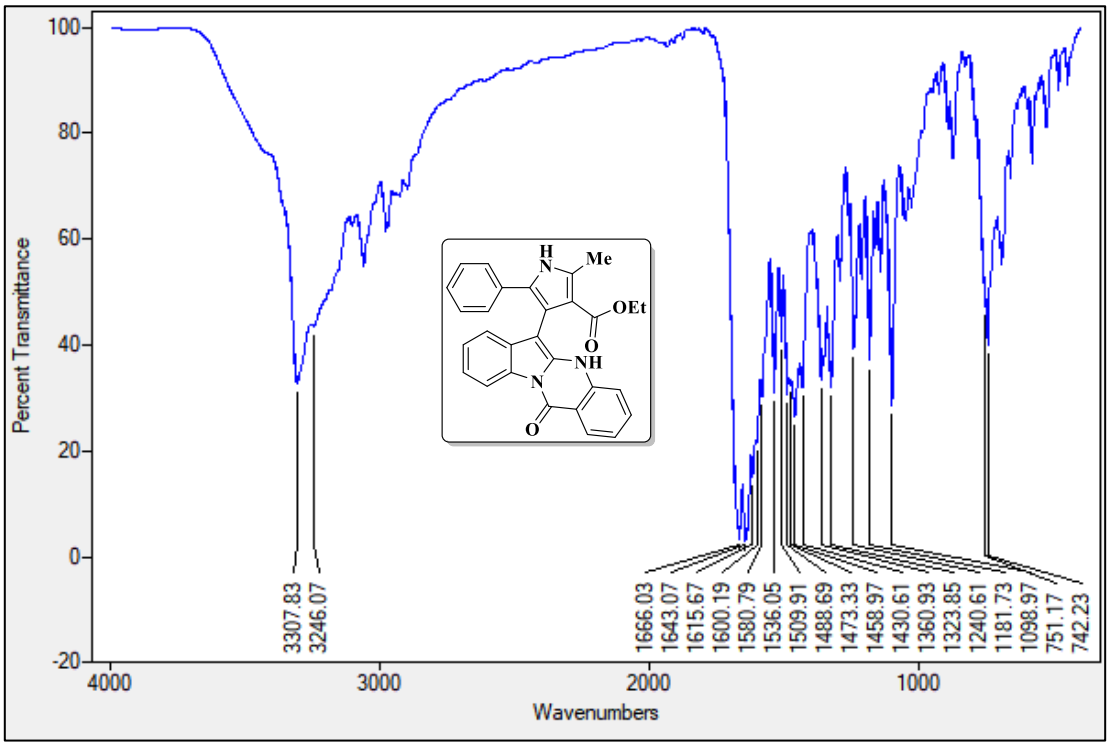

IR spectrum of the compound **4a**

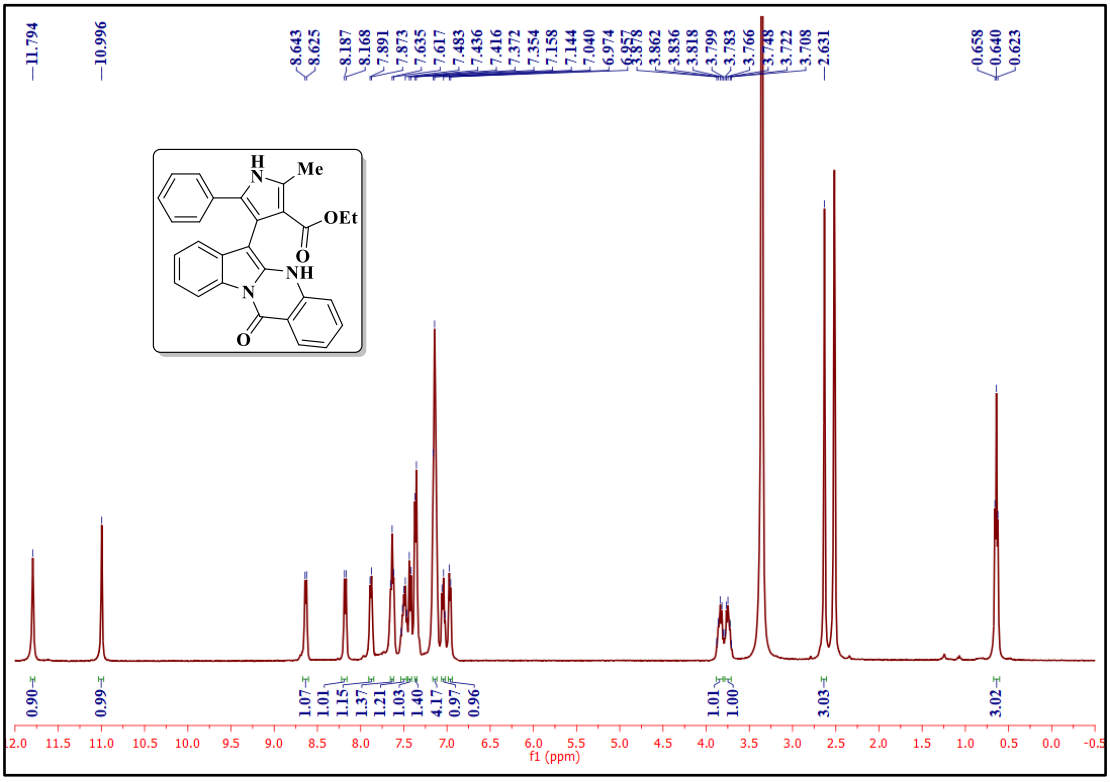

^{1}H NMR spectrum of the compound **4a**

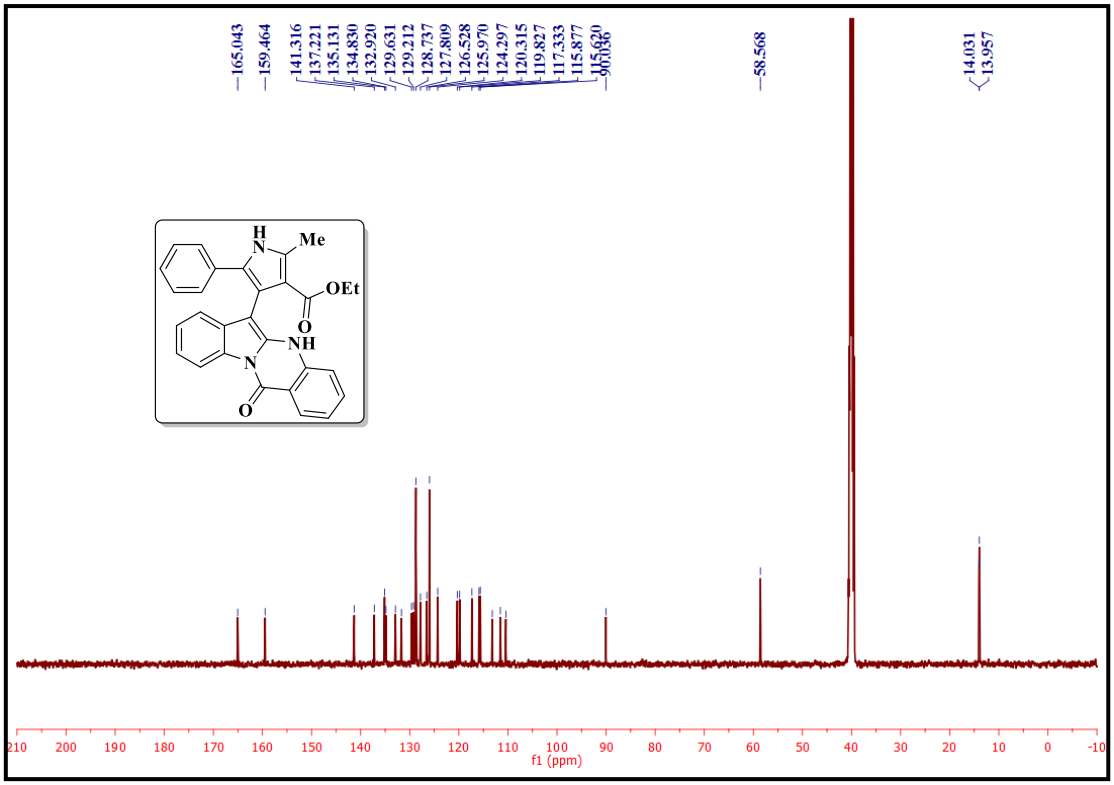

^{13}C NMR spectrum of the compound **4a**

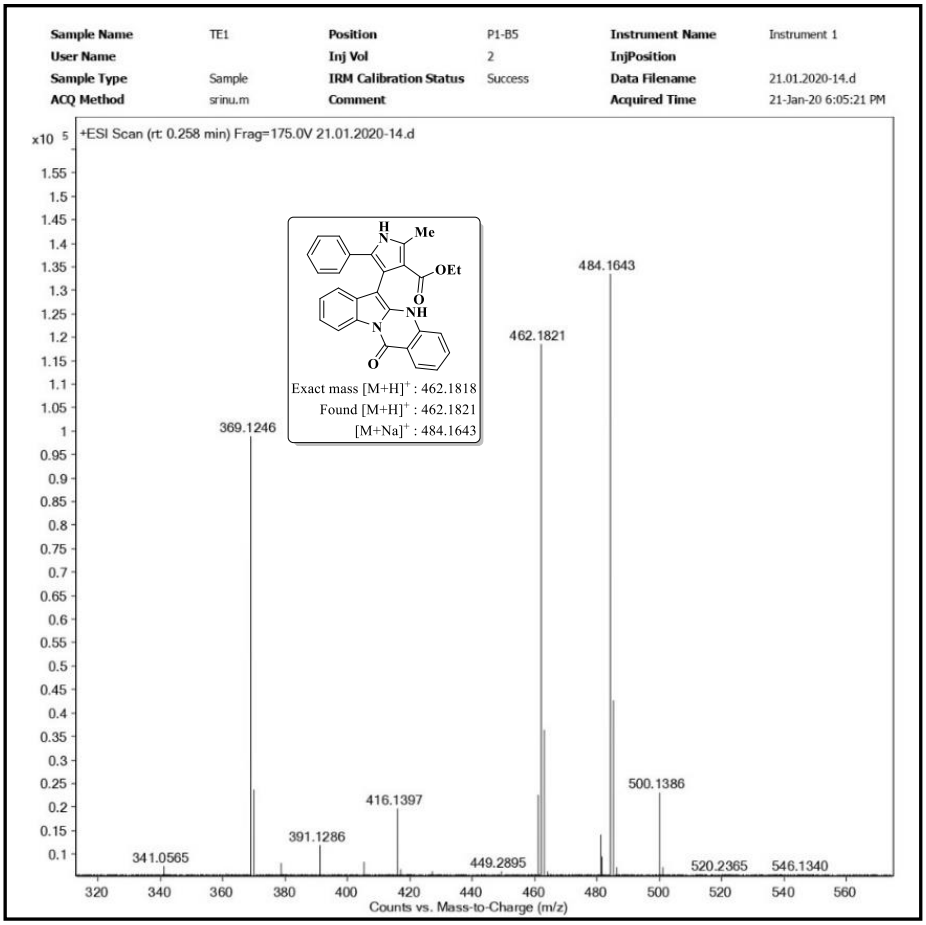

Mass spectrum of the compound **4a**

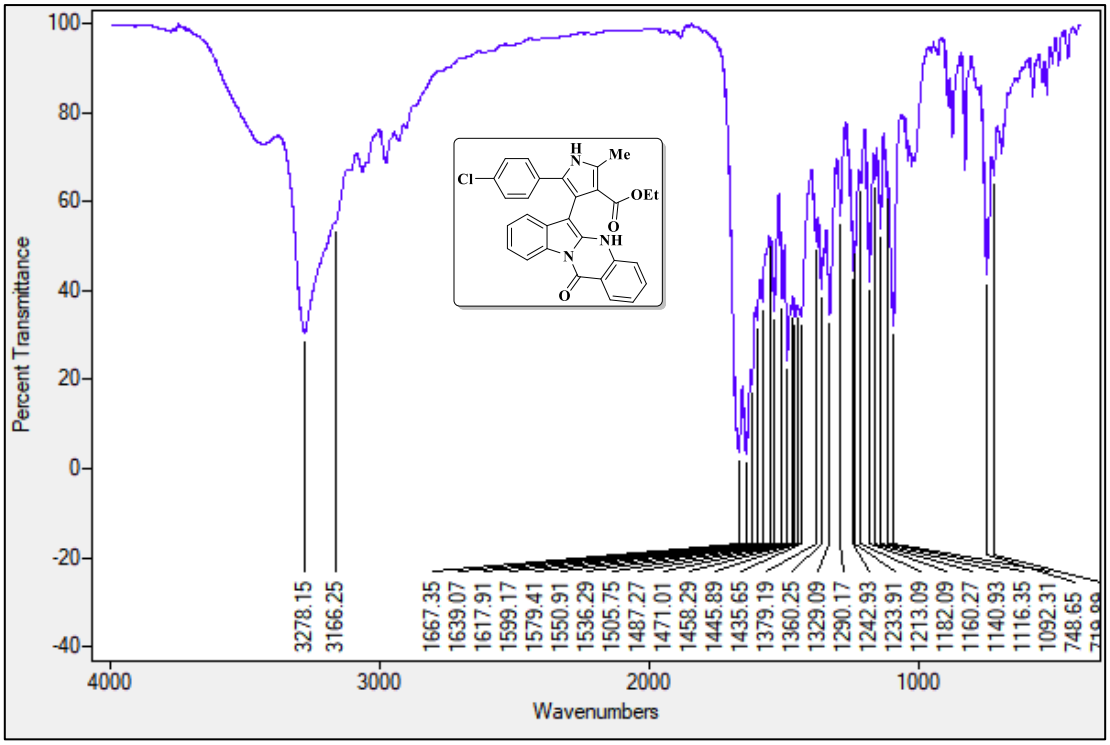

IR spectrum of the compound **4c**

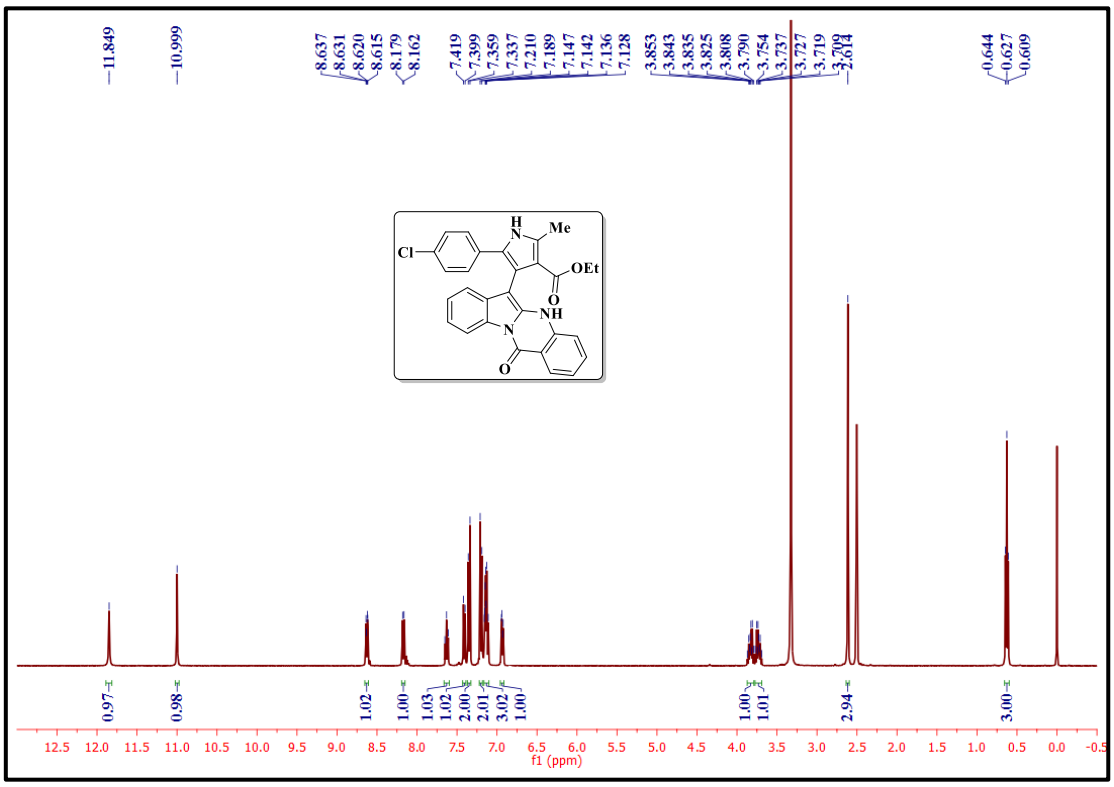

^{1}H NMR spectrum of the compound **4c**

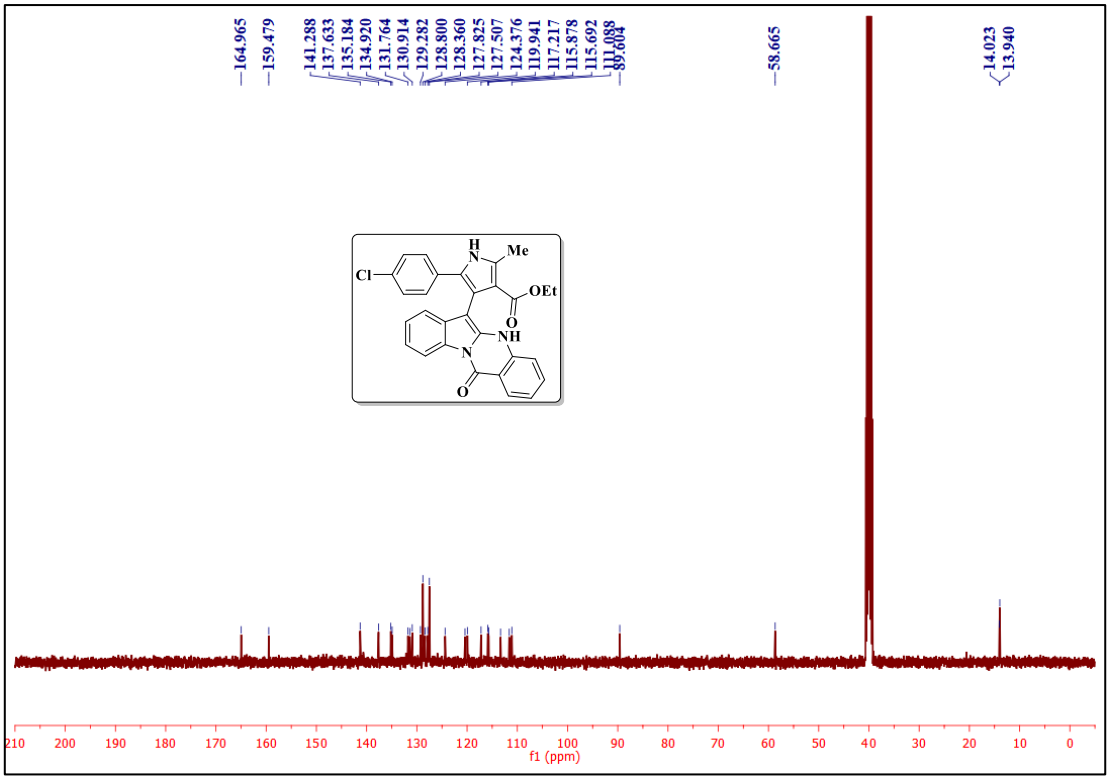

^{13}C NMR spectrum of the compound **4c**

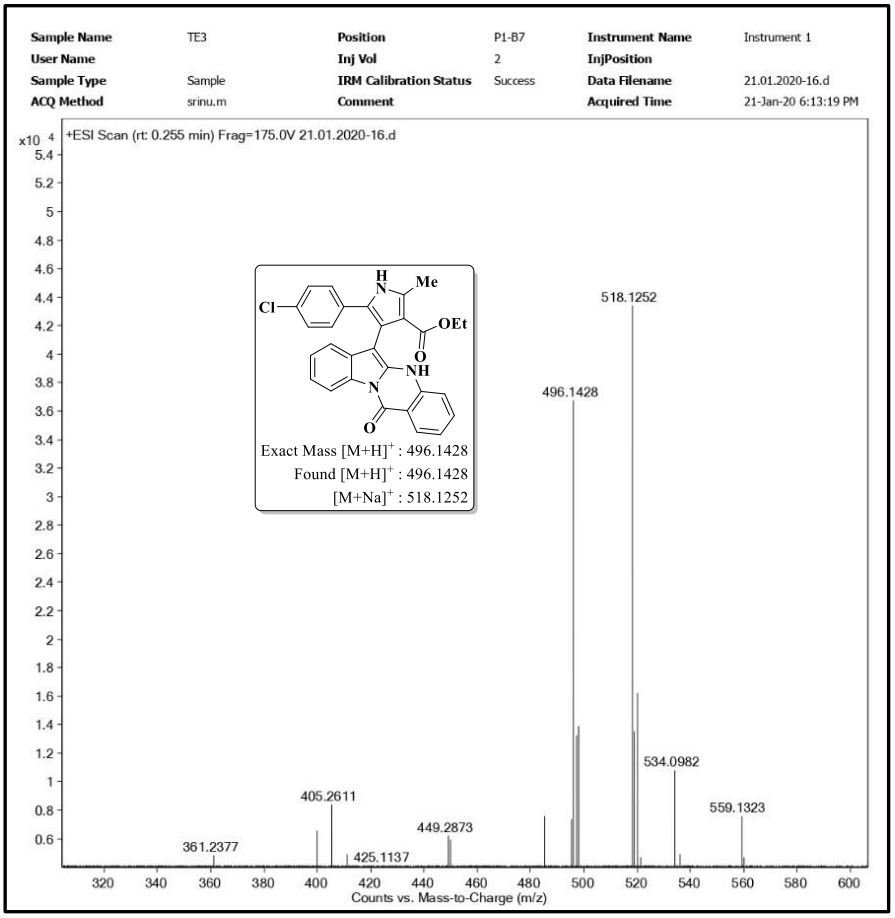

Mass spectrum of the compound **4c**

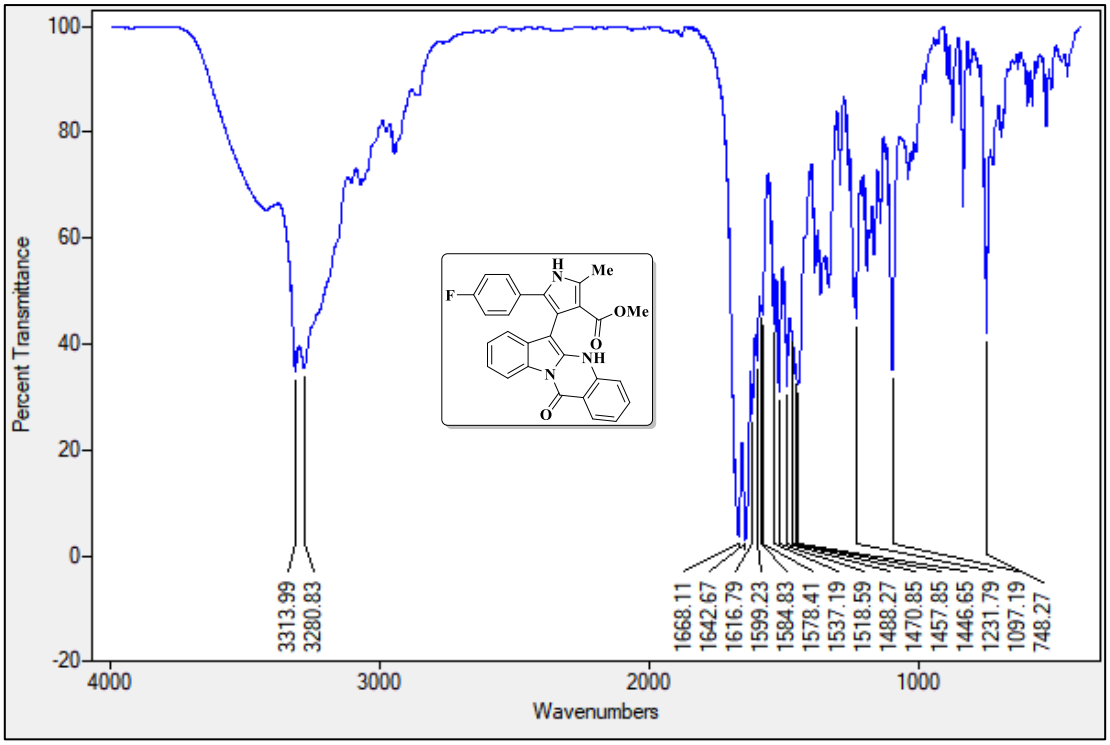

IR spectrum of the compound **4h**

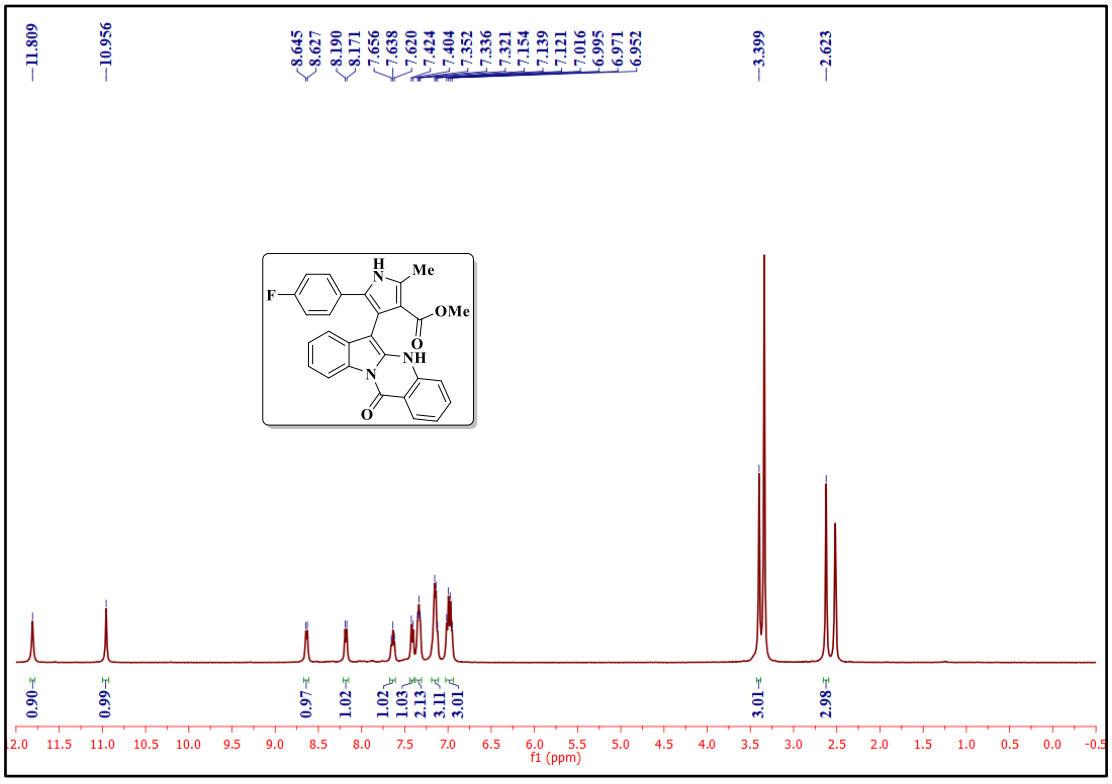

^{1}H NMR spectrum of the compound **4h**

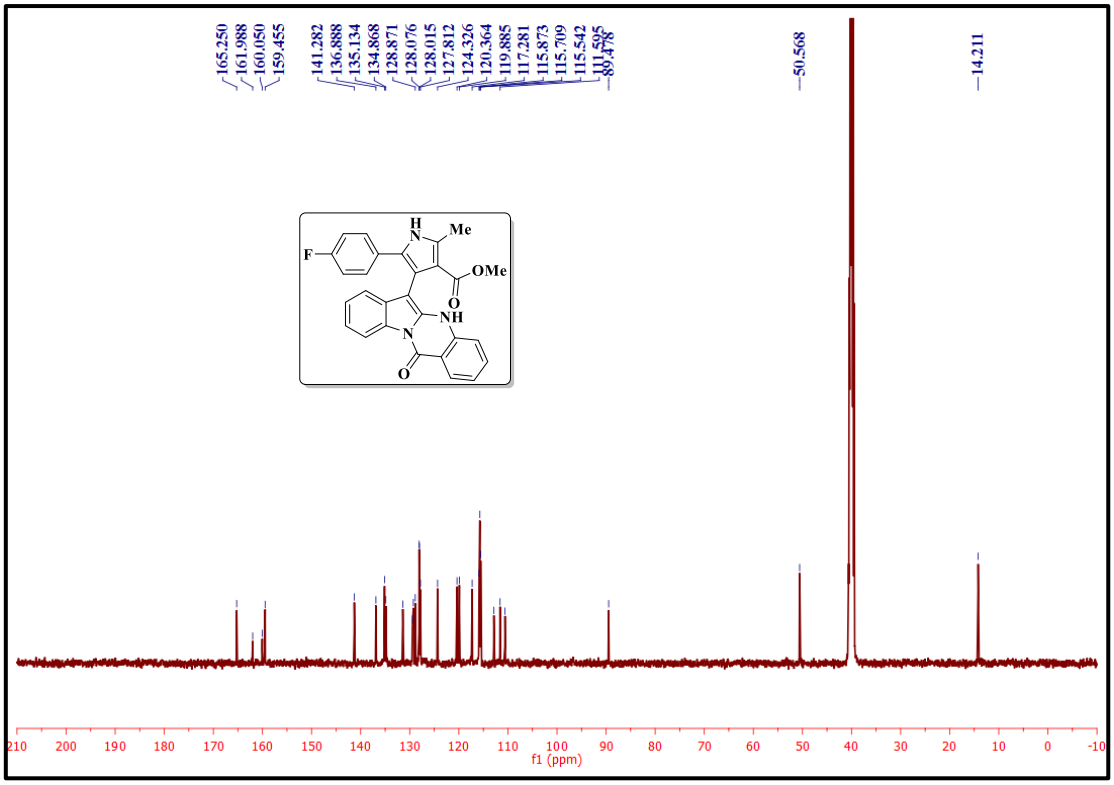

^{13}C NMR spectrum of the compound **4h**

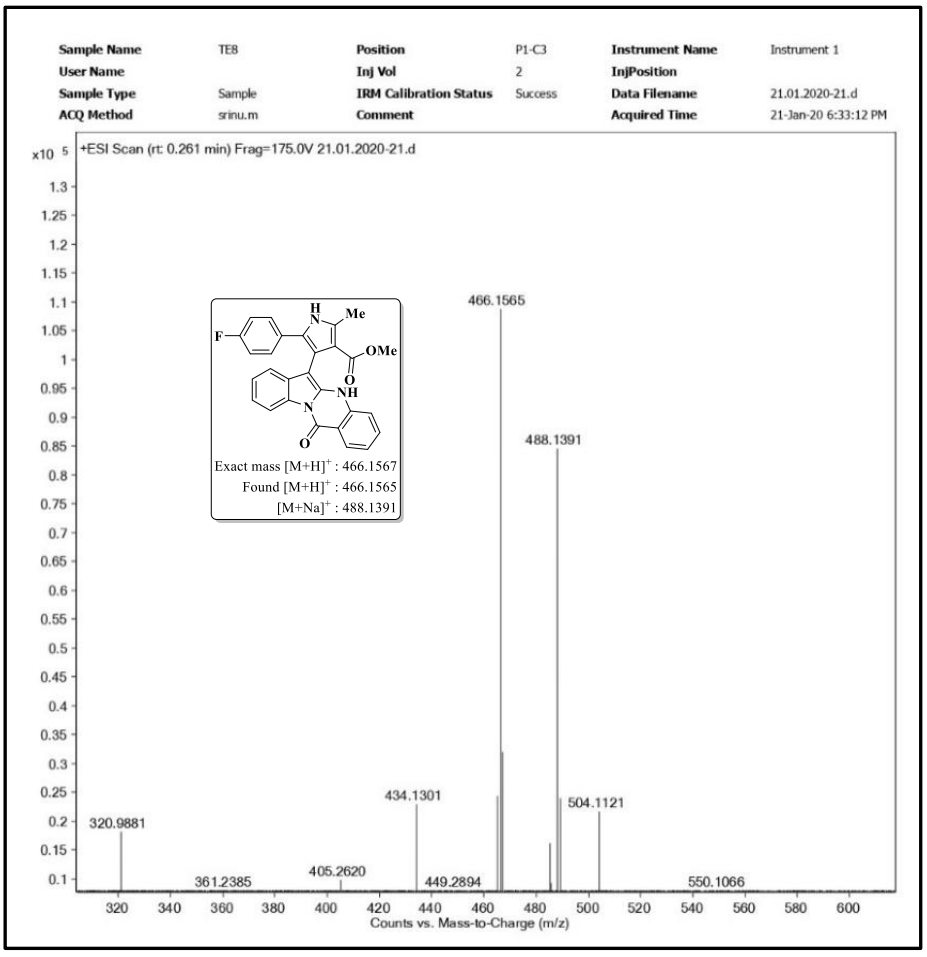

Mass spectrum of the compound **4h**

CHAPTER-II
Section-B

Transition metal- and oxidant-free regioselective synthesis of 3,4,5-trisubstituted pyrazoles *via* [3+2] cycloaddition reaction

2B.1. Introduction

Pyrazoles are ubiquitous in biological systems displaying diverse applications in medicinal and in synthetic chemistry [1,2]. Many of the pyrazole derivatives have received significant attention as building blocks for drug discovery [3]. In the past few decades, pyrazole analogs have gained renewed interest due to their wide range of biological activities, including anti-cancer [4], anti-tubercular [5], anti-bacterial [6], anti-obesity [7], anti-inflammatory [8-10] etc.

As demonstrated by the examples shown in Figure 2B.1, fipronil is a broadly used insecticide that belongs to the phenylpyrazole chemical family [11]. Pyrazofurin, isolated in 1969 from fermentation of a strain of Streptomyces candidus, is used as an effective drug against HIV [12]. Rimonabant shows beneficial effects for the treatment of obesity and tuberculosis [13]. Whereas, the drug celecoxib is a nonsteroidal anti-inflammatory drug, specifically used as COX-2 inhibitor [14]. Difenamizole is also a nonsteroidal anti-inflammatory drug [15], and the compound CDPPB (3-cyano-*N*-(1,3-diphenyl-1*H*-pyrazol-5-yl)benzamide) used in scientific community as anti-psychotic drug [16] (Figure 2B.1).

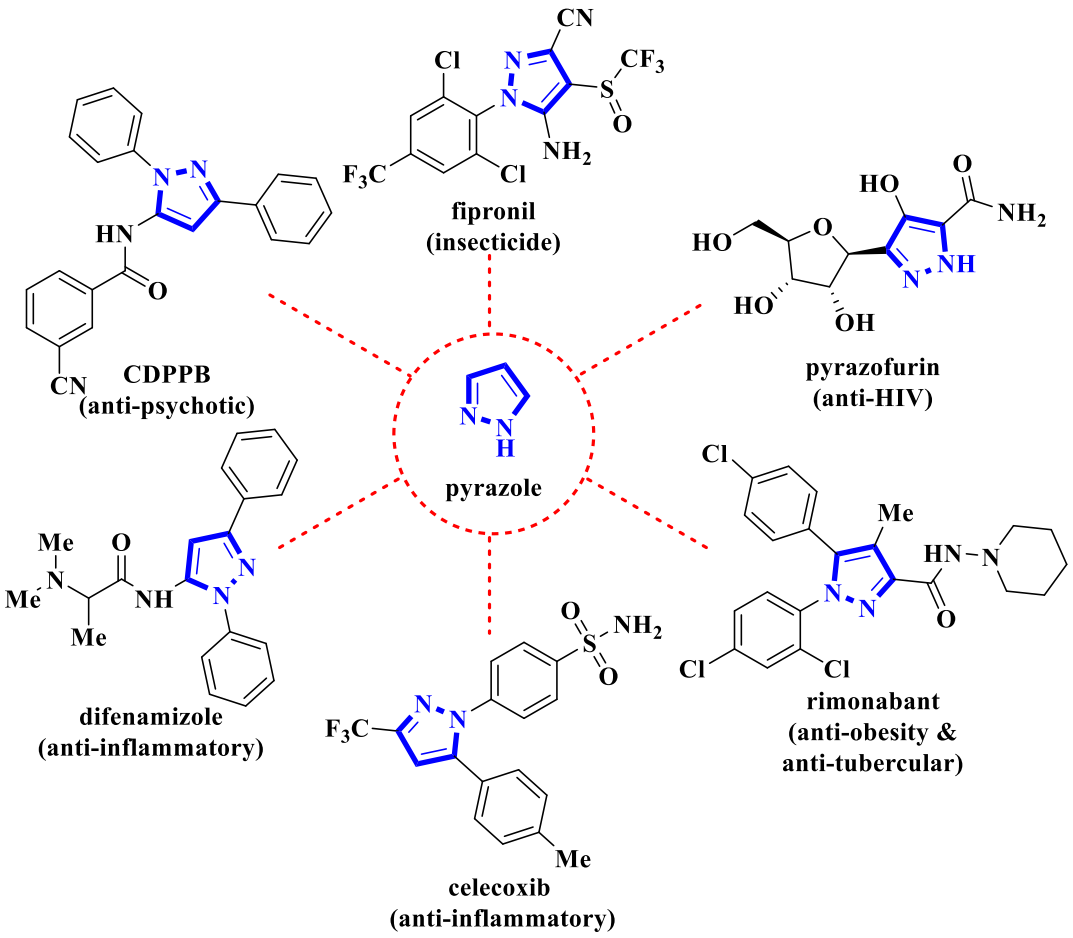

Figure 2B.1. Biologically potent drugs possessing pyrazole scaffold.

Apart from the biological activity, pyrazoles play vital role as various building blocks in agrochemicals [17,18], polymers [19], dyes and pigments [20]. They have also displayed various applications in the preparation of high performance energetic materials [21], functional metal-organic complexes [22], electroluminescent materials [23] etc. Besides these, they have also been used as bifunctional ligands in transition metal-catalyzed reactions, and as artificial receptors [24].

Owing to its versatile applications, the synthesis of pyrazoles has been a subject of extensive research. The synthetic methodologies for the preparation of this important scaffold involves transition metal catalyzed cross-coupling reactions [25], [3+2] cycloaddition reactions of Bestmann-Ohira reagent and Seyferth-Gilbert reagent with olefinic derivatives [26], [4+1] annulation using hydrazones [27], Knorr condensation of hydrazines with 1,3-dicarbonyl compounds [28]. Despite the availability of these numerous synthetic pathways, the reaction of a hydrazine with a 1,3-electrophilic substrate like 1,3-dicarbonyl substrates, tertiary enamines and Michael acceptors remains the predominant options [29]. However, these methods suffer from use of hazardous transition metals, lack of commercially available starting materials, and use of carcinogenic substituted hydrazines.

On the other hand, *N*-tosylhydrazones which are rapidly obtained from aldehydes or ketones have been utilized as a versatile synthons for the generation of large number of heterocycles [30]. A wide range of transformations have been performed using *N*-tosylhydrazones, including cyclization, coupling, insertion, alkynylation and olefination reactions [31,32]. They have also been used as a safe and easily available precursors of diazo compounds [33].

2B.1.1. Reported methods for the preparation of pyrazoles

Marzouk et al. reported the design, synthesis, biological evaluation, and computational studies of the novel thiazolo-pyrazole compounds (Figure 2B.2). The ability of the synthesized compounds for COX-2 inhibition was evaluated using *in vitro* COX-1/COX-2 enzyme inhibition and *in vivo* anti-inflammatory assays. These studies were further supported by *in silico* molecular docking analysis and drug likeness properties [34].

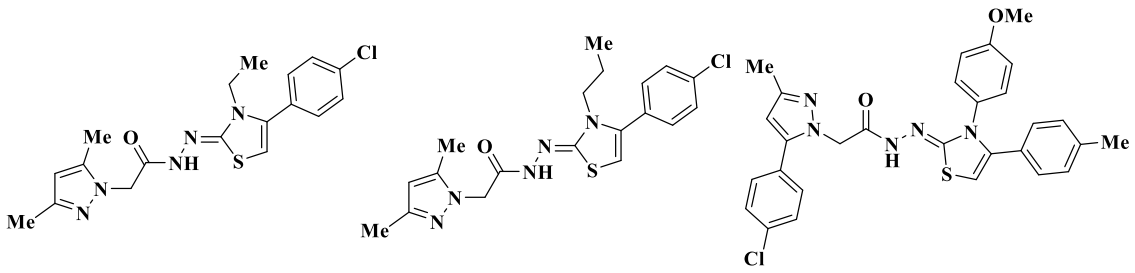

Figure 2B.2

Tang and co-workers designed and synthesized the novel pyrazole-benzimidazole derivatives, evaluated their *in vitro* anti-prolifirative activity against HCT116, MCF-7 and Huh-7 cell lines (Figure 2B.3). Moreover, fluorescent staining and cell cycle arrest studies were performed on the most potent molecules. In addition, ADME calculations were also evaluated to study the drug likeness properties of the synthesized compounds [35].

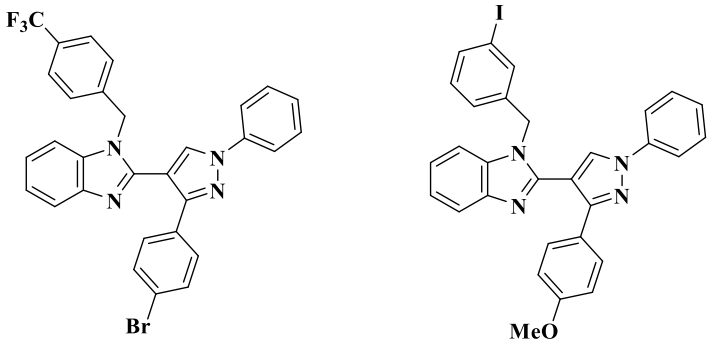

Figure 2B.3

Perez-Aguilar et al. employed a novel and general approach for the regioselective synthesis of substituted pyrazoles from alkynes and *N*-tosylhydrazones through a catalyst free [3+2] cycloaddition and [1,5] sigmatropic rearrangement process (Scheme 2B.1) [36].

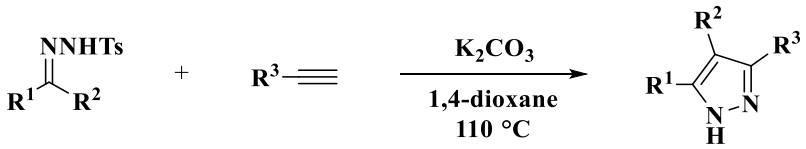

Scheme 2B.1

Kamal and co-workers developed an operationally simple and high yielding protocol for the synthesis of 3,4,5-trisubstituted pyrazoles by using aldehydes, 1,3-dicarbonyls and tosylhydrazones in a one pot three component system (Scheme 2B.2). The reaction proceeds through a tandem Knoevenagel condensation, 1,3-dipolar cycloaddition, and external oxidant-free oxidative aromatization by utilizing atmospheric oxygen as a green oxidant [37].

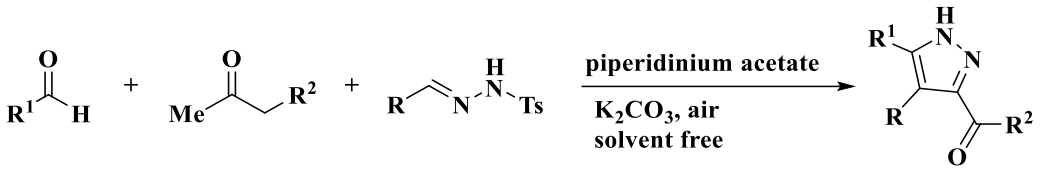

Scheme 2B.2

Ma et al. described the divergent synthesis of 1,3,5-tri and 1,3-disubstituted pyrazoles under transition metal-free three component reaction using aldehydes, ethyl acrylate and *N*-tosylhydrazones as the initial substrates (Scheme 2B.3) [38].

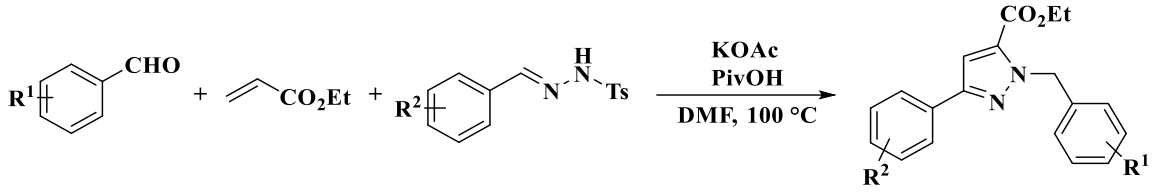

Scheme 2B.3

Guo et al. demonstrated a domino C−H sulfonylation and pyrazole annulation for the synthesis of fully substituted pyrazoles in water using hydrophilic enamines and sulfonyl hydrazines (Scheme 2B.4). The reaction proceeded smoothly with good substrate tolerance without using any metal catalyst [39].

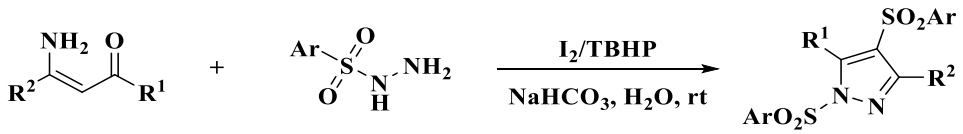

Scheme 2B.4

Pearce et al. introduced a multicomponent oxidative coupling reaction of alkynes, nitriles, and titanium complexes for the synthesis of polysubstituted pyrazoles (Scheme 2B.5). This synthetic protocol avoids the use of potentially hazardous reactants like hydrazine, instead forming the N−N bond in the final step *via* titanium mediated electrocyclic pathway [40].

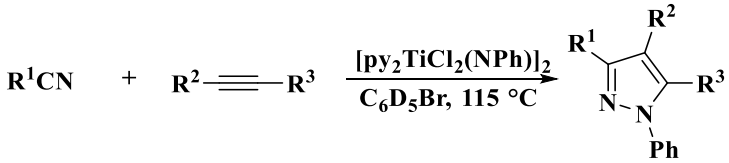

Scheme 2B.5

Shi et al. reported a sequential [3+2] annulation reaction of the propynylsulfonium salts and hydrazonyl chlorides for the generation of pyrazoles (Scheme 2B.6). This reaction provides easy access to synthesize various functionalized pyrazoles in good yields with a wide range of substrates [41].

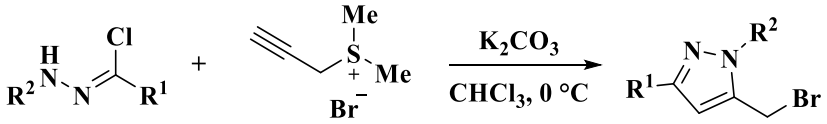

Scheme 2B.6

Shao and co-workers developed a novel divergent domino annulation reaction for the generation of polysubstituted pyrazoles using sulfur ylides and aryldiazonium tetrafluoroborates (Scheme 2B.7). In this one pot reaction, three molecules of sulfur ylides were utilized as C_1 synthon to construct the highly substituted pyrazoles with five new chemical bonds [42].

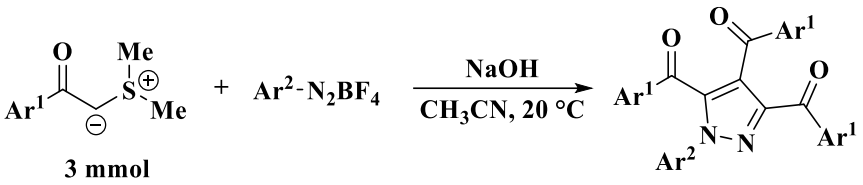

Scheme 2B.7

Gulia and co-workers produced a new method for the preparation of *N*-substituted pyrazoles directly from primary amines and diketones (Scheme 2B.8). The features like without involvement of inorganic reagents, short reaction time, mild conditions, and the use of commercially available starting materials make this protocol more efficient [43].

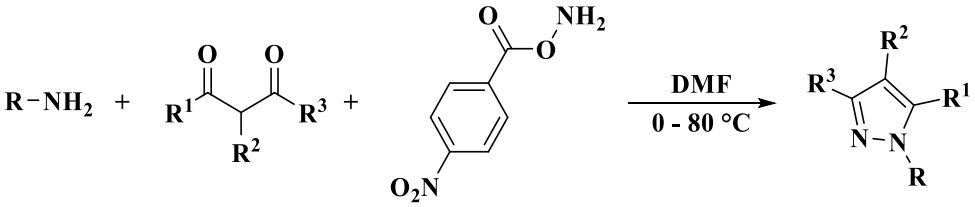

Scheme 2B.8

2B.2. Present work

In view of the foregoing literature reports and considering the significance of pyrazole moiety, we have developed a new approach for the regioselective synthesis of 3,4,5-trisubstituted pyrazoles *via* [3+2] cycloaddition of thiazolidinedione chalcones with *N*-tosylhydrazones under transition metal-, and oxidant-free conditions.

2B.2.1. Synthesis of thiazolidinedione chalcone 1

To a stirred solution of thiazolidinedione **A** (1.0 mmol) and K_2CO_3 (1.5 equiv) in acetonitrile (3 mL) was added methyl iodide **B** (1.2 mmol) slowly at room temperature. The resultant mixture was kept at 50 °C for 4 h. After cooling, the solvent was evaporated

and added water, the resulting solid product **1'** was collected and used for next step without further purification. Later, the obtained intermediate **1'** (1.0 mmol) was treated with *p*-anisaldehyde **C** (1.0 mmol) and piperidine (20 mol%) in methanol (3 mL) under reflux for 6 h. After cooling, the resultant solid was collected and recrystallized from methanol to produce thiazolidinedione chalcone **1** with 78**%** yield (Scheme 2B.9) [44].

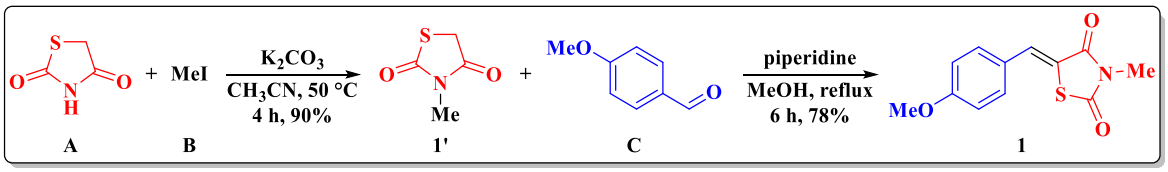

Scheme 2B.9

The title compounds **4a-y** were synthesized by using thiazolidinedione chalcones **1a-e**, benzaldehydes **2a-k** and tosylhydrazine **3** in DMF (Scheme 2B.10). Further, all the synthesized compounds were screened for the *in vitro* anti-tubercular activity and *in silico* molecular docking and ADME prediction.

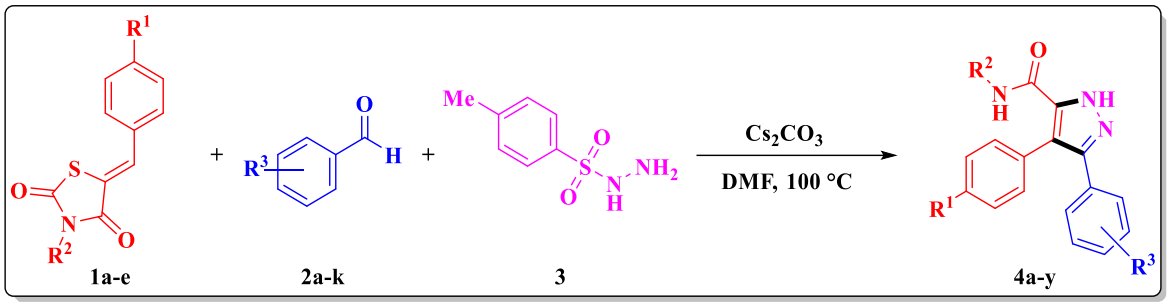

Scheme 2B.10. Synthesis of 3,4,5-trisubstituted pyrazoles **4a-y**.

2B.2.2. Results and discussion

The reaction of benzaldehyde **2a** (1.0 mmol) and tosylhydrazine **3** (1.0 mmol) with 5-(4-methoxybenzylidene)-3-methyl-thiazolidine-2,4-dione **1a** (1.0 mmol) was investigated using different solvents and bases (Table 2B.1). In the initial attempt with Cs_2CO_3 (1.0 equiv) in DMF at room temperature led to desired product **4a** in 30% (entry 1). However, increasing the reaction temperature to 100 °C in presence of Cs_2CO_3 (1.0 equiv) resulted 60% of yield (entry 2). Excellent yields were occurred with increase in the amount of Cs_2CO_3 from 1.0 to 2.0 equiv and then to 3.0 equiv (entries 3 and 4). Other bases such as K_2CO_3, Et_3N, DBU, NaOAc and DABCO could not give better yields (entries 5-9). No product was detected without base (entry 10). Replacing DMF with other solvents such as DMSO, CH_3CN, EtOH and toluene had an negative effect on the reaction rate and product yield (entries 11-14). There was no reaction in H_2O, leading to recovery of starting materials (entry 15). The reaction gave a lower yield of **4a** either decreasing or increasing

the temperature (entries 16 and 17). On the basis of above results, the optimal reaction condition for the generation of **4a** was Cs_2CO_3 (3.0 equiv) as the base in DMF at 100 °C (entry 4).

Table 2B.1. Optimization of the reaction conditions[a]

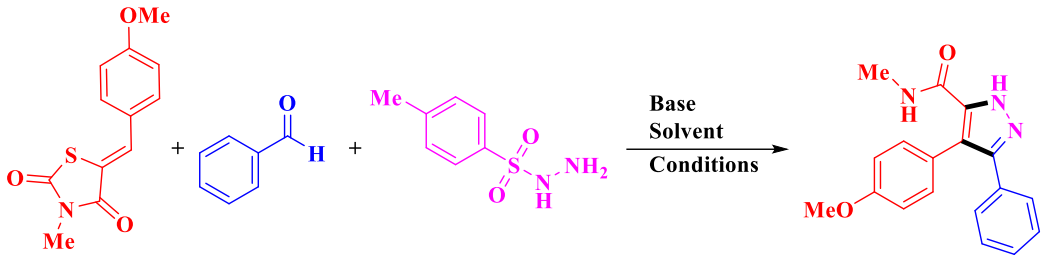

Entry	Base	Equiv	Solvent	Temp (°C)	Time (h)	Yield (%)[b]
1	Cs_2CO_3	1	DMF	RT	12	30
2	Cs_2CO_3	2	DMF	100	10	60
3	Cs_2CO_3	3	DMF	100	8	78
4	**Cs_2CO_3**	**3**	**DMF**	**100**	**6**	**85**
5	K_2CO_3	3	DMF	100	6	75
6	Et_3N	3	DMF	100	10	40
7	DBU	3	DMF	100	8	60
8	NaOAc	3	DMF	100	8	65
9	DABCO	3	DMF	100	8	65
10	--	--	DMF	100	10	ND
11	Cs_2CO_3	3	DMSO	100	6	80
12	Cs_2CO_3	3	CH_3CN	reflux	8	60
13	Cs_2CO_3	3	EtOH	reflux	8	55
14	Cs_2CO_3	3	Toluene	100	8	70
15	Cs_2CO_3	3	H_2O	100	10	ND
16	Cs_2CO_3	3	DMF	80	8	80
17	Cs_2CO_3	3	DMF	120	6	82

[a]Reaction condition: compound **1a** (1.0 mmol), benzaldehyde **2a** (1.0 mmol), tosylhydrazine **3** (1.0 mmol), base and solvent (3 mL). [b]Isolated yields. RT: room temperature. ND: not determined.

The reaction generality and substrate scope of this transformation were further explored (Table 2B.2). Various benzaldehydes having both electron donating group (EDG) and electron withdrawing group (EWG) were investigated. EDG (–Me, –OMe), EWG (–CN, $–NO_2$) and halogen (–F, –Cl, –Br) on the aromatic ring underwent the conversion smoothly to afford the corresponding products in good yields. It was also found that the positions of the substituents on benzaldehydes had no significant effect on the product

yield. In addition, EWG (–CN, –NO_2) on thiazolidinedione chalcones also obtain the target compounds in good yields. However, the reaction was not successful with aliphatic aldehydes, resulting in the recovery of starting materials.

Table 2B.2. Substrate scope of regioselective 3,4,5-trisubstituted pyrazoles **4a-y**[a,b]

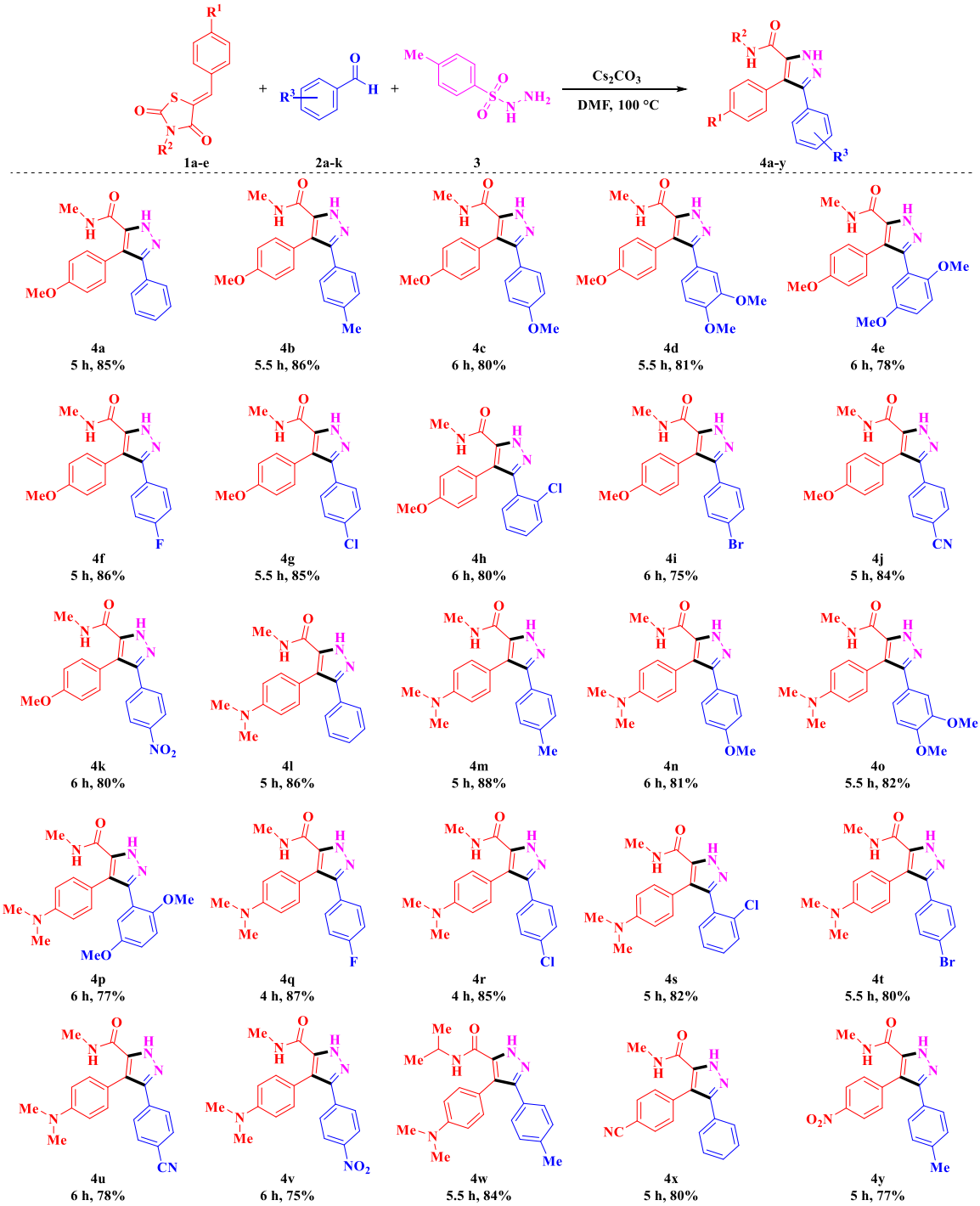

[a]Reaction condition: thiazolidinedione chalcones **1a-e** (1.0 mmol), benzaldehydes **2a-k** (1.0 mmol), tosylhydrazine **3** (1.0 mmol) and Cs_2CO_3 (3.0 equiv) in 3 mL of DMF at 100 °C. [b]Isolated yields.

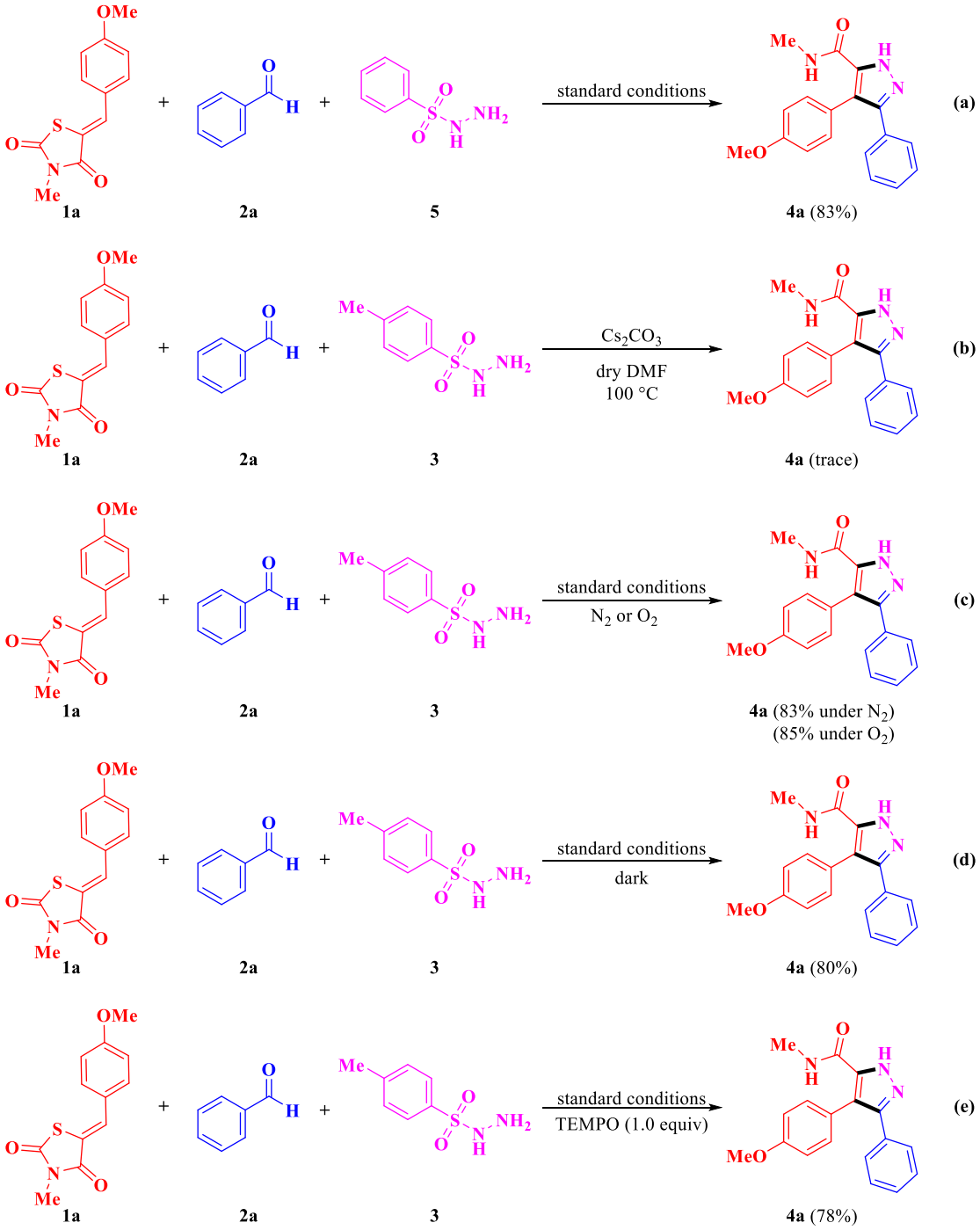

Scheme 2B.11. Control experiments.

To illustrate the reaction mechanism, some control experiments were carried out. Initially, reaction of thiazolidinedione chalcone **1a**, benzaldehyde **2a** worked well with benzenesulfonyl hydrazide **5** under standard conditions, resulting the product **4a** in 83% yield (Scheme 2B.11a). A trace amount of product formation under dry condition demonstrates the essential role of water (Scheme 2B.11b). Reaction proceeded smoothly in the presence of N_2 or O_2 atmosphere (Scheme 2B.11c). To check the feasibility of reaction

under sunlight, we conducted the reaction under dark condition, 80% of yield was obtained (Scheme 2B.11d). This indicates that the reaction is light independent. The reaction efficiency was not influenced in the presence of radical inhibitor TEMPO (Scheme 2B.11e). Which rule out the possibility of radical pathway.

Based on control experiments a plausible reaction mechanism was illustrated in Scheme 2B.12. Initially, reaction of benzaldehyde **2a** with tosylhydrazine **3** generates intermediate **A**, which converts into diazo intermediate **B** in the presence of Cs_2CO_3. The subsequent loss of TsH from **B** provides dipole intermediate **C** [45]. Further, the *in situ* generated intermediate **C** undergoes [3+2] cycloaddition reaction with **1a** produces the intermediate **D,** which converts into intermediate **E** in the presence of water and base [46]. From this, intermediate **F** is formed with the loss of carbonyl sulfide and H_2O [47]. This undergoes tautomerism to produce the desired product **4a**.

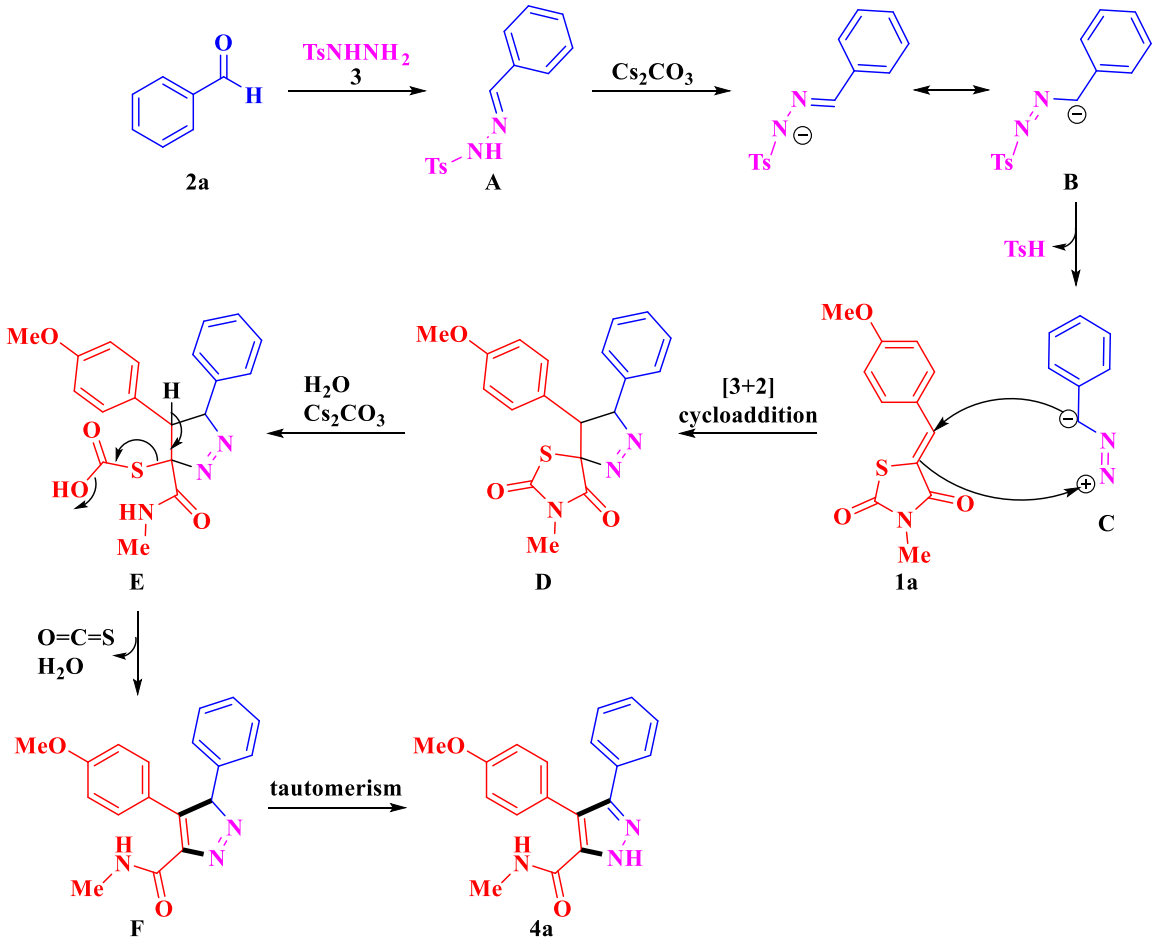

Scheme 2B.12. Plausible reaction mechanism.

The chemical structures of **4a-y** were identified from their FT-IR, ^{1}H NMR, ^{13}C NMR and mass spectral data, and were supported by single crystal X-ray diffraction analysis of compound **4a** (Figure 2B.4). For instance, the IR spectrum of **4a** shows the

bands at 3273 cm^{-1} and 3175 cm^{-1} represents –NH stretching frequencies. The band at 1635 cm^{-1} represents the –C=O stretching frequency of the amide functional group. In the ^{1}H NMR spectrum, a peak showed as singlet at δ 13.49 represents the –NH proton of the pyrazole ring, and a singlet at δ 8.03 represents the –NH proton of the amide moiety. The ^{13}C NMR showed a peak at δ 163.28 corresponds –C=O carbon of the amide group [48].Whereas, the compounds **4f** and **4q** exhibited heteronuclear coupling (C–F) in ^{13}C NMR spectrum with coupling constant values around *J*(*ipso*) = 245.0 Hz, *J*(*ortho*) = 20.0 Hz, *J*(*meta*) = 8.0 Hz and *J*(*para*) = 2.0 Hz. The molecular weight of the compound **4a** was determined by the peak at *m/z* 308.1397 corresponds $[M+H]^{+}$ in HRMS spectrum. The crystallographic data with CCDC number 2110703 and structure refinement parameters of the compound **4a** were shown in Table 2B.3.

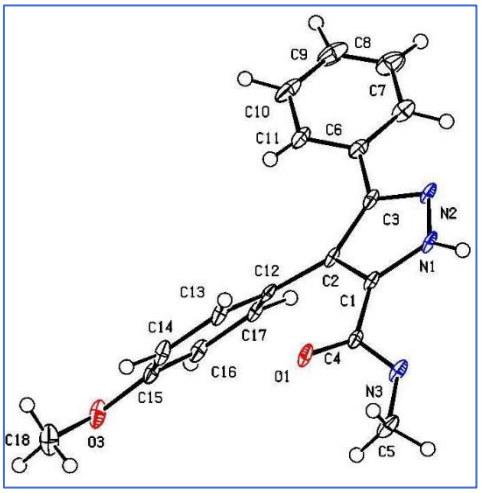

Figure 2B.4. ORTEP representation of the compound **4a** and the thermal ellipsoids are drawn at 50% probability level.

Table 2B.3. Salient crystallographic data and refinement parameters of the compound **4a**

Identification code	**4a**
Empirical formula	$C_{18}H_{17}N_3O_2$
Formula weight	307.1321
Crystal system	Monoclinic
Space group	$P2_1/c$
T (K)	100
a (Å)	13.046 (3)
b (Å)	16.071 (3)
c (Å)	15.202 (3)
α (°)	90
β (°)	103.55
γ (°)	90
Z	8
V ($Å^3$)	3098.6 (12)
D_{calc} (g/cm^3)	1.313

F (000)	1288.0
μ (mm^{-1})	0.088
Θ (°)	26.997
Index ranges	-16 ≤ h ≤ 16 -20 ≤ k ≤ 20 -19 ≤ l ≤ 19
N-total	6771
Parameters	436
R_1 *[I > 2 σ (I)]*	0.0843
wR_2 (all data)	0.2421 (6218)
GOF	1.033
CCDC	2110703

2B.2.3. Biological activity

2B.2.3.1. Anti-tubercular activity (anti-TB)

The anti-tubercular activity of the synthesized 3,4,5-trisubstituted pyrazoles **4a-y** were examined using the Microplate Alamar Blue Assay (MABA) method against *Mycobacterium tuberculosis* H37Rv (ATCC27294) strain and ethambutol as a standard drug [49]. The experiments were conducted in duplicates and the MIC values (μg/mL) are listed in Table 2B.4.

The results of anti-TB activity indicate that all the screened compounds exhibited potent to poor activity with the MIC values ranging from 3.125 μg/mL to >25.00 μg/mL. Among these, two compounds **4e** and **4o** exhibited potent activity with MIC value 3.125 μg/mL when compared to the standard drug ethambutol (MIC: 1.56 μg/mL). Whereas, two compounds **4i** and **4v** showed significant activity with MIC value 6.25 μg/mL. On the other hand, two compounds **4c** and **4w** displayed moderate anti-TB activity (12.5 μg/mL). The remaining derivatives showed poor anti-TB potency.

Table 2B.4. *In vitro* anti-tubercular activity of the synthesized compounds **4a-y**

Entry	Compound	MIC (μg/mL)	% of Inhibition @25μM[a]
1	**4a**	25	ND[b]
2	**4b**	25	ND
3	**4c**	12.5	ND
4	**4d**	25	ND
5	**4e**	**3.125**	**19.04**
6	**4f**	>25	ND
7	**4g**	>25	ND
8	**4h**	>25	ND
9	**4i**	6.25	23.68

10	**4j**	>25	ND
11	**4k**	25	ND
12	**4l**	>25	ND
13	**4m**	25	ND
14	**4n**	>25	ND
15	**4o**	**3.125**	**21.04**
16	**4p**	>25	ND
17	**4q**	25	ND
18	**4r**	25	ND
19	**4s**	>25	ND
20	**4t**	>25	ND
21	**4u**	25	ND
22	**4v**	6.25	24.76
23	**4w**	12.5	ND
24	**4x**	25	ND
25	**4y**	25	ND
26	**Ethambutol**	**1.56**	ND

[a] % inhibition was examined using RAW 264.7 cell line, [b] ND = not determined.

2B.2.3.2. Cytotoxicity studies

The promising anti-TB active compounds have been tested for their safety profile by the evaluation of cytotoxicity on normal RAW 264.7 cells at 25 µg/mL [50] and the results were depicted in Table 2B.4. In this study, the promising anti-TB compounds **4e**, **4i**, **4o** and **4v** exhibited less percentage of inhibition such as 19.04, 23.68, 21.04 and 24.76% respectively to the normal RAW 264.7 cell line.

2B.2.3.3. Structure activity relationship studies

In the structure activity relationship (SAR) studies, diverse donor and acceptor abilities of substituted groups on the phenyl ring and structural changes are crucial in their anti-tubercular activity of the title compounds. SAR studies reveal that the presence of methoxy (–OMe) substitution on the phenyl ring is significantly enhances the anti-tubercular activity when compared to other substitutions.

2B.3. Molecular docking studies

The outcome of the molecular docking study revealed that all the synthesized compounds **4a-y** were successfully docked, and efficiently fit into the active sites of the *Mycobacterium tuberculosis* protein (PDB ID: 1DF7) [51]. The results of the molecular docking study were depicted in Table 2B.5. Among all the screened compounds, the compounds **4h**, **4k**, **4o** and **4s** showed good binding energies -9.37, -9.31, -9.46 nd -9.41

kcal/mol respectively. Among these, the compound **4o** exhibited more negative binding energy -9.46 kcal/mol, forms five hydrogen bonds with the amino acid residues TRP6 (2.85 Å), ALA7 (2.25 Å), ASP27 (3.20 Å), TYR100 (1.84 Å), GLU111 (3.55 Å) respectively and forms seven hydrophobic (π···π and mixed π···alkyl) interactions with the amino acids. Whereas, the compound **4s** showed binding energy -9.41 kcal/mol, forms six hydrogen bonds with the amino acid residues TRP6 (2.85 Å), ALA7 (2.11 Å), ASP27 (3.41 Å), TYR100 (2.23 Å, 3.41 Å), GLU111 (3.57 Å) and shows three hydrophobic (π···π and π···alkyl) interactions with the amino acids. The ligand interactions of the compounds **4o** and **4s** are presented in Figure 2B.5 and Figure 2B.6.

Table 2B.5. Docking results of the compounds **4a-y** against 1DF7 protein

En-try	Compound	Binding energy (kcal/mol)	No. of hydrogen bonds	Residues involved in the hydrogen bonding	Hydrogen bond length (Å)
1	**4a**	-9.13	5	TRP6, ALA7, ASP27, TYR100	1.89, 2.28, 2.99, 3.21, 3.46
2	**4b**	-9.23	4	TRP6, ALA7, ASP27, TYR100	2.08, 2.16, 3.03, 3.16
3	**4c**	-9.21	4	TRP6, ALA7, ASP27, TYR100	1.89, 2.10, 3.01, 3.40
4	**4d**	-9.15	4	TRP6, ALA7, ASP27, TYR100	1.85, 2.15, 2.98, 3.51
5	**4e**	-9.24	4	TRP6, ALA7, LEU24, GLN28	2.24, 2.84, 2.88, 3.63
6	**4f**	-9.12	5	TRP6, ALA7, TYR100	1.95, 2.21, 2.30, 3.21, 3.36
7	**4g**	-9.12	4	TRP6, ALA7, ASP27, TYR100	1.98, 2.19, 3.06, 3.33
8	**4h**	-9.37	5	TRP6, ALA7, ASP27, TYR100	2.05, 2.15, 2.21, 3.11, 3.22
9	**4i**	-9.01	3	TRP6, GLN28, TYR100	2.20, 2.65, 3.03
10	**4j**	-8.97	4	TRP6, ALA7, ASP27, TYR100	2.01, 2.21, 2.99, 3.21
11	**4k**	-9.31	7	ALA7, GLY18, ILE20, ARG45, SER49, GLN98, TYR100	1.65, 1.92, 1.92, 2.05, 2.32, 2.70, 3.32
12	**4l**	-9.12	6	TRP6, ALA7, ASP27, TYR100, GLU111	2.08, 2.18, 2.89, 3.33, 3.36, 3.56
13	**4m**	-9.07	5	TRP6, ALA7, ASP27, TYR100, GLU111	1.88, 2.23, 2.83, 3.13, 3.56
14	**4n**	-9.13	5	TRP6, ALA7, ASP27, TYR100, GLU111	1.98, 2.14, 2.84, 3.17, 3.56
15	**4o**	**-9.46**	5	TRP6, ALA7, ASP27, TYR100, GLU111	2.85, 2.27, 3.20, 1.84, 3.55

16	**4p**	-8.38	4	LEU24, ASP27, GLN28	2.04, 2.79, 2.98, 3.15
17	**4q**	-9.04	5	TRP6, ALA7, ASP27, TYR100, GLU111	1.97, 2.14, 2.84, 3.42, 3.57
18	**4r**	-8.99	6	TRP6, TRP22, LEU24, ASP27, TYR100	2.89, 3.00, 3.03, 3.15, 3.51, 3.66
19	**4s**	**-9.41**	6	TRP6, ALA7, ASP27, TYR100, GLU111	2.85, 2.11,3.41, 2.23, 3.41, 3.57
20	**4t**	-9.23	4	TRP6, LEU24, TYR100	2.85, 3.03, 3.05, 3.54
21	**4u**	-9.18	6	ILE5, TRP6, TRP22, LEU24, ASP27, TYR100	2.72, 2.87, 3.06, 3.36, 3.49, 3.75
22	**4v**	-8.90	4	ARG32, SER49, ARG60, ILE94	1.67, 2.06, 3.12, 3.67
23	**4w**	-8.95	6	SER49, GLY95, GLY96, TYR100	1.72, 2.23, 3.19, 3.29, 3.66, 3.79
24	**4x**	-8.48	4	TRP6, ASP27, GLU111	1.73, 2.14, 3.22, 3.74
25	**4y**	-8.95	5	GLN28, LYS53, ARG60	1.67, 1.85, 2.32, 2.35, 2.59

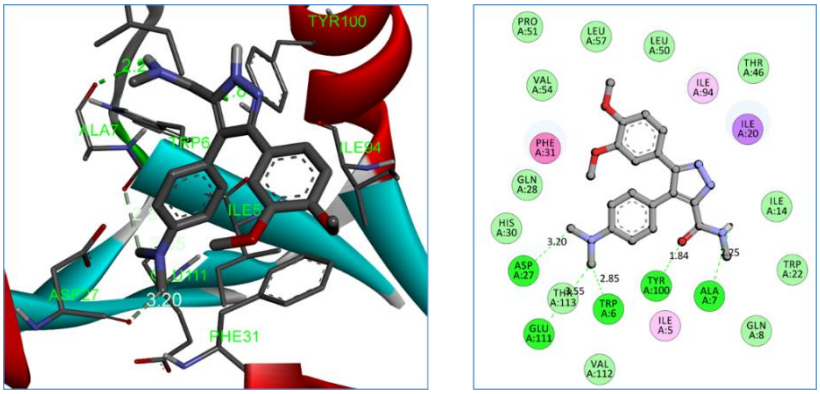

Figure 2B.5. Binding interactions of the compound **4o** with active site of 1DF7.

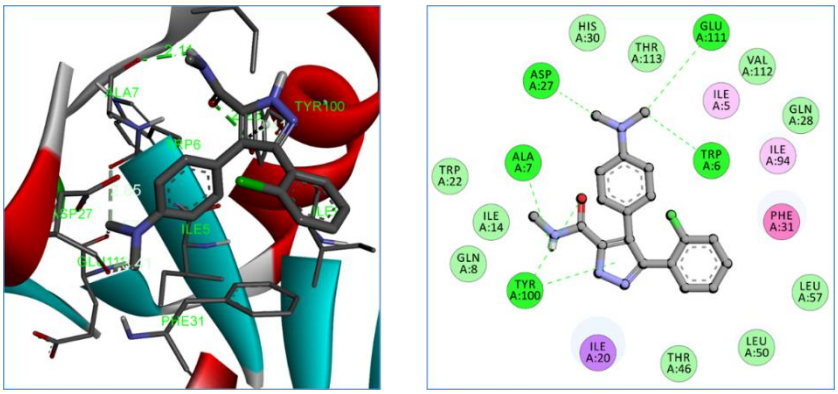

Figure 2B.6. Binding interactions of the compound **4s** with active site of 1DF7.

2B.4. ADME prediction

The measurement of absorption, distribution, metabolism and excretion (ADME) makes it easier to identify molecules at the therapeutic dose with a high safety profile.

Moreover, the use of *in silico* pharmacokinetic parameters prediction lowers the risk of drug failure during the final stages of a clinical study. ADME prediction results of the synthesized compounds are presented in Table 2B.6.

LogP is the measure of octanol/water partition co-efficient (lipophilicity). The predicted lipophilicity values are in the ranging from 2.682 to 4.471, and these values revealed that optimal lipophilicity of the compounds. The predicted aqueous solubility (LogS) values for the synthesized compounds varied from -3.122 to -4.739, which indicates their good solubility in aqueous media because of lipophilic groups present in the molecules. However, the topological polar surface area (TPSA) values (≤ 140 Å) reveal that the compounds have excellent oral bioavailability. The results from logarithm of the apparent permeability co-efficient (logPapp) suggests that all the compounds have acceptable Caco-2 permeability in the range of -0.572 x 10^{-6} to 1.280 x 10^{-6}. Remarkably, all the synthesized compounds have moderate human intestinal absorption (HIA: 84.012–97.97%). Blood-brain partition co-efficient (logBB) values of the synthesized compounds are in acceptable range to cross the blood-brain barrier (BBB). The reported drug like properties and *in silico* ADME prediction revealed that the title compounds **4a-y** exhibit adequate pharmacokinetic parameters and can be considered as lead molecules for the development of future pharmacophores.

Table 2B.6. Drug likeliness and *in silico* ADME properties of the compounds **4a-y**

Entry	Mol. Wt	H-donor	H-acceptor	No. of rotatable bonds	LogP	LogS	TPSA (Å)	Caco-2 Permeability (logPapp in 10^{-6} cm/s)	HIA (% absorbed)	BBB permeability (log BB)
	≤500	**≤5**	**≤10**	**≤10**	**≤5**	**<0.5**	**≤140**	**>8x10^{-6}**	**70 - 100%**	**-3.0 - 1.2**
4a	307.35	2	5	5	2.989	-3.788	67.01	0.961	96.718	-0.003
4b	321.38	2	5	5	3.462	-4.233	67.01	1.074	96.691	-0.042
4c	337.379	2	6	6	3.056	-4.084	76.24	1.051	97.607	-1.012
4d	367.405	2	7	7	2.793	-3.982	85.47	0.771	97.849	-1.108
4e	367.405	2	7	7	2.947	-4.635	85.47	1.049	96.942	-0.986
4f	325.343	2	5	5	3.103	-4.095	67.01	1.032	96.236	0.114
4g	341.798	2	5	5	3.677	-4.516	67.01	1.052	95.233	-0.055
4h	341.798	2	5	5	3.453	-4.739	67.01	0.956	95.140	0.072
4i	386.249	2	5	5	3.830	-4.581	67.01	1.048	95.166	-0.056
4j	332.363	2	6	5	2.769	-4.409	90.80	1.098	97.673	-0.957
4k	352.35	2	8	6	3.010	-4.490	110.15	-0.605	84.937	-1.107
4l	320.396	2	5	5	3.217	-3.128	61.02	1.109	97.017	0.19
4m	334.423	2	5	5	3.745	-3.514	61.02	1.280	96.990	0.151
4n	350.422	2	6	6	3.238	-3.330	70.25	1.083	97.907	-0.92

4o	380.448	2	7	7	2.950	-3.122	79.48	1.049	98.148	-1.015
4p	380.448	2	7	7	3.182	-3.841	79.48	1.082	97.241	-0.893
4q	338.386	2	5	5	3.304	-3.469	61.02	1.099	96.535	0.307
4r	354.841	2	5	5	3.998	-4.261	61.02	1.278	95.532	0.138
4s	354.841	2	5	5	3.789	-4.524	61.02	1.059	95.439	0.145
4t	399.292	2	5	5	4.124	-4.346	61.02	1.276	95.465	0.137
4u	345.406	2	6	5	2.938	-4.151	84.81	1.13	97.972	-0.865
4v	365.393	2	8	6	3.208	-4.546	104.16	-0.603	84.012	-1.015
4w	362.477	2	5	6	4.471	-4.448	61.02	1.269	95.874	-0.01
4x	302.337	2	5	4	2.682	-4.034	81.57	1.001	96.782	-0.811
4y	336.351	2	7	5	3.380	-4.373	100.92	-0.572	86.955	-0.981

Mol. Wt: molecular weight; **H-donor**: number of hydrogen bond donors; **H-acceptor**: number of hydrogen bond acceptors; **LogP**: octanol/water partition coefficient; **LogS**: aqua solubility parameter; **TPSA**: topological polar surface area; **Caco-2**: cell permeability; **HIA**: human intestinal absorption; **LogBB**: blood/brain partition co-efficient.

2B.5. Conclusion

In this chapter we have demonstrated a highly efficient and convenient route for the construction of 3,4,5-trisubstituted pyrazoles from thiazolidinedione chalcones, benzaldehydes and *N*-tosylhydrazine with Cs_2CO_3 as a base. The reaction proceeds smoothly under mild reaction conditions and was free of transition metal and external oxidant. A range of poly functionalized pyrazoles were obtained in moderate to good yields from easily available starting materials. All the synthesized compounds were well characterized by spectral data and screened their *in vitro* anti-TB activity against *Mycobacterium tuberculosis* H37Rv. Among all, two compounds **4e** and **4o** exhibited potent activity with MIC value 3.125 µg/mL and the compounds **4i** and **4v** showed good activity with MIC value 6.25 µg/mL when compared to the standard drug ethambutol (MIC: 1.56 µg/mL). The active compounds were showed relatively low levels of cytotoxicity against the normal cell line RAW 264.7. In addition, *in silico* molecular docking studies and ADME prediction revealed that the title compounds could be regarded as potential scaffolds which are useful in the development of lead molecules for the treatment of tuberculosis.

2B.6. Experimental Section

2B.6.1. General procedure for 3,4,5-trisubstituted 1*H*-pyrazoles (4a-y)

To a solution of benzaldehyde **2** (1.0 mmol) in 3 mL DMF, tosylhydrazine **3** (1.0 mmol) was added and continued the reaction for 10 min at room temperature, to this thiazolidinedione chalcones **1** (1.0 mmol) and Cs_2CO_3 (3.0 equiv) were added. The reaction mixture was stirred at 100 °C for 4-6 h. The progress of the reaction was monitored by

TLC. After completion, the reaction mixture was cooled to room temperature and added water. The resulting solid product was filtered and dried under vacuum. The purification of crude material by silica gel column chromatography (ethyl acetate / petroleum ether, 30:70 to 40:60 V/V) furnished the targeted compounds **4a–y**.

2B.6.2. Protocol for the anti-TB screening

The MIC of the generated compounds was tested using *in vitro* Microplate Alamar Blue Assay protocol [52]. The *Mycobacterium tuberculosis* H37Rv strain (ATCC27294) was used for the screening. The inoculum was prepared from fresh LJ medium re-suspended in 7H9-S medium (7H9 broth, 0.1% casitone, 0.5% glycerol, supplemented oleic acid, albumin, dextrose, and catalase [OADC]), adjusted to a OD_{590} 1.0, and diluted 1:20; 100 µL was used as inoculum. Each drug stock solution was thawed and diluted in 7H9-S at four-fold the final highest concentration tested. Serial two-fold dilutions of each drug were prepared directly in a sterile 96-well microtiter plate using 100 µL 7H9-S. A growth control containing no antibiotic and a sterile control were also prepared on each plate. Sterile water was added to all perimeter wells to avoid evaporation during the incubation. The plate was covered, sealed in plastic bags and incubated at 37 ^{o}C in normal atmosphere. After 7 days incubation, 30 µL of alamar blue solution was added to each well, and the plate was re-incubated overnight. A change in colour from blue (oxidized state) to pink (reduced) indicated the growth of bacteria, and the MIC was defined as the lowest concentration of drug that prevented this change in colour.

2B.6.3. *In vitro* cytotoxicity screening

The *in vitro* cytotoxicity of the privileged anti-TB active analogues with lower MIC value were assessed by 3-(4,5-dimethylthiazol-2-yl)-2,5-diphenyltetrazolium bromide (MTT) assay against growth inhibition of RAW 264.7 cells at 25 µg/mL concentration [53]. Cell lines were maintained at 37 °C in a humidified 5% CO_2 incubator (Thermo scientific). Detached the adhered cells and followed by centrifugation to get cell pellet. Fresh media was added to the pellet to make a cell count using haemocytometer and plate 100 µL of media with cells ranging from 5,000 - 6,000 per well in a 96-well plate. The plate was incubated overnight in CO_2 incubator for the cells to adhere and regain its shape. After 24 h cells were treated with the test compounds at 25 µg/mL diluted using the media to deduce the percentage inhibition on normal cells. The cells were incubated for 48 h to assay the effect of the test compounds on different cell lines. Zero hour reading was noted down with untreated cells and also control with 1% DMSO to subtract further from the 48 h reading.

After 48 h incubation, cells were treated by MTT (4,5-dimethylthiazol-2-yl)-2,5-diphenyltetrazolium bromide) dissolved in PBS (5 mg/mL) and incubated for 3-4 h at 37 °C. The formazan crystals thus formed were dissolved in 100 µL of DMSO and the viability was measured at 540 nm on a multimode reader (Spectra max). The values were further calculated for percentage inhibition which in turn helps us to know the cytotoxicity of the test compounds.

2B.6.4. Molecular docking protocol

The docking studies are prominent tools for the assessment of the binding affinity to the ligand-protein receptor. All the synthesized compounds were subjected to *in silico* molecular docking studies by using the AutoDockTools (ADT) version 1.5.6 and AutoDock version 4.2.5.1 docking program [54]. The 3D-structures of all the synthesized compounds were prepared by using chem3D pro 12.0 software. The optimized 3D structures were saved in pdb format. The structure of the dihydrofolate reductase of *Mycobacterium tuberculosis* (PDB code: 1DF7) protein was extracted from the protein data bank (http://www.rcsb.org/pdb). The bound ligand and water molecules in protein were removed by using Discovery Studio Visualizer version 4.0 to prepare the protein. Non polar hydrogens were merged and gasteiger charges were added to the protein. The grid file was saved in gpf format. The three dimensional grid box having dimensions 60 x 60 x 60 $Å^3$ was created around the protein with spacing 0.3750 Å. The genetic algorithm was carried out with the population size and the maximum number of evaluations were 150 and 25,00,000 respectively. The docking output file was saved as Lamarckian Ga (4.2) in dpf format. The ligand-protein complex binding sites were visualized by Discovery Studio Visualizer version 4.0.

2B.6.5. ADME prediction

In silico ADME properties and pharmacokinetic parameters of the synthesized compounds were calculated by using the online servers ADMETlab 2.0 and pkCSM [55]. The ADMET properties, human intestinal absorption (HIA), Caco-2 cell permeability, plasma protein binding and blood brain barrier penetration (BBB) were predicted using this program.

2B.7. Spectral data of synthesized compounds 4a-y

4-(4-methoxyphenyl)-*N*-methyl-3-phenyl-1*H*-pyrazole-5-carboxamide (4a)

White solid. mp: 247-249 °C. IR (KBr, cm^{-1}): 3273, 3175, 2956, 1635, 1527, 1414. ^{1}H NMR (400 MHz, DMSO-d_6) δ: 13.49 (s, 1H), 8.03 (s, 1H), 7.31 (d, J = 15.2 Hz, 5H), 7.12 (d, J = 7.6 Hz, 2H), 6.85 (d, J = 7.6 Hz, 2H), 3.75 (s, 3H), 2.69 (d, J = 3.6 Hz, 3H). ^{13}C NMR (100 MHz, DMSO-d_6) δ: 163.28, 158.50, 145.20, 140.99, 132.05, 129.68, 129.07, 128.67, 128.05, 125.20, 118.88, 113.67, 55.43, 25.99. HRMS (ESI, m/z): $[M+H]^+$ calcd. for $C_{18}H_{18}N_3O_2$: 308.1399; found: 308.1397.

4-(4-methoxyphenyl)-*N*-methyl-3-(*p*-tolyl)-1*H*-pyrazole-5-carboxamide (4b)

Off-white solid. mp: 244-246 °C. IR (KBr, cm^{-1}): 3388, 3150, 2934, 1637, 1527, 1414. ^{1}H NMR (400 MHz, DMSO-d_6) δ: 13.43 (s, 1H), 8.01 (s, 1H), 7.15 (s, 4H), 7.11 (d, J = 8.4 Hz, 2H), 6.84 (d, J = 7.2 Hz, 2H), 3.75 (s, 3H), 2.68 (d, J = 3.6 Hz, 3H), 2.27 (s, 3H). ^{13}C NMR (100 MHz, DMSO-d_6) δ: 163.33, 158.45, 145.14, 141.05, 138.14, 132.04, 129.63, 127.93, 126.82, 125.31, 118.58, 113.64, 55.43, 25.98, 21.21. HRMS (ESI, m/z): $[M+H]^+$ calcd. for $C_{19}H_{20}N_3O_2$: 322.1556; found: 322.1560.

3,4-bis(4-methoxyphenyl)-*N*-methyl-1*H*-pyrazole-5-carboxamide (4c)

Off-white solid. mp: 222-224 °C. IR (KBr, cm^{-1}): 3390, 3152, 2934, 1636, 1526, 1415. ^{1}H NMR (400 MHz, DMSO-d_6) δ: 13.37 (s, 1H), 8.01 (s, 1H), 7.21 (d, J = 7.2 Hz, 2H), 7.12 (d, J = 6.4 Hz, 2H), 6.91 (d, J = 6.8 Hz, 2H), 6.86 (s, 2H), 3.75 (s, 3H), 3.74 (s, 3H), 2.68 (s, 3H). ^{13}C NMR (100 MHz, DMSO-d_6) δ: 163.36, 159.59, 158.41, 145.08, 140.90, 132.06, 129.36, 125.42, 121.99, 118.22, 114.54, 113.65, 55.61, 55.41, 25.98. HRMS (ESI, m/z): $[M+H]^+$ calcd. for $C_{19}H_{20}N_3O_3$: 338.1505; found: 338.1505.

3-(3,4-dimethoxyphenyl)-4-(4-methoxyphenyl)-*N*-methyl-1*H*-pyrazole-5-carboxamide (4d)

White solid. mp: 228-230 °C. IR (KBr, cm^{-1}): 3382, 3134, 2931, 1626, 1528, 1456. ^{1}H NMR (400 MHz, DMSO-d_6) δ: 13.40 (s, 1H), 8.00 (d, J = 4.4 Hz, 1H), 7.14 (d, J = 8.4 Hz, 2H), 6.92 (d, J = 8.8 Hz, 1H), 6.87 (d, J = 8.4 Hz, 2H), 6.85 (d, J = 2.0 Hz, 1H), 6.83 (s, 1H), 3.75 (s, 3H), 3.73 (s, 3H), 3.54 (s, 3H), 2.68 (d, J = 4.8 Hz, 3H). ^{13}C NMR (100 MHz, DMSO-d_6) δ: 163.28, 158.51, 149.15, 148.82, 145.12, 140.95, 132.17, 125.66, 122.01, 120.28, 118.32, 113.69, 112.22, 111.59, 55.93, 55.55, 55.50, 25.96. HRMS (ESI, m/z): $[M+H]^+$ calcd. for $C_{20}H_{22}N_3O_4$: 368.1610; found: 368.1611.

3-(2,5-dimethoxyphenyl)-4-(4-methoxyphenyl)-*N*-methyl-1*H*-pyrazole-5-carboxamide (4e)

Plae brown solid. mp: 195-197 °C. IR (KBr, cm^{-1}): 3409, 3279, 2948, 1649, 1547. ^1H NMR (400 MHz, DMSO-d_6) δ: 13.19 (s, 1H), 8.00 (d, J = 4.0 Hz, 1H), 7.08 (d, J = 8.4 Hz, 2H), 6.98 (d, J = 9.2 Hz, 1H), 6.90 (dd, J = 8.8, 2.8 Hz, 1H), 6.79 (d, J = 8.8 Hz, 2H), 6.61 (d, J = 2.4 Hz, 1H), 3.71 (s, 3H), 3.57 (s, 3H), 3.53 (s, 3H), 2.70 (d, J = 4.8 Hz, 3H). ^{13}C NMR (100 MHz, DMSO-d_6) δ: 163.58, 158.23, 153.07, 151.50, 144.08, 137.98, 131.45, 125.68, 120.00, 119.37, 117.07, 115.36, 113.35, 56.20, 55.74, 55.42, 26.04. HRMS (ESI, m/z): $[M+H]^+$ calcd. for $C_{20}H_{22}N_3O_4$: 368.1610; found: 368.1613.

3-(4-fluorophenyl)-4-(4-methoxyphenyl)-*N*-methyl-1*H*-pyrazole-5-carboxamide (4f)

Off-white solid. mp: 218-220 °C. IR (KBr, cm^{-1}): 3387, 3265, 2936, 1656, 1526, 1414. ^1H NMR (400 MHz, DMSO-d_6) δ: 13.53 (s, 1H), 8.04 (s, 1H), 7.31 (dd, J = 8.4, 5.6 Hz, 2H), 7.22 – 7.18 (m, 2H), 7.12 (d, J = 8.0 Hz, 2H), 6.86 (d, J = 7.2 Hz, 2H), 3.76 (s, 3H), 2.68 (d, J = 4.8 Hz, 3H). ^{13}C NMR (100 MHz, DMSO-d_6) δ: 163.21, 162.30 (d, J = 245.0 Hz), 158.57, 145.16, 140.10, 132.02, 130.26 (d, J = 8.4 Hz), 126.18, 125.00, 118.88, 116.21 (d, J = 21.8 Hz), 113.74, 55.43, 26.00. HRMS (ESI, m/z): $[M+H]^+$ calcd. for $C_{18}H_{17}FN_3O_2$: 326.1305; found: 326.1307.

3-(4-chlorophenyl)-4-(4-methoxyphenyl)-*N*-methyl-1*H*-pyrazole-5-carboxamide (4g)

White solid. mp: 263-265 °C. IR (KBr, cm^{-1}): 3383, 3091, 2940, 1638, 1527, 1415. ^1H NMR (400 MHz, DMSO-d_6) δ: 13.58 (s, 1H), 8.05 (s, 1H), 7.43 (d, J = 7.6 Hz, 2H), 7.28 (d, J = 8.4 Hz, 2H), 7.13 (d, J = 8.0 Hz, 2H), 6.86 (d, J = 7.6 Hz, 2H), 3.76 (s, 3H), 2.68 (d, J = 4.4 Hz, 3H). ^{13}C NMR (100 MHz, DMSO-d_6) δ: 163.14, 158.60, 145.25, 139.85, 133.41, 132.02, 129.76, 129.18, 128.52, 124.85, 119.19, 113.78, 55.44, 26.00. HRMS (ESI, m/z): $[M+H]^+$ calcd. for $C_{18}H_{17}ClN_3O_2$: 342.1009; found: 342.1007.

3-(2-chlorophenyl)-4-(4-methoxyphenyl)-*N*-methyl-1*H*-pyrazole-5-carboxamide (4h)

Off-white solid. mp: 190-192 °C. IR (KBr, cm^{-1}): 3413, 3185, 2937, 1649, 1523. ^1H NMR (400 MHz, DMSO-d_6) δ: 13.44 (s, 1H), 8.10 (d, J = 4.4 Hz, 1H), 7.53 (d, J = 7.6 Hz, 1H), 7.44 (t, J = 8.0 Hz, 1H), 7.37 (d, J = 7.6 Hz, 1H), 7.33 (d, J = 7.6 Hz, 1H), 7.06 (d, J = 8.4 Hz, 2H), 6.75 (d, J = 8.4 Hz, 2H), 3.69 (s, 3H), 2.71 (d, J = 4.8 Hz, 3H). ^{13}C NMR (100 MHz, DMSO-d_6) δ: 163.43, 158.29, 144.08, 138.81, 133.87, 133.21, 131.30, 130.07, 129.36, 127.68, 124.78, 120.62, 113.41, 55.36, 26.06. HRMS (ESI, m/z): $[M+H]^+$ calcd. for $C_{18}H_{17}ClN_3O_2$: 342.1009; found: 342.1006.

3-(4-bromophenyl)-4-(4-methoxyphenyl)-*N*-methyl-1*H*-pyrazole-5-carboxamide (4i)

Off-white solid. mp: 277-279 °C. IR (KBr, cm^{-1}): 3383, 3088, 2937, 1639, 1527, 1416. ^1H NMR (400 MHz, DMSO-d_6) δ: 13.59 (s, 1H), 8.05 (s, 1H), 7.56 (d, J = 7.2 Hz, 2H), 7.22 (d, J = 8.4 Hz, 2H), 7.13 (d, J = 8.0 Hz, 2H), 6.86 (d, J = 7.6 Hz, 2H), 3.76 (s, 3H), 2.68 (d, J = 4.4 Hz, 3H). ^{13}C NMR (100 MHz, DMSO-d_6) δ: 163.14, 158.61, 145.26, 139.90, 132.09, 132.00, 131.37, 130.01, 128.89, 124.84, 122.06, 119.19, 113.79, 55.45, 26.00. HRMS (ESI, m/z): $[M+H]^+$ calcd. for $C_{18}H_{17}BrN_3O_2$: 386.0504; found: 386.0504.

3-(4-cyanophenyl)-4-(4-methoxyphenyl)-*N*-methyl-1*H*-pyrazole-5-carboxamide (4j)

White solid. mp: 265-267 °C. IR (KBr, cm^{-1}): 3375, 3275, 2934, 2226, 1635, 1528, 1411. ^1H NMR (400 MHz, DMSO-d_6) δ: 7.89 (d, J = 4.0 Hz, 1H), 7.76 (d, J = 8.0 Hz, 2H), 7.47 (d, J = 8.4 Hz, 2H), 7.14 (d, J = 8.4 Hz, 2H), 6.89 (d, J = 8.4 Hz, 2H), 3.77 (s, 3H), 2.68 (d, J = 4.8 Hz, 3H). ^{13}C NMR (100 MHz, DMSO-d_6) δ: 162.68, 158.66, 143.32, 142.36, 136.54, 132.81, 131.96, 128.16, 125.31, 119.92, 119.24, 113.99, 110.10, 55.45, 26.03. HRMS (ESI, m/z): $[M+H]^+$ calcd. for $C_{19}H_{17}N_4O_2$: 333.1352; found: 333.1346.

4-(4-methoxyphenyl)-*N*-methyl-3-(4-nitrophenyl)-1*H*-pyrazole-5-carboxamide (4k)

Brown solid. mp: 283-285 °C. IR (KBr, cm^{-1}): 3396, 3212, 2937, 1655, 1525, 1415. ^1H NMR (400 MHz, DMSO-d_6) δ: 13.87 (s, 1H), 8.20 (d, J = 1.2 Hz, 2H), 8.11 (s, 1H), 7.54 (d, J = 4.4 Hz, 2H), 7.16 (d, J = 3.2 Hz, 2H), 6.90 (d, J = 1.6 Hz, 2H), 3.78 (s, 3H), 2.69 (s, 3H). ^{13}C NMR (100 MHz, DMSO-d_6) δ: 158.84, 147.14, 139.71, 139.03, 131.96, 128.84, 128.56, 124.51, 124.30, 114.50, 114.00, 55.49, 26.06. HRMS (ESI, m/z): $[M+H]^+$ calcd. for $C_{18}H_{17}N_4O_4$: 353.1250; found: 353.1255.

4-(4-(dimethylamino)phenyl)-*N*-methyl-3-phenyl-1*H*-pyrazole-5-carboxamide (4l)

Off-white solid. mp: 204-206 °C. IR (KBr, cm^{-1}): 3395, 3175, 2938, 1626, 1529, 1441. ^1H NMR (400 MHz, DMSO-d_6) δ: 13.40 (s, 1H), 7.97 (d, J = 4.4 Hz, 1H), 7.34 – 7.28 (m, 5H), 7.02 (d, J = 8.4 Hz, 2H), 6.63 (d, J = 8.4 Hz, 2H), 2.89 (s, 6H), 2.68 (d, J = 4.4 Hz, 3H). ^{13}C NMR (100 MHz, DMSO-d_6) δ: 163.52, 149.54, 145.36, 140.62, 131.45, 129.40, 129.01, 128.84, 128.52, 127.99, 120.38, 119.32, 112.21, 40.52, 26.02. HRMS (ESI, m/z): $[M+H]^+$ calcd. for $C_{19}H_{21}N_4O$: 321.1715; found: 321.1710.

4-(4-(dimethylamino)phenyl)-*N*-methyl-3-(*p*-tolyl)-1*H*-pyrazole-5-carboxamide (4m)

White solid. mp: 225-227 °C. IR (KBr, cm^{-1}): 3386, 3151, 2921, 1632, 1532, 1443. ^1H NMR (400 MHz, DMSO-d_6) δ: 13.33 (s, 1H), 7.95 (s, 1H), 7.19 (d, J = 7.6 Hz, 2H), 7.14

(d, *J* = 6.8 Hz, 2H), 7.02 (d, *J* = 8.4 Hz, 2H), 6.63 (d, *J* = 7.6 Hz, 2H), 2.89 (s, 6H), 2.67 (d, *J* = 4.0 Hz, 3H), 2.28 (s, 3H). ^{13}C NMR (100 MHz, DMSO-d_6) δ: 163.55, 149.52, 145.30, 140.67, 137.93, 131.45, 129.56, 127.88, 127.12, 120.55, 119.00, 112.20, 40.54, 26.01, 21.21. HRMS (ESI, m/z): $[M+H]^+$ calcd. for $C_{20}H_{23}N_4O$: 335.1872; found: 335.1867.

4-(4-(dimethylamino)phenyl)-3-(4-methoxyphenyl)-*N*-methyl-1*H*-pyrazole-5-carboxamide (4n)

Pale yellow solid. mp: 160-162 °C. IR (KBr, cm^{-1}): 3403, 2924, 1614, 1531, 1443. ^{1}H NMR (400 MHz, DMSO-d_6) δ: 13.27 (s, 1H), 7.93 (d, *J* = 3.6 Hz, 1H), 7.23 (d, *J* = 8.4 Hz, 2H), 7.02 (d, *J* = 8.0 Hz, 2H), 6.90 (d, *J* = 8.0 Hz, 2H), 6.64 (d, *J* = 7.2 Hz, 2H), 3.74 (s, 3H), 2.89 (s, 6H), 2.67 (d, *J* = 4.4 Hz, 3H). ^{13}C NMR (100 MHz, DMSO-d_6) δ: 163.57, 159.49, 149.45, 140.52, 131.47, 129.31, 122.33, 120.68, 118.65, 114.50, 112.20, 55.60, 40.55, 25.99. HRMS (ESI, m/z): $[M+H]^+$ calcd. for $C_{20}H_{23}N_4O_2$: 351.1821; found: 351.1819.

3-(3,4-dimethoxyphenyl)-4-(4-(dimethylamino)phenyl)-*N*-methyl-1*H*-pyrazole-5-carboxamide (4o)

Off-white solid. mp: 203-205 °C. IR (KBr, cm^{-1}): 3399, 3204, 2935, 1650, 1512, 1464. ^{1}H NMR (400 MHz, DMSO-d_6) δ: 13.32 (s, 1H), 7.94 (d, *J* = 4.4 Hz, 1H), 7.05 (d, *J* = 8.8 Hz, 2H), 6.91 (t, *J* = 8.4 Hz, 1H), 6.88 (d, *J* = 9.2 Hz, 2H), 6.68 (d, *J* = 8.8 Hz, 2H), 3.74 (s, 3H), 3.55 (s, 3H), 2.89 (s, 6H), 2.69 (d, *J* = 4.8 Hz, 3H). ^{13}C NMR (100 MHz, DMSO-d_6) δ: 163.47, 149.67, 149.04, 148.78, 145.28, 140.61, 131.58, 122.31, 121.00, 120.18, 118.78, 112.38, 112.19, 111.58, 55.92, 55.54, 40.68, 25.97. HRMS (ESI, m/z): $[M+H]^+$ calcd. for $C_{21}H_{25}N_4O_3$: 381.1927; found: 381.1922.

3-(2,5-dimethoxyphenyl)-4-(4-(dimethylamino)phenyl)-*N*-methyl-1*H*-pyrazole-5-carboxamide (4p)

White solid. mp: 180-182 °C. IR (KBr, cm^{-1}): 3402, 3091, 2936, 1656, 1526, 1465. ^{1}H NMR (400 MHz, DMSO-d_6) δ: 13.09 (s, 1H), 7.94 (d, *J* = 4.4 Hz, 1H), 6.99 (d, *J* = 8.4 Hz, 3H), 6.89 (dd, *J* = 8.8, 2.8 Hz, 1H), 6.59 (d, *J* = 8.4 Hz, 3H), 3.57 (s, 3H), 3.56 (s, 3H), 2.85 (s, 6H), 2.69 (d, *J* = 4.4 Hz, 3H). ^{13}C NMR (100 MHz, DMSO-d_6) δ: 163.80, 153.04, 151.62, 149.41, 144.17, 137.55, 130.95, 130.78, 121.09, 120.39, 119.70, 117.13, 115.19, 113.30, 112.12, 56.29, 55.71, 40.55, 26.04. HRMS (ESI, m/z): $[M+H]^+$ calcd. for $C_{21}H_{25}N_4O_3$: 381.1927; found: 381.1925.

4-(4-(dimethylamino)phenyl)-3-(4-fluorophenyl)-*N*-methyl-1*H*-pyrazole-5-carboxamide (4q)

Off-white solid. mp: 241-243 °C. IR (KBr, cm^{-1}): 3402, 3229, 2934, 1638, 1534, 1444. ^{1}H NMR (400 MHz, DMSO-d_6) δ: 13.42 (s, 1H), 7.97 (s, 1H), 7.330 (t, J = 8.0 Hz, 2H), 7.20 (t, J = 7.2 Hz, 2H), 7.02 (d, J = 7.6 Hz, 2H), 6.64 (d, J = 6.4 Hz, 2H), 2.90 (s, 6H), 2.67 (d, J = 4.4 Hz, 3H). ^{13}C NMR (100 MHz, DMSO-d_6) δ: 163.44 (d, J = 248.0 Hz), 149.59, 145.33, 139.74, 131.42, 130.18 (d, J = 8.0 Hz) 126.45, 120.16, 119.33, 116.12 (d, J = 20.0 Hz), 112.24 (d, J = 1.6 Hz), 40.48, 26.02. HRMS (ESI, m/z): $[M+H]^+$ calcd. for $C_{19}H_{20}FN_4O$: 339.1621; found: 339.1615.

3-(4-chlorophenyl)-4-(4-(dimethylamino)phenyl)-*N*-methyl-1*H*-pyrazole-5-carboxamide (4r)

Off-white solid. mp: 257-259 °C. IR (KBr, cm^{-1}): 3377, 3143, 2907, 1634, 1532, 1349. ^{1}H NMR (400 MHz, DMSO-d_6) δ: 13.48 (s, 1H), 7.99 (s, 1H), 7.42 (d, J = 7.2 Hz, 2H), 7.30 (d, J = 8.0 Hz, 3H), 7.02 (d, J = 7.2 Hz, 2H), 6.64 (d, J = 6.8 Hz, 1H), 2.90 (s, 6H), 2.68 (s, 3H). ^{13}C NMR (100 MHz, DMSO-d_6) δ: 163.41, 149.61, 145.38, 139.49, 133.27, 131.42, 129.73, 129.15, 128.79, 119.93, 119.66, 112.25, 40.52, 26.03. HRMS (ESI, m/z): $[M+H]^+$ calcd. for $C_{19}H_{20}ClN_4O$: 355.1326; found: 355.1333.

3-(2-chlorophenyl)-4-(4-(dimethylamino)phenyl)-*N*-methyl-1*H*-pyrazole-5-carboxamide (4s)

White solid. mp: 227-229 °C. IR (KBr, cm^{-1}): 3383, 3218, 1646, 1563, 1433. ^{1}H NMR (400 MHz, DMSO-d_6) δ: 13.34 (s, 1H), 8.05 (d, J = 4.4 Hz, 1H), 7.54 (d, J = 7.6 Hz, 1H), 7.43 (t, J = 6.8 Hz, 1H), 7.35 (t, J = 7.6 Hz, 1H), 7.33 – 7.28 (m, 1H), 6.97 (d, J = 8.8 Hz, 2H), 6.53 (d, J = 8.8 Hz, 2H), 2.83 (s, 6H), 2.71 (d, J = 4.4 Hz, 3H). ^{13}C NMR (100 MHz, DMSO-d_6) δ: 163.66, 149.33, 144.15, 138.36, 133.95, 133.24, 131.17, 130.74, 130.31, 130.04, 129.73, 127.63, 121.03, 120.11, 111.97, 40.50, 26.07. HRMS (ESI, m/z): $[M+H]^+$ calcd. for $C_{19}H_{20}ClN_4O$: 355.1326; found: 355.1327.

3-(4-bromophenyl)-4-(4-(dimethylamino)phenyl)-*N*-methyl-1*H*-pyrazole-5-carboxamide (4t)

White solid. mp: 239-241 °C. IR (KBr, cm^{-1}): 3395, 3090, 2906, 1633, 1531, 1414. ^{1}H NMR (400 MHz, DMSO-d_6) δ: 13.50 (s, 1H), 7.99 (s, 1H), 7.55 (d, J = 4.4 Hz, 2H), 7.24 (d, J = 6.0 Hz, 2H), 7.03 (d, J = 6.8 Hz, 2H), 6.66 (s, 2H), 2.90 (s, 6H), 2.68 (s, 3H). ^{13}C NMR (100 MHz, DMSO-d_6) δ: 163.35, 149.62, 145.44, 139.50, 132.03, 131.41, 129.97,

129.20, 121.84, 119.96, 119.65, 112.25, 40.91, 26.02. HRMS (ESI, m/z): $[M+H]^+$ calcd. for $C_{19}H_{20}BrN_4O$: 399.0820; found: 399.0819.

3-(4-cyanophenyl)-4-(4-(dimethylamino)phenyl)-*N*-methyl-1*H*-pyrazole-5-carboxamide (4u)

White solid. mp: 260-262 °C. IR (KBr, cm^{-1}): 3370, 3095, 2887, 2226, 1636, 1533, 1356. ^1H NMR (400 MHz, DMSO-d_6) δ: 13.72 (s, 1H), 8.05 (s, 1H), 7.80 (s, 2H), 7.49 (d, J = 8.0 Hz, 2H), 7.05 (d, J = 8.0 Hz, 2H), 6.69 (s, 2H), 2.92 (s, 6H), 2.68 (d, J = 4.4 Hz, 3H). ^{13}C NMR (100 MHz, DMSO-d_6) δ: 149.87, 132.91, 131.33, 128.32, 128.20, 120.60, 119.10, 112.51, 112.45, 112.38, 40.62, 26.15. HRMS (ESI, m/z): $[M+H]^+$ calcd. for $C_{20}H_{20}N_5O$: 346.1668; found: 346.1675.

4-(4-(dimethylamino)phenyl)-*N*-methyl-3-(4-nitrophenyl)-1*H*-pyrazole-5-carboxamide (4v)

Plae brown solid. mp: 250-252 °C. IR (KBr, cm^{-1}): 3403, 3226, 2939, 1646, 1512, 1338. ^1H NMR (400 MHz, DMSO-d_6) δ: 13.79 (s, 1H), 8.37 (s, 1H), 8.19 (d, J = 5.2 Hz, 2H), 7.57 (d, J = 7.2 Hz, 2H), 7.06 (d, J = 7.6 Hz, 2H), 6.70 (d, J = 2.4 Hz, 2H), 2.92 (s, 6H), 2.68 (d, J = 4.4 Hz, 3H). ^{13}C NMR (100 MHz, DMSO-d_6) δ: 149.92, 146.96, 139.69, 138.71, 131.60, 131.33, 129.48, 128.67, 124.75, 124.22, 112.48, 112.29, 40.53, 26.14. HRMS (ESI, m/z): $[M+H]^+$ calcd. for $C_{19}H_{20}N_5O_3$: 366.1566; found: 366.1561.

4-(4-(dimethylamino)phenyl)-*N*-isopropyl-3-(*p*-tolyl)-1*H*-pyrazole-5-carboxamide (4w)

Off-white solid. mp: 210-212 °C. IR (KBr, cm^{-1}): 3429, 3388, 2924, 1645, 1537, 1362. ^1H NMR (400 MHz, DMSO-d_6) δ: 13.35 (s, 1H), 7.58 (s, 1H), 7.18 (bs, 2H), 7.13 (bs, 2H), 7.01 (d, J = 8.0 Hz, 2H), 6.65 (bs, 2H), 2.88 (s, 6H), 2.26 (s, 3H), 1.22 (bs, 1H), 1.07 (bs, 6H). ^{13}C NMR (100 MHz, DMSO-d_6) δ: 163.55, 149.54, 145.33, 140.70, 137.96, 131.47, 131.22, 129.59, 127.90, 127.19, 127.15, 120.58, 119.03, 112.23, 40.57, 26.04, 21.24, 21.02. ESI-MS (m/z): $[M+H]^+$ calcd. for $C_{22}H_{27}N_4O$: 363; found: 363.

4-(4-cyanophenyl)-*N*-methyl-3-phenyl-1*H*-pyrazole-5-carboxamide (4x)

White solid. mp: 255-257 °C. IR (KBr, cm^{-1}): 3375, 3092, 2933, 2227, 1634, 1528, 1411. ^1H NMR (400 MHz, DMSO-d_6) δ: 13.48 (s, 1H), 8.29 (d, J = 8.8 Hz, 2H), 7.69 (d, J = 5.2 Hz, 2H), 7.67 (s, 1H), 7.47 – 7.43 (m, 1H), 7.30 (q, J = 8.0 Hz, 4H), 3.07 (d, J = 5.2 Hz, 3H). ^{13}C NMR (100 MHz, $CDCl_3$) δ: 161.12, 159.42, 147.47, 138.10, 131.89, 131.80,

128.83, 124.08, 123.91, 118.13, 114.53, 113.91, 113.81, 26.08. ESI-MS (m/z): $[M+Na]^+$ calcd. for $C_{18}H_{14}N_4NaO$: 325; found: 325.

***N*-methyl-4-(4-nitrophenyl)-3-(*p*-tolyl)-1*H*-pyrazole-5-carboxamide (4y)**

Off-white solid. mp: 247-249 °C. IR (KBr, cm^{-1}): 3423, 3281, 2924, 1655, 1510, 1347. ^1H NMR (400 MHz, DMSO-d_6) δ: 13.72 (s, 1H), 8.21 (d, J = 2.8 Hz, 1H), 8.15 (d, J = 8.0 Hz, 2H), 7.47 (d, J = 8.0 Hz, 2H), 7.17 (dd, J = 14.8, 7.2 Hz, 4H), 2.71 (d, J = 4.4 Hz, 3H), 2.29 (s, 3H). ^{13}C NMR (100 MHz, DMSO-d_6) δ: 162.83, 146.49, 144.87, 142.16, 141.06, 138.85, 132.22, 129.89, 128.32, 125.92, 123.25, 117.17, 26.03, 21.23. ESI-MS (m/z): $[M+H]^+$ calcd. for $C_{18}H_{17}N_4O_3$: 337; found: 337.

2B.8. References

[1] V. Kumar, K. Kaur, G. K. Gupta, A. K. Sharma, *Eur. J. Med. Chem.* **2013**, *69*, 735–753.

[2] A. Ansari, A. Ali, M. Asif, S. Shamsuzzaman, *New J. Chem.* **2017**, *41*, 16–41.

[3] O. Kuleshova, O. Khilya, Y. Volovenko, S. Mallet-Ladeira, V. Dyakonenko, E. Gras, *ACS Omega* **2017**, *2*, 8911–8927.

[4] F. E. Bennani, L. Doudach, Y. Cherrah, Y. Ramli, K. Karrouchi, M. Ansar, M. E. A. Faouzi, *Bioorg. Chem.* **2020**, *97*, 103470–103531.

[5] Z. Xu, C. Gao, Q. C. Ren, X. F. Song, L. S. Feng, Z. S. Lv, *Eur. J. Med. Chem.* **2017**, *139*, 429–440.

[6] I. Saleh, H. Raj KC, S. Roy, M. K. Abugazleh, H. Ali, D. Gilmore, M. A. Alam, *RSC Med. Chem.* **2021**, *12*, 1690–1697.

[7] M. Alvarado, P. Goya, M. Macías-González, F. J. Pavón, A. Serrano, N. Jagerovic, J. Elguero, A. Gutiérrez-Rodríguez, S. García-Granda, M. Suardíaz, F. Rodríguez de Fonseca, *Bioorg. Med. Chem.* **2008**, *16*, 10098–10105.

[8] A. Masih, A. K. Agnihotri, J. K. Srivastava, N. Pandey, H. R. Bhat, U. P. Singh, *J. Biochem. Mol. Toxicol.* **2021**, *35*, 1–9.

[9] R. Hanachi, R. Ben Said, H. Allal, S. Rahali, M. A. M. Alkhalifah, F. Alresheedi, B. Tangour, M. Hochlaf, *New J. Chem.* **2021**, *45*, 17796–17807.

[10] Y. G. Zheng, J. A. Wang, L. Meng, X. Pei, L. Zhang, L. An, C. L. Li, Y. L. Miao,

Eur. J. Med. Chem. **2021**, *209*, 112934–112946.

[11] R. M. Kartheek, M. David, *Toxicol. Reports* **2018**, *5*, 448–456.

[12] E. De Clercq, *Chem. – An Asian J.* **2019**, *14*, 3962–3968.

[13] R. S. Padwal, S. R. Majumdar, *Lancet* **2007**, *369*, 71–77.

[14] G. Szabó, J. Fischer, Á. Kis-Varga, K. Gyires, *J. Med. Chem.* **2008**, *51*, 142–147.

[15] K. Tsutomu, N. Toshitaka, *Neuropharmacology* **1978**, *17*, 249–256.

[16] S. Parmentier-Batteur, J. A. Obrien, S. Doran, S. J. Nguyen, R. B. Flick, J. M. Uslaner, H. Chen, E. N. Finger, T. M. Williams, M. A. Jacobson, P. H. Hutson, *Neuropharmacology* **2012**, *62*, 1453–1460.

[17] P. A. Moraes, E. S. Brum, I. Brusco, M. A. Marangoni, M. M. Lobo, A. F. Camargo, P. A. Nogara, H. G. Bonacorso, M. A. P. Martins, J. B. T. Da Rocha, S. M. Oliveira, N. Zanatta, *ChemistrySelect* **2020**, *5*, 14620–14625.

[18] D. Xia, X. Cheng, X. Liu, C. Zhang, Y. Wang, Q. Liu, Q. Zeng, N. Huang, Y. Cheng, X. Lv, *J. Agric. Food Chem.* **2021**, *69*, 8358–8365.

[19] Y. Zhang, N. Zhou, X. Zhu, X. He, *Polym. Chem.* **2021**, *12*, 5535–5541.

[20] A. Demirçalı, *J. Mol. Struct.* **2021**, *1231*, 129960–129967.

[21] P. Yin, J. Zhang, C. He, D. A. Parrish, J. M. Shreeve, *J. Mater. Chem. A* **2014**, *2*, 3200–3208.

[22] J. Y. Zhang, X. Wang, Z. Chang, Z. Zhang, X. Wang, H. Lin, *Inorg. Chem. Commun.* **2021**, *129*, 108580–108583.

[23] W. Yan, L. Wang, H. Qi, G. Zhan, P. Fang, Z. Liu, Z. Bian, *Inorg. Chem.* **2021**, *60*, 18103–18111.

[24] Y. Kashiwame, S. Kuwata, T. Ikariya, *Chem. - A Eur. J.* **2010**, *16*, 766–770.

[25] X. Li, L. He, H. Chen, W. Wu, H. Jiang, *J. Org. Chem.* **2013**, *78*, 3636–3646.

[26] Y. T. Tian, F. G. Zhang, J. A. Ma, *J. Org. Chem.* **2021**, *86*, 3574–3582.

[27] J. M. Yu, G. P. Lu, C. Cai, *Chem. Commun.* **2017**, *53*, 5342–5345.

[28] Y. Du, Y. Xu, C. Qi, C. Wang, *Tetrahedron Lett.* **2019**, *60*, 1999–2004.

[29] A. S. Komendantova, K. A. Lyssenko, I. V. Zavarzin, Y. A. Volkova, *Org. Chem. Front.* **2020**, *7*, 1640–1646.

[30] Z. Wei, Q. Zhang, M. Tang, S. Zhang, Q. Zhang, *Org. Lett.* **2021**, *23*, 4436–4440.

[31] J. Radolko, P. Ehlers, P. Langer, *Adv. Synth. Catal.* **2021**, *363*, 3616–3654.

[32] Z. Sun, J. He, W. Li, X. Li, Y. Feng, Y. Liu, P. Liu, S. Han, *ChemistrySelect* **2020**, *5*, 7396–7399.

[33] Y. Liu, X. Ma, Y. Ding, Z. Yang, H. W. Roesky, *Organometallics* **2018**, *37*, 3839–3845.

[34] A. A. Marzouk, E. S. Taher, M. S. A. Shaykoon, P. Lan, W. H. Abd-Allah, A. M. Aboregela, M. F. El-Behairy, *Bioorg. Chem.* **2021**, *111*, 104883–104896.

[35] B. Ren, R. C. Liu, K. Ji, J. J. Tang, J. M. Gao, *Bioorg. Med. Chem. Lett.* **2021**, *43*, 128097–128102.

[36] M. C. Pérez-Aguilar, C. Valdés, *Angew. Chemie - Int. Ed.* **2013**, *52*, 7219–7223.

[37] A. Kamal, K. N. V. Sastry, D. Chandrasekhar, G. S. Mani, P. R. Adiyala, J. B. Nanubolu, K. K. Singarapu, R. A. Maurya, *J. Org. Chem.* **2015**, *80*, 4325–4335.

[38] L. Ma, P. Ou, X. Huang, *Org. Biomol. Chem.* **2020**, *18*, 6487–6491.

[39] Y. Guo, G. Wang, L. Wei, J. P. Wan, *J. Org. Chem.* **2019**, *84*, 2984–2990.

[40] A. J. Pearce, R. P. Harkins, B. R. Reiner, A. C. Wotal, R. J. Dunscomb, I. A. Tonks, *J. Am. Chem. Soc.* **2020**, *142*, 4390–4399.

[41] T. Shi, Z. Wu, T. Jia, C. Zhang, L. Zeng, R. Zhuang, J. Zhang, S. Liu, J. Shao, H. Zhu, *Chem. Commun.* **2021**, *57*, 8460–8463.

[42] F. Qiu, Y. Cao, L. Zeng, C. Zhang, L. Fu, J. Zhang, H. Zhu, J. Shao, *J. Org. Chem.* **2021**, *86*, 8997–9006.

[43] N. Gulia, M. Małecki, S. Szafert, *J. Org. Chem.* **2021**, *86*, 9353–9359.

[44] G. Huang, C. M. Solano, J. Melendez, S. Yu-Alfonzo, R. Boonhok, H. Min, J. Miao, D. Chakrabarti, Y. Yuan, *Eur. J. Med. Chem.* **2021**, *209*, 112889–112904.

[45] S. Panda, P. Maity, D. Manna, *Org. Lett.* **2017**, *19*, 1534–1537.

[46] J. Sun, L. L. Zhang, E. Y. Xia, C. G. Yan, *J. Org. Chem.* **2009**, *74*, 3398–3401.

[47] A. M. Youssef, A. K. EL-Ziaty, W. S. I. Abou-Elmagd, S. K. Ramadan, *J. Heterocycl. Chem.* **2015**, *52*, 278–283.

[48] A. J. Flynn, A. Ford, U. B. R. Khandavilli, S. E. Lawrence, A. R. Maguire, *European J. Org. Chem.* **2019**, *2019*, 5368–5384.

[49] S. G. Franzblau, R. S. Witzig, J. C. Mclaughlin, P. Torres, G. Madico, A. Hernandez, M. T. Degnan, M. B. Cook, V. K. Quenzer, R. M. Ferguson, R. H. Gilman, *J. Clin. Microbiol.* **1998**, *36*, 362–366.

[50] P. Suman, C. Dayakar, K. Rajkumar, B. Yashwanth, P. Yogeeswari, D. Sriram, J. V. Rao, B. C. Raju, *Bioorg. Med. Chem. Lett.* **2015**, *25*, 2390–2394.

[51] M. Kumar, R. Vijayakrishnan, G. Subba Rao, *Mol. Divers.* **2010**, *14*, 595–604.

[52] J. M. Nguta, R. Appiah-Opong, A. K. Nyarko, D. Yeboah-Manu, P. G. A. Addo, I. Otchere, A. Kissi-Twum, *J. Ethnopharmacol.* **2016**, *182*, 10–15.

[53] M. F. Abo-Ashour, W. M. Eldehna, R. F. George, M. M. Abdel-Aziz, M. M. Elaasser, N. M. Abdel Gawad, A. Gupta, S. Bhakta, S. M. Abou-Seri, *Eur. J. Med. Chem.* **2018**, *160*, 49–60.

[54] L. Ravi, K. Krishnan, *Innovare J. Med. Sci.* **2016**, *4*, 1–6.

[55] D. E. V. Pires, T. L. Blundell, D. B. Ascher, *J. Med. Chem.* **2015**, *58*, 4066–4072.

2B.9. Selected IR, NMR (^{1}H and ^{13}C) and Mass spectra

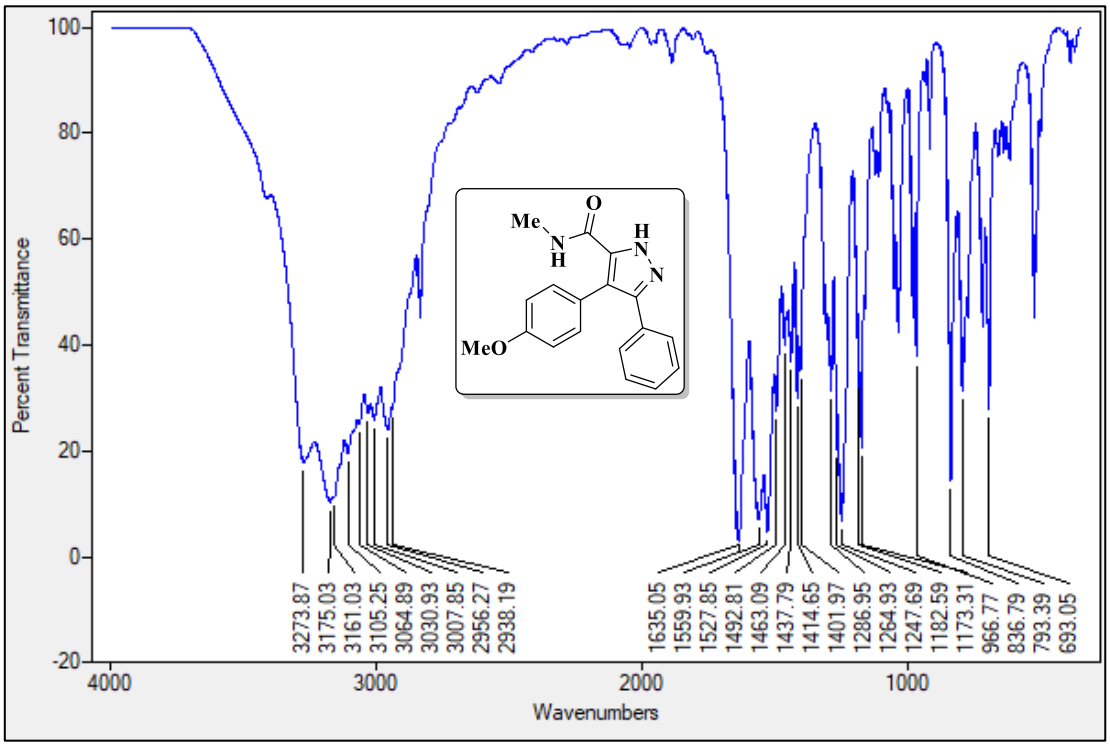

IR spectrum of the compound **4a**

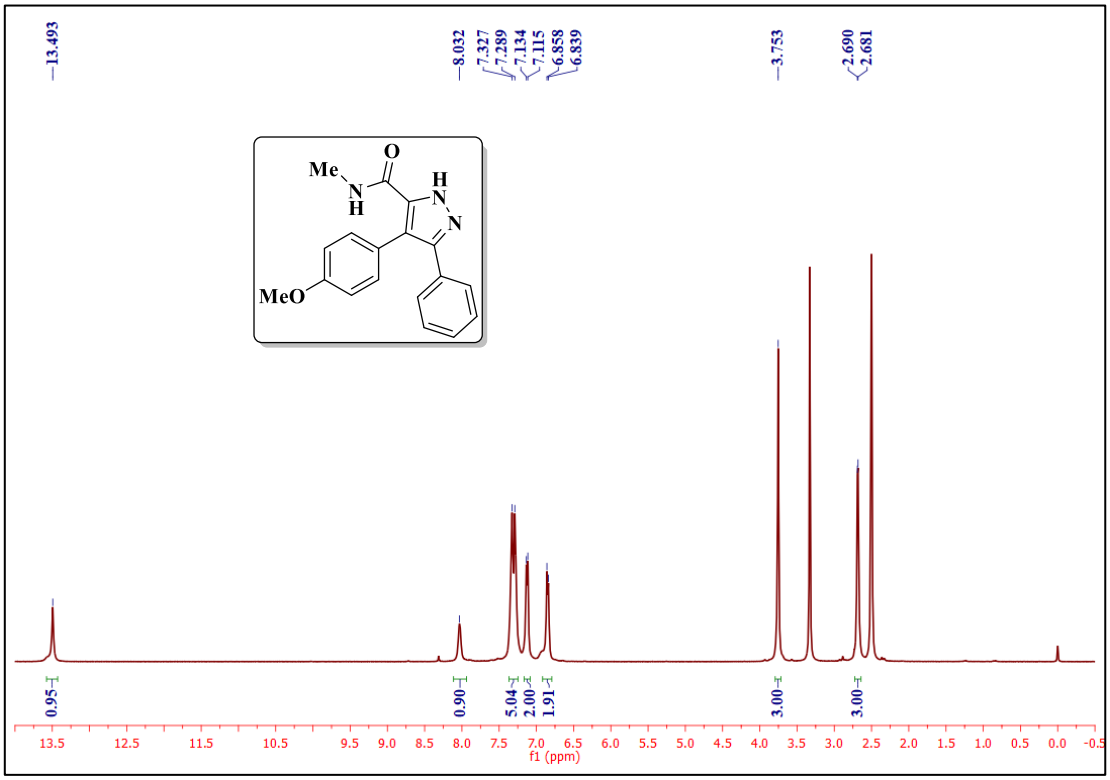

^{1}H NMR spectrum of the compound **4a**

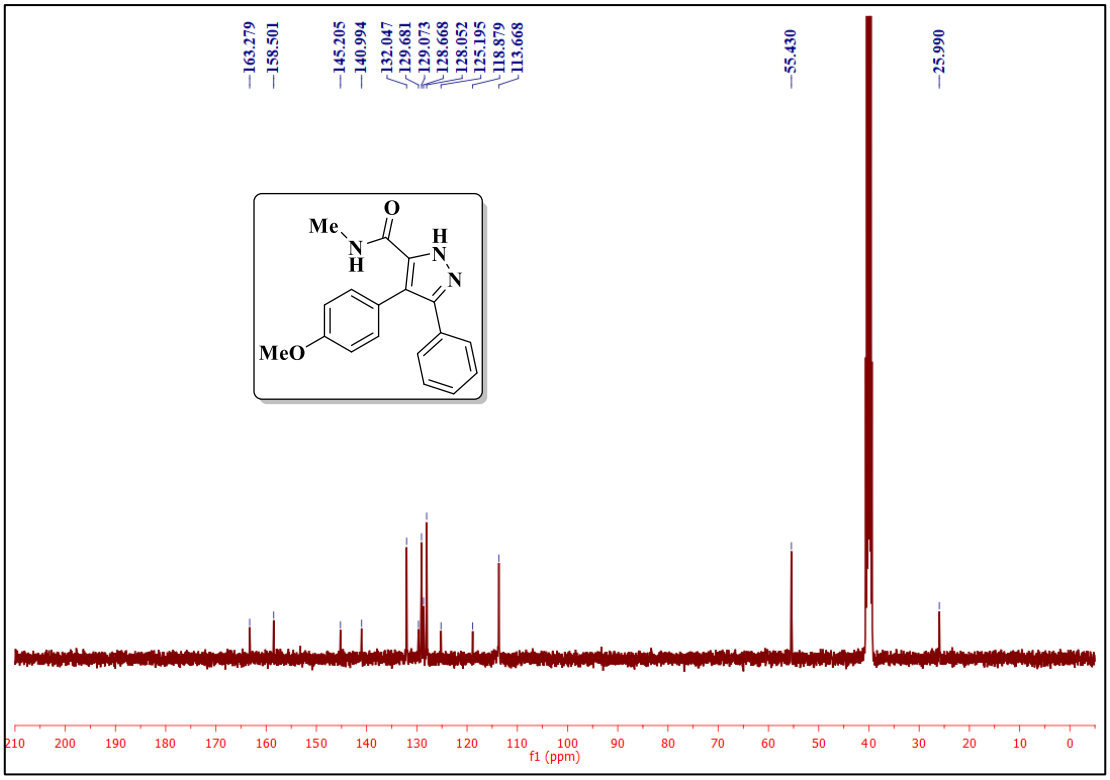

^{13}C NMR spectrum of the compound **4a**

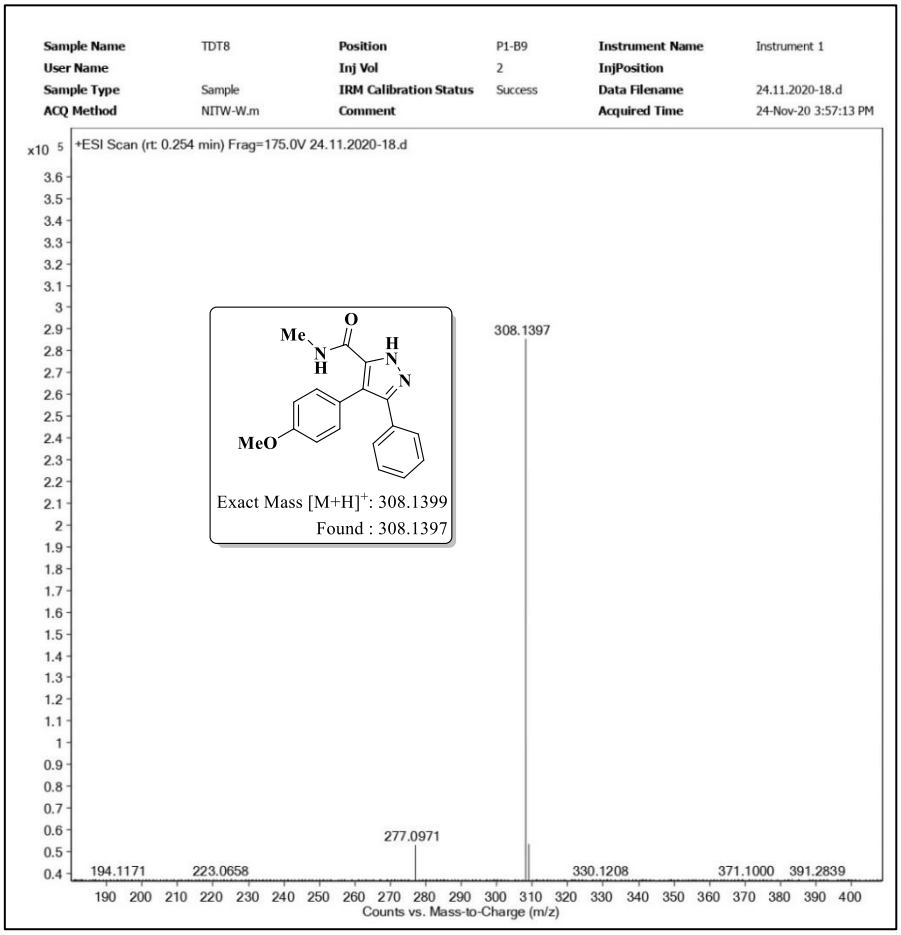

Mass spectrum of the compound **4a**

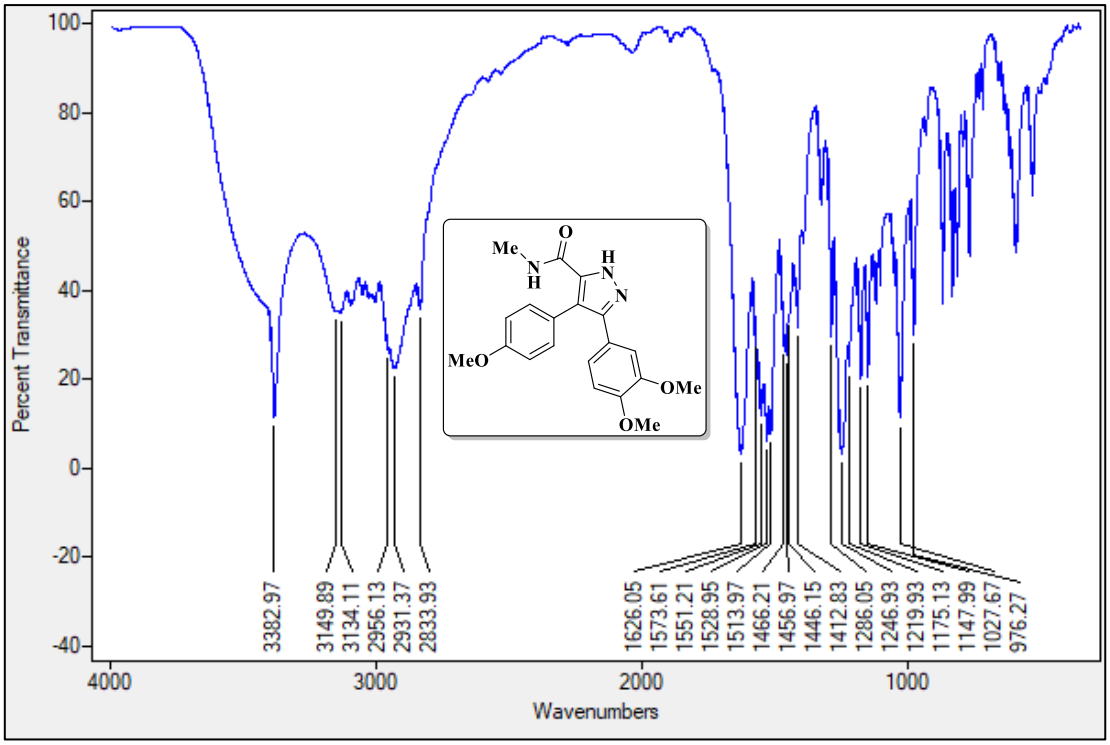

IR spectrum of the compound **4d**

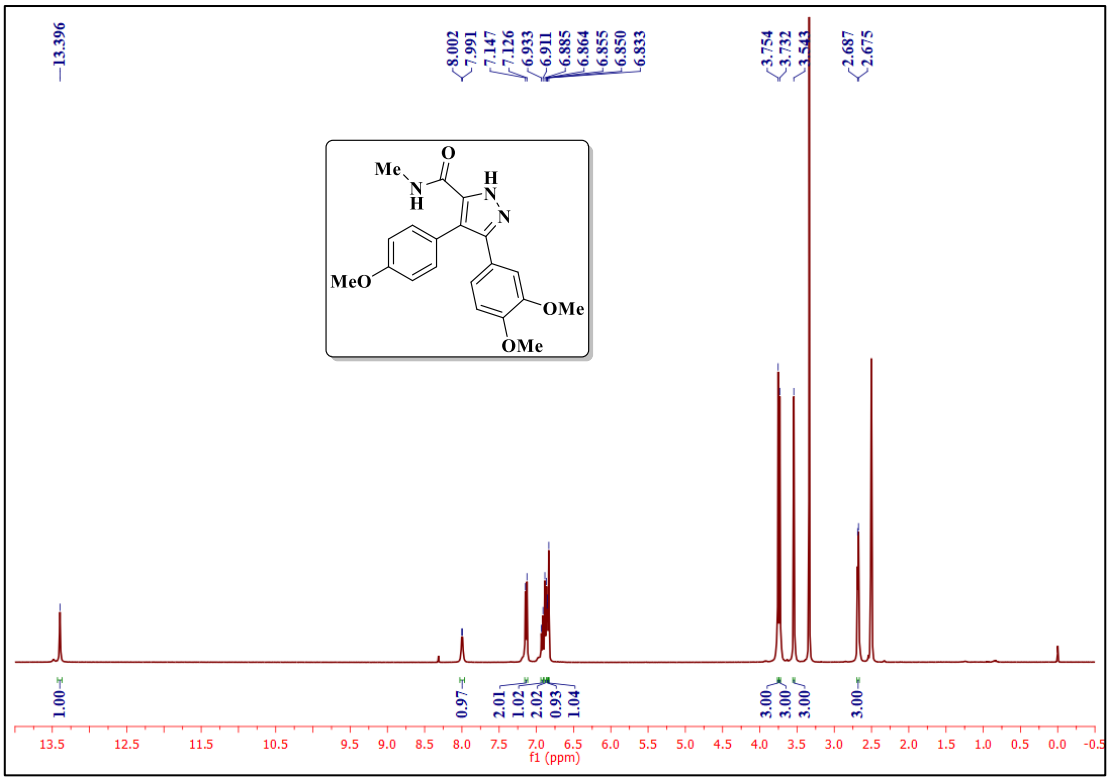

^{1}H NMR spectrum of the compound **4d**

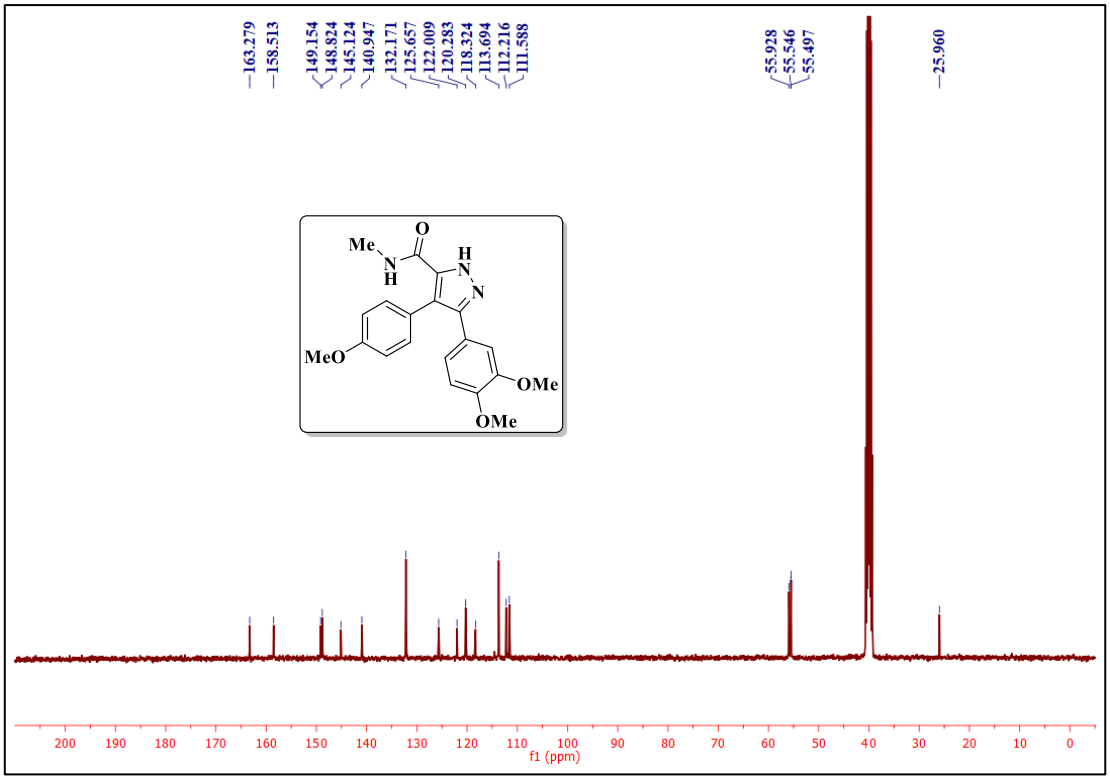

^{13}C NMR spectrum of the compound **4d**

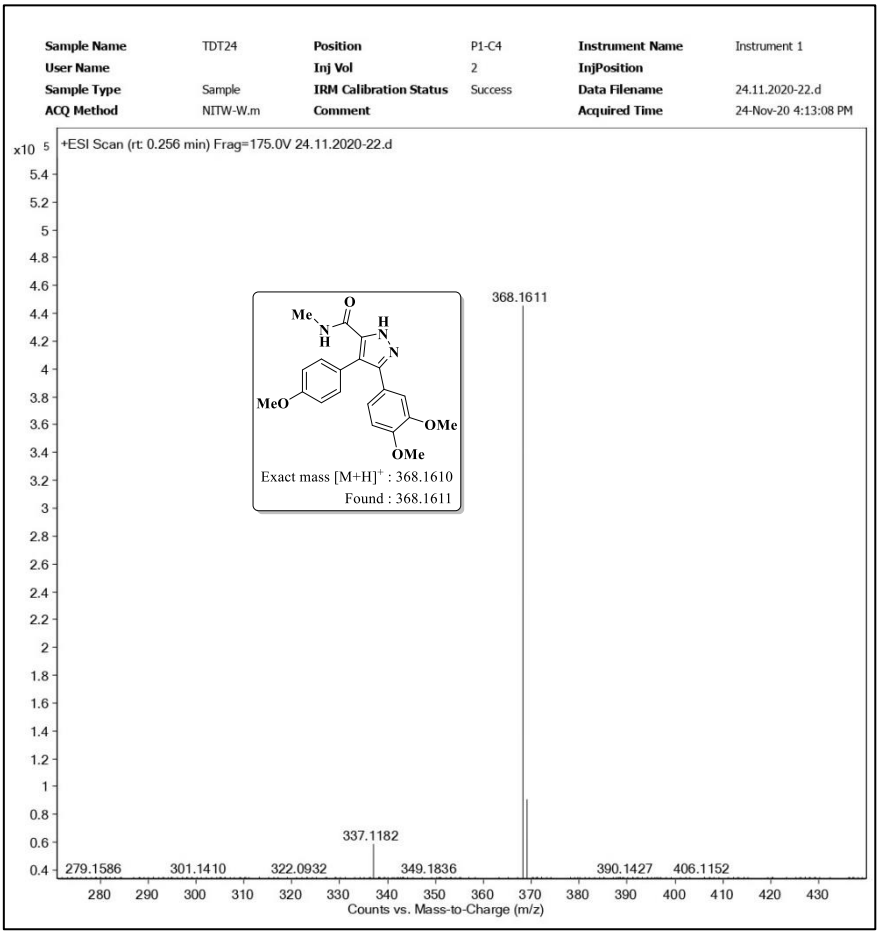

Mass spectrum of the compound **4d**

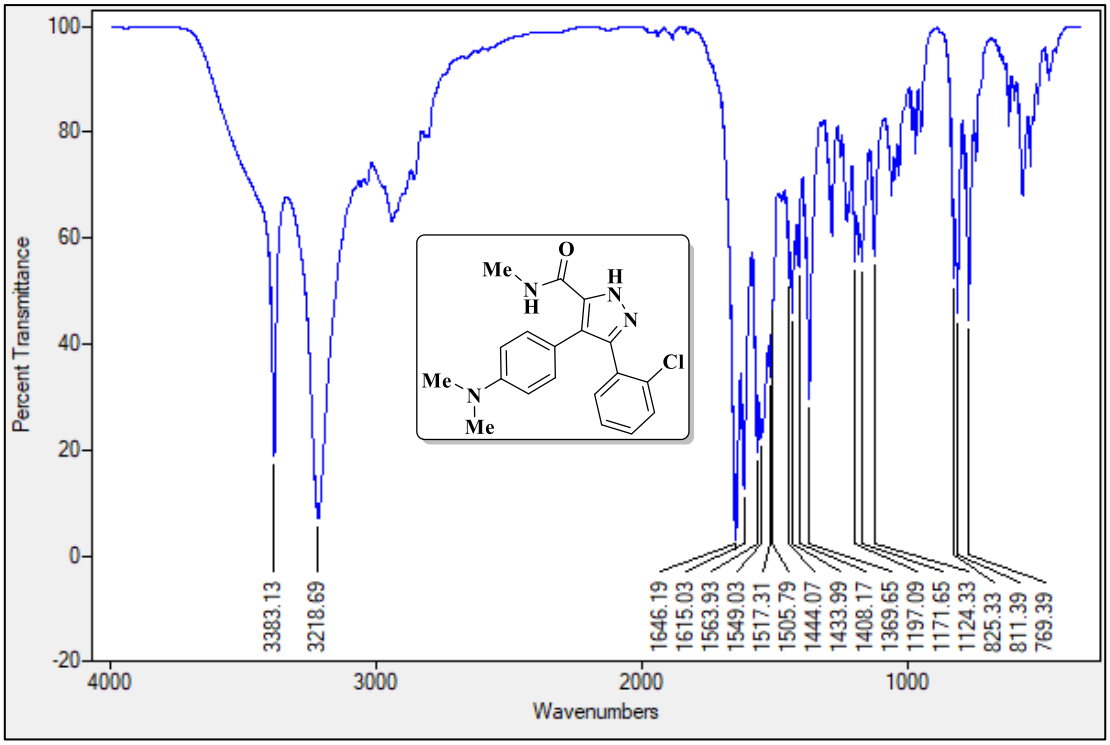

IR spectrum of the compound **4s**

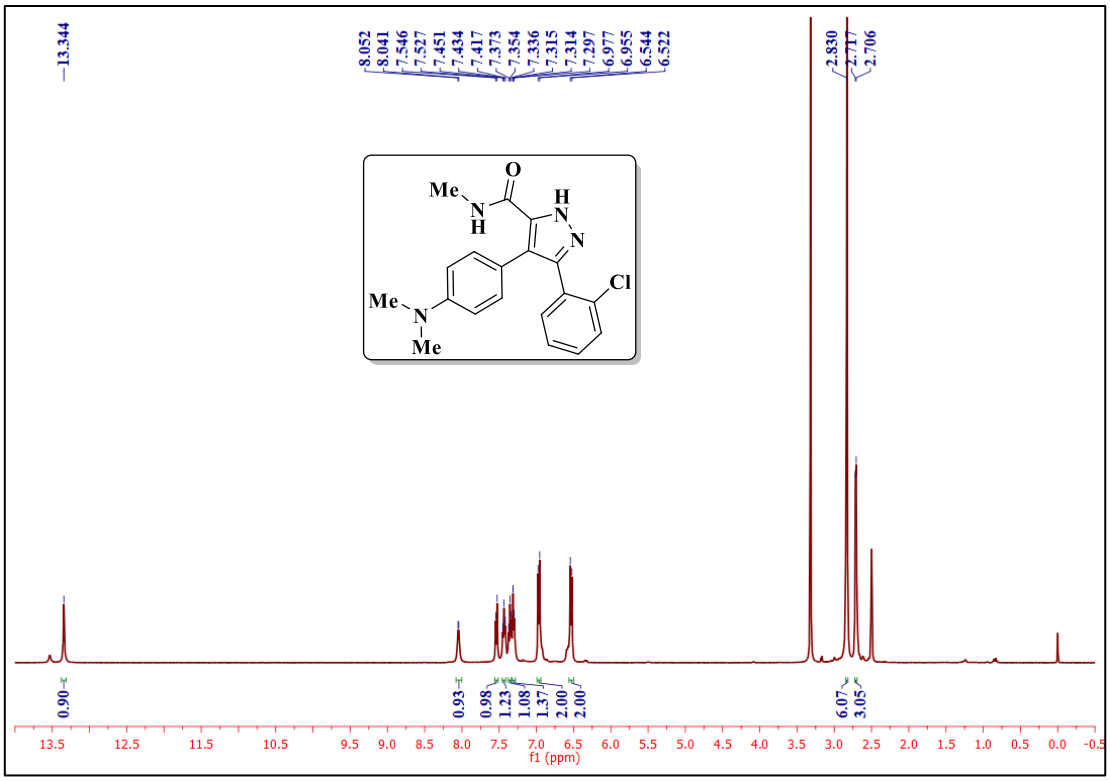

^{1}H NMR spectrum of the compound **4s**

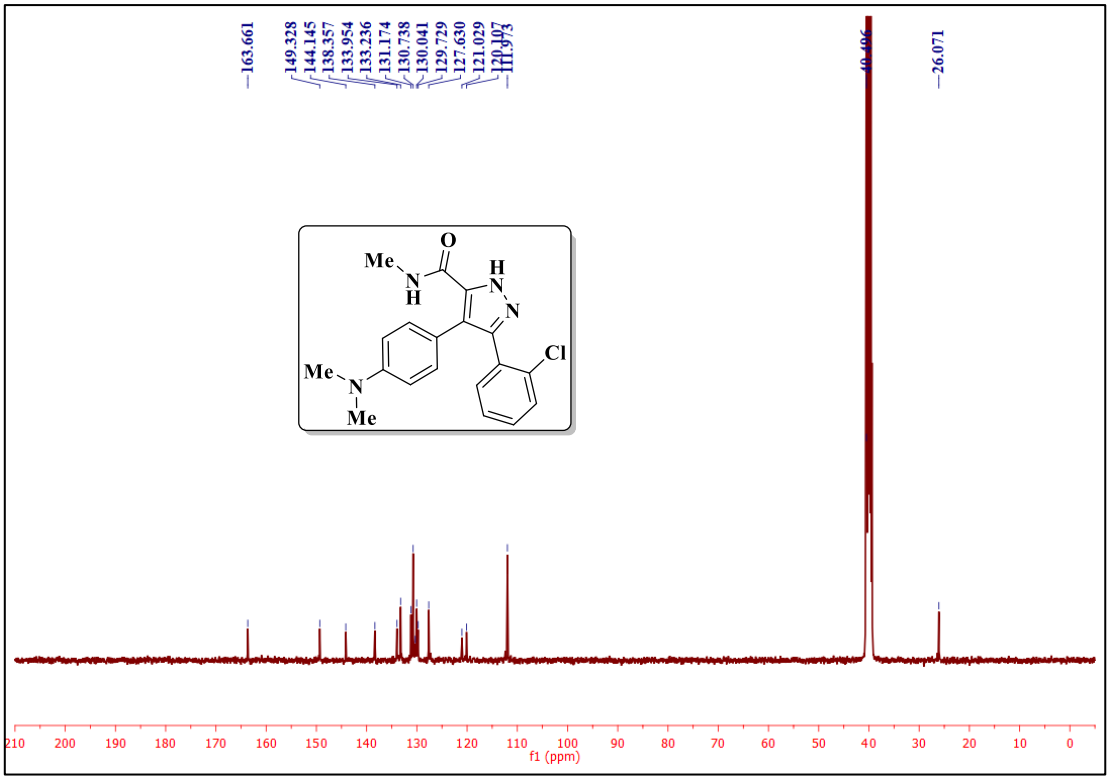

^{13}C NMR spectrum of the compound **4s**

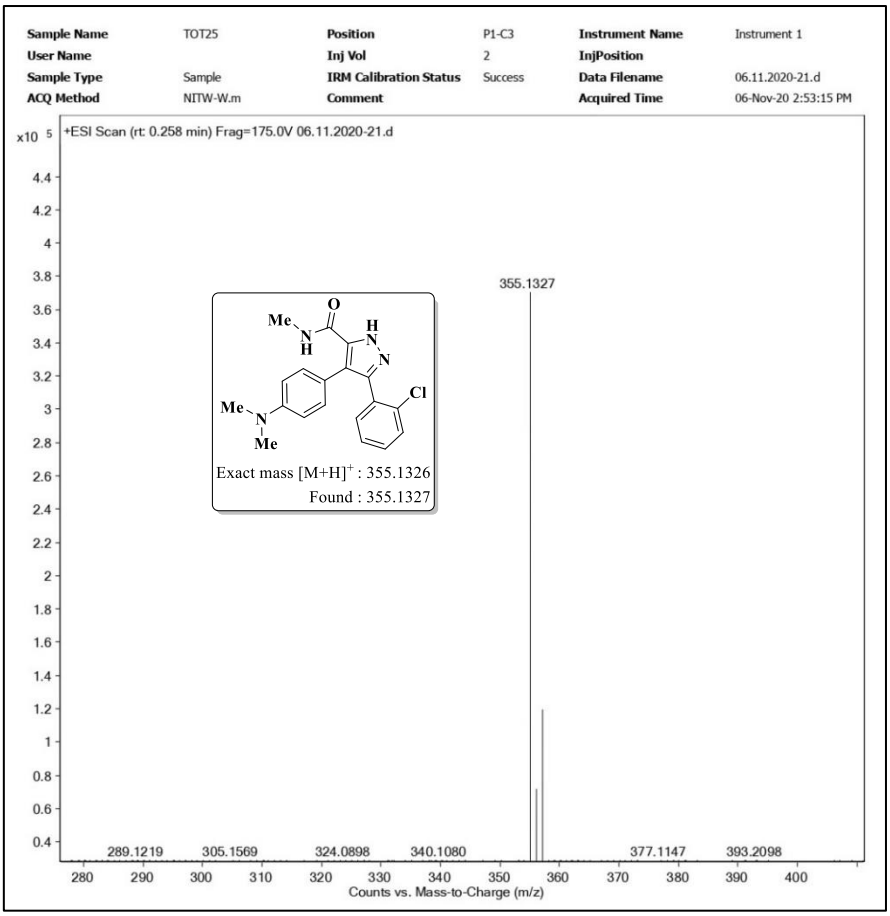

HRMS spectrum of the compound **4s**

CHAPTER-III

A photoinduced multicomponent regioselective synthesis of 1,4,5-trisubstituted-1,2,3-triazoles: Transition metal-, azide- and oxidant-free protocol

3.1. Introduction

Triazoles constitute a major role in chemical community due to their wide range of applications in medicinal and in organic synthesis [1]. Significantly, 1,2,3-triazoles show a broad spectrum of biological activities such as anti-cancer [2], anti-viral [3], analgesic [4], anti-fungal [5], anti-bacterial [6], anti-tubercular [7], anti-inflammatory [8], anti-pyretic [9-11] etc. For the prevention of disease in humans, there are several drugs available in the market containing the triazole as a core moiety namely, cefatrizine (anti-bacterial) [12], tazobactam (anti-biotic) [13], *tert*-butyldimethylsilyl-spiroaminooxathioledioxide (TSAO) (anti-HIV) [14], carboxyamidotriazole (anti-cancer) [15], rufinamide (anti-epileptic) [16], suvorexant (anti-insomnia) [17], and the drug DA-6886 is used as anti-intestinal [18]. They also play a vital role as key precursors in many industrial applications like photostabilizers [19], agrochemicals [20], polymers [21], corrosion retardants [22], pigments and dyes [23]. Some of the biologically active triazoles were shown in Figure 3.1.

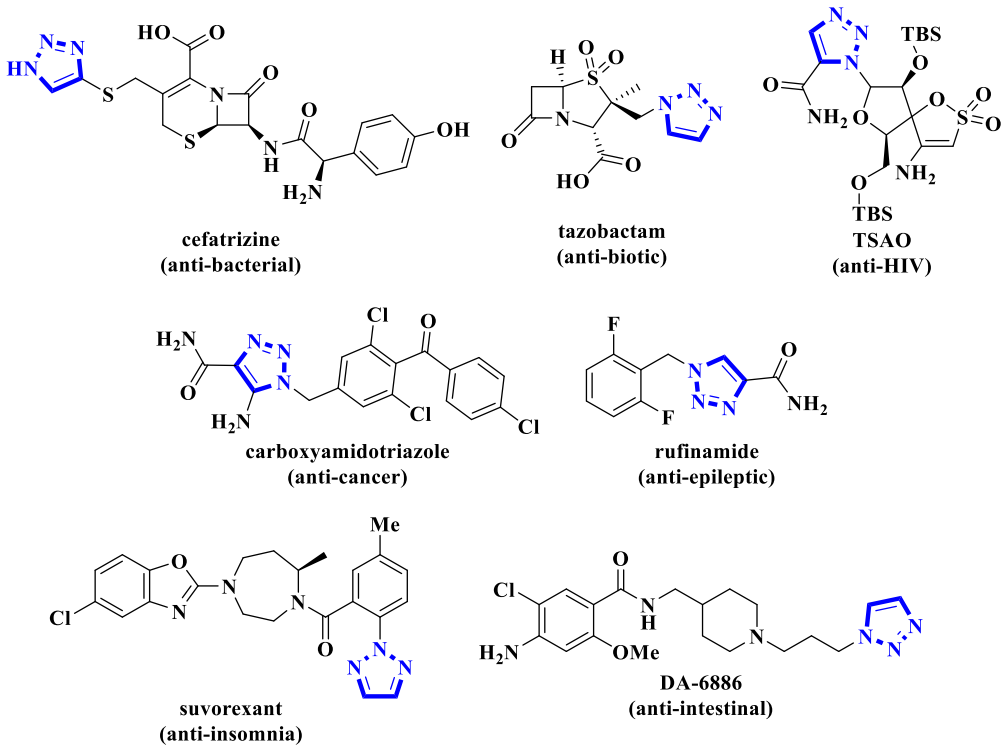

Figure 3.1. Biologically potent drugs having 1,2,3-triazole.

Because of their diverse applications in the field of medicinal and material sciences, several methodologies have been demonstrated to construct these triazole moieties [24]. Among them, the Huisgen azide-alkyne dipolar cycloaddition (AAC) is the most universally employed method for the synthesis of 1,2,3-triazoles [25]. However, this transformation suffers from poor regioselectivity and limited substrate scope [26]. Later,

the copper catalyzed azide-alkyne cycloaddition reaction (CuAAC) discovered by Sharpless and Meldal has led to the most prominent strategy in 1,2,3-triazole chemistry due to their excellent regioselectivity [27].

3.1.1. Synthetic methods for the preparation of 1,2,3-triazoles

Ramachary and co-workers developed DBU catalyzed [3+2] cycloaddition reaction of readily available cyclic/acyclic enones with less reactive vinyl/aryl azides under ambient conditions for the synthesis of medicinally important 1,2,3-triazoles (Scheme 3.1) [28].

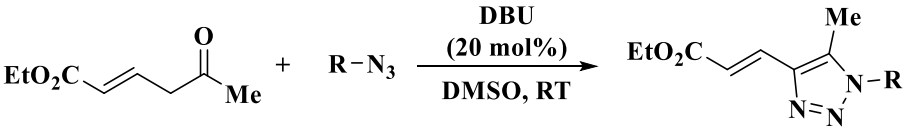

Scheme 3.1

Thomas et al. reported an approach for the direct and selective preparation of 1,5-disubstituted-1,2,3-triazoles from readily available building blocks such as primary amines, enolizable ketones and 4-nitrophenyl azide *via* an organo cascade process (Scheme 3.2). This protocol makes use of readily available organic azides and amines as the sources of nitrogen of the triazole heterocycles [29].

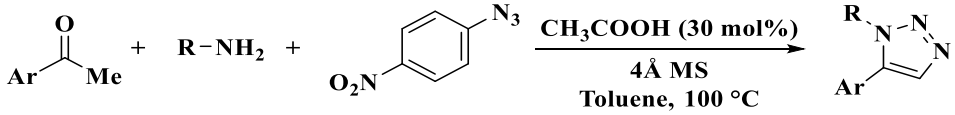

Scheme 3.2

Westermann and co-workers introduced tosylhydrazone based triazole formation from the readily accessible primary amines with α,α-dichlorotosylhydrozones under ambient conditions (Scheme 3.3). This method offers azide- and metal- free route for the regioselective synthesis of 1,4-substituted triazoles [30].

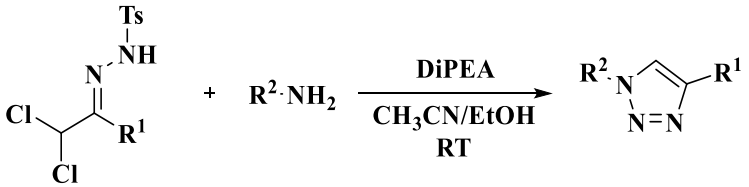

Scheme 3.3

Wang and co-workers described an efficient I_2/TBPB mediated oxidative [4+1] cycloaddition of *N*-tosylhydrazones with anilines for the construction of 1,4-disubstituted 1,2,3-triazoles under metal- and azide- free conditions (Scheme 3.4). This protocol involves the of formation of C–N/N–N bonds and the cleavage of S–N bond in a single operation [31].

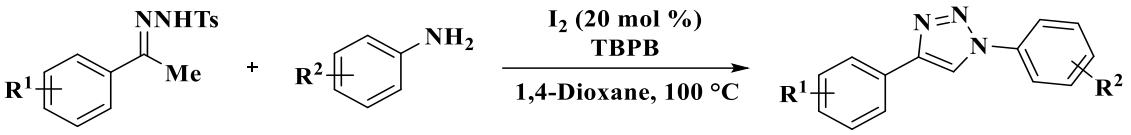

Scheme 3.4

Zhou et al. used a transition metal-, azide- and oxidant- free [4+1] cycloaddition strategy to synthesize 1,2,3-triazoles from *α,α*-difluoro-*N*-tosylhydrazone and amine (Scheme 3.5). The reaction proceeded smoothly in high yields with good functional group tolerance through C–F bond cleavage [32].

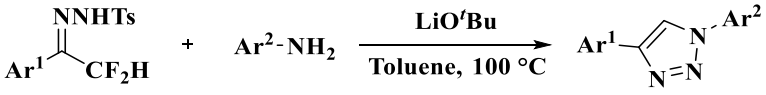

Scheme 3.5

Zhang and co-workers employed a transition metal free approach for the construction of 5-amino-1,2,3-triazoles using carbodiimides and diazo compounds *via* base promoted nucleophilic addition/cyclization process under mild conditions (Scheme 3.6) [33].

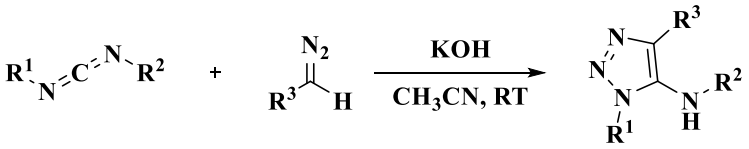

Scheme 3.6

Huang et al. reported the direct synthesis of 4-aryl-1,2,3-triazoles through iodine mediated formal [2+2+1] cyclization under metal- and azide- free conditions (Scheme 3.7). In this method, tosylhydrazine and 1-aminopyridinium iodide were utilized as nitrogen sources to generate *NH*-1,2,3-triazoles [34].

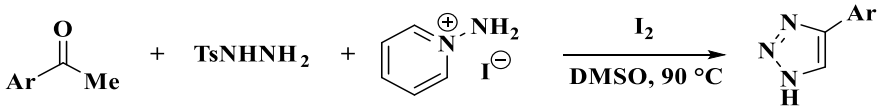

Scheme 3.7

3.2. Present work

Considering the significance of 1,2,3-trialzoles herewith, we have developed a photoinduced one-pot three component reaction involving isatin Schiff bases, aromatic aldehydes and tosylhydrazine in DMF to produce the desired compounds **4a-al** (Scheme 3.8). All the synthesized compounds were tested for the *in vitro* antitubercular activity and *in silico* molecular docking and ADME prediction.

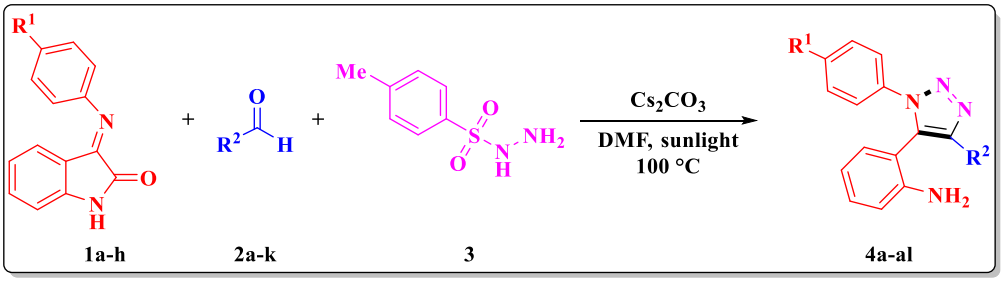

Scheme 3.8. Synthesis of 1,4,5-trisubstituted-1,2,3-triazoles **4a-al**.

With this proposed methodology we have prepared various 1,4,5-trisubstituted-1,2,3-triazoles under transition metal-, azide- and oxidant- free conditions.

3.2.1. Results and discussion

To optimize the reaction, 3-(phenylimino)indolin-2-one **1a**, benzaldehyde **2a** and tosylhydrazine **3** were considered for our study. The reaction of **1a** (1.0 mmol), **2a** (1.0 mmol) and **3** (1.0 mmol) in the presence of Cs_2CO_3 (1.0 equiv) in DMF was initially examined under sunlight to obtain 1,4,5-trisubstituted-1,2,3-triazole **4a** with poor yield (Table 3.1, entry 1). Then the experiment was carried out in the absence of base at 100 °C resulting no desired product **4a** (Table 3.1, entry 2). Further the reaction was conducted in the presence of Cs_2CO_3 (1.0 equiv) in DMF at 100 °C resulted **4a** with moderate yield (Table 3.1, entry 3). Since we have not satisfied with these yields, we have checked the reaction by increasing the equivalents of Cs_2CO_3. To our delight, the desired product was obtained with a better yield in the presence of 3 equivalents of Cs_2CO_3 in DMF at 100 °C (Table 3.1, entry 4).

We have also tried with other bases such as K_2CO_3, NaH, Na_2CO_3, DBU, NaOAc and Et_3N (Table 3.1, entries 5-10), among these Cs_2CO_3 was chosen as a suitable base for the generation of desired product **4a**. Then various solvents such as DMSO, CH_3CN and EtOH were investigated to optimize the yield (Table 3.1, entries 11, 12, 15) and DMF was found to be the best optimal solvent w.r.t. yield of the desired product. Use of H_2O as solvent resulted no formation of required product (Table 3.1, entry 16). Further, we have tried the reaction at 120 °C in DMF lead to a lower yield of **4a** (Table 3.1, entry 14). It is noteworthy that increasing the base would reduce the yield of **4a** (Table 3.1, entry 13), and the optimized reaction conditions were established with Cs_2CO_3 as an efficient base and DMF as a suitable solvent for the generation of desired product **4a**.

Table 3.1. Optimization of the reaction conditions[a]

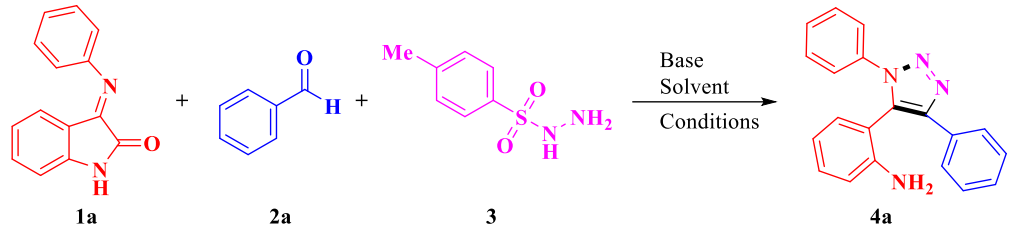

1a 2a 3 4a

Entry	Base	Base equivalents	Solvent	Temp (°C)	Time (h)	Yield (%)[b]
1	Cs_2CO_3	1	DMF	RT	12	45
2	-	-	DMF	100	12	ND
3	Cs_2CO_3	1	DMF	100	8	65
4	**Cs_2CO_3**	**3**	**DMF**	**100**	**6**	**89**
5	K_2CO_3	3	DMF	100	8	70
6	NaH	3	DMF	100	10	40
7	Na_2CO_3	3	DMF	100	10	60
8	DBU	3	DMF	100	8	65
9	NaOAc	3	DMF	100	8	63
10	Et_3N	3	DMF	100	10	36
11	Cs_2CO_3	3	DMSO	100	6	85
12	Cs_2CO_3	3	CH_3CN	Reflux	8	56
13	Cs_2CO_3	4	DMF	100	6	86
14	Cs_2CO_3	3	DMF	120	6	85
15	Cs_2CO_3	3	EtOH	Reflux	10	48
16	Cs_2CO_3	3	H_2O	100	10	ND

[a]Reaction condition: Compound **1a** (1.0 mmol), benzaldehyde **2a** (1.0 mmol) and tosylhydrazine **3** (1.0 mmol) under sunlight. [b]Isolated yields. RT: room temperature. ND: not determined.

The above optimized conditions were explored for reaction generality and scope of the substrates (Table 3.2). In general, a wide range of isatin Schiff bases and benzaldehydes can react smoothly and offer the desired products in good to excellent yields. Electron donating (–CH_3, –OCH_3), withdrawing (–NO_2, –CN) and hetero aryl (pyridine) groups had no substantial impact on the efficiency of the reaction.

Table 3.2. Substrate scope of regioselective 1,4,5-trisubstituted-1,2,3-triazoles **4a-al**[a,b]

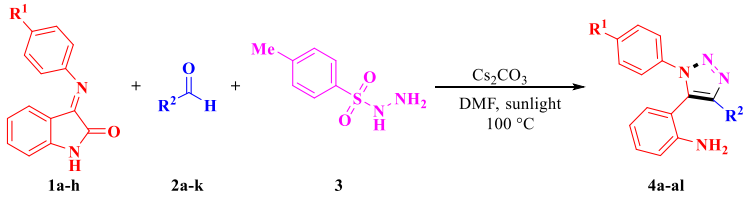

1a-h 2a-k 3 4a-al

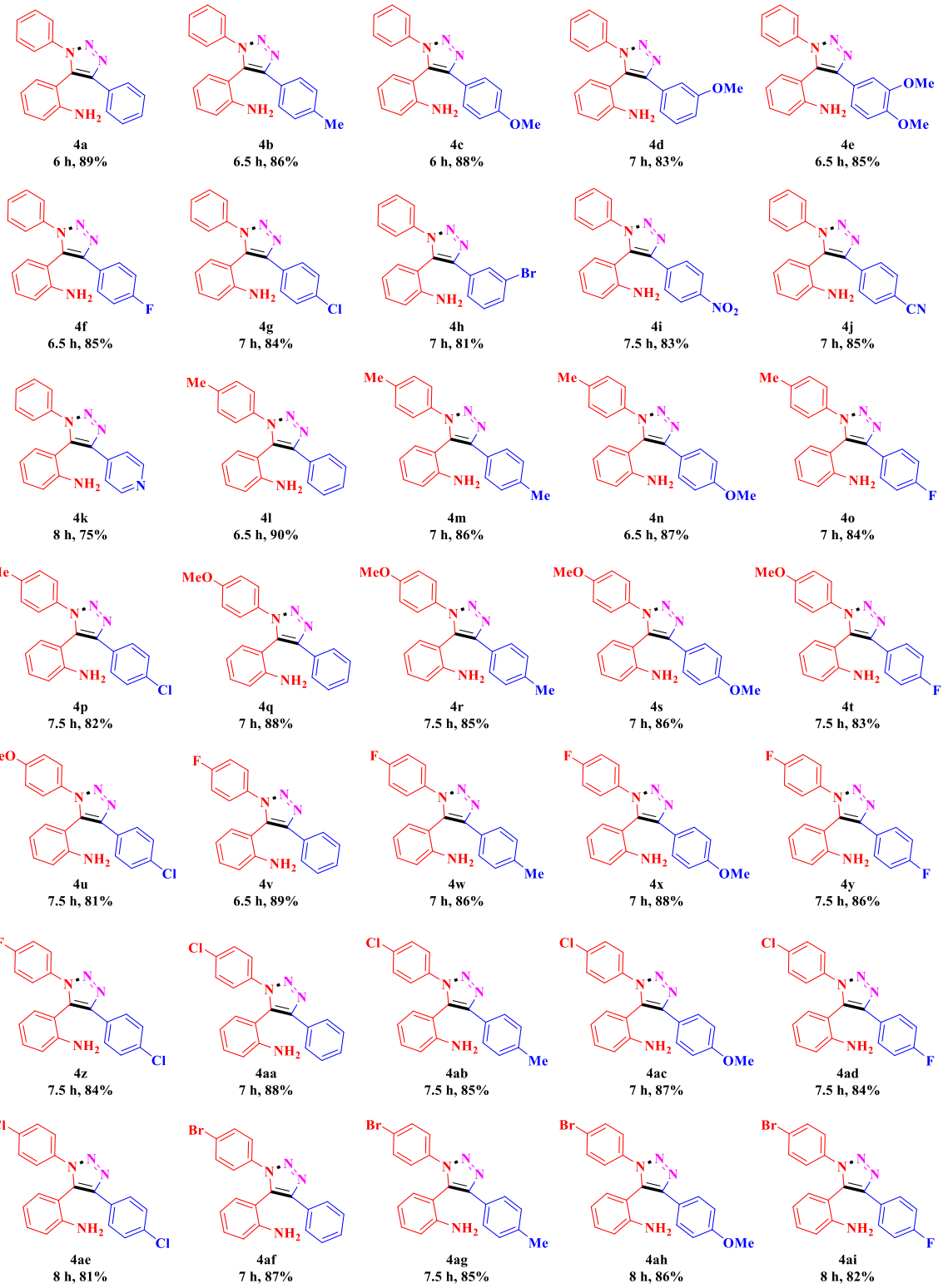

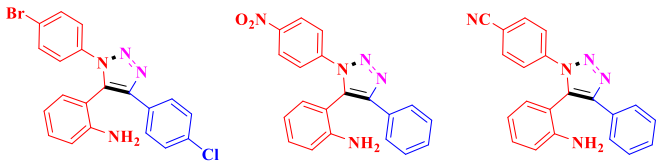

4aj 8 h, 81% **4ak** 8 h, 78% **4al** 7.5 h, 80%

[a]Reaction condition: isatin Schiff bases **1a-h** (1.0 mmol), benzaldehydes **2a-k** (1.0 mmol), tosylhydrazine **3** (1.0 mmol) and Cs_2CO_3 (3.0 equiv) in 3 mL DMF at 100 °C under sunlight. [b]Isolated yields

In order to gain insight into the reaction process, a series of control experiments were carried out as shown in Scheme 3.9. First, the isatin Schiff base **1a**, benzaldehyde **2a** were reacted with benzenesulfonyl hydrazide **5** under the established reaction conditions and obtained the desired product **4a** in 87% yield (eqn 1). The low reaction yield under an inert (N_2) atmosphere showed that oxygen atmosphere plays an important role in this reaction (eqn 2). To investigate the interference of light on our strategy, we have performed the reaction in dark condition and observed a trace amount product formation. The result indicated that this reaction is light dependent (eqn 3). When conducting the reaction with *N*-substituted isatin Schiff base **6** instead of **1a** did not furnish the desired product **7** (eqn 4). Which indicates the essential role of free –NH group. Next, acyclic α-ketoamide **8** led to no desired product **9** (eqn 5) when employed under optimized conditions instead of **1a**.

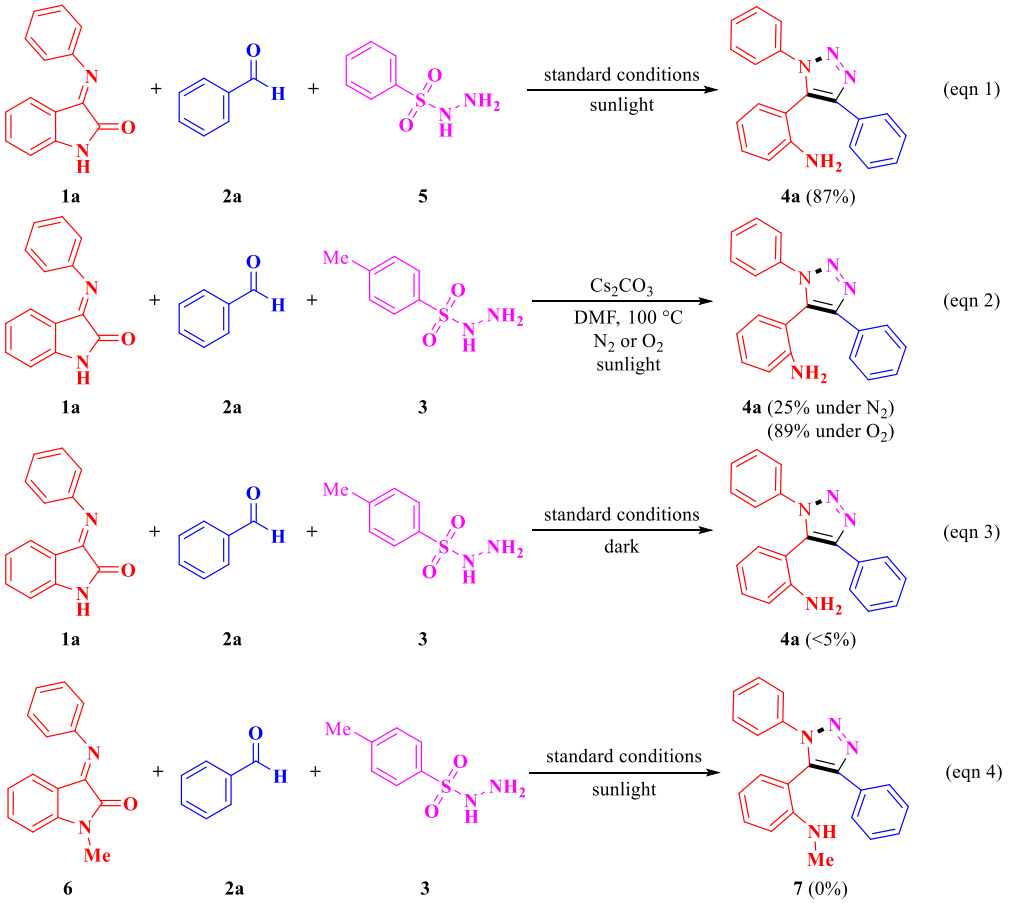

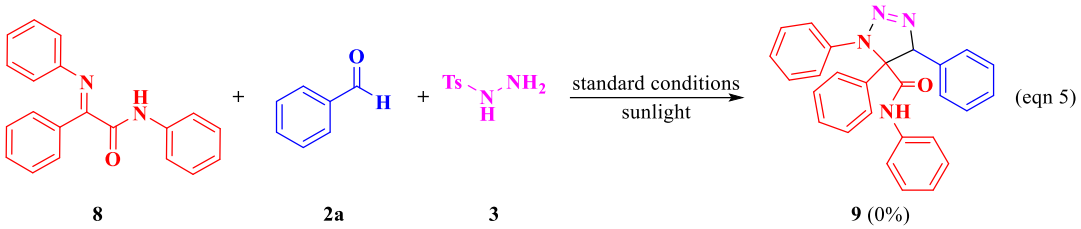

Scheme 3.9. Control experiments.

On the basis of above controlled experiments, the plausible reaction mechanism for the synthesis of target compounds **4a-al** is illustrated in Scheme 3.10. Initially, *N*-tosylhydrazone intermediate **A** forms from aldehyde **2a** and tosylhydrazine **3**, which converts into diazo intermediate **B** in the presence of Cs_2CO_3. Then intermediate **B** undergoes excitation (**C**) in the presence of sunlight. Further, it converts into radical intermediate **D** in the presence of atmospheric oxygen. Oxygen may serve as an oxidant to oxidize the *in situ* formed anion **C** into radical **D** [35]. Further, the radical intermediate **D** on reaction with **1a** generates the intermediate **E**. Next, a subsequent intramolecular radical attack and the elimination of Ts radical produces the spiro cyclic intermediate **F,** which then react with water to form intermediate **H** by the cleavage of isatin ring [36]. This undergoes decarboxylation and dehydrogenation to yield the desired product 1,2,3-triazole **4a**.

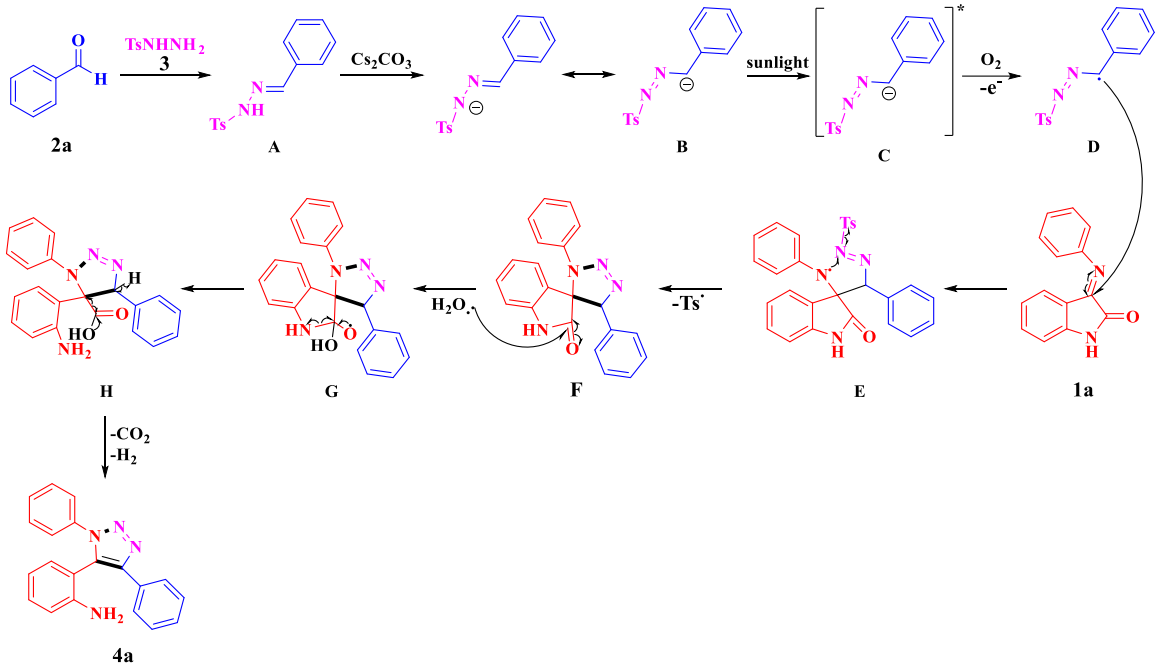

Scheme 3.10. Plausible mechanism for the generation of target compounds **4a-al**.

The synthesized compounds **4a-al** were characterized by IR, ^{1}H NMR, ^{13}C NMR and mass spectral data. For instance, the IR spectrum of **4g** shows the bands at 3457 cm^{-1}

and 3360 cm^{-1} represents the NH_2 group. The band at 1621 cm^{-1} represents the C=C stretching frequency of triazole moiety, and the C–N stretching mode of triazole ring observed at 1401 cm^{-1} [37]. In the ^1H NMR spectrum the peak showed a singlet at δ 5.23 *ppm* represents the NH_2 protons. The ^{13}C NMR showed the peaks at δ 147.92 and δ 138.63 *ppm* corresponds to C_9 and C_{10} carbons of triazole ring respectively [38]. The molecular weight of the compound was confirmed by the peak at *m/z* 395.41 $[M+H]^+$ in mass spectrum. Additionally, fragmentation pathway of the compound **4g** was supported by the MS/MS spectrum analysis. Further, the regiochemistry and structures of the derivatives were determined by the single crystal X-ray diffraction (SCXRD) method (**4g**). The Oak Ridge thermal ellipsoid plot (ORTEP) representation of **4g** was given in Figure 3.2. The crystallographic data with CCDC number 2070199 and structure refinement parameters of the compound **4g** were shown in Table 3.3.

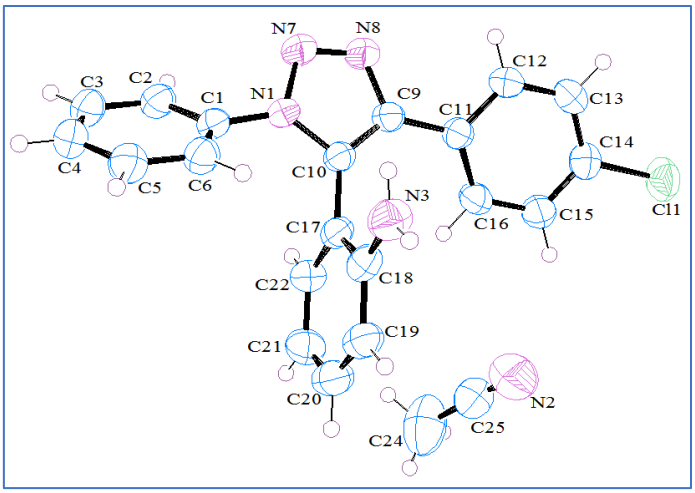

Figure 3.2. ORTEP representation of the compound **4g** and the thermal ellipsoids are drawn at 50% probability level. The crystal **4g** is the acetonitrile solvate.

Table 3.3. Salient crystallographic data and refinement parameters of the compound **4g**

Identification code	**4g**
Empirical formula	$C_{22}H_{18}ClN_5$
Formula weight	387.87
Crystal system	Monoclinic
Space group	$P2_1/n$
T (K)	100
a (Å)	5.7459 (6)
b (Å)	21.858 (2)
c (Å)	15.4874 (18)
α (°)	90
β (°)	92.156 (4)

γ (°)	90
Z	4
V (Å^3)	1943.8 (4)
D_{calc} (g/cm^3)	1.325
F (000)	808.9
μ (mm^{-1})	0.214
Θ (°)	27
Index ranges	-7 ≤ h ≤ 7 -27 ≤ k ≤ 27 -19 ≤ l ≤ 19
N-total	9529
N-independent	4247
N-observed	3646
Parameters	255
R_1 *[I > 2 σ (I)]*	0.0645
wR_2 (all data)	0.1765 (4233)
GOF	1.057
CCDC	2070199

3.2.2. Biological activity

3.2.2.1. Anti-tubercular activity (anti-TB)

The anti-tubercular activity of the synthesized 1,4,5-trisubstituted-1,2,3-triazoles **4a-al** were examined using the Microplate Alamar Blue Assay (MABA) method against *Mycobacterium tuberculosis* H37Rv (ATCC27294) strain and ethambutol as a standard drug [39]. The experiments were conducted in duplicates and the MIC values (μg/mL) are listed in Table 3.4.

The results of anti-TB activity indicate that all the screened compounds exhibited significant to poor activity with the MIC values ranging from 6.25 μg/mL to >25.00 μg/mL. Among these, three compounds **4a**, **4o** and **4z** exhibited significant activity with MIC value 6.25 μg/mL when compared to the standard drug ethambutol (MIC: 1.56 μg/mL). On the other hand, six compounds **4e**, **4k**, **4p**, **4u**, **4x**, and **4ak** displayed moderate anti-TB activity with the MIC value 12.5 μg/mL. The remaining derivatives showed poor anti-TB potency.

Table 3.4. *In vitro* anti-tubercular activity of title compounds **4a-al**

Entry	Compound	MIC (μg/mL)	% of Inhibition @25μM[a]
1	**4a**	**6.25**	**27.72**
2	**4b**	>25	ND[b]
3	**4c**	25	ND

4	**4d**	25	ND
5	**4e**	12.5	ND
6	**4f**	>25	ND
7	**4g**	>25	ND
8	**4h**	>25	ND
9	**4i**	25	ND
10	**4j**	25	ND
11	**4k**	12.5	ND
12	**4l**	>25	ND
13	**4m**	>25	ND
14	**4n**	>25	ND
15	**4o**	**6.25**	**18.25**
16	**4p**	12.5	ND
17	**4q**	>25	ND
18	**4r**	25	ND
19	**4s**	>25	ND
20	**4t**	>25	ND
21	**4u**	12.5	ND
22	**4v**	>25	ND
23	**4w**	>25	ND
24	**4x**	12.5	ND
25	**4y**	25	ND
26	**4z**	**6.25**	**19.04**
27	**4aa**	>25	ND
28	**4ab**	>25	ND
29	**4ac**	25	ND
30	**4ad**	>25	ND
31	**4ae**	25	ND
32	**4af**	>25	ND
33	**4ag**	>25	ND
34	**4ah**	>25	ND
35	**4ai**	>25	ND
36	**4aj**	>25	ND
37	**4ak**	12.5	ND
38	**4al**	25	ND
39	**Ethambutol**	**1.56**	ND

[a] % inhibition was examined using RAW 264.7 cell line, [b] ND = not determined.

3.2.2.2. Cytotoxicity studies

The promising anti-TB active compounds have been screened for their safety profile by the evaluation of cytotoxicity on normal RAW 264.7 cells at 25 µg/mL [40] and the results were depicted in Table 3.4. In this study, the promising anti-TB compounds **4a**, **4o**, and **4z** showed lower percentage of inhibition i.e., 27.72, 18.25 and 19.04% respectively to the normal RAW 264.7 cell line.

3.2.2.3. Structure activity relationship studies

The structure activity relationship (SAR) studies unveils that the diverse donor and acceptor abilities of substituted groups on the phenyl ring and presence of hetero aryl groups are crucial in their anti-tubercular activity of the synthesized compounds. The presence of Fluoro (–F) substitution on the phenyl ring is significantly enhances the anti-tubercular activity when compared to other substitutions.

3.3. Molecular docking studies

The outcome of the molecular docking study revealed that all the synthesized compounds **4a-al** were successfully docked, and efficiently fit into the active sites of the *Mycobacterium tuberculosis* protein (PDB ID: 1DF7) [41]. The results of the molecular docking study were presented in Table 3.5. Among all the screened compounds, thirteen compounds **4h**, **4i**, **4n**, **4o**, **4r**, **4u**, **4z**, **4ac**, **4ae**, **4ag**, **4ah**, **4aj** and **4ak** exhibit good binding energies as -1055, -10.49, -10.42, -10.82, -10.43, -10.50, -10.65, -10.41, -10.46, -10.56, -10.75, -10.59 and -10.49 kcal/mol respectively. Among these, the compound **4o** exhibits more negative binding energy -10.82, forms four hydrogen bonds with the amino acid residues ALA7 (2.21 Å), THR46 (2.44 Å), ILE94 (2.06 Å), TYR100 (2.26 Å) and shows two hydrophobic (π···π and π···alkyl) interactions with the amino acids. The compound **4z** exhibits binding energy -10.65 kcal/mol, forms five hydrogen bonds with the amino acid residues ALA7 (2.42 Å), THR46 (2.47 Å), ILE94 (2.04 Å), TYR100 (2.00 Å, 2.29 Å) and shows a hydrophobic (π···alkyl) interaction with the amino acid. Whereas, the compound **4ah** shows binding energy -10.75 kcal/mol, forms five hydrogen bonds with the amino acid residues ALA7 (2.24 Å), ASP27 (2.85 Å), THR46 (2.45 Å), ILE94 (2.05 Å), TYR100 (2.31 Å) and forms two hydrophobic (π···π and π···alkyl) interactions with the amino acids. The ligand interactions of the compounds **4o**, **4z** and **4ah** are presented in Figure 3.3, Figure 3.4 and Figure 3.5.

Table 3.5. Docking results of the compounds **4a-al** against 1DF7 protein

En-try	Com-pound	Binding energy (kcal/mol)	No. of hydrogen bonds	Residues involved in the hydrogen bonding	Hydrogen bond length (Å)
1	**4a**	-9.69	3	ALA7, ILE94, TYR100	1.88, 2.14, 2.65
2	**4b**	-10.02	3	ALA7, ILE94, TYR100	1.79, 2.09, 2.82
3	**4c**	-9.84	4	ALA7, ILE94, GLY97, TYR100	1.84, 2.17, 2.66, 2.78
4	**4d**	-10.16	5	ALA7, GLY18, SER49, ILE94, TYR100	1.96, 2.10, 2.40, 2.65, 3.35

5	**4e**	-9.94	6	ALA7, GLY18, THR46, SER49, ILE94, TYR100	1.71, 2.11, 2.12, 2.77, 2.88, 3.49
6	**4f**	-9.61	4	ALA7, THR46, ILE94, TYR100	2.05, 2.22, 2.23, 2.50
7	**4g**	-10.14	3	ALA7, ILE94, TYR100	1.84, 2.20, 2.70
8	**4h**	-10.55	4	ALA7, HIS30, ILE94, TYR100	1.74, 2.17, 3.05, 3.71
9	**4i**	-10.49	5	ALA7, THR46, ILE94, GLY97, TYR100	1.79, 2.07, 2.08, 2.76, 2.80
10	**4j**	-10.25	3	ALA7, ILE94, TYR100	1.75, 2.02, 3.00
11	**4k**	-9.54	4	ALA7, THR46, ILE94, TYR100	1.99, 2.20, 2.22, 2.35
12	**4l**	-9.90	4	ALA7, THR46, ILE94, TYR100	2.03, 2.36, 2.40, 2.50
13	**4m**	-10.16	4	ALA7, THR46, ILE94, TYR100	2.06, 2.42, 2.43, 2.49
14	**4n**	-10.42	5	ALA7, ASP27, THR46, ILE94, TYR100	2.04, 2.27, 2.27, 2.46, 2.84
15	**4o**	**-10.82**	4	ALA7, THR46, ILE94, TYR100	2.21, 2.44, 2.06, 2.26
16	**4p**	-10.29	3	ALA7, ILE94, TYR100	1.93, 2.41, 2.79
17	**4q**	-9.79	4	ALA7, THR46, ILE94, TYR100	2.03, 2.21, 2.23, 2.48
18	**4r**	-10.43	7	ALA7, ASP27, THR46, ILE94, TYR100	1.96, 2.07, 2.25, 2.44, 2.44, 2.85, 3.78
19	**4s**	-10.17	7	ALA7, ASP27, THR46, ILE94, TYR100	1.96, 2.01, 2.29, 2.36, 2.49, 2.85, 3.75
20	**4t**	-9.98	5	ALA7, ASP27, THR46, ILE94, TYR100	2.03, 2.33, 2.43, 2.44, 2.84
21	**4u**	-10.50	7	ALA7, ASP27, THR46, ILE94, TYR100	1.94, 2.03, 2.27, 2.39, 2.49, 2.86, 3.74
22	**4v**	-9.53	3	ALA7, ILE94, TYR100	1.88, 2.00, 2.35
23	**4w**	-9.82	4	ALA7, THR46, ILE94, TYR100	2.04, 2.29, 2.35, 2.40
24	**4x**	-9.55	5	ALA7, THR46, ILE94, TYR100	1.96, 2.04, 2.29, 2.37, 2.49
25	**4y**	-9.50	4	ALA7, THR46, ILE94, TYR100	2.06, 2.22, 2.22, 2.50
26	**4z**	**-10.65**	5	ALA7, THR46, ILE94, TYR100	2.42, 2.47, 2.04, 2.00, 2.29
27	**4aa**	-9.93	3	ALA7, ILE94, TYR100	1.81, 1.98, 2.85
28	**4ab**	-10.33	4	ALA7, THR46, ILE94, TYR100	2.04, 2.29, 2.35, 2.43
29	**4ac**	-10.41	5	ALA7, ASP27, THR46, ILE94, TYR100	2.15, 2.22, 2.24, 2.42, 2.87

30	**4ad**	-10.01	4	ALA7, THR46, ILE94, TYR100	2.04, 2.18, 2.25, 2.53
31	**4ae**	-10.46	4	ALA7, HIS30, ILE94, TYR100	1.98, 2.41, 2.58, 3.54
32	**4af**	-10.17	3	ALA7, ILE94, TYR100	1.86, 1.87, 2.63
33	**4ag**	-10.56	4	ALA7, THR46, ILE94, TYR100	2.05, 2.24, 2.42, 2.50
34	**4ah**	**-10.75**	5	ALA7, ASP27, THR46, ILE94, TYR100	2.24, 2.85, 2.45, 2.05, 2.31
35	**4ai**	-10.23	4	ALA7, THR46, ILE94, TYR100	2.06, 2.21, 2.23, 2.48
36	**4aj**	-10.59	4	ALA7, THR46, ILE94, TYR100	2.05, 2.25, 2.45, 2.53
37	**4ak**	-10.49	5	ALA7, THR46, ILE94, GLY97, TYR100	1.84, 1.93, 2.01, 2.69, 3.02
38	**4al**	-10.21	3	ALA7, ILE94, TYR100	1.76, 2.05, 2.96

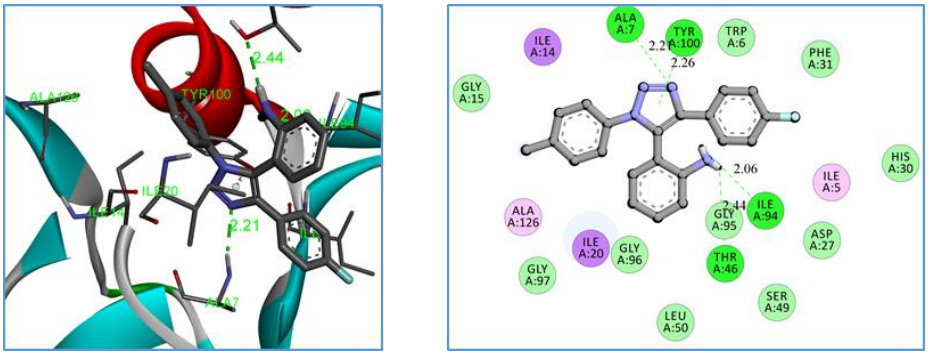

Figure 3.3. Binding interactions between compound **4o** with active site of 1DF7.

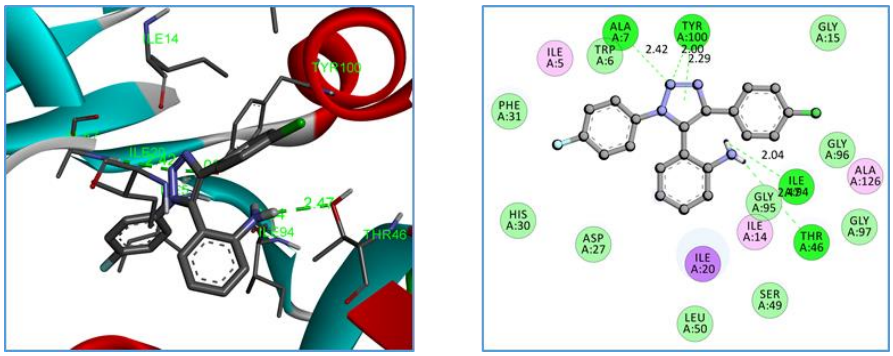

Figure 3.4. Binding interactions between compound **4z** with active site of 1DF7.

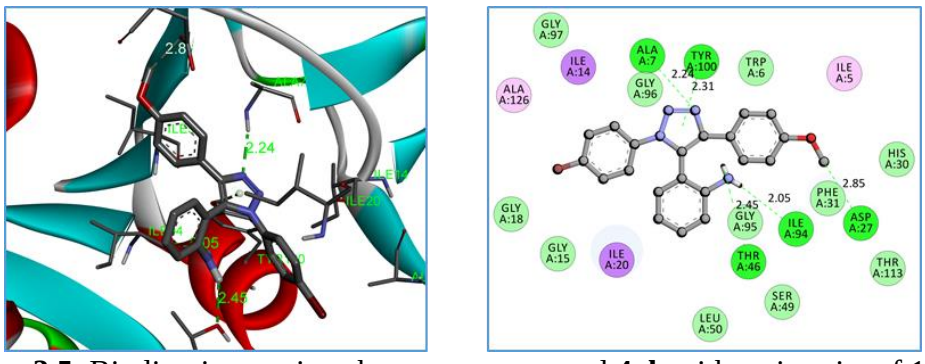

Figure 3.5. Binding interactions between compound **4ah** with active site of 1DF7.

3.4. ADME prediction

Absorption, distribution, metabolism and excretion (ADME) data improves the selection and identification of molecules at the therapeutic dose with an optimal safety profile. Also, *in silico* prediction of pharmacokinetic parameters lowers the risk of failure of drug at the final stages of clinical trials. ADME prediction results of the synthesized compounds were illustrated in Table 3.6.

Estimation of octanol/water partition coefficient (lipophilicity) is examined by LogP. The predicted lipophilicity values are in the ranging from 3.578 to 5.599, and these values revealed that moderate lipophilicity of the compounds. The predicted aqueous solubility (LogS) values of the synthesized compounds ranging from -3.535 to -6.597, which reflects their moderate solubility in water due to presence of lipophilic groups. On the other hand, the topological polar surface area (TPSA) values (≤140 Å) reveals that the compounds' oral bioavailability is high. In general, higher the logarithm of the apparent permeability coefficient (logPapp) higher will be the Caco-2 permeability. From the results, it is predicted that all the compounds have shown medium Caco-2 permeability in the range from 0.44 x 10^{-6} to 1.36 x 10^{-6}. Interestingly, all the synthesized compounds exhibit high human intestinal absorption (HIA: 95.638–100%). Blood/brain partition co-efficient (logBB) value is a measure of the ability of a drug to cross the blood-brain barrier (BBB). The target compounds are in considerable range of BBB. The observed drug like properties and *in silico* ADME prediction suggests that the synthesized compounds **4a-al** exhibit acceptable pharmacokinetic parameters and can be considered as lead molecules for the development of novel drugs.

Table 3.6. Drug likeliness and *in silico* ADME properties of the compounds **4a-al**

En-try	**Mol. Wt**	**H-donor**	**H-acceptor**	**No. of rotatable bonds**	**LogP**	**LogS**	**TPSA (Å)**	**Caco-2 Permeability (logPapp in 10^{-6} cm/s)**	**HIA (% absorbed)**	**BBB permeability (log BB)**
	≤500	**≤5**	**≤10**	**≤10**	**≤5**	**<0.5**	**≤140**	**>8x10^{-6}**	**70 - 100%**	**-3.0 - 1.2**
4a	312.376	1	4	3	4.1835	-4.755	56.73	1.366	98.755	0.327
4b	326.403	1	4	3	4.4919	-5.212	56.73	1.366	98.7	0.293
4c	342.402	1	5	4	4.1921	-4.973	65.96	0.522	99.642	0.19
4d	342.402	1	5	4	4.1921	-4.966	65.96	0.446	99.42	0.153
4e	372.428	1	6	5	4.2007	-4.665	75.19	0.972	100	-0.809
4f	330.366	1	4	3	4.3226	-5.045	56.73	1.357	98.234	0.312
4g	346.821	1	4	3	4.8369	-5.730	56.73	1.025	97.242	0.28
4h	391.272	1	4	3	4.946	-5.820	56.73	1.022	97.853	0.293
4i	357.373	1	6	4	4.0917	-5.680	99.87	1.086	99.085	-0.868

4j	337.386	1	5	3	4.0552	-5.443	80.52	0.519	99.719	-0.5
4k	313.364	1	5	3	3.5785	-3.535	69.62	0.855	100	-0.565
4l	326.403	1	4	3	4.4919	-5.188	56.73	1.366	98.677	0.293
4m	340.43	1	4	3	4.8003	-5.608	56.73	1.021	98.622	0.259
4n	356.429	1	5	4	4.5005	-5.365	65.96	0.593	99.564	0.156
4o	344.393	1	4	3	4.6310	-5.452	56.73	1.068	98.156	0.279
4p	360.848	1	4	3	5.1453	-6.149	56.73	1.019	97.164	0.246
4q	342.402	1	5	4	4.1921	-4.945	65.96	0.502	99.7	0.03
4r	356.429	1	5	4	4.5005	-5.365	65.96	0.574	99.645	-0.004
4s	372.428	1	6	5	4.2007	-5.192	75.19	0.92	100	-0.834
4t	360.392	1	5	4	4.3312	-5.287	65.96	0.883	99.179	0.016
4u	376.847	1	5	4	4.8455	-5.950	65.96	0.524	98.186	-0.017
4v	330.366	1	4	3	4.3226	-5.008	56.73	1.358	98.287	0.154
4w	344.393	1	4	3	4.6310	-5.452	56.73	1.065	98.232	0.12
4x	360.392	1	5	4	4.3312	-5.287	65.96	0.88	99.174	0.017
4y	348.356	1	4	3	4.4617	-5.364	56.73	1.112	97.766	0.139
4z	364.811	1	4	3	4.976	-6.057	56.73	1.063	96.774	0.107
4aa	346.821	1	4	3	4.8369	-5.689	56.73	1.026	97.219	0.28
4ab	360.848	1	4	3	5.1453	-6.149	56.73	1.019	97.164	0.246
4ac	376.847	1	5	4	4.8455	-5.950	65.96	0.544	98.106	0.143
4ad	364.811	1	4	3	4.976	-6.057	56.73	1.066	96.698	0.266
4ae	381.266	1	4	3	5.4903	-6.479	56.73	1.017	95.705	0.233
4af	391.272	1	4	3	4.946	-5.801	56.73	1.023	97.152	0.278
4ag	405.299	1	4	3	5.2544	-6.281	56.73	1.017	97.097	0.245
4ah	421.298	1	5	4	4.9546	-6.070	65.96	0.535	98.039	0.142
4ai	409.262	1	4	3	5.0851	-6.182	56.73	1.064	96.631	0.264
4aj	425.717	1	4	3	5.5994	-6.597	56.73	1.015	95.638	0.232
4ak	357.373	1	6	4	4.0917	-5.642	99.87	1.095	99.085	-0.877
4al	337.386	1	5	3	4.0552	-5.409	80.52	0.522	99.7	-0.509

Mol. Wt: molecular weight; **H-donor**: number of hydrogen bond donors; **H-acceptor**: number of hydrogen bond acceptors; **LogP**: octanol/water partition coefficient; **LogS**: aqua solubility parameter; **TPSA**: topological polar surface area; **Caco-2**: cell permeability; **HIA**: human intestinal absorption; **LogBB**: blood/brain partition co-efficient.

3.5. Conclusion

In this chapter we have introduced a photoinduced regioselective synthesis of 1,4,5-trisubstituted-1,2,3-triazoles under transition metal-, azide- and oxidant- free protocol. From this method a library of 38 compounds were synthesized with wide variety of functional groups. This method is amicable with most of the functional groups and able to produce title compounds in good to excellent yields. Further, *in vitro* anti-TB activity of the synthesized compounds were investigated against *Mycobacterium tuberculosis* H37Rv. Among them, three compounds **4o**, **4z** and **4ah** exhibited significant activity with MIC value 6.25 µg/mL, whereas the compounds **4e**, **4k**, **4p**, **4u**, **4x** and **4ak** showed moderate activity with MIC value 12.5 µg/mL when compared to the standard drug ethambutol (MIC:

1.56 µg/mL). The significant active compounds were exhibited relatively low levels of cytotoxicity against RAW 264.7 cell line. In addition, *in silico* molecular docking studies and ADME prediction revealed that the title compounds could be considered as lead molecules in future research.

3.6. Experimental Section

3.6.1. General procedure for 1,4,5-trisubstituted-1,2,3-triazoles (4a-al)

To a solution of aldehyde **2** (1.0 mmol) in DMF, tosylhydrazine **3** was added (1.0 mmol) and continued the reaction for 10 min, to this isatin Schiff base **1** (1.0 mmol) and Cs_2CO_3 (3.0 equiv) were added. The mixture was heated to 100 °C for 6-8 h under sunlight. The progress of the reaction was monitored by TLC. After completion, the reaction mixture was cooled to room temperature and added water. The resulting solid product was filtered and dried under vacuum. The residue was purified by column chromatography on silica gel with ethyl acetate in *n*-hexane (5-10% V/V) as an eluent to afford the targeted compounds.

3.6.2. Protocol for the anti-TB screening

The MIC of the synthesized compounds was tested using *in vitro* Microplate Alamar Blue Assay using the reported protocol [42]. The *Mycobacterium tuberculosis* H37Rv strain (ATCC27294) was used for the screening. The inoculum was prepared from fresh LJ medium re-suspended in 7H9-S medium (7H9 broth, 0.1% casitone, 0.5% glycerol, supplemented oleic acid, albumin, dextrose, and catalase [OADC]), adjusted to a OD_{590} 1.0, and diluted 1:20; 100 µL was used as inoculum. Each drug stock solution was thawed and diluted in 7H9-S at four-fold the final highest concentration tested. Serial two-fold dilutions of each drug were prepared directly in a sterile 96-well microtiter plate using 100 µL 7H9-S. A growth control containing no antibiotic and a sterile control were also prepared on each plate. Sterile water was added to all perimetre wells to avoid evaporation during the incubation. The plate was covered, sealed in plastic bags and incubated at 37 ^oC in normal atmosphere. After 7 days incubation, 30 µL of alamar blue solution was added to each well, and the plate was re-incubated overnight. A change in colour from blue (oxidised state) to pink (reduced) indicated the growth of bacteria, and the MIC was defined as the lowest concentration of drug that prevented this change in colour.

3.6.3. *In vitro* cytotoxicity screening

The *in vitro* cytotoxicity of the privileged anti-tubercular active analogues with lower MIC value were assessed by 3-(4,5-dimethylthiazol-2-yl)-2,5-diphenyltetrazolium

bromide (MTT) assay against growth inhibition of RAW 264.7 cells at 25 μg/mL concentration [43]. Cell lines were maintained at 37 °C in a humidified 5% CO_2 incubator (Thermo scientific). Detached the adhered cells and followed by centrifugation to get cell pellet. Fresh media was added to the pellet to make a cell count using haemocytometer and plate 100 μL of media with cells ranging from 5,000 - 6,000 per well in a 96-well plate. The plate was incubated overnight in CO_2 incubator for the cells to adhere and regain its shape. After 24 h cells were treated with the test compounds at 25 μg/mL diluted using the media to deduce the percentage inhibition on normal cells. The cells were incubated for 48 h to assay the effect of the test compounds on different cell lines. Zero hour reading was noted down with untreated cells and also control with 1% DMSO to subtract further from the 48 h reading. After 48 h incubation, cells were treated by MTT (4,5-dimethylthiazol-2-yl)-2,5-diphenyltetrazolium bromide) dissolved in PBS (5 mg/mL) and incubated for 3-4 h at 37 °C. The formazan crystals thus formed were dissolved in 100 μL of DMSO and the viability was measured at 540 nm on a multimode reader (Spectra max). The values were further calculated for percentage inhibition which in turn helps us to know the cytotoxicity of the test compounds.

3.6.4. Molecular docking protocol

The docking studies are prominent tools for the assessment of the binding affinity to the ligand-protein receptor. All the synthesized compounds were subjected to *in silico* molecular docking studies by using the AutoDockTools (ADT) version 1.5.6 and AutoDock version 4.2.5.1 docking program [44]. The 3D-structures of all the synthesized compounds were prepared by using chem3D pro 12.0 software. The optimized 3D structures were saved in pdb format. The structure of the dihydrofolate reductase of *Mycobacterium tuberculosis* (PDB code: 1DF7) protein was extracted from the protein data bank (http://www.rcsb.org/pdb). The bound ligand and water molecules in protein were removed by using Discovery Studio Visualizer version 4.0 to prepare the protein. Non polar hydrogens were merged and gasteiger charges were added to the protein. The grid file was saved in gpf format. The three dimensional grid box having dimensions 60 x 60 x 60 $Å^3$ was created around the protein with spacing 0.3750 Å. The genetic algorithm was carried out with the population size and the maximum number of evaluations were 150 and 25,00,000 respectively. The docking output file was saved as Lamarckian Ga (4.2) in dpf format. The ligand-protein complex binding sites were visualized by Discovery Studio Visualizer version 4.0.

3.6.5. ADME prediction

In silico ADME properties of these synthesized compounds were calculated by using the online servers ADMETlab 2.0 and pkCSM [45]. The ADMET properties, human intestinal absorption (HIA), Caco-2 cell permeability, plasma protein binding and blood brain barrier penetration (BBB) were predicted using this program.

3.7. Characterization data of products 4a-al

2-(1,4-diphenyl-1*H*-1,2,3-triazol-5-yl)aniline (4a)

White solid. mp: 187-189 °C. IR (KBr, cm^{-1}): 3458, 3368, 1618. ^1H NMR (400 MHz, DMSO-d_6) δ: 7.65 (d, J = 7.6 Hz, 2H), 7.53 (s, 1H), 7.50 (d, J = 6.4 Hz, 2H), 7.44 (d, J = 6.0 Hz, 2H), 7.35 (t, J = 7.2 Hz, 2H), 7.29 (d, J = 6.8 Hz, 1H), 7.12 (t, J = 7.6 Hz, 1H), 6.90 (d, J = 7.6 Hz, 1H), 6.71 (d, J = 8.4 Hz, 1H), 6.50 (t, J = 7.2 Hz, 1H), 5.21 (s, 2H). ^{13}C NMR (125 MHz, DMSO-d_6) δ: 161.96, 148.15, 144.31, 136.90, 134.26, 132.29, 131.61, 131.57, 131.26, 129.58, 129.52, 129.01, 128.15, 126.28, 125.33, 116.37, 115.30, 110.87. HRMS (ESI, m/z): $[M+H]^+$ calcd. for $C_{20}H_{17}N_4$: 313.1453; found: 313.1445.

2-(1-phenyl-4-(*p*-tolyl)-1*H*-1,2,3-triazol-5-yl)aniline (4b)

Off-white solid. mp: 170-172 °C. IR (KBr, cm^{-1}): 3451, 3365, 1618. ^1H NMR (400 MHz, DMSO-d_6) δ: 7.52 – 7.47 (m, 4H), 7.43 (d, J = 2.8 Hz, 3H), 7.15 – 7.11 (m, 3H), 6.87 (d, J = 6.0 Hz, 1H), 6.70 (d, J = 6.8 Hz, 1H), 6.49 (s, 1H), 5.17 (s, 2H), 2.27 (s, 3H). ^{13}C NMR (125 MHz, DMSO-d_6) δ: 162.15, 148.01, 145.27, 139.01, 133.33, 132.84, 132.22, 130.34, 128.36, 128.29, 126.96, 117.75, 117.22, 117.04, 116.12, 111.07, 21.62. HRMS (ESI, m/z): $[M+H]^+$ calcd. for $C_{21}H_{19}N_4$: 327.1610; found: 327.1593.

2-(4-(4-methoxyphenyl)-1-phenyl-1*H*-1,2,3-triazol-5-yl)aniline (4c)

Pale yellow solid. mp: 150-152 °C. IR (KBr, cm^{-1}): 3424, 3336, 1616. ^1H NMR (400 MHz, DMSO-d_6) δ: 7.82 (d, J = 8.8 Hz, 2H), 7.48 (t, J = 7.2 Hz, 2H), 7.44 (d, J = 6.0 Hz, 2H), 7.11 (t, J = 8.0 Hz, 1H), 7.06 (d, J = 8.4 Hz, 2H), 6.92 (d, J = 8.8 Hz, 2H), 6.71 (d, J = 8.4 Hz, 1H), 6.50 (t, J = 7.2 Hz, 1H), 5.17 (s, 2H), 3.83 (s, 3H). ^{13}C NMR (125 MHz, DMSO-d_6) δ: 162.15, 160.98, 148.12, 136.96, 131.67, 131.32, 131.19, 130.47, 129.51, 127.62, 125.25, 124.00, 116.41, 115.28, 114.87, 114.48, 111.06, 55.54. HRMS (ESI, m/z): $[M+H]^+$ calcd. for $C_{21}H_{19}N_4O$: 343.1559; found: 343.1551.

2-(4-(3-methoxyphenyl)-1-phenyl-1*H*-1,2,3-triazol-5-yl)aniline (4d)

White solid. mp: 153-155 °C. IR (KBr, cm^{-1}): 3427, 3378, 1615. ^{1}H NMR (400 MHz, DMSO-d_6) δ: 8.63 (s, 1H), 7.82 (d, J = 8.4 Hz, 2H), 7.57 – 7.51 (m, 4H), 7.06 (d, J = 8.4 Hz, 2H), 6.91 (t, J = 8.4 Hz, 2H), 6.71 (d, J = 8.4 Hz, 1H), 6.52 (t, J = 7.2 Hz, 1H), 5.19 (s, 2H), 3.83 (s, 3H). ^{13}C NMR (100 MHz, DMSO-d_6) δ: 148.19, 132.80, 132.44, 131.61, 131.25, 130.09, 129.53, 125.39, 125.34, 119.42, 118.60, 117.71, 116.39, 114.11, 113.76, 113.14, 111.61, 110.93, 55.18. ESI-MS (m/z): $[M+H]^+$ calcd. for $C_{21}H_{19}N_4O$: 343.15; found: 343.15.

2-(4-(3,4-dimethoxyphenyl)-1-phenyl-1*H*-1,2,3-triazol-5-yl)aniline (4e)

Off-white solid. mp: 166-168 °C. IR (KBr, cm^{-1}): 3365, 3236, 1617. ^{1}H NMR (400 MHz, DMSO-d_6) δ: 7.52 – 7.46 (m, 2H), 7.44 (d, J = 6.4 Hz, 1H), 7.25 – 7.18 (m, 3H), 7.12 (t, J = 6.8 Hz, 1H), 6.98 (d, J = 7.2 Hz, 1H), 6.95 – 6.91 (m, 1H), 6.88 (d, J = 5.6 Hz, 1H), 6.73 (d, J = 8.0 Hz, 1H), 6.51 (t, J = 7.6 Hz, 1H), 5.21 (s, 2H), 3.73 (s, 3H), 3.57 (s, 3H). ^{13}C NMR (100 MHz, DMSO-d_6) δ: 148.96, 148.86, 148.27, 131.72, 131.15, 130.08, 129.54, 129.08, 125.25, 118.71, 117.71, 116.41, 115.24, 114.13, 112.38, 109.97, 55.94, 55.38. ESI-MS (m/z): $[M+H]^+$ calcd. for $C_{22}H_{21}N_4O_2$: 373.17; found: 373.15.

2-(4-(4-fluorophenyl)-1-phenyl-1*H*-1,2,3-triazol-5-yl)aniline (4f)

White solid. mp: 176-178 °C. IR (KBr, cm^{-1}): 3454, 3365, 1616. ^{1}H NMR (400 MHz, DMSO-d_6) δ: 7.65 (bs, 2H), 7.45 (bs, 5H), 7.19 (bs, 2H), 7.11 (s, 1H), 6.88 (d, J = 4.0 Hz, 1H), 6.70 (t, J = 6.4 Hz, 1H), 6.49 (d, J = 8.4 Hz, 1H), 5.22 (s, 2H). ^{13}C NMR (125 MHz, DMSO-d_6) δ: 163.14 (d, J = 243.6 Hz), 148.15, 143.54, 136.85, 132.15, 131.59, 131.34, 129.61, 129.53, 128.30 (d, J = 7.6 Hz), 128.09, 125.32, 116.42, 116.01(d, J = 21.4 Hz), 115.35, 110.58. HRMS (ESI, m/z): $[M+H]^+$ calcd. for $C_{20}H_{16}FN_4$: 331.1359; found: 331.1341.

2-(4-(4-chlorophenyl)-1-phenyl-1*H*-1,2,3-triazol-5-yl)aniline (4g)

White solid. mp: 184-186 °C. IR (KBr, cm^{-1}): 3457, 3360, 1621. ^{1}H NMR (400 MHz, DMSO-d_6) δ: 7.64 (d, J = 7.2 Hz, 2H), 7.53 (q, J = 8.4 Hz, 4H), 7.34 (t, J = 7.6 Hz, 2H), 7.29 (d, J = 7.2 Hz, 1H), 7.14 (t, J = 7.6 Hz, 1H), 6.92 (d, J = 7.2 Hz, 1H), 6.71 (d, J = 8.0 Hz, 1H), 6.52 (t, J = 7.2 Hz, 1H), 5.23 (s, 2H). ^{13}C NMR (125 MHz, DMSO-d_6) δ: 148.07, 143.29, 136.77, 132.84, 132.59, 131.53, 131.41, 130.45, 130.07, 129.55, 129.12, 127.90, 125.35, 116.46, 115.39, 110.42. HRMS (ESI, m/z): $[M+H]^+$ calcd. for $C_{20}H_{16}ClN_4$: 347.1063; found: 347.1058.

2-(4-(3-bromophenyl)-1-phenyl-1*H*-1,2,3-triazol-5-yl)aniline (4h)

Off-white solid. mp: 142-144 °C. IR (KBr, cm^{-1}): 3427, 3379, 1618. ^1H NMR (400 MHz, DMSO-d_6) δ: 7.64 (d, J = 7.6 Hz, 2H), 7.53 (d, J = 14.0 Hz, 3H), 7.44 (d, J = 8.0 Hz, 2H), 7.33 (t, J = 8.0 Hz, 2H), 7.13 (t, J = 7.6 Hz, 1H), 6.92 (d, J = 6.8 Hz, 1H), 6.71 (d, J = 8.0 Hz, 1H), 6.52 (t, J = 6.8 Hz, 1H), 5.28 (s, 2H). ^{13}C NMR (100 MHz, DMSO-d_6) δ: 148.14, 142.83, 136.75, 133.94, 133.90, 131.50, 131.32, 130.70, 130.08, 129.57, 128.78, 127.20, 125.36, 125.03, 122.37, 117.71, 116.44, 115.36, 110.27. ESI-MS (m/z): $[M+H]^+$ calcd. for $C_{20}H_{16}BrN_4$: 391.05; found: 391.05.

2-(4-(4-nitrophenyl)-1-phenyl-1*H*-1,2,3-triazol-5-yl)aniline (4i)

Yellow solid. mp: 174-176 °C. IR (KBr, cm^{-1}): 3457, 3360, 1621. ^1H NMR (400 MHz, DMSO-d_6) δ: 8.23 (d, J = 8.8 Hz, 2H), 7.88 (d, J = 8.8 Hz, 2H), 7.50 (s, 2H), 7.47 (d, J = 5.2 Hz, 3H), 7.16 (t, J = 8.0 Hz, 1H), 6.93 (d, J = 7.2 Hz, 1H), 6.74 (d, J = 8.4 Hz, 1H), 6.52 (t, J = 7.6 Hz, 1H), 5.32 (s, 2H). ^{13}C NMR (100 MHz, DMSO-d_6) δ: 148.10, 146.99, 142.44, 138.12, 136.61, 134.25, 131.64, 131.43, 130.08, 129.86, 129.60, 126.85, 125.47, 124.46, 117.70, 116.52, 115.54, 109.90. ESI-MS (m/z): $[M+H]^+$ calcd. for $C_{20}H_{16}N_5O_2$: 358.13; found: 358.15.

4-(5-(2-aminophenyl)-1-phenyl-1*H*-1,2,3-triazol-4-yl)benzonitrile (4j)

White solid. mp: 164-166 °C. IR (KBr, cm^{-1}): 3444, 3354, 2227, 1613. ^1H NMR (400 MHz, DMSO-d_6) δ: 7.63 (d, J = 7.2 Hz, 2H), 7.34 (dd, J = 16.4, 7.6 Hz, 4H), 7.28 (d, J = 7.2 Hz, 1H), 7.23 (d, J = 8.0 Hz, 2H), 7.11 (t, J = 7.6 Hz, 1H), 6.88 (d, J = 7.2 Hz, 1H), 6.70 (d, J = 8.0 Hz, 1H), 6.49 (t, J = 7.2 Hz, 1H), 5.17 (s, 2H). ^{13}C NMR (100 MHz, DMSO-d_6) δ: 148.10, 142.68, 136.64, 136.17, 133.12, 131.59, 131.43, 130.08, 129.82, 129.58, 128.70, 126.58, 125.44, 119.26, 117.70, 116.48, 115.48, 110.50, 110.05. ESI-MS (m/z): $[M+H]^+$ calcd. for $C_{21}H_{16}N_5$: 338.14; found: 338.15.

2-(1-phenyl-4-(pyridin-4-yl)-1*H*-1,2,3-triazol-5-yl)aniline (4k)

White solid. mp: 155-157 °C. IR (KBr, cm^{-1}): 3363, 3235, 1617. ^1H NMR (400 MHz, DMSO-d_6) δ: 8.54 (d, J = 0.4 Hz, 2H), 7.55 (d, J = 0.4 Hz, 2H), 7.50 (bs, 2H), 7.46 (bs, 3H), 7.15 (t, J = 6.4 Hz, 1H), 6.92 (d, J = 6.8 Hz, 1H), 6.74 (d, J = 7.2 Hz, 1H), 6.52 (t, J = 8.0 Hz, 1H), 5.30 (s, 2H). ^{13}C NMR (100 MHz, DMSO-d_6) δ: 150.50, 148.08, 141.84, 138.80, 136.59, 134.31, 131.62, 131.37, 129.85, 129.59, 125.45, 120.20, 116.46, 115.46, 109.97. ESI-MS (m/z): $[M+H]^+$ calcd. for $C_{19}H_{16}N_5$: 314.14; found: 314.10.

2-(4-phenyl-1-(*p*-tolyl)-1*H*-1,2,3-triazol-5-yl)aniline (4l)

Off-white solid. mp: 209-211 °C. IR (KBr, cm^{-1}): 3447, 3360, 1619. ^{1}H NMR (400 MHz, DMSO-d_6) δ: 7.64 (d, J = 7.2 Hz, 2H), 7.38-7.32 (m, 4H), 7.28 (d, J = 7.2 Hz, 1H), 7.24 (d, J = 8.0 Hz, 2H), 7.11 (t, J = 7.6 Hz, 1H), 6.88 (d, J = 7.2 Hz, 1H), 6.70 (d, J = 8.0 Hz, 1H), 6.50 (t, J = 7.6 Hz, 1H), 5.17 (s, 2H), 2.31 (s, 3H). ^{13}C NMR (125 MHz, DMSO-d_6) δ: 148.07, 143.17, 139.35, 134.38, 132.78, 132.58, 131.54, 131.34, 130.54, 129.95, 129.11, 127.86, 125.22, 116.42, 115.36, 110.53, 21.10. HRMS (ESI, m/z): $[M+H]^+$ calcd. for $C_{21}H_{19}N_4$: 327.1610; found: 327.1600.

2-(1,4-di-*p*-tolyl-1*H*-1,2,3-triazol-5-yl)aniline (4m)

Off-white solid. mp: 180-182 °C. IR (KBr, cm^{-1}): 3448, 3366, 1614. ^{1}H NMR (400 MHz, DMSO-d_6) δ: 7.51 (d, J = 8.0 Hz, 2H), 7.36 (d, J = 8.0 Hz, 2H), 7.23 (d, J = 8.0 Hz, 2H), 7.14 (d, J = 8.0 Hz, 2H), 7.10 (d, J = 7.2 Hz, 1H), 6.86 (d, J = 7.2 Hz, 1H), 6.70 (d, J = 8.0 Hz, 1H), 6.49 (t, J = 7.6 Hz, 1H), 5.14 (s, 2H), 2.31 (s, 3H), 2.27 (s, 3H). ^{13}C NMR (125 MHz, DMSO-d_6) δ: 148.06, 144.31, 139.18, 137.42, 134.53, 131.89, 131.63, 131.13, 129.92, 129.56, 128.80, 126.23, 125.16, 116.36, 115.25, 111.08, 21.23, 21.09. HRMS (ESI, m/z): $[M+H]^+$ calcd. for $C_{22}H_{21}N_4$: 341.1766; found: 341.1761.

2-(4-(4-methoxyphenyl)-1-(*p*-tolyl)-1*H*-1,2,3-triazol-5-yl)aniline (4n)

Pale yellow solid. mp: 197-199 °C. IR (KBr, cm^{-1}): 3435, 3337, 1618. ^{1}H NMR (400 MHz, DMSO-d_6) δ: 7.55 (d, J = 7.6 Hz, 2H), 7.35 (d, J = 8.0 Hz, 2H), 7.23 (d, J = 7.6 Hz, 2H), 7.12 – 7.05 (m, 1H), 6.91 (d, J = 8.4 Hz, 2H), 6.86 (d, J = 7.2 Hz, 1H), 6.70 (d, J = 7.6 Hz, 1H), 6.49 (t, J = 7.6 Hz, 1H), 5.14 (s, 2H), 3.73 (s, 3H), 2.31 (s, 3H). ^{13}C NMR (125 MHz, DMSO-d_6) δ: 159.93, 148.06, 144.15, 137.38, 132.04, 131.67, 131.10, 129.99, 129.56, 128.86, 126.86, 126.20, 119.95, 116.34, 115.24, 114.54, 111.93, 111.12, 55.87, 21.23. HRMS (ESI, m/z): $[M+H]^+$ calcd. for $C_{22}H_{21}N_4O$: 357.1715; found: 357.1708.

2-(4-(4-fluorophenyl)-1-(*p*-tolyl)-1*H*-1,2,3-triazol-5-yl)aniline (4o)

White solid. mp: 139-141 °C. IR (KBr, cm^{-1}): 3447, 3353, 1621. ^{1}H NMR (400 MHz, DMSO-d_6) δ: 7.65 (t, J = 6.4 Hz, 2H), 7.36 (d, J = 7.6 Hz, 2H), 7.24 (d, J = 8.4 Hz, 3H), 7.18 (d, J = 8.8 Hz, 1H), 7.12 (t, J = 7.6 Hz, 1H), 6.88 (d, J = 7.2 Hz, 1H), 6.70 (d, J = 7.6 Hz, 1H), 6.50 (t, J = 8.0 Hz, 1H), 5.20 (s, 2H), 2.31 (s, 3H). ^{13}C NMR (125 MHz, DMSO-d_6) δ: 163.12 (d, J = 243.5 Hz), 148.12, 143.44, 139.30, 134.44, 132.14, 131.61, 131.29 129.95, 128.27 (d, J = 8.1 Hz), 125.19, 116.42, 116.01(d, J = 21.4 Hz), 115.33, 110.70, 21.09. HRMS (ESI, m/z): $[M+H]^+$ calcd. for $C_{21}H_{18}FN_4$: 345.1515; found: 345.1511.

2-(4-(4-chlorophenyl)-1-(*p*-tolyl)-1*H*-1,2,3-triazol-5-yl)aniline (4p)

Off-white solid. mp: 204-206 °C. IR (KBr, cm^{-1}): 3451, 3354, 1623. ^1H NMR (400 MHz, DMSO-d_6) δ: 7.63 (d, J = 8.4 Hz, 2H), 7.42 (d, J = 8.8 Hz, 2H), 7.36 (d, J = 8.4 Hz, 2H), 7.24 (d, J = 8.4 Hz, 2H), 7.12 (t, J = 7.6 Hz, 1H), 6.88 (d, J = 6.8 Hz, 1H), 6.70 (d, J = 8.0 Hz, 1H), 6.50 (t, J = 7.6 Hz, 1H), 5.21 (s, 2H), 2.31 (s, 3H). ^{13}C NMR (100 MHz, DMSO-d_6) δ: 148.05, 143.20, 139.40, 134.37, 132.82, 132.59, 131.55, 131.37, 130.52, 129.98, 129.12, 127.89, 125.23, 116.48, 115.39, 110.55, 21.12. HRMS (ESI, m/z): $[M+H]^+$ calcd. for $C_{21}H_{18}ClN_4$: 361.1220; found: 361.1208.

2-(1-(4-methoxyphenyl)-4-phenyl-1*H*-1,2,3-triazol-5-yl)aniline (4q)

Off-white solid. mp: 157-159 °C. IR (KBr, cm^{-1}): 3450, 3329, 1611. ^1H NMR (400 MHz, DMSO-d_6) δ: 7.63 (d, J = 7.6 Hz, 2H), 7.42 (d, J = 8.8 Hz, 2H), 7.34 (t, J = 7.6 Hz, 2H), 7.28 (d, J = 7.2 Hz, 1H), 7.11 (t, J = 8.0 Hz, 1H), 6.98 (d, J = 8.8 Hz, 2H), 6.90 (d, J = 7.6 Hz, 1H), 6.70 (d, J = 8.0 Hz, 1H), 6.50 (t, J = 7.6 Hz, 1H), 5.17 (s, 2H), 3.76 (s, 3H). ^{13}C NMR (125 MHz, DMSO-d_6) δ: 159.96, 148.10, 144.04, 132.42, 131.65, 131.17, 129.84, 128.99, 128.06, 126.89, 126.21, 119.95, 116.35, 115.27, 115.19, 114.55, 113.91, 111.93, 111.00, 55.88. HRMS (ESI, m/z): $[M+H]^+$ calcd. for $C_{21}H_{19}N_4O$: 343.1559; found: 343.1550.

2-(1-(4-methoxyphenyl)-4-(*p*-tolyl)-1*H*-1,2,3-triazol-5-yl)aniline (4r)

Off-white solid. mp: 140-142 °C. IR (KBr, cm^{-1}): 3471, 3379, 1618. ^1H NMR (400 MHz, DMSO-d_6) δ: 7.51 (d, J = 8.0 Hz, 2H), 7.41 (d, J = 8.8 Hz, 2H), 7.14 (d, J = 8.0 Hz, 2H), 7.09 (d, J = 7.2 Hz, 1H), 6.97 (d, J = 8.8 Hz, 2H), 6.88 (d, J = 7.6 Hz, 1H), 6.69 (d, J = 8.0 Hz, 1H), 6.50 (t, J = 7.6 Hz, 1H), 5.13 (s, 2H), 3.76 (s, 3H), 2.27 (s, 3H). ^{13}C NMR (125 MHz, DMSO-d_6) δ: 159.93, 148.03, 132.04, 131.66, 131.11, 130.00, 129.56, 128.80, 126.87, 126.20, 119.96, 116.37, 115.25, 115.19, 114.54, 111.10, 55.87, 21.22. HRMS (ESI, m/z): $[M+H]^+$ calcd. for $C_{22}H_{21}N_4O$: 357.1715; found: 357.1700.

2-(1,4-bis(4-methoxyphenyl)-1*H*-1,2,3-triazol-5-yl)aniline (4s)

Off-white solid. mp: 141-143 °C. IR (KBr, cm^{-1}): 3470, 3380, 1604. ^1H NMR (400 MHz, DMSO-d_6) δ: 7.55 (d, J = 8.8 Hz, 2H), 7.41 (d, J = 8.8 Hz, 2H), 7.06 (d, J = 8.8 Hz, 2H), 6.97 (d, J = 8.8 Hz, 2H), 6.91 (d, J = 8.8 Hz, 2H), 6.70 (d, J = 8.4 Hz, 1H), 6.50 (t, J = 7.2 Hz, 1H), 5.13 (s, 2H), 3.76 (s, 3H), 3.74 (s, 3H). ^{13}C NMR (125 MHz, DMSO-d_6) δ: 160.97, 148.10, 134.67, 131.71, 131.09, 130.45, 129.94, 127.54, 126.83, 125.43, 124.15, 119.95,

116.36, 115.24, 114.87, 114.54, 114.46, 111.20, 55.86, 55.53. HRMS (ESI, m/z): $[M+H]^+$ calcd. for $C_{22}H_{21}N_4O_2$: 373.1665; found: 373.1653.

2-(4-(4-fluorophenyl)-1-(4-methoxyphenyl)-1*H*-1,2,3-triazol-5-yl)aniline (4t)

Off-white solid. mp: 137-139 °C. IR (KBr, cm^{-1}): 3448, 3328, 1610. ^1H NMR (400 MHz, DMSO-d_6) δ: 7.64 (s, 2H), 7.41 (s, 2H), 7.33 (s, 1H), 7.18 (s, 2H), 6.98 (s, 2H), 6.90 (s, 1H), 6.70 (s, 1H), 6.49 (s, 1H), 5.19 (s, 2H), 3.76 (s, 3H). ^{13}C NMR (125 MHz, DMSO-d_6) δ: 162.13 (d, J = 243.4 Hz), 148.10, 143.28, 134.68, 132.28, 131.64, 131.26, 129.79, 128.22 (d, J = 7.3 Hz), 126.89, 125.42, 119.95, 116.41, 116.01, (d, J = 21.4 Hz), 115.33, 115.19, 114.56, 110.73, 55.87. HRMS (ESI, m/z): $[M+H]^+$ calcd. for $C_{21}H_{18}FN_4O$: 361.1465; found: 361.1460.

2-(4-(4-chlorophenyl)-1-(4-methoxyphenyl)-1*H*-1,2,3-triazol-5-yl)aniline (4u)

White solid. mp: 138-140 °C. IR (KBr, cm^{-1}): 3475, 3370, 1619. ^1H NMR (400 MHz, DMSO-d_6) δ: 7.62 (d, J = 6.4 Hz, 2H), 7.41 (d, J = 2.4 Hz, 4H), 7.11 (t, J = 7.2 Hz, 1H), 6.98 (d, J = 6.8 Hz, 2H), 6.89 (d, J = 5.6 Hz, 1H), 6.70 (d, J = 6.8 Hz, 1H), 6.50 (t, J = 5.6 Hz, 1H), 5.20 (s, 2H), 3.76 (s, 3H). ^{13}C NMR (100 MHz, DMSO-d_6) δ: 164.79, 152.79, 147.80, 137.53, 136.34, 136.10, 135.32, 134.84, 134.47, 134.14, 133.87, 132.60, 131.69, 127.77, 121.23, 120.14, 119.35, 115.34, 60.66. HRMS (ESI, m/z): $[M+H]^+$ calcd. for $C_{21}H_{18}ClN_4O$: 377.1169; found: 377.1163.

2-(1-(4-fluorophenyl)-4-phenyl-1*H*-1,2,3-triazol-5-yl)aniline (4v)

White solid. mp: 183-185 °C. IR (KBr, cm^{-1}): 3445, 3359, 1617. ^1H NMR (400 MHz, DMSO-d_6) δ: 7.64 (d, J = 7.6 Hz, 2H), 7.57-7.53 (m, 2H), 7.36 – 7.31 (m, 4H), 7.29 (t, J = 4.0 Hz, 1H), 7.12 (t, J = 7.2 Hz, 1H), 6.92 (d, J = 7.6 Hz, 1H), 6.71 (d, J = 8.4 Hz, 1H), 6.52 (t, J = 7.2 Hz, 1H), 5.21 (s, 2H). ^{13}C NMR (125 MHz, DMSO-d_6) δ: 162.51 (d, J = 246.0 Hz), 147.61, 144.47, 132.87, 132.55, 131.59, 129.14, 128.69, 128.61, 127.80 (d, J = 8.7 Hz), 126.33, 116.95, 116.59 (d, J = 22.7 Hz), 115.48, 110.41. HRMS (ESI, m/z): $[M+H]^+$ calcd. for $C_{20}H_{16}FN_4$: 331.1359; found:331.1349.

2-(1-(4-fluorophenyl)-4-(*p*-tolyl)-1*H*-1,2,3-triazol-5-yl)aniline (4w)

White solid. mp: 177-179 °C. IR (KBr, cm^{-1}): 3448, 3362, 1618. ^1H NMR (400 MHz, DMSO-d_6) δ: 7.55-7.50 (m, 4H), 7.31 (t, J = 8.4 Hz, 2H), 7.14 (d, J = 8.0 Hz, 2H), 7.10 (d, J = 7.2 Hz, 1H), 6.90 (d, J = 7.6 Hz, 1H), 6.69 (d, J = 8.0 Hz, 1H), 6.50 (t, J = 7.2 Hz, 1H), 5.18 (s, 2H), 2.27 (s, 3H). ^{13}C NMR (125 MHz, DMSO-d_6) δ: 161.54, 147.40, 144.67,

138.41, 132.72, 132.24, 131.62, 129.74, 127.76, (d, *J* = 9.6 Hz), 126.36, 117.15, 116.60 (d, *J* = 22.8 Hz), 115.52, 110.47, 21.02. HRMS (ESI, m/z): $[M+H]^+$ calcd. for $C_{21}H_{18}FN_4$: 345.1515; found: 345.1497.

2-(1-(4-fluorophenyl)-4-(4-methoxyphenyl)-1*H*-1,2,3-triazol-5-yl)aniline (4x)

Off-white solid. mp: 146-148 °C. IR (KBr, cm^{-1}): 3442, 3338, 1604. ^1H NMR (400 MHz, DMSO-d_6) δ: 7.57-7.51 (m, 4H), 7.31 (t, *J* = 8.8 Hz, 2H), 7.12 (t, *J* = 7.2 Hz, 1H), 7.05 (d, *J* = 8.8 Hz, 3H), 6.70 (d, *J* = 8.4 Hz, 1H), 6.51 (t, *J* = 7.2 Hz, 1H), 5.18 (s, 2H), 3.74 (s,3H). ^{13}C NMR (125 MHz, DMSO-d_6) δ: 159.44, 147.43, 135.47, 131.63, 131.13, 130.70, 130.20, 127.88, 127.71 (d, *J* = 9.2 Hz), 117.19, 116.60 (d, *J* = 22.7 Hz), 115.54, 114.96, 114.92, 114.51, 55.52. HRMS (ESI, m/z): $[M+H]^+$ calcd. for $C_{21}H_{18}FN_4O$: 361.1465; found: 361.1451.

2-(1,4-bis(4-fluorophenyl)-1*H*-1,2,3-triazol-5-yl)aniline (4y)

White solid. mp: 170-172 °C. IR (KBr, cm^{-1}): 3479, 3317, 1635. ^1H NMR (400 MHz, DMSO-d_6) δ: 7.65 (dd, *J* = 8.4, 5.6 Hz, 2H), 7.54 (dd, *J* = 8.8, 5.2 Hz, 2H), 7.32 (t, *J* = 8.8 Hz, 2H), 7.21 (t, *J* = 8.8 Hz, 2H), 7.12 (t, *J* = 8.4 Hz, 1H), 6.92 (d, *J* = 7.2 Hz, 1H), 6.71 (d, *J* = 8.4 Hz, 1H), 6.51 (t, *J* = 7.2 Hz, 1H), 5.24 (s, 2H). ^{13}C NMR (125 MHz, DMSO-d_6) δ: 163.44 (d, *J* = 245.1 Hz), 163.16 (d, *J* = 243.4 Hz), 160.90, 148.12, 143.47, 133.25, 132.40, 131.63 (d, *J* = 27.1 Hz), 131.20 (d, *J* = 8.8 Hz), 128.29 (d, *J* = 8.0 Hz), 128.04 (d, *J* = 2.0 Hz), 127.81 (d, *J* = 8.8 Hz), 116.63, 116.58, 116.45, 116.39, 116.10 (d, *J* = 21.4 Hz), 115.93, 115.39, 110.31. HRMS (ESI, m/z): $[M+H]^+$ calcd. for $C_{20}H_{15}F_2N_4$: 349.1265; found: 349.1247.

2-(4-(4-chlorophenyl)-1-(4-fluorophenyl)-1*H*-1,2,3-triazol-5-yl)aniline (4z)

White solid. mp: 151-153 °C. IR (KBr, cm^{-1}): 3456, 3360, 1624. ^1H NMR (400 MHz, DMSO-d_6) δ: 7.63 (d, *J* = 7.6 Hz, 2H), 7.54 (s, 2H), 7.43 (d, *J* = 8.0 Hz, 2H), 7.32 (t, *J* = 8.0 Hz, 2H), 7.12 (t, *J* = 7.6 Hz, 1H), 6.92 (d, *J* = 6.8 Hz, 1H), 6.70 (d, *J* = 8.0 Hz, 1H), 6.51 (t, *J* = 6.8 Hz, 1H), 5.27 (s, 2H). ^{13}C NMR (125 MHz, DMSO-d_6) δ: 163.46, (d, *J* = 245.0 Hz), 148.05, 143.21, 133.16, 132.88, 132.84, 131.56, 131.48, 130.50, 130.39, 129.57, 129.40, 129.14, 127.85 (d, *J* = 11.5 Hz), 116.59, 116.48 (d, *J* = 23 Hz), 115.43, 110.14. HRMS (ESI, m/z): $[M+H]^+$ calcd. for $C_{20}H_{15}ClFN_4$: 365.0969; found:365.0951.

2-(1-(4-chlorophenyl)-4-phenyl-1*H*-1,2,3-triazol-5-yl)aniline (4aa)

Off-white solid. mp: 183-185 °C. IR (KBr, cm^{-1}): 3446, 3353, 1624. ^{1}H NMR (400 MHz, DMSO-d_6) δ: 7.63 (d, J = 2.0 Hz, 2H), 7.44 (bs, 7H), 7.14 – 7.10 (m, 1H), 6.91-6.87 (m, 1H), 6.71 (d, J = 3.2 Hz, 1H), 6.51 – 6.47 (m, 1H), 5.23 (s, 2H). ^{13}C NMR (125 MHz, DMSO-d_6) δ: 148.10, 144.40, 135.71, 134.23, 132.40, 131.61, 131.41, 129.61, 129.30, 129.04, 128.23, 127.08, 126.30, 116.45, 115.38, 110.45. HRMS (ESI, m/z): $[M+H]^+$ calcd. for $C_{20}H_{16}ClN_4$: 347.1063; found: 347.1055.

2-(1-(4-chlorophenyl)-4-(*p*-tolyl)-1*H*-1,2,3-triazol-5-yl)aniline (4ab)

White solid. mp: 202-204 °C. IR (KBr, cm^{-1}): 3443, 3362, 1616. ^{1}H NMR (400 MHz, DMSO-d_6) δ: 7.77 (d, J = 8.0 Hz, 1H), 7.52 (q, J = 8.8 Hz, 4H), 7.32 (d, J = 8.0 Hz, 1H), 7.14 (d, J = 8.0 Hz, 3H), 6.90 (d, J = 7.2 Hz, 1H), 6.70 (d, J = 8.4 Hz, 1H), 6.51 (t, J = 7.2 Hz, 1H), 5.20 (s, 2H), 2.28 (s, 3H). ^{13}C NMR (125 MHz, DMSO-d_6) δ: 148.09, 144.57, 137.61, 136.19, 132.56, 131.99, 131.65, 131.37, 129.63, 128.60, 127.30, 126.31, 122.75, 116.46, 115.37, 110.57, 21.26. HRMS (ESI, m/z): $[M+H]^+$ calcd. for $C_{21}H_{18}ClN_4$: 361.1220; found: 361.1201.

2-(1-(4-chlorophenyl)-4-(4-methoxyphenyl)-1*H*-1,2,3-triazol-5-yl)aniline (4ac)

Pale yellow solid. mp: 164-166 °C. IR (KBr, cm^{-1}): 3436, 3329, 1603. ^{1}H NMR (400 MHz, DMSO-d_6) δ: 7.82 (d, J = 8.4 Hz, 2H), 7.57-7.48 (m, 5H), 7.06 (d, J = 8.4 Hz, 3H), 6.71 (d, J = 8.4 Hz, 1H), 6.52 (t, J = 7.2 Hz, 1H), 5.19 (s, 2H), 3.74 (s, 3H). ^{13}C NMR (125 MHz, DMSO-d_6) δ: 147.23, 132.68, 132.61, 131.03, 130.17, 129.71, 129.62, 129.04, 116.33, 115.30, 114.96, 114.53, 114.27, 114.18, 114.11, 56.05. HRMS (ESI, m/z): $[M+H]^+$ calcd. for $C_{21}H_{18}ClN_4O$: 377.1169; found: 377.1154.

2-(1-(4-chlorophenyl)-4-(4-fluorophenyl)-1*H*-1,2,3-triazol-5-yl)aniline (4ad)

Off-white solid. mp: 165-167 °C. IR (KBr, cm^{-1}): 3453, 3354, 1623. ^{1}H NMR (400 MHz, DMSO-d_6) δ: 7.65 (dd, J = 8.0, 6.0 Hz, 2H), 7.53 (q, J = 8.8 Hz, 4H), 7.21 (t, J = 8.8 Hz, 2H), 7.14 (t, J = 7.6 Hz, 1H), 6.92 (d, J = 7.2 Hz, 1H), 6.71 (d, J = 8.0 Hz, 1H), 6.52 (t, J = 7.2 Hz, 1H), 5.25 (s, 2H).^{13}C NMR (125 MHz, DMSO-d_6) δ: 163.18(d, J = 243.3 Hz), 148.10, 143.63, 135.65, 134.28, 132.26, 131.60, 131.50, 131.20, 129.63, 129.31, 128.34 (d, J = 8.1 Hz), 127.94, 127.07, 123.04, 116.52, 116.11 (d, J = 21.5 Hz), 115.44, 110.18. HRMS (ESI, m/z): $[M+H]^+$ calcd. for $C_{20}H_{15}ClFN_4$: 365.0969; found: 365.0956.

2-(1,4-bis(4-chlorophenyl)-1*H*-1,2,3-triazol-5-yl)aniline (4ae)

White solid. mp: 180-182 °C. IR (KBr, cm^{-1}): 3454, 3358, 1624. ^{1}H NMR (400 MHz, DMSO-d_6) δ: 7.61 (d, J = 7.2 Hz, 2H), 7.51 (d, J = 6.4 Hz, 4H), 7.42 (d, J = 9.6 Hz, 2H), 7.14 (t, J = 9.2 Hz, 1H), 6.91 (d, J = 7.6 Hz, 1H), 6.71 (d, J = 9.2 Hz, 1H), 6.52 (d, J = 8.4 Hz, 1H), 5.25 (s, 2H) ^{13}C NMR (100 MHz, DMSO-d_6) δ: 148.05, 143.39, 135.60, 134.36, 132.95, 132.73, 131.55, 130.32, 129.67, 129.18, 127.94, 127.13, 116.56, 115.49, 110.03. HRMS (ESI, m/z): $[M+H]^+$ calcd. for $C_{20}H_{15}Cl_2N_4$: 381.0674; found: 381.0689.

2-(1-(4-bromophenyl)-4-phenyl-1*H*-1,2,3-triazol-5-yl)aniline (4af)

White solid. mp: 186-188 °C. IR (KBr, cm^{-1}): 3449, 3354, 1624. ^{1}H NMR (400 MHz, DMSO-d_6) δ: 7.63 (s, 3H), 7.43 (bs, 3H), 7.33 (bs, 3H), 7.11 (s, 1H), 6.89 (s, 1H), 6.68 (s, 1H), 6.53 (s, 1H), 5.20 (s, 2H). ^{13}C NMR (125 MHz, DMSO-d_6) δ: 148.07, 144.43, 136.10, 132.56, 132.35, 131.60, 131.42, 129.53, 129.04, 128.25, 127.31, 126.30, 125.32, 122.79, 116.48, 115.38, 110.43. HRMS (ESI, m/z): $[M+H]^+$ calcd. for $C_{20}H_{16}BrN_4$: 391.0558; found: 391.0557.

2-(1-(4-bromophenyl)-4-(*p*-tolyl)-1*H*-1,2,3-triazol-5-yl)aniline (4ag)

Off-white solid. mp: 217-219 °C. IR (KBr, cm^{-1}): 3443, 3360, 1615. ^{1}H NMR (400 MHz, DMSO-d_6) δ: 7.66 (s, 2H), 7.50 (d, J = 4.8 Hz, 2H), 7.42 (s, 2H), 7.14 (d, J = 4.0 Hz, 3H), 6.89 (s, 1H), 6.70 (s, 1H), 6.51 (s, 1H), 5.19 (s, 2H), 2.27 (s, 3H). ^{13}C NMR (125 MHz, DMSO-d_6) δ: 148.60, 145.08, 138.12, 136.70, 133.07, 132.50, 132.16, 131.88, 130.14, 129.11, 127.81, 126.82, 123.26, 116.97, 115.89, 111.08, 21.77. HRMS (ESI, m/z): $[M+H]^+$ calcd. for $C_{21}H_{18}BrN_4$: 405.0715; found: 405.0709.

2-(1-(4-bromophenyl)-4-(4-methoxyphenyl)-1*H*-1,2,3-triazol-5-yl)aniline (4ah)

Pale yellow solid. mp: 203-205 °C. IR (KBr, cm^{-1}): 3434, 3333, 1615. ^{1}H NMR (400 MHz, DMSO-d_6) δ: 7.65 (s, 2H), 7.55 (s, 2H), 7.41 (s, 2H), 7.11 (s, 1H), 6.90 (s, 3H), 6.68 (s, 1H), 6.51 (s, 1H), 5.18 (s, 2H), 3.72 (s, 3H). ^{13}C NMR (125 MHz, DMSO-d_6) δ: 160.02, 148.05, 143.01, 132.73, 131.57, 131.32, 130.59, 129.72, 129.37, 129.10, 127.82, 126.92, 116.41, 115.35, 114.58, 110.56, 55.88. HRMS (ESI, m/z): $[M+H]^+$ calcd. for $C_{21}H_{18}BrN_4O$: 421.0664; found: 421.0658.

2-(1-(4-bromophenyl)-4-(4-fluorophenyl)-1*H*-1,2,3-triazol-5-yl)aniline (4ai)

White solid. mp: 184-186 °C. IR (KBr, cm^{-1}): 3455, 3362, 1622. ^{1}H NMR (400 MHz, DMSO-d_6) δ: 7.70-7.63 (m, 4H), 7.43 (d, J = 8.4 Hz, 2H), 7.22 (d, J = 8.8 Hz, 2H), 7.14 (t,

J = 7.2 Hz, 1H), 6.92 (d, *J* = 8.0 Hz, 1H), 6.72 (d, *J* = 8.4 Hz, 1H), 6.52 (t, *J* = 7.6 Hz, 1H), 5.25 (s, 2H). ^{13}C NMR (125 MHz, DMSO-d_6) δ: 163.18 (d, *J* = 243.4 Hz), 148.11, 143.65, 136.08, 135.75, 132.58, 131.90, 131.60, 131.50, 128.32 (d, *J* = 8.0 Hz), 127.31, 123.03, 122.82, 116.50, 116.10 (d, *J* = 21.4 Hz), 115.44, 110.17. HRMS (ESI, m/z): $[M+H]^+$ calcd. for $C_{20}H_{15}BrFN_4$: 409.0464; found: 409.0456.

2-(1-(4-bromophenyl)-4-(4-chlorophenyl)-1*H*-1,2,3-triazol-5-yl)aniline (4aj)

Off-white solid. mp: 196-198 °C. IR (KBr, cm^{-1}): 3455, 3365, 1616. ^{1}H NMR (400 MHz, DMSO-d_6) δ: 7.68 (d, *J* = 8.4 Hz, 2H), 7.63 (d, *J* = 8.4 Hz, 2H), 7.43 (d, *J* = 8.0 Hz, 4H), 7.14 (t, *J* = 7.6 Hz, 1H), 6.92 (d, *J* = 7.2 Hz, 1H), 6.71 (d, *J* = 8.0 Hz, 1H), 6.52 (t, *J* = 7.2 Hz, 1H), 5.26 (s, 2H). ^{13}C NMR (100 MHz, DMSO-d_6) δ: 147.81, 143.15, 135.35, 134.12, 132.71, 132.48, 131.31, 130.08, 129.42, 128.93, 127.70, 126.89, 116.32, 115.25, 109.79. HRMS (ESI, m/z): $[M+H]^+$ calcd. for $C_{20}H_{15}BrClN_4$: 425.0169; found: 425.0162.

2-(1-(4-nitrophenyl)-4-phenyl-1*H*-1,2,3-triazol-5-yl)aniline (4ak)

White solid. mp: 185-187 °C. IR (KBr, cm^{-1}): 3425, 3338, 1604. ^{1}H NMR (400 MHz, $CDCl_3$) δ: 7.71 (d, *J* = 6.0 Hz, 2H), 7.34 (d, *J* = 4.0 Hz, 4H), 7.31 (d, *J* = 6.8 Hz, 2H), 7.26 (s, 2H), 6.92 (d, *J* = 7.2 Hz, 1H), 6.75 (t, *J* = 8.4 Hz, 2H), 3.66 (s, 2H). ^{13}C NMR (100 MHz, DMSO-d_6) δ: 148.12, 143.47, 135.67, 134.43, 133.02, 132.80, 131.63, 130.39, 129.74, 129.25, 128.01, 127.21, 116.64, 115.57, 110.11. ESI-MS (m/z): $[M+H]^+$ calcd. for $C_{20}H_{16}N_5O_2$: 358.13; found: 358.10.

4-(5-(2-aminophenyl)-4-phenyl-1*H*-1,2,3-triazol-1-yl)benzonitrile (4al)

Off-white solid. mp: 153-155 °C. IR (KBr, cm^{-1}): 3321, 3191, 2218, 1586. ^{1}H NMR (400 MHz, DMSO-d_6) δ: 7.67 (d, *J* = 8.4 Hz, 2H), 7.62 (d, *J* = 8.4 Hz, 2H), 7.48 (d, *J* = 9.2 Hz, 1H), 7.43 (d, *J* = 8.0 Hz, 4H), 7.14 (t, *J* = 7.6 Hz, 1H), 6.91 (d, *J* = 7.2 Hz, 1H), 6.71 (d, *J* = 8.0 Hz, 1H), 6.52 (t, *J* = 7.6 Hz, 1H), 5.25 (s, 2H). ^{13}C NMR (100 MHz, DMSO-d_6) δ: 148.89, 139.35, 133.40, 132.07, 131.10, 131.05, 129.97, 129.37, 128.83, 128.32, 128.04, 126.98, 124.21, 123.01, 120.54, 114.85. ESI-MS (m/z): $[M+H]^+$ calcd. for $C_{21}H_{16}N_5$: 338.14; found: 338.15.

3.8. References

[1] J. Huo, H. Hu, M. Zhang, X. Hu, M. Chen, D. Chen, J. Liu, G. Xiao, Y. Wang, Z. Wen, *RSC Adv.* **2017**, *7*, 2281–2287.

[2] Z. Xu, S. J. Zhao, Y. Liu, *Eur. J. Med. Chem.* **2019**, *183*, 111700.

[3] I. A. Seliem, S. S. Panda, A. S. Girgis, Y. Moatasim, A. Kandeil, A. Mostafa, M. A. Ali, E. S. Nossier, F. Rasslan, A. M. Srour, R. Sakhuja, T. S. Ibrahim, Z. K. M. Abdel-samii, A. M. M. Al-Mahmoudy, *Bioorg. Chem.* **2021**, *114*, 105117.

[4] S. Gharehnaghadeh, P. Salehi, M. Bararjanian, Ł. Pecio, K. Babanezhad-Harikandei, M. Khoramjouy, S. Shahhosseini, M. Faizi, *ChemistrySelect* **2020**, *5*, 14753–14758.

[5] Z. C. Dai, Y. F. Chen, M. Zhang, S. K. Li, T. T. Yang, L. Shen, J. X. Wang, S. S. Qian, H. L. Zhu, Y. H. Ye, *Org. Biomol. Chem.* **2015**, *13*, 477–486.

[6] Z. Xu, *Eur. J. Med. Chem.* **2020**, *206*, 112686.

[7] S. Zhang, Z. Xu, C. Gao, Q. C. Ren, L. Chang, Z. S. Lv, L. S. Feng, *Eur. J. Med. Chem.* **2017**, *138*, 501–513.

[8] P. Sambasiva Rao, C. Kurumurthy, B. Veeraswamy, G. Santhosh Kumar, Y. Poornachandra, C. Ganesh Kumar, S. B. Vasamsetti, S. Kotamraju, B. Narsaiah, *Eur. J. Med. Chem.* **2014**, *80*, 184–191.

[9] A. Sahu, D. Das, R. K. Agrawal, A. Gajbhiye, *Life Sci.* **2019**, *228*, 176–188.

[10] S. G. Agalave, S. R. Maujan, V. S. Pore, *Chem. - An Asian J.* **2011**, *6*, 2696–2718.

[11] S. Ferreira, A. C. R. Sodero, M. F. C. Cardoso, E. S. Lima, C. R. Kaiser, F. P. Silva, V. F. Ferreira, *J. Med. Chem.* **2010**, *53*, 2364–2375.

[12] R. P. Lewis, R. D. Meyer, L. L. Kraus, *Antimicrob. Agents Chemother.* **1976**, *9*, 780–786.

[13] M. Bassetti, N. Castaldo, A. Cattelan, C. Mussini, E. Righi, C. Tascini, F. Menichetti, C. M. Mastroianni, M. Tumbarello, P. Grossi, S. Artioli, N. Carannante, L. Cipriani, D. Coletto, A. Russo, M. Digaetano, A. R. Losito, M. Peghin, A. Capone, S. Nicolè, A. Vena, *Int. J. Antimicrob. Agents* **2019**, *53*, 408–415.

[14] M.-J. Camarasa, A. San-Felix, S. Velazquez, M.-J. Perez-Perez, F. Gago, J. Balzarini, *Curr. Top. Med. Chem.* **2004**, *4*, 945–963.

[15] M. J. Soltis, H. J. Yeh, K. A. Cole, N. Whittaker, R. P. Wersto, E. C. Kohn, *Drug Metab. Dispos.* **1996**, *24*, 799–806.

[16] J. W. Wheless, B. Vazquez, *Epilepsy Curr.* **2010**, *10*, 1–6.

[17] D. Minehira, S. Takahara, I. Adachi, N. Toyooka, *Tetrahedron Lett.* **2014**, *55*, 5778–5780.

[18] M. J. Lee, K. H. Cho, H. M. Park, H. J. Sung, S. Choi, W. Im, *Eur. J. Pharmacol.* **2014**, *735*, 115–122.

[19] J. Huo, Z. Hu, D. Chen, S. Luo, Z. Wang, Y. Gao, M. Zhang, H. Chen, *ACS Omega* **2017**, *2*, 5557–5564.

[20] X. Wang, Z. C. Dai, Y. F. Chen, L. L. Cao, W. Yan, S. K. Li, J. X. Wang, Z. G. Zhang, Y. H. Ye, *Eur. J. Med. Chem.* **2017**, *126*, 171–182.

[21] S. Kantheti, R. Narayan, K. V. S. N. Raju, *RSC Adv.* **2015**, *5*, 3687–3708.

[22] Q. Ma, S. Qi, X. He, Y. Tang, G. Lu, *Corros. Sci.* **2017**, *129*, 91–101.

[23] D. Brunel, F. Dumur, *New J. Chem.* **2020**, *44*, 3546–3561.

[24] J. John, J. Thomas, W. Dehaen, *Chem. Commun.* **2015**, *51*, 10797–10806.

[25] A. Garg, N. Khupse, A. Bordoloi, D. Sarma, *New J. Chem.* **2019**, *43*, 19331–19337.

[26] H. M. F. Elnagdy, K. Gogoi, A. A. Ali, D. Sarma, *Appl. Organomet. Chem.* **2018**, *32*, 1–6.

[27] E. Haldón, M. C. Nicasio, P. J. Pérez, *Org. Biomol. Chem.* **2015**, *13*, 9528–9550.

[28] G. Surendra Reddy, A. Suresh Kumar, D. B. Ramachary, *Org. Biomol. Chem.* **2020**, *18*, 4470–4478.

[29] J. Thomas, S. Jana, J. John, S. Liekens, W. Dehaen, *Chem. Commun.* **2016**, *52*, 2885–2888.

[30] S. S. Vanberkel, S. Brauch, L. Gabriel, M. Henze, S. Stark, D. Vasilev, L. A. Wessjohann, M. Abbas, B. Westermann, *Angew. Chemie - Int. Ed.* **2012**, *51*, 5343–5346.

[31] Z.-J. Cai, X.-M. Lu, Y. Zi, C. Yang, L.-J. Shen, J. Li, S.-Y. Wang, S.-J. Ji, *Org. Lett.* **2014**, *16*, 5108–5111.

[32] Q. Zhou, Z. Fu, L. Yu, J. Wang, *Asian J. Org. Chem.* **2019**, *8*, 646–649.

[33] S. Wang, Y. Zhang, G. Liu, H. Xu, L. Song, J. Chen, J. Li, Z. Zhang, *Org. Chem.*

Front. **2021**, *8*, 599–604.

[34] C. Huang, X. Geng, P. Zhao, Y. Zhou, X.-X. Yu, L.-S. Wang, Y.-D. Wu, A.-X. Wu, *J. Org. Chem.* **2021**, *86*, 13664–13672.

[35] T. Zhang, Y. Meng, J. Lu, Y. Yang, G. Q. Li, C. Zhu, *Adv. Synth. Catal.* **2018**, *360*, 3063–3068.

[36] M. Singh, Vaishali, A. K. Paul, V. Singh, V. Singh, *Org. Biomol. Chem.* **2020**, *18*, 4459–4469.

[37] Y. Sert, G. A. El-Hiti, H. Gökce, F. Ucun, B. F. Abdel-Wahab, B. M. Kariuki, *J. Mol. Struct.* **2020**, *1211*, 128077.

[38] Z. Xu, G. Cheng, S. Zhu, Q. Lin, H. Yang, *J. Mater. Chem. A* **2018**, *6*, 2239–2248.

[39] V. S. Krishna, S. Zheng, E. M. Rekha, L. W. Guddat, D. Sriram, *J. Comput. Aided. Mol. Des.* **2019**, *33*, 357–366.

[40] K. K. Alluri, R. S. Reshma, R. Suraparaju, S. Gottapu, D. Sriram, *Bioorganic Med. Chem.* **2018**, *26*, 1462–1469.

[41] R. Li, R. Sirawaraporn, P. Chitnumsub, W. Sirawaraporn, J. Wooden, F. Athappilly, S. Turley, W. G. J. Hol, *J. Mol. Biol.* **2000**, *295*, 307–323.

[42] L. A. Collins, S. G. Franzblau, *Antimicrob. Agents Chemother.* **1997**, *41*, 1004–1009.

[43] J. van Meerloo, G. J. L. Kaspers, J. Cloos, in *Cancer Cell Cult.*, **2011**, pp. 237–245.

[44] G. M. Morris, R. Huey, A. J. Olson, *Curr. Protoc. Bioinforma.* **2008**, *24*, 1–40.

[45] D. E. V. Pires, T. L. Blundell, D. B. Ascher, *J. Med. Chem.* **2015**, *58*, 4066–4072.

3.9. Selected IR, NMR (^{1}H and ^{13}C) and Mass spectra

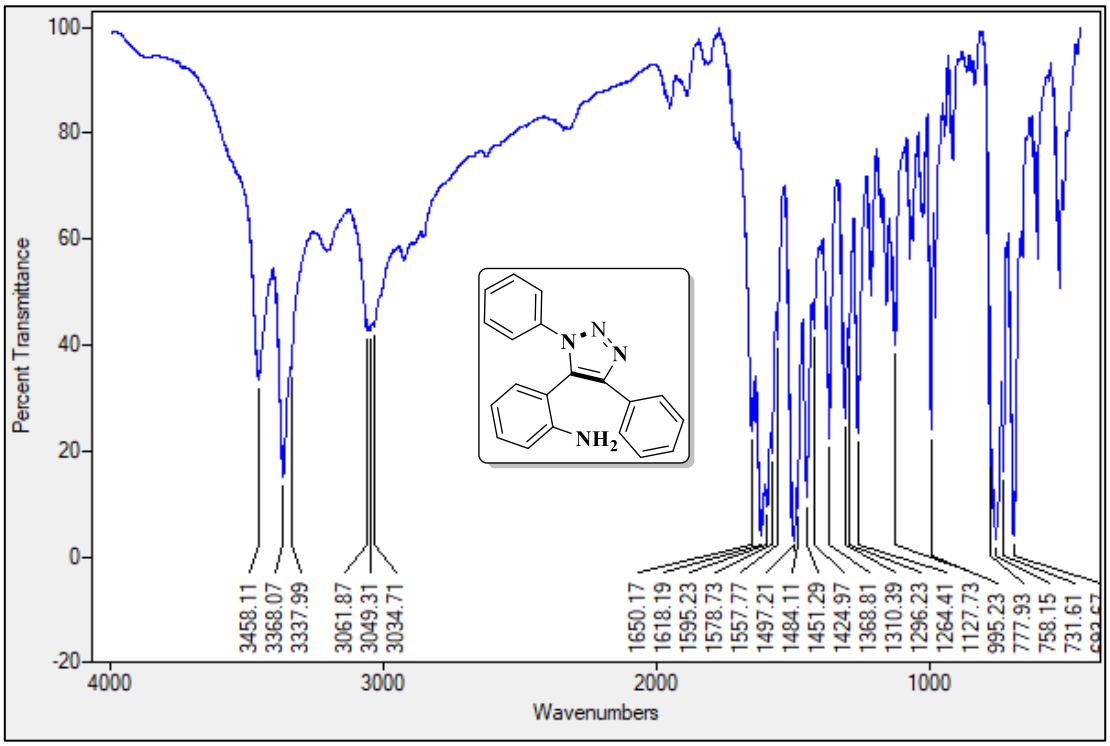

IR spectrum of the compound **4a**

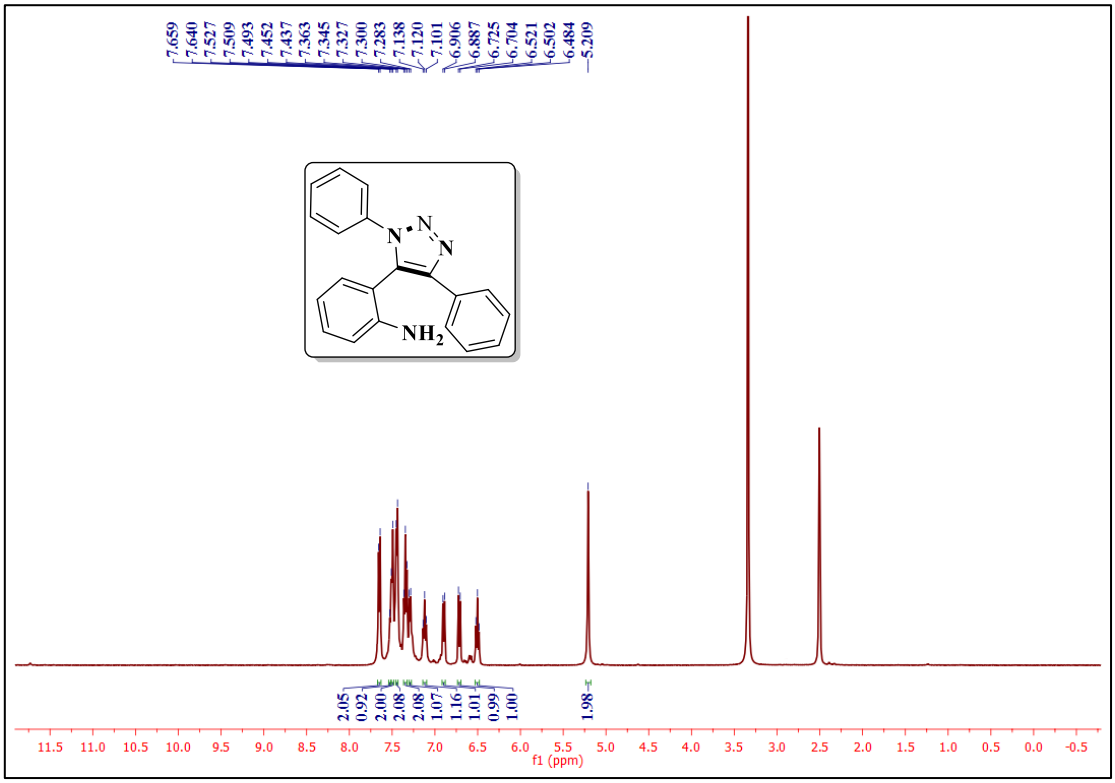

^{1}H NMR spectrum of the compound **4a**

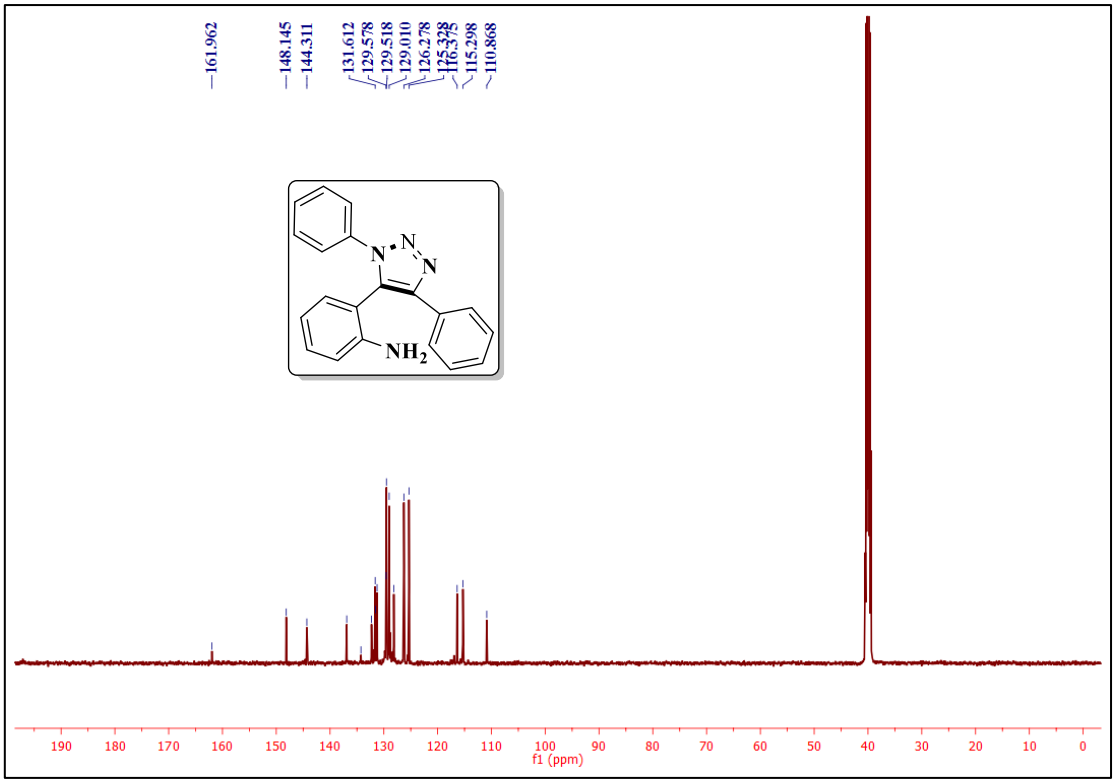

^{13}C NMR spectrum of the compound **4a**

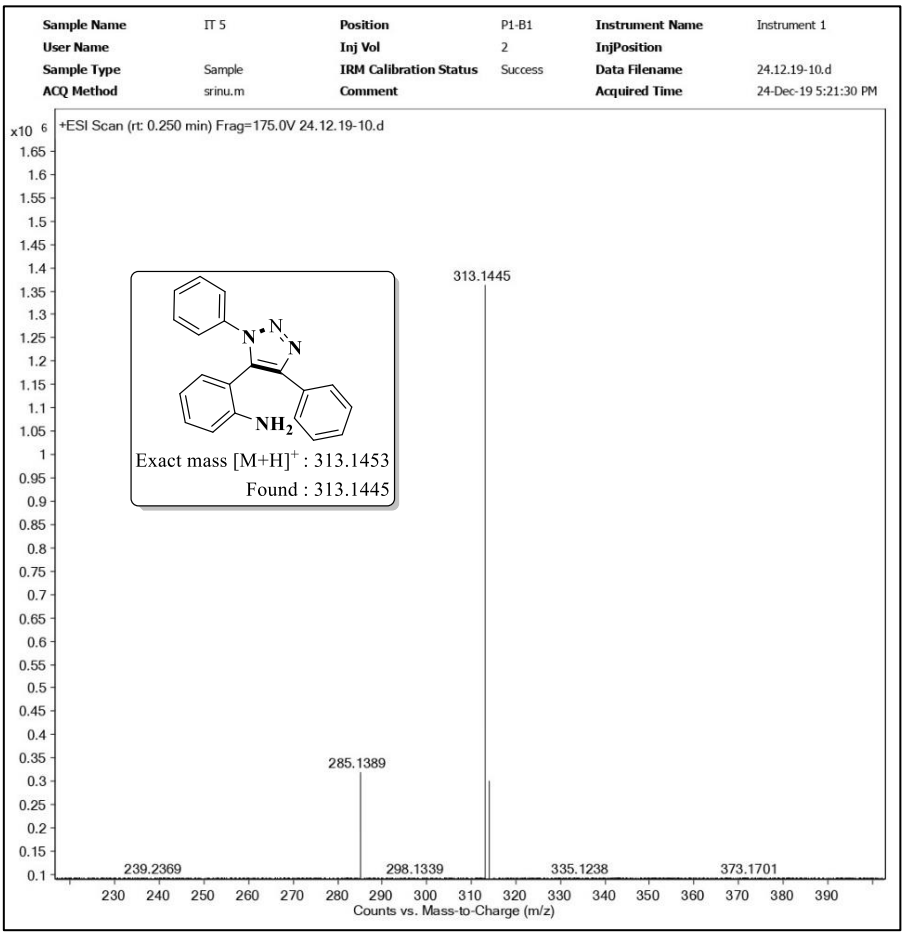

Mass spectrum of the compound **4a**

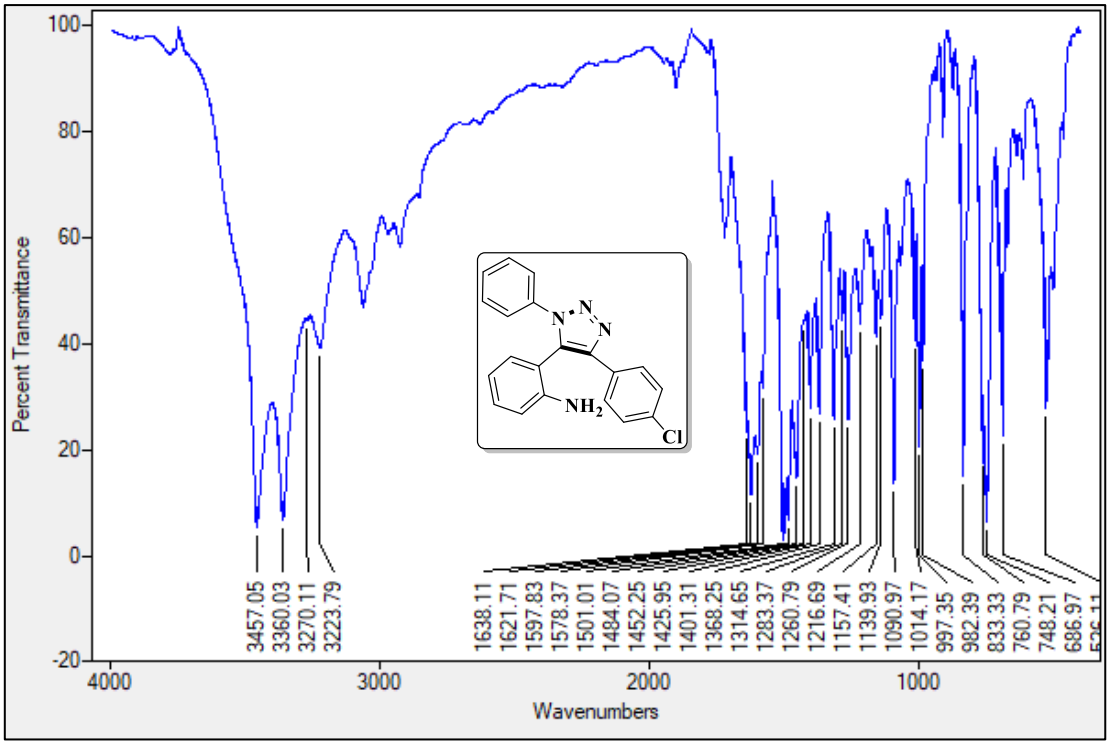

IR spectrum of the compound **4g**

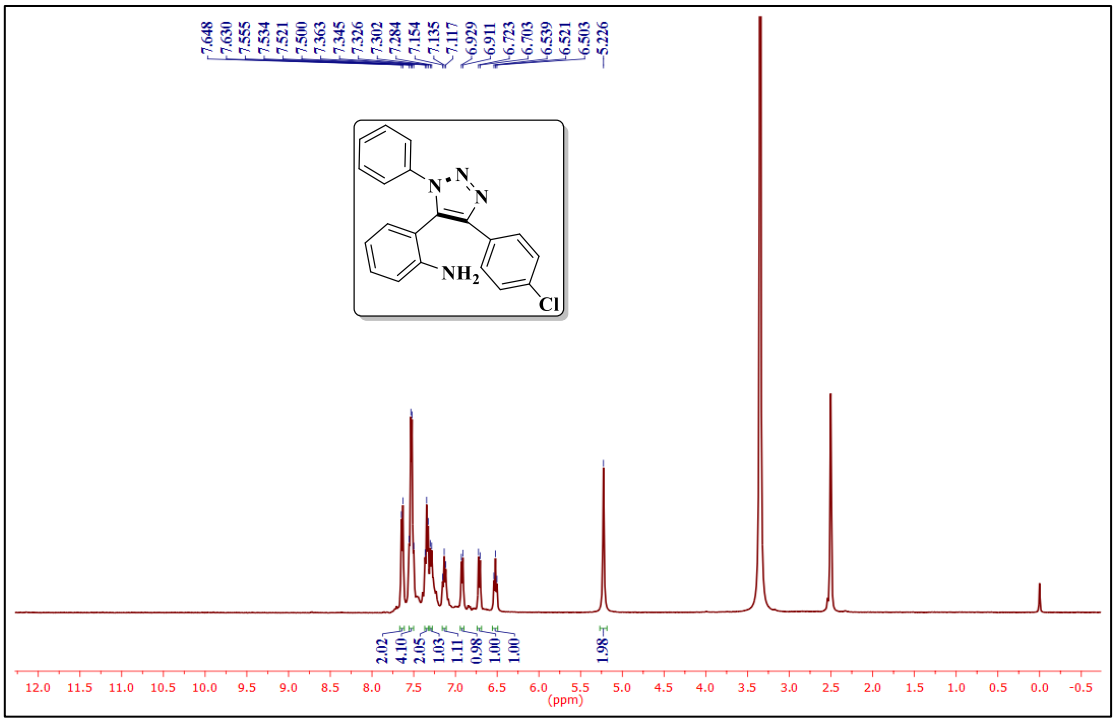

^{1}H NMR spectrum of the compound **4g**

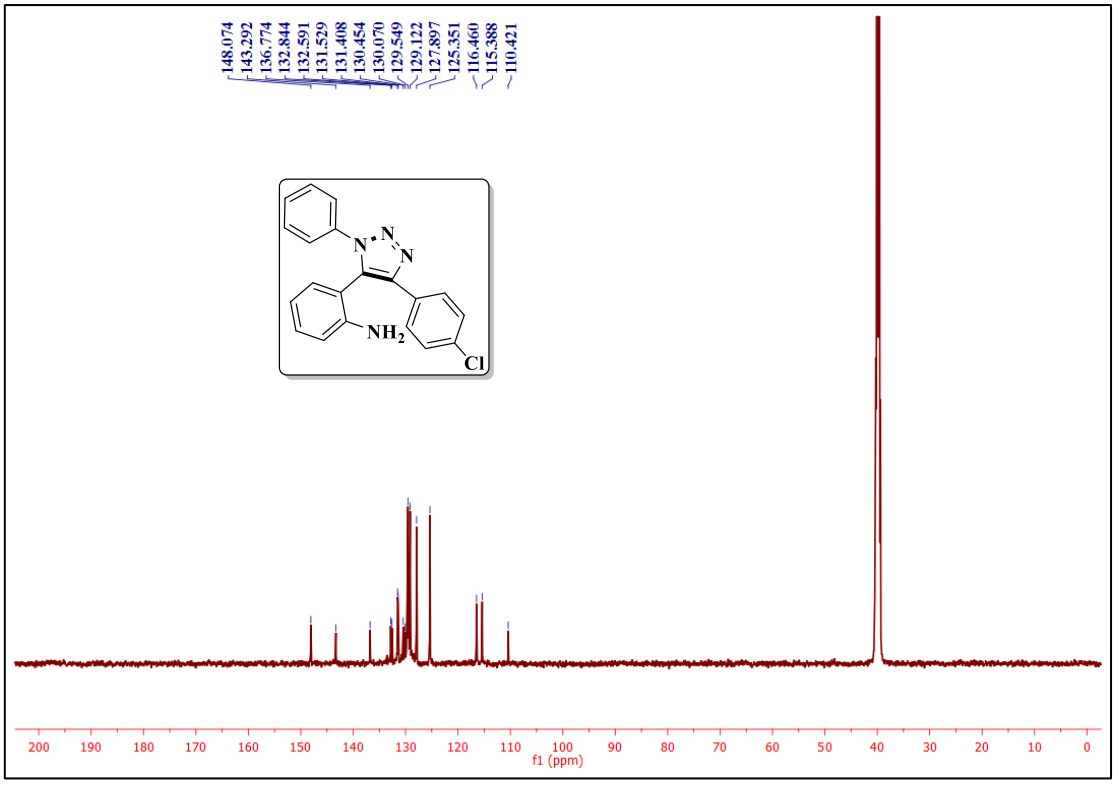

^{13}C NMR spectrum of the compound **4g**

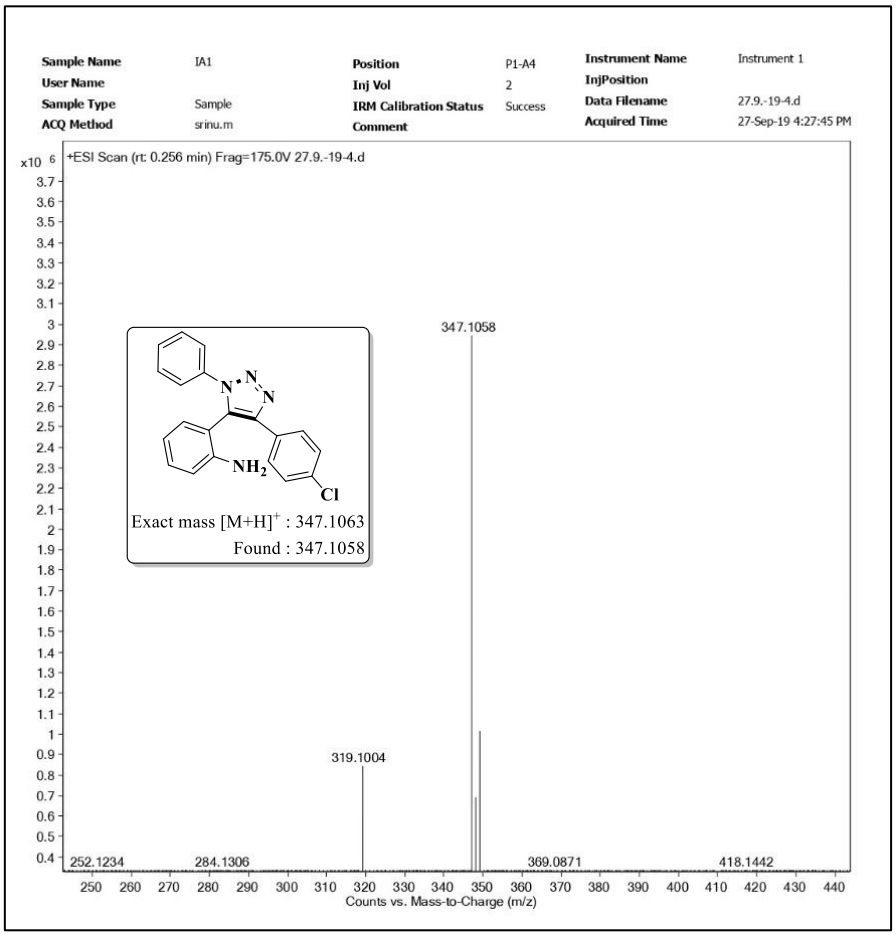

Mass spectrum of the compound **4g**

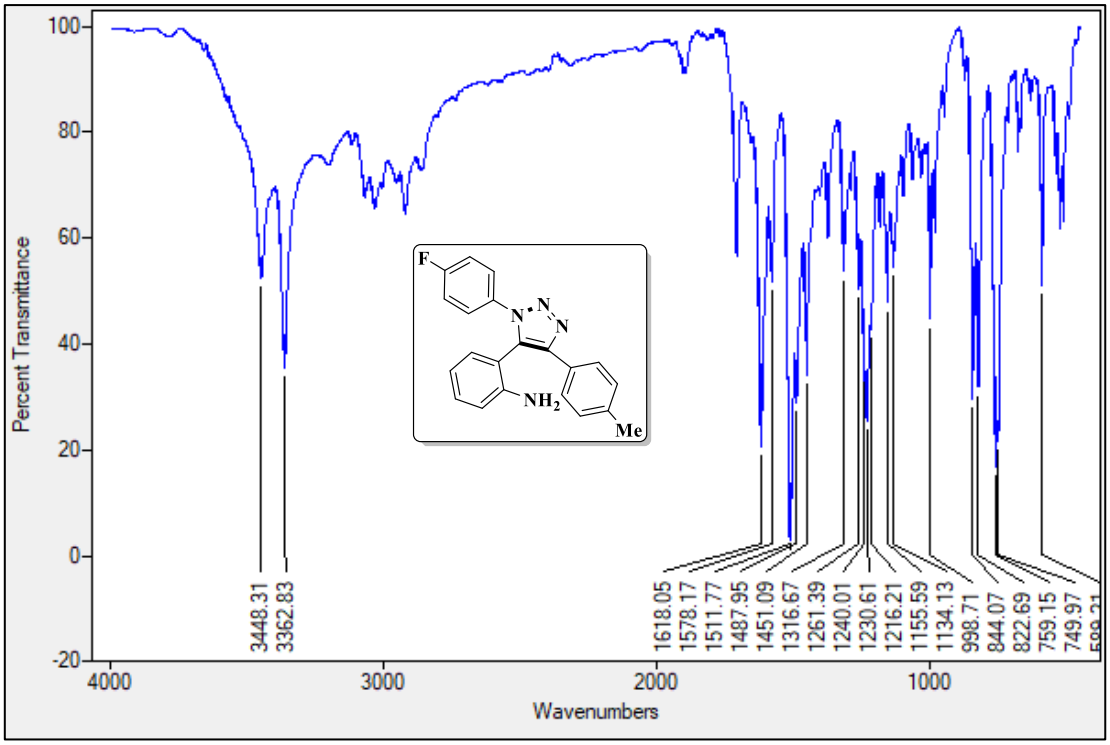

IR spectrum of the compound **4w**

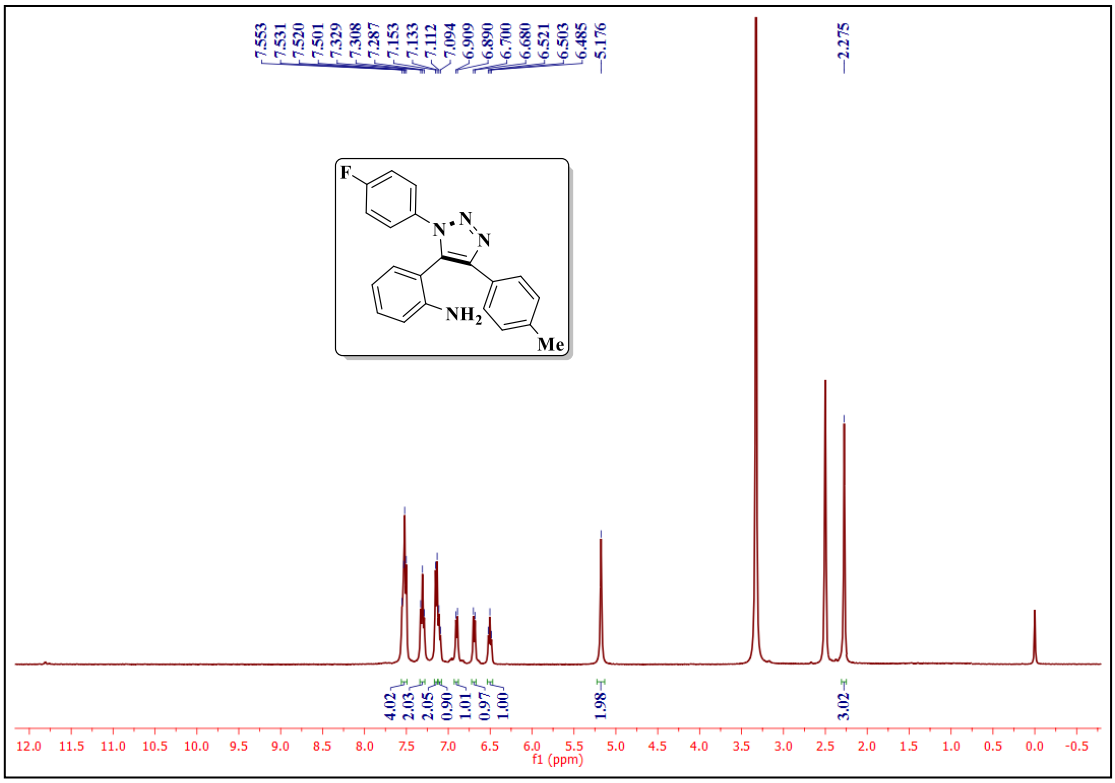

^{1}H NMR spectrum of the compound **4w**

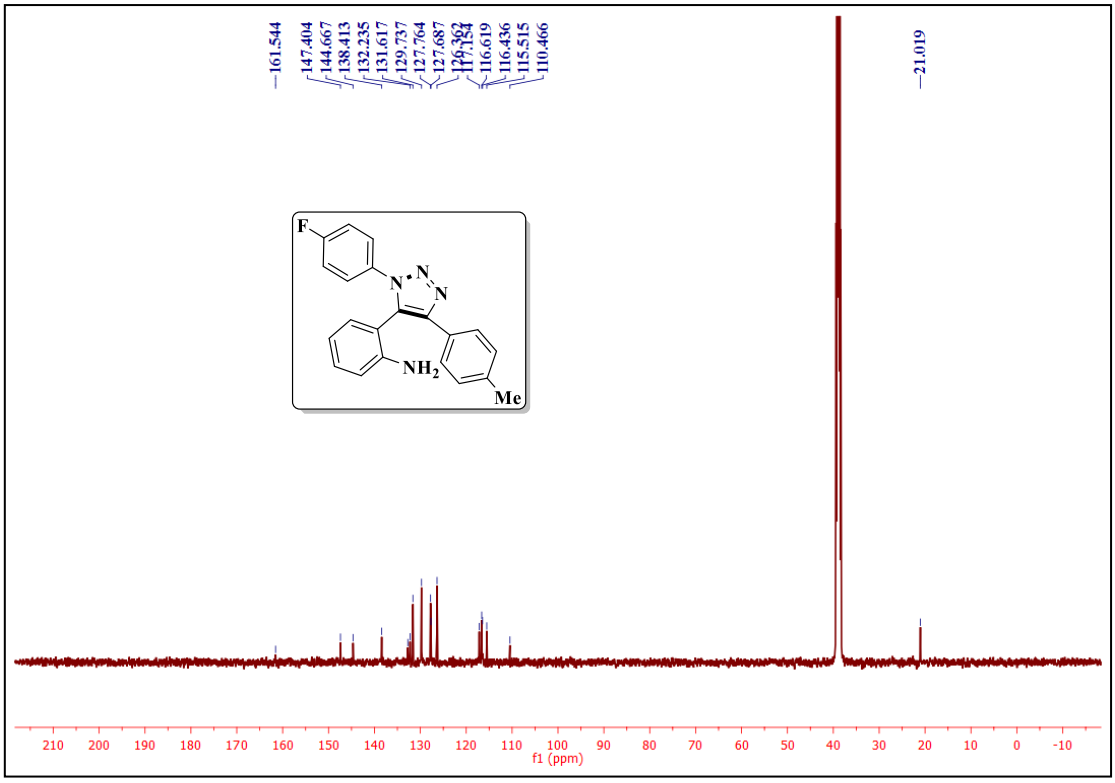

^{13}C NMR spectrum of the compound **4w**

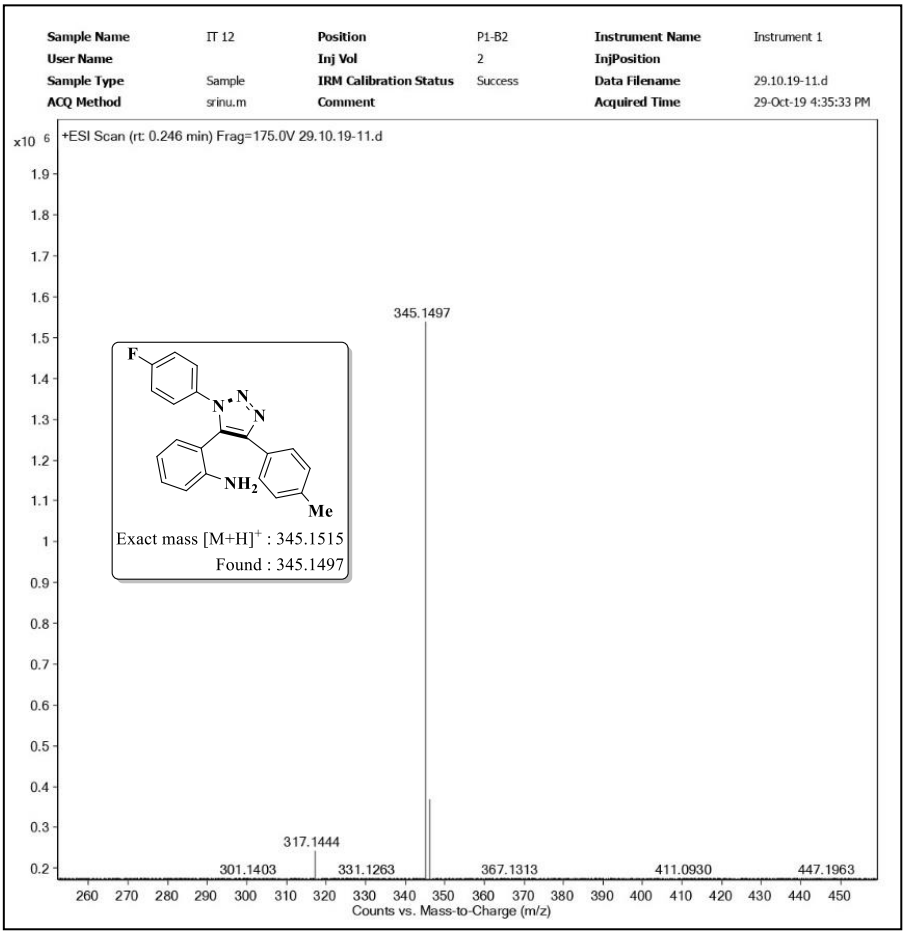

Mass spectrum of the compound **4w**

CHAPTER-IV
Section-A

One-pot multicomponent reaction for the synthesis of functionalized 2'-oxo-spiro[furo-pyrrolo[2,1-*a*]isoquinolino-indolines

4A.1. Introduction

Spirooxindoles are important class of heterocyclic compounds in medicinal chemistry due to their privileged biological properties such as anti-cancer [1], anti-microbial [2], anti-tubercular [3], anti-HIV [4], anti-bacterial [5], anti-inflammatory [6]. They also act as potential synthetic intermediates for alkaloids [7], drug like molecules [8] and pharmaceutical agents [9]. The incorporation of two or more pharmacophores in oxindole skeleton could significantly enhance the biological activity and lead to generate new therapeutic candidates [10].

In particular, spirooxindole having five membered oxa-heterocycles like hydrofurans and dihydrohydrofurans found in various natural products [11] and biologically active compounds [12]. For example, tryptoquivaline is the natural alkaloid which can be isolated from the marine derived fungi, exhibits anti-bacterial and anti-biofilm activities [13,14]. Pteropodine is an oxindole alkaloid specifically isolated from cat's claw used as traditional medicine to exhibit anti-inflammatory and anti-mutagenic activities [15,16]. Whereas, aspergilline-A is an indole-tetrahedrofuran derived alkaloid, isolated from the endophytic fungus Aspergillus versicolor exhibits various activities such as anti-cancer, anti-microbial and anti-oxidant [17,18].

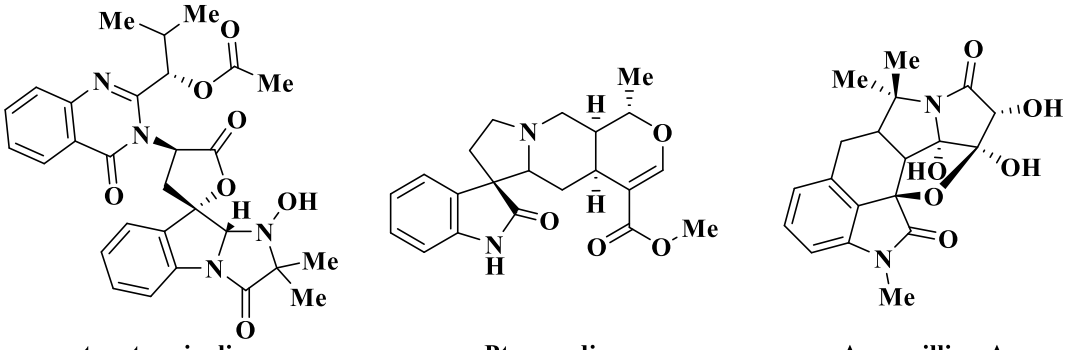

Figure 4A.1. Examples of some natural and bioactive compounds having spirooxindoles.

4A.1.1. Reported methods for the synthesis and biological evaluation of spirooxindolo-furans

Wu and co-workers developed a series of spirooxindole tetrahydrofuran derivatives *via* base-mediated cascade [3+2] Michael reactions under mild reaction conditions (Figure 4A.2). Subsequently, *in vitro* antifungal activities of all the synthesized compounds were evaluated against five pathogenic fungi using the mycelium growth rate method and the results demonstrated that some of the compounds exhibit potent inhibition [19].

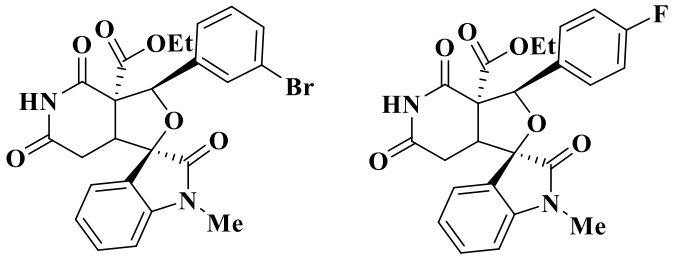

Figure 4A.2

Gupta et al. synthesized as series of substituted spirooxindolo dihydrofurans by simple tandem Michael cyclization in aqueous medium using DABCO as catalyst (Figure 4A.3). Further, *in vitro* anti-bacterial activity of the synthesized compounds were evaluated in both gram positive and gram negative bacterial strains and the IC_{50} values of the compounds showed better than the standard antibiotic ampicillin [20].

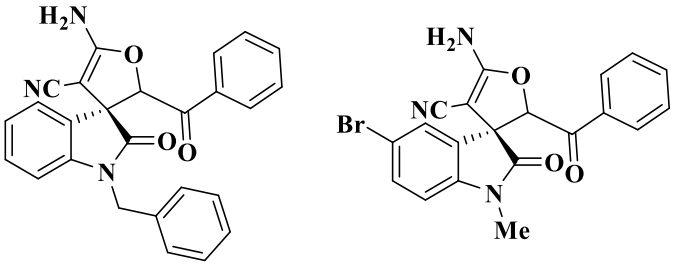

Figure 4A.3

Kamal and co-workers demonstrated a simple and efficient method for the synthesis of pyrazolopyridine based spirooxindolo furans by three-component reaction using sulfamic acid (H_2NSO_3H) as a green catalyst (Figure 4A.4). The synthesized compounds were investigated for *in vitro* cytotoxicity against human cancer cell lines and some of the compounds exhibited remarkable cytotoxicity against breast cancer cell line [21].

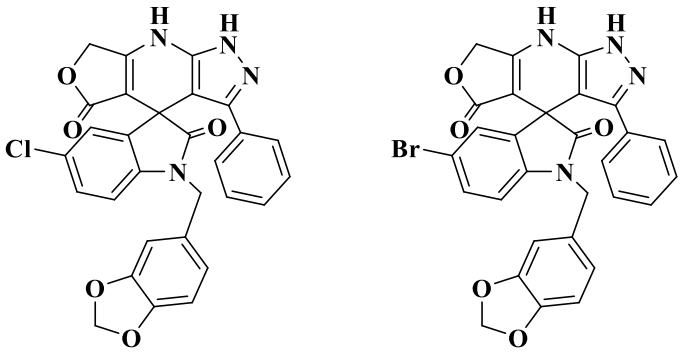

Figure 4A.4

Tang et al. disclosed isocyanide based three-component bicyclization reaction with allenoates and isatin for the construction of structurally complex spirooxindolo furans

(Scheme 4A.1). This reaction proceeds through Michael addition, double cyclization and [1,5]-hydride shift pathway [22].

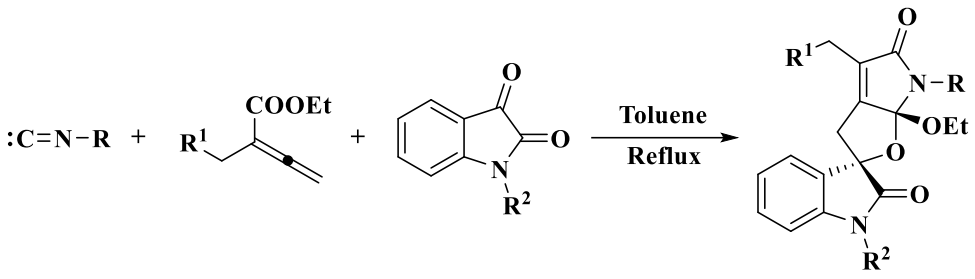

Scheme 4A.1

Vivekanand et al. established spirooxindole containing tetrahydro-cyclopenta[*b*]furan frameworks from isatin derived aldehydes and 1,3-dicarbonyl compounds using piperidine as catalyst (Scheme 4A.2). Generation of four new bonds, two new rings and single diastereomer of spirooxindole with five consecutive asymmetric carbons were the main features of this protocol [23].

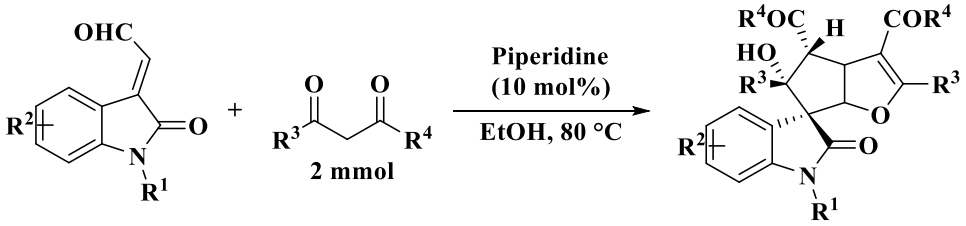

Scheme 4A.2

Murphy and co-workers reported an iodine mediated reaction between cyclic iodonium ylides and alkylidene-oxindoles for the preparation of spirooxindolo dihydrofurans (Scheme 4A.3). The reaction was catalyzed by Bu_4NI and tolerated on both electron rich and electron poor oxindoles in excellent yields [24].

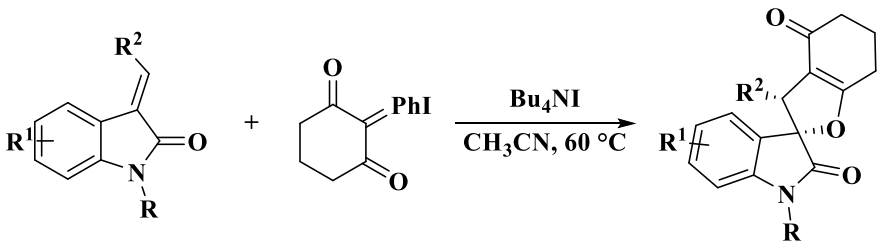

Scheme 4A.3

Yang et al. employed the selective construction of functionalized spiro-indoline-tetrapheno-furans from *o*-arylalkynylacetophenones and phenacylideneoxindoles using $Cu(OTf)_2$/HOTf as catalyst (Scheme 4A.4). This protocol established the practical application of the domino C–C coupling reaction in organic synthesis [25].

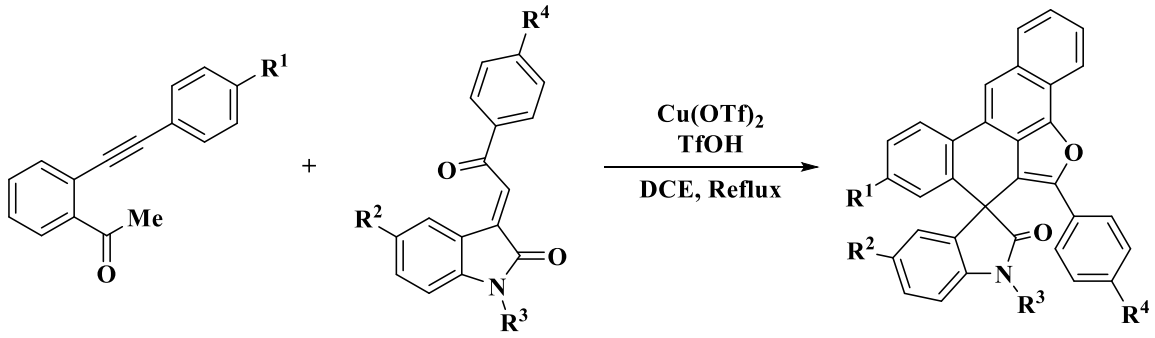

Scheme 4A.4

Baharfar and co-workers demonstrated a simple and efficient protocol for the synthesis of novel spirooxindolo furan derivatives using isatins, 1,3-dicarbonyl compounds and *N*-phenacyl pyridinium salts as the starting materials (Scheme 4A.5). Mild reaction conditions and simple work-up procedures were the advantages of this protocol [26].

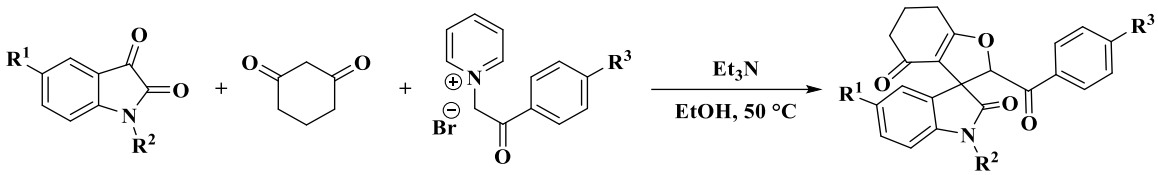

Scheme 4A.5

Azimi et al. produced a facile and efficient protocol for the diastereoselective construction of novel spirooxindolo dihydrofurans by the three-component reaction of isatins, 3-cyanoacetyl indole and *N*-phenacylpyridinium bromides (Scheme 4A.6). Preparation of highly functionalized spirooxindoles using commercially available starting materials in a single synthetic operation without isolating any intermediates were the main features of this reaction [27].

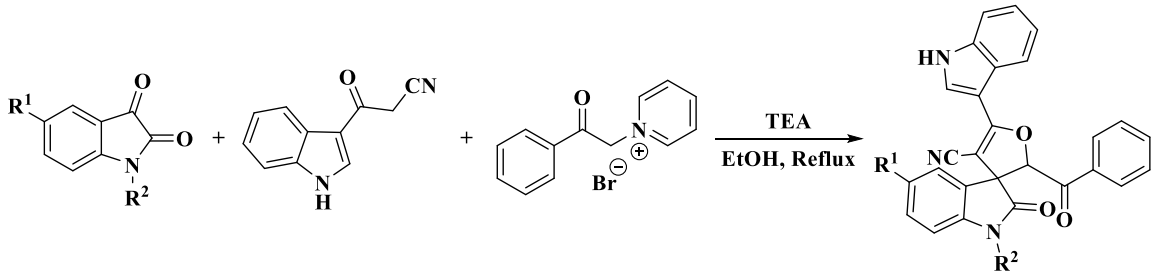

Scheme 4A.6

4A.2. Present work

In view of the aforementioned literature reports and considering the importance of spirooxindolo-furan moiety, herein we report an efficient three-component reaction of isatins **1a-f**, malononitrile **2** and *N*-phenacylisoquinolinium bromides **3a-e** for the

construction of isoquinoline based spirooxindolo-furans through [3+2] cycloaddition strategy (Scheme 4A.7). In addition, all the synthesized compounds were evaluated for *in silico* molecular docking and ADME prediction.

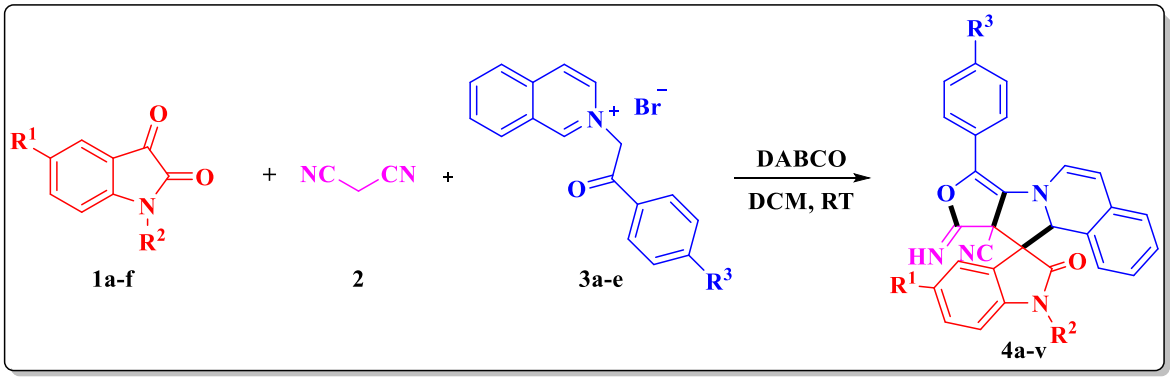

Scheme 4A.7. Synthesis of isoquinoline based spirooxindolo-furans **4a-v**.

4A.2.1. Results and discussion

We began our study by choosing isatin **1a** (1.0 mmol), malononitrile **2** (1.0 mmol) and 2-(2-oxo-2-phenylethyl)isoquinolin-2-ium bromide **3a** (1.0 mmol) as initial starting materials and investigating the effect of solvents and bases on the product yield (Table 4A.1). When the reaction was performed in DCM at room temperature without any base, the target product **4a** was obtained in 10% yield (Table 4A.1, entry 1). However, a significant improvement in the yield was observed in the presence of Et_3N in DCM (Table 4A.1, entry 2). Later, we tried to explore the reaction in different solvents such as $CHCl_3$, THF, 1,4-dioxane and water (Table 4A.1, entries 3-6). Among all, DCM is the best solvent for this cascade reaction (Table 4A.1, entry 2). Encouraged by these results, other bases such as DMAP, DABCO, DBU and K_2CO_3 were explored in DCM (Table 4A.1, entries 7-10) and found that DABCO was the efficient base to produce the desired product **4a** (Table 4A.1 entry 8). Next, we screened different amounts of DABCO and found that the yield of the product decreased slightly when the amount of DABCO was 1.0 equiv and 2.0 equiv (Table 4A.1, entries 11,12). From these results, we determined that DABCO (1.5 equiv) as base in DCM at room temperature (Table 4A.1, entry 8) is the optimal reaction condition for the construction of desired product **4a**.

Table 4A.1. Optimization of the reaction conditions[a]

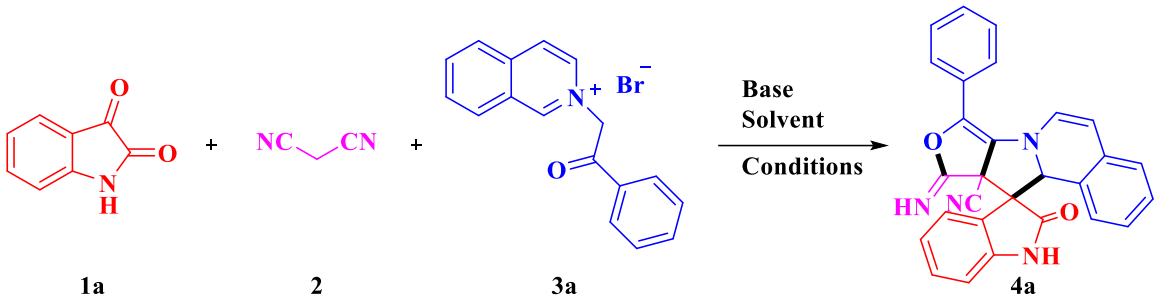

1a 2 3a 4a

Entry	Solvent	Base	Time (h)	Yield (%)[b]
1	DCM	--	24	10
2	DCM	Et_3N	8	70
3	$CHCl_3$	Et_3N	8	65
4	THF	Et_3N	10	50
5	1,4-Dioxane	Et_3N	10	50
6	H_2O	Et_3N	24	20
7	DCM	DMAP	6	75
8	**DCM**	**DABCO**	**4**	**85**
9	DCM	DBU	6	75
10	DCM	K_2CO_3	6	60
11[c]	DCM	DABCO	6	75
12[d]	DCM	DABCO	4	82

[a]Reaction condition: isatin **1a** (1.0 mmol), malononitrile **2** (1.0 mmol), compound **3a** (1.0 mmol) and base (1.5 equiv) in solvent (3 mL) at room temperature. [b]Isolated yields. [c]1.0 equiv of base was used. [d]2.0 equiv of base was used.

The above optimized conditions were explored for the reaction generality and scope of the substrates (Table 4A.2). In general, different substituted isatins **1a-f** and isoquinolinium bromides **3a-e** can react smoothly and offered the desire products in good yields. Electron donating (–CH_3), withdrawing (–NO_2) and halo (–Cl, –Br) substitutions on isoquinolinium bromide had no substantial impact on the efficiency of the reaction.

Table 4A.2. Synthesis of isoquinoline based spirooxindolo-furans **4a-v**[a,b]

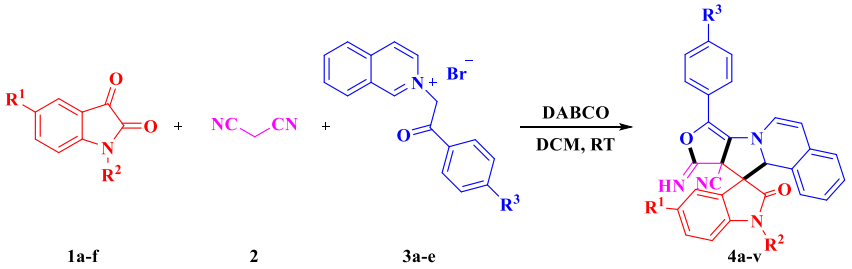

1a-f 2 3a-e 4a-v

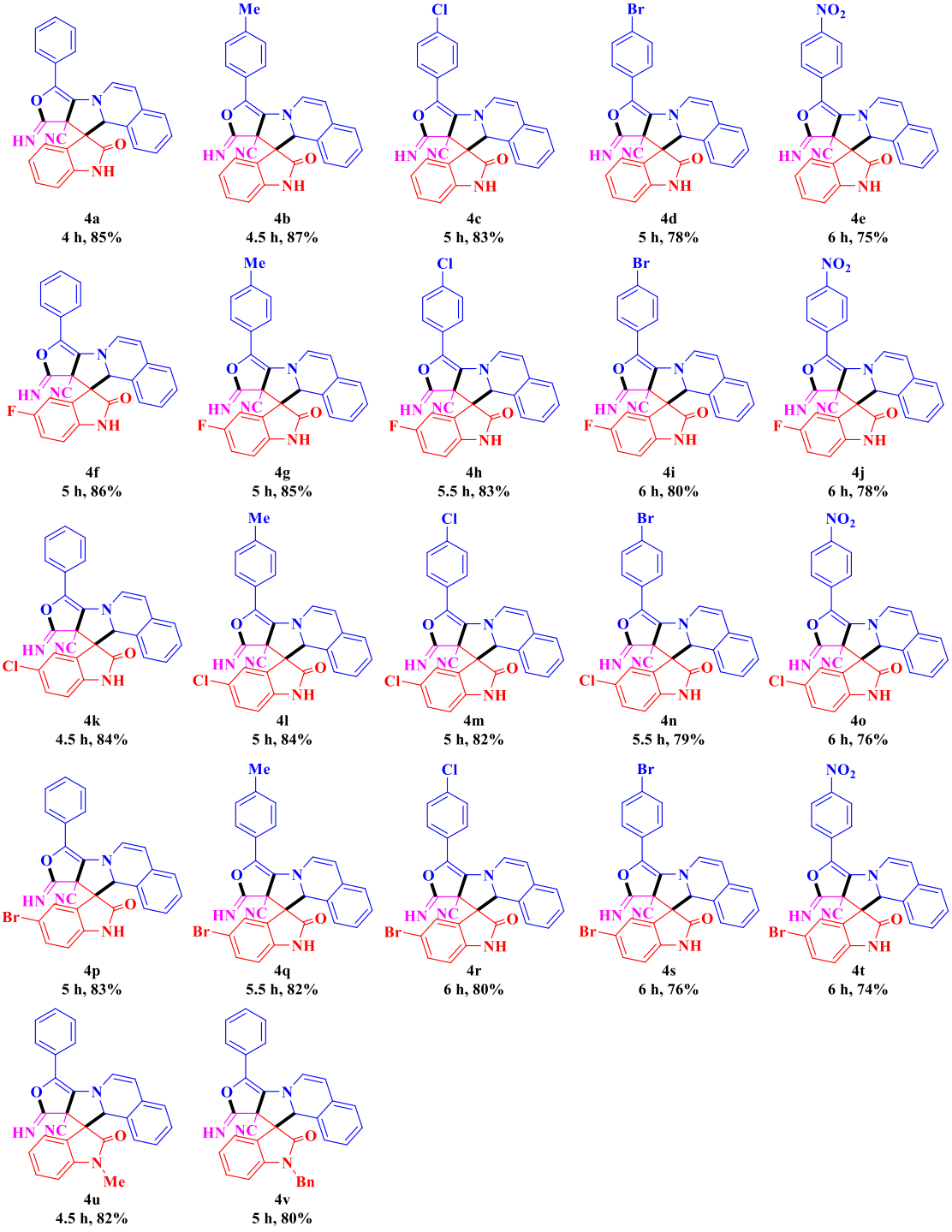

[a]Reaction condition: isatins **1a-f** (1.0 mmol), malononitrile **2** (1.0 mmol), compounds **3a-e** (1.0 mmol) and DABCO (1.5 equiv) in 3 mL of DCM at room temperature. [b]Isolated yields.

The plausible reaction mechanism for the generation of target compounds **4a-v** was presented in Scheme 4A.8. Initially, isatin **1a** on reaction with malononitrile **2** produces the intermediate **A.** On the other hand, *N*-phenacylisoquinolinium bromide **3a** converts in to dipolar intermediate **B** in the presence of DABCO [28]. Further, this *in situ* generated ylide (**B**) undergoes [3+2] cycloaddition with **A** generates the intermediate **C** [29]. From this, the de-protonation and intramolecular annulation (**E**) produces the target compound **4a** [30].

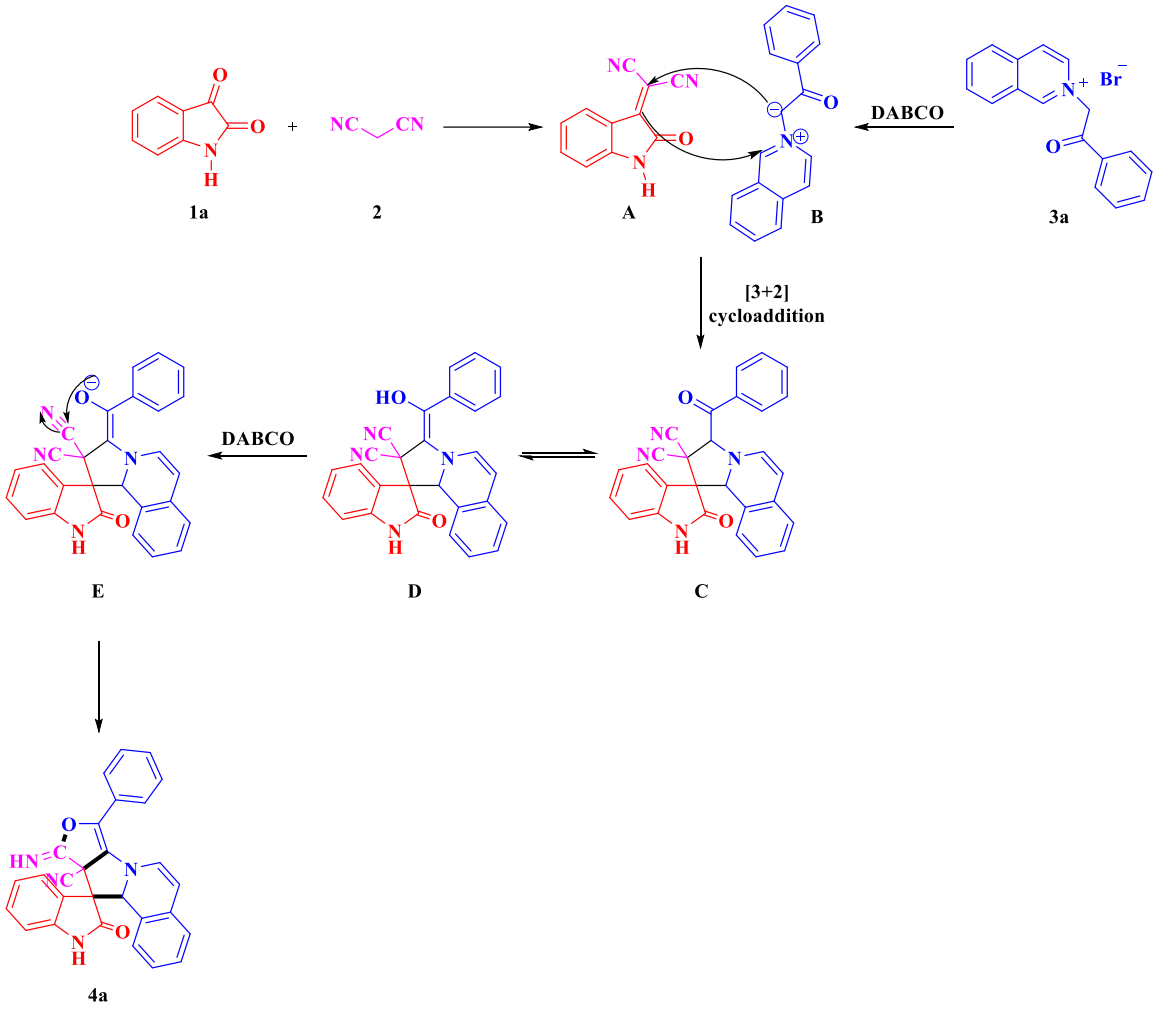

Scheme 4A.8. Plausible reaction mechanism for the generation of target compounds **4**.

The structure of the target compounds (**4a-v**) were analyzed by IR, ^{1}H NMR, ^{13}C NMR and mass spectral data. In this, the IR spectrum of compound **4m** shows the band at 3157 cm^{-1} represents the –NH stretching frequency [31]. The ^{1}H NMR spectrum of the compound **4m** showed two singlets at δ 11.16 *ppm* and δ 9.59 *ppm* corresponds to the two N–H protons of isatin and imine moieties [32,33]. The two –NH protons were further confirmed by D_2O exchange ^{1}H NMR spectrum (**4a**). In the ^{13}C NMR spectrum the peak appeared at δ 87.14 *ppm* corresponds the spiro carbon, which was further determined by the absence of this spiro carbon peak in DEPT-135 NMR spectrum. The molecular weight

of the compound **4m** was determined by the peak at *m/z* 511.1382 $[M+H]^+$ in mass spectrum.

4A.3. Molecular docking studies

All the synthesized compounds were successfully docked against *Mycobacterium tuberculosis* protein and the outcome of the results revealed that all the synthesized compounds **4a-v** were efficiently fit into the active sites of the protein (PDB ID: 1DF7) [34]. The results of the molecular docking study were presented in Table 4A.3. Among all, the compounds **4a, 4b, 4d, 4e, 4j, 4k, 4m**, **4n, 4o** and **4v** were showed good binding energies as -9.77, -9.75, -9.87, -10.32, -10.01, -9.78, -10.79, -10.99, -10.49 and -9.78 kcal/mol respectively. Among these, the compound **4n** exhibited more negative binding energy -10.99 kcal/mol, forms a hydrogen bond with the amino acid residue SER49 (2.70 Å) and also forms four hydrophobic interactions (π···π and π···alkyl) with the amino acids ILE5 (3.96 Å), ILE20 (4.36 and 4.66 Å) and PHE31 (4.54 Å). Whereas, the compound **4m** displayed binding energy -10.79 kcal/mol and forms a hydrogen bond with the amino acid residue SER49 (2.69 Å) and also exhibit four hydrophobic interactions (π···π and π···alkyl) with the amino acids ILE5 (3.88 Å), ILE20 (4.35 and 4.70 Å) and PHE31 (4.46 Å). The ligand interactions of the compounds **4m** and **4n** with 1DF7 protein were presented in Figure 4A.5 and Figure 4A.6.

Table 4A.3. Docking results of the compounds **4a-v** against 1DF7

Ent-ry	Compound	Binding energy (kcal/mol)	No. of hydrogen bonds	Residues involved in the hydrogen bonding	Hydrogen bond length (Å)
1	**4a**	-9.77	1	SER49	2.71
2	**4b**	-9.75	2	THR46, SER49	2.90, 2.63
3	**4c**	-9.66	3	HIS30, THR46, SER49	3.76, 2.85, 2.65
4	**4d**	-9.87	3	HIS30, THR46, SER49	3.77, 2.85, 2.66
5	**4e**	-10.32	1	ARG32	2.21
6	**4f**	-9.44	1	SER49	2.72
7	**4g**	-9.41	2	THR46, SER49	2.87, 2.64
8	**4h**	-9.35	2	THR46, SER49	2.85, 2.67
9	**4i**	-9.56	3	HIS30, THR46, SER49	3.77, 2.85, 2.66
10	**4j**	-10.01	2	ARG32, PRO51	2.15, 3.33
11	**4k**	-9.78	1	SER49	2.73
12	**4l**	-9.69	2	THR46, SER49	2.87, 2.64

13	**4m**	**-10.79**	1	SER49	2.69
14	**4n**	**-10.99**	1	SER49	2.70
15	**4o**	-10.49	3	ARG32, PRO51	2.03, 2.85, 3.18
16	**4p**	-8.80	0	--	--
17	**4q**	-9.24	0	--	--
18	**4r**	-9.33	0	--	--
19	**4s**	-9.55	0	--	--
20	**4t**	-7.89	2	GLY15, SER49	3.63, 2.31
21	**4u**	-9.48	0	--	--
22	**4v**	-9.78	1	PRO51	2.95

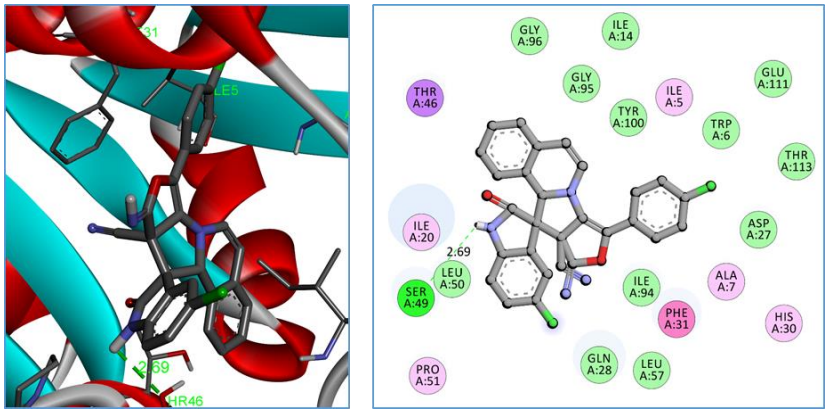

Figure 4A.5. Binding interactions between compound **4m** and active site of 1DF7.

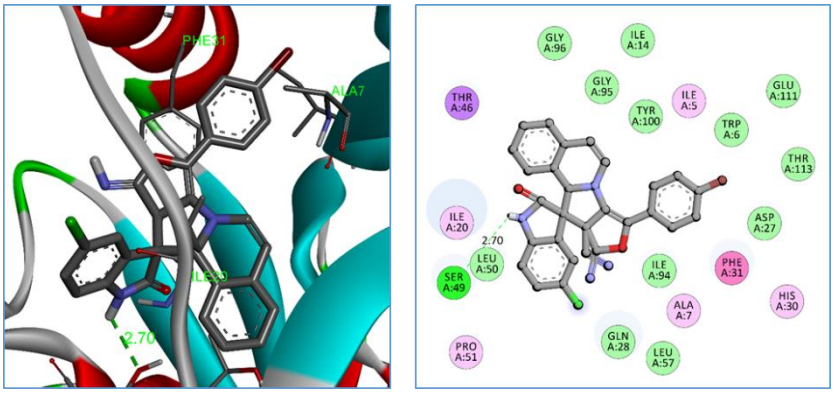

Figure 4A.6. Binding interactions between compound **4n** and active site of 1DF7.

4A.4. ADME prediction

Absorption, distribution, metabolism and excretion (ADME) data improves the selection and identification of molecules at the therapeutic dose with an optimal safety profile. Also, *in silico* prediction of pharmacokinetic parameters lowers the risk of failure of drug at the final stages of clinical trials [35]. The ADME prediction of the synthesized compounds **4a-v** were illustrated in Table 4A.4.

Estimation of octanol/water partition coefficient (lipophilicity) is examined by LogP. The predicted lipophilicity values are in the ranging from 3.953 to 5.653, and these values revealed that good lipophilicity of the compounds. The predicted aqueous solubility (LogS) values of the synthesized compounds ranging from -4.525 to -5.471, which reflects their moderate solubility in water due to presence of lipophilic groups. On the other hand, the topological polar surface area (TPSA) values (80.42-132.35) reveals that the compounds' oral bioavailability is high. In general, higher the logarithm of the apparent permeability coefficient (logPapp) higher will be the Caco-2 permeability. From the results, it is predicted that all the compounds have shown moderate Caco-2 permeability in the range from 0.366 x 10^{-6} to 0.686 x 10^{-6}. Interestingly, all the synthesized compounds exhibit high human intestinal absorption (HIA: 89-100%). Blood/brain partition coefficient (logBB) value is a measure of the ability of a drug to cross the blood-brain barrier (BBB). The target compounds are in considerable range of BBB. The observed drug like properties and *in silico* ADME prediction suggests that the target compounds **4a-v** exhibit acceptable pharmacokinetic parameters and can be considered as lead molecules for the development of future drugs.

Table 4A.4. Drug likeness and *in silico* ADME properties of the target compounds **4a-v**

Entry	Mol.Wt	H-donor	H-acceptor	No. of rotatable bonds	LogP	LogS	TPSA (Å)	Caco-2 Permeability (logPapp in 10^{-6} cm/s)	HIA (% absorbed)	BBB permeability (log BB)
	≤500	**≤5**	**≤10**	**≤10**	**≤5**	**<0.5**	**≤140**	**>8x10^{-6}**	**70 - 100%**	**-3.0 - 1.2**
4a	442.47	2	6	1	4.064	-4.738	89.21	0.574	92.708	-0.372
4b	456.50	2	6	1	4.520	-4.930	89.21	0.643	92.756	-0.397
4c	476.91	2	6	1	4.742	-4.806	89.21	0.593	91.297	-0.551
4d	521.37	2	6	1	4.882	-4.815	89.21	0.585	91.230	-0.571
4e	487.47	2	9	2	3.998	-4.525	132.35	0.686	100	-0.591
4f	460.46	2	6	1	4.161	-4.748	89.21	0.615	92.015	-0.58
4g	474.49	2	6	1	4.627	-4.936	89.21	0.685	92.062	-0.605
4h	494.91	2	6	1	4.860	-4.837	89.21	0.635	90.604	-0.758
4i	439.35	2	6	1	5.000	-4.849	89.21	0.627	90.537	-0.779
4j	505.46	2	9	2	4.085	-4.548	132.35	0.659	100	-0.798
4k	476.92	2	6	1	4.681	-4.828	89.21	0.593	90.947	-0.556
4l	490.15	2	6	1	5.126	-5.029	89.21	0.662	90.995	-0.58
4m	511.36	2	6	1	5.364	-4.934	89.21	0.613	89.537	-0.734
4n	555.81	2	6	1	5.505	-4.959	89.21	0.604	89.469	-0.754

4o	521.92	2	9	2	4.608	-4.630	132.35	0.591	100	-0.774
4p	521.36	2	6	1	4.810	-4.852	89.21	0.584	90.88	-0.576
4q	535.40	2	6	1	5.255	-5.058	89.21	0.654	90.928	-0.601
4r	555.81	2	6	1	5.497	-4.970	89.21	0.604	89.469	-0.754
4s	600.26	2	6	1	5.653	-5.005	89.21	0.596	89.402	-0.775
4t	566.37	2	9	2	4.765	-4.654	132.35	0.594	100	-0.794
4u	456.50	1	6	1	3.953	-4.970	80.42	0.528	95.533	-0.052
4v	532.60	1	6	3	5.216	-5.471	80.42	0.366	96.442	-0.102

Mol. Wt: molecular weight; **H-donor**: number of hydrogen bond donors; **H-acceptor**: number of hydrogen bond acceptors; **LogP**: octanol/water partition coefficient; **LogS**: aqua solubility parameter; **TPSA**: topological polar surface area; **Caco-2**: cell permeability; **HIA**: human intestinal absorption; **LogBB**: blood/brain partition co-efficient.

4A.5. Conclusion

In this chapter, we have successfully established an efficient protocol for the generation of isoquinoline based spirooxindolo-furans through [3+2] cycloaddition of isatin malononitrile adducts with isoquinolinium ylides. This method exhibits the advantages of mild reaction conditions, easy operation and broad substrate scope. Further, *in silico* molecular docking study, ADME prediction and drug likeness profiles reveal that the target compounds represent a promising platform for the development of novel therapeutic agents.

4A.6. Experimental Section

4A.6.1. General procedure for isoquinoline based spirooxindolo-furans (4a-v)

To a solution of isatin **1** (1.0 mmol) in DCM, malononitrile **2** was added (1.0 mmol) and continued the reaction for 10 min, to this *N*-phenacylisoquinolinium bromides **3** (1.0 mmol) and DABCO (1.5 equiv) were added and continue the reaction at room temperature. The progress of the reaction was monitored by TLC. After completion, the reaction mixture was filtered and the resulting solid product was recrystallized from methanol to afford the targeted compounds.

4A.6.2. Molecular docking protocol

The docking studies are prominent tools for the assessment of the binding affinity to the ligand-protein receptor. All the synthesized compounds were subjected to *in silico* molecular docking studies by using the AutoDockTools (ADT) version 1.5.6 and AutoDock version 4.2.5.1 docking program [36]. The 3D-structures of all the synthesized compounds were prepared by using chem3D pro 12.0 software. The optimized 3D

structures were saved in pdb format. The structure of the dihydrofolate reductase of *Mycobacterium tuberculosis* (PDB code: 1DF7) protein was extracted from the protein data bank (http://www.rcsb.org/pdb). The bound ligand and water molecules in protein were removed by using Discovery Studio Visualizer version 4.0 to prepare the protein. Non polar hydrogens were merged and gasteiger charges were added to the protein. The grid file was saved in gpf format. The three dimensional grid box having dimensions 60 x 60 x 60 $Å^3$ was created around the protein with spacing 0.3750 Å. The genetic algorithm was carried out with the population size and the maximum number of evaluations were 150 and 25,00,000 respectively. The docking output file was saved as Lamarckian Ga (4.2) in dpf format. The ligand-protein complex binding sites were visualized by Discovery Studio Visualizer version 4.0.

4A.6.3. ADME prediction

In silico ADME properties and pharmacokinetic parameters of the synthesized compounds were calculated by using the online servers ADMETlab 2.0 and pkCSM [37,38]. The ADMET properties, human intestinal absorption (HIA), Caco-2 cell permeability, plasma protein binding and blood brain barrier penetration (BBB) were predicted using this program.

4A.7. Spectral data of synthesized compounds 4a-v

10-imino-2'-oxo-8-phenyl-11*aH*-spiro[furo[3',4':4,5]pyrrolo[2,1-*a*]isoquinoline-11,3'-indoline]-10*a*(10*H*)-carbonitrile (4a)

Yellow solid. mp: 175-177 °C. IR (KBr, cm^{-1}): 3162, 3030, 1656, 1572, 1468. ^{1}H NMR (400 MHz, DMSO-d_6) δ: 11.00 (s, 1H), 9.55 (s, 1H), 7.61 (s, 2H), 7.49 (s, 4H), 7.45 (d, J = 6.0 Hz, 2H), 7.38 (d, J = 1.6 Hz, 2H), 7.18 (t, J = 7.6 Hz, 1H), 7.13 (d, J = 7.6 Hz, 1H), 7.05 (t, J = 7.2 Hz, 1H), 6.93 (d, J = 6.8 Hz, 1H), 6.49 (d, J = 6.8 Hz, 1H), 5.95 (s, 1H). ^{13}C NMR (100 MHz, DMSO-d_6) δ: 171.23, 155.78, 139.62, 136.14, 130.85, 130.65, 130.36, 129.33, 128.95, 128.17, 127.31, 127.07, 126.70, 124.15, 123.00, 122.04, 121.93, 112.17, 112.12, 112.01, 110.58, 102.27, 87.47, 64.82, 55.38. ESI-MS (m/z): $[M+H]^+$ calcd. for $C_{28}H_{19}N_4O_2$: 443.1508; found: 443.1517.

10-imino-2'-oxo-8-(*p*-tolyl)-11*aH*-spiro[furo[3',4':4,5]pyrrolo[2,1-*a*]isoquinoline-11,3'-indoline]-10*a*(10*H*)-carbonitrile (4b)

Brown solid. mp: 190-192 °C. IR (KBr, cm^{-1}): 3166, 2922, 1653, 1566, 1467. ^{1}H NMR (400 MHz, DMSO-d_6) δ: 10.99 (s, 1H), 9.49 (s, 1H), 7.49 (d, J = 8.0 Hz, 2H), 7.46 – 7.41

(m, 3H), 7.37 (d, *J* = 6.8 Hz, 2H), 7.29 (d, *J* = 8.0 Hz, 2H), 7.17 (t, *J* = 7.6 Hz, 1H), 7.12 (d, *J* = 7.6 Hz, 1H), 7.05 (t, *J* = 7.6 Hz, 1H), 6.92 (d, *J* = 7.6 Hz, 1H), 6.48 (d, *J* = 7.6 Hz, 1H), 5.91 (s, 1H), 2.34 (s, 3H). ^{13}C NMR (100 MHz, DMSO-d_6) δ: 171.22, 155.97, 140.27, 139.60, 133.15, 130.84, 130.35, 129.89, 128.94, 128.19, 127.25, 127.03, 126.73, 124.15, 122.97, 122.06, 121.90, 111.95, 110.55, 102.22, 87.44, 64.83, 52.19, 21.21. ESI-MS (m/z): $[M+H]^+$ calcd. for $C_{29}H_{21}N_4O_2$: 457.1665; found: 457.1657.

8-(4-chlorophenyl)-10-imino-2'-oxo-11*aH*-spiro[furo[3',4':4,5]pyrrolo[2,1-*a*]isoquinoline-11,3'-indoline]-10*a*(10*H*)-carbonitrile (4c)

Brown solid. mp: 183-185 °C. IR (KBr, cm^{-1}): 3160, 3087, 1659, 1579, 1466. ^{1}H NMR (400 MHz, DMSO-d_6) δ: 11.05 (s, 1H), 9.59 (s, 1H), 7.64 (d, *J* = 8.4 Hz, 2H), 7.56 (d, *J* = 8.0 Hz, 2H), 7.48 – 7.44 (m, 3H), 7.38 (d, *J* = 7.2 Hz, 2H), 7.18 (t, *J* = 7.6 Hz, 1H), 7.12 (d, *J* = 7.6 Hz, 1H), 7.05 (t, *J* = 7.6 Hz, 1H), 6.94 (d, *J* = 7.6 Hz, 1H), 6.49 (d, *J* = 7.6 Hz, 1H), 6.03 (s, 1H). ^{13}C NMR (100 MHz, DMSO-d_6) δ: 171.21, 155.10, 139.65, 135.49, 135.20, 130.78, 130.39, 129.37, 128.99, 128.07, 127.32, 127.16, 126.65, 124.20, 123.07, 121.97, 112.03, 110.64, 102.31, 87.05, 64.67, 52.11. ESI-MS (m/z): $[M+H]^+$ calcd. for $C_{28}H_{18}ClN_4O_2$: 477.1118; found: 477.1117.

8-(4-bromophenyl)-10-imino-2'-oxo-11*aH*-spiro[furo[3',4':4,5]pyrrolo[2,1-*a*]isoquinoline-11,3'-indoline]-10*a*(10*H*)-carbonitrile (4d)

Yellow solid. mp: 183-185 °C. IR (KBr, cm^{-1}): 3156, 3085, 1658, 1577, 1465. ^{1}H NMR (400 MHz, DMSO-d_6) δ: 11.05 (s, 1H), 9.59 (s, 1H), 7.70 (d, *J* = 8.8 Hz, 2H), 7.57 (d, *J* = 8.4 Hz, 2H), 7.50 – 7.42 (m, 3H), 7.38 (d, *J* = 8.0 Hz, 2H), 7.18 (t, *J* = 7.6 Hz, 1H), 7.11 (d, *J* = 7.6 Hz, 1H), 7.05 (t, *J* = 7.6 Hz, 1H), 6.94 (d, *J* = 7.6 Hz, 1H), 6.48 (d, *J* = 7.6 Hz, 1H), 6.03 (s, 1H). ^{13}C NMR (100 MHz, DMSO-d_6) δ: 171.21, 155.06, 139.65, 135.63, 132.29, 130.78, 130.39, 129.62, 128.99, 128.06, 127.33, 127.17, 126.65, 124.29, 124.20, 123.07, 121.97, 112.04, 110.65, 102.31, 87.11, 64.65, 52.04. ESI-MS (m/z): $[M+H]^+$ calcd. for $C_{28}H_{18}BrN_4O_2$: 521.0613; found: 521.0613.

10-imino-8-(4-nitrophenyl)-2'-oxo-11*aH*-spiro[furo[3',4':4,5]pyrrolo[2,1-*a*]isoquinoline-11,3'-indoline]-10*a*(10*H*)-carbonitrile (4e)

Yellow solid. mp: 178-180 °C. IR (KBr, cm^{-1}): 3211, 3083, 1659, 1579, 1466. ^{1}H NMR (400 MHz, DMSO-d_6) δ: 11.08 (s, 1H), 9.75 (s, 1H), 8.33 (d, *J* = 8.8 Hz, 2H), 7.93 (d, *J* = 8.4 Hz, 2H), 7.49 7.44 (m, 3H), 7.39 (t, *J* = 8.8 Hz, 2H), 7.20 (t, *J* = 7.6 Hz, 1H), 7.14 (d, *J* = 7.2 Hz, 1H), 7.07 (t, *J* = 7.6 Hz, 1H), 6.94 (d, *J* = 7.6 Hz, 1H), 6.51 (d, *J* = 7.6 Hz, 1H),

6.14 (s, 1H). ^{13}C NMR (100 MHz, DMSO-d_6) δ: 171.19, 154.36, 149.07, 143.20, 139.70, 130.72, 130.48, 129.22, 129.07, 127.98, 127.40, 126.47, 124.31, 123.20, 122.08, 121.87, 112.07, 111.78, 110.73, 102.53, 86.92, 64.59, 52.07. ESI-MS (m/z): $[M+H]^+$ calcd. for $C_{28}H_{18}N_5O_4$: 488.1359; found: 488.1348.

5'-fluoro-10-imino-2'-oxo-8-phenyl-11*aH*-spiro[furo[3',4':4,5]pyrrolo[2,1-*a*]isoquinoline-11,3'-indoline]-10*a*(10*H*)-carbonitrile (4f)

Yellow solid. mp: 180-182 °C. IR (KBr, cm^{-1}): 3155, 3063, 1665, 1569. ^{1}H NMR (400 MHz, DMSO-d_6) δ: 11.03 (s, 1H), 9.59 (s, 1H), 7.62 (d, J = 4.0 Hz, 2H), 7.53 – 7.47 (m, 5H), 7.44 (dd, J = 6.0, 2.8 Hz, 1H), 7.39 (d, J = 7.2 Hz, 1H), 7.17 – 7.14 (m, 2H), 7.03 (td, J = 9.2, 2.4 Hz, 1H), 6.91 (dd, J = 8.4, 4.8 Hz, 1H), 6.56 (d, J = 7.6 Hz, 1H), 6.02 (s, 1H). ^{13}C NMR (100 MHz, DMSO-d_6) δ: 171.25, 159.16 (d, J = 233.2 Hz), 135.98 (d, J = 23.0 Hz), 131.06, 130.72, 130.59, 130.44, 129.37, 129.16, 127.83, 127.54, 127.25, 126.74, 124.17, 123.28 (d, J = 9.6 Hz), 113.31, 113.08, 112.69, 112.07, 111.18 (d, J = 9.0 Hz), 110.17, 109.91, 101.74, 87.54, 64.96, 52.29. ESI-MS (m/z): $[M+H]^+$ calcd. for $C_{28}H_{18}FN_4O_2$: 461.1414; found: 461.1409.

5'-fluoro-10-imino-2'-oxo-8-(*p*-tolyl)-11*aH*-spiro[furo[3',4':4,5]pyrrolo[2,1-*a*]isoquinoline-11,3'-indoline]-10*a*(10*H*)-carbonitrile (4g)

Yellow solid. mp: 188-190 °C. IR (KBr, cm^{-1}): 3163, 3082, 1655, 1566, 1478. ^{1}H NMR (400 MHz, DMSO-d_6) δ: 11.01 (s, 1H), 9.53 (s, 1H), 7.48 (d, J = 8.4 Hz, 4H), 7.45 (s, 1H), 7.38 (d, J = 6.8 Hz, 1H), 7.29 (d, J = 7.6 Hz, 2H), 7.14 (d, J = 8.0 Hz, 2H), 7.02 (t, J = 8.4 Hz, 1H), 6.90 (dd, J = 8.0, 4.8 Hz, 1H), 6.54 (d, J = 7.6 Hz, 1H), 5.98 (s, 1H), 2.34 (s, 3H). ^{13}C NMR (100 MHz, DMSO-d_6) δ: 171.25, 159.15 (d, J = 233.2 Hz), 157.03, 140.35, 135.73, 133.00, 130.59 (d, J = 16.8 Hz), 129.92, 129.14, 127.84 (d, J = 32.2 Hz), 127.18, 126.76, 124.17, 123.30, 123.20, 113.27, 113.03, 112.60, 112.13, 111.14 (d, J = 8.0 Hz), 110.14, 109.88, 101.67, 87.51, 64.98, 52.32, 21.20. ESI-MS (m/z): $[M+H]^+$ calcd. for $C_{29}H_{20}FN_4O_2$: 475.1570; found: 475.1572.

8-(4-chlorophenyl)-5'-fluoro-10-imino-2'-oxo-11*aH*-spiro[furo[3',4':4,5]pyrrolo[2,1-*a*]isoquinoline-11,3'-indoline]-10*a*(10*H*)-carbonitrile (4h)

Yellow solid. mp: 185-187 °C. IR (KBr, cm^{-1}): 3167, 3086, 1660, 1579, 1478. ^{1}H NMR (400 MHz, DMSO-d_6) δ: 11.06 (s, 1H), 9.63 (s, 1H), 7.64 (d, J = 8.8 Hz, 2H), 7.57 (d, J = 8.8 Hz, 2H), 7.48 (s, 2H), 7.44 (dd, J = 6.4, 3.2 Hz, 1H), 7.39 (d, J = 7.2 Hz, 1H), 7.14 (d, J = 7.6 Hz, 2H), 7.01 (dd, J = 9.2, 2.4 Hz, 1H), 6.91 (dd, J = 8.4, 4.8 Hz, 1H), 6.55 (d, J =

7.6 Hz, 1H), 6.09 (s, 1H). ^{13}C NMR (100 MHz, DMSO-d_6) δ: 171.24, 159.16 (d, J = 233.4 Hz), 156.14, 135.79, 135.56, 135.04, 130.53 (d, J = 7.2 Hz), 129.94, 129.40 (d, J = 7.8 Hz), 129.20, 127.73, 127.55, 126.68, 124.22, 123.21, 123.11, 113.40 (d, J = 23.4 Hz), 112.72, 111.98, 111.89, 111.15, 110.26, 109.99, 101.76, 87.12, 64.81, 52.23. ESI-MS (m/z): $[M+H]^+$ calcd. for $C_{28}H_{17}ClFN_4O_2$: 495.1024; found: 495.1020.

8-(4-bromophenyl)-5'-fluoro-10-imino-2'-oxo-11*aH*-spiro[furo[3',4':4,5]pyrrolo[2,1-*a*]isoquinoline-11,3'-indoline]-10*a*(10*H*)-carbonitrile (4i)

Brown solid. mp: 176-178 °C. IR (KBr, cm^{-1}): 3169, 3085, 1660, 1579, 1479. ^{1}H NMR (400 MHz, DMSO-d_6) δ: 11.07 (s, 1H), 9.62 (s, 1H), 7.70 (d, J = 8.8 Hz, 2H), 7.56 (d, J = 8.8 Hz, 2H), 7.46 (s, 2H), 7.38 (d, J = 6.8 Hz, 2H), 7.13 (d, J = 8.0 Hz, 1H), 7.03 (t, J = 9.2 Hz, 1H), 6.92 (d, J = 4.8 Hz, 1H), 6.55 (d, J = 7.6 Hz, 1H), 6.09 (s, 1H), 5.75 (s, 1H). ^{13}C NMR (100 MHz, DMSO-d_6) δ: 171.23, 157.78 (d, J = 243.4 Hz), 139.68, 137.17, 131.80, 130.68 (d, J = 9.2 Hz), 129.36, 128.98, 128.19, 127.51, 127.04, 125.79, 124.19, 123.10, 122.35, 120.96, 112.37 (d, J = 24.6 Hz), 111.31, 110.18, 103.28, 88.47, 63.84, 55.28. ESI-MS (m/z): $[M+H+2]^+$ calcd. for $C_{28}H_{17}BrFN_4O_2$: 541.0474; found: 541.0473.

5'-fluoro-10-imino-8-(4-nitrophenyl)-2'-oxo-11*aH*-spiro[furo[3',4':4,5]pyrrolo[2,1-*a*]isoquinoline-11,3'-indoline]-10*a*(10*H*)-carbonitrile (4j)

Yellow solid. mp: 177-179 °C. IR (KBr, cm^{-1}): 3239, 3081, 1661, 1578, 1480. ^{1}H NMR (400 MHz, DMSO-d_6) δ: 11.10 (s, 1H), 9.80 (s, 1H), 8.33 (d, J = 8.8 Hz, 2H), 7.93 (d, J = 8.4 Hz, 2H), 7.49 (s, 2H), 7.45 (dd, J = 6.0, 2.8 Hz, 1H), 7.40 (d, J = 7.2 Hz, 1H), 7.19 – 7.14 (m, 2H), 7.04 (td, J = 9.2, 2.4 Hz, 1H), 6.92 (dd, J = 8.4, 4.8 Hz, 1H), 6.58 (d, J = 7.6 Hz, 1H), 6.20 (s, 1H). ^{13}C NMR (100 MHz, DMSO-d_6) δ: 171.22, 159.20 (d, J = 233.4 Hz), 155.37, 149.11, 143.03, 135.83, 130.55 (d, J = 8.4 Hz), 129.27, 129.16, 127.63, 126.50, 124.34, 124.28, 123.10 (d, J = 9.4 Hz), 113.58 (d, J = 23.6 Hz), 112.75, 111.78, 111.63, 111.34, 110.41, 110.14, 101.93, 86.98, 64.74, 52.18. ESI-MS (m/z): $[M+H]^+$ calcd. for $C_{28}H_{17}FN_5O_4$: 506.1265; found: 506.2248.

5'-chloro-10-imino-2'-oxo-8-phenyl-11*aH*-spiro[furo[3',4':4,5]pyrrolo[2,1-*a*]isoquinoline-11,3'-indoline]-10*a*(10*H*)-carbonitrile (4k)

Orange solid. mp: 178-180 °C. IR (KBr, cm^{-1}): 3409, 3094, 1669, 1574, 1411. ^{1}H NMR (400 MHz, DMSO-d_6) δ: 11.12 (s, 1H), 9.54 (s, 1H), 7.61 (d, J = 4.0 Hz, 2H), 7.49 (d, J = 4.4 Hz, 5H), 7.45 – 7.42 (m, 1H), 7.38 (d, J = 7.6 Hz, 1H), 7.36 (d, J = 1.2 Hz, 1H), 7.22 (dd, J = 8.4, 2.0 Hz, 1H), 7.13 (d, J = 7.6 Hz, 1H), 6.93 (d, J = 8.4 Hz, 1H), 6.53 (d, J = 7.6

Hz, 1H), 6.05 (s, 1H). ^{13}C NMR (100 MHz, DMSO-d_6) δ: 171.00, 156.97, 138.12, 136.02, 130.72, 130.49, 129.36, 129.20, 127.80, 127.57, 127.25, 126.57, 126.41, 125.85, 124.28, 123.84, 122.51, 112.26, 112.08, 111.75, 101.18, 87.55, 64.97, 52.52. ESI-MS (m/z): $[M+H]^+$ calcd. for $C_{28}H_{18}ClN_4O_2$: 477.1118; found: 477.1131.

5'-chloro-10-imino-2'-oxo-8-(*p*-tolyl)-11*aH*-spiro[furo[3',4':4,5]pyrrolo[2,1-*a*]isoquinoline-11,3'-indoline]-10*a*(10*H*)-carbonitrile (4l)

Yellow solid. mp: 186-188 °C. IR (KBr, cm^{-1}): 3136, 3075, 1655, 1565, 1417. ^{1}H NMR (400 MHz, DMSO-d_6) δ: 11.11 (s, 1H), 9.49 (s, 1H), 7.49 (s, 1H), 7.48 (s, 3H), 7.45 – 7.42 (m, 1H), 7.38 (d, *J* = 7.2 Hz, 1H), 7.35 (s, 1H), 7.29 (d, *J* = 7.6 Hz, 2H), 7.21 (dd, *J* = 8.4, 1.2 Hz, 1H), 7.11 (d, *J* = 7.6 Hz, 1H), 6.93 (d, *J* = 8.0 Hz, 1H), 6.52 (d, *J* = 7.2 Hz, 1H), 6.02 (s, 1H), 2.33 (s, 3H). ^{13}C NMR (100 MHz, DMSO-d_6) δ: 171.00, 157.17, 140.35, 138.11, 133.03, 130.49, 129.91, 129.18, 127.81, 127.56, 127.18, 126.59, 126.36, 125.82, 124.28, 123.85, 122.48, 112.15, 111.71, 101.14, 87.53, 64.98, 52.56, 21.20. ESI-MS (m/z): $[M+H]^+$ calcd. for $C_{29}H_{20}ClN_4O_2$: 491.1275; found: 491.1270.

5'-chloro-8-(4-chlorophenyl)-10-imino-2'-oxo-11*aH*-spiro[furo[3',4':4,5]pyrrolo[2,1-*a*]isoquinoline-11,3'-indoline]-10*a*(10*H*)-carbonitrile (4m)

Yellow solid. mp: 180-182 °C. IR (KBr, cm^{-1}): 3157, 3063, 1659, 1576, 1416. ^{1}H NMR (400 MHz, DMSO-d_6) δ: 11.16 (s, 1H), 9.59 (s, 1H), 7.64 (d, *J* = 8.4 Hz, 2H), 7.57 (d, *J* = 8.8 Hz, 2H), 7.48 (d, *J* = 2.8 Hz, 2H), 7.44 (dd, *J* = 5.6, 3.2 Hz, 1H), 7.39 (d, *J* = 7.2 Hz, 1H), 7.36 (d, *J* = 1.2 Hz, 1H), 7.22 (dd, *J* = 8.4, 2.0 Hz, 1H), 7.11 (d, *J* = 7.6 Hz, 1H), 6.94 (d, *J* = 8.0 Hz, 1H), 6.53 (d, *J* = 7.6 Hz, 1H), 6.12 (s, 1H). ^{13}C NMR (100 MHz, DMSO-d_6) δ: 170.99, 156.25, 138.16, 135.57, 135.08, 130.52, 130.42, 129.40, 129.32, 129.24, 127.70, 127.60, 126.50, 125.89, 124.34, 123.75, 122.60, 112.29, 112.00, 111.80, 101.23, 87.14, 64.82, 52.47. ESI-MS (m/z): $[M+H]^+$ calcd. for $C_{28}H_{17}Cl_2N_4O_2$: 511.0729; found: 511.1382.

8-(4-bromophenyl)-5'-chloro-10-imino-2'-oxo-11*aH*-spiro[furo[3',4':4,5]pyrrolo[2,1-*a*]isoquinoline-11,3'-indoline]-10*a*(10*H*)-carbonitrile (4n)

Yellow solid. mp: 181-183 °C. IR (KBr, cm^{-1}): 3164, 3064, 1659, 1576, 1416. ^{1}H NMR (400 MHz, DMSO-*d*6) δ: 11.16 (s, 1H), 9.59 (s, 1H), 7.70 (d, *J* = 8.8 Hz, 2H), 7.56 (d, *J* = 8.4 Hz, 2H), 7.48 (s, 2H), 7.46 – 7.43 (m, 1H), 7.39 (d, *J* = 7.2 Hz, 1H), 7.35 (d, *J* = 1.2 Hz, 1H), 7.22 (dd, *J* = 8.4, 2.0 Hz, 1H), 7.11 (d, *J* = 7.6 Hz, 1H), 6.94 (d, *J* = 8.4 Hz, 1H), 6.53 (d, *J* = 7.2 Hz, 1H), 6.12 (s, 1H). ^{13}C NMR (100 MHz, DMSO-*d*6) δ: 170.99, 156.21,

138.16, 135.51, 132.32, 130.52, 130.42, 129.56, 129.24, 127.69, 127.60, 126.49, 125.89, 124.34, 123.75, 122.60, 112.30, 112.00, 111.81, 101.22, 87.20, 64.81, 52.40. ESI-MS (m/z): $[M+H]^+$ calcd. for $C_{28}H_{17}BrClN_4O_2$: 555.0223; found: 555.0228.

5'-chloro-10-imino-8-(4-nitrophenyl)-2'-oxo-11*aH*-spiro[furo[3',4':4,5]pyrrolo[2,1-*a*]isoquinoline-11,3'-indoline]-10*a*(10*H*)-carbonitrile (4o)

Yellow solid. mp: 179-181 °C. IR (KBr, cm^{-1}): 3181, 3088, 1661, 1576, 1473. ^1H NMR (400 MHz, DMSO-d_6) δ: 11.19 (s, 1H), 9.77 (s, 1H), 8.33 (d, J = 8.4 Hz, 2H), 7.93 (d, J = 8.4 Hz, 2H), 7.49 (s, 2H), 7.47 – 7.43 (m, 1H), 7.40 (d, J = 7.2 Hz, 2H), 7.24 (d, J = 7.2 Hz, 1H), 7.13 (d, J = 7.6 Hz, 1H), 6.94 (d, J = 8.0 Hz, 1H), 6.55 (d, J = 7.6 Hz, 1H), 6.23 (s, 1H). ^{13}C NMR (100 MHz, DMSO-d_6) δ: 170.96, 155.47, 149.11, 143.08, 138.21, 130.61, 130.35, 129.32, 129.16, 127.67, 127.61, 126.67, 126.29, 125.97, 124.41, 124.34, 123.65, 122.75, 111.89, 101.45, 87.00, 64.75, 52.44. ESI-MS (m/z): $[M+H]^+$ calcd. for $C_{28}H_{17}ClN_5O_4$: 522.0969; found: 522.0967.

5'-bromo-10-imino-2'-oxo-8-phenyl-11*aH*-spiro[furo[3',4':4,5]pyrrolo[2,1-*a*]isoquinoline-11,3'-indoline]-10*a*(10*H*)-carbonitrile (4p)

Yellow solid. mp: 184-186 °C. IR (KBr, cm^{-1}): 3158, 3095, 1671, 1572, 1467. ^1H NMR (400 MHz, DMSO-d_6) δ: 11.01 (s, 1H), 9.57 (s, 1H), 7.60 (d, J = 8.0 Hz, 2H), 7.49-7.46 (m, 4H), 7.37 (d, J = 7.2 Hz, 2H), 7.15 (d, J = 7.2 Hz, 2H), 7.03-6.97 (m, 2H), 6.91 (d, J = 4.8 Hz, 1H), 6.54 (d, J = 7.2 Hz, 1H), 6.03 (s, 1H). ^{13}C NMR (100 MHz, DMSO-d_6) δ: 171.31, 158.09, 139.67, 134.63, 132.28, 131.79, 130.39, 129.12, 128.66, 128.04, 127.63, 127.15, 126.55, 124.21, 124.10, 123.19, 112.64, 110.67, 102.32, 87.41, 64.85, 52.08. ESI-MS (m/z): $[M+H]^+$ calcd. for $C_{28}H_{18}BrN_4O_2$: 521.0613; found: 521.0645.

5'-bromo-10-imino-2'-oxo-8-(*p*-tolyl)-11a*H*-spiro[furo[3',4':4,5]pyrrolo[2,1-a]isoquinoline-11,3'-indoline]-10a(10*H*)-carbonitrile (4q)

Yellow solid. mp: 187-189 °C. IR (KBr, cm^{-1}): 3135, 2852, 1657, 1567, 1469. ^1H NMR (400 MHz, DMSO-d_6) δ: 11.13 (s, 1H), 9.50 (s, 1H), 7.59 (s, 1H), 7.46 (s, 3H), 7.46 – 7.41 (m, 1H), 7.39 (d, J = 8.0 Hz, 1H), 7.36 (s, 1H), 7.30 (d, J = 7.6 Hz, 2H), 7.21-7.16 (m, 1H), 7.10 (d, J = 8.0 Hz, 1H), 6.92 (d, J = 7.6 Hz, 1H), 6.53 (d, J = 7.2 Hz, 1H), 5.96 (s, 1H), 2.33 (s, 3H). ^{13}C NMR (100 MHz, DMSO-d_6) δ: 170.96, 157.18, 139.85, 138.10, 132.06, 130.59, 129.94, 129.10, 127.85, 127.49, 126.69, 126.48, 125.85, 124.36, 123.82, 122.82, 112.85, 111.11, 101.18, 87.56, 64.78, 52.86, 21.15. ESI-MS (m/z): $[M+H]^+$ calcd. for $C_{29}H_{20}BrN_4O_2$: 535.0770; found: 535.1691.

5'-bromo-8-(4-chlorophenyl)-10-imino-2'-oxo-11aH-spiro[furo[3',4':4,5]pyrrolo[2,1-a]isoquinoline-11,3'-indoline]-10a(10H)-carbonitrile (4r)

Yellow solid. mp: 182-184 °C. IR (KBr, cm^{-1}): 3140, 2837, 1659, 1567, 1415. ^1H NMR (400 MHz, DMSO-d_6) δ: 11.06 (s, 1H), 9.66 (s, 1H), 7.66 (d, J = 8.4 Hz, 2H), 7.53 (d, J = 8.4 Hz, 2H), 7.47 (s, 2H), 7.45-7.40 (m, 1H), 7.38 (d, J = 7.6 Hz, 1H), 7.14 (d, J = 7.6 Hz, 2H), 7.04 (m, 1H), 6.91 (dd, J = 8.8, 4.4 Hz, 1H), 6.57 (d, J = 8.8 Hz, 1H), 6.09 (s, 1H). ^{13}C NMR (100 MHz, DMSO-d_6) δ: 171.26, 159.16, 156.14, 135.89, 135.66, 132.04, 130.63, 129.98, 129.22, 127.78, 126.80, 124.44, 123.22, 114.08, 112.62, 111.65, 110.98, 110.24, 108.98, 101.66, 87.10, 64.86, 52.26. ESI-MS (m/z): $[M+H]^+$ calcd. for $C_{28}H_{17}BrClN_4O_2$: 555.0223; found: 555.1730.

5'-bromo-8-(4-bromophenyl)-10-imino-2'-oxo-11*aH*-spiro[furo[3',4':4,5]pyrrolo[2,1-*a*]isoquinoline-11,3'-indoline]-10*a*(10*H*)-carbonitrile (4s)

Yellow solid. mp: 184-186 °C. IR (KBr, cm^{-1}): 3142, 2835, 1660, 1575, 1469. ^1H NMR (400 MHz, DMSO-d_6) δ: 11.18 (s, 1H), 9.60 (s, 1H), 7.72 (d, J = 8.4 Hz, 2H), 7.56 (d, J = 8.4 Hz, 2H), 7.50 (s, 2H), 7.45 – 7.43 (m, 1H), 7.38 (d, J = 7.6 Hz, 1H), 7.34 (s, 1H), 7.22-7.16 (m, 1H), 7.10 (d, J = 7.6 Hz, 1H), 6.96 (d, J = 8.8 Hz, 1H), 6.56 (d, J = 7.6 Hz, 1H), 6.12 (s, 1H). ^{13}C NMR (100 MHz, DMSO-d_6) δ: 171.20, 156.22, 139.56, 136.52, 133.32, 130.58, 130.40, 129.56, 127.70, 126.47, 125.80, 124.42, 123.76, 122.62, 112.32, 112.08, 111.80, 101.12, 88.20, 65.01, 53.06. ESI-MS (m/z): $[M+H]^+$ calcd. for $C_{28}H_{17}Br_2N_4O_2$: 598.9718; found: 598.9482.

5'-bromo-10-imino-8-(4-nitrophenyl)-2'-oxo-11*aH*-spiro[furo[3',4':4,5]pyrrolo[2,1-*a*]isoquinoline-11,3'-indoline]-10*a*(10*H*)-carbonitrile (4t)

Yellow solid. mp: 183-185 °C. IR (KBr, cm^{-1}): 3074, 2873, 1661, 1576, 1470. ^1H NMR (400 MHz, DMSO-d_6) δ: 11.12 (s, 1H), 9.68 (s, 1H), 8.32 (d, J = 9.2 Hz, 2H), 7.96 (d, J = 8.8 Hz, 2H), 7.49 (s, 2H), 7.45 – 7.40 (m, 1H), 7.38 (d, J = 7.2 Hz, 1H), 7.20 – 7.16 (m, 2H), 7.04 – 6.98 (m, 1H), 6.92 (dd, J = 9.2, 5.2 Hz, 1H), 6.60 (d, J = 8.0 Hz, 1H), 6.20 (s, 1H). ^{13}C NMR (100 MHz, DMSO-d_6) δ: 171.24, 159.18 155.26, 149.24, 143.53, 135.93, 132.56, 129.24, 129.10, 127.62, 126.51, 124.31, 124.18, 113.68, 112.95, 111.88, 111.64, 110.46, 101.93, 87.08, 64.68, 53.02. ESI-MS (m/z): $[M+H]^+$ calcd. for $C_{28}H_{17}BrN_5O_4$: 566.0464; found: 566.1340.

10-imino-1'-methyl-2'-oxo-8-phenyl-11*aH*-spiro[furo[3',4':4,5]pyrrolo[2,1-*a*]isoquinoline-11,3'-indoline]-10*a*(10*H*)-carbonitrile (4u)

Yellow solid. mp: 171-173 °C. IR (KBr, cm^{-1}): 3429, 2924, 1651, 1564, 1409. ^{1}H NMR (400 MHz, DMSO-*d*6) δ: 9.29 (s, 1H), 7.63 (d, *J* = 3.6 Hz, 2H), 7.50 (d, *J* = 3.2 Hz, 3H), 7.46 (s, 1H), 7.44 (d, *J* = 8.8 Hz, 2H), 7.42 – 7.36 (m, 2H), 7.27 (t, *J* = 7.6 Hz, 1H), 7.13 (dd, *J* = 13.2, 8.4 Hz, 3H), 6.54 (d, *J* = 7.2 Hz, 1H), 5.95 (s, 1H), 3.16 (s, 3H). ^{13}C NMR (100 MHz, DMSO-*d*6) δ: 169.17, 155.72, 140.83, 135.87, 130.90, 130.72, 130.35, 129.40, 129.01, 128.16, 127.32, 127.27, 127.02, 126.92, 124.02, 122.74, 122.51, 121.08, 112.77, 112.13, 112.02, 109.61, 101.05, 87.53, 64.78, 51.92, 26.65. ESI-MS (m/z): $[M+H]^+$ calcd. for $C_{29}H_{21}N_4O_2$: 457.1665; found: 457.1666.

1'-benzyl-10-imino-2'-oxo-8-phenyl-11a*H*-spiro[furo[3',4':4,5]pyrrolo[2,1-*a*]isoquinoline-11,3'-indoline]-10*a*(10*H*)-carbonitrile (4v)

Brown solid. mp: 167-169 °C. IR (KBr, cm^{-1}): 3084, 2917, 1660, 1574, 1475. ^{1}H NMR (400 MHz, DMSO-d_6) δ: 11.10 (s, 1H), 9.67 (s, 1H), 8.33 (d, *J* = 8.4 Hz, 2H), 8.12 (s, 1H), 7.65 (d, *J* = 7.6 Hz, 2H), 7.40 (d, *J* = 8.4 Hz, 4H), 7.35 (t, *J* = 7.2 Hz, 2H), 7.31 – 7.27 (m, 2H), 7.19 (d, *J* = 7.6 Hz, 2H), 7.16 – 7.11 (m, 3H), 6.85 (t, *J* = 7.6 Hz, 2H), 6.77 (d, *J* = 7.6 Hz, 1H), 6.20 (s, 1H). ^{13}C NMR (100 MHz, DMSO-d_6) δ: 171.04, 155.67, 149.11, 143.72, 143.08, 138.21, 137.61, 136.39, 130.35, 130.23, 129.05, 128.58, 128.06, 127.88, 127.49, 127.07, 123.35, 122.42, 119.17, 115.14, 113.59, 112.87, 112.32, 110.01, 101.56, 87.08, 64.82, 52.64. ESI-MS (m/z): $[M+H]^+$ calcd. for $C_{35}H_{25}N_4O_2$: 533.1978; found: 533.1978.

4A.8. References

[1] K. R. Senwar, P. Sharma, T. S. Reddy, M. K. Jeengar, V. L. Nayak, V. G. M. Naidu, A. Kamal, N. Shankaraiah, *Eur. J. Med. Chem.* **2015**, *102*, 413–424.

[2] K. Parthasarathy, C. Praveen, J. C. Jeyaveeran, A. A. M. Prince, *Bioorg. Med. Chem. Lett.* **2016**, *26*, 4310–4317.

[3] Z. M. Darvish, B. Mirza, S. Makarem, *J. Heterocycl. Chem.* **2017**, *54*, 1763–1766.

[4] T. Ponpandian, S. Muthusubramanian, *Synth. Commun.* **2014**, *44*, 868–874.

[5] M. A. El-Hashash, S. A. Rizk, *J. Heterocycl. Chem.* **2017**, *54*, 1776–1784.

[6] J. Liu, Y. Sun, X. Zhang, X. Liang, Y. Wu, Y. Wang, X. Jiang, *Inflamm. Cell Signal.* **2014**, *1*, 1–4.

[7] K. Guo, T. Fang, J. Wang, A. A. Wu, Y. Wang, J. Jiang, X. Wu, S. Song, W. Su, Q. Xu, X. Deng, *Bioorg. Med. Chem. Lett.* **2014**, *24*, 4995–4998.

[8] L. M. Zhou, R. Y. Qu, G. F. Yang, *Expert Opin. Drug Discov.* **2020**, *15*, 603–625.

[9] K. Ding, Y. Lu, Z. N. Coleska, G. Wang, S. Qiu, S. Shangary, W. Gao, D. Qin, J. Stuckey, K. Krajewski, P. P. Roller, S. Wang, *J. Med. Chem.* **2006**, *49*, 3432–3435.

[10] S. Mathusalini, T. Arasakumar, K. Lakshmi, C. H. Lin, P. S. Mohan, M. G. Ramnath, R. Thirugnanasampandan, *New J. Chem.* **2016**, *40*, 5164–5169.

[11] A. P. Antonchick, C. Gerding-Reimers, M. Catarinella, M. Schürmann, H. Preut, S. Ziegler, D. Rauh, H. Waldmann, *Nat. Chem.* **2010**, *2*, 735–740.

[12] L. Zhang, W. Ren, X. Wang, J. Zhang, J. Liu, L. Zhao, X. Zhang, *Eur. J. Med. Chem.* **2017**, *126*, 1071–1082.

[13] N. M. Gomes, L. J. Bessa, S. Buttachon, P. M. Costa, J. Buaruang, T. Dethoup, A. M. S. Silva, A. Kijjoa, *Mar. Drugs* **2014**, *12*, 822–839.

[14] G. Büchi, K. C. Luk, B. Kobbe, J. M. Townsend, *J. Org. Chem.* **1977**, *42*, 244–246.

[15] T. H. Kang, K. Matsumoto, M. Tohda, Y. Murakami, H. Takayama, M. Kitajima, N. Aimi, H. Watanabe, *Eur. J. Pharmacol.* **2002**, *444*, 39–45.

[16] R. P. Pérez, E. M. Bujaidar, D. M. Jasso, S. R. Cadena, I. Á. González, L. S. Chapul, J. P. Gallaga, *Basic Clin. Pharmacol. Toxicol.* **2009**, *104*, 222–227.

[17] M. Zhou, M. M. Miao, G. Du, X. N. Li, S. Z. Shang, W. Zhao, Z. H. Liu, G. Y. Yang, C. T. Che, Q. F. Hu, X. M. Gao, *Org. Lett.* **2014**, *16*, 5016–5019.

[18] M. C. Nakhla, J. L. Wood, *J. Am. Chem. Soc.* **2017**, *139*, 18504–18507.

[19] J. S. Wu, X. Zhang, Y. L. Zhang, J. W. Xie, *Org. Biomol. Chem.* **2015**, *13*, 4967–4975.

[20] N. Gupta, G. Bhojani, R. Tak, A. Jakhar, N. ul H. Khan, S. Chatterjee, R. I. Kureshy, *ChemistrySelect* **2017**, *2*, 10902–10907.

[21] A. Kamal, K. S. Babu, M. V. P. S. Vishnu Vardhan, S. M. A. Hussaini, R. Mahesh, S. P. Shaik, A. Alarifi, *Bioorg. Med. Chem. Lett.* **2015**, *25*, 2199–2202.

[22] Z. Tang, Z. Liu, Y. An, R. Jiang, X. Zhang, C. Li, X. Jia, J. Li, *J. Org. Chem.* **2016**,

81, 9158–9166.

[23] T. Vivekanand, B. S. Vachan, M. Karuppasamy, I. Muthukrishnan, C. U. Maheswari, S. Nagarajan, N. Bhuvanesh, V. Sridharan, *J. Org. Chem.* **2019**, *84*, 4009–4016.

[24] B. A. Laevens, J. Tao, G. K. Murphy, *J. Org. Chem.* **2017**, *82*, 11903–11908.

[25] R. Y. Yang, J. Sun, Q. Sun, C. G. Yan, *Org. Biomol. Chem.* **2017**, *15*, 6353–6357.

[26] R. Baharfar, S. Asghari, F. Zaheri, N. Shariati, *Comptes Rendus Chim.* **2017**, *20*, 359–364.

[27] R. Azimi, R. Baharfar, H. Bagheri, *Polycycl. Aromat. Compd.* **2021**, *1*, 1–10.

[28] L. Wu, J. Sun, C. G. Yan, *Org. Biomol. Chem.* **2012**, *10*, 9452–9463.

[29] Q. Fu, C. G. Yan, *Tetrahedron* **2013**, *69*, 5841–5849.

[30] J. Sun, M. R. Y. Yang, C. G. Yan, *ChemistrySelect* **2017**, *2*, 304–308.

[31] S. J. Garden, C. R. Werneck Guimarães, M. B. Corréa, C. A. Fernandes de Oliveira, A. Da Cunha Pinto, R. Bicca de Alencastro, *J. Org. Chem.* **2003**, *68*, 8815–8822.

[32] A. Dandia, H. Taneja, R. Gupta, S. Paul, *Synth. Commun.* **2002**, *29*, 2323–2335.

[33] Y. J. Xie, J. Sun, C. G. Yan, *RSC Adv.* **2014**, *4*, 44537–44546.

[34] P. S. Kharkar, V. M. Kulkarni, *Org. Biomol. Chem.* **2003**, *1*, 1315–1322.

[35] A. Boobis, U. Gundert-Remy, P. Kremers, P. Macheras, O. Pelkonen, *Eur. J. Pharm. Sci.* **2002**, *17*, 183–193.

[36] H. Riza, A. Fahrurroji, A. Wicaksono, A. K. Nugroho, S. Martono, *Int. J. Pharm. Pharm. Sci.* **2018**, *10*, 85–89.

[37] R. Jyothi, R. Yaligar, I. R. Jyothi, I. G. Narappa, I. M. Ravi, *J. Pharmacogn. Phytochem.* **2020**, *9*, 1799–1809.

[38] M. S. Reddy, N. S. Thirukovela, S. Narsimha, M. Ravinder, S. K. Nukala, *J. Mol. Struct.* **2022**, *1250*, 131747–131754.

4A.9. Selected IR, NMR (^{1}H and ^{13}C) and Mass spectra

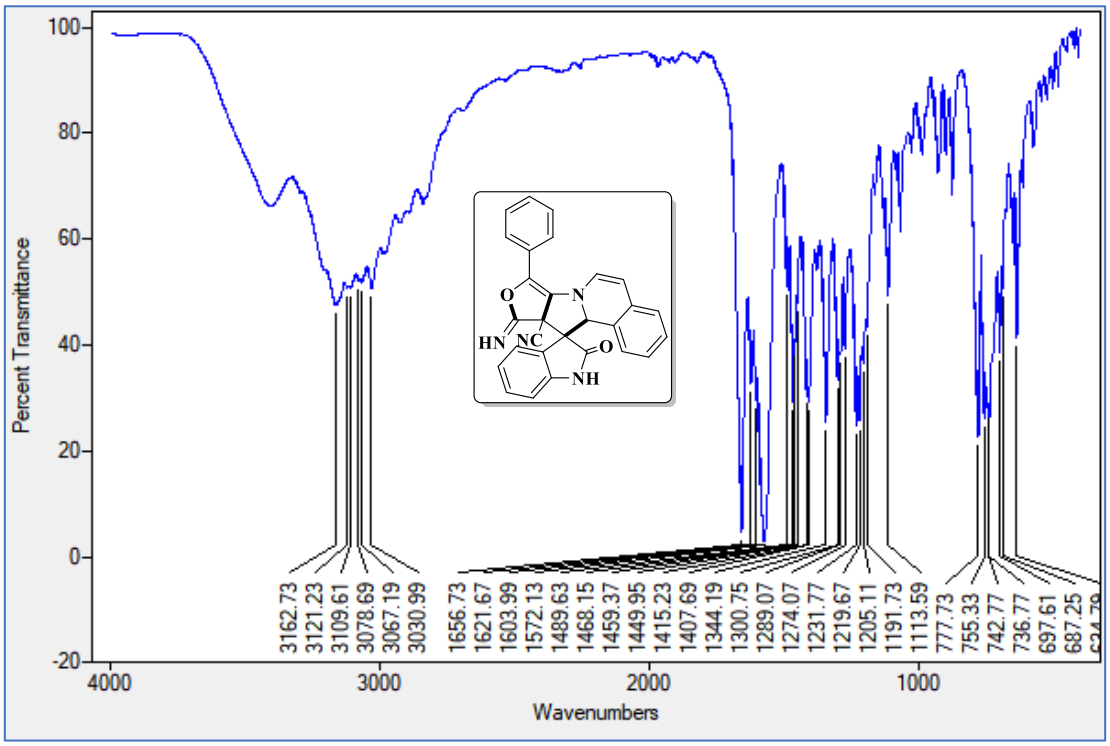

IR spectrum of the compound **4a**

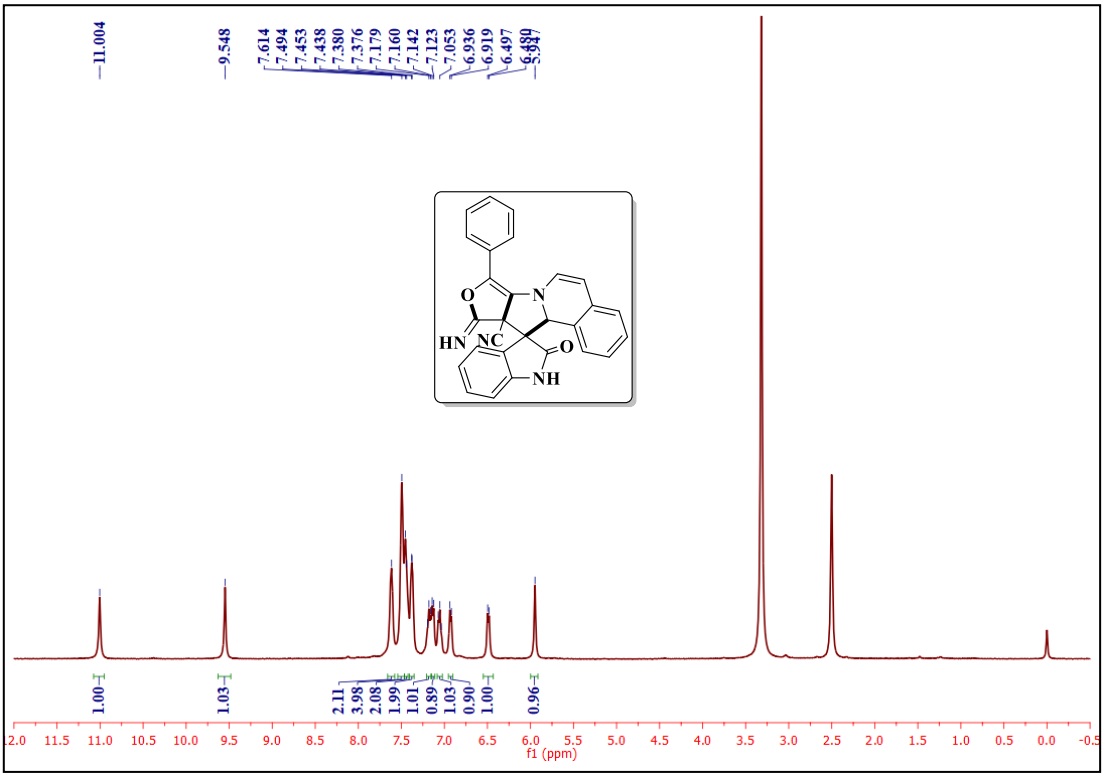

^{1}H NMR spectrum of the compound **4a**

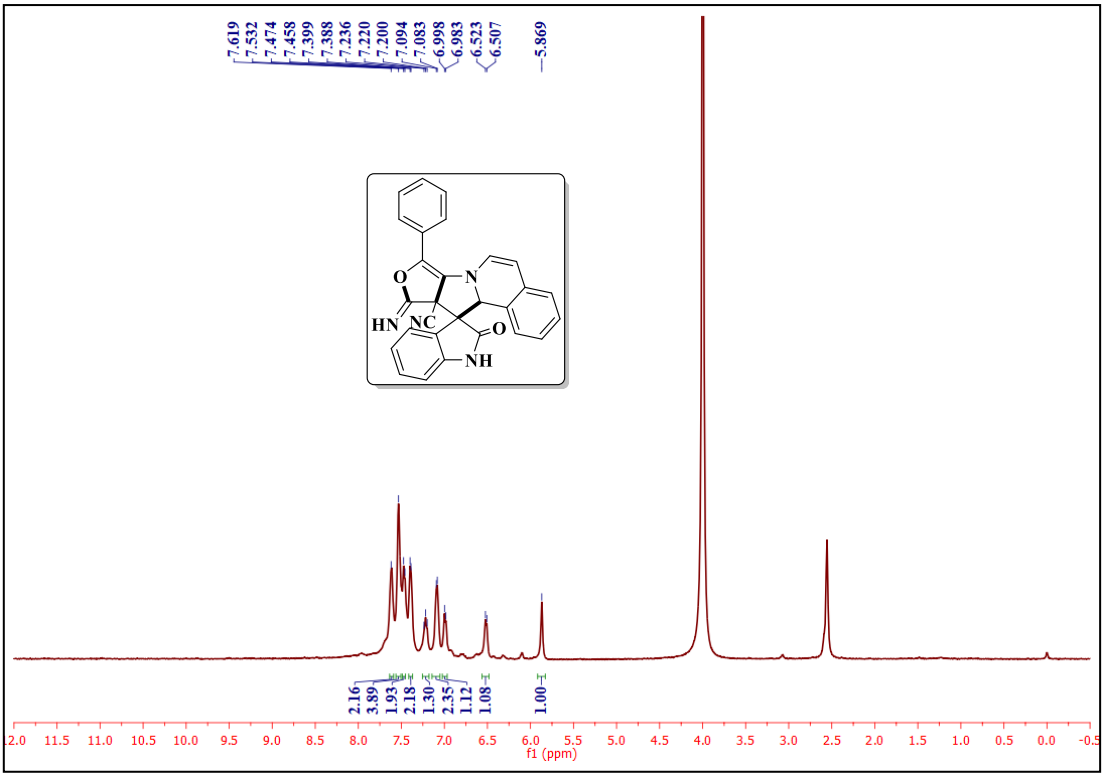

^{1}H NMR (D_2O exchange) spectrum of the compound **4a**

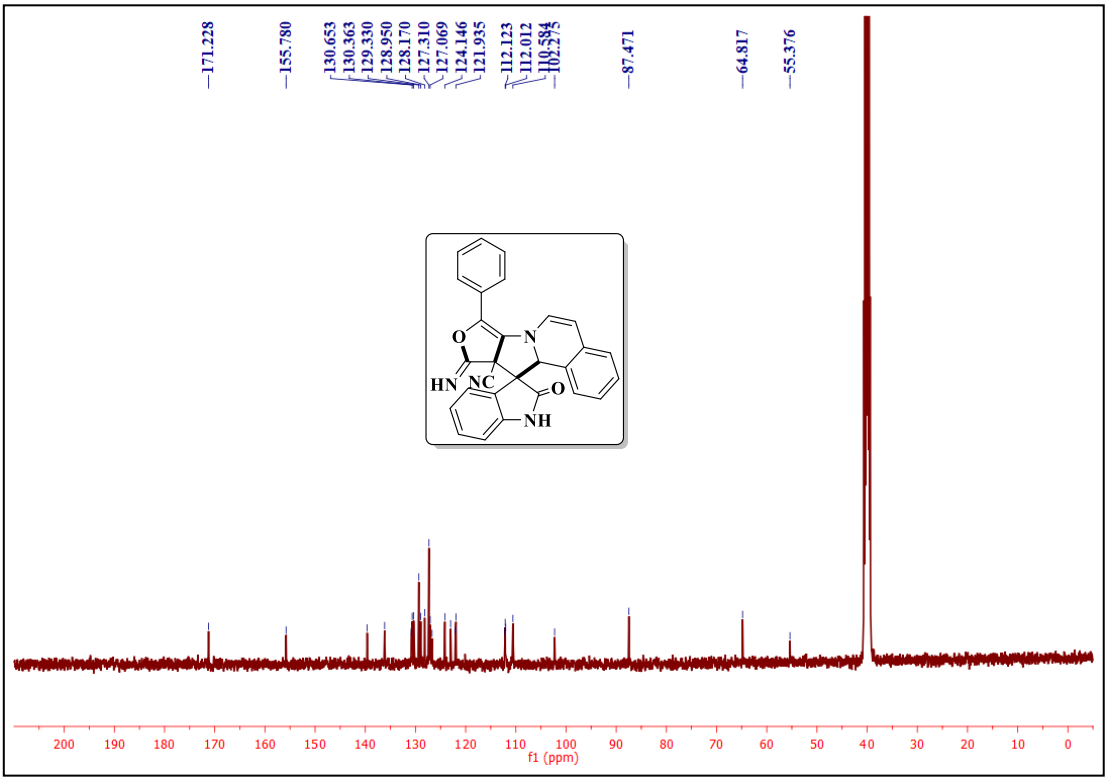

^{13}C NMR spectrum of the compound **4a**

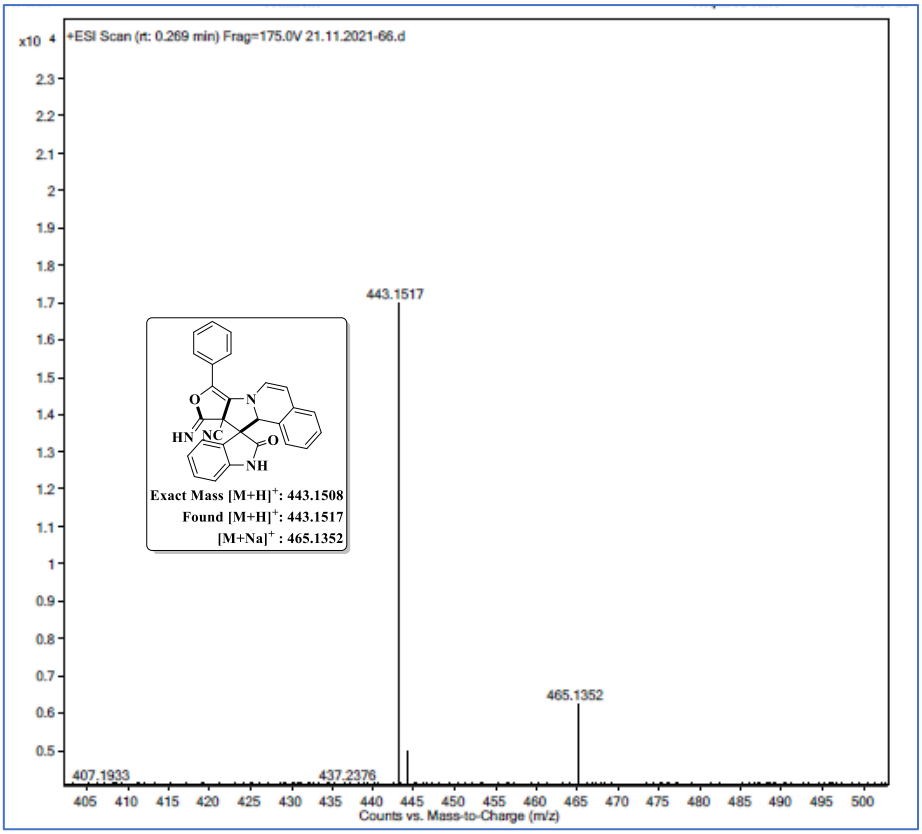

Mass spectrum of the compound **4a**

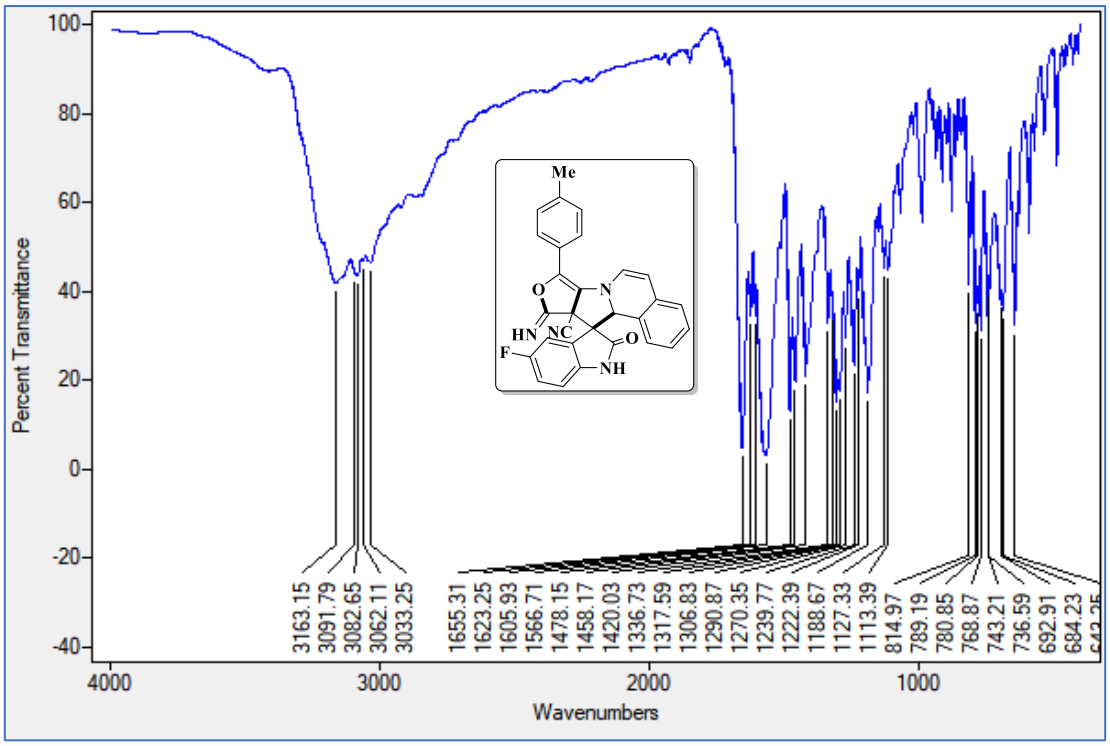

IR spectrum of the compound **4g**

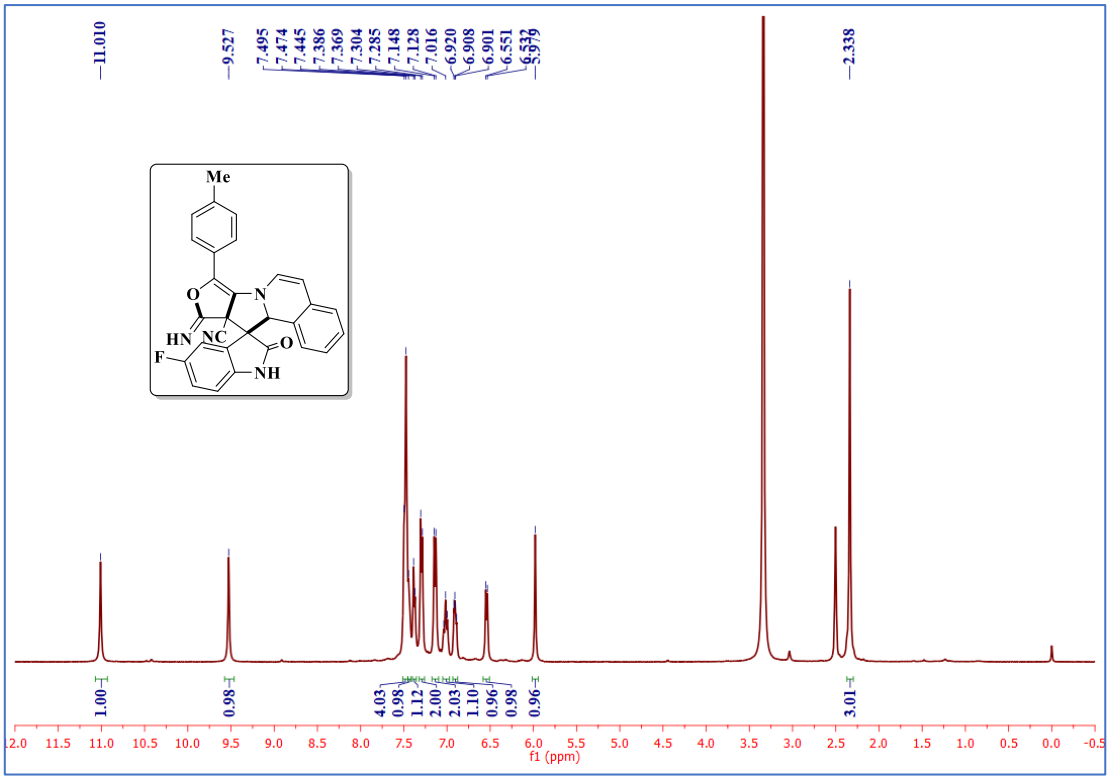

^{1}H NMR spectrum of the compound **4g**

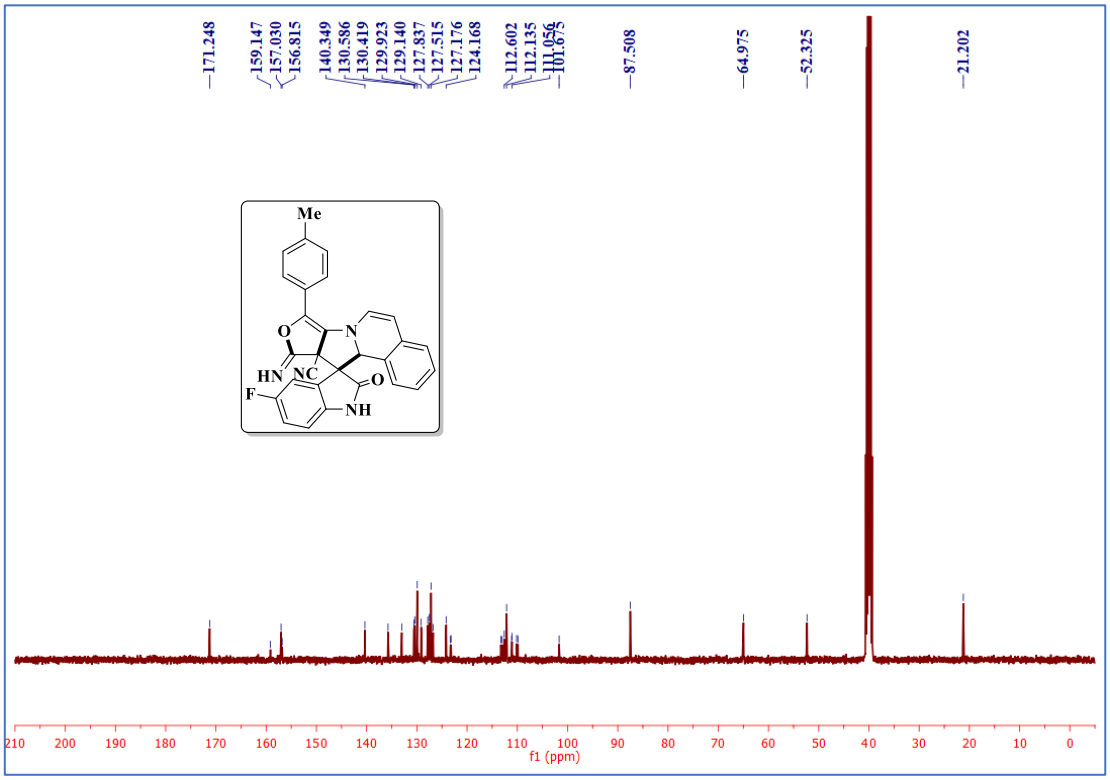

^{13}C NMR spectrum of the compound **4g**

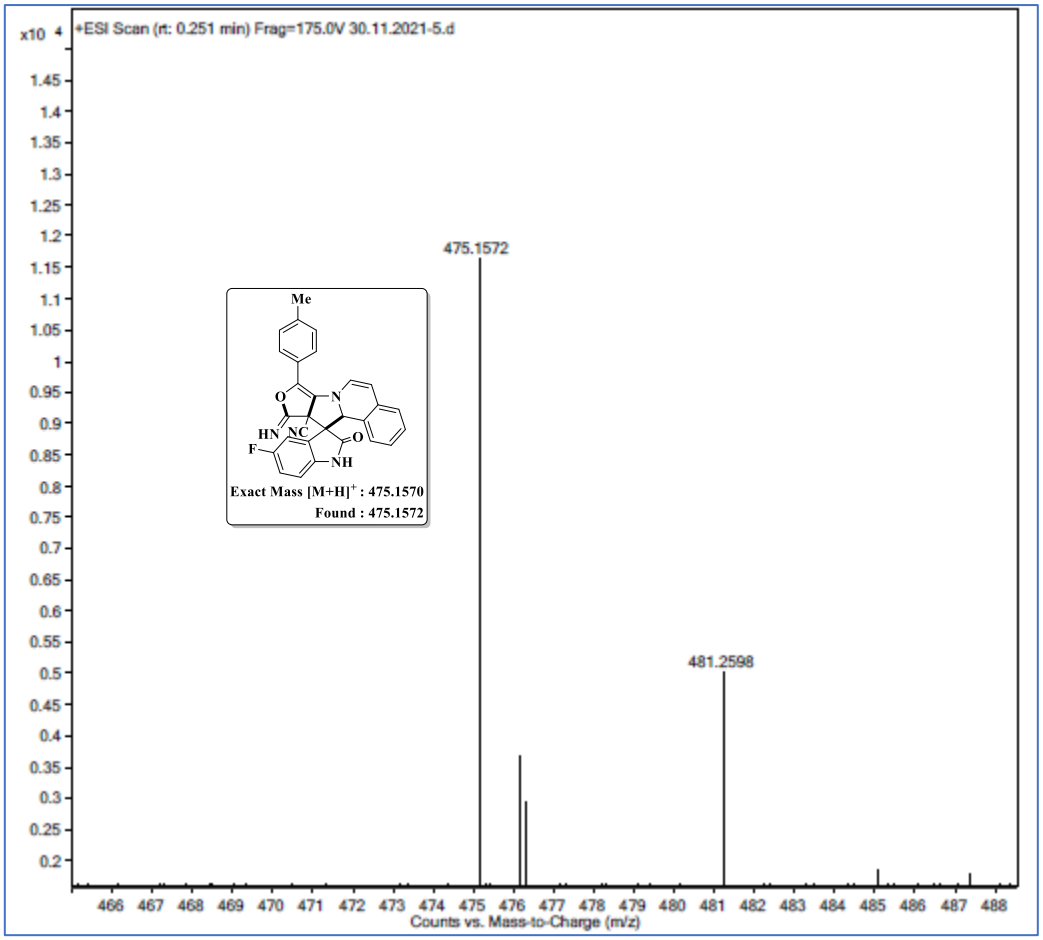

Mass spectrum of the compound **4g**

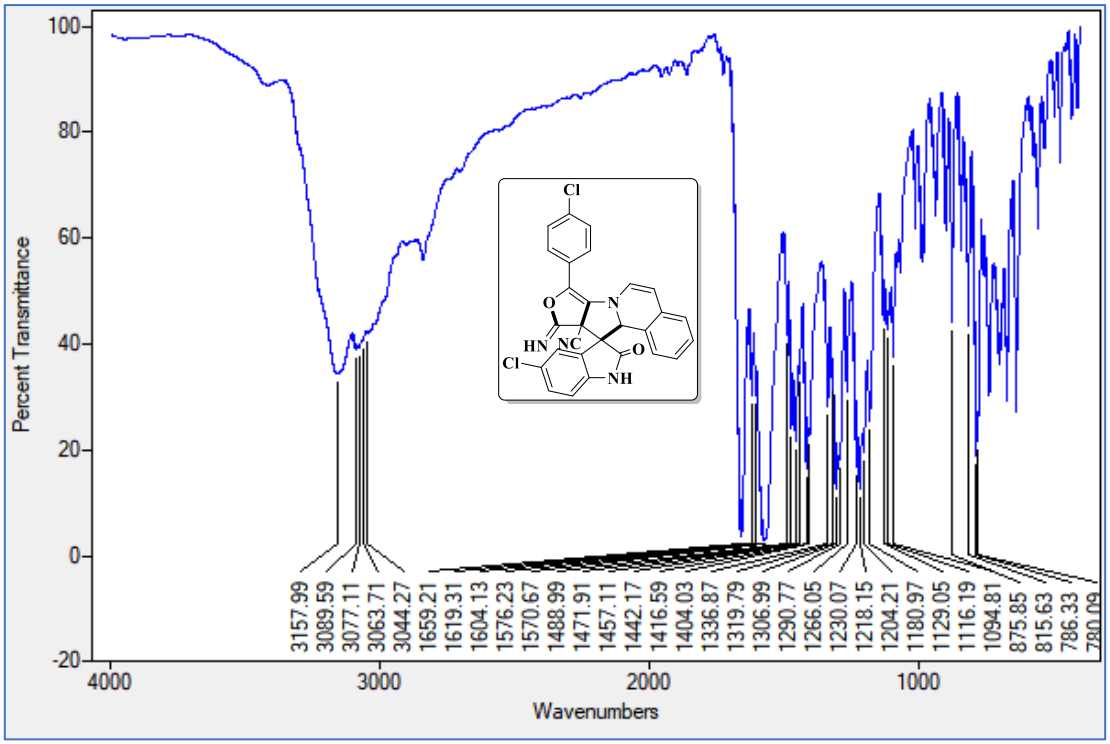

IR spectrum of the compound **4m**

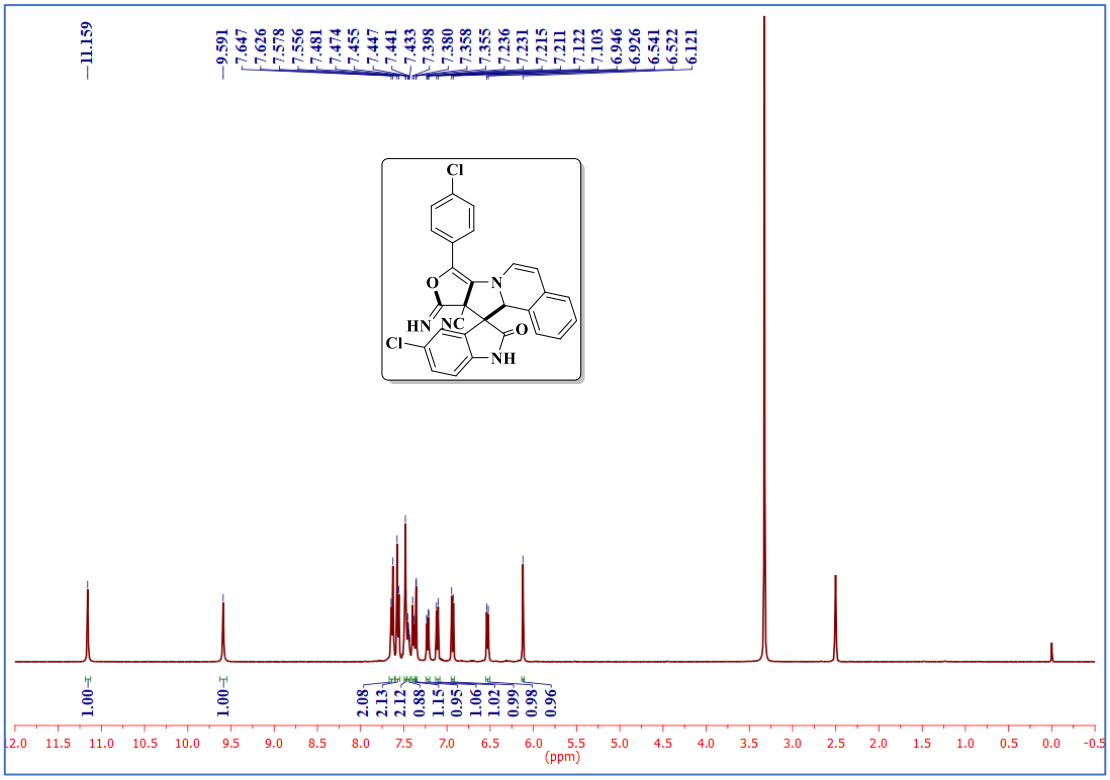

^{1}H NMR spectrum of the compound **4m**

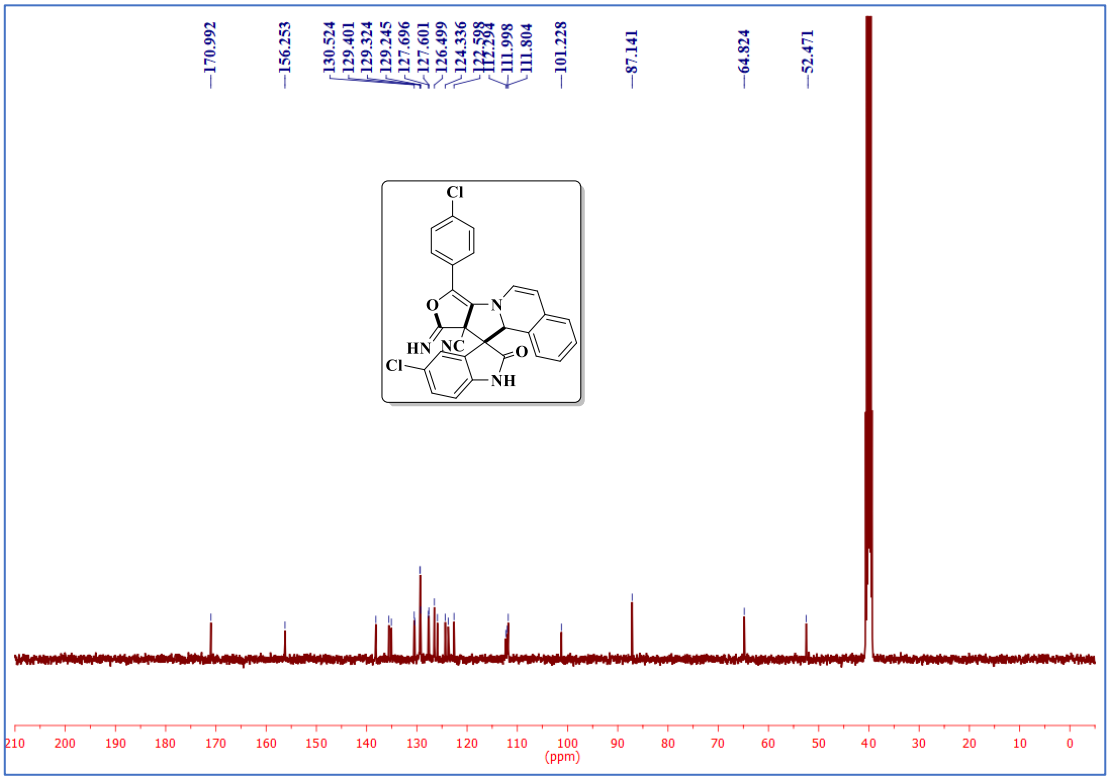

^{13}C NMR spectrum of the compound **4m**

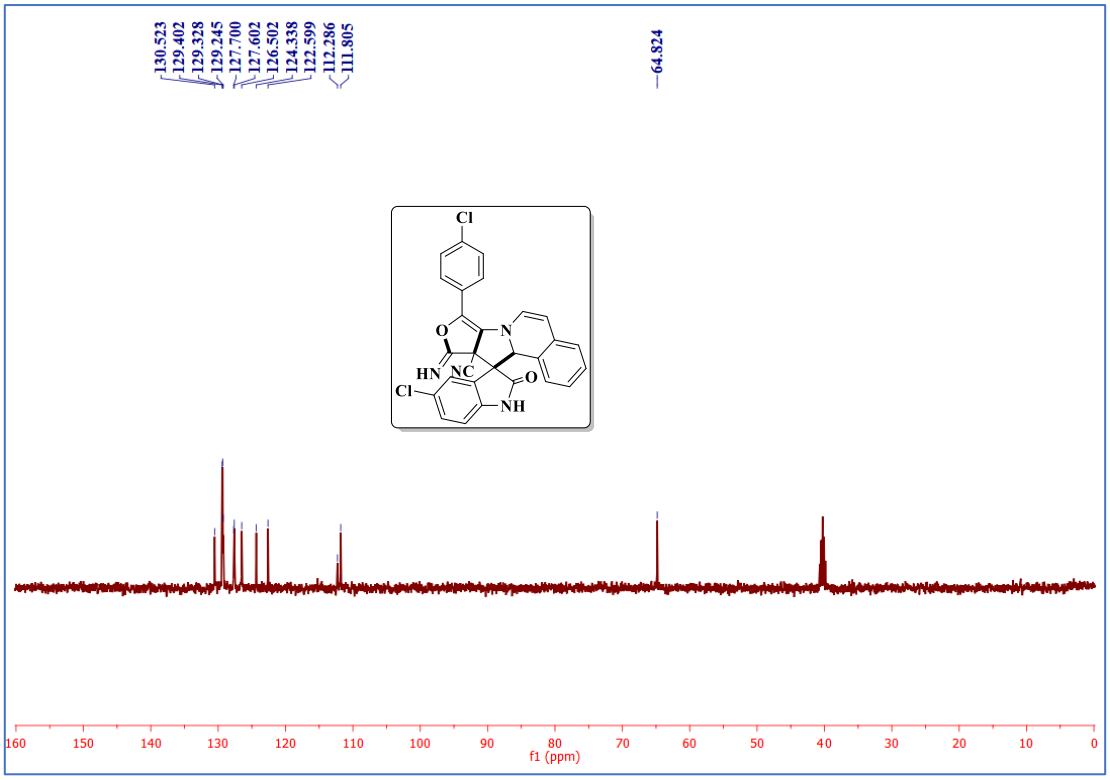

DEPT-135 NMR spectrum of the compound **4m**

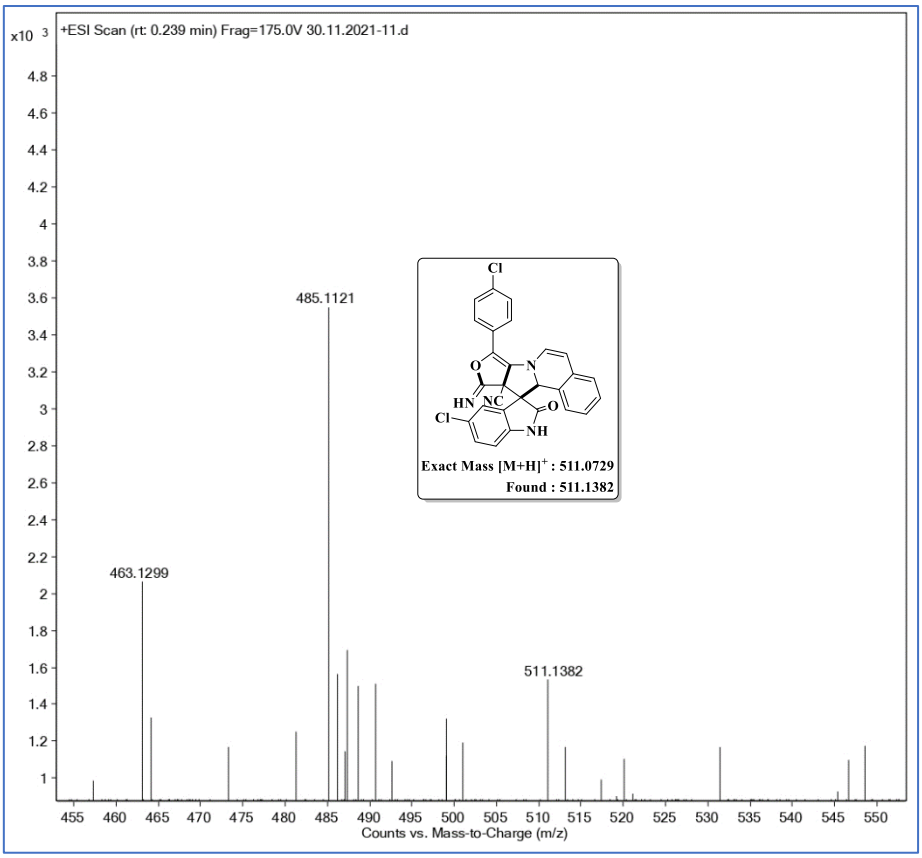

Mass spectrum of the compound **4m**

CHAPTER-IV
Section-B

A three component [3+2] cycloaddition reaction for the synthesis of spirooxindolo-pyrrolizidines

4B.1. Introduction

Ultrasound irradiation has long been considered as a clean and efficient technique in organic synthesis [1]. The prominent features of ultrasound irradiation are energy saving, enhanced reaction rates, formation of pure products in high yields, shorter reaction times and operational simplicity compared with traditional methods [2,3]. Ultrasound produces both chemical and physical effects because of cavitational collapse and it induce the formation of chemical species which are not easily attained under conventional methods [4]. Also, multicomponent reactions (MCRs) are special type of synthetically prominent organic reactions in combinatorial and medicinal chemistry, in which three or more starting materials react together in a single pot to produce final product without isolating intermediates [5,6]. MCRs offer significant advantages like operational simplicity, lessening of energy consumption and high degree of atom economy [7].

On the other hand, spirooxindoles gained much attention in heterocyclic chemistry because of their highly pronounced pharmacological and biological activities [8,9]. A number of spirooxindoles were present in natural products such as spirotryprostatin A is an indolic alkaloid found in Aspergillus fumigatus fungus and can be serve as an anti-cancer drug [10]. Whereas, horsfiline is an oxindole alkaloid found in the plant horsfieldia superba, which is used in traditional herbal medicine as anti-analgesic [11]. Mitraphylline is an active alkaloid displaying various biological activities like anti-proliferative, non-narcotic drug and anti-cancer (Figure 4B.1) [12,13].

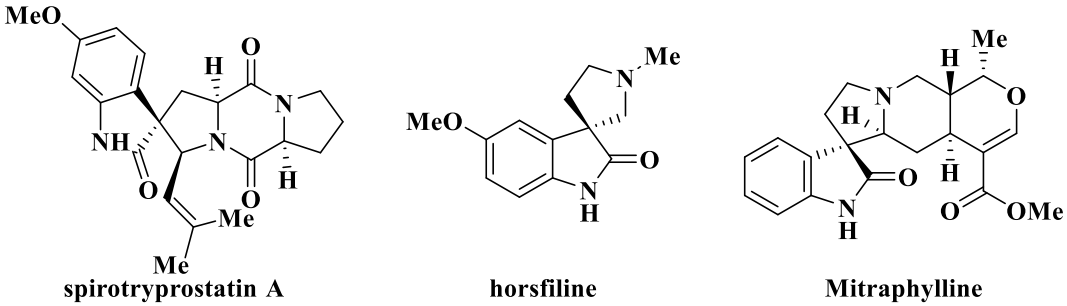

Figure 4B.1

Spirooxindoles can also serve as synthetic intermediates for drug precursors or pharmaceuticals [14,15]. Therefore, finding an efficient and concise methods for the preparation of this type of moieties is a fascinating area in chemistry [16]. In recent years, many methods have been utilized to construct structurally diverse spirooxindoles [17].

4B.1.1. Reported methods for the synthesis and biological activity of spirooxindoles

Kumar et al. reported an efficient synthesis of spiro-pyrido-pyrrolizines under solvent-free microwave irradiation (Figure 4B.2). The synthesized compounds were screened for *in vitro* activity against mycobacterium tuberculosis H37Rv (MTB), multi-drug resistant M. tuberculosis (MDR-TB) and mycobacterium smegmatis (MC2) using agar dilution method and some compounds found to be most active against MTB and MDR-TB [18].

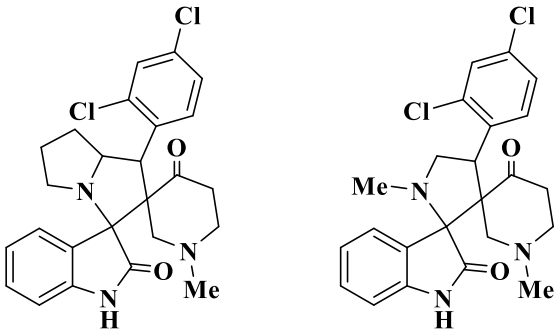

Figure 4B.2

Gollner and co-workers presented spirooxindole compounds as chemically stable and orally active inhibitors of the MDM2−p53 interaction (Figure 4B.3). Further structure based optimization resulted these compounds to bind MDM2 protein and to interrupt its protein-protein interaction (PPI) with TP53 and the compounds showed *in vivo* efficacy in a mouse SJSA-1 xenograft study [19].

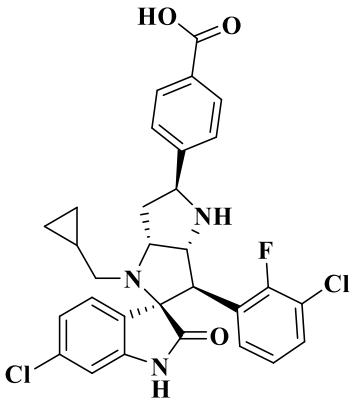

Figure 4B.3

Toumi et al. disclosed a series of rhodanine fused spirooxindolo-pyrrolidines by one-pot three component [3+2] cycloaddition (Figure 4B.4). Further, all the cycloadducts were evaluated for *in vitro* α-amylase inhibitory activity and showed good inhibition with respect to standard drug acarbose. In addition, the potent compounds were studied their *in silico* molecular docking analysis and *in vivo* hypoglycemic activity in alloxan-induced diabetic rats [20].

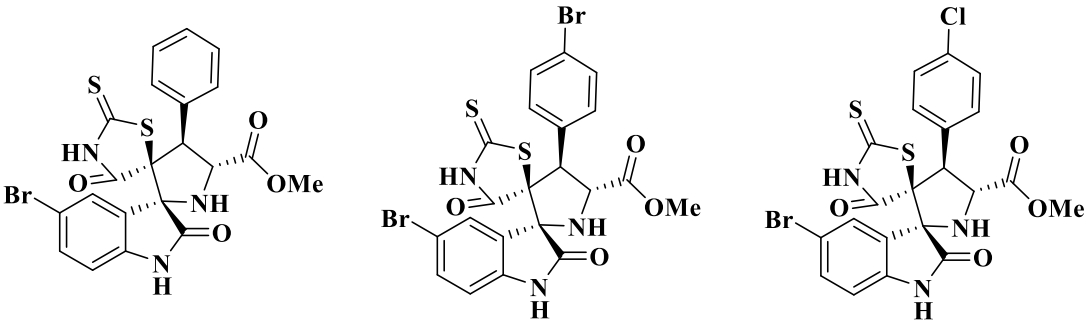

Figure 4B.4

de Silva et al. employed spirooxindolo-pyrrolizidine analogues by microwave assisted one-pot three component [3+2] cycloaddition reaction (Figure 4B.5). Further, the synthesized compounds were tested for *in vitro* anti-amyloidogenic activity for the treatment of Alzheimer's disease with MTT assay [21].

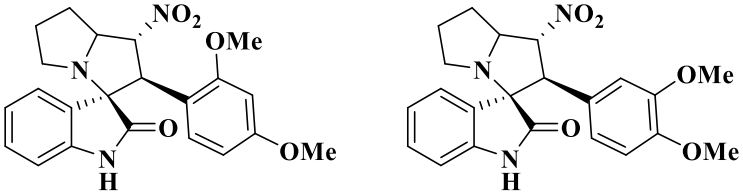

Figure 4B.5

Kumar and co-workers design and synthesized bioisosteres of spirooxindole as inhibitors of the MDM2–p53 interaction for anti-breast cancer agents (Figure 4B.6). Further, *in vivo* efficacy was also investigated on xenograft tumors in athymic nude mice and the most active compound induced G1/S phase arrest and thus inhibited the growth of breast cancer cells [22].

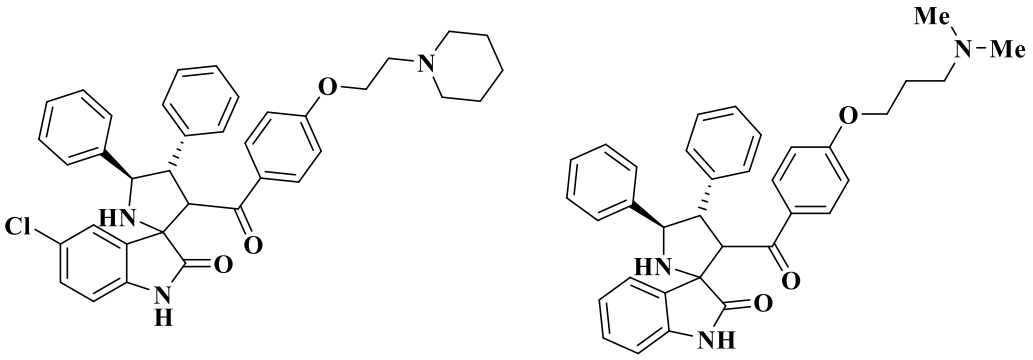

Figure 4B.6

Prasanna et al. described a regio and stereoselective [3+2] cycloaddition for the synthesis of novel spiro-pyrrolothiazolyloxindoles (Figure 4B.7). The synthesized compounds were screened for their *in vitro* activity against mycobacterium tuberculosis H37Rv (MTB) using

agar dilution method and some compounds displayed potent activity than standard drugs ciprofloxacin and ethambutol [23].

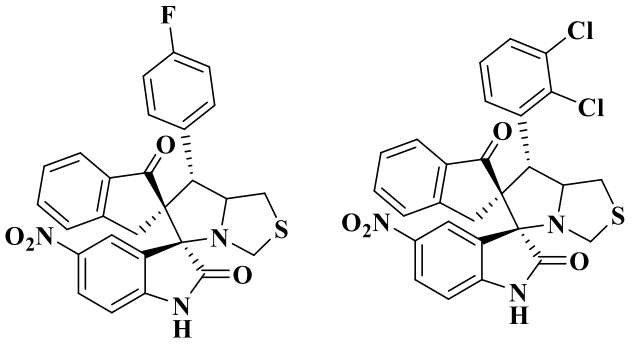

Figure 4B.7

Barakat and co-workers employed a rapid combinatorial approach to produce a series of hybrid spirooxindole based MDM2 inhibitors (Figure 4B.8). Further, the selected compounds were screened for *in vitro* cytotoxic activity using MTT assay. In addition, *in silico* ADMET prediction and drug likeness properties were evaluated for the active compounds, the results showed no Lipinski violation [24].

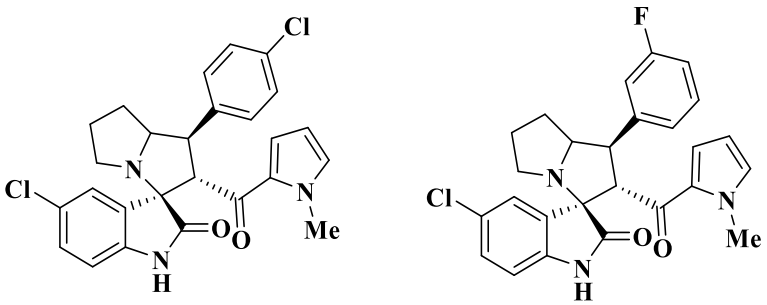

Figure 4B.8

Huang et al. demonstrated the acetic acid catalyzed three-component reaction of pyrrolidine, aldehydes and phenacylideneoxindoles to afford functionalized spirooxindolo-pyrrolizines (Scheme 4B.1). The obtained spirooxindole derivatives were evaluated *in vitro* against mouse colon cancer cells CT26 and human liver cancer cells HepG2 by MTT assay [25].

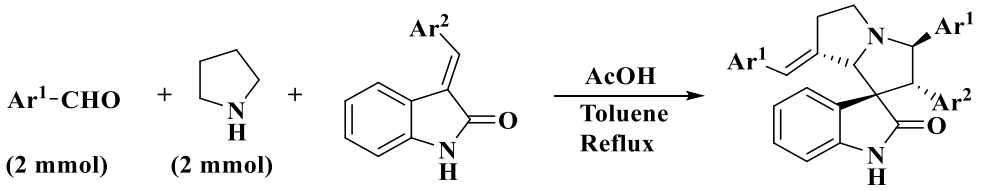

Scheme 4B.1

Sun et al. established a general and practical route for the *in situ* generation of azomethine ylide and its 1,3-dipolar cycloaddition reaction for the production of functionalized spirooxindolo-pyrrolizines (Scheme 4B.2). Comemercially available starting materials, milder reaction conditions and molecular diversity were the advantages of this reaction [26].

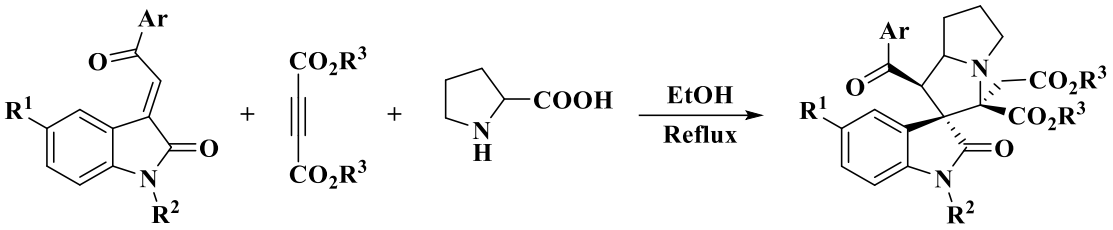

Scheme 4B.2

Ganesh and co-workers developed a highly diastereoselective [3+2] cycloaddition strategy using oxindoles and α,β-disubstituted nitroethylenes to access tetra-substituted spiropyrrolidines (Scheme 4B.3). Further, the synthesized compounds were evaluated for *in vitro* anti-bacterial activity against gram-positive bacteria S. aureus [27].

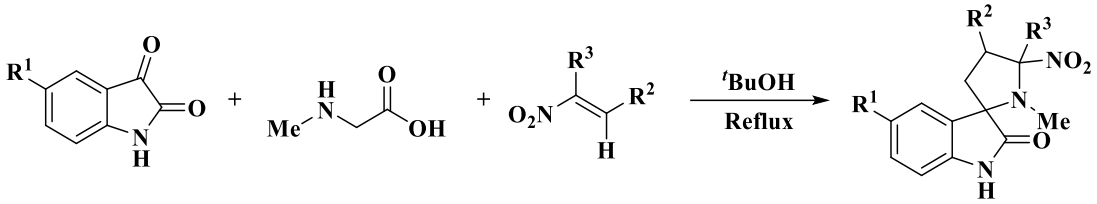

Scheme 4B.3

Sakly et al. disclosed one-pot four component domino strategy for the generation of novel spirooxindolo-1,2,3-triazoles through stereo and regioselective [3+2] cycloaddition (Scheme 4B.4). Further, the synthesized compounds were screened for *in vitro* anti-fungal and anti-bacterial activities using agar dilution method [28].

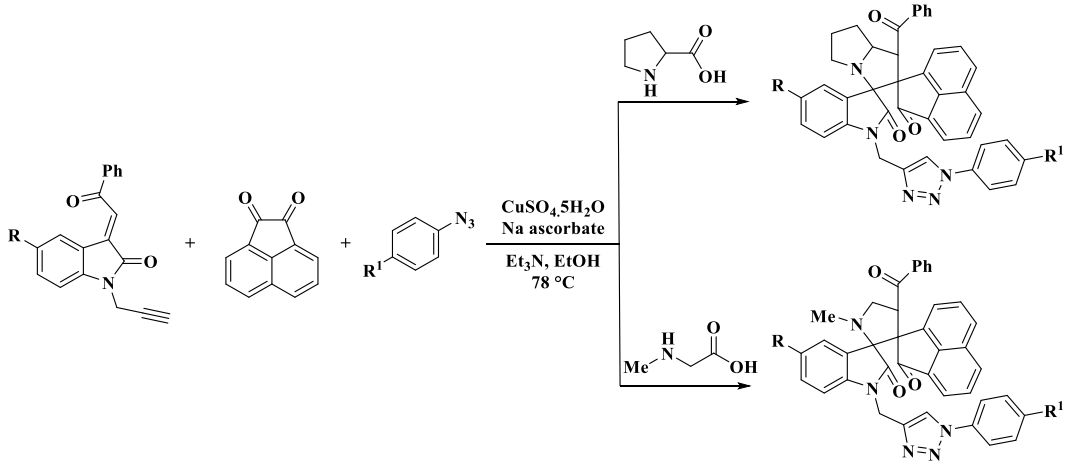

Scheme 4B.4

Parthasarathy and co-workers described the synthesis of fused spiropyrrolizidine oxindoles *via* 1,3-dipolar cycloaddition of azomethine ylides with heterobicyclic alkenes (Scheme 4B.5). Utilization of heterobicyclic alkenes as dipolarophile was the main advantage of this reaction [29].

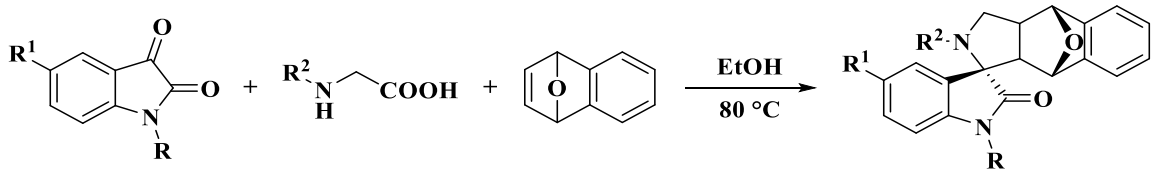

Scheme 4B.5

4B.2. Present work

Encouraged by the aforementioned literature reports and considering the significance of spirooxindoles, herein we have demonstrated a highly regioselective synthesis of aza-spirooxindoles from one-pot three component reaction *via* [3+2] cycloaddition between isatin-malononitrile adducts **1a-j** and azomethine ylides, generated *in situ* from quinolinyl aldehydes **2a-b** and cyclic α-amino acid **3** (Scheme 4B.6). In addition, all the synthesized compounds were screened for *in silico* molecular docking and ADME prediction.

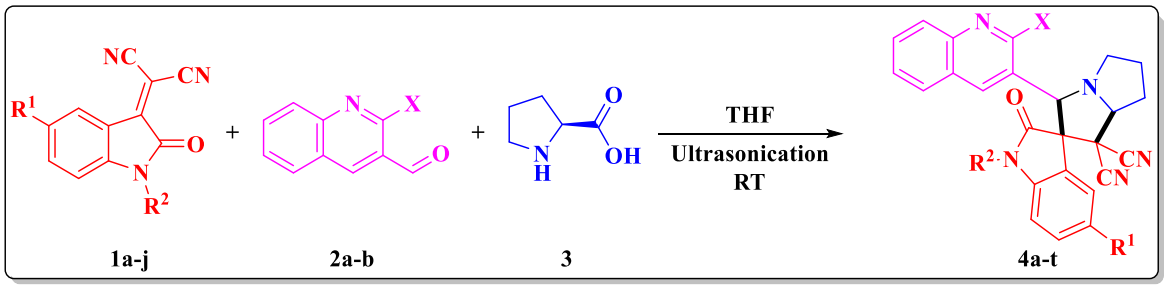

Scheme 4B.6. Synthesis of quinoline based spirooxindolo-pyrrolizidines **4a-t**.

4B.2.1. Results and discussion

We commenced our study by choosing 2-(2-oxoindolin-3-ylidene)malononitrile **1a**, chloroquinolinyl aldehyde **2a** and L-proline **3** as the model reactants to get the optimized reaction parameters (Table 4B.1). When the reaction was performed in MeOH at room temperature, the target product **4a** was obtained with 45% yield in 20 h (Table 4B.1, entry 1). The product yield increased with the rising reaction temperatures (Table 4B.1, entries 2-6). Further, the reaction was conducted in different solvents such as EtOH, THF, CH_3CN, toluene (Table 4B.1, entries 3-6). Among these, highest yield was obtained in THF (Table 4B.1, entry 4). To increase the product yield and environmental concerns an attempt was

made under ultrasonication (RT and 60 °C) and to our delight, the reaction was feasible (Table 4B.1, entry 7-11). The highest yield of product was obtained when the reaction was carried out in THF at room temperature (Table 4B.1, entry 9). However, increasing reaction temperature and time had no significant impact on the yield (Table 4B.1, entries 10,11). Therefore, 1.0 mmol of **1a**, 1.0 mmol of **2a** and 1.0 mmol of **3** in 3 mL of THF at room temperature under ultrasonication (Table 4B.1, entry 9) is the best reaction condition for the generation of target compounds **4a-t**.

Table 4B.1. Optimization of the reaction conditions[a]

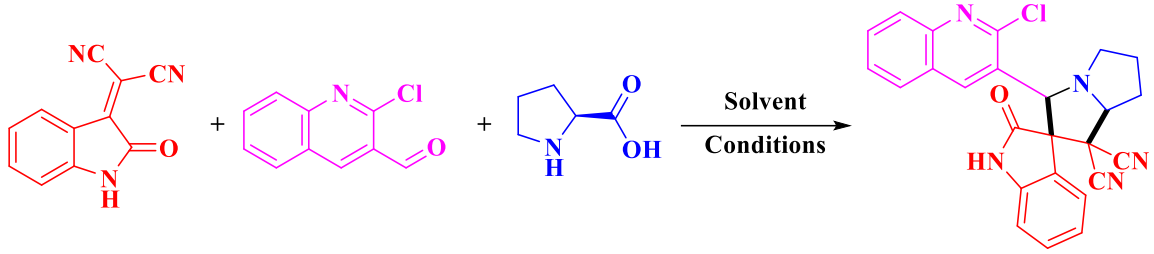

1a **2a** **3** **4a**

Entry	Solvent	Method	Temp (°C)	Time	Yield (%)[b]
1	MeOH	Conventional	RT	20 h	45
2	MeOH	Conventional	Reflux	8 h	60
3	EtOH	Conventional	Reflux	8 h	65
4	THF	Conventional	Reflux	6 h	67
5	CH_3CN	Conventional	Reflux	6 h	65
6	Toluene	Conventional	Reflux	10 h	48
7	CH_3CN	Ultrasonication	RT	60 min	70
8	MeOH	Ultrasonication	RT	60 min	75
9	**THF**	**Ultrasonication**	**RT**	**40 min**	**83**
10	THF	Ultrasonication	60	30 min	80
11	THF	Ultrasonication	RT	90 min	84

[a]Reaction condition: compound **1a** (1.0 mmol), chloroquinolinyl aldehyde **2a** (1.0 mmol), and L-proline **3** (1.0 mmol), solvent (3 mL). [b]Isolated yields.

With the optimized reaction conditions in hand, we have explored the substrate scope by taking various isatin-malononitrile adducts **1a-j**, quinolinyl aldehydes **2a-b** and L-proline **3** (Table 4B.2). Isatin-malononitrile adducts having electron donating (–Me, –OMe), electron withdrawing ($–NO_2$) and halogen (–F, –Cl, –Br, –I) substitutions have no substantial impact on the efficiency of the reaction.

Table 4B.2. Synthesis of quinoline based spirooxindolo-pyrrolizidines **4**[a,b]

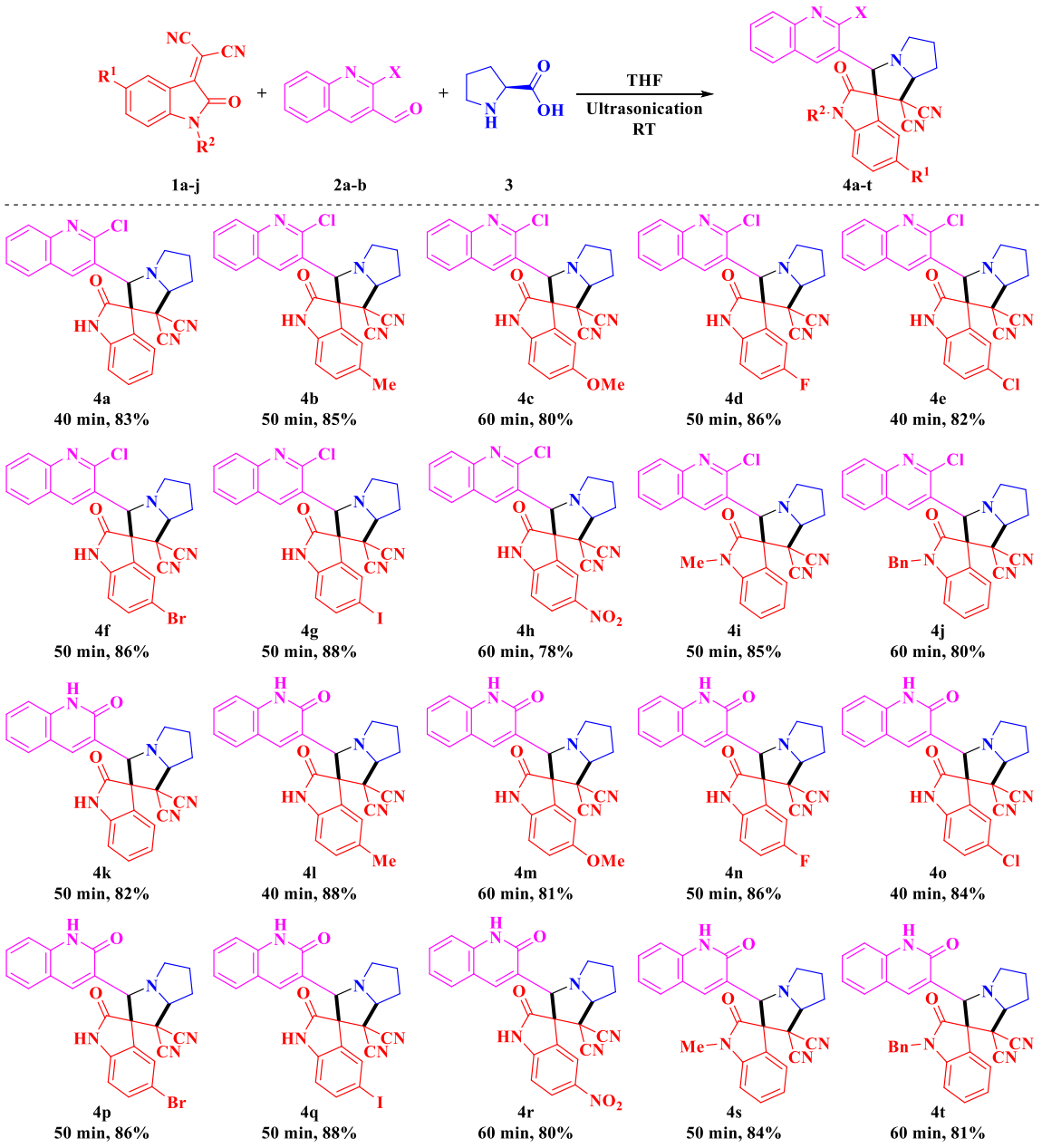

[a]Reaction condition: compounds **1a-j** (1.0 mmol), quinolinyl aldehydes **2a-b** (1.0 mmol), L-proline **3** (1.0 mmol) in 3 mL of THF at room temperature under ultrasonication. [b]Isolated yields.

The plausible reaction mechanism for the generation of target compounds **4** is illustrated in Scheme 4B.7. Initially, azomethine ylide **6** has generated *via* intermediate **5** formation between chloroquinolinyl aldehyde **2a** and cyclic α-amino acid (L-proline) **3**, by the elimination of H_2O and CO_2 [30]. Later, it undergoes [3+2] cycloaddition reaction with isatin-malononitrile adduct **1a** generates the target compound **4a**.

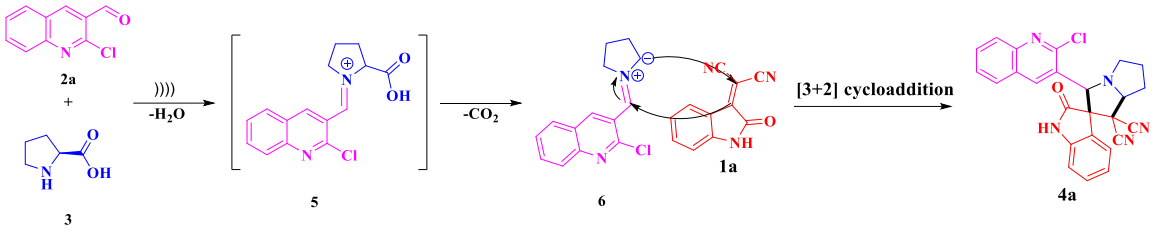

Scheme 4B.7. Plausible reaction mechanism for the generation of target compounds **4**.

The structure of the target compounds (**4a-t**) were analyzed by IR, ^{1}H NMR, ^{13}C NMR and mass spectral data. In this context, IR spectrum of the compound **4l** showed a band at 3213 cm^{-1} corresponds to –NH group and the bands at 1730 cm^{-1} and 1699 cm^{-1} represents the amide carbonyls of oxindole and quinoline moieties respectively [31,32]. The ^{1}H NMR spectrum of compound **4l** showed the singlet signal corresponding to isatin –NH proton at δ 11.47 *ppm*. Whereas, the multiplet in the range from δ 3.23 to δ 2.14 *ppm* attributed to the protons of pyrrolizidine ring. In the ^{13}C NMR spectrum the peak appeared at δ 65.95 *ppm* corresponds the spiro carbon, which was further determined by the absence of this spiro carbon peak in DEPT-135 NMR spectrum. The mass spectrum of compound **4l** displayed a molecular ion peak at *m/z* 436.1804 $[M+H]^{+}$. Furthermore, the regiochemistry of the target compounds were determined by SXRD method (**4e** and **4n**). The ORTEP representation of the compounds **4e** and **4n** have shown in Figures 4B.9 and Figure 4B.10. The CCDC deposition numbers and salient features of crystallographic information of **4e** and **4n** have shown in Table 4B.3.

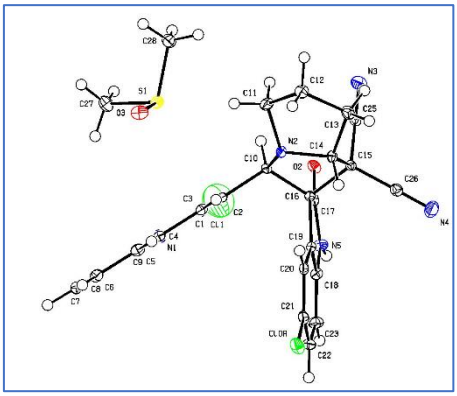

Figure 4B.9. ORTEP representation of **4e** and the thermal ellipsoids are drawn at 50% probability level. The crystal **4e** is the dimethyl sulfoxide solvate.

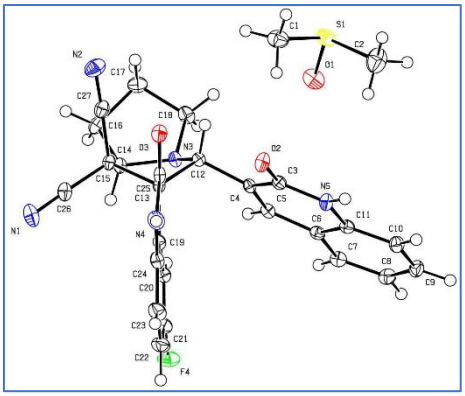

Figure 4B.10. ORTEP representation of **4n** and the thermal ellipsoids are drawn at 50% probability level. The crystal **4n** is the dimethyl sulfoxide solvate.

Table 4B.3. Crystallographic data and refinement parameters of compounds **4e** and **4n**

Identification code	**4e**	**4n**
Empirical formula	$C_{25}H_{17}Cl_2N_5O$	$C_{25}H_{18}FN_5O_2$
Formula weight	473.0810	439.1445
Crystal system	Monoclinic	Triclinic
Space group	$P2_1/c$	P-1
T (K)	100	100
a (Å)	17.1969 (19)	8.981 (2)
b (Å)	9.5687 (10)	9.583 (3)
c (Å)	17.1149 (17)	15.412 (4)
α (°)	90	103.053 (13)
β (°)	115.186(3)	97.931 (12)
γ (°)	90	100.656 (12)
Z	4	2
V (Å^3)	2548.6(5)	1247.3 (6)
D_{calc} (g/cm^3)	1.440	1.378
F (000)	1144.0	540.0
μ (mm^{-1})	0.373	0.177
Θ (°)	27	27
Index ranges	$-21 \le h \le 21$ $-12 \le k \le 12$ $-21 \le l \le 21$	$-11 \le h \le 11$ $-12 \le k \le 12$ $-19 \le l \le 19$
N-total	5556	5446
Parameters	337	349
R_1 $[I > 2\ \sigma\ (I)]$	0.0747	0.0447
wR_2 (all data)	0.2433 (5492)	0.1693 (5323)
GOF	0.915	1.862
CCDC	2129897	2129929

4B.3. Molecular docking studies

In order to get a deeper insight into binding interactions of the targeted compounds, molecular docking studies were performed against dihydrofolate reductase of

mycobacterium tuberculosis (PDB code: 1DF7) [33]. The observed binding energies were depicted in Table 4B.4. The docked compounds (**4a-t**) were well fitted in the binding site of the protein 1DF7 and gives different polar and non-polar interactions with amino acid residues. Among all, the compounds **4j**, **4m**, **4r** and **4t** were showed good binding energies as -10.83, -9.88, -10.28 and -10.54 kcal/mol respectively. Among these, the compound **4j** exhibited more negative binding energy -10.83 kcal/mol, forms two hydrogen bonds with the amino acid residue GLN28 (2.57 and 2.78 Å) and forms three hydrophobic interactions (π···π and π···alkyl) with the amino acid residues. Whereas, the compound **4t** showed binding energy -10.54 kcal/mol, forms three hydrogen bonds with amino acid residues ASP27 (2.42 and 3.11 Å), GLN28 (3.35 Å) and forms two hydrophobic interactions (π···π) with the amino acids. The ligand interaction diagrams of the compounds **4j** and **4t** were presented in Figure 4B.11 and Figure 4B.12.

Table 4B.4 Docking results of the compounds **4a-t** against 1DF7

Ent-ry	Compound	Binding energy (kcal/mol)	No. of hydrogen bonds	Residues involved in the hydrogen bonding	Hydrogen bond length (Å)
1	**4a**	-8.70	1	ALA7	2.81
2	**4b**	-7.82	1	PRO51	3.35
3	**4c**	-8.27	2	ALA7	2.05, 3.19
4	**4d**	-7.55	2	SER49, PRO51	2.87, 3.37
5	**4e**	-7.94	1	PRO51	3.37
6	**4f**	-8.02	1	PRO51	3.38
7	**4g**	-8.01	1	PRO51	3.46
8	**4h**	-8.94	2	GLY95, TYR100	3.66, 2.47
9	**4i**	-7.71	3	ASP27, GLN28	3.25, 3.54, 1.97
10	**4j**	**-10.83**	2	GLN28	2.57, 2.78
11	**4k**	-9.04	2	THR46, ILE94	3.01, 2.39
12	**4l**	-9.36	2	THR46, ILE94	2.97, 2.39
13	**4m**	-9.88	4	ALA7, THR46, ILE94	2.01, 3.29, 3.01, 2.28
14	**4n**	-9.04	3	ALA7, THR46, ILE94	2.12, 3.02, 2.38
15	**4o**	-9.29	2	THR46, ILE94	2.93, 2.50
16	**4p**	-9.46	3	THR46, SER49, ILE94	2.58, 3.25, 2.94
17	**4q**	-9.45	3	THR46, SER49, ILE94	2.66, 3.17, 2.75
18	**4r**	-10.28	2	ILE94, TYR100	2.00, 2.13
19	**4s**	-8.47	2	ASP27, SER49	3.45, 2.04

20	**4t**	**-10.54**	3	ASP27, GLN28	2.42, 3.11, 3.35

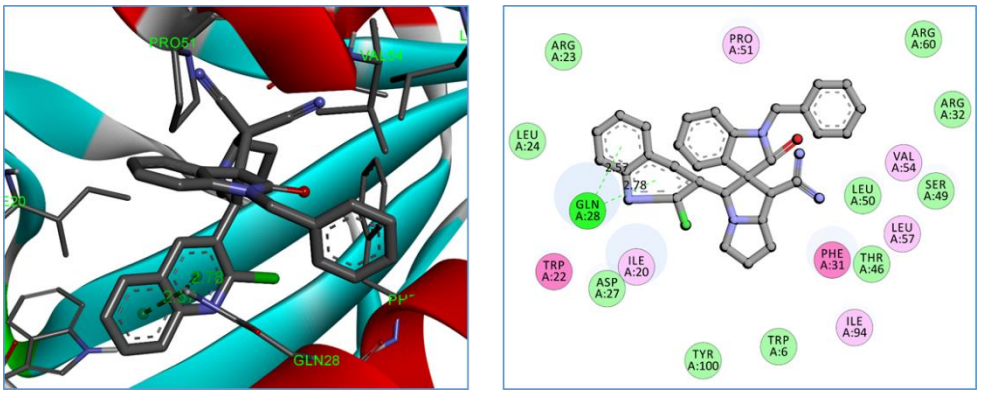

Figure 4B.11. Binding interactions between compound **4j** and active site of 1DF7.

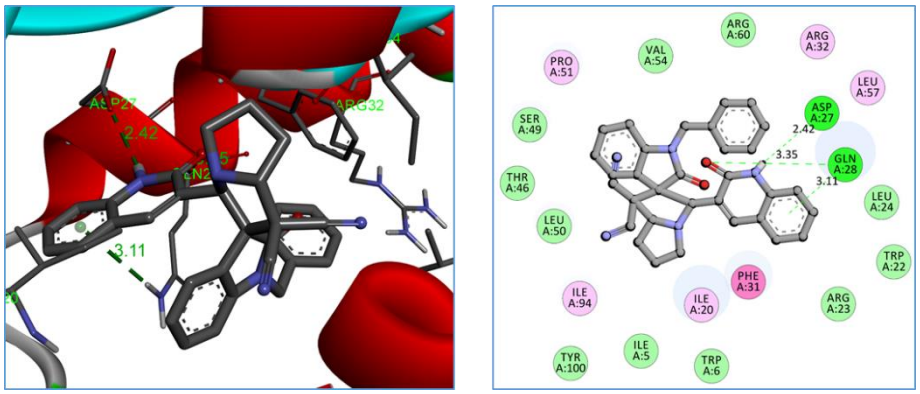

Figure 4B.12. Binding interactions between compound **4t** and active site of 1DF7.

4B.4. ADME prediction

Absorption, distribution, metabolism and excretion (ADME) data improves the selection and identification of molecules at the therapeutic dose with an optimal safety profile. Also, *in silico* prediction of pharmacokinetic parameters lowers the risk of failure of drug at the final stages of clinical trials [34]. The ADME prediction of the synthesized compounds **4a-t** were presented in Table 4B.5.

Estimation of octanol/water partition coefficient (lipophilicity) is examined by LogP. The predicted lipophilicity values are in the ranging from 2.371 to 4.500, and these values revealed that high lipophilicity of the compounds. The predicted aqueous solubility (LogS) values of the synthesized compounds ranging from -3.288 to -5.217, which reflects their excellent solubility in water due to presence of lipophilic groups. On the other hand, the topological polar surface area (TPSA) values ($\leq$ 140 Å) revealed that the compounds' oral bioavailability is high. In general, higher the logarithm of the apparent permeability coefficient (logPapp) higher will be the Caco-2 permeability. From the results, it is predicted that all the compounds have shown high Caco-2 permeability in the range from -

0.219 to 0.751. Interestingly, all the synthesized compounds exhibit high human intestinal absorption (HIA: 90.793-100%). Blood/brain partition coefficient (logBB) value is a measure of the ability of a drug to cross the blood-brain barrier (BBB). The target compounds are in considerable range of BBB. The observed drug like properties and *in silico* ADME prediction suggests that the target compounds **4a-t** exhibit acceptable pharmacokinetic parameters and can be considered as lead molecules for the development of new drugs.

Table 4B.5. Drug likeness and *in silico* ADME properties of the target compounds **4a-t**

En-try	**Mol. Wt.**	**H-donor**	**H-acceptor**	**No. of rotatable bonds**	**LogP**	**LogS**	**TPSA (Å)**	**Caco-2 Permeability (logPapp in 10^{-6} cm/s)**	**HIA (% absorbed)**	**BBB permeability (log BB)**
	≤500	**≤5**	**≤10**	**≤10**	**≤5**	**<0.5**	**≤140**	**>8x10^{-6}**	**70 - 100%**	**-3.0 - 1.2**
4a	439.90	1	6	1	3.273	-3.841	92.81	0.378	100	-0.314
4b	453.92	1	6	1	3.683	-4.188	92.81	0.373	100	-0.345
4c	469.92	1	7	2	3.369	-3.988	102.04	0.396	100	-0.491
4d	457.89	1	6	1	3.359	-3.978	92.81	0.410	100	-0.479
4e	474.35	1	6	1	3.935	-4.710	92.81	0.260	100	-0.52
4f	518.80	1	6	1	4.066	-4.833	92.81	0.265	100	-0.528
4g	565.80	1	6	1	4.340	-5.217	92.81	0.281	100	-0.532
4h	484.89	1	9	2	3.283	-4.547	135.95	-0.219	99.158	-0.843
4i	453.92	0	6	1	3.200	-4.094	84.02	0.722	93.923	-0.335
4j	530.03	0	6	3	4.500	-4.981	84.02	0.522	92.124	-0.353
4k	421.45	2	7	1	2.428	-3.288	112.78	0.403	94.241	-0.520
4l	435.48	2	7	1	2.839	-3.695	112.78	0.398	94.794	-0.551
4m	451.48	2	8	2	2.503	-3.479	112.01	0.421	90.793	-0.653
4n	439.44	2	7	1	2.508	-3.415	112.78	0.436	92.706	-0.668
4o	455.90	2	7	1	3.118	-3.906	112.78	0.286	95.502	-0.704
4p	500.35	2	7	1	3.262	-4.085	112.78	0.290	95.238	-0.724
4q	547.35	2	7	1	3.628	-4.266	112.78	0.306	93.400	-0.711
4r	466.45	2	10	2	2.465	-3.841	155.92	-0.694	91.095	-0.727
4s	435.48	1	7	1	2.371	-3.420	103.99	0.751	97.496	0.242
4t	511.58	1	7	3	3.687	-4.584	103.99	0.587	100	0.357

Mol. Wt: molecular weight; **H-donor**: number of hydrogen bond donors; **H-acceptor**: number of hydrogen bond acceptors; **LogP**: octanol/water partition coefficient; **LogS**: aqua solubility parameter; **TPSA**: topological polar surface area; **Caco-2**: cell permeability; **HIA**: human intestinal absorption; **LogBB**: blood/brain partition co-efficient.

4B.5. Conclusion

This chapter describes the utilization of ultrasound irradiation as green protocol for the synthesis of quinoline based spirooxindolo-pyrrolizidines through [3+2] cycloaddition of isatin malononitrile adducts with azomethine ylides. This methodology has the advantages of mild reaction conditions, easy operation and broad substrate scope. Subsequently, *in silico* molecular docking study, ADME prediction and drug likeness profiles revealed that the synthesized compounds can serve as lead molecules in future research.

4B.6. Experimental Section

4B.6.1. General procedure for quinoline based spirooxindolo-pyrrolizidines (4a-t)

A mixture of isatin malononitrile adducts **1** (1.0 mmol), quinolinyl aldehydes **2** (1.0 mmol) and L-proline **3** (1.0 mmol) in 3 mL of THF were kept at room temperature under ultrasonication for 40-60 min. After the complete consumption of starting materials (monitored by TLC), the resulting solid was filtered and recrystallized from acetone to furnish the desired products.

4B.6.2. Molecular docking protocol

The docking studies are prominent tools for the assessment of the binding affinity to the ligand-protein receptor. All the synthesized compounds were subjected to *in silico* molecular docking studies by using the AutoDockTools (ADT) version 1.5.6 and AutoDock version 4.2.5.1 docking program [35]. The 3D-structures of all the synthesized compounds were prepared by using chem3D pro 12.0 software. The optimized 3D structures were saved in pdb format. The structure of the dihydrofolate reductase of *Mycobacterium tuberculosis* (PDB code: 1DF7) protein was extracted from the protein data bank (http://www.rcsb.org/pdb). The bound ligand and water molecules in protein were removed by using Discovery Studio Visualizer version 4.0 to prepare the protein. Non polar hydrogens were merged and gasteiger charges were added to the protein. The grid file was saved in gpf format. The three dimensional grid box having dimensions 60 x 60 x 60 $Å^3$ was created around the protein with spacing 0.3750 Å. The genetic algorithm was carried out with the population size and the maximum number of evaluations were 150 and 25,00,000 respectively. The docking output file was saved as Lamarckian Ga (4.2) in dpf format. The ligand-protein complex binding sites were visualized by Discovery Studio Visualizer version 4.0.

4B.6.3. ADME prediction

In silico ADME properties and pharmacokinetic parameters of the synthesized compounds were calculated by using the online servers ADMETlab 2.0 and pkCSM [36,37]. The ADMET properties, human intestinal absorption (HIA), Caco-2 cell permeability, plasma protein binding and blood brain barrier penetration (BBB) were predicted using this program.

4B.7. Spectral data of synthesized compounds 4a-t

3'-(2-chloroquinolin-3-yl)-2-oxo-5',6',7',7a'-tetrahydro-1'*H*,3'*H*-spiro[indoline-3,2'-pyrrolizine]-1',1'-dicarbonitrile (4a)

White solid. mp: 219-221 °C. IR (KBr, cm^{-1}): 3383, 2974, 2247, 1737, 1653, 1473. ^1H NMR (400 MHz, DMSO-d_6) δ: 11.13 (s, 1H), 8.72 (s, 1H), 7.95 (d, J = 6.0 Hz, 1H), 7.84 – 7.75 (m, 2H), 7.60 (bs, 1H), 7.51 (d, J = 6.0 Hz, 1H), 7.11 (s, 1H), 6.86 (s, 1H), 6.74 (d, J = 6.0 Hz, 1H), 5.14 (s, 1H), 4.92 – 4.91 (m, 1H), 3.07 (bs, 1H), 2.93 (bs, 1H), 2.47 – 2.40 (m, 2H), 2.33 – 2.29 (m, 1H), 2.19 – 2.14 (m, 1H). ^{13}C NMR (100 MHz, DMSO-d_6) δ: 171.93, 148.87, 146.71, 142.50, 140.76, 131.68, 131.12, 129.34, 128.63, 127.95, 127.90, 127.71, 126.75, 123.13, 122.18, 113.01, 111.99, 110.82, 71.91, 69.29, 66.25, 53.26, 48.47, 28.30, 26.49. ESI-MS (m/z): $[M+H]^+$ calcd. for $C_{25}H_{19}ClN_5O$: 440.1278; found: 440.1241.

3'-(2-chloroquinolin-3-yl)-5-methyl-2-oxo-5',6',7',7a'-tetrahydro-1'*H*,3'*H*-spiro[indoline-3,2'-pyrrolizine]-1',1'-dicarbonitrile (4b)

Off-white solid. mp: 219-221 °C. IR (KBr, cm^{-1}): 3213, 2987, 2247, 1730, 1645, 1495. ^1H NMR (400 MHz, DMSO-d_6) δ: 11.47 (s, 1H), 8.11 (s, 1H), 7.65 (d, J = 6.4 Hz, 1H), 7.40 (d, J = 7.2 Hz, 1H), 7.14 (d, J = 7.2 Hz, 2H), 7.03 (s, 1H), 6.92 (d, J = 7.2 Hz, 1H), 6.66 (d, J = 7.2 Hz, 1H), 4.70 (d, J = 3.6 Hz, 1H), 4.64 (s, 1H), 3.21 – 3.20 (m, 1H), 2.96 – 2.86 (m, 1H), 2.45 – 2.41 (m, 1H), 2.33 – 2.32(m, 2H), 2.24 – 2.16 (m, 1H), 2.03 (s, 3H). ^{13}C NMR (100 MHz, DMSO-d_6) δ: 172.17, 161.18, 140.82, 138.21, 137.56, 130.80, 130.49, 130.35, 128.37, 127.84, 124.08, 122.27, 119.20, 115.08, 113.08, 112.46, 110.06, 72.11, 67.63, 65.95, 54.01, 48.60, 27.58, 26.78, 20.91. ESI-MS (m/z): $[M+H]^+$ calcd. for $C_{26}H_{21}ClN_5O$: 454.1435; found: 454.1445.

3'-(2-chloroquinolin-3-yl)-5-methoxy-2-oxo-5',6',7',7a'-tetrahydro-1'*H*,3'*H*-spiro[indoline-3,2'-pyrrolizine]-1',1'-dicarbonitrile (4c)

Off-white solid. mp: 207-209 °C. IR (KBr, cm^{-1}): 3266, 2973, 2248, 1726, 1646, 1489. ^1H NMR (400 MHz, DMSO-d_6) δ: 10.97 (s, 1H), 8.82 (s, 1H), 7.99 (d, J = 8.0 Hz, 1H), 7.82

(d, J = 8.8 Hz, 1H), 7.78 – 7.72 (m, 1H), 7.63 (t, J = 7.2 Hz, 1H), 6.96 (s, 1H), 6.68 (s, 2H), 5.12 (s, 1H), 4.96 (t, J = 5.6 Hz, 1H), 3.52 (s, 3H), 3.14 – 3.08 (m, 1H), 2.99 (s, 1H), 2.46 – 2.39 (m, 2H), 2.31 – 2.28 (m, 1H), 2.20 – 2.13 (m, 1H). ^{13}C NMR (100 MHz, DMSO-d_6) δ: 172.16, 154.97, 148.87, 146.72, 140.56, 135.92, 131.66, 129.76, 128.97, 128.53, 128.31, 128.04, 127.89, 127.74, 126.82, 124.28, 116.81, 114.33, 113.55, 113.10, 112.14, 111.38, 72.11, 69.42, 66.73, 56.23, 53.33, 48.72, 28.15, 26.29. ESI-MS (m/z): $[M+H]^+$ calcd. for $C_{26}H_{21}ClN_5O_2$: 470.1384; found: 470.1208.

3'-(2-chloroquinolin-3-yl)-5-fluoro-2-oxo-5',6',7',7a'-tetrahydro-1'*H*,3'*H*-spiro[indoline-3,2'-pyrrolizine]-1',1'-dicarbonitrile (4d)

White solid. mp: 209-211 °C. IR (KBr, cm^{-1}): 3429, 2918, 1733, 1644, 1487. ^{1}H NMR (400 MHz, DMSO-d_6) δ: 11.19 (s, 1H), 8.78 (s, 1H), 7.97 (d, J = 8.4 Hz, 1H), 7.83 (d, J = 8.4 Hz, 1H), 7.77 (t, J = 8.0 Hz, 1H), 7.63 (t, J = 7.6 Hz, 1H), 7.45 (d, J = 6.8 Hz, 1H), 6.98 (td, J = 8.8, 2.0 Hz, 1H), 6.75 (dd, J = 8.4, 4.4 Hz, 1H), 5.14 (s, 1H), 4.97 (t, J = 6.4 Hz, 1H), 3.11 – 3.06 (m, 1H), 2.97 – 2.91 (m, 1H), 2.47 – 2.37 (m, 2H), 2.34 – 2.26 (m, 1H), 2.20 – 2.09 (m, 1H). ^{13}C NMR (100 MHz, DMSO-d_6) δ: 171.89, 159.12 (d, J = 240.0 Hz), 148.75, 146.75, 140.72, 138.88 (d, J = 1.8 Hz), 131.79, 129.22, 128.56, 128.11, 127.75, 126.77, 124.70 (d, J = 8.6 Hz), 117.83 (d, J = 23.6 Hz), 115.78 (d, J = 26.2 Hz), 112.88, 111.78, 71.84, 69.29, 66.68, 53.21, 48.37, 28.27, 26.47. ESI-MS (m/z): $[M+H]^+$ calcd. for $C_{25}H_{18}ClFN_5O$: 458.1184; found: 458.1186.

5-chloro-3'-(2-chloroquinolin-3-yl)-2-oxo-5',6',7',7a'-tetrahydro-1'*H*,3'*H*-spiro[indoline-3,2'-pyrrolizine]-1',1'-dicarbonitrile (4e)

White solid. mp: 232-234 °C. IR (KBr, cm^{-1}): 3432, 2991, 2244, 1736, 1644, 1479. ^{1}H NMR (400 MHz, DMSO-d_6) δ: 11.55 (s, 1H), 8.14 (s, 1H), 7.68 (d, J = 7.6 Hz, 1H), 7.43 (t, J = 7.6 Hz, 1H), 7.21 – 7.13 (m, 4H), 6.81 (d, J = 8.8 Hz, 1H), 4.73 (dd, J = 7.2, 4.0 Hz, 1H), 4.62 (s, 1H), 3.24 – 3.21 (m, 1H), 2.94 (dd, J = 15.2, 8.8 Hz, 1H), 2.46 – 2.38 (m, 1H), 2.35 – 2.28 (m, 2H), 2.21 – 2.14 (m, 1H). ^{13}C NMR (100 MHz, DMSO-d_6) δ: 172.20, 161.22, 142.38, 138.23, 137.54, 130.67, 130.59, 130.41, 128.49, 127.04, 126.01, 125.45, 122.41, 119.16, 115.19, 112.90, 111.82, 72.30, 67.74, 66.09, 54.06, 48.47, 27.53, 26.61. ESI-MS (m/z): $[M+H]^+$ calcd. for $C_{25}H_{18}Cl_2N_5O$: 474.0888; found: 474.1086.

5-bromo-3'-(2-chloroquinolin-3-yl)-2-oxo-5',6',7',7a'-tetrahydro-1'*H*,3'*H*-spiro[indoline-3,2'-pyrrolizine]-1',1'-dicarbonitrile (4f)

White solid. mp: 235-237 °C. IR (KBr, cm^{-1}): 3166, 2989, 2245, 1737, 1644, 1475. ^{1}H NMR (400 MHz, DMSO-d_6) δ: 11.45 (s, 1H), 8.12 (s, 1H), 7.69 (d, J = 8.0 Hz, 1H), 7.43 (d, J = 7.6 Hz, 1H), 7.27 – 7.20 (m, 4H), 6.82 (d, J = 8.4 Hz, 1H), 4.75 – 4.70 (m, 1H), 4.63 (s, 1H), 3.26 – 3.23 (m, 1H), 2.99 – 2.90 (m, 1H), 2.47 – 2.39 (m, 1H), 2.35 – 2.26 (m, 2H), 2.21 – 2.15 (m, 1H). ^{13}C NMR (100 MHz, DMSO-d_6) δ: 173.25, 162.22, 143.38, 139.24, 137.55, 131.69, 130.49, 128.59, 127.64, 126.20, 125.47, 122.43, 119.18, 115.29, 112.92, 111.84, 72.20, 68.46, 66.19, 54.02, 48.27, 28.23, 26.51. ESI-MS (m/z): $[M+H]^+$ calcd. for $C_{25}H_{18}BrClN_5O$: 518.0383; found: 518.0482.

3'-(2-chloroquinolin-3-yl)-5-iodo-2-oxo-5',6',7',7a'-tetrahydro-1'*H*,3'*H*-spiro[indoline-3,2'-pyrrolizine]-1',1'-dicarbonitrile (4g)

White solid. mp: 240-242 °C. IR (KBr, cm^{-1}): 3458, 2990, 1737, 1648, 1476. ^{1}H NMR (400 MHz, DMSO-d_6) δ: 11.27 (s, 1H), 8.74 (s, 1H), 7.98 (d, J = 8.0 Hz, 1H), 7.83 (d, J = 8.0 Hz, 1H), 7.81 – 7.76 (m, 1H), 7.73 (s, 1H), 7.65 (t, J = 7.2 Hz, 1H), 7.43 (dd, J = 8.4, 1.2 Hz, 1H), 6.58 (d, J = 8.0 Hz, 1H), 5.12 (s, 1H), 4.95 (t, J = 6.8 Hz, 1H), 3.14 – 3.04 (m, 1H), 2.98 – 2.91 (m, 1H), 2.46 – 2.36 (m, 2H), 2.31 – 2.25 (m, 1H), 2.20 – 2.13 (m, 1H). ^{13}C NMR (100 MHz, DMSO-d_6) δ: 171.55, 148.65, 146.75, 142.19, 140.73, 139.63, 135.94, 131.80, 129.27, 128.49, 128.06, 127.75, 126.76, 125.53, 113.05, 112.97, 111.80, 85.05, 72.06, 69.44, 66.30, 53.23, 48.28, 28.25, 26.39. ESI-MS (m/z): $[M+H]^+$ calcd. for $C_{25}H_{18}ClIN_5O$: 566.0245; found: 565.9703.

3'-(2-chloroquinolin-3-yl)-5-nitro-2-oxo-5',6',7',7a'-tetrahydro-1'*H*,3'*H*-spiro[indoline-3,2'-pyrrolizine]-1',1'-dicarbonitrile (4h)

Off-white solid. mp: 297-299 °C. IR (KBr, cm^{-1}): 3434, 2924, 2247, 1739, 1653, 1521. ^{1}H NMR (400 MHz, DMSO-d_6) δ: 11.30 (s, 1H), 8.82 (s, 1H), 8.13 (d, J = 8.8, 1H), 7.86 (s, 1H), 7.70 (d, J = 7.6 Hz, 1H), 7.52 – 7.43 (m, 1H), 7.14 (d, J = 8.0 Hz, 1H), 7.08 – 7.02 (m, 2H), 4.80 – 4.75 (m, 1H), 4.66 (s, 1H), 3.06 – 2.98 (m, 1H), 2.86 – 2.80 (m, 1H), 2.45 – 2.39 (m, 1H), 2.36 – 2.25 (m, 2H), 2.23 – 2.08 (m, 1H).^{13}C NMR (100 MHz, DMSO-d_6) δ: 172.20, 152.63, 147.38, 142.57, 136.58, 132.85, 132.30, 130.31, 129.71, 128.60, 128.15, 126.53, 113.63, 110.65, 87.02, 72.59, 64.10, 57.82, 48.02, 28.85, 26.13. ESI-MS (m/z): $[M+H]^+$ calcd. for $C_{25}H_{18}ClN_6O_3$: 485.1129; found: 485.0795.

3'-(2-chloroquinolin-3-yl)-1-methyl-2-oxo-5',6',7',7a'-tetrahydro-1'*H*,3'*H*-spiro[indoline-3,2'-pyrrolizine]-1',1'-dicarbonitrile (4i)

White solid. mp: 239-241 °C. IR (KBr, cm^{-1}): 3168, 2956, 2242, 1730, 1650, 1476. ^{1}H NMR (400 MHz, DMSO-d_6) δ: 8.21 (s, 1H), 7.69 (d, J = 7.2 Hz, 1H), 7.48 – 7.40 (m, 1H), 7.26 – 7.10 (m, 4H), 7.01 (d, J = 7.2 Hz, 1H), 6.84 (d, J = 7.6 Hz, 1H), 4.74 – 7.70 (m, 1H), 4.64 (s, 1H), 3.22 (s, 3H), 2.99 (bs, 2H), 2.42 – 2.38 (m, 1H), 2.35 – 2.32 (m, 2H), 2.20 – 2.12 (m, 1H). ^{13}C NMR (100 MHz, DMSO-d_6) δ: 172.85, 152.63, 147.80, 144.13, 136.58, 132.30, 130.03, 129.71, 128.15, 127.93, 126.53, 122.28, 113.63, 110.33, 72.32, 67.76, 66.19, 54.08, 48.47, 32.85 27.63, 26.62. ESI-MS (m/z): $[M+H]^+$ calcd. for $C_{26}H_{21}ClN_5O$: 454.1435; found: 454.1536.

1-benzyl-3'-(2-chloroquinolin-3-yl)-2-oxo-5',6',7',7a'-tetrahydro-1'*H*,3'*H*-spiro[indoline-3,2'-pyrrolizine]-1',1'-dicarbonitrile (4j)

White solid. mp: 244-246 °C. IR (KBr, cm^{-1}): 3368, 2954, 2245, 1736, 1648, 1475. ^{1}H NMR (400 MHz, DMSO-d_6) δ: 8.11 (s, 1H), 7.66 (d, J = 8.0 Hz, 1H), 7.50 (d, J = 8.0 Hz, 3H), 7.39 (t, J = 7.2 Hz, 2H), 7.32 – 7.29 (m, 2H), 7.19 – 7.12 (m, 3H), 6.89 (d, J = 7.6 Hz, 1H), 6.74 (d, J = 8.0 Hz, 1H), 5.10 (bs 1H), 4.84 (s, 1H), 4.76 (s, 2H), 3.29 – 3.25 (m, 1H), 2.98 – 2.83 (m, 1H), 2.46 – 2.40 (m, 1H), 2.35 – 2.31 (m, 2H), 2.24 – 2.14 (m, 1H). ^{13}C NMR (100 MHz, DMSO-d_6) δ: 171.45, 152.63, 145.08, 144.13, 136.92, 136.58, 132.30, 130.31, 130.03, 129.93, 129.71, 128.78, 128.78, 128.57, 128.57, 128.15, 128.03, 126.53, 122.28, 113.63, 113.63, 112.05, 74.59, 65.10, 57.42, 55.02, 46.84, 27.85, 25.13. ESI-MS (m/z): $[M+H]^+$ calcd. for $C_{32}H_{25}ClN_5O$: 530.1748; found: 530.1890.

2-oxo-3'-(2-oxo-1,2-dihydroquinolin-3-yl)-5',6',7',7a'-tetrahydro-1'*H*,3'*H*-spiro[indoline-3,2'-pyrrolizine]-1',1'-dicarbonitrile (4k)

Off-white solid. mp: 233-235 °C. IR (KBr, cm^{-1}): 3358, 2952, 2243, 1752, 1651, 1473. ^{1}H NMR (400 MHz, DMSO-d_6) δ: 11.49 (s, 1H), 10.81 (s, 1H), 8.11 (s, 1H), 7.65 (d, J = 7.6 Hz, 1H), 7.41 (t, J = 7.6 Hz, 1H), 7.16 – 7.10 (m, 4H), 6.80 (d, J = 7.6 Hz, 1H), 6.75 (t, J = 7.6 Hz, 1H), 4.67 (dd, J = 7.6, 4.4 Hz, 1H), 4.63 (s, 1H), 3.27 – 3.21 (m, 1H), 2.95 (dd, J = 15.6, 8.8 Hz, 1H), 2.47 – 2.40 (m, 1H), 2.37 – 2.29 (m, 2H), 2.22 – 2.13 (m, 1H). ^{13}C NMR (100 MHz, DMSO-d_6) δ: 172.51, 161.21, 143.34, 138.23, 137.29, 130.72, 130.56, 130.51, 128.54, 127.10, 124.15, 122.25, 121.48, 119.19, 115.10, 113.00, 112.48, 110.42, 72.41, 67.77, 65.95, 54.11, 48.74, 27.46, 26.64. ESI-MS (m/z): $[M+H]^+$ calcd. for $C_{25}H_{20}N_5O_2$: 422.1617; found: 422.1814.

5-methyl-2-oxo-3'-(2-oxo-1,2-dihydroquinolin-3-yl)-5',6',7',7a'-tetrahydro-1'*H*,3'*H*-spiro [indoline-3,2'-pyrrolizine]-1',1'-dicarbonitrile (4l)

White solid. mp: 219-221 °C. IR (KBr, cm^{-1}): 3213, 2988, 1730, 1699, 1644, 1495. ^1H NMR (400 MHz, DMSO-d_6) δ: 11.47 (s, 1H), 10.68 (s, 1H), 8.11 (s, 1H), 7.65 (d, J = 7.6 Hz, 1H), 7.44 – 7.38 (m, 1H), 7.14 (d, J = 7.6 Hz, 2H), 7.03 (s, 1H), 6.92 (d, J = 7.6 Hz, 1H), 6.66 (d, J = 8.0 Hz, 1H), 4.70 (dd, J = 7.6, 4.4 Hz, 1H), 4.64 (d, J = 0.8 Hz, 1H), 3.23 – 3.18 (m, 1H), 2.94 – 2.88 (m, 1H), 2.47 – 2.40 (m, 1H), 2.36 – 2.28 (m, 2H), 2.23 – 2.14 (m, 1H), 2.03 (s, 3H). ^{13}C NMR (100MHz, DMSO-d_6) δ: 172.17, 161.18, 140.82, 138.21, 137.55, 130.80, 130.49, 130.34, 128.36, 127.84, 124.08, 122.27, 119.20, 115.08, 113.07, 112.46, 110.06, 72.11, 67.63, 65.95, 54.01, 48.60, 27.57, 26.78, 20.91. ESI-MS (m/z): $[M+H]^+$ calcd. for $C_{26}H_{22}N_5O_2$: 436.1773; found: 436.1804.

5-methoxy-2-oxo-3'-(2-oxo-1,2-dihydroquinolin-3-yl)-5',6',7',7a'-tetrahydro-1'*H*,3'*H*-spiro [indoline-3,2'-pyrrolizine]-1',1'-dicarbonitrile (4m)

Off-white solid. mp: 244-246 °C. IR (KBr, cm^{-1}): 3433, 2917, 2243, 1726, 1653, 1491. ^1H NMR (400 MHz, DMSO-d_6) δ: 11.49 (s, 1H), 10.63 (s, 1H), 8.17 (s, 1H), 7.68 (d, J = 5.6 Hz, 1H), 7.43 (d, J = 7.2 Hz, 1H), 7.15 (d, J = 5.2 Hz, 2H), 6.71 (bs, 3H), 4.71 (d, J = 3.6 Hz, 1H), 4.63 (s, 1H), 3.46 (s, 3H), 3.23 (s, 1H), 2.96 – 2.94 (m, 1H), 2.46 – 2.38 (m, 1H), 2.37 – 2.26 (m, 2H), 2.23 – 2.15 (m, 1H). ^{13}C NMR (100 MHz, DMSO-d_6) δ: 172.45, 161.17, 154.38, 138.26, 137.28, 136.74, 130.80, 130.52, 128.42, 125.19, 122.31, 119.23, 115.89, 115.13, 113.98, 113.09, 112.52, 110.83, 72.31, 67.74, 66.34, 55.97, 54.05, 48.72, 27.49, 26.52. ESI-MS (m/z): $[M+H]^+$ calcd. for $C_{26}H_{22}N_5O_3$: 452.1723; found: 452.1560.

5-fluoro-2-oxo-3'-(2-oxo-1,2-dihydroquinolin-3-yl)-5',6',7',7a'-tetrahydro-1'*H*,3'*H*-spiro [indoline-3,2'-pyrrolizine]-1',1'-dicarbonitrile (4n)

White solid. mp: 218-220 °C. IR (KBr, cm^{-1}): 3450, 2984, 2246, 1733, 1644, 1488. ^1H NMR (400 MHz, DMSO-d_6) δ: 11.54 (s, 1H), 10.86 (s, 1H), 8.15 (s, 1H), 7.68 (d, J = 7.6 Hz, 1H), 7.43 (t, J = 7.6 Hz, 1H), 7.16 (d, J = 7.6 Hz, 2H), 7.07 (dd, J = 8.8, 2.4 Hz, 1H), 6.99 (td, J = 9.6, 2.4 Hz, 1H), 6.80 (dd, J = 8.4, 4.4 Hz, 1H), 4.74 (dd, J = 7.6, 4.4 Hz, 1H), 4.64 (s, 1H), 3.28 – 3.20 (m, 1H), 2.96 (dd, J = 15.6, 8.8 Hz, 1H), 2.47 – 2.39 (m, 1H), 2.36 – 2.29 (m, 2H), 2.21 – 2.14 (m, 1H). ^{13}C NMR (100 MHz, DMSO-d_6) δ: 172.49, 161.20, 158.60 (d, J = 238.0 Hz), 139.76, 138.26, 137.45, 130.63 (d, J = 16.8 Hz), 128.54, 125.68 (d, J = 8.4 Hz), 122.37, 119.15, 117.25 (d, J = 23.2 Hz), 115.17, 115.00, 114.74, 112.90,

112.26, 111.25 (d, *J* = 7.8 Hz), 72.33, 67.78, 66.35, 54.07, 48.56, 27.48, 26.56. ESI-MS (m/z): $[M+H]^+$ calcd. for $C_{25}H_{19}FN_5O_2$: 440.1523; found: 440.1443.

5-chloro-2-oxo-3'-(2-oxo-1,2-dihydroquinolin-3-yl)-5',6',7',7a'-tetrahydro-1'*H*,3'*H*-spiro [indoline-3,2'-pyrrolizine]-1',1'-dicarbonitrile (4o)

White solid. mp: 240-242 °C. IR (KBr, cm^{-1}): 3201, 2990, 1736, 1698, 1643, 1478. ^1H NMR (400 MHz, DMSO-d_6) δ: 11.55 (s, 1H), 10.98 (s, 1H), 8.15 (s, 1H), 7.68 (d, *J* = 8.0 Hz, 1H), 7.44 (t, *J* = 7.6 Hz, 1H), 7.22 – 7.14 (m, 4H), 6.82 (d, *J* = 9.2 Hz, 1H), 4.73 (dd, *J* = 7.2, 4.0 Hz, 1H), 4.62 (s, 1H), 3.27 – 3.21 (m, 1H), 2.94 (dd, *J* = 15.6, 8.8 Hz, 1H), 2.46 – 2.40 (m, 1H), 2.35 – 2.31 (m, 2H), 2.25 – 2.15 (m, 1H). ^{13}C NMR (100 MHz, DMSO-d_6) δ: 172.21, 161.22, 142.35, 138.21, 137.57, 130.69, 130.60, 130.38, 128.50, 127.04, 126.00, 125.47, 122.44, 119.16, 115.19, 112.19, 111.83, 72.30, 67.72, 66.09, 54.06, 48.48, 27.53, 26.61. ESI-MS (m/z): $[M+H]^+$ calcd. for $C_{25}H_{19}ClN_5O_2$: 456.1227; found: 456.1008.

5-bromo-2-oxo-3'-(2-oxo-1,2-dihydroquinolin-3-yl)-5',6',7',7a'-tetrahydro-1'*H*,3'*H*-spiro [indoline-3,2'-pyrrolizine]-1',1'-dicarbonitrile (4p)

Off-white solid. mp: 237-239 °C. IR (KBr, cm^{-1}): 3432, 2988, 2244, 1737, 1644, 1475. ^1H NMR (400 MHz, DMSO-d_6) δ: 11.56 (s, 1H), 10.98 (s, 1H), 8.14 (s, 1H), 7.91 (bs, 1H), 7.69 (s, 1H), 7.45 (s, 1H), 7.30 (s, 1H), 7.17 (s, 2H), 6.76 (s, 1H), 5.14 – 4.96 (m, 1H), 4.67 (bs, 1H), 3.26 – 3.16 (m, 1H), 2.98 – 2.94 (m, 1H), 2.44 – 2.37 (m, 1H), 2.37 – 2.21 (m, 3H). ^{13}C NMR (100 MHz, DMSO-d_6) δ: 172.09, 161.21, 142.75, 138.22, 137.55, 133.77, 133.43, 130.67, 130.39, 129.76, 128.47, 126.36, 122.41, 119.17, 115.19, 113.02, 112.30, 72.30, 67.74, 66.03, 54.05, 48.46, 27.54, 26.61. ESI-MS (m/z): $[M+H]^+$ calcd. for $C_{25}H_{19}BrN_5O_2$: 500.0722; found: 500.0841.

5-iodo-2-oxo-3'-(2-oxo-1,2-dihydroquinolin-3-yl)-5',6',7',7a'-tetrahydro-1'*H*,3'*H*-spiro [indoline-3,2'-pyrrolizine]-1',1'-dicarbonitrile (4q)

White solid. mp: 245-247 °C. IR (KBr, cm^{-1}): 3458, 2991, 1738, 1642, 1458. ^1H NMR (400 MHz, DMSO-d_6) δ: 11.54 (s, 1H), 10.96 (s, 1H), 8.13 (s, 1H), 7.69 (d, *J* = 8.4 Hz, 1H), 7.48 – 7.43 (m, 2H), 7.41 (d, *J* = 1.2 Hz, 1H), 7.18 (d, *J* = 7.2 Hz, 2H), 6.65 (d, *J* = 8.4 Hz, 1H), 4.68 (dd, *J* = 7.6, 4.4 Hz, 1H), 4.61 (d, *J* = 0.8 Hz, 1H), 3.25 – 3.20 (m, 1H), 2.94 (dd, *J* = 16.0, 8.4 Hz, 1H), 2.47 – 2.40 (m, 1H), 2.35 – 2.27 (m, 2H), 2.22 – 2.14 (m, 1H). ^{13}C NMR (100 MHz, DMSO-d_6) δ: 171.94, 161.21, 143.12, 139.14, 138.22, 137.56, 135.37, 130.65, 130.41, 128.44, 126.55, 122.39, 119.17, 115.18, 112.74, 112.22, 83.97, 72.34,

67.74, 65.84, 54.01, 48.43, 27.54, 26.57. ESI-MS (m/z): $[M+H]^+$ calcd. for $C_{25}H_{19}IN_5O_2$: 548.0583; found: 548.0621.

5-nitro-2-oxo-3'-(2-oxo-1,2-dihydroquinolin-3-yl)-5',6',7',7a'-tetrahydro-1'*H*,3'*H*-spiro [indoline-3,2'-pyrrolizine]-1',1'-dicarbonitrile (4r)

Off-white solid. mp: 302-304 °C. IR (KBr, cm^{-1}): 3433, 2974, 2247, 1738, 1652, 1521. ^1H NMR (400 MHz, DMSO-d_6) δ: 11.71 (s, 1H), 11.60 (s, 1H), 8.22 (d, J = 6.0 Hz, 1H), 8.13 (dd, J = 9.2, 1.2 Hz, 1H), 7.88 (s, 1H), 7.71 (d, J = 7.2 Hz, 1H), 7.49 – 7.40 (m, 1H), 7.14 (d, J = 8.4 Hz, 2H), 7.02 (dd, J = 15.2, 8.8 Hz, 1H), 4.78 – 4.75 (m, 1H), 4.65 (s, 1H), 3.04 – 2.98 (m, 1H), 2.85 – 2.79 (m, 1H), 2.47 – 2.40 (m, 1H), 2.38 – 2.25 (m, 2H), 2.23 – 2.05 (m, 1H). ^{13}C NMR (100 MHz, DMSO-d_6) δ: 172.97, 161.31, 149.91, 141.67, 138.14, 137.67, 130.80, 130.27, 128.58, 127.94, 124.93, 123.21, 122.54, 115.22, 111.96, 110.77, 72.58, 67.84, 65.74, 54.23, 48.40, 27.51, 26.48. ESI-MS (m/z): $[M+H]^+$ calcd. for $C_{25}H_{19}N_6O_4$: 467.1468; found: 467.1501.

1-methyl-2-oxo-3'-(2-oxo-1,2-dihydroquinolin-3-yl)-5',6',7',7a'-tetrahydro-1'*H*,3'*H*-spiro [indoline-3,2'-pyrrolizine]-1',1'-dicarbonitrile (4s)

Off-white solid. mp: 313-315 °C. IR (KBr, cm^{-1}): 3437, 2940, 2245, 1727, 1651, 1493. ^1H NMR (400 MHz, DMSO-d_6) δ: 11.58 (s, 1H), 8.11 (s, 1H), 7.67 (d, J = 6.0 Hz, 1H), 7.46 – 7.40 (m, 1H), 7.24 – 7.09 (m, 4H), 7.01 (d, J = 6.0 Hz, 1H), 6.81 (d, J = 7.2 Hz, 1H), 4.73 – 7.71 (m, 1H), 4.62 (s, 1H), 3.20 (s, 3H), 2.98 (bs, 2H), 2.46 – 2.41 (m, 1H), 2.36 – 2.34 (m, 2H), 2.24 – 2.19 (m, 1H). ^{13}C NMR (100 MHz, DMSO-d_6) δ: 171.43, 161.30, 144.72, 138.14, 137.16, 130.82, 130.69, 130.53, 128.56, 126.78, 123.52, 122.31, 122.13, 119.18, 115.07, 109.39, 72.77, 68.44, 65.44, 54.32, 48.58, 27.44, 27.31, 26.64. ESI-MS (m/z): $[M+H]^+$ calcd. for $C_{26}H_{22}N_5O_2$: 436.1773; found: 436.1579.

1-benzyl-2-oxo-3'-(2-oxo-1,2-dihydroquinolin-3-yl)-5',6',7',7a'-tetrahydro-1'*H*,3'*H*-spiro [indoline-3,2'-pyrrolizine]-1',1'-dicarbonitrile (4t)

White solid. mp: 255-257 °C. IR (KBr, cm^{-1}): 3444, 2974, 2248, 1732, 1647, 1488. ^1H NMR (400 MHz, DMSO-d_6) δ: 11.64 (s, 1H), 8.12 (s, 1H), 7.65 (d, J = 7.6 Hz, 1H), 7.40 (d, J = 8.4 Hz, 3H), 7.35 (t, J = 7.2 Hz, 2H), 7.31 – 7.27 (m, 2H), 7.16 – 7.11 (m, 3H), 6.85 (t, J = 7.6 Hz, 1H), 6.77 (d, J = 7.6 Hz, 1H), 5.09 (d, J = 16.0 Hz, 1H), 4.82 (bs, 1H), 4.76 (s, 2H), 3.27 – 3.23 (m, 1H), 2.99 – 2.93 (m, 1H), 2.48 – 2.41 (m, 1H), 2.39 – 2.32 (m, 2H), 2.25 – 2.15 (m, 1H). ^{13}C NMR (100 MHz, DMSO-d_6) δ: 171.04, 161.38, 143.72, 138.21, 137.72, 136.39, 130.71, 130.23, 129.05, 128.58, 127.88, 127.49, 127.07, 123.35, 122.42,

119.17, 115.14, 112.87, 112.32, 110.01, 72.19, 67.78, 65.48, 54.09, 48.68, 43.98, 27.74, 26.73. ESI-MS (m/z): $[M+H]^+$ calcd. for $C_{32}H_{26}N_5O_2$: 512.2087; found: 512.2499.

4B.8. References

[1] M. J. Lo Fiego, A. S. Lorenzetti, G. F. Silbestri, C. E. Domini, *Ultrason. Sonochem.* **2021**, *80*, 105834–105880.

[2] E. Ruiz, H. Rodríguez, J. Coro, V. Niebla, A. Rodríguez, R. Martínez-Alvarez, H. N. De Armas, M. Suárez, N. Martín, *Ultrason. Sonochem.* **2012**, *19*, 221–226.

[3] A. L. S. Eh, S. G. Teoh, *Ultrason. Sonochem.* **2012**, *19*, 151–159.

[4] N. S. M. Yusof, B. Babgi, Y. Alghamdi, M. Aksu, J. Madhavan, M. Ashokkumar, *Ultrason. Sonochem.* **2016**, *29*, 568–576.

[5] T. Zarganes-Tzitzikas, A. L. Chandgude, A. Dömling, *Chem. Rec.* **2015**, *15*, 981–996.

[6] J. D. Sunderhaus, S. F. Martin, *Chem. - A Eur. J.* **2009**, *15*, 1300–1308.

[7] H. Farhid, V. Khodkari, M. T. Nazeri, S. Javanbakht, A. Shaabani, *Org. Biomol. Chem.* **2021**, *19*, 3318–3358.

[8] M. Xia, R.-Z. Ma, *J. Heterocycl. Chem.* **2014**, *51*, 539–554.

[9] G. Molteni, A. Silvani, *European J. Org. Chem.* **2021**, *2021*, 1653–1675.

[10] T. Onishi, P. R. Sebahar, R. M. Williams, *Org. Lett.* **2003**, *5*, 3135–3137.

[11] B. M. Trost, M. K. Brennan, *Org. Lett.* **2006**, *8*, 2027–2030.

[12] R. Rojas-Duran, G. González-Aspajo, C. Ruiz-Martel, G. Bourdy, V. H. Doroteo-Ortega, J. Alban-Castillo, G. Robert, P. Auberger, E. Deharo, *J. Ethnopharmacol.* **2012**, *143*, 801–804.

[13] E. García Prado, M. D. García Gimenez, R. De la Puerta Vázquez, J. L. Espartero Sánchez, M. T. Sáenz Rodríguez, *Phytomedicine* **2007**, *14*, 280–284.

[14] D. B. Ramachary, C. Venkaiah, R. Madhavachary, *Org. Lett.* **2013**, *15*, 3042–3045.

[15] W. Luo, B. Shao, J. Li, X. Xiao, D. Song, F. Ling, W. Zhong, *Org. Chem. Front.* **2020**, *7*, 1016–1021.

[16] A. P. Sakla, P. Kansal, N. Shankaraiah, *Org. Biomol. Chem.* **2020**, *18*, 8572–8596.

[17] F. Yu, R. Huang, H. Ni, J. Fan, S. Yan, J. Lin, *Green Chem.* **2013**, *15*, 453–462.

[18] R. R. Kumar, S. Perumal, P. Senthilkumar, P. Yogeeswari, D. Sriram, *Eur. J. Med. Chem.* **2009**, *44*, 3821–3829.

[19] A. Gollner, D. Rudolph, H. Arnhof, M. Bauer, S. M. Blake, G. Boehmelt, X. L. Cockroft, G. Dahmann, P. Ettmayer, T. Gerstberger, J. Karolyi-Oezguer, D. Kessler, C. Kofink, J. Ramharter, J. Rinnenthal, A. Savchenko, R. Schnitzer, H. Weinstabl, U. Weyer-Czernilofsky, T. Wunberg, D. B. McConnell, *J. Med. Chem.* **2016**, *59*, 10147–10162.

[20] A. Toumi, S. Boudriga, K. Hamden, M. Sobeh, M. Cheurfa, M. Askri, M. Knorr, C. Strohmann, L. Brieger, *Bioorg. Chem.* **2021**, *106*, 104507–104523.

[21] N. H. de Silva, S. Pyreddy, E. W. Blanch, H. M. Hügel, S. Maniam, *Bioorg. Chem.* **2021**, *114*, 105128–105138.

[22] A. Kumar, G. Gupta, A. K. Bishnoi, R. Saxena, K. S. Saini, R. Konwar, S. Kumar, A. Dwivedi, *Bioorg. Med. Chem.* **2015**, *23*, 839–848.

[23] P. Prasanna, K. Balamurugan, S. Perumal, P. Yogeeswari, D. Sriram, *Eur. J. Med. Chem.* **2010**, *45*, 5653–5661.

[24] G. Lotfy, Y. M. Abdel Aziz, M. M. Said, E. S. H. El Ashry, E. S. H. El Tamany, M. M. Abu-Serie, M. Teleb, A. Dömling, A. Barakat, *Bioorg. Chem.* **2021**, *117*, 105427–105448.

[25] Y. Huang, H. L. Fang, Y. X. Huang, J. Sun, C. G. Yan, *J. Org. Chem.* **2019**, *84*, 12437–12451.

[26] J. Sun, L. Chen, H. Gong, C. G. Yan, *Org. Biomol. Chem.* **2015**, *13*, 5905–5917.

[27] M. P. Rao, S. S. Gunaga, J. Zuegg, R. Pamarthi, M. Ganesh, *Org. Biomol. Chem.* **2019**, *17*, 9390–9402.

[28] R. Sakly, H. Edziri, M. Askri, M. Knorr, C. Strohmann, M. Mastouri, *Comptes Rendus Chim.* **2018**, *21*, 41–53.

[29] S. Kumaran, R. Saritha, P. Gurumurthy, K. Parthasarathy, *Eur. J. Org. Chem.* **2020**, *2020*, 2725–2729.

[30] I. Coldham, R. Hufton, *Chem. Rev.* **2005**, *105*, 2765–2809.

[31] A. Boukaoud, Y. Chiba, D. Sebbar, M. Dehbaoui, N. Guechi, *Brazilian J. Phys.* **2021**, *51*, 1207–1214.

[32] M. M. Kaddah, A. R. I. Morsy, A. A. Fahmi, M. M. Kamel, M. M. Elsafty, S. A. Rizk, S. K. Ramadan, *Synth. Commun.* **2021**, *51*, 3366–3378.

[33] G. P. Riboldi, R. Zigweid, P. J. Myler, S. J. Mayclin, R. M. Couñago, B. L. Staker, *RSC Med. Chem.* **2021**, *12*, 103–109.

[34] I. Amine Khodja, H. Boulebd, *Mol. Divers.* **2021**, *25*, 279–290.

[35] D. J. Boruah, D. Kathirvelan, S. Borra, R. A. Maurya, P. Yuvaraj, *New J. Chem.* **2022**, *1*, 1–6.

[36] F. X. Domínguez-Villa, N. A. Durán-Iturbide, J. G. Ávila-Zárraga, *Bioorg. Chem.* **2021**, *106*, 104497–104501.

[37] J. A. Souza Silva, L. G. Tunes, R. S. Coimbra, D. B. Ascher, D. E. V. Pires, R. L. Monte-Neto, *Biomed. Pharmacother.* **2021**, *133*, 111049–111058.

4B.9. Selected IR, NMR (^{1}H and ^{13}C) and Mass spectra

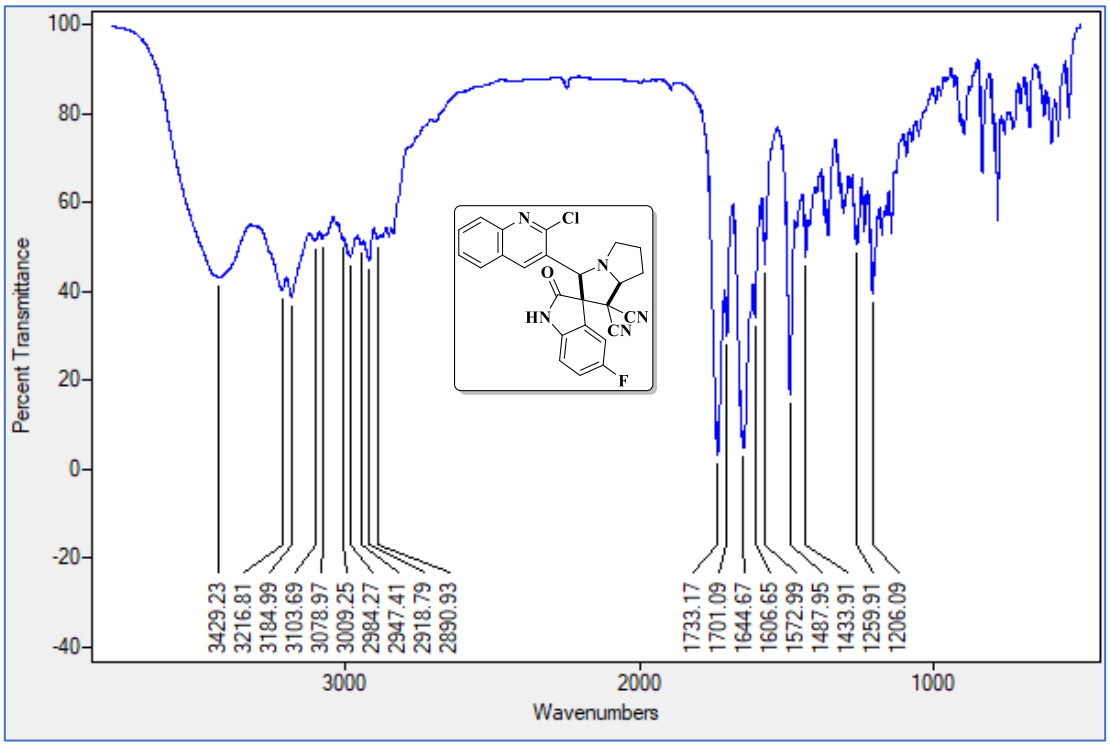

IR spectrum of the compound **4d**

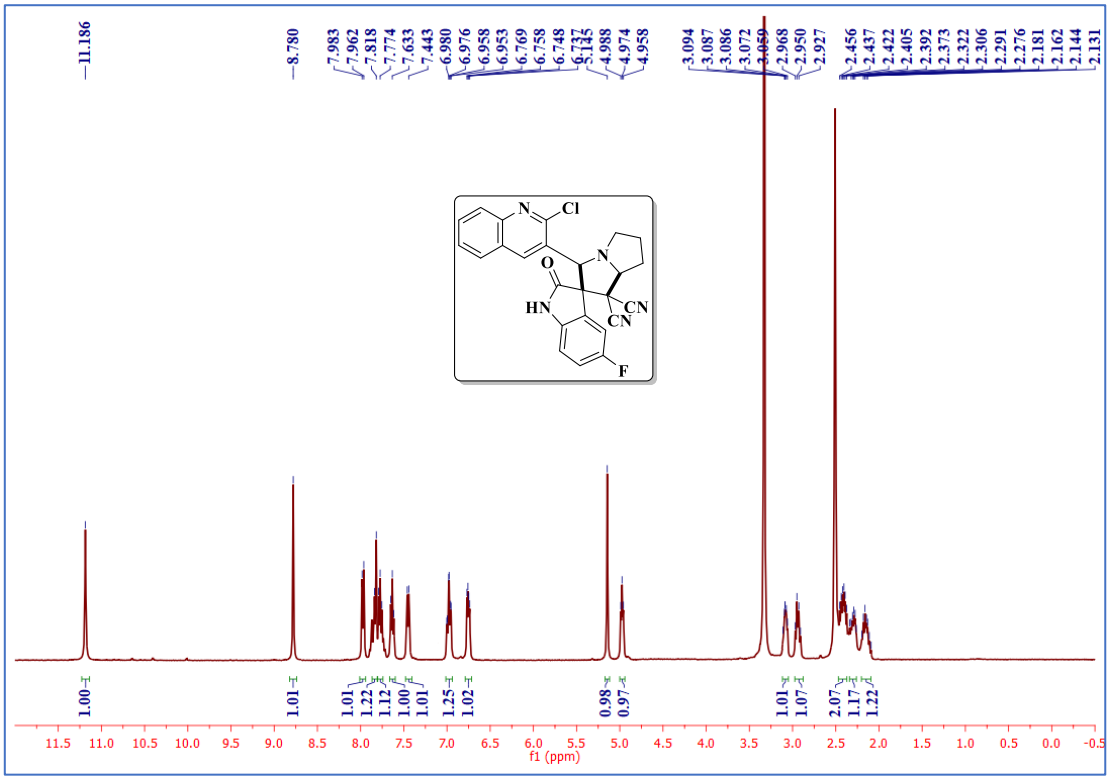

^{1}H NMR spectrum of the compound **4d**

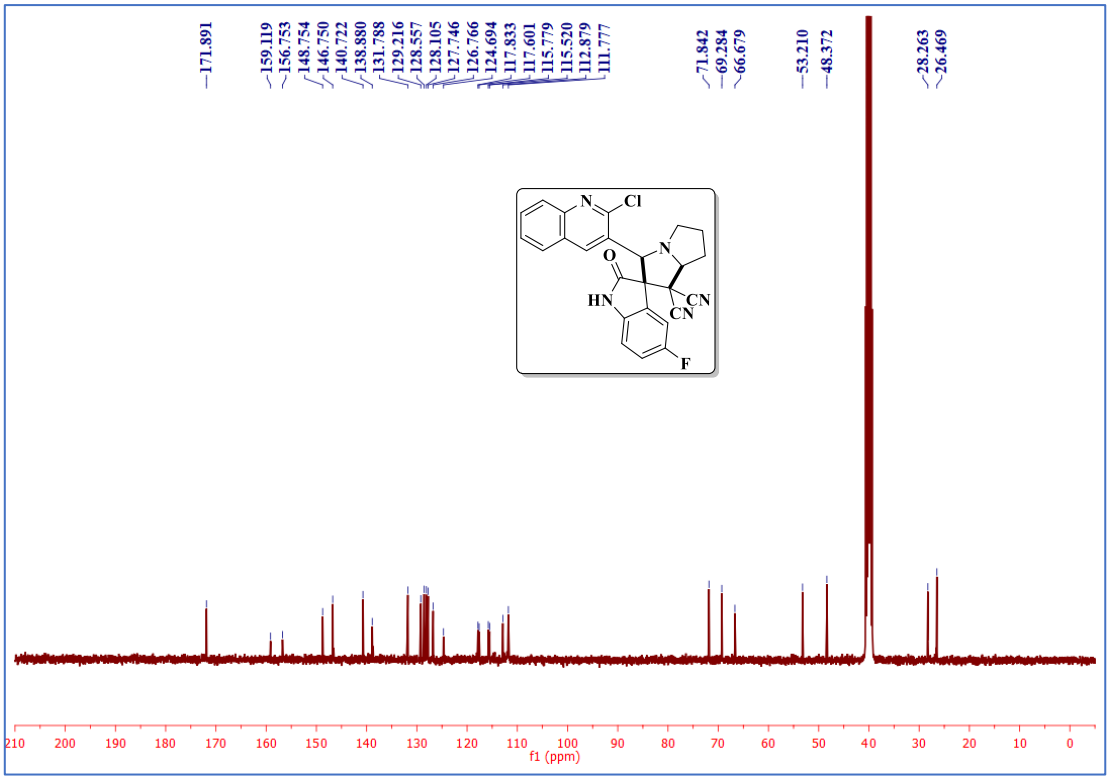

^{13}C NMR spectrum of the compound **4d**

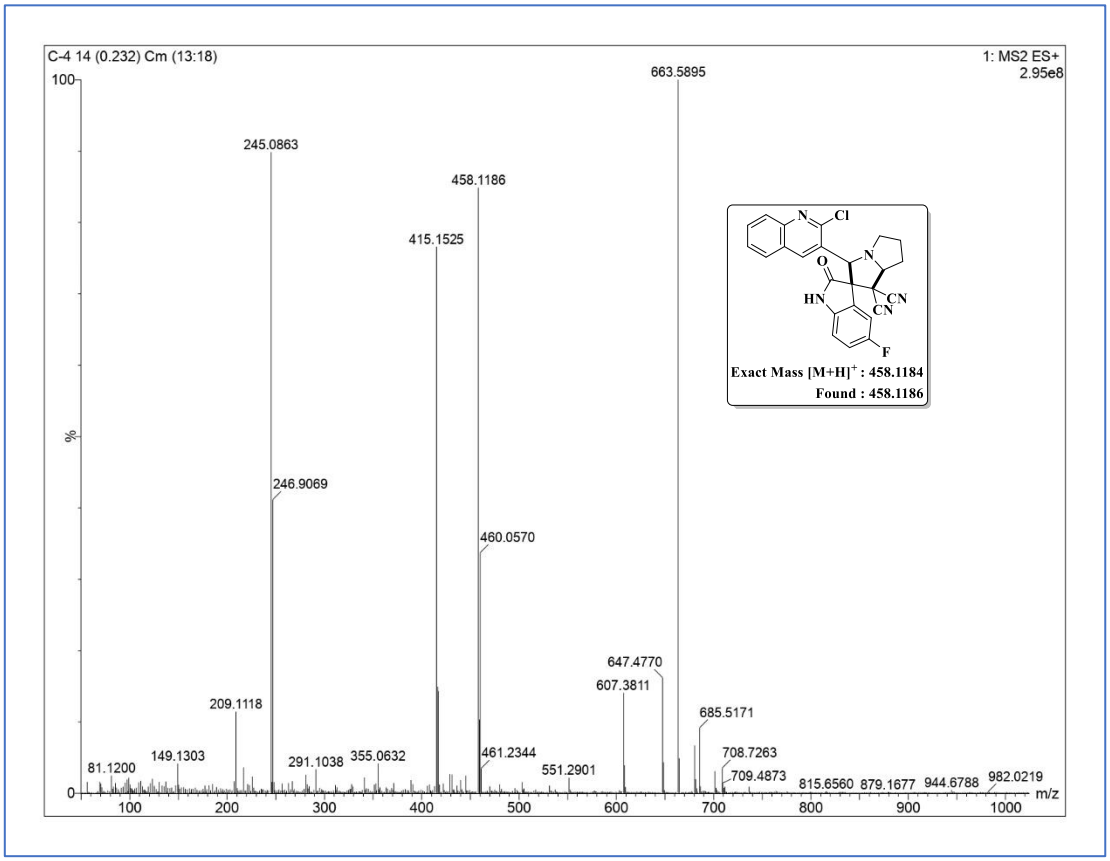

Mass spectrum of the compound **4d**

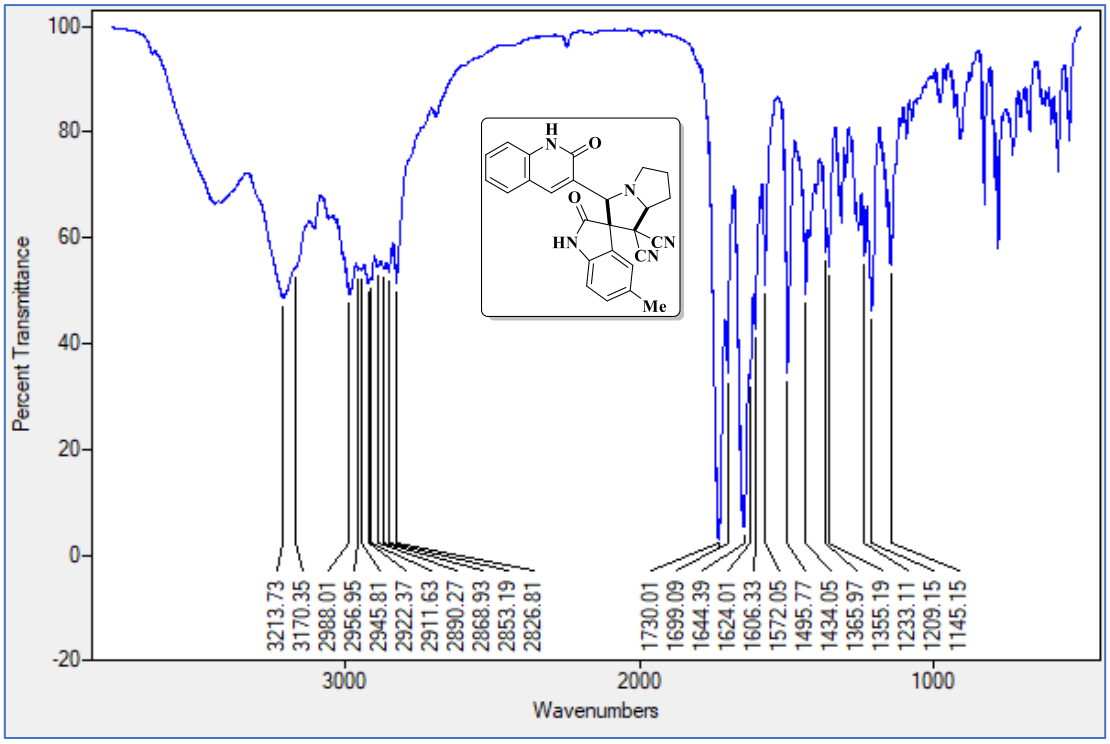

IR spectrum of the compound **4l**

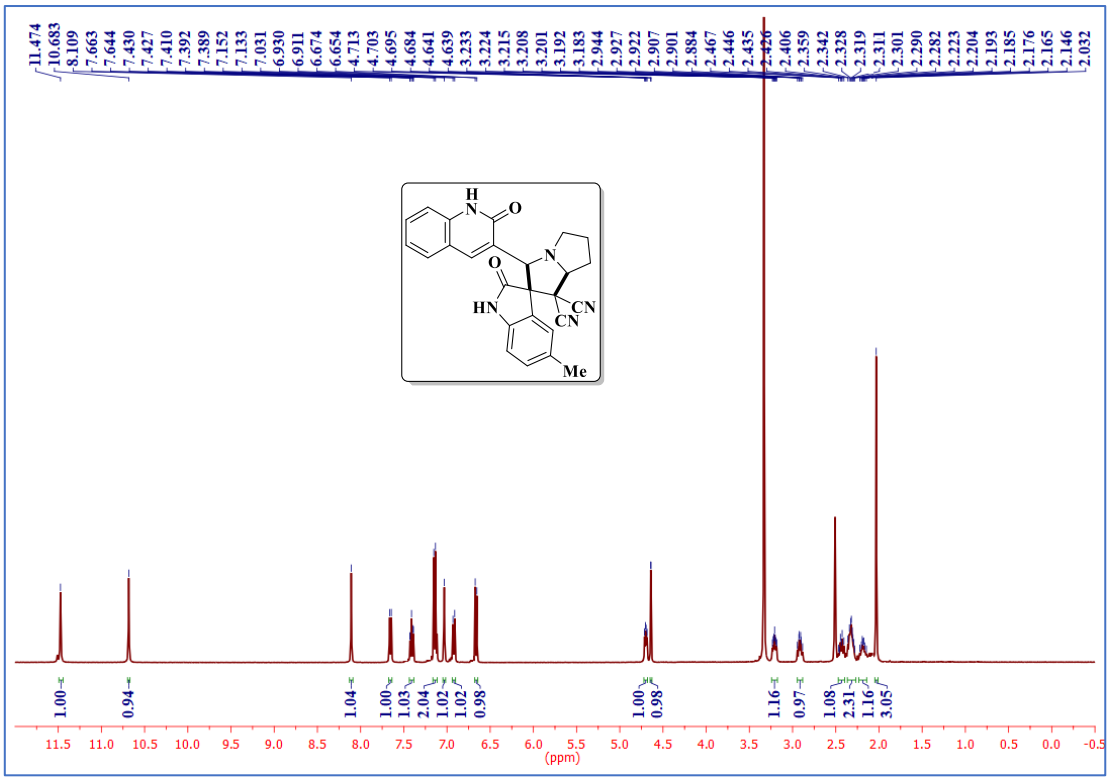

^{1}H NMR spectrum of the compound **4l**

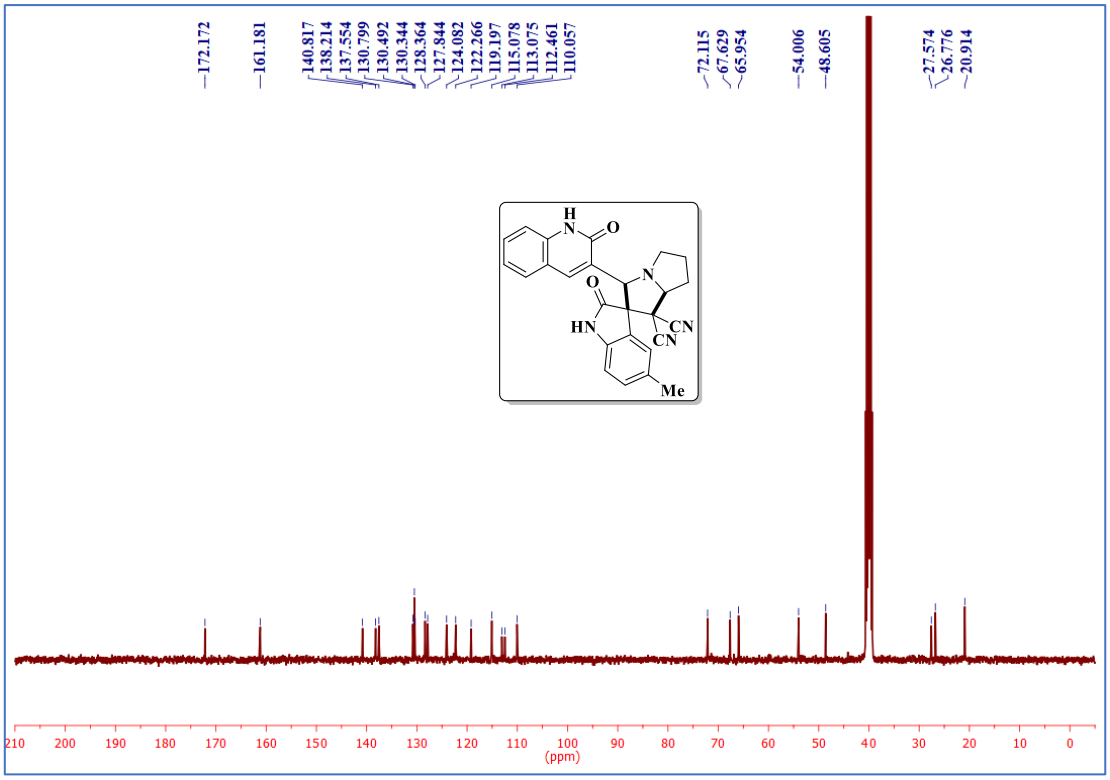

^{13}C NMR spectrum of the compound **4l**

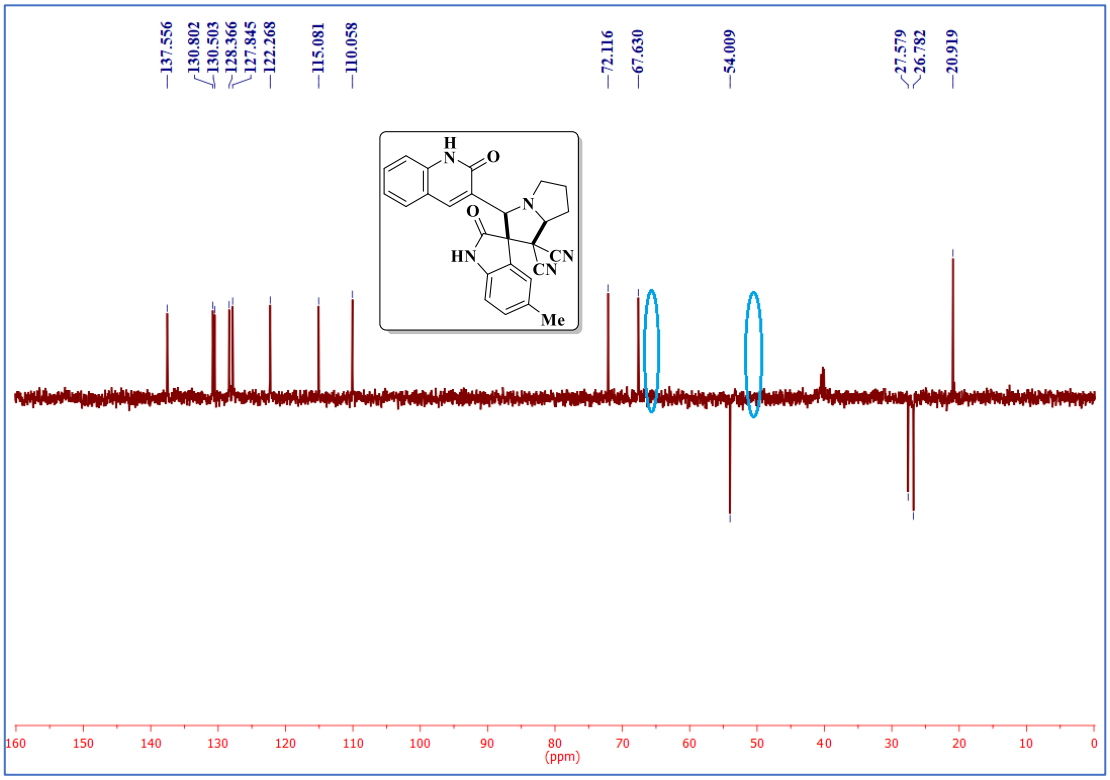

DEPT-135 NMR spectrum of the compound **4l**

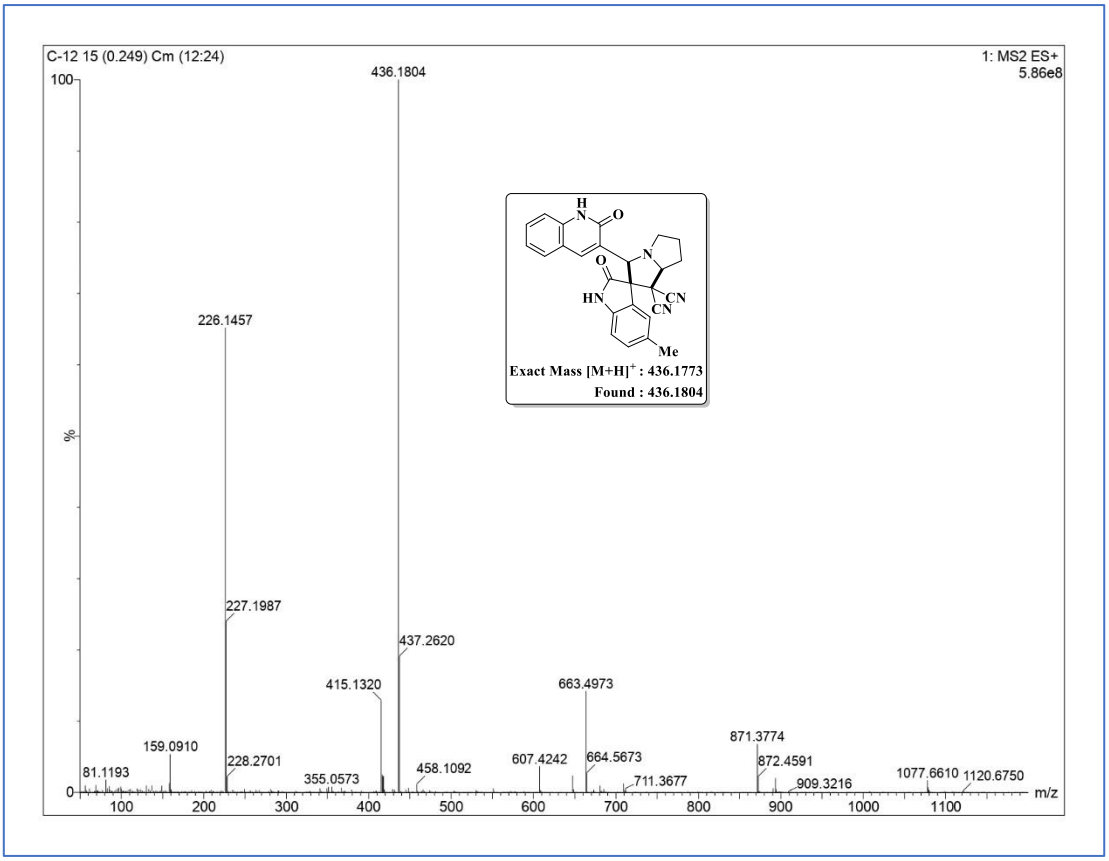

Mass spectrum of the compound **4l**

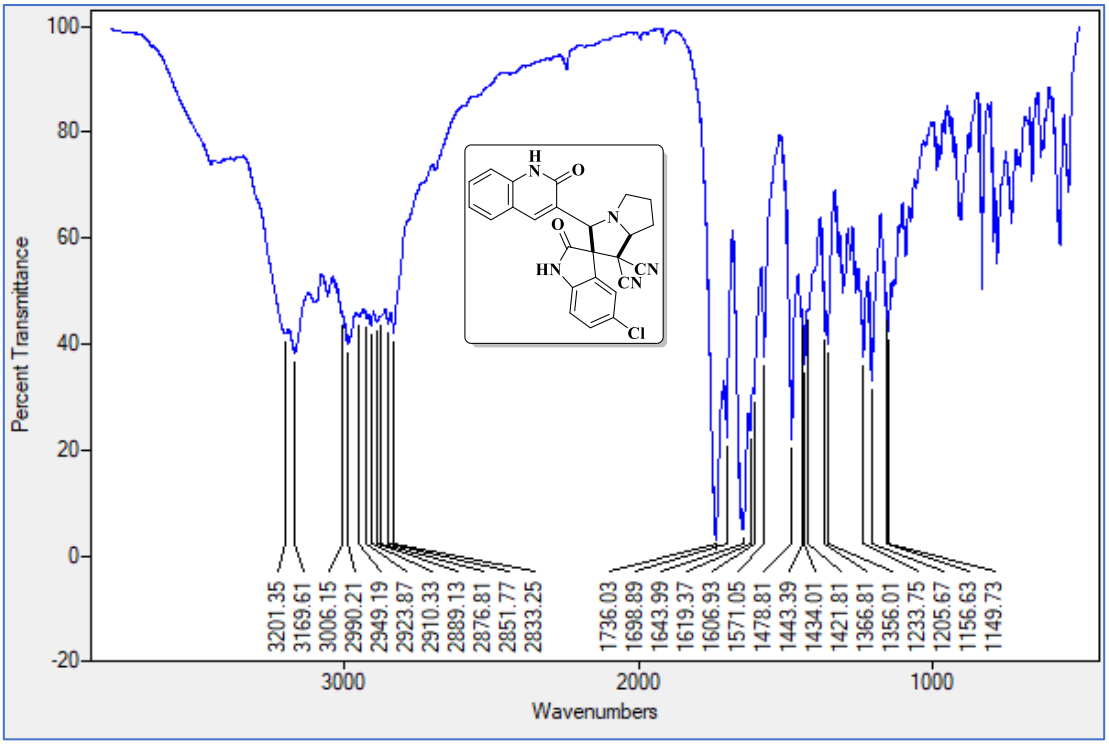

IR spectrum of the compound **4o**

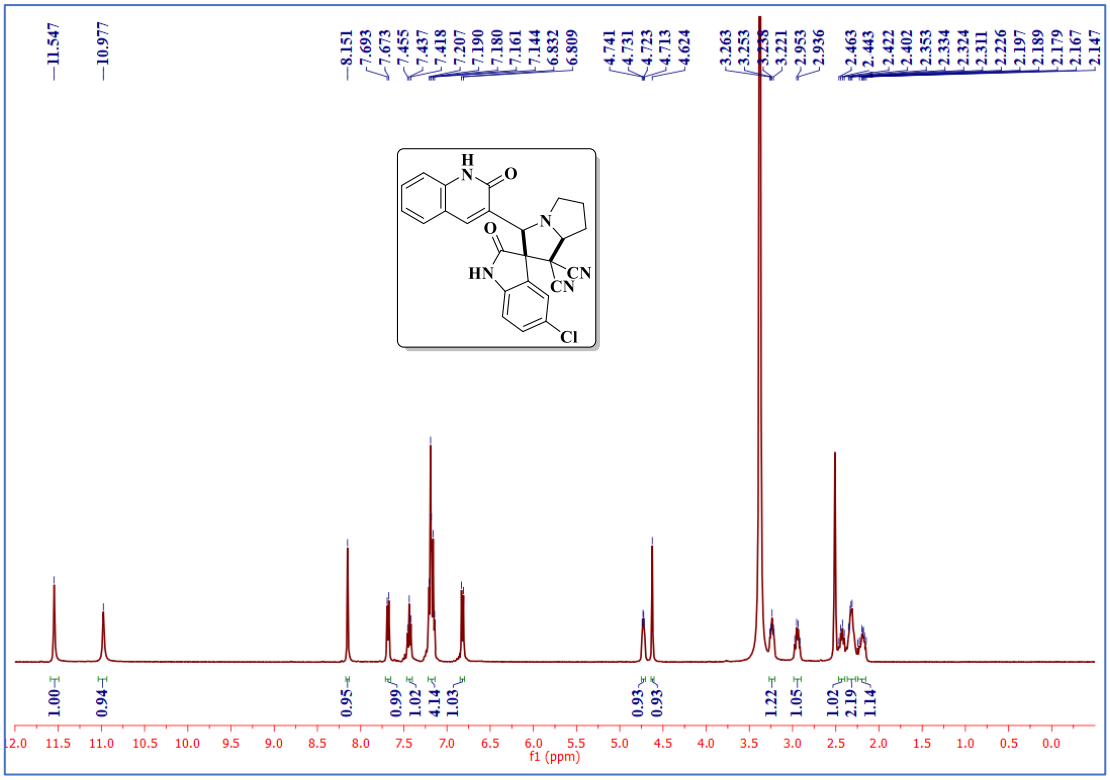

^{1}H NMR spectrum of the compound **4o**

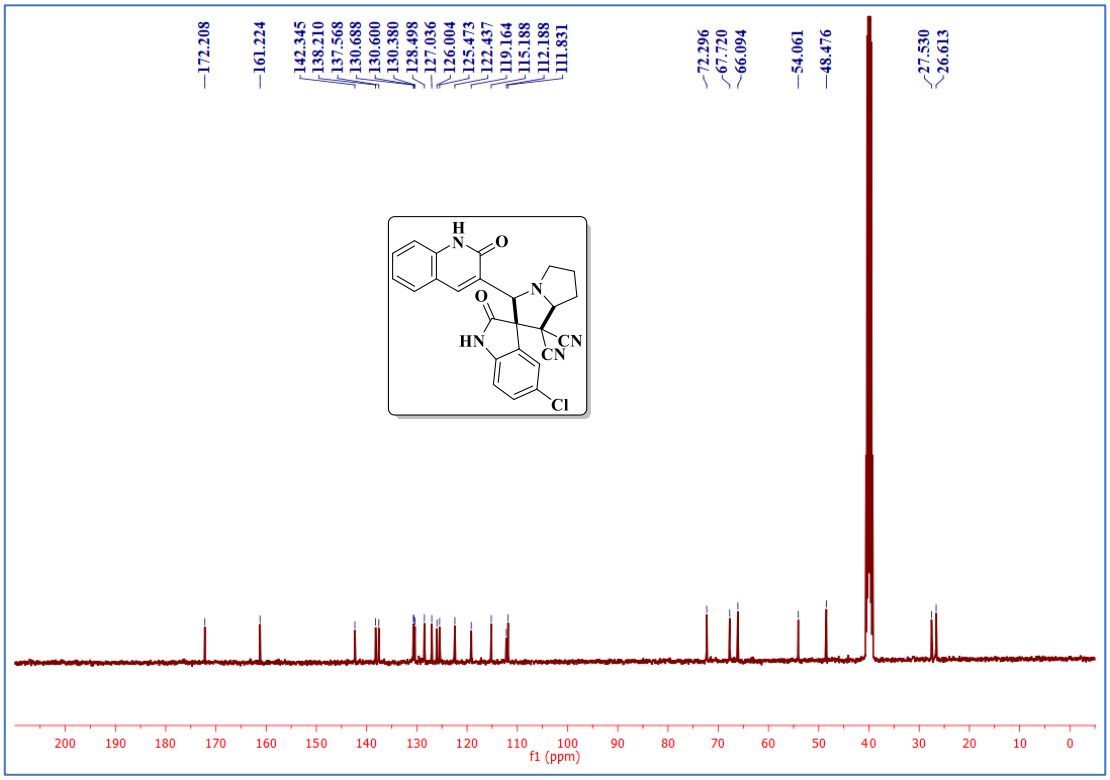

^{13}C NMR spectrum of the compound **4o**

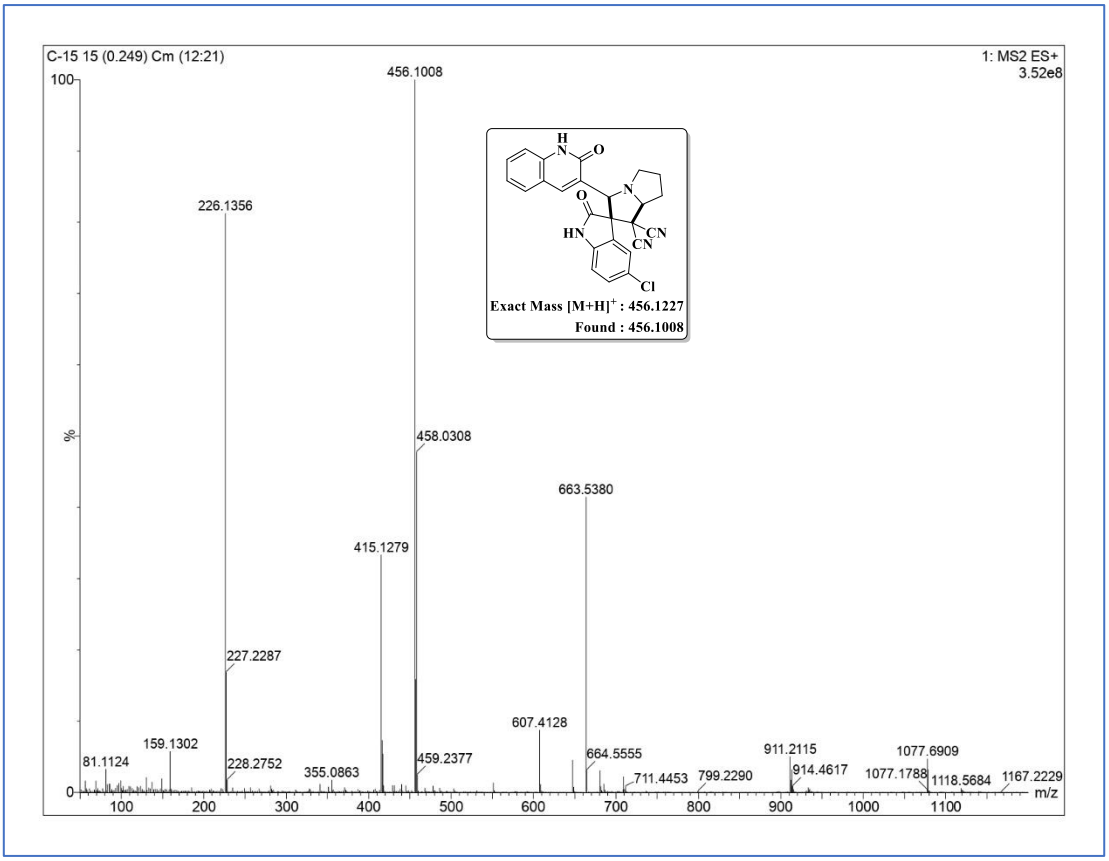

Mass spectrum of the compound **4o**

CHAPTER-V
Section-A

Quinazolinone based spirooxadiazole hybrids: Design, synthesis and anti-tubercular activity

5A.1. Introduction

1,2,4-oxadiazoles are important five membered heterocycles which are widely exist in natural products and used as drugs in various pharmaceuticals [1]. The number of published research articles and patents on 1,2,4-oxadiazoles keep rising, reflecting that the area is still growing [2]. The high percentage of patents demonstrate a wide range of essential applications of 1,2,4-oxadiazoles as pharmacophores from pharmaceuticals to materials research [3]. There are numerous examples in the literature of 1,2,4-oxadiazole having structures displaying anti-cancer [4], anti-bacterial [5], anti-inflammatory [6], anti-tubercular [7] and anti-oxidant activities [8].

Nowadays, there are few commercially available drugs having 1,2,4-oxadiazole moiety such as pleconaril is an anti-viral drug for the prevention of asthma exacerbations in patients exposed to picornavirus respiratory infections [9]. The drug proxazole is used as anti-biotic for the treatment of functional gastrointestinal disorders [10]. Whereas, oxolamine is an anti-inflammatory drug, which is also used as cough suppressant and is available as a generic drug in many juridictions [11]. On the other hand, ataluren, a small molecular drug sold under the brand name translarna, which is currently utilized as a medication for the treatment of duchenne muscular dystrophy (anti-inflammatory) [12]. The drug fasiplon is a nonbenzodiazepine anxiolytic drug from the imidazopyrimidine family of drugs [13] and the drug prenoxdiazine, marketed as libexin is used as anti-tussive [14].

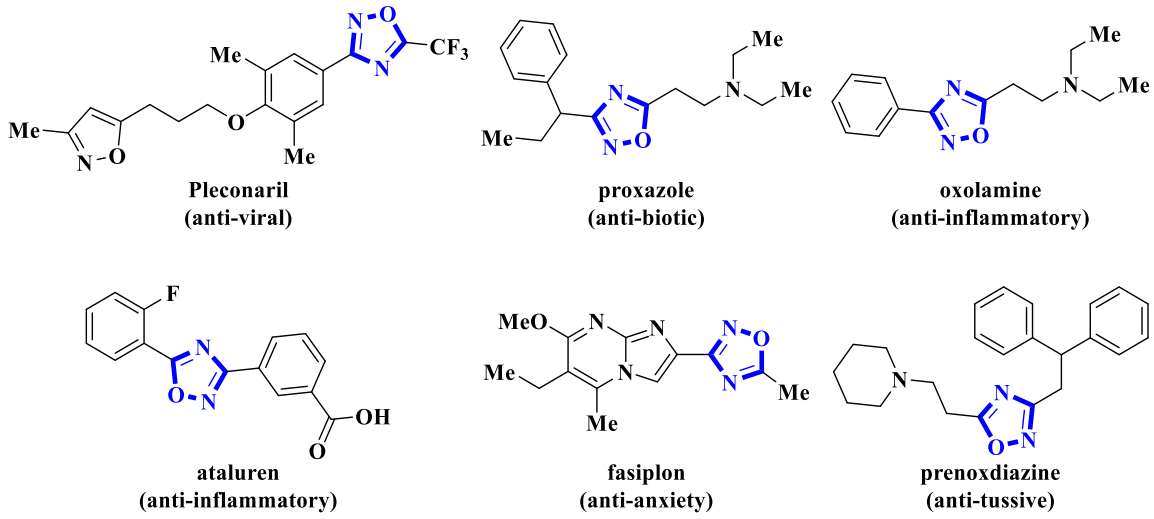

Figure 5A.1. Biologically potent drugs having 1,2,4-oxadiazole moiety.

In addition to their therapeutic significance, they have also drawn considerable attention in material science due to their thermal, electrical and optical properties [15].

1,2,4-oxadiazoles are employed as building blocks for organic solar cells and light emitting diodes [16]. These moieties can also be utilized as high energy density materials [17].

On the other hand, quinazolinone and its derivatives attain a great deal of interest from synthetic as well as medicinal chemists due to their pharmacological properties [18]. They have shown broad spectrum of biological activities like anti-cancer, anti-bacterial, anti-microbial and anti-diabetic etc [19].

5A.1.1. Reported methods for the preparation of 1,2,4-oxadiazoles

Loboda et al. designed and synthesized a new class of 3,5-disubstituted 1,2,4-oxadiazoles as catalytic inhibitors of human topo IIα (Figure 5A.2). Inhibitor binding geometries in molecular dynamic simulations were evaluated for a deeper insight into molecular recognition with its macromolecular target. They have also tested for *in vitro* cytotoxicity of the selected compounds on MCF-7 cancer cell line [20].

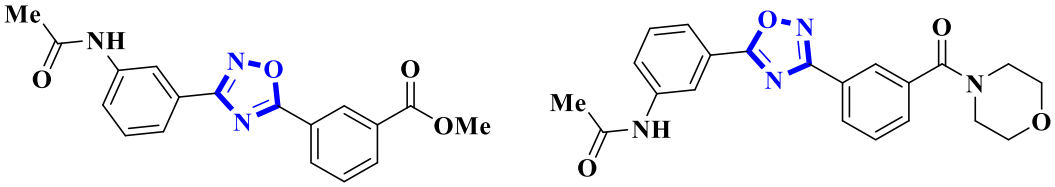

Figure 5A.2

Li and co-workers reported 1,2,4-oxadiazole derivatives as novel GSK-3β inhibitors and evaluated their potential as multifunctional anti-alzheimer agents (Figure 5A.3). The synthesized compounds were also assessed their bidirectional transport studies for blood-brain barrier permeability. Further, *in vivo* experiments revealed that a compound improved cognitive impairment in scopolamine-induced mouse models [21].

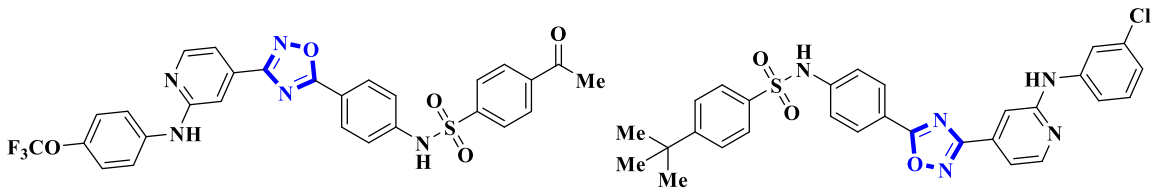

Figure 5A.3

Potenza et al. developed structure based screening for the detection of 1,2,4-oxadiazoles as promising leads for the development of new anti-inflammatory agents through eicosanoid biosynthetic pathways (Figure 5A.4). Moreover, *in vivo* results of the synthesized compounds demonstrated that the compounds were able to attenuate leukocyte migration [22].

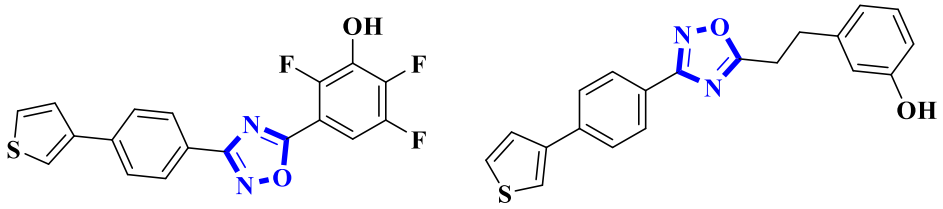

Figure 5A.4

Oliveira et al. produced alkylated 1,2,4-oxadiazole glycoconjugates for the usage in chemotherapy against lung carcinoma and mycobacterium tuberculosis (Figure 5A.5). Further, *in vitro* cytotoxicity was screened against RAW 264.7 and HepG2 cells and the most promising anti-tubercular compounds showed better selective index. In addition, *in silico* molecular docking studies were evaluated to understand possible interactions and their stability within the binding pocket of the proteins [23].

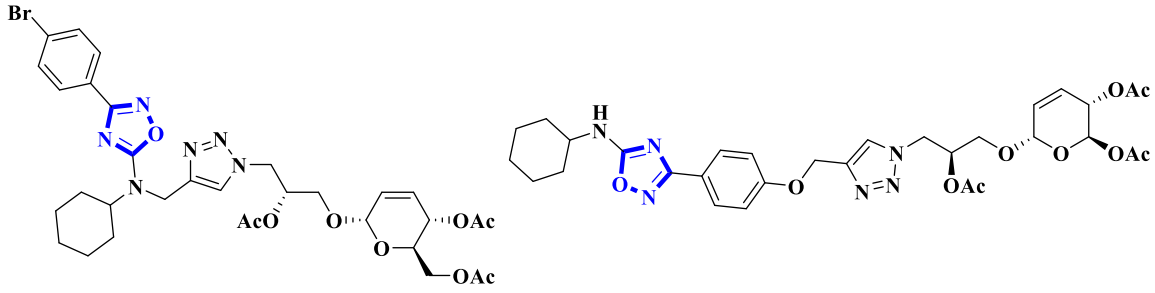

Figure 5A.5

Mohamed and co-workers demonstrated novel 3-aryl-1,2,4-oxadiazoles derived from indomethacin as potent anti-inflammatory agents (Figure 5A.6). Moreover, *in vivo* anti-inflammatory studies of synthesized compounds were evaluated. Molecular docking and ADME analysis were revealed that the compounds have reasonable drug-likeness with acceptable physicochemical properties [24].

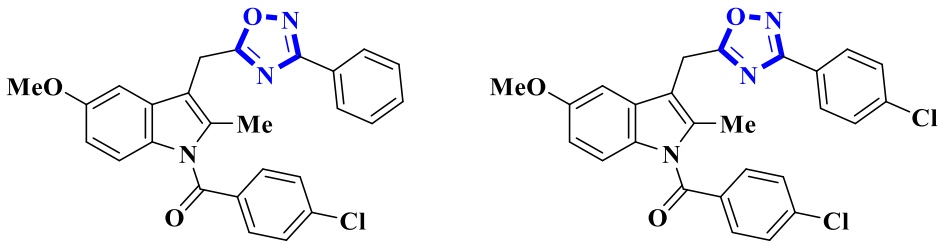

Figure 5A.6

Golushko et al. reported a tandem reaction of nitroalkenes with arenes and nitriles in the presence of superacid TfOH for the production of 1,2,4-oxadiazoles (Scheme 5A.1). The reaction occurs through a consequent interaction of arenes and nitriles, as nucleophiles with intermediate cationic species generated by the protonation of nitroalkenes in TfOH [25].

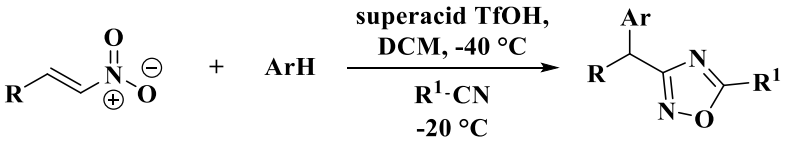

Scheme 5A.1

Bian et al. employed a direct strategy for the selective synthesis of 3-acyl-1,2,4-oxadiazoles from alkynes and nitriles under iron nitrate mediated conditions (Scheme 5A.2). In this reaction iron nitrate plays a dual role in the nitration of alkynes and in the activation of nitriles [26].

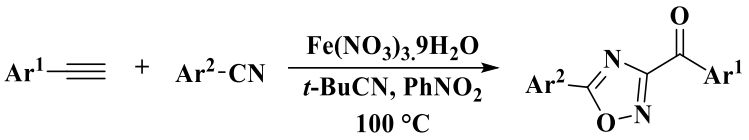

Scheme 5A.2

Tron and co-workers developed a one pot route for the synthesis of 5-amino-1,2,4-oxadiazoles using multicomponent reaction of chlorooximes, isocyanides and hydroxylamines *via* [3+1] cycloaddition reaction (Scheme 5A.3) [27].

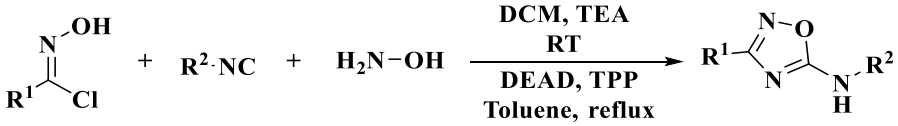

Scheme 5A.3

Liu and co-workers described the copper catalyzed three component synthetic strategy for substituted 1,2,4-oxadiazole derivatives from readily available benzaldehyde, hydroxylamine and benzylamine (Scheme 5A.4). The construction of 1,2,4-oxadiazole possess [2+2+1] annulation *via* copper catalyzed dehydrogenative cyclization reaction [28].

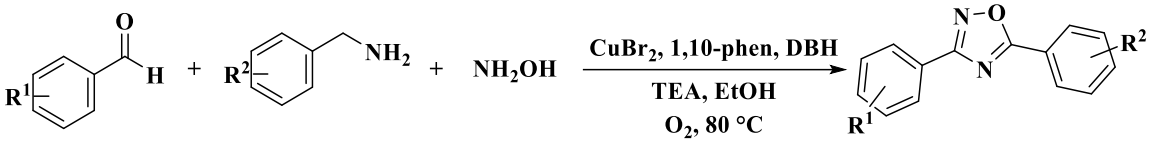

Scheme 5A.4

Wang and co-workers demonstrated a convenient and efficient approach for the synthesis of 5-amino-1,2,4-oxadiazoles through palladium catalyzed cyclization of isocyanides and amidoximes (Scheme 5A.5). The reaction proceeds *via* C–N and C–C bond formations under mild reaction conditions [29].

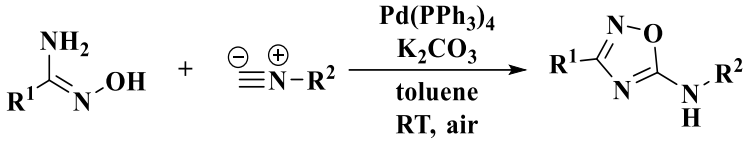

Scheme 5A.5

Zhang et al. employed an efficient domino protocol for the synthesis of 1,2,4-oxadiazoles using 1-(2-oxo-2-arylethyl)pyridin-1-iums and benzamidines as precursors (Scheme 5A.6). This protocol exhibited excellent functional group tolerance and proceeded under mild reaction conditions [30].

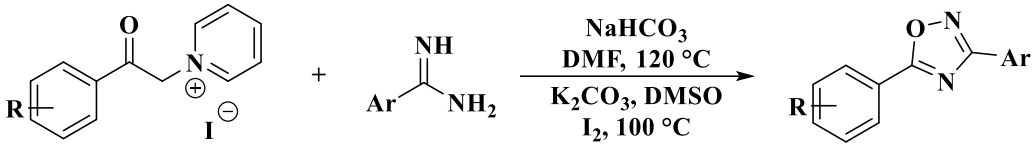

Scheme 5A.6

5A.2. Present work and design strategy

Lu et al. described quinazolinones (Figure 5A.7. compound **A**) as novel anti-tuberculosis agents [31]. **Chakraborti and co-workers** reported quinazolinone derivatives (Figure 5A.7. compound **B**) as anti-tubercular agents [32]. **Borsoi et al.** reported the therapeutic potential of quinoline and its derivatives (Figure 5A.7. compound **C**) as anti-tuberculosis agents [33]. **Patel et al.** described quinolines (Figure 5A.7. compound **D**) as anti-tuberculosis agents [34]. **Subramanian and co-workers** reported anti-tuberculosis studies of new quinoline derivatives carrying 1,2,4-oxadiazole moiety (Figure 5A.7. compound **E**) [35]. **Kumar et al.** disclosed anti-tubercular activity of novel 1,2,4-oxadiazole hybrids (Figure 5A.7. compound **F**) [36].

Encouraged by the above findings and considering the importance of 1,2,4-oxadiazole moiety, we have designed and synthesized a new spiro heterocyclic system possessing quinazolinone-quinoline core connected by biologically prominent 1,2,4-oxadiazole moiety.

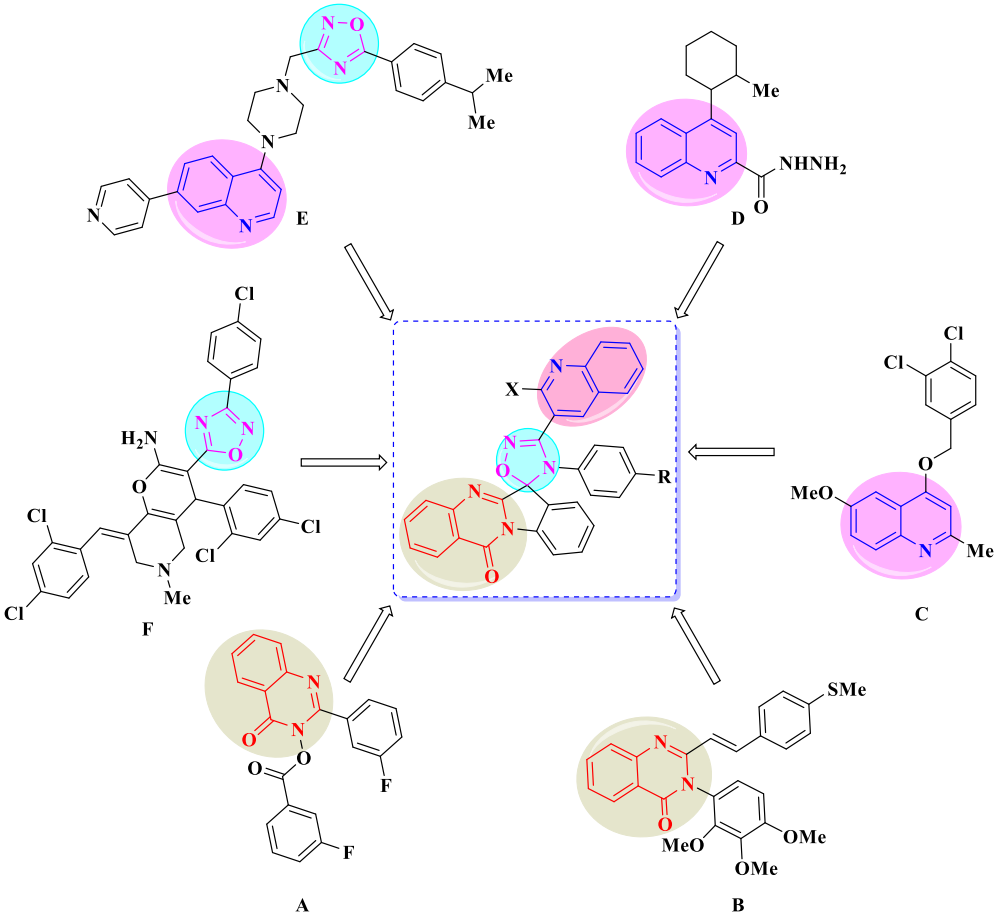

Figure 5A.7. Design strategy of quinolinyl spiroquinazolinoneoxadiazoles for anti-tubercular activity.

5A.2.1. Synthesis of quinazolinyl Schiff's base 1

Aniline **B′** (1.0 mmol) was added to a stirred solution of indolo[2,1-*b*]quinazoline-6,12-dione **A′** (1.0 mmol) in methanol (3 mL) at room temperature. To this $BF_3.Et_2O$ (20 mol%) was added and the mixture was stirred under reflux (Scheme 5A.7) until complete consumption of starting materials (judged by TLC). Reaction mixture was then brought to room temperature, the precipitated product was filtered and further it was purified by recrystallization from methanol [37].

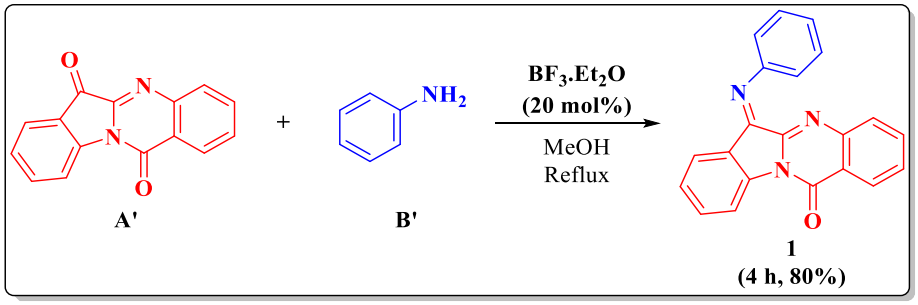

Scheme 5A.7

The target spiroquinazolinoneoxadiazoles **3a-o** were synthesized by taking quinazolinyl Schiff's bases **1a-h** and *N*-hydroxycarbimidoyl chlorides **2a-b** in DCM having Et_3N as base at room temperature (Scheme 5A.8). The structures of all the synthesized compounds were well characterized by spectral data and were tested for *in vitro* anti-tubercular activity.

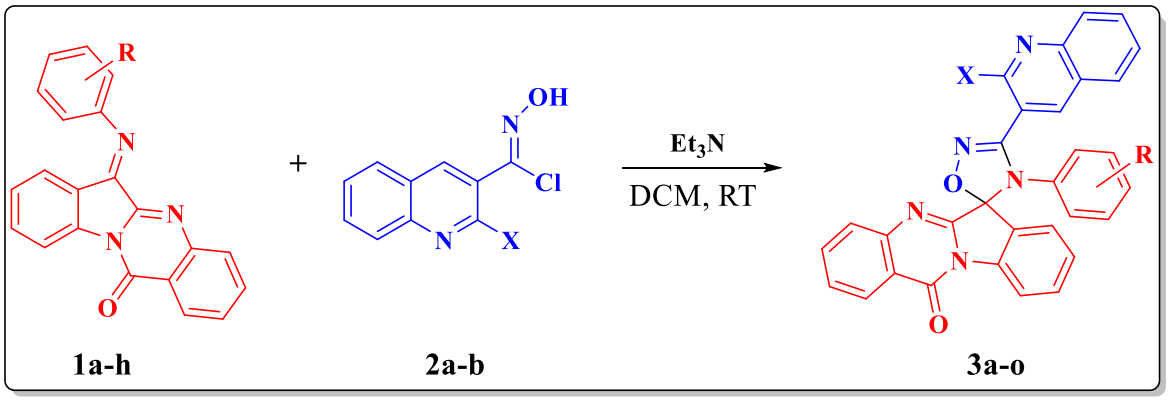

Scheme 5A.8. Synthesis of quinolinyl spiroquinazolinoneoxadiazoles **3a-o**.

5A.2.2. Results and discussion

6-(phenylimino)indolo[2,1-*b*]quinazolin-12(6*H*)-one **1a** and *N*-hydroxy-carbimidoyl chloride **2a** were considered to optimize the reaction parameters (Table 5A.1). Initially, an attempt was carried in dichloromethane (DCM) at room temperature, trace amount of the desired product **3a** was obtained (Table 5A.1, entry 1). Then the reaction was conducted in presence of Et_3N in DCM at room temperature for 4 h. To our delight, the desired product **3a** was obtained in 85% yield (Table 5A.1, entry 2). Further, a series of solvents including Et_2O, H_2O, MeOH and THF were screened (Table 5A.1, entries 3-6), and the results showed that DCM as best solvent to achieve target compound **3a**. In order to find the efficiency, various bases such as DMAP, DABCO, DBU and K_2CO_3 were examined (Table 5A.1, entries 7-10) and it was found that Et_3N as an efficient base for the generation of target compound **3a**. Further, varying the base equivalents as 1.5 and 2.5 led to the negative influence on the product yield (Table 5A.1, entries 11,12). Therefore, it can be concluded that 1.0 mmol of **1a**, 1.1 mmol of **2a** and 2.0 equiv of Et_3N in DCM at room temperature (Table 5A.1, entry 2) is the optimal reaction condition for the generation of target compounds.

Table 5A.1. Optimization of the reaction conditions[a]

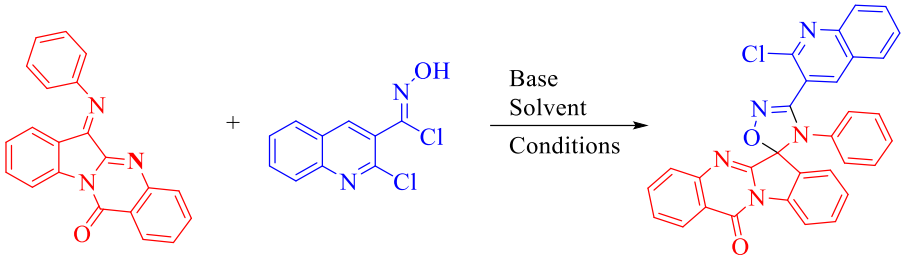

1a **2a** **3a**

Entry	Solvent	Base	Time (h)	Yield (%)[b]
1	DCM	--	12	trace
2	**DCM**	**Et_3N**	**4**	**85**
3	Et_2O	Et_3N	10	55
4	H_2O	Et_3N	12	25
5	MeOH	Et_3N	8	60
6	THF	Et_3N	8	70
7	DCM	DMAP	6	75
8	DCM	DABCO	6	80
9	DCM	DBU	6	70
10	DCM	K_2CO_3	6	60
11[c]	DCM	Et_3N	4	75
12[d]	DCM	Et_3N	6	80

[a]Reaction condition: compound **1a** (1.0 mmol), *N*-hydroxycarbimidoyl chloride **2a** (1.1 mmol), base (2.0 equiv) and solvent (3 mL) at room temperature. [b]Isolated yields. [c]1.5 equiv of base. [d]2.5 equiv of base.

The optimized reaction condition was used to explore the substrate scope by taking various substituted quinazolinone Schiff's bases **1a-h** and *N*-hydroxycarbimidoyl chlorides **2a-b** (Table 5A.2). Quinazolinone Schiff's bases having electron donating (–Me, –OMe) and halo substituted (–F, Cl, Br) groups have no substantial impact on the efficiency of the reaction. It was also found that the positions of the substituents on quinazolinone Schiff's bases had no significant effect on reaction efficiency.

Table 5A.2. Synthesis of quinolinyl spiroquinazolinoneoxadiazoles **3a-o**[a,b]

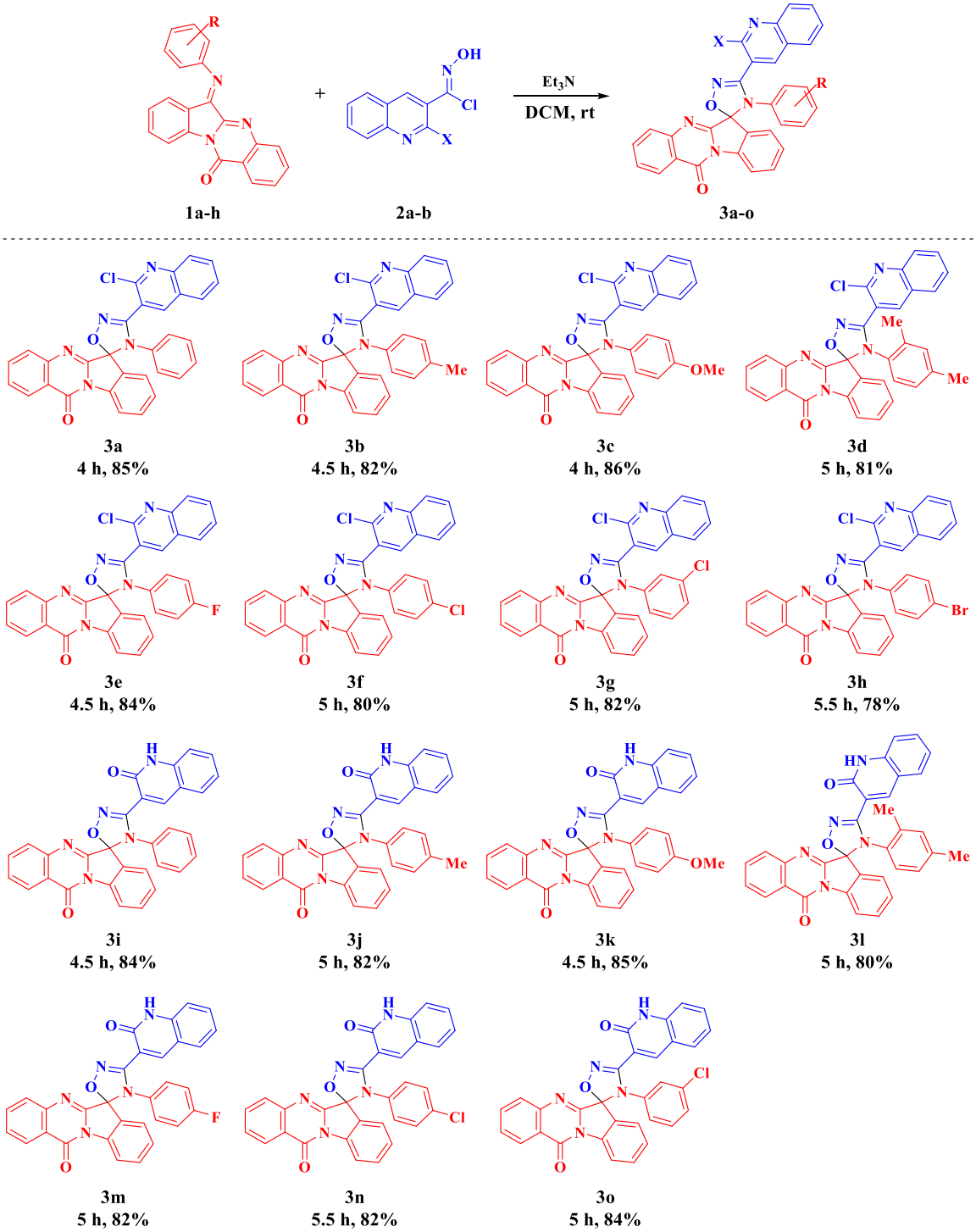

[a]Reaction condition: compounds **1a-h** (1.0 mmol), *N*-hydroxycarbimidoyl chlorides **2a-b** (1.1 mmol) and Et_3N (2.0 equiv) in 3 mL of DCM at room temperature. [b]Isolated yields.

A plausible reaction mechanism for the generation of target compounds **3** was depicted in Scheme 5A.9. Initially *N*-hydroxycarbimidoyl chloride **2a** reacted with Et_3N to generate *N*-oxide. This *in situ* generated *N*-oxide undergoes 1,3-dipolar cycloaddition reaction with quinazolinone Schiff's base **1a** produces the target compound **3a** [38].

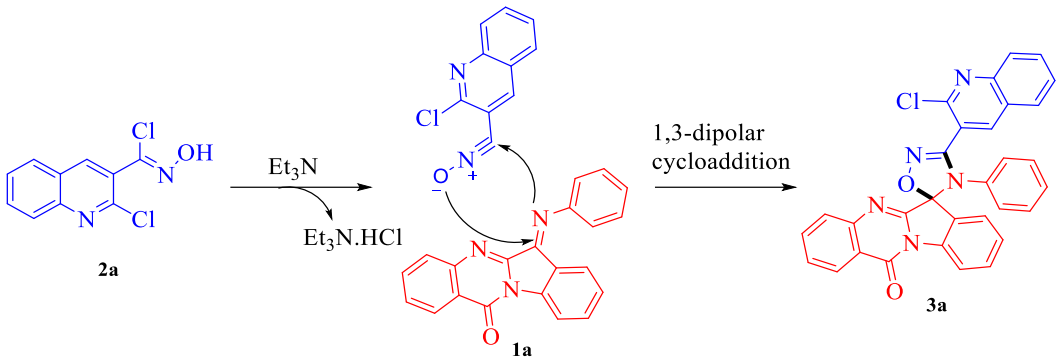

Scheme 5A.9. Plausible reaction pathway for the generation of target compounds **3a-o**.

The structures of target compounds **3a-o** were elucidated by IR, ^{1}H, ^{13}C NMR and mass spectral methods. Further, the structures were authenticated by single crystal X-ray diffraction of **3a** (Figure 5A.8). The IR spectrum of the compound **3a** showed a peak at 1697 cm^{-1} corresponds to amide carbonyl of quinazolinone moiety. In the ^{1}H NMR spectrum, a singlet at δ 8.71 *ppm* corresponds to the –CH proton of quinoline ring which is adjacent to the oxadiazole moiety. A peak at δ 101.63 *ppm* in the ^{13}C NMR represents the spiro carbon, which was further confirmed by the absence of this spiro carbon peak in DEPT-135 NMR spectrum of **3a**. In the mass spectrum, the molecular ion peak at *m/z* 528.0686 $[M+H]^{+}$ determines the molecular weight of the compound **3a**. Further, X-ray analysis data of compound **3a** (*CCDC*:2108237) demonstrates the regiochemistry of the generated compounds and the structure refinement parameters of the compound **3a** were represented in Table 5A.3.

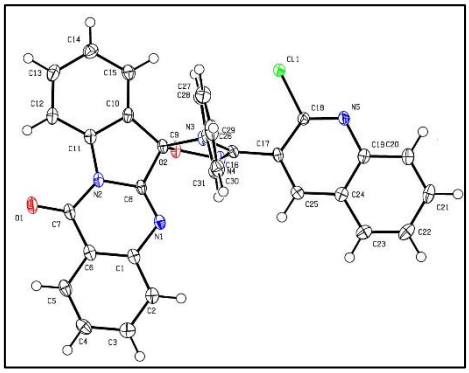

Figure 5A.8. ORTEP representation of the compound **3a** and the thermal ellipsoids were drawn at 50% probability level.

Table 5A.3. Salient features and crystallographic information of **3a**

Identification code	**3a**
Empirical formula	$C_{31}H_{18}ClN_5O_2$
Formula weight	527.1149

Crystal system	Monoclinic
Space group	$P2_1/c$
T (K)	293 K
a (Å)	12.0315 (14)
b (Å)	11.8354 (12)
c (Å)	17.3663 (19)
α (°)	90
β (°)	100.098 (5)
γ (°)	90
Z	4
V (Å^3)	2434.6 (5)
D_{calc} (g/cm^3)	1.440
F (000)	1088.0
μ (mm^{-1})	0.199
Θ (°)	26.368
Index ranges	$-15 \leq h \leq 15$ $-14 \leq k \leq 14$ $-21 \leq k \leq 21$
N-total	4967
Parameters	4728
R_1 $[I > 2\ \sigma\ (I)]$	0.0331
wR_2 (all data)	0.0805
GOF	1.052
CCDC	2108237

5A.2.3. Biological activity

5A.2.3.1. Anti-tubercular activity (anti-TB)

The *in vitro* anti-tubercular screening of the target compounds **3a-o** were evaluated against *Mycobacterium tuberculosis* (Mtb) H37Rv (ATCC27294) by the microplate alamar blue assay (MABA) method [39]. The minimum inhibitory concentration (MIC) values of **3a-o** along with standard drugs (Isoniazid, Rifampicin and Ethambutol) are provided in Table 5A.4. In comparison to the first line anti-TB drugs, compounds **3a-o** exhibited potent to moderate activity against Mtb with MIC values ranging from 0.78 μg/mL to 25 μg/mL. Among them, seven compounds exhibit potent activity with MIC values less than or equal that of the standard drug, ethambutol (MIC = 1.56 μg/mL). Compounds **3b**, **3e**, **3f**, **3h** and **3l** exhibit higher potency (MIC = 0.78 μg/mL) than the standard drug ethambutol. The compounds **3j** and **3o** display significant activity (MIC = 1.56 μg/mL). Whereas, the compounds **3i**, **3k** and **3m** show good activity with MIC value 3.125 μg/mL. While the remaining compounds exhibit moderate to poor activity.

Table 5A.4. *In vitro* anti-tubercular activity of the target compounds **3a-o**

Entry	Compound	MIC (µg/mL)	% of Inhibition @25 µM[a]
1	**3a**	25	ND[b]
2	**3b**	**0.78**	**25.69**
3	**3c**	12.5	ND
4	**3d**	12.5	ND
5	**3e**	**0.78**	**22.71**
6	**3f**	**0.78**	**23.86**
7	**3g**	25	ND
8	**3h**	**0.78**	**27.72**
9	**3i**	3.125	19.91
10	**3j**	**1.56**	**20.94**
11	**3k**	3.125	21.87
12	**3l**	**0.78**	**23.88**
13	**3m**	3.125	19.04
14	**3n**	12.5	ND
15	**3o**	**1.56**	**24.16**
16	Isoniazid	0.05	ND
17	Rifampicin	0.1	ND
18	Ethambutol	1.56	ND

[a]% inhibition was examined using RAW 264.7 cell line, [b]ND = not determined.

5A.2.3.2. Cytotoxicity studies

The active analogues (**3b**, **3e**, **3f**, **3h**, **3i**, **3j**, **3k**, **3l**, **3m** and **3o**) were also evaluated for their *in vitro* cytotoxicity effect against RAW 264.7 cells at 25µM concentration using MTT assay [40]. The percentage of inhibition data is summarized in Table 5A.4. From this data, it has been concluded that the most potent analogues were less toxic to RAW 264.7 cells and are suitable for further mechanistic studies (Figure 5A.9).

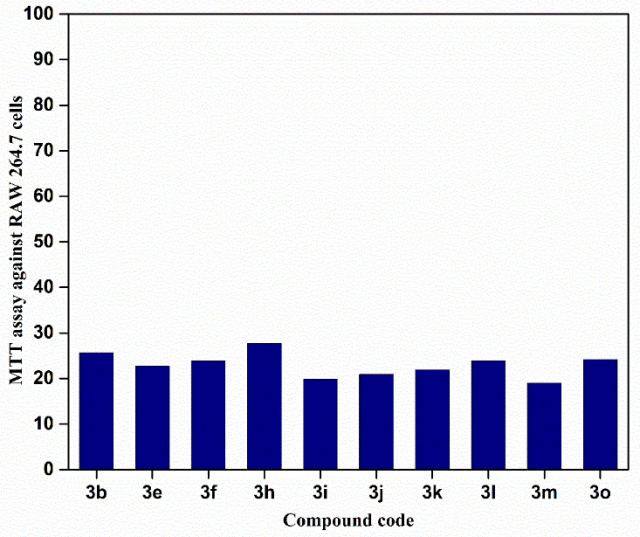

Figure 5A.9. % inhibition of potent anti-tubercular compounds on RAW 264.7 cell line at 25 µM concentration.

5A.2.3.3. Structure activity relationship studies

In the structure activity relationship (SAR) studies, diverse donor and acceptor abilities of substituted groups on the phenyl ring and structural changes are crucial in their anti-tubercular activity of the title compounds. SAR studies reveal that the presence of halogens on the phenyl ring significantly enhances anti-tubercular activity. Whereas, the compounds having methyl group on phenyl ring exhibit potent activity than other electron releasing groups (–OMe). However, the –Cl substitution on the quinoline moiety at 2-position shows potent activity than oxygen (2-oxo) derivatives.

5A.3. Molecular docking studies

The molecular docking studies were carried out against *Mycobacterium tuberculosis* protein (PDB ID: 1DF7) [41]. In the protein 1DF7, the best active molecules **3b**, **3e**, **3f**, **3g**, **3h**, **3j**, **3k**, **3m**, **3n** and **3o** forming the π···π stacking interactions with GLN28 (compound **3o** with ALA7), and –C=O oxygen of quinazolinone ring forms hydrogen bonding interactions with TYR100 having dock scores -12.53, -11.94, -12.73, -11.93, -12.92, -12.13, -11.86, -11.52, -12.33 and -11.87 respectively. From the docking scores, all the synthesized compounds have a good affinity towards anti-tubercular activity. The compound **3f** showed binding energy -12.73 kcal/mol, forms three H-bonds with the amino acid residues GLN28 (2.76 Å), PRO51 (3.07 Å) and TYR100 (2.13 Å) and exhibited four hydrophobic interactions (π···alkyl) with the amino acids ILE20 (4.73 Å), LEU24 (5.24 Å), LEU50 (4.81 Å) and PRO51 (5.01 Å) respectively. Whereas, the compound **3h** exhibited more negative binding energy -12.92 kcal/mol, forms three hydrogen bonds with the amino acid residues GLN28 (2.76 Å), PRO51 (3.05 Å) and TYR100 (2.14 Å). Also, it forms four hydrophobic interactions (π···alkyl) with the amino acids ILE20 (4.82 Å), LEU24 (5.15 Å), LEU50 (4.81 Å) and PRO51 (5.01 Å) respectively. The ligand interaction diagrams of the best active molecules (**3f** and **3h**) were depicted in Figure 5A.10 and Figure 5A.11. The detailed hydrogen bonding profile of the target compounds with the protein 1DF7 is given in Table 5A.5.

Table 5A.5. Molecular docking results of the target compounds **3a-o** against 1DF7

S No.	Compound	Binding energy (kcal/mol)	No. of hydrogen bonds	Residues involved in the hydrogen bonding	Hydrogen bond length (Å)
1	**3a**	-11.26	4	ALA7, GLN28, PRO51, TYR100	2.06, 2.76, 2.84, 3.61

2	**3b**	-12.53	3	GLN28, PRO51, TYR100	1.98, 2.76, 3.10
3	**3c**	-11.62	6	ALA7, TRP22, GLN28, PHE31, PRO51	1.81, 2.71, 2.92, 2.95, 3.38, 3.65
4	**3d**	-11.16	3	SER49, LEU50, PRO51	3.32, 3.34, 3.36
5	**3e**	-11.94	5	TRP22, LEU24, GLN28, PRO51, TYR100,	1.98, 2.76, 2.87, 3.08, 3.76
6	**3f**	**-12.73**	3	GLN28, PRO51, TYR100	2.76, 3.07, 2.13
7	**3g**	-11.93	5	ALA7, GLN28, PHE31, PRO51, TYR100	1.81, 2.73, 2.94, 3.38, 3.63
8	**3h**	**-12.92**	3	GLN28, PRO51, TYR100	2.76, 3.05, 2.14
9	**3i**	-10.99	3	ALA7, GLN28, PHE31	1.84, 2.77, 2.97
10	**3j**	-12.13	2	GLN28, TYR100	2.12, 2.79
11	**3k**	-11.86	3	TRP22, GLN28, TYR100	1.95, 2.78, 2.81
12	**3l**	-10.94	3	GLY18, GLN28, SER49	2.24, 3.00, 3.04
13	**3m**	-11.52	4	TRP22, LEU24, GLN28, TYR100	1.98, 2.77, 2.89, 3.74
14	**3n**	-12.33	2	GLN28, TYR100	2.13, 2.78
15	**3o**	-11.87	2	ALA7, TYR100	1.77. 2.39

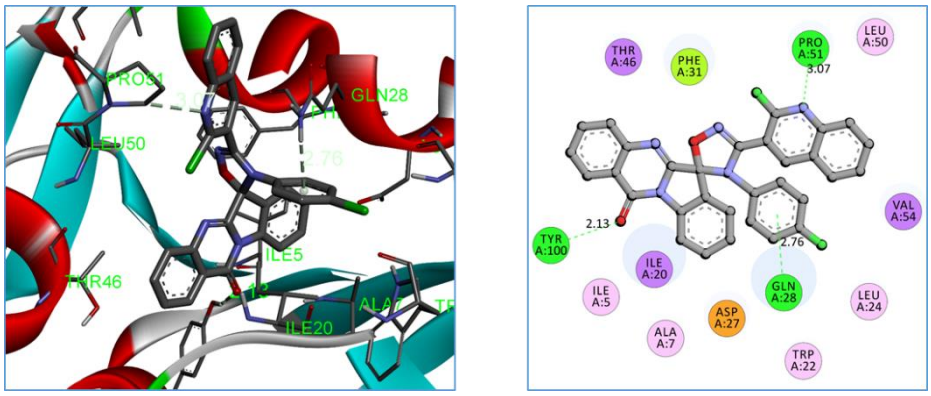

Figure 5A.10. Binding interactions between compound **3f** and active site of 1DF7.

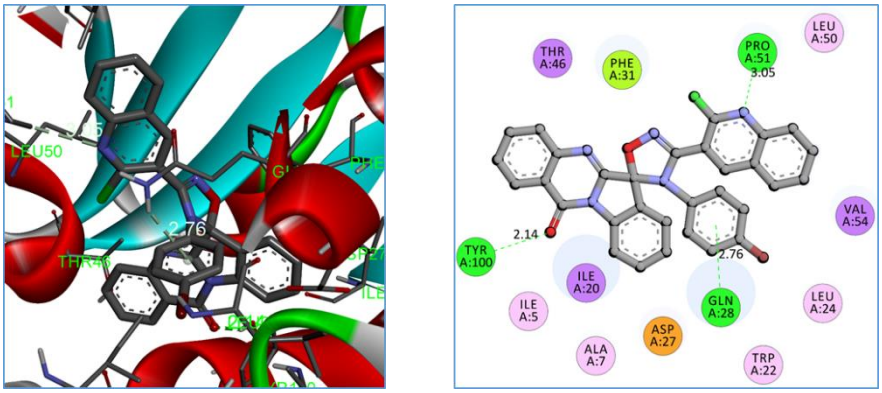

Figure 5A.11. Binding interactions between compound **3h** and active site of 1DF7.

5A.4. ADME prediction

The ADME properties of all the compounds **3a-o** have shown satisfactory results [42]. All the compounds have shown good intestinal absorption which are nearer to 100. The compounds have shown moderate permeability for *in silico* Caco2 cells and MDCK cells. Blood-brain barrier penetration results demonstrated that all the compounds have high absorption into the CNS, and this indicates that these compounds have more capability to cross the CNS. All the compounds exhibit maximum skin permeability. From these results, we observed that the synthesized quinolinyl spiroquinazolinoneoxadiazoles have good ADME properties and all the obtained parameters are summarized in Table 5A.6.

Table 5A.6. Prediction of ADME Properties of the title compounds **3a-o**

Entry	Mol. wt.	[a]HIA	[b]Caco2	[c]MDCK	[d]Plasma Protein Binding	[e]BBB	[f]Skin Permeability	[g]Rule of five
3a	527.97	98.32	35.62	0.762	100.00	2.68	-2.17	2
3b	541.99	98.21	33.32	0.054	99.36	1.80	-2.24	2
3c	557.99	98.26	33.02	0.045	96.55	3.91	-2.35	2
3d	556.02	98.38	34.33	0.060	93.20	2.42	-2.16	2
3e	545.95	98.32	32.94	0.051	99.36	3.50	-2.48	2
3f	562.41	98.45	35.14	0.061	100.00	2.99	-2.20	2
3g	562.41	98.45	35.62	1.563	99.81	3.36	-2.20	2
3h	606.86	98.52	35.37	0.019	100.00	2.87	-2.15	2
3i	509.52	97.62	26.79	0.134	99.61	1.94	-2.65	2
3j	523.55	97.69	29.11	0.047	95.53	2.30	-2.60	2
3k	539.55	97.50	29.75	0.044	95.53	1.33	-2.78	2
3l	537.58	97.76	31.35	0.045	91.75	2.28	-2.53	2
3m	527.51	97.63	27.35	0.046	99.21	1.85	-2.97	2
3n	543.96	97.92	24.18	0.046	100.00	2.24	-2.67	2
3o	543.96	97.92	24.25	0.081	100.00	2.39	-2.67	2

[a] Human intestinal absorption, 70-100% good absorption; [b] >90 high permeability; [c] from $3.4x10^{-6}$ to $20.2x10^{-6}$; [d] >90% strongly plasma protein binding; [e] >0.40 CNS active compound; [f] ranging from -6.1 to -0.19; [g] n-violation ≤1.

5A.5. Conclusion

In this chapter a series of quinolinyl spiroquinazolinoneoxadiazoles were designed and synthesized. These compounds were screened for their *in vitro* anti-tubercular activity against *mycobacterium tuberculosis* H37Rv. Among them, **3b**, **3e**, **3f**, **3h** and **3l** (MIC = 0.78 µg/mL) were considered to be most active compounds than the standard drug ethambutol (MIC = 1.56 µg/mL). Whereas, the compounds **3i**, **3j**, **3k**, **3m** and **3o** exhibited significant activity with MIC values ranging from 1.56 to 3.125 µg/mL. The potent anti-tubercular activity of the compounds was accompanied with relatively low levels of

cytotoxicity, which revealed their therapeutic potential in the field of anti-tubercular agents. Structure activity studies indicated that methyl, fluoro, chloro and bromo substitution on phenyl ring may enhance the anti-tubercular activity. Furthermore, the molecular docking studies support that our best active compounds are showing relatively good interactions with *Mycobacterium tuberculosis* protein (1DF7) and also ADME properties of the target compounds were found to be in significantly acceptable ranges. Altogether, these compounds could pave the way for the development of future lead molecules for the generation of new anti-TB drugs.

5A.6. Experimental Section

5A.6.1. General procedure for the generation of target compounds 3a-o

To a solution of quinazolinone Schiff's bases **1a-h** (1.0 mmol) and *N*-hydroxycarbimidoyl chlorides **2a-b** (1.1 mmol) in DCM (3 mL) was added Et_3N (2.0 equiv) drop wise about 10 min. The reaction was allowed to stir at room temperature for appropriate time. After completion of the reaction (monitored by TLC), reaction mixture was concentrated under reduced pressure and the residue was recrystallized from methanol to afford the desired products **3a-o**.

5A.6.2. Protocol for the anti-TB screening

The MIC of the synthesized compounds was tested using *in vitro* microplate alamar blue assay method [43]. The *Mycobacterium tuberculosis* H37Rv strain (ATCC27294) was used for the screening. The inoculum was prepared from fresh LJ medium re-suspended in 7H9-S medium (7H9 broth, 0.1% casitone, 0.5% glycerol, supplemented oleic acid, albumin, dextrose, and catalase [OADC]), adjusted to a OD_{590} 1.0, and diluted 1:20; 100 µL was used as inoculum. Each drug stock solution was thawed and diluted in 7H9-S at four-fold the final highest concentration tested. Serial two-fold dilutions of each drug were prepared directly in a sterile 96-well microtiter plate using 100 µL 7H9-S. A growth control containing no antibiotic and a sterile control were also prepared on each plate. Sterile water was added to all perimeter wells to avoid evaporation during the incubation. The plate was covered, sealed in plastic bags and incubated at 37 ^{o}C in normal atmosphere. After 7 days incubation, 30 µL of alamar blue solution was added to each well, and the plate was re-incubated overnight. A change in colour from blue (oxidised state) to pink (reduced) indicated the growth of bacteria, and the MIC was defined as the lowest concentration of drug that prevented this change in colour.

5A.6.3. *In vitro* cytotoxicity screening

The *in vitro* cytotoxicity of the privileged anti-tubercular active analogues with lower MIC value were assessed by 3-(4,5-dimethylthiazol-2-yl)-2,5-diphenyltetrazolium bromide (MTT) assay against growth inhibition of RAW 264.7 cells at 25 μM concentration [44]. Cell lines were maintained at 37 °C in a humidified 5% CO_2 incubator (Thermo scientific). Detached the adhered cells and followed by centrifugation to get cell pellet. Fresh media was added to the pellet to make a cell count using haemocytometer and plate 100 μL of media with cells ranging from 5,000 - 6,000 per well in a 96-well plate. The plate was incubated overnight in CO_2 incubator for the cells to adhere and regain its shape. After 24 h cells were treated with the test compounds at 25 μg/mL diluted using the media to deduce the percentage inhibition on normal cells. The cells were incubated for 48 h to assay the effect of the test compounds on different cell lines. Zero hour reading was noted down with untreated cells and also control with 1% DMSO to subtract further from the 48 h reading. After 48 h incubation, cells were treated by MTT (4,5-dimethylthiazol-2-yl)-2,5-diphenyltetrazolium bromide) dissolved in PBS (5 mg/mL) and incubated for 3-4 h at 37 °C. The formazan crystals thus formed were dissolved in 100 μL of DMSO and the viability was measured at 540 nm on a multimode reader (Spectra max). The values were further calculated for percentage inhibition which in turn helps us to know the cytotoxicity of the test compounds.

5A.6.4. Molecular docking protocol

The docking studies are predominating tools for the assessment of the binding affinity to the ligand-protein receptor. All the synthesized compounds were subjected to *in silico* molecular docking studies by using the AutoDockTools (ADT) version 1.5.6 and AutoDock version 4.2.5.1 docking program [45]. The 3D-structures of all the synthesized compounds were prepared by using chem3D pro 12.0 software. The optimized 3D structures were saved in pdb format. The structure of the dihydrofolate reductase of *Mycobacterium tuberculosis* (PDB code: 1DF7) protein was extracted from the protein data bank (http://www.rcsb.org/pdb). The bound ligand and water molecules in protein were removed by using Discovery Studio Visualizer version 4.0 to prepare the protein. Non polar hydrogens were merged and gasteiger charges were added to the protein. The grid file was saved in gpf format. The three dimensional grid box having dimensions 60 x 60 x 60 $Å^3$ was created around the protein with spacing 0.3750 Å. The genetic algorithm was carried out with the population size and the maximum number of evaluations were 150 and

25,00,000 respectively. The docking output file was saved as Lamarckian Ga (4.2) in dpf format. The ligand-protein complex binding sites were visualized by Discovery Studio Visualizer version 4.0.

5A.6.5. ADME prediction

In silico ADME prediction of the synthesized compounds were calculated by using the online servers ADMETlab 2.0 and pkCSM [46]. The ADMET properties, human intestinal absorption (HIA), Caco-2 cell permeability, plasma protein binding and blood brain barrier penetration (BBB) were predicted using this program.

5A.7. Spectral data of the synthesized compounds 3a-o

3'-(2-chloroquinolin-3-yl)-4'-phenyl-4'*H*,12*H*-spiro[indolo[2,1-*b*]quinazoline-6,5'-[1,2,4] oxadiazol]-12-one (3a)

White solid. mp: 249-251 ℃. IR (KBr, cm^{-1}): 1697, 1654. ^{1}H NMR (400 MHz, $CDCl_3$) δ: 8.71 (s, 1H), 8.52 (d, J = 6.8 Hz, 1H), 8.36 (d, J = 7.6 Hz, 1H), 8.06 - 8.00 (m, 2H), 7.97 – 7.91 (m, 2H), 7.81 (d, J = 7.2 Hz, 2H), 7.66 – 7.62 (m, 2H), 7.56 (s, 1H), 7.51 (s, 1H) 6.92 (s, 3H), 6.81 (s, 2H). ^{13}C NMR (100 MHz, $CDCl_3$) δ: 159.18, 153.57, 148.23, 147.99, 146.98, 139.71, 134.87, 134.64, 133.08, 132.30, 129.41, 129.28, 129.22, 129.16, 128.66, 128.42, 128.03, 127.59, 127.12, 126.98, 126.82, 126.38, 126.29, 126.12, 122.46, 118.63, 117.57, 117.45, 101.63. HRMS (ESI, m/z): calcd. for $C_{31}H_{19}ClN_5O_2$ $[M+H]^+$: 528.1227; found: 528.0686.

3'-(2-chloroquinolin-3-yl)-4'-(*p*-tolyl)-4'*H*,12*H*-spiro[indolo[2,1-*b*]quinazoline-6,5'-[1,2,4] oxadiazol]-12-one (3b)

White solid. mp: 255-257 ℃. IR (KBr, cm^{-1}): 1688, 1647. ^{1}H NMR (400 MHz, DMSO-d_6) δ: 9.11 (s, 1H), 8.40 (d, J = 6.8 Hz, 1H), 8.30 (d, J = 4.8 Hz, 1H), 8.23 (d, J = 6.8 Hz, 1H), 8.09 (d, J = 7.2 Hz, 1H), 7.96 (s, 4H), 7.77 (d, J = 8.0 Hz, 1H), 7.69 (s, 2H), 7.56 (d, J = 3.6 Hz, 1H), 6.78 (s, 4H), 1.98 (s, 3H). ^{13}C NMR (100 MHz, DMSO-d_6) δ: 158.32, 153.68, 152.62, 147.40, 147.11, 146.42, 143.00, 139.09, 137.32, 135.20, 133.18, 132.84, 131.67, 129.79, 128.74, 128.29, 127.75, 127.60, 126.76, 126.55, 125.85, 122.00, 117.70, 116.56, 100.81, 20.20. HRMS (ESI, m/z): calcd. for $C_{32}H_{21}ClN_5O_2$ $[M+H]^+$: 542.1384; found: 542.1383.

3'-(2-chloroquinolin-3-yl)-4'-(4-methoxyphenyl)-4'*H*,12*H*-spiro[indolo[2,1-*b*]quinazoline-6, 5'-[1,2,4]oxadiazol]-12-one (3c)

White solid. mp: 230-232 ℃. IR (KBr, cm^{-1}): 1694, 1655. ^{1}H NMR (400 MHz, $CDCl_3$) δ: 8.67 (s, 1H), 8.49 (d, J = 7.6 Hz, 1H), 8.35 (d, J = 7.6 Hz, 1H), 8.09 (d, J = 6.8 Hz, 1H), 8.00 (d, J = 8.4 Hz, 1H), 7.95 (d, J = 7.6 Hz, 2H), 7.82 (t, J = 7.6 Hz, 2H), 7.66 – 7.50 (m, 4H), 6.82 (d, J = 8.0 Hz, 2H), 6.41 (d, J = 8.4 Hz, 2H), 3.51 (s, 3H). ^{13}C NMR (100 MHz, DMSO-d_6) δ: 158.35, 153.80, 152.88, 147.41, 147.20, 146.45, 143.04, 139.10, 135.25, 133.20, 132.86, 129.16, 128.74, 128.36, 127.79, 127.63, 126.64, 126.40, 125.96, 125.82, 122.01, 117.67, 116.57, 114.40, 100.84, 54.96. HRMS (ESI, m/z): calcd. for $C_{32}H_{21}ClN_5O_3$ $[M+H]^+$: 558.1333; found: 558.1330.

3'-(2-chloroquinolin-3-yl)-4'-(2,4-dimethylphenyl)-4'*H*,12*H*-spiro[indolo[2,1-*b*]quinazoline-6,5'-[1,2,4]oxadiazol]-12-one (3d)

White solid. mp: 245-247 ℃. IR (KBr, cm^{-1}): 1687, 1651. ^{1}H NMR (400 MHz, $CDCl_3$) δ: 8.64 (s, 1H), 8.51 (s, 1H), 8.36 (t, J = 8.0 Hz, 1H), 7.99 (d, J = 7.2 Hz, 2H), 7.89 (d, J = 8.0 Hz, 2H), 7.81 (d, J = 6.4 Hz, 2H), 7.63 – 7.54 (m, 3H), 7.49 – 7.43 (m, 1H), 6.62 (dt, J = 15.6, 7.6 Hz, 3H), 2.20 (s, 3H), 1.98 (s, 3H). ^{13}C NMR (100 MHz, DMSO-d_6) δ: 158.18, 147.25, 147.06, 146.24, 142.95, 138.12, 136.37, 135.30, 133.09, 132.87, 132.01, 129.56, 128.74, 128.66, 128.30, 128.08, 127.66, 127.02, 126.90, 126.67, 125.64, 117.77, 116.52, 100.92, 20.13, 17.92. HRMS (ESI, m/z): calcd. for $C_{33}H_{23}ClN_5O_2$ $[M+H]^+$: 556.1540; found: 556.1530.

3'-(2-chloroquinolin-3-yl)-4'-(4-fluorophenyl)-4'*H*,12*H*-spiro[indolo[2,1-*b*]quinazoline-6,5'- [1,2,4]oxadiazol]-12-one (3e)

White solid. mp: 250-252 ℃. IR (KBr, cm^{-1}): 1690, 1652. ^{1}H NMR (400 MHz, DMSO-d_6) δ: 9.18 (s, 1H), 8.40 (d, J = 7.6 Hz, 1H), 8.31 (d, J = 8.0 Hz, 1H), 8.25 (d, J = 8.0 Hz, 1H), 8.10 (d, J = 6.8 Hz, 1H), 7.97 (s, 4H), 7.80 (t, J = 7.2 Hz, 1H), 7.70 (t, J = 7.6 Hz, 2H), 7.56 (t, J = 7.6 Hz, 1H), 6.96 (d, J = 3.6 Hz, 2H), 6.89 (t, J = 8.4 Hz, 2H). ^{13}C NMR (100 MHz, DMSO-d_6) δ: 161.78 (d, J = 244.6 Hz), 158.34, 153.51, 152.47, 147.45, 146.94, 146.39, 143.20, 139.21, 135.14, 133.28, 132.90, 130.70, 129.16 (d, J = 9.0 Hz), 128.75, 128.36 (d, J = 8.8 Hz), 127.77 (d, J = 21.0 Hz), 126.66, 126.56, 125.79, 125.37, 122.10, 117.37, 116.59, 116.40, 116.17, 100.80. HRMS (ESI, m/z): calcd. for $C_{31}H_{18}ClFN_5O_2$ $[M+H]^+$: 546.1133; found: 546.1122.

4'-(4-chlorophenyl)-3'-(2-chloroquinolin-3-yl)-4'*H*,12*H*-spiro[indolo[2,1-*b*]quinazoline-6,5'- [1,2,4]oxadiazol]-12-one (3f)

White solid. mp: 256-258 ℃. IR (KBr, cm^{-1}): 1690, 1650. ^{1}H NMR (400 MHz, DMSO-d_6) δ: 9.20 (s, 1H), 8.42 (d, J = 8.0 Hz, 1H), 8.32 (d, J = 8.0 Hz, 1H), 8.26 (d, J = 8.0 Hz, 1H), 8.05 (d, J = 7.6 Hz, 1H), 8.00-7.93 (m, 4H), 7.81 (t, J = 7.2 Hz, 1H), 7.71 (dd, J = 12.0, 6.4 Hz, 2H), 7.54 (t, J = 7.6 Hz, 1H), 7.10 (d, J = 8.4 Hz, 2H), 6.88 (d, J = 8.4 Hz, 2H). ^{13}C NMR (100 MHz, DMSO-d_6) δ: 158.37, 153.41, 152.21, 147.50, 146.83, 146.39, 143.24, 139.28, 135.13, 133.62, 133.36, 132.95, 131.69, 129.42, 128.82, 128.40, 128.28, 127.79, 127.71, 127.57, 126.69, 126.51, 125.84, 125.15, 122.18, 117.35, 116.66, 100.75. HRMS (ESI, m/z): calcd. for $C_{31}H_{18}Cl_2N_5O_2$ $[M+H]^+$: 562.0838; found: 562.0844.

4'-(3-chlorophenyl)-3'-(2-chloroquinolin-3-yl)-4'*H*,12*H*-spiro[indolo[2,1-*b*]quinazoline-6,5'- [1,2,4]oxadiazol]-12-one (3g)

White solid. mp: 227-229 ℃. IR (KBr, cm^{-1}): 1693, 1657. ^{1}H NMR (400 MHz, DMSO-d_6) δ: 9.23 (s, 1H), 8.42 (d, J = 8.0 Hz, 1H), 8.29 (dd, J = 15.2, 8.0 Hz, 2H), 8.08 (d, J = 7.2 Hz, 1H), 8.03-7.93 (m, 4H), 7.82 (t, J = 7.6 Hz, 1H), 7.72 (t, J = 7.6 Hz, 2H), 7.55 (t, J = 7.6 Hz, 1H), 7.06 (d, J = 5.2 Hz, 2H), 6.91 (s, 1H), 6.84 – 6.81 (m, 1H). ^{13}C NMR (100 MHz, DMSO-d_6) δ: 158.40, 153.34, 152.07, 147.52, 146.86, 146.39, 143.34, 139.34, 136.15, 135.20, 133.47, 133.09, 133.06, 131.06, 128.83, 128.49, 128.29, 127.83, 127.63, 127.42, 126.73, 126.60, 125.81, 125.77, 125.04, 124.59, 122.19, 117.32, 116.68, 100.76. HRMS (ESI, m/z): calcd. for $C_{31}H_{18}Cl_2N_5O_2$ $[M+H]^+$: 562.0838; found: 562.0832.

4'-(4-bromophenyl)-3'-(2-chloroquinolin-3-yl)-4'*H*,12*H*-spiro[indolo[2,1-*b*]quinazoline-6,5'- [1,2,4]oxadiazol]-12-one (3h)

White solid. mp: 267-269 ℃. IR (KBr, cm^{-1}): 1689, 1651. ^{1}H NMR (400 MHz, DMSO-d_6) δ: 9.19 (s, 1H), 8.42 (d, J = 8.0 Hz, 1H), 8.32 (d, J = 7.6 Hz, 1H), 8.26 (d, J = 8.0 Hz, 1H), 8.04 (d, J = 7.6 Hz, 1H), 8.01 – 7.92 (m, 4H), 7.81 (t, J = 7.6 Hz, 1H), 7.71 (dd, J = 11.6, 6.8 Hz, 2H), 7.53 (t, J = 7.6 Hz, 1H), 7.23 (d, J = 8.0 Hz, 2H), 6.80 (d, J = 8.4 Hz, 2H). ^{13}C NMR (100 MHz, DMSO-d_6) δ: 158.37, 153.39, 152.14, 147.50, 146.81, 146.38, 143.23, 139.28, 135.12, 134.07, 133.36, 132.95, 132.34, 128.81, 128.39, 128.27, 127.88, 127.80, 127.56, 126.69, 126.49, 125.84, 125.12, 122.19, 120.11, 117.34, 116.66, 100.70. HRMS (ESI, m/z): calcd. for $C_{31}H_{18}BrClN_5O_2$ $[M+H]^+$: 606.0332; found: 606.0344.

3'-(2-oxo-1,2-dihydroquinolin-3-yl)-4'-phenyl-4'*H*,12*H*-spiro[indolo[2,1-*b*]quinazoline-6,5'- [1,2,4]oxadiazol]-12-one (3i)

White solid. mp: 260-262 ℃. IR (KBr, cm^{-1}): 1665, 1601. ^{1}H NMR (400 MHz, DMSO-d_6) δ: 11.95 (s, 1H), 8.60 (s, 1H), 8.38 (d, J = 7.6 Hz, 1H), 8.28 (d, J = 7.2 Hz, 1H), 7.98 (d, J = 6.0 Hz, 1H), 7.94 (s, 2H), 7.87 (d, J = 5.2 Hz, 1H), 7.68 (d, J = 6.8 Hz, 2H), 7.59 (t, J = 6.8 Hz, 1H), 7.52 (t, J = 6.8 Hz, 1H), 7.31 – 7.26 (m, 3H), 7.01 (d, J = 7.2 Hz, 2H), 6.83 (d, J = 6.0 Hz, 2H). ^{13}C NMR (100 MHz, DMSO-d_6) δ: 158.43, 146.42, 143.47, 135.81, 135.22, 132.27, 129.01, 128.77, 128.28, 127.58, 126.82, 126.77, 126.69, 126.58, 126.38, 126.29, 125.43, 122.44, 121.96, 118.18, 117.27, 116.59, 115.24, 100.66. HRMS (ESI, m/z): calcd. for $C_{31}H_{20}N_5O_3$ $[M+H]^+$: 510.1566; found: 510.1565.

3'-(2-oxo-1,2-dihydroquinolin-3-yl)-4'-(*p*-tolyl)-4'*H*,12*H*-spiro[indolo[2,1-*b*]quinazoline-6,5' -[1,2,4]oxadiazol]-12-one (3j)

White solid. mp: 264-266 ℃. IR (KBr, cm^{-1}): 1688, 1651. ^{1}H NMR (400 MHz, $CDCl_3$) δ: 11.42 (s, 1H), 8.50 (d, J = 8.0 Hz, 1H), 8.41 (s, 1H), 8.36 (d, J = 8.0 Hz, 1H), 8.15 (d, J = 7.2 Hz, 1H), 7.92 (d, J = 8.0 Hz, 1H), 7.79 (t, J = 7.6 Hz, 1H), 7.67 (d, J = 8.0 Hz, 1H), 7.61 (t, J = 8.0 Hz, 1H), 7.59 – 7.47 (m, 3H), 7.29 (s, 1H), 7.24 (s, 1H), 6.80 (d, J = 8.0 Hz, 2H), 6.69 (d, J = 8.0 Hz, 2H), 2.01 (s, 3H).^{13}C NMR (100 MHz, DMSO-d_6) δ: 158.42, 158.35, 153.87, 153.19, 146.41, 143.37, 139.61, 138.56, 136.53, 135.17, 132.92, 132.87, 132.17, 129.45, 128.95, 128.70, 128.26, 127.53, 126.69, 126.64, 126.30, 126.04, 122.35, 121.91, 118.13, 117.30, 116.52, 115.18, 100.64, 20.27. HRMS (ESI, m/z): calcd. for $C_{32}H_{22}N_5O_3$ $[M+H]^+$: 524.1723; found: 524.1717.

4'-(4-methoxyphenyl)-3'-(2-oxo-1,2-dihydroquinolin-3-yl)-4'*H*,12*H*-spiro[indolo[2,1-*b*] quinazoline-6,5'-[1,2,4]oxadiazol]-12-one (3k)

White solid. mp: 273-275 ℃. IR (KBr, cm^{-1}): 1684, 1650. ^{1}H NMR (400 MHz, DMSO-d_6) δ: 11.95 (s, 1H), 8.56 (s, 1H), 8.36 (d, J = 8.0 Hz, 1H), 8.28 (d, J = 8.0 Hz, 1H), 8.06 (d, J = 7.2 Hz, 1H), 7.97 (d, J = 5.2 Hz, 2H), 7.86 (d, J = 7.6 Hz, 1H), 7.68 (dd, J = 15.2, 6.8 Hz, 2H), 7.61 – 7.54 (m, 2H), 7.30 – 7.24 (m, 2H), 6.86 (d, J = 8.4 Hz, 2H), 6.57 (d, J = 8.8 Hz, 2H), 3.50 (s, 3H). ^{13}C NMR (100 MHz, DMSO-d_6) δ: 158.44, 158.32, 158.03, 153.95, 153.45, 146.41, 143.37, 139.58, 138.55, 135.16, 132.86, 132.11, 128.89, 128.63, 128.23, 127.53, 126.74, 126.62, 126.31, 122.31, 121.88, 118.08, 117.21, 116.47, 115.16, 113.97, 100.68, 54.90. HRMS (ESI, m/z): calcd. for $C_{32}H_{22}N_5O_4$ $[M+H]^+$: 540.1672; found: 540.1678.

4'-(2,4-dimethylphenyl)-3'-(2-oxo-1,2-dihydroquinolin-3-yl)-4'*H*,12*H*-spiro [indolo[2,1-*b*] quinazoline-6,5'-[1,2,4]oxadiazol]-12-one (3l)

White solid. mp: 252-254 ℃. IR (KBr, cm^{-1}): 1696, 1653. ^{1}H NMR (400 MHz, DMSO-d_6) δ: 11.88 (s, 1H), 8.53 (s, 1H), 8.35 (d, J = 8.4 Hz, 1H), 8.26 (d, J = 6.0 Hz, 1H), 8.05 (d, J = 6.8 Hz, 1H), 7.98 – 7.90 (m, 2H), 7.81 (d, J = 6.0 Hz, 1H), 7.67 (d, J = 6.8 Hz, 2H), 7.55 (d, J = 7.6 Hz, 2H), 7.25 – 7.21 (m, 2H), 6.75 (d, J = 7.6 Hz, 1H), 6.71 (s, 1H), 6.64 (d, J = 7.6 Hz, 1H), 2.15 (s, 3H), 1.98 (s, 3H). ^{13}C NMR (100 MHz, DMSO-d_6) δ: 158.44, 158.22, 153.61, 146.25, 143.08, 139.50, 138.09, 137.68, 135.25, 132.79, 132.14, 131.60, 131.00, 130.87, 129.66, 128.87, 128.68, 128.07, 127.00, 126.84, 126.52, 122.28, 121.78, 117.94, 117.26, 115.09, 100.70, 20.23, 18.04. HRMS (ESI, m/z): calcd. for $C_{33}H_{24}N_5O_3$ $[M+H]^+$: 538.1879; found: 538.1864.

4'-(4-fluorophenyl)-3'-(2-oxo-1,2-dihydroquinolin-3-yl)-4'*H*,12*H*-spiro[indolo[2,1-*b*] quinazoline-6,5'-[1,2,4]oxadiazol]-12-one (3m)

White solid. mp: 261-263 ℃. IR (KBr, cm^{-1}): 1685, 1651. ^{1}H NMR (400 MHz, DMSO-d_6) δ: 11.98 (s, 1H), 8.63 (s, 1H), 8.38 (d, J = 8.0 Hz, 1H), 8.29 (d, J = 7.6 Hz, 1H), 8.02 (d, J = 7.6 Hz, 1H), 7.96 (d, J = 2.4 Hz, 2H), 7.89 (d, J = 7.6 Hz, 1H), 7.69 (d, J = 8.0 Hz, 2H), 7.61 (t, J = 7.6 Hz, 1H), 7.54 (t, J = 7.6 Hz, 1H), 7.31-7.25 (m, 2H), 6.93-6.87 (m, 4H). ^{13}C NMR (100 MHz, DMSO-d_6) δ: 161.59 (d, J = 243.6 Hz) 158.32, 153.71, 153.22, 146.39, 143.69, 139.69, 138.69, 135.15, 133.04, 132.27, 131.91, 129.01 (d, J = 29.0 Hz), 128.47 (d, J = 8.8 Hz), 128.26, 127.54, 126.65, 126.32 (d, J = 4.8 Hz), 122.40, 122.00, 118.14, 116.87, 116.57, 115.95, 115.72, 115.22, 100.70. HRMS (ESI, m/z): calcd. for $C_{31}H_{19}FN_5O_3$ $[M+H]^+$: 528.1472; found: 528.1481.

4'-(4-chlorophenyl)-3'-(2-oxo-1,2-dihydroquinolin-3-yl)-4'*H*,12*H*-spiro[indolo[2,1-*b*] quinazoline-6,5'-[1,2,4]oxadiazol]-12-one (3n)

White solid. mp: 263-265 ℃. IR (KBr, cm^{-1}): 1687, 1651. ^{1}H NMR (400 MHz, DMSO-d_6) δ: 12.00 (s, 1H), 8.66 (s, 1H), 8.41 (d, J = 7.6 Hz, 1H), 8.30 (d, J = 7.2 Hz, 1H), 7.99 – 7.94 (m, 3H), 7.90 (d, J = 7.6 Hz, 1H), 7.69 (d, J = 5.2 Hz, 2H), 7.62 (t, J = 7.2 Hz, 1H), 7.52 (t, J = 6.8 Hz, 1H), 7.33 – 7.28 (m, 2H), 7.11 (d, J = 8.0 Hz, 2H), 6.86 (d, J = 8.0 Hz, 2H). ^{13}C NMR (100 MHz, DMSO-d_6) δ: 158.37, 158.22, 153.56, 152.89, 146.36, 143.67, 139.72, 138.69, 135.10, 134.93, 133.08, 132.29, 130.94, 129.00, 128.71, 128.25, 127.52, 126.87, 126.65, 126.21, 126.07, 122.39, 122.05, 118.16, 116.81, 116.62, 115.23, 100.57. HRMS (ESI, m/z): calcd. for $C_{31}H_{19}ClN_5O_3$ $[M+H]^+$: 544.1176; found: 544.1181.

4'-(3-chlorophenyl)-3'-(2-oxo-1,2-dihydroquinolin-3-yl)-4'*H*,12*H*-spiro[indolo[2,1-*b*] quinazoline-6,5'-[1,2,4]oxadiazol]-12-one (3o)

White solid. mp: 236-238 ℃. IR (KBr, cm^{-1}): 1687, 1665. ^{1}H NMR (400 MHz, DMSO-d_6) δ: 12.03 (s, 1H), 8.67 (s, 1H), 8.41 (d, J = 7.6 Hz, 1H), 8.29 (d, J = 7.2 Hz, 1H), 7.99 (d, J = 7.2 Hz, 1H), 7.94 (s, 2H), 7.91 (d, J = 8.0 Hz, 1H), 7.69 (t, J = 7.6 Hz, 2H), 7.62 (t, J = 8.8 Hz, 1H), 7.56 – 7.51 (m, 1H), 7.30 (dd, J = 16.8, 8.0 Hz, 2H), 7.05 (d, J = 8.4 Hz, 2H), 6.88 (s, 1H), 6.80 (d, J = 7.6 Hz, 1H).^{13}C NMR (100 MHz, DMSO-d_6) δ: 158.66, 153.69, 152.97, 146.49, 144.14, 139.87, 138.92, 137.52, 135.55, 133.55, 133.07, 130.92, 129.37, 129.16, 128.44, 127.94, 127.09, 126.95, 126.57, 126.17, 125.17, 124.12, 122.90, 122.16, 118.39, 116.83, 115.54, 100.83. HRMS (ESI, m/z): calcd. for $C_{31}H_{19}ClN_5O_3$ $[M+H]^+$: 544.1176; found: 544.1157.

5A.8. References

[1] J. Boström, A. Hogner, A. Llinàs, E. Wellner, A. T. Plowright, *J. Med. Chem.* **2012**, *55*, 1817–1830.

[2] P. G. Sasikumar, M. Ramachandra, S. S. S. Naremaddepalli, (**2015**). 1,2,4-oxadiazole derivatives as immunomodulators. WO 2015/033299 Al, filed 5 September 2014 and issued 12 March 2015.

[3] T. S. Ibrahim, A. J. Almalki, A. H. Moustafa, R. M. Allam, G. E. D. A. Abuo-Rahma, H. I. El Subbagh, M. F. A. Mohamed, *Bioorg. Chem.* **2021**, *111*, 104885–104897.

[4] A. E. El Mansouri, A. Oubella, M. Maatallah, M. Y. AitItto, M. Zahouily, H. Morjani, H. B. Lazrek, *Bioorg. Med. Chem. Lett.* **2020**, *30*, 127438–127446.

[5] M. A. Boudreau, D. Ding, J. E. Meisel, J. Janardhanan, E. Spink, Z. Peng, Y. Qian, T. Yamaguchi, S. A. Testero, P. I. O'Daniel, E. Leemans, E. Lastochkin, W. Song, V. A. Schroeder, W. R. Wolter, M. A. Suckow, S. Mobashery, M. Chang, *ACS Med. Chem. Lett.* **2020**, *11*, 322–326.

[6] Y. Y. Zhang, Q. Q. Zhang, J. Zhang, J. L. Song, J. C. Li, K. Han, J. T. Huang, C. S. Jiang, H. Zhang, *Bioorg. Med. Chem. Lett.* **2020**, *30*, 127373–127378.

[7] A. Atmaram Upare, P. K. Gadekar, H. Sivaramakrishnan, N. Naik, V. M. Khedkar, D. Sarkar, A. Choudhari, S. Mohana Roopan, *Bioorg. Chem.* **2019**, *86*, 507–512.

[8] M. S. Ayoup, M. M. Abu-Serie, H. Abdel-Hamid, M. Teleb, *Eur. J. Med. Chem.* **2021**, *220*, 113475–113494.

[9] J. R. Romero, *Expert Opin. Investig. Drugs* **2001**, *10*, 369–379.

[10] E. Gaetani, C. Laureri, M. Vitto, *J. Pharm. Biomed. Anal.* **1995**, *13*, 335–337.

[11] K. A. Min, X. Zhu, J. M. Oh, W. G. Shin, *Am. J. Heal. Pharm.* **2006**, *63*, 153–156.

[12] C. M. McDonald, C. Campbell, R. E. Torricelli, R. S. Finkel, K. M. Flanigan, N. Goemans, G. Vita, *Lancet* **2017**, *390*, 1489–1498.

[13] K. Biernacki, M. Daśko, O. Ciupak, K. Kubiński, J. Rachon, S. Demkowicz, *Pharmaceuticals* **2020**, *13*, 1–45.

[14] Z. Bártfai, A. Somosközi, E. H. Puhó, A. E. Czeizel, *Congenit. Anom. (Kyoto).* **2007**, *47*, 16–21.

[15] H. Wei, C. He, J. Zhang, J. M. Shreeve, *Angew. Chemie - Int. Ed.* **2015**, *54*, 9367–9371.

[16] R. Agneeswari, V. Tamilavan, M. Song, M. H. Hyun, *J. Mater. Chem. C* **2014**, *2*, 8515–8524.

[17] H. Xiong, H. Yang, C. Lei, P. Yang, W. Hu, G. Cheng, *Dalt. Trans.* **2019**, *48*, 14705–14711.

[18] Z. Xing, W. Wu, Y. Miao, Y. Tang, Y. Zhou, L. Zheng, Y. Fu, Z. Song, Y. Peng, *Org. Chem. Front.* **2021**, *8*, 1867–1889.

[19] I. Khan, S. Zaib, S. Batool, N. Abbas, Z. Ashraf, J. Iqbal, A. Saeed, *Bioorg. Med. Chem.* **2016**, *24*, 2361–2381.

[20] K. B. Loboda, K. Valjavec, M. Štampar, G. Wolber, B. Žegura, M. Filipič, M. S. Dolenc, A. Perdih, *Bioorg. Chem.* **2020**, *99*, 103828–103846.

[21] M. Wang, T. Liu, S. Chen, M. Wu, J. Han, Z. Li, *Eur. J. Med. Chem.* **2021**, *209*, 112874–113031.

[22] M. Potenza, M. Sciarretta, M. G. Chini, A. Saviano, F. Maione, M. V. D'Auria, S. De Marino, A. Giordano, R. K. Hofstetter, C. Festa, O. Werz, G. Bifulco, *Eur. J. Med. Chem.* **2021**, *224*, 113693–113705.

[23] V. N. Melo de Oliveira, C. Flávia do Amaral Moura, A. dos S. Peixoto, V. P. Gonçalves Ferreira, H. M. Araújo, L. M. Lapa Montenegro Pimentel, C. do Ó. Pessoa, R. Nicolete, J. Versiani dos Anjos, P. P. Sharma, B. Rathi, L. J. Pena, P. Rollin, A. Tatibouët, R. Nascimento de Oliveira, *Eur. J. Med. Chem.* **2021**, *220*, 113472–113491.

[24] M. F. A. Mohamed, A. A. Marzouk, A. Nafady, D. A. El-Gamal, R. M. Allam, G. E. D. A. Abuo-Rahma, H. I. El Subbagh, A. H. Moustafa, *Bioorg. Chem.* **2020**, *105*, 104439–104451.

[25] A. A. Golushko, O. V. Khoroshilova, A. V. Vasilyev, *J. Org. Chem.* **2019**, *84*, 7495–7500.

[26] Q. Bian, C. Wu, J. Yuan, Z. Shi, T. Ding, Y. Huang, H. Xu, Y. Xu, *J. Org. Chem.* **2020**, *85*, 4058–4066.

[27] V. Mercalli, A. Massarotti, M. Varese, M. Giustiniano, F. Meneghetti, E. Novellino, G. C. Tron, *J. Org. Chem.* **2015**, *80*, 9652–9661.

[28] C. Wang, X. Rui, D. Si, R. Dai, Y. Zhu, H. Wen, W. Li, J. Liu, *Adv. Synth. Catal.* **2021**, *363*, 2825–2833.

[29] X. Wang, J. P. Fu, J. X. Xie, Q. H. Teng, H. T. Tang, Y. M. Pan, *Org. Biomol. Chem.* **2020**, *18*, 4936–4940.

[30] Y. Zhang, C. Wu, X. Wan, C. Wang, *J. Heterocycl. Chem.* **2021**, 1–11.

[31] W. Lu, I. A. Baig, H. J. Sun, C. J. Cui, R. Guo, I. P. Jung, D. Wang, M. Dong, M. Y. Yoon, J. G. Wang, *Eur. J. Med. Chem.* **2015**, *94*, 298–305.

[32] P. S. Jadhavar, T. M. Dhameliya, M. D. Vaja, D. Kumar, J. P. Sridevi, P. Yogeeswari, D. Sriram, A. K. Chakraborti, *Bioorg. Med. Chem. Lett.* **2016**, *26*, 2663–2669.

[33] A. F. Borsoi, J. D. Paz, B. L. Abbadi, F. S. Macchi, N. Sperotto, K. Pissinate, R. S. Rambo, A. S. Ramos, D. Machado, M. Viveiros, C. V. Bizarro, L. A. Basso, P. Machado, *Eur. J. Med. Chem.* **2020**, *192*, 112179–112188.

[34] S. R. Patel, R. Gangwal, A. T. Sangamwar, R. Jain, *Eur. J. Med. Chem.* **2015**, *93*, 511–522.

[35] T. G. Shruthi, S. Eswaran, P. Shivarudraiah, S. Narayanan, S. Subramanian, *Bioorg. Med. Chem. Lett.* **2019**, *29*, 97–102.

[36] R. Ranjith Kumar, S. Perumal, J. C. Menéndez, P. Yogeeswari, D. Sriram, *Bioorg. Med. Chem.* **2011**, *19*, 3444–3450.

[37] J. Azizian, M. K. Mohammadi, O. Firuzi, N. Razzaghi-asl, R. Miri, *Med. Chem. Res.* **2012**, *21*, 3730–3740.

[38] G. Shi, X. He, Y. Shang, L. Xiang, C. Yang, G. Han, B. Du, *Chinese J. Chem.* **2016**, *34*, 901–909.

[39] S. K. Marvadi, V. S. Krishna, D. Sriram, S. Kantevari, *Eur. J. Med. Chem.* **2019**, *164*, 171–178.

[40] V. S. Krishna, S. Zheng, E. M. Rekha, R. Nallangi, D. V. Sai Prasad, S. E. George, L. W. Guddat, D. Sriram, *Eur. J. Med. Chem.* **2020**, *193*, 112178–112190.

[41] N. Wang, J. X. Ren, Y. Xie, *J. Biomol. Struct. Dyn.* **2019**, *37*, 1054–1061.

[42] J. C. Dearden, *Expert Opin. Drug Metab. Toxicol.* **2007**, *3*, 635–639.

[43] H. Veeravarapu, V. Malkhed, K. K. Mustyala, R. Vadija, R. Malikanti, U. Vuruputuri, M. K. K. Muthyala, *Mol. Divers.* **2021**, *25*, 351–366.

[44] P. I. Jalava, R. O. Salonen, A. S. Pennanen, M. S. Happo, P. Penttinen, A. I. Hälinen, M. Sillanpää, R. Hillamo, M. R. Hirvonen, *Toxicol. Appl. Pharmacol.* **2008**, *229*, 146–160.

[45] M. M. Kamel, H. I. Ali, M. M. Anwar, N. A. Mohamed, A. M. M. Soliman, *Eur. J. Med. Chem.* **2010**, *45*, 572–580.

[46] G. Xiong, Z. Wu, J. Yi, L. Fu, Z. Yang, C. Hsieh, M. Yin, X. Zeng, C. Wu, A. Lu, X. Chen, T. Hou, D. Cao, *Nucleic Acids Res.* **2021**, *49*, 5–14.

5A.9. Selected IR, NMR (^{1}H and ^{13}C) and Mass spectra

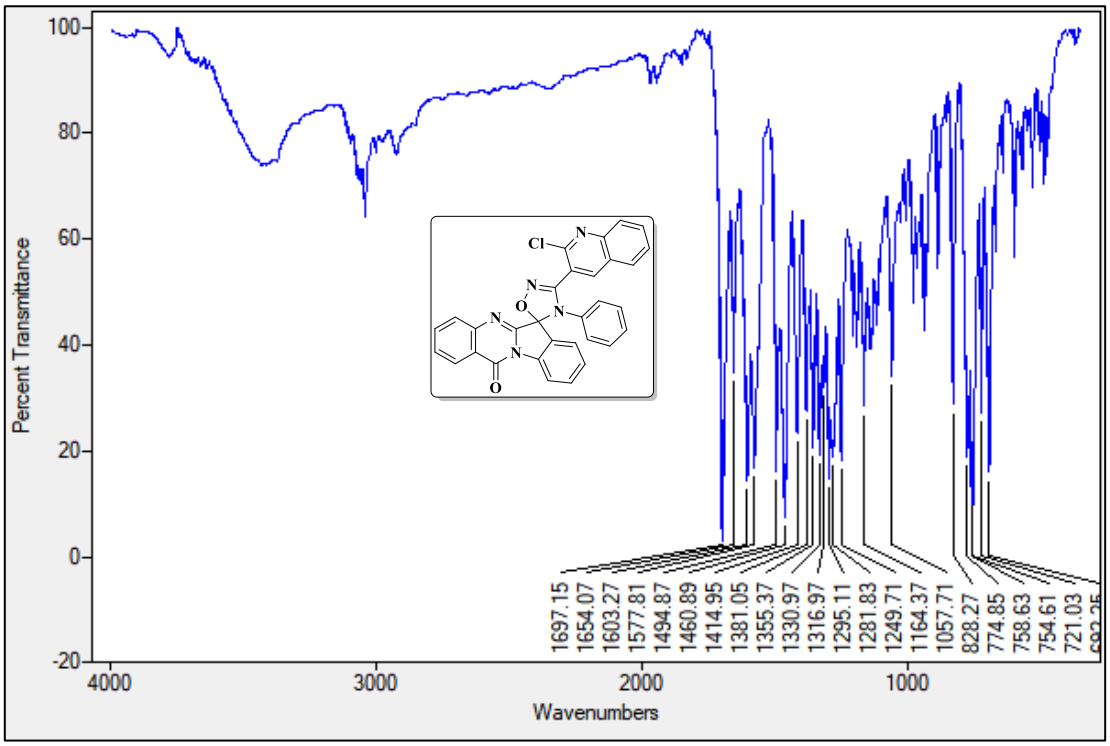

IR spectrum of the compound **3a**

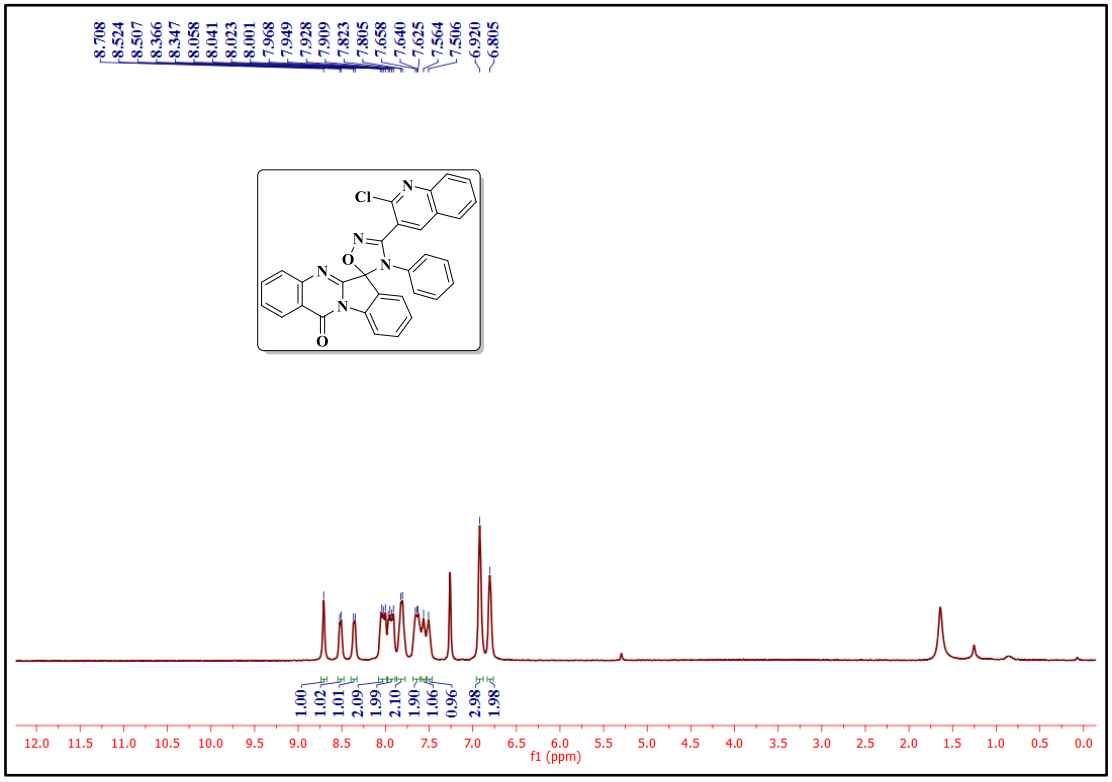

^{1}H NMR spectrum of the compound **3a**

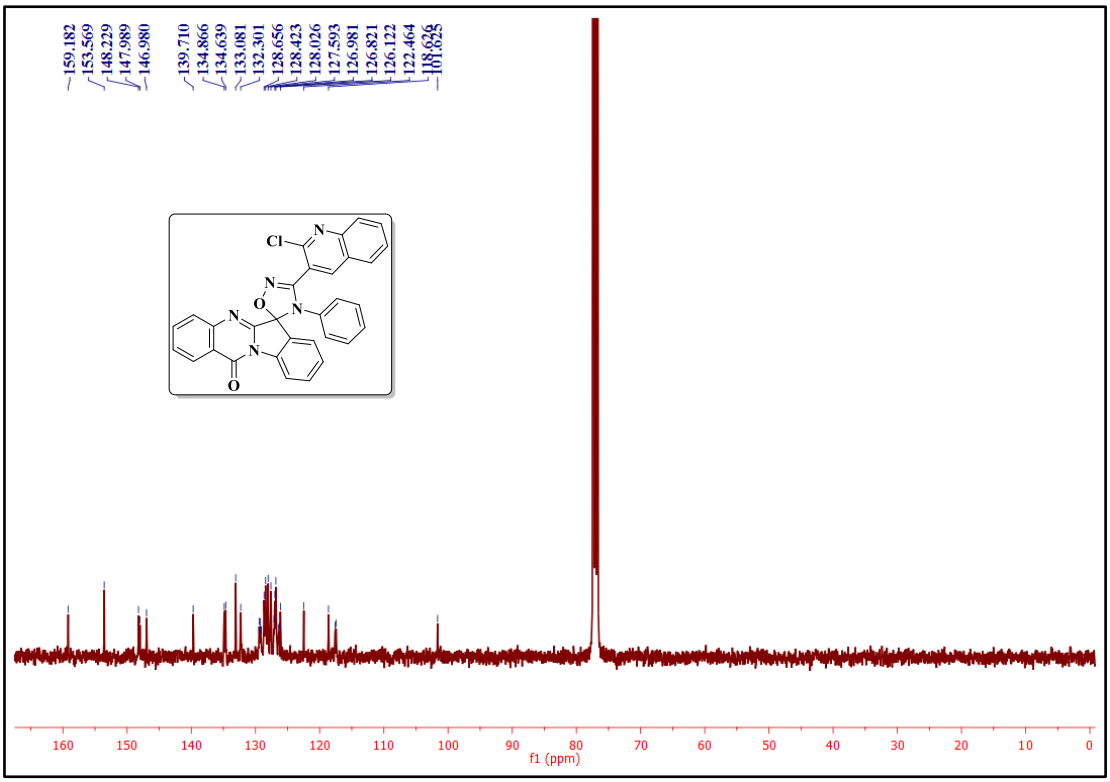

^{13}C NMR spectrum of the compound **3a**

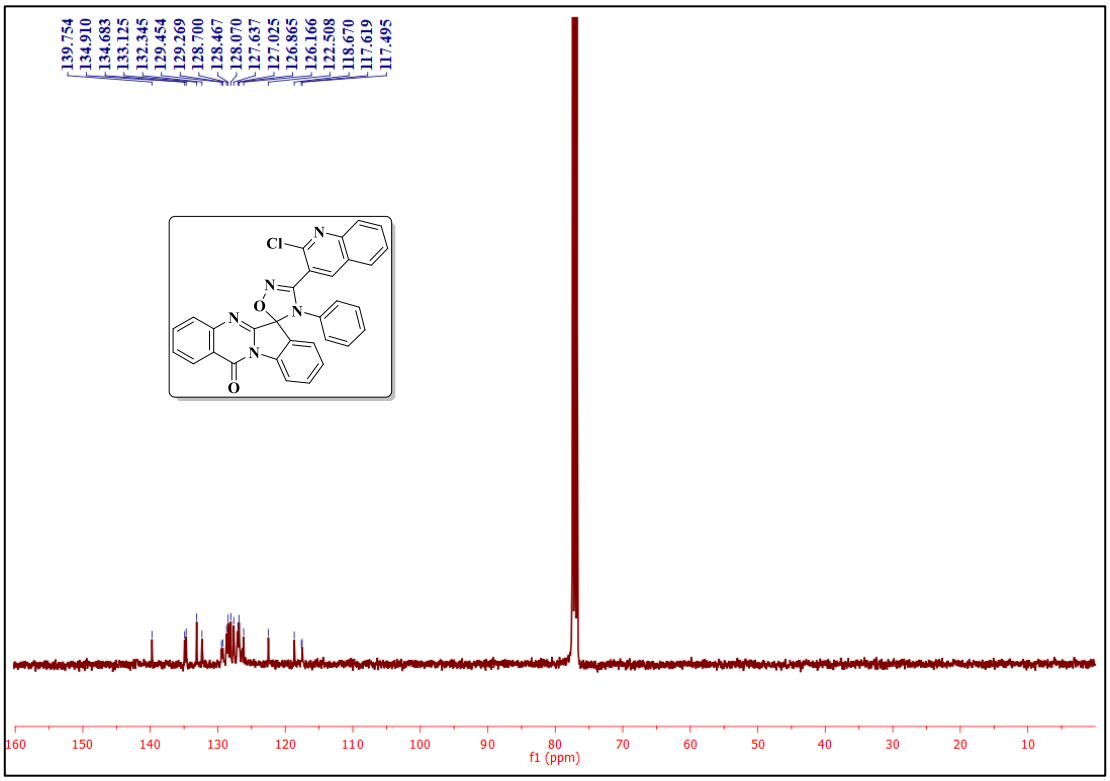

DEPT-135 NMR spectrum of the compound **3a**

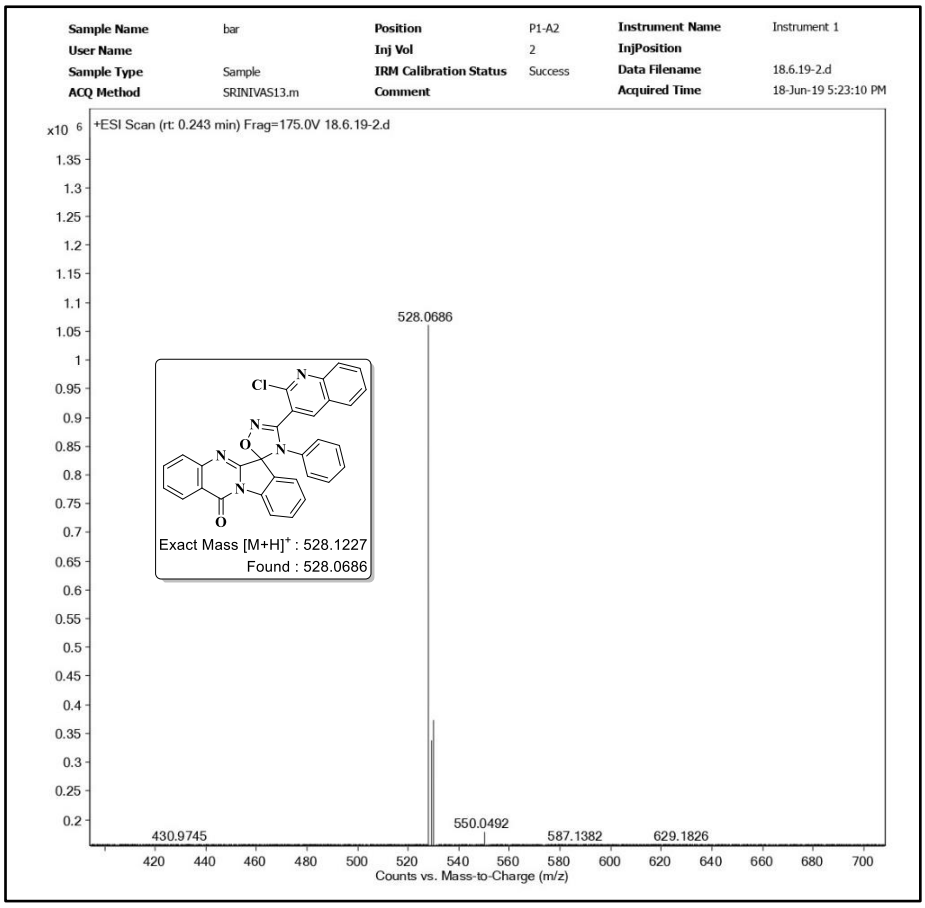

Mass spectrum of the compound **3a**

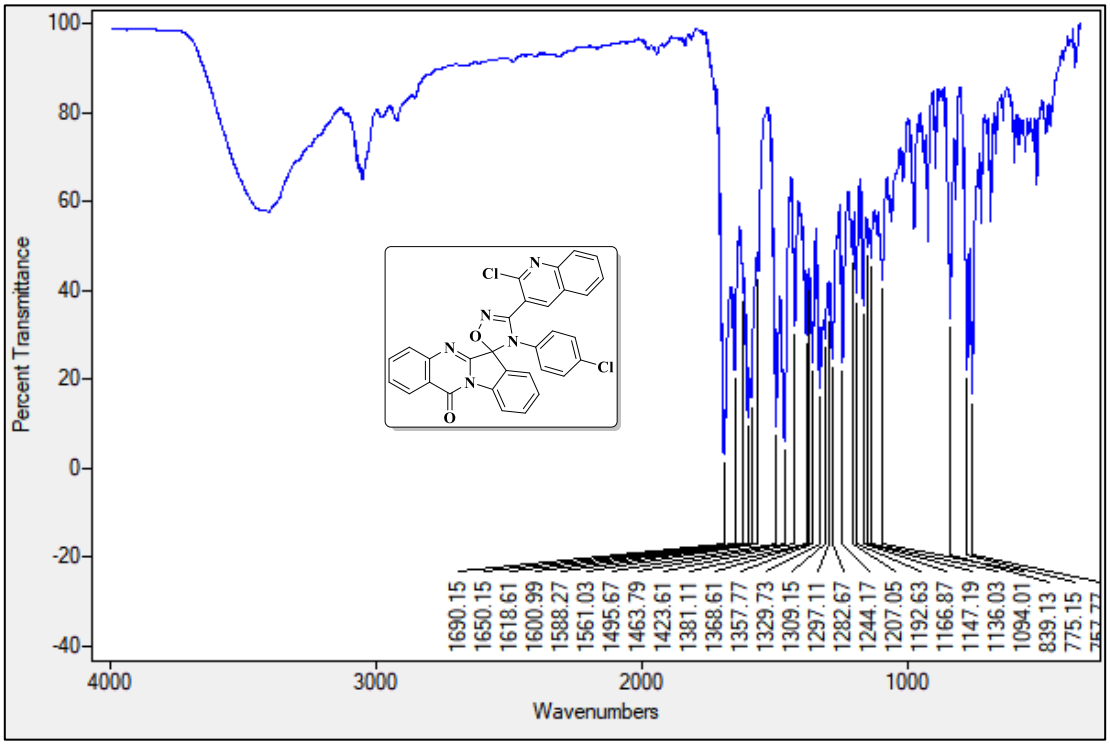

IR spectrum of the compound **3f**

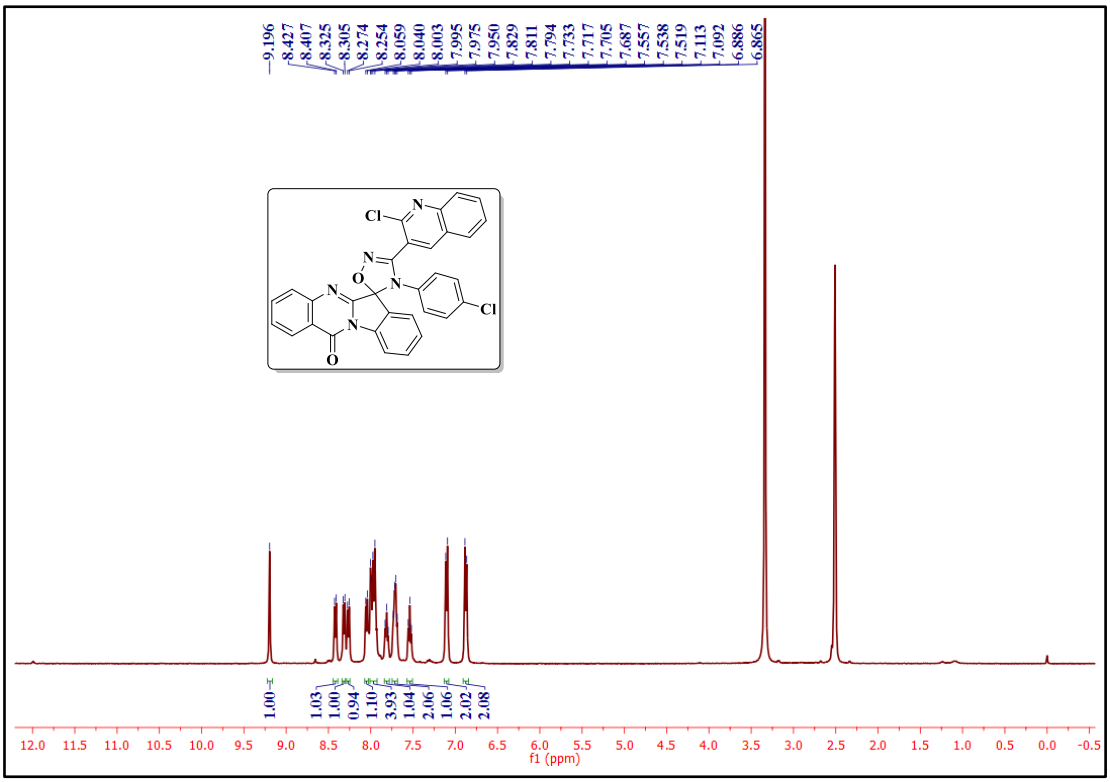

^{1}H NMR spectrum of the compound **3f**

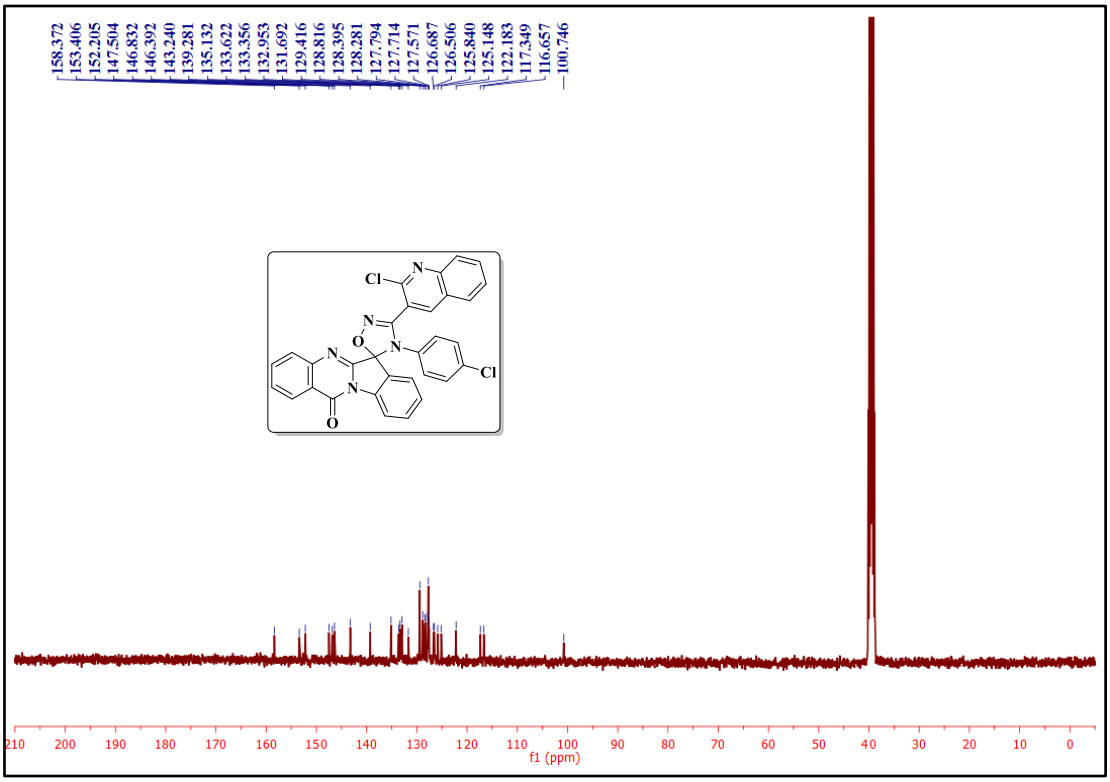

^{13}C NMR spectrum of the compound **3f**

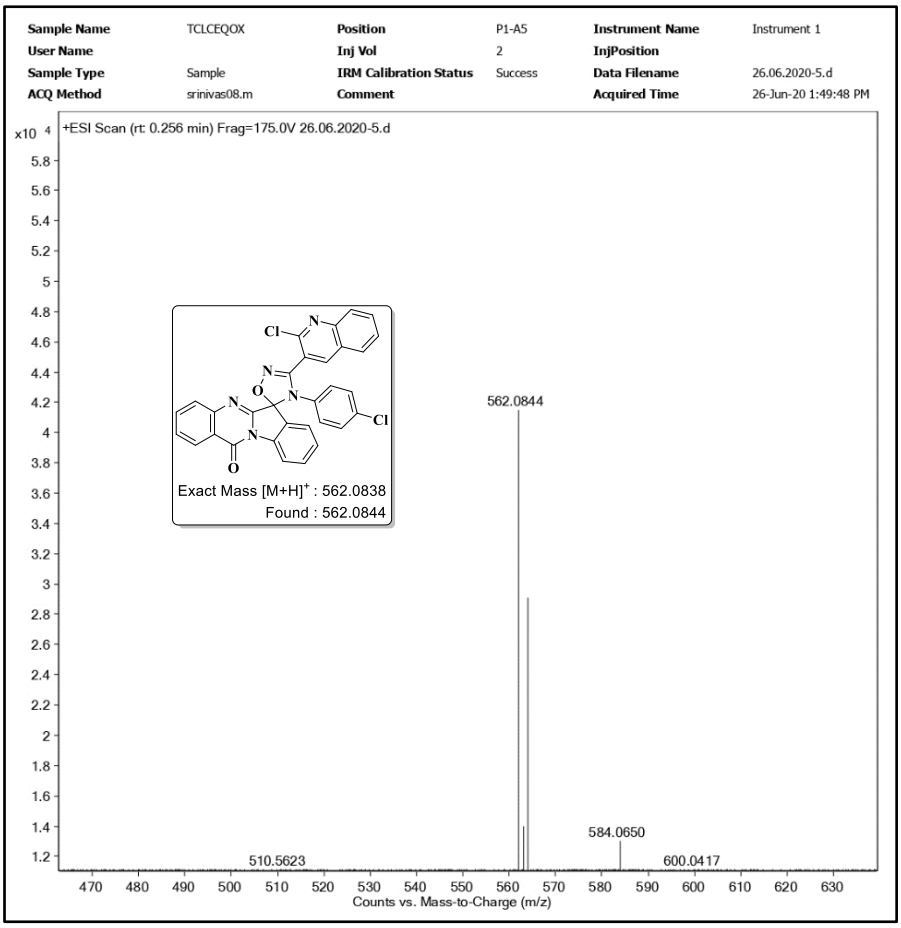

Mass spectrum of the compound **3f**

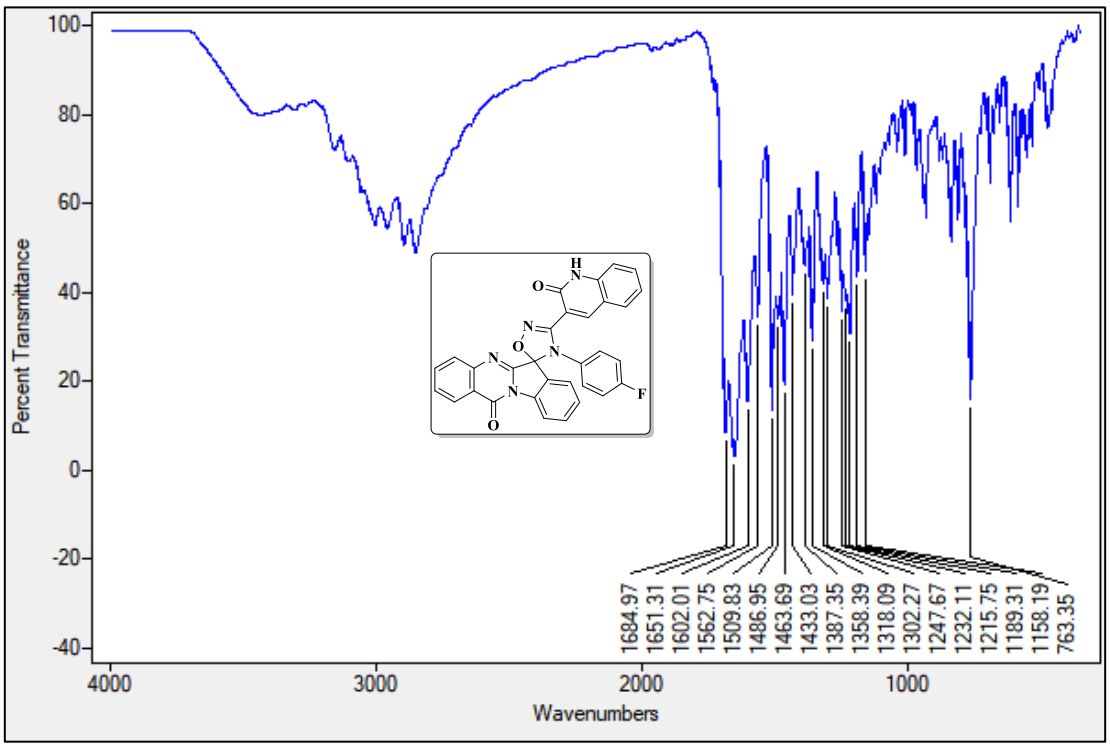

IR spectrum of the compound **3m**

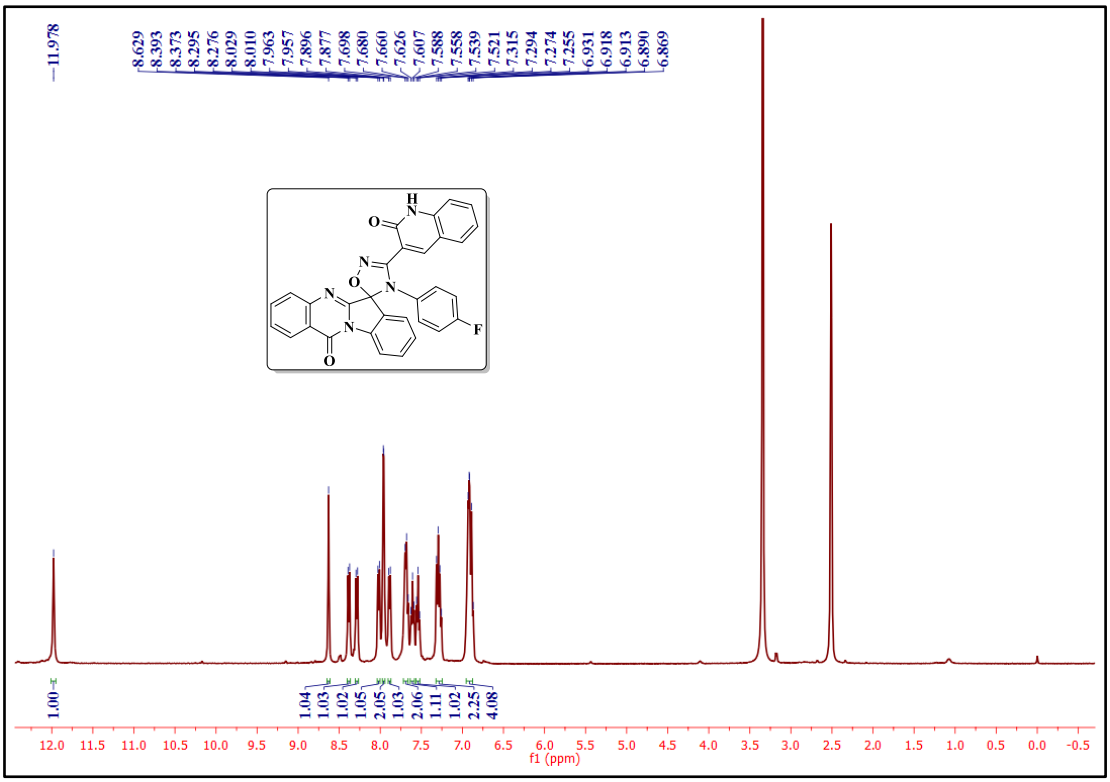

^{1}H NMR spectrum of the compound **3m**

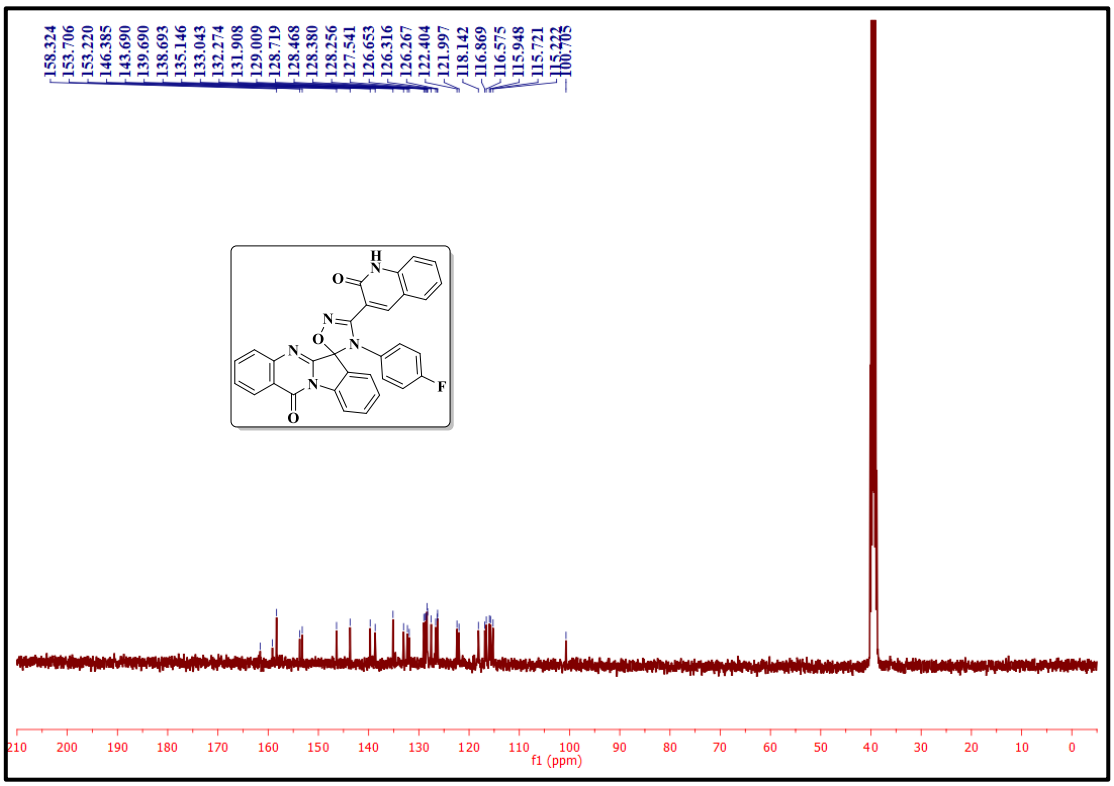

^{13}C NMR spectrum of the compound **3m**

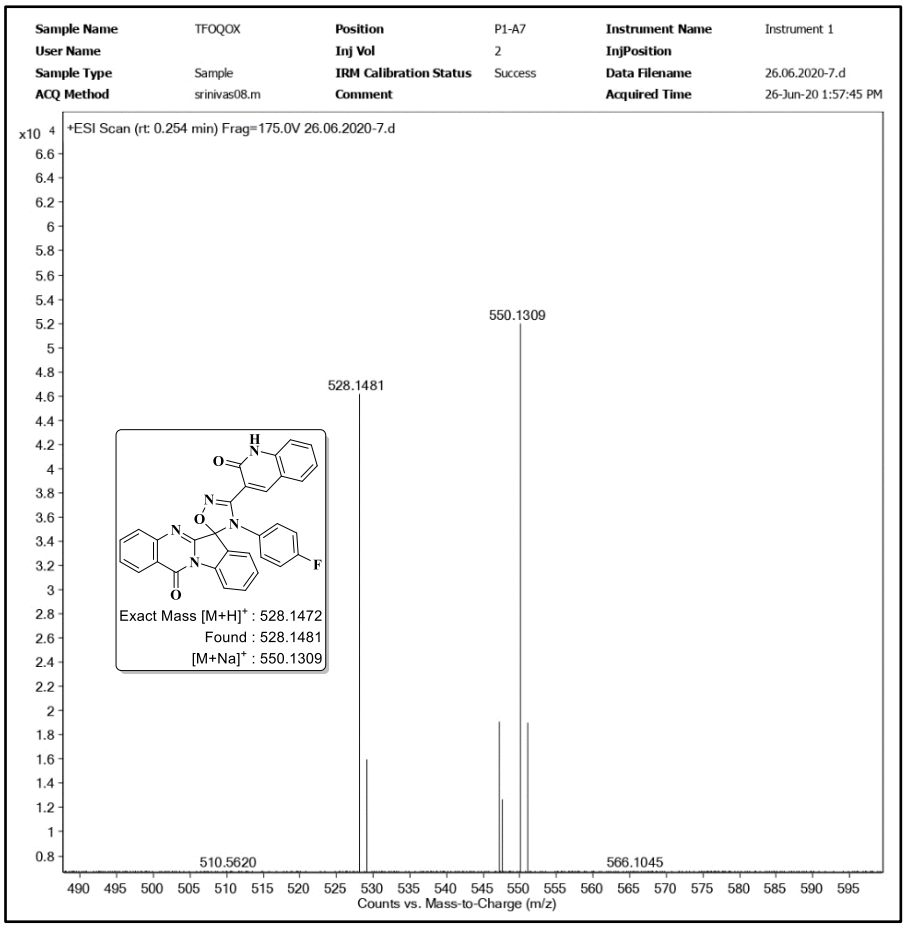

Mass spectrum of the compound **3m**

CHAPTER-V
Section-B

One-pot multicomponent synthesis of novel quinazolinone based spirocyclopropane hybrids and their *in silico* molecular docking studies

5B.1. Introduction

The construction of spirocyclopropanes with inherent three dimensional rigidity and unique metabolic stability has received great attention in organic and medicinal chemistry [1]. Spirocyclopropane moiety is found to be an important scaffold of many synthetic as well as natural products of biological interest [2,3]. spirocyclopropanes have been used as diverse pharmaceutical drugs such as anti-cancer agents [4], HIV inhibitors [5], kinase inhibitors [6], and anti-obesity agents [7]. For instance, the natural product ptaquiloside **A** (Figure 5B.1) exhibits anti-cancer activity [8]. Spirocyclopropane linked oxindoles **B** and **C** (Figure 5B.1) have been found as potent anti-cancer and HIV-1 inhibitors [9,10]. Also, spirocyclopropane linked pyrazolone **D** (Figure 5B.1) exhibits anti-fungal activity [11]. Whereas, the compound **E** (Figure 5B.1) acts as progesterone antagonist [12]. Naturally occurring hapalindolinone **F** (Figure 5B.1) is reported as vasopressin antagonist [13], and also the compound **G** in Figure 5B.1 (CFI-400945) is an orally available PLK4 inhibitor for the treatment of cancer [14].

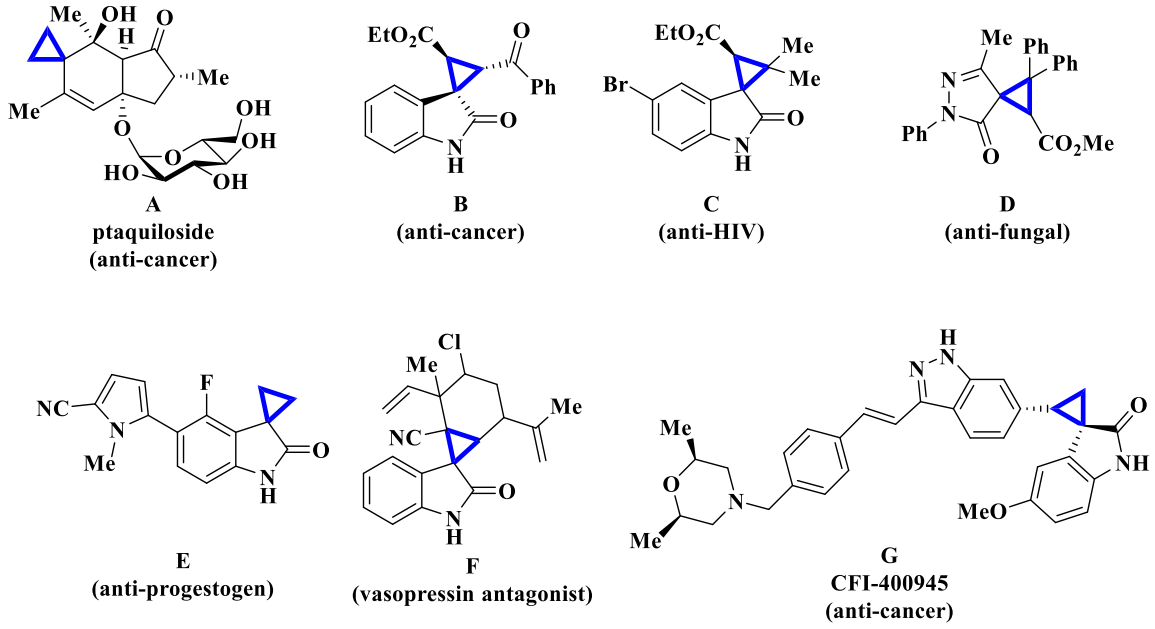

Figure 5B.1. Biologically potent drugs having spirocyclopropane moiety.

In addition to their medicinal importance, they have also got lot of interest in functional materials [15], and also serve as key precursors in synthetic organic chemistry [16]. The structural and biological importance of these moieties promoted the development of numerous methodologies, including Simmons-Smith type reactions [17], Michael initiated ring closure [18], Corey-Chaykovsky reaction with sulfonium ylides [19] and with diazo compounds.

On the other hand, quinazolinone forms a main group of nitrogen heterocycles exhibit broad spectrum of biological applications such as anti-cancer [20], anti-bacterial [21], anti-inflammatory [22], anti-tubercular [23] etc. Nevertheless, multicomponent reactions (MCRs) are considered to be most efficient strategies for the generation of drug like complex molecules without isolating the intermediates [24,25]. Among these, [3+2] cycloaddition MCRs has been extensively used for the synthesis of nitrogen heterocycles [26].

5B.1.1. Reported methods for the preparation of spirocyclopropanes

Chen and co-workers described a novel Michael/alkylation cascade reaction of 3-bromooxindoles with α,β-unsaturated acyl phosphonates for the construction of spirocyclopropyl oxindoles (Scheme 5B.1). In this reaction DABCO wielding as a robust catalyst and the synthetic methodology has applicable for the generation of a high active non-nucleoside reverse transcriptase (NNRT1) inhibitors against HIV-1 [27].

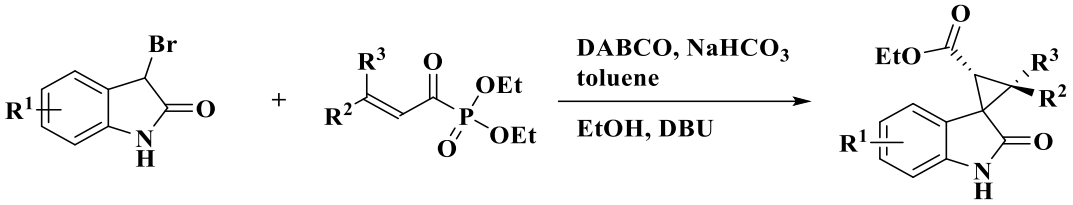

Scheme 5B.1

Mei et al. reported a highly efficient asymmetric ring-opening/cyclopropanation reaction of 3-(oxyethylidene)-2-oxoindolines with cyclic sulfur ylides for the synthesis of sulfur-containing spirocyclopropyl oxindoles (Scheme 5B.2). The reaction offered an efficient method to produce numerous chiral sulfur-containing compounds having vicinal tertiary or quaternary carbon chiral centers [28].

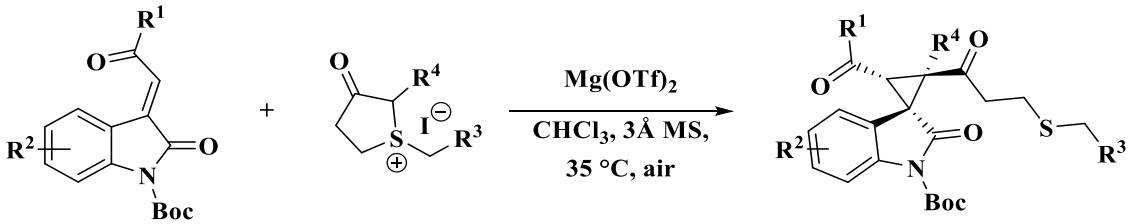

Scheme 5B.2

Wang et al. described a new enantioselective cyclopropanation of 3-alkenyl-oxindoles with sulfoxonium ylides by utilizing a chiral *N,N'*-dioxide/$Mg(OTf)_2$ complex as the catalyst (Scheme 5B.3). In this reaction the corresponding chiral spirocyclopropyl oxindoles having three continuous chiral carbon centres were obtained in good yields [29].

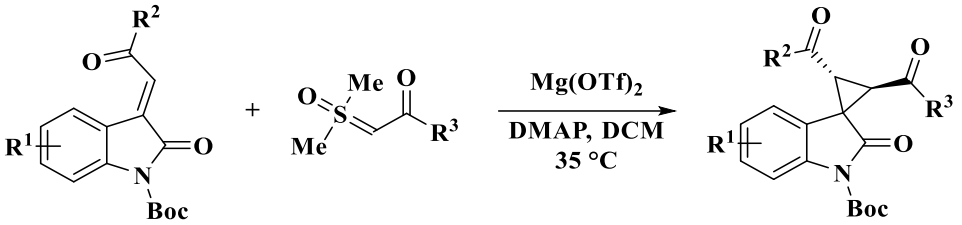

Scheme 5B.3

You and co-workers presented an efficient and divergent synthesis of spirocyclopropyl oxindoles *via* controllable reaction of isatin-derived para-quinone methides with sulfur ylides without a catalyst and an additive (Scheme 5B.4) [30].

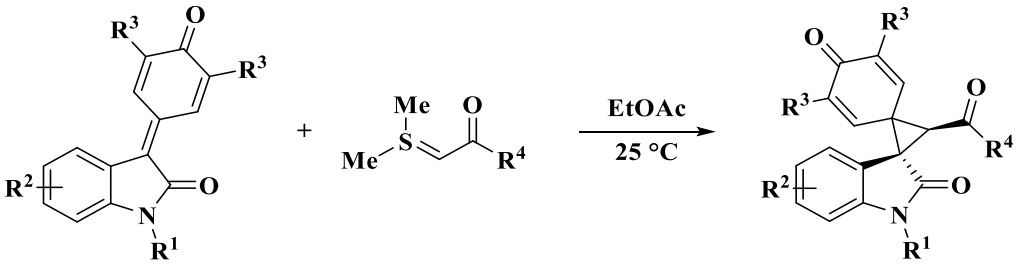

Scheme 5B.4

Su and co-workers developed sulfide catalyzed diastereoselective spirocyclopropanation reaction for the generation of spirocyclopropanyl-pyrazolones through [2+1] annulation (Scheme 5B.5). High diastereoselectivity, short reaction times and broad substrate scope are the main advantages of this methodology [31].

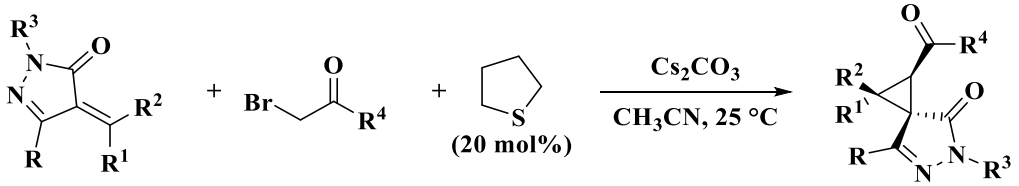

Scheme 5B.5

Li et al. employed an efficient synthesis of spirocyclopropanes *via* a multicomponent reaction of aldehydes, Meldrum's acid and sulfoxonium ylides (Scheme 5B.6). In this reaction both aryl and alkyl aldehydes were well tolerated to produce broad range of cyclopropanes in good yields [32].

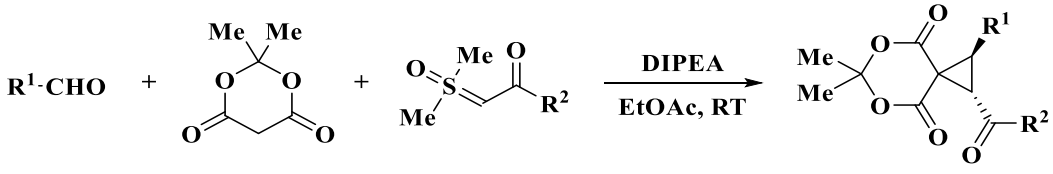

Scheme 5B.6

Liu et al. demonstrated a highly efficient and metal free tandem annulation approach for the synthesis of novel spirocyclopropyl fused pyrazolinones from pyrazole ketones and two component sulfur ylides in an acidic medium (Scheme 5B.7) [33].

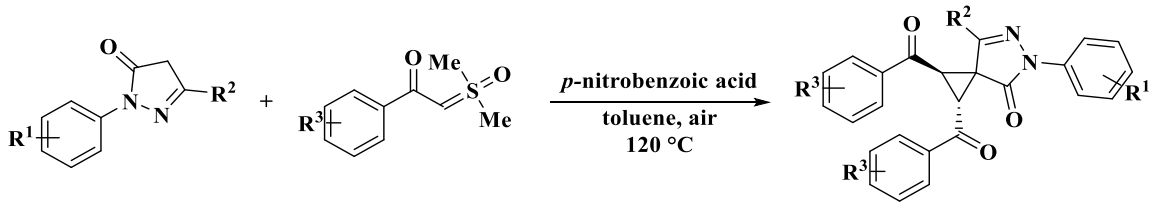

Scheme 5B.7

Fang et al. displayed a base mediated [2+1] cycloaddition reaction for the regio- and diastereo-selective spirocyclopropanation of benzofuran derived azadienes *via* 1,4-addition/dearomatization under mild reaction conditions (Scheme 5B.8) [34].

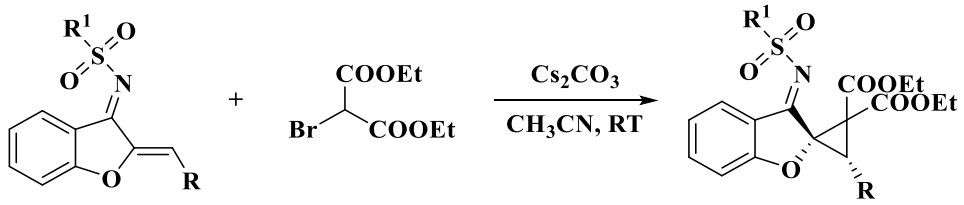

Scheme 5B.8

Zhao et al. developed a Michael/alkylation cascade reaction for the generation of nitro-spirocyclopropanes by using arylenechromanone and bromonitroalkane as reactants (Scheme 5B.9). This reaction produces broad range of spirocyclopropanes containing three adjacent stereogenic centers [35].

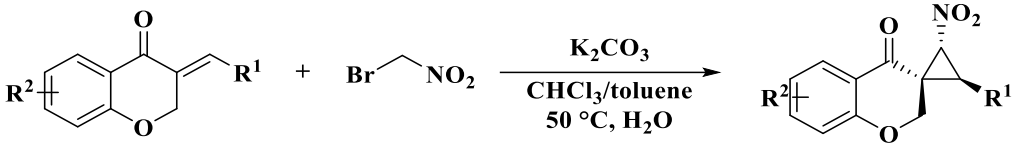

Scheme 5B.9

5B.2. Present work

In view of the aforementioned literature reports and considering the importance of spirocyclopropane moiety, herein we report an efficient three-component reaction of aldehydes **1a-i**, tosylhydrazine **2** and quinazolinyl chalcones **3a-c** for the construction of spirocyclopropane-indoloquinazolinones through [3+2] cycloaddition strategy (Scheme 5B.10). In addition, all the synthesized compounds were evaluated their *in silico* molecular docking and ADME prediction.

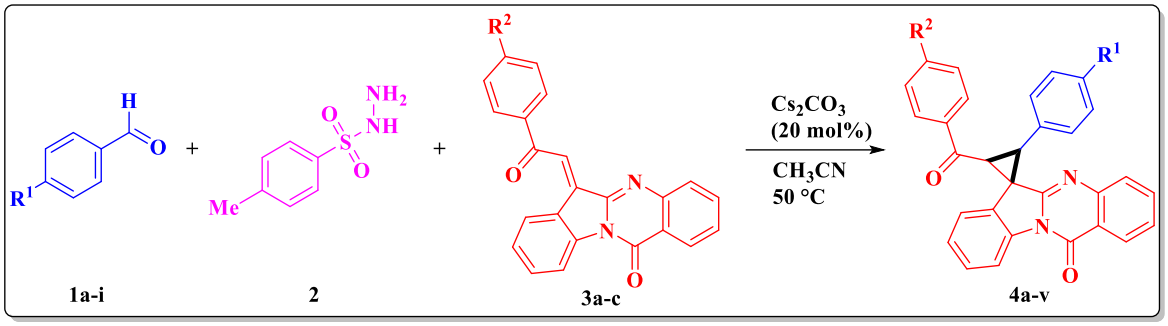

Scheme 5B.10. Synthesis of quinazolinone based spirocyclopropanes **4a-v**.

5B.2.1. Results and discussion

We began our study by choosing benzaldehyde **1a** (1.0 mmol), tosylhydrazine **2** and 6-(2-(4-methoxyphenyl)-2-oxoethylidene)indolo[2,1-*b*]quinazolin-12(6*H*)-one **3a** (1.0 mmol) as initial starting materials and investigating the effect of solvents and bases on the product yield (Table 5B.1). When the reaction was performed in methanol under reflux without any base, the target spirocyclopropane product **4a** was obtained in 12% yield (Table 5B.1, entry 1). However, a significant improvement in the yield (40%) was observed in the presence of Cs_2CO_3 (20 mol%) in methanol (Table 5B.1, entry 2). Later, we tried to explore the reaction in different solvents such as EtOH, CH_3CN, DMF and DMSO (Table 5B.1, entries 3-6). Among all CH_3CN is the best solvent for this cascade reaction (Table 5B.1, entry 4). We further conducted the reaction in different temperatures (Table 5B.1, entries 7,8) and found that 50 °C was the efficient temperature to give the desired product **4a**. Encouraged by these results, other bases such as K_2CO_3, DABCO, DMAP and Et_3N in CH_3CN were explored (Table 5B.1, entries 9-12), but could not get the satisfactory results. Next, we screened different amounts of Cs_2CO_3 and found that the yield of the product decreased slightly when the weight of Cs_2CO_3 was 10 mol% and 30 mol% (Table 5B.1, entries 13,14). From these results, the optimal reaction condition for the preparation of desired product **4a** was determined to be Cs_2CO_3 (20 mol%) in CH_3CN at 50 °C (Table 5B.1, entry 7).

Table 5B.1. Optimization of the reaction conditions[a]

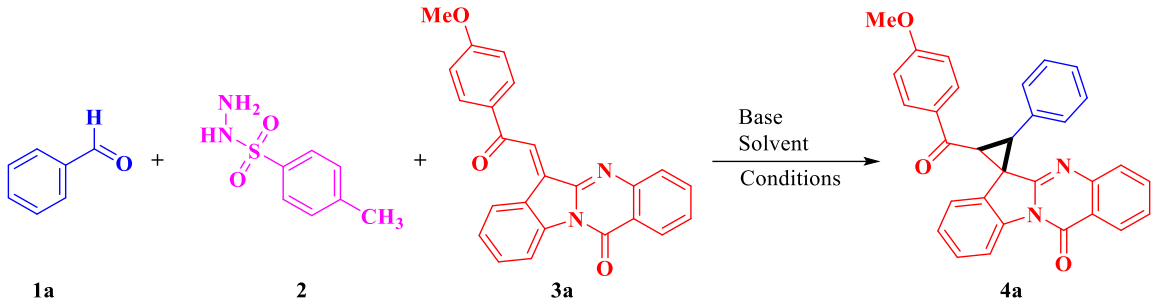

1a 2 3a 4a

Entry	Base (20 mol%)	Solvent	Temp (°C)	Time (h)	Yield (%)[b]
1	-	MeOH	Reflux	24	12
2	Cs_2CO_3	MeOH	Reflux	8	40
3	Cs_2CO_3	EtOH	Reflux	8	50
4	Cs_2CO_3	CH_3CN	Reflux	3	80
5	Cs_2CO_3	DMF	100	5	72
6	Cs_2CO_3	DMSO	100	5	70
7	**Cs_2CO_3**	**CH_3CN**	**50**	**2.5**	**83**
8	Cs_2CO_3	CH_3CN	RT	8	62
9	K_2CO_3	CH_3CN	50	4	75
10	DABCO	CH_3CN	50	4	60
11	DMAP	CH_3CN	50	6	55
12	Et_3N	CH_3CN	50	6	50
13[c]	Cs_2CO_3	CH_3CN	50	3	75
14[d]	Cs_2CO_3	CH_3CN	50	3	80

[a]Reaction condition: benzaldehyde **1a** (1.0 mmol), tosylhydrazine **2** (1.0 mmol), compound **3a** (1.0 mmol), and base (20 mol%) in solvent (3 mL). [b]Isolated yields. [c]10 mol% of base was used. [d]30 mol% of base was used. RT = room temperature.

Under the optimal reaction conditions, the substrate scope of this protocol was investigated with various benzaldehydes **1a-i** (Table 5B.2). Different substituted aromatic benzaldehydes were well tolerated and provided the targeted compounds **4a-v** in good yields. The benzene ring bearing a methyl (–Me) group at *para*-position react smoothly under optimized conditions afford the target product in high yield. The aromatic ring having electron donating (–OMe) group regardless of substituted positions (*meta*- or *para*-) were produced the corresponding products in good yield. The phenyl group having halogens (–F, –Cl, –Br) either at *para*-position or at the *ortho*-position (–Cl) afforded the

corresponding products in good yields. In addition, presence of electron withdrawing group (–CN) had also no substantial impact on the product yield.

Table 5B.2. Synthesis of quinazolinone based spirocyclopropanes **4a-v**[a,b]

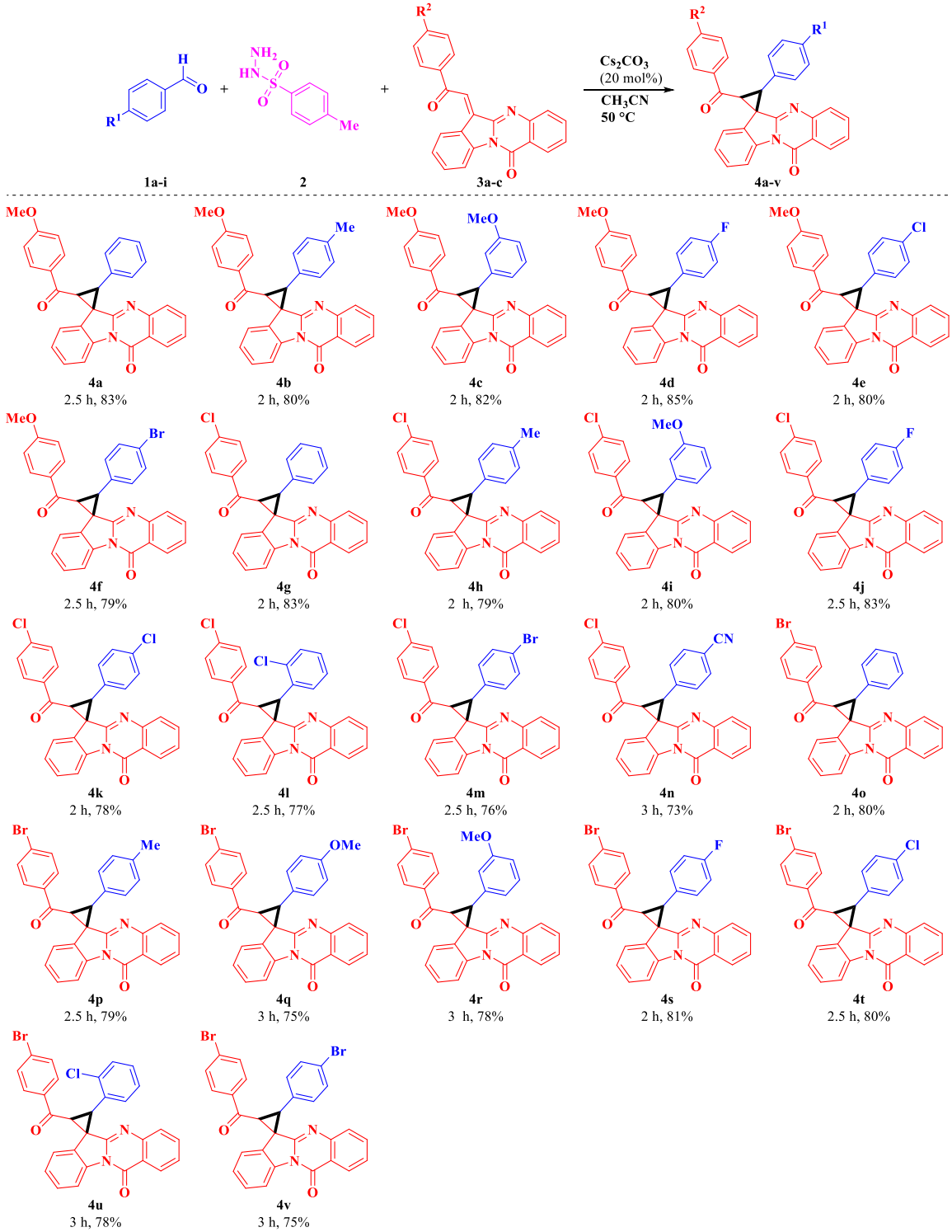

[a]Reaction condition: aldehydes **1a-i** (1.0 mmol), tosylhydrazine **2** (1.0 mmol), chalcones **3a-c** (1.0 mmol) and Cs_2CO_3 (20 mol%) in 3 mL of CH_3CN at 50 °C. [b]Isolated yields.

The plausible reaction mechanism for the generation of target compounds **4a-v** was depicted in Scheme 5B.11. Initially, benzaldehyde **1a** on reaction with tosylhydrazine **2** produces the tosylhydrazone **A.** Then, the intermediate **B** is generated from tosylhydrazone **A** by treating with Cs_2CO_3. The *in situ* generated intermediate **C** (from **B**) undergoes [3+2] cycloaddition reaction with compound **3a** followed by the subsequent loss of nitrogen affords the target compound **4a**.

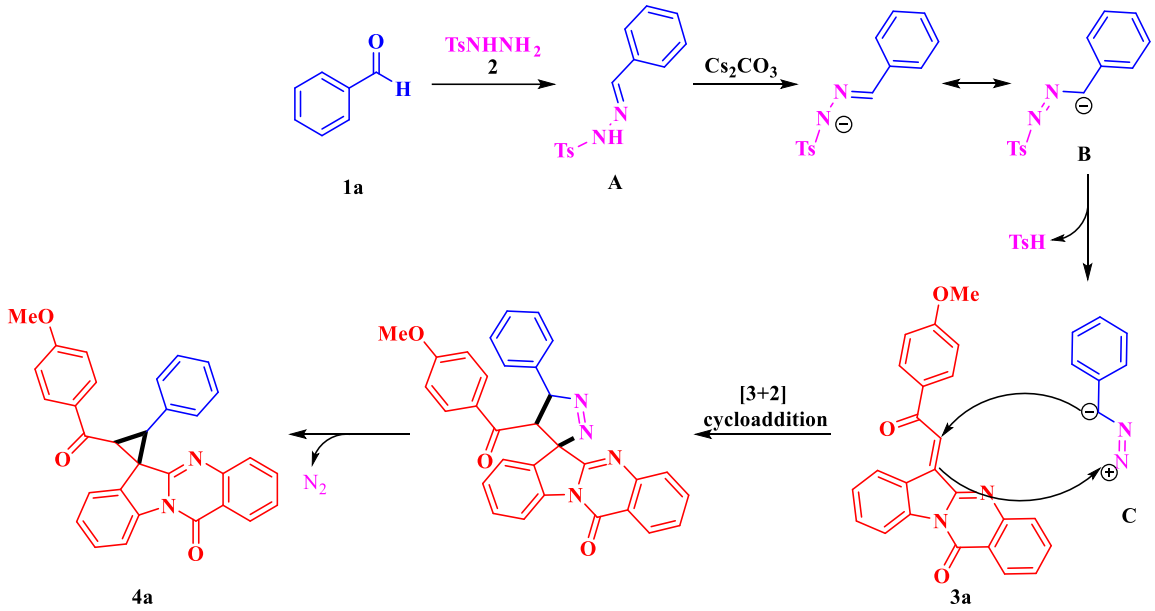

Scheme 5B.11. Plausible reaction pathway for the generation of target compounds **4**.

The structure of the target compounds (**4a-v**) were analyzed by IR, ^{1}H NMR, ^{13}C NMR and mass spectral data. In this, the IR spectrum of compound **4j** shows the bands at 1680 cm^{-1} and 1637 cm^{-1} represents the benzoyl carbonyl group and quinazolinone carbonyl group respectively [36,37]. The ^{1}H NMR spectrum of the compound **4j** showed two signals at δ 4.74 *ppm* and δ 4.30 *ppm* corresponds to the two C–H protons of spirocyclopropane moiety. In the ^{13}C NMR spectrum the peak appeared at δ 40.63 *ppm* corresponds the spiro carbon, which was further determined by the absence of this spiro carbon peak in DEPT-135 NMR spectrum (**4a**). The mass spectrum of compound **4j** displayed a molecular ion peak at *m/z* 493.17 $[M+H]^+$. Furthermore, the regiochemistry of the target compounds were determined by SCXRD method (**4j**, **4p** and **4s**). The ORTEP representation of the compounds **4j**, **4p** and **4s** have shown in Figures 5B.2, 5B.3 and 5B.4. The CCDC deposition numbers and salient features of crystallographic information of **4j**, **4p** and **4s** have shown in Table 5B.3.

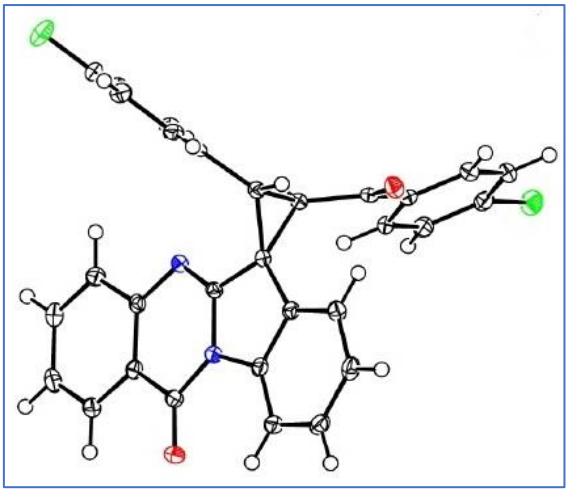

Figure 5B.2. ORTEP representation of **4j** and the thermal ellipsoids are drawn at 50% probability level.

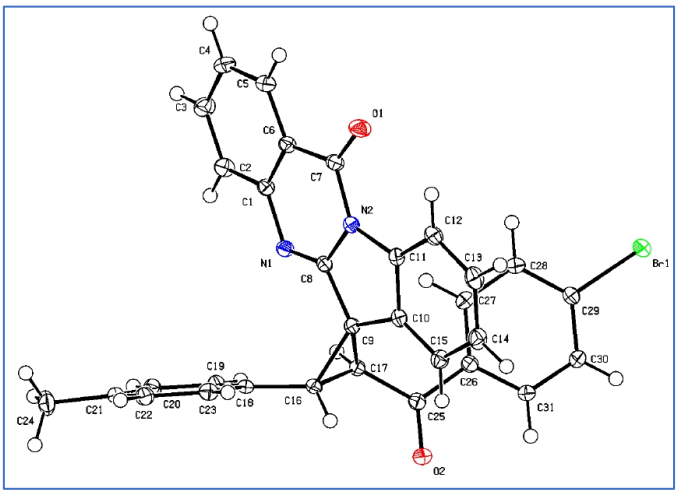

Figure 5B.3. ORTEP representation of **4p** and the thermal ellipsoids are drawn at 50% probability level.

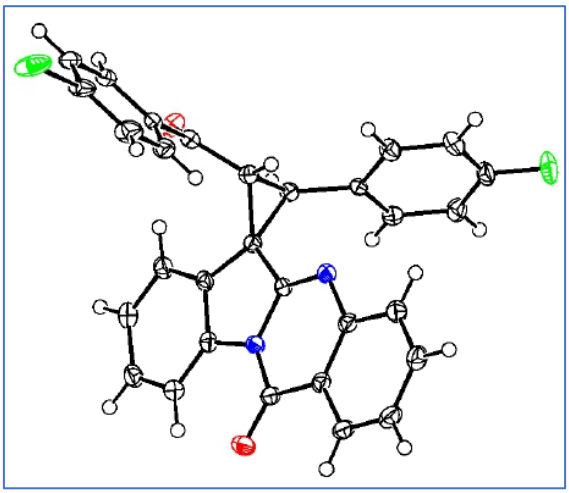

Figure 5B.4. ORTEP representation of **4s** and the thermal ellipsoids are drawn at 50% probability level.

Table 5B.3. Crystallographic data and refinement parameters of compounds **4j**, **4p** and **4s**

Identification code	**4j**	**4p**	**4s**
Empirical formula	$C_{30}H_{18}ClFN_2O_2$	$C_{31}H_{21}BrN_2O_2$	$C_{30}H_{18}BrFN_2O_2$
Formula weight	492.1041	532.0786	536.0536
Crystal system	Triclinic	Triclinic	Triclinic
Space group	*P*-1	*P*-1	*P*-1
T (K)	100	100	100
a (Å)	12.0460(15)	8.9166(16)	12.058(5)
b (Å)	14.3604(17)	10.0403(18)	14.560(5)
c (Å)	15.1144(18)	14.995(3)	15.168(4)
α (°)	106.245(4)	73.860(5)	107.431(10)
β (°)	108.930(4)	80.662(6)	107.212(14)
γ (°)	99.535(4)	66.181(5)	100.582(16)
Z	4	2	4
V (Å^3)	2277.8(5)	1177.8(4)	2316.1(14)
D_{calc} (g/cm^3)	1.437	1.504	1.541
F (000)	1016.0	544.0	1088.0
μ (mm^{-1})	0.209	1.779	1.815
Θ (°)	26.998	26.999	27.000
Index ranges	-15 ≤ h ≤ 15 -18 ≤ k ≤ 18 -19 ≤ l ≤ 19	-11 ≤ h ≤ 11 -12 ≤ k ≤ 12 -19 ≤ l ≤ 19	-15 ≤ h ≤ 15 -18 ≤ k ≤ 18 -19 ≤ l ≤ 19
N-total	9967	5146	10127
Parameters	650	327	650
R_1 *[I > 2 σ (I)]*	0.0468	0.0271	0.0420
wR_2 (all data)	0.1208(9961)	0.0963(5053)	0.1168(10110)
GOF	1.132	1.353	1.225
CCDC	2131180	2131181	2131182

5B.3. Molecular docking studies

Molecular docking is an essential tool employed in the study of binding interactions between target proteins and ligands. It is proficient in the virtual screening of drug like compounds and determining the ligand's binding conformations and affinities to the protein, thereby resulting in the amelioration of drug development research [38]. Three *Mycobacterium tuberculosis* proteins PDB ID: 1DF7, 1P44 and 4TZK were taken as target proteins for molecular docking study of the synthesized compounds to rationalize their anti-tubercular property. The outcome of the molecular docking study revealed that all the synthesized compounds were successfully docked, and efficiently fit into the active sites of the proteins. The results of the molecular docking study were presented in Table 5B.4. Among all the screened compounds, the compounds **4i** and **4r** showed more negative binding energies. The compound **4i** displayed better binding energy (-11.48 kcal/mol) with two hydrogen bond interactions to the active site of 1DF7, displayed the negative binding

energy (-10.99 kcal/mol) to the active site of 1P44, and also exhibited -10.69 kcal/mol binding energy with four hydrogen bond interactions to the protein 4TZK. The binding interactions were depicted in Figure 5B.5a, b and c. Likewise, the compound **4r** interacts with binding site of 1DF7 (-11.59 kcal/mol) with three hydrogen bonds. However, **4r** displayed more negative binding energy (-11.03 kcal/mol) with two hydrogen bond interactions to the protein 1P44, and also exhibited better binding energy (-10.65 kcal/mol) with four hydrogen bonds to the active site of 4TZK as depicted in Figure 5B.6a, b and c. Whereas, the compounds **4l**, **4m**, **4n**, **4u** and **4v** exhibits good binding energies -11.32, -11.35, -11.32, -11.37 and -11.46 respectively with the protein 1DF7. From these results, it is revealed that all the synthesized compounds exhibit better binding energies (-8.56 to -11.59 kcal/mol) than the standard drug isoniazid, and may serve as potential anti-tubercular leads.

Table 5B.4. Docking results of the title compounds **4a-v** against target proteins

Entry	1DF7		1P44		4TZK	
	Binding energy (kcal/mol)	**No. of hydrogen bonds**	**Binding energy (kcal/mol)**	**No. of hydrogen bonds**	**Binding energy (kcal/mol)**	**No. of hydrogen bonds**
4a	-10.65	4	-10.06	4	-9.87	4
4b	-11.00	3	-10.33	5	-9.91	3
4c	-11.18	4	-10.20	3	-9.91	3
4d	-10.52	3	-9.62	1	-9.82	3
4e	-11.05	3	-9.71	2	-9.84	3
4f	-11.21	4	-9.63	3	-9.32	3
4g	-10.93	2	-8.56	0	-10.15	1
4h	-11.21	2	-10.49	0	-10.31	3
4i	**-11.48**	**2**	**-10.99**	**0**	**-10.69**	**4**
4j	-10.81	2	-10.40	1	-10.12	3
4k	-11.20	2	-10.65	0	-10.29	3
4l	-11.32	2	-10.12	1	-10.28	2
4m	-11.35	1	-10.78	2	-10.37	3
4n	-11.32	2	-10.93	2	-10.31	3
4o	-11.02	2	-10.66	1	-10.36	3
4p	-11.27	1	-10.76	1	-10.49	3
4q	-11.25	4	-10.96	2	-10.26	2
4r	**-11.59**	**3**	**-11.03**	**2**	**-10.65**	**4**
4s	-10.87	2	-10.68	2	-10.32	3
4t	-11.29	2	-10.92	0	-10.49	3
4u	-11.37	0	-11.07	1	-10.51	0
4v	-11.46	2	-11.04	0	-10.56	3
Isoni-azid	-5.23	5	-5.72	3	-5.58	4

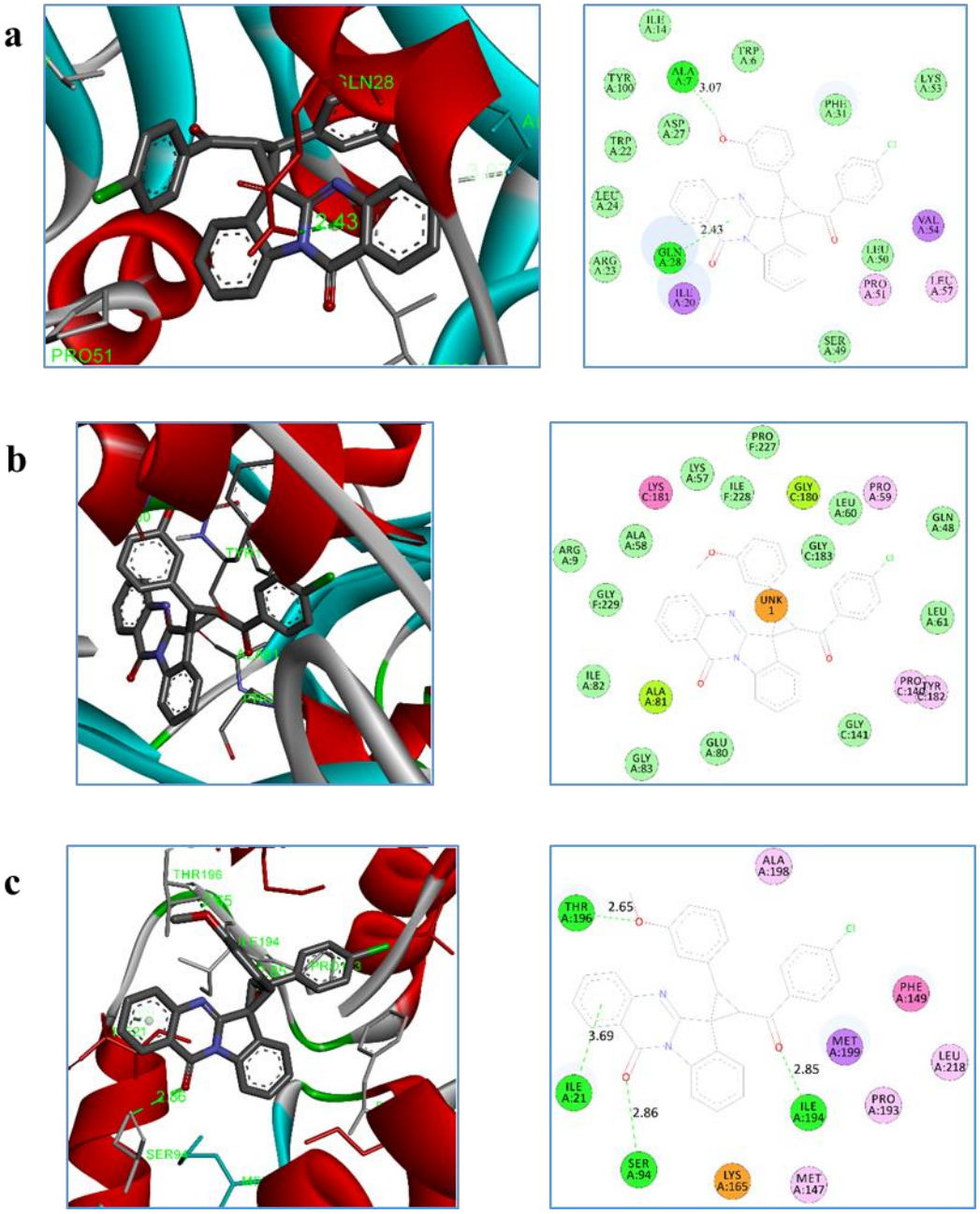

Figure 5B.5. 3D and 2D interaction poses of compound **4i** to the binding site residues of target proteins a) 1DF7; b) 1P44; c) 4TZK.

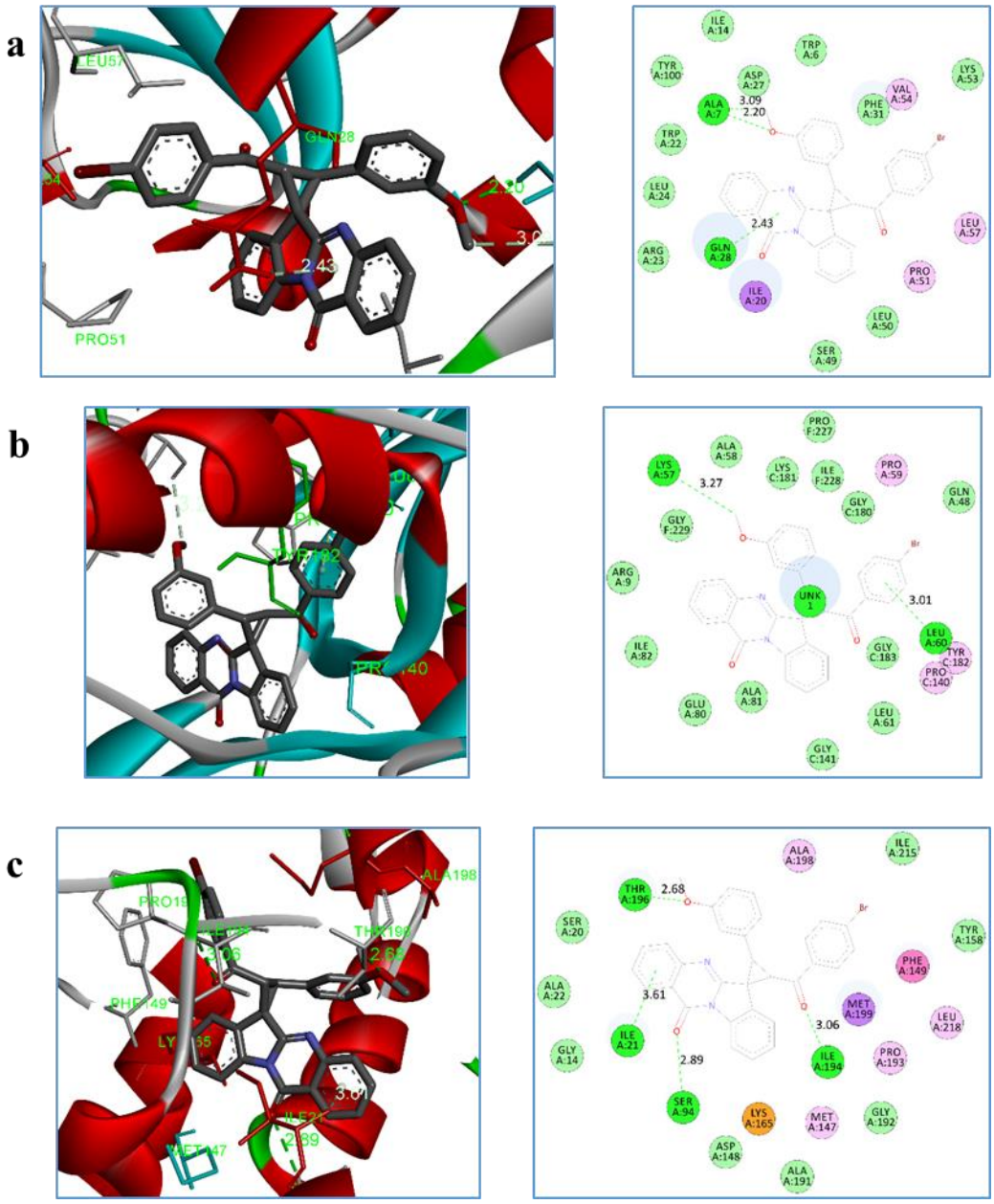

Figure 5B.6. 3D and 2D interaction poses of compound **4r** to the binding site residues of target proteins a) 1DF7; b) 1P44; c) 4TZK.

5B.4. ADME prediction

Absorption, distribution, metabolism and excretion (ADME) data improves the selection and identification of molecules at the therapeutic dose with an optimal safety profile. Also, *in silico* prediction of pharmacokinetic parameters lowers the risk of failure of drug at the final stages of clinical trials [39]. The ADME prediction of the synthesized compounds **4a-v** were illustrated in Table 5B.5.

Estimation of octanol/water partition coefficient (lipophilicity) is examined by LogP. The predicted lipophilicity values are in the ranging from 4.385 to 6.034, and these values revealed that moderate lipophilicity of the compounds. The predicted aqueous

solubility (LogS) values of the synthesized compounds ranging from -5.032 to -6.980, which reflects their moderate solubility in water due to presence of lipophilic groups. On the other hand, the topological polar surface area (TPSA) values reveals that the compounds' oral bioavailability is high. In general, higher the logarithm of the apparent permeability coefficient (logPapp) higher will be the Caco-2 permeability. From the results, it is predicted that all the compounds except **4c** and **4n** have shown high Caco-2 permeability in the range from 0.868 to 0.914. Interestingly, all the synthesized compounds exhibit high human intestinal absorption (HIA:100%). Blood/brain partition coefficient (logBB) value is a measure of the ability of a drug to cross the blood-brain barrier (BBB). The target compounds are in considerable range of BBB. The observed drug like properties and *in silico* ADME prediction suggests that the target compounds **4a-v** exhibit acceptable pharmacokinetic parameters and can be considered as lead molecules for the development of novel drugs.

Table 5B.5. Drug likeness and *in silico* ADME properties of the target compounds **4a-v**

Entry	**Mol. Wt**	**H-donor**	**H-acceptor**	**No. of rotatable bonds**	**LogP**	**LogS**	**TPSA (Å)**	**Caco-2 Permeability (logPapp in 10^{-6} cm/s)**	**HIA (% absorbed)**	**BBB permeability (log BB)**
	≤500	**≤5**	**≤10**	**≤10**	**≤5**	**<0.5**	**≤140**	**>8x10^{-6}**	**70 - 100%**	**-3.0 - 1.2**
4a	470.16	0	5	4	4.385	-6.154	61.19	0.885	100	-0.622
4b	484.17	0	5	4	4.918	-6.113	61.19	0.874	100	-0.634
4c	500.17	0	6	5	4.47	-5.250	70.42	0.365	100	-0.717
4d	488.15	0	5	4	4.558	-5.032	61.19	0.913	100	-0.773
4e	504.12	0	5	4	5.144	-6.031	61.19	0.872	100	-0.647
4f	548.07	0	5	4	5.310	-6.017	61.19	0.869	100	-0.648
4g	474.11	0	4	3	5.068	-6.980	51.96	0.886	100	-0.532
4h	488.13	0	4	3	5.572	-6.929	51.96	0.875	100	-0.544
4i	504.12	0	5	4	5.146	-6.109	61.19	0.887	100	-0.93
4j	492.10	0	4	3	5.226	-5.937	51.96	0.914	100	-0.683
4k	508.07	0	4	3	5.77	-6.813	51.96	0.873	100	-0.557
4l	508.07	0	4	3	5.615	-6.834	51.96	0.897	100	-0.488
4m	552.02	0	4	3	5.904	-6.793	51.96	0.871	100	-0.558
4n	499.11	0	5	3	4.757	-6.646	75.75	0.325	100	-0.623

4o	518.06	0	4	3	5.234	-6.963	51.96	0.884	100	-0.533
4p	532.08	0	4	3	5.713	-6.910	51.96	0.873	100	-0.545
4q	548.07	0	5	4	5.31	-5.822	61.19	0.878	100	-0.824
4r	548.07	0	5	4	5.318	-6.094	61.19	0.885	100	-0.932
4s	536.05	0	4	3	5.395	-5.924	51.96	0.912	100	-0.684
4t	552.02	0	4	3	5.904	-6.793	51.96	0.871	100	-0.558
4u	552.02	0	4	3	5.765	-6.814	51.96	0.895	100	-0.489
4v	595.97	0	4	3	6.034	-6.771	51.96	0.868	100	-0.559

MW: molecular weight; **H-donor**: number of hydrogen bond donors; **H-acceptor**: number of hydrogen bond acceptors; **LogP**: octanol/water partition coefficient; **LogS**: aqua solubility parameter; **TPSA**: topological polar surface area; **Caco-2**: cell permeability; **HIA**: human intestinal absorption; **LogBB**: blood/brain partition co-efficient.

5B.5. Conclusion

In this chapter, we have successfully established an efficient protocol for the synthesis of quinazolinone based spirocyclopropanes through [3+2] cycloaddition reaction of quinazolinone chalcones with tosylhydrazones. The advantages of this methodology are mild reaction conditions, easy operation and high tolerance of various functional groups on aromatic ring. Further, *in silico* Molecular docking study, ADME prediction and drug likeness profiles reveal that the title compounds represent a promising platform for the development of new therapeutic agents.

5B.6. Experimental Section

5B.6.1. General procedure for the generation of target compounds (4a-v)

In 3 mL of acetonitrile, aldehydes **1a-i** (1.0 mmol) and tosylhydrazine **2** (1.0 mmol) were added and stirred at room temperature for 10 min. To this quinazolinyl chalcones **3a-c** (1.0 mmol) and Cs_2CO_3 (20 mol%) were added and kept the reaction at 50 °C for appropriate time. After completion of the reaction (monitored by TLC), reaction mixture was concentrated under reduced pressure and the residue was chromatographed on silica gel (EtOAc/*n*-hexane 1:10-1:9) to afford the desired products **4a-v**.

5B.6.2. Molecular docking protocol

The docking studies are prominent tools for the assessment of the binding affinity to the ligand-protein receptor. All the synthesized compounds were subjected to *in silico* molecular docking studies by using the AutoDockTools (ADT) version 1.5.6 and AutoDock version 4.2.5.1 docking program [40]. The 3D-structures of all the synthesized

compounds were prepared by using chem3D pro 12.0 software. The optimized 3D structures were saved in pdb format. The structure of the dihydrofolate reductase of *Mycobacterium tuberculosis* (PDB code: 1DF7) protein and enoyl reductase proteins 1P44 and 4TZK were extracted from the protein data bank (http://www.rcsb.org/pdb). The bound ligand and water molecules in protein were removed by using Discovery Studio Visualizer version 4.0 to prepare the protein. Non polar hydrogens were merged and gasteiger charges were added to the protein. The grid file was saved in gpf format. The three dimensional grid box having dimensions 60 x 60 x 60 $Å^3$ was created around the protein with spacing 0.3750 Å. The genetic algorithm was carried out with the population size and the maximum number of evaluations were 150 and 25,00,000 respectively. The docking output file was saved as Lamarckian Ga (4.2) in dpf format. The ligand-protein complex binding sites were visualized by Discovery Studio Visualizer version 4.0.

5B.6.3. ADME prediction

In silico ADME properties and pharmacokinetic parameters of the synthesized compounds were calculated by using the online servers ADMETlab 2.0 and pkCSM [41]. The ADMET properties, human intestinal absorption (HIA), Caco-2 cell permeability, plasma protein binding and blood brain barrier penetration (BBB) were predicted using this program.

5B.7. Spectral data of synthesized compounds 4a-v

2-(4-methoxybenzoyl)-3-phenyl-12'*H*-spiro[cyclopropane-1,6'-indolo[2,1-*b*]quinazolin]-12'-one (4a)

White solid. mp: 185-187 °C. IR (KBr, cm^{-1}): 1684, 1637, 1600, 1465. ^{1}H NMR (400 MHz, DMSO-d_6) δ: 8.52 (d, J = 8.0 Hz, 1H), 8.25 (dd, J = 8.0, 1.2 Hz, 1H), 7.87 (d, J = 8.8 Hz, 2H), 7.79 (td, J = 8.4, 1.6 Hz, 1H), 7.55 – 7.49 (m, 3H), 7.46 – 7.40 (m, 2H), 7.34 – 7.22 (m, 5H), 6.96 (d, J = 9.2 Hz, 2H), 4.73 (d, J = 8.8 Hz, 1H), 4.27 (d, J = 8.8 Hz, 1H), 3.75 (s, 3H). ^{13}C NMR (100 MHz, DMSO-d_6) δ: 191.02, 164.16, 159.71, 155.47, 147.02, 139.80, 134.92, 132.94, 131.16, 130.55, 129.88, 129.09, 128.35, 128.04, 127.79, 127.63, 126.98, 126.75, 126.60, 121.74, 120.93, 116.66, 114.70, 55.99, 42.89, 41.94, 40.86. HRMS (ESI, m/z): $[M+H]^+$ calcd. for $C_{31}H_{23}N_2O_3$: 471.1709; found: 471.1691.

2-(4-methoxybenzoyl)-3-(*p*-tolyl)-12'*H*-spiro[cyclopropane-1,6'-indolo[2,1-*b*]quinazolin]-12'-one (4b)

White solid. mp: 213-215 °C. IR (KBr, cm^{-1}): 3052, 2966, 1686, 1639, 1600, 1465. ^1H NMR (400 MHz, DMSO-d_6) δ: 8.51 (d, J = 8.0 Hz, 1H), 8.24 (dd, J = 8.0, 1.2 Hz, 1H), 7.87 (d, J = 8.8 Hz, 2H), 7.82 – 7.78 (m, 1H), 7.53 (td, J = 8.0, 1.2 Hz, 1H), 7.49 (d, J = 8.0 Hz, 1H), 7.44 (dd, J = 6.4, 2.0 Hz, 1H), 7.41 (d, J = 8.0 Hz, 2H), 7.33 – 7.27 (m, 2H), 7.09 (d, J = 8.0 Hz, 2H), 6.96 (d, J = 9.2 Hz, 2H), 4.73 (d, J = 9.2 Hz, 1H), 4.20 (d, J = 8.8 Hz, 1H), 3.74 (s, 3H), 2.24 (s, 3H). ^{13}C NMR (100 MHz, DMSO-d_6) δ: 191.08, 164.16, 159.71, 155.47, 147.06, 139.73, 136.93, 134.96, 131.14, 130.39, 129.88, 129.71, 129.19, 128.63, 128.29, 127.71, 126.98, 126.77, 126.60, 121.69, 120.93, 116.64, 114.71, 56.00, 42.88, 42.15, 41.05, 21.21. ESI-MS (m/z): $[M+H]^+$ calcd. for $C_{32}H_{25}N_2O_3$: 485.19; found: 485.27.

2-(4-methoxybenzoyl)-3-(3-methoxyphenyl)-12'*H*-spiro[cyclopropane-1,6'-indolo[2,1-*b*] quinazolin]-12'-one (4c)

White solid. mp: 161-163 °C. IR (KBr, cm^{-1}): 3000, 2932, 1683, 1636, 1596, 1466. ^1H NMR (400 MHz, DMSO-d_6) δ: ^1H NMR (400 MHz, DMSO) δ 8.52 (d, J = 8.0 Hz, 1H), 8.25 (dd, J = 8.0, 1.6 Hz, 1H), 7.87 (d, J = 8.8 Hz, 2H), 7.81 (td, J = 8.4, 1.6 Hz,, 1H), 7.53 (td, J = 8.0, 1.6 Hz,, 1H), 7.46 (d, J = 8.8 Hz, 1H), 7.43 (dd, J = 8.0, 1.6 Hz, 1H), 7.33 – 7.26 (m, 2H), 7.19 – 7.15 (m, 2H), 7.06 (d, J = 7.6 Hz, 1H), 6.95 (d, J = 8.8 Hz, 2H), 6.80 (dd, J = 8.0, 2.4 Hz, 1H), 4.77 (d, J = 8.8 Hz, 1H), 4.24 (d, J = 8.8 Hz, 1H), 3.74 (s, 3H), 3.74 (s, 3H). ^{13}C NMR (100 MHz, DMSO-d_6) δ: 191.01, 164.15, 159.72, 159.22, 155.51, 147.04, 139.78, 134.98, 134.46, 131.17, 129.87, 129.10, 129.00, 128.35, 127.63, 127.01, 126.79, 126.59, 122.94, 121.70, 120.97, 116.66, 115.76, 114.69, 113.86, 55.99, 55.60, 43.00, 42.01, 40.98. ESI-MS (m/z): $[M+H]^+$ calcd. for $C_{32}H_{25}N_2O_4$: 501.18; found: 501.24.

2-(4-fluorophenyl)-3-(4-methoxybenzoyl)-12'*H*-spiro[cyclopropane-1,6'-indolo[2,1-*b*] quinazolin]-12'-one (4d)

White solid. mp: 223-225 °C. IR (KBr, cm^{-1}): 3077, 2925, 1671, 1637, 1599, 1466. ^1H NMR (400 MHz, DMSO-d_6) δ: 8.52 (d, J = 8.0 Hz, 1H), 8.25 (dd, J = 8.0, 1.2 Hz, 1H), 7.86 (d, J = 9.2 Hz, 2H), 7.80 (td, J = 8.4, 1.6 Hz, 1H), 7.59 – 7.52 (m, 3H), 7.45 (d, J = 8.4 Hz, 2H), 7.33 – 7.26 (m, 2H), 7.10 (t, J = 8.8 Hz, 2H), 6.96 (d, J = 8.8 Hz, 2H), 4.71 (d, J = 8.8 Hz, 1H), 4.27 (d, J = 8.8 Hz, 1H), 3.75 (s, 3H). ^{13}C NMR (100 MHz, DMSO-d_6) δ: 190.92, 164.16, 163.14 (d, J = 242 Hz), 159.72, 155.48, 147.02, 139.84, 134.98,

132.67 (d, *J* = 9.0 Hz), 131.18, 129.86, 129.24 (d, *J* = 3.0 Hz), 128.95, 128.38, 127.62, 127.02, 126.76, 126.57, 121.74, 120.96, 116.66, 114.87 (d, *J* = 18 Hz), 114.66, 56.00, 43.14, 40.80, 40.63. ESI-MS (m/z): $[M+H]^+$ calcd. for $C_{31}H_{22}FN_2O_3$: 489.16; found: 489.23.

2-(4-chlorophenyl)-3-(4-methoxybenzoyl)-12'*H*-spiro[cyclopropane-1,6'-indolo[2,1-*b*] quinazolin]-12'-one (4e)

White solid. mp: 190-192 °C. IR (KBr, cm^{-1}): 3066, 2931, 1685, 1637, 1600, 1466. ^1H NMR (400 MHz, DMSO-d_6) δ: 8.52 (d, *J* = 8.0 Hz, 1H), 8.26 (dd, *J* = 7.6, 1.2 Hz, 1H), 7.86 (d, *J* = 9.2 Hz, 2H), 7.84 – 7.79 (td, *J* = 8.4, 1.6 Hz, 1H), 7.57 (d, *J* = 8.4 Hz, 2H), 7.56 – 7.52 (m, 1H), 7.47 (d, *J* = 8.0 Hz, 1H), 7.44 (dd, *J* = 8.0, 1.6 Hz, 1H), 7.34 (d, *J* = 8.4 Hz, 2H), 7.32 – 7.26 (m, 2H), 6.96 (d, *J* = 8.8 Hz, 2H), 4.73 (d, *J* = 8.8 Hz, 1H), 4.27 (d, *J* = 8.8 Hz, 1H), 3.75 (s, 3H). ^{13}C NMR (100 MHz, DMSO-d_6) δ: 190.83, 164.17, 159.70, 155.43, 146.98, 139.86, 135.01, 132.51, 132.37, 132.06, 131.19, 129.82, 128.82, 128.44, 127.92, 127.64, 127.06, 126.77, 126.58, 121.79, 120.98, 116.66, 114.69, 55.99, 42.95, 40.82, 40.74. ESI-MS (m/z): $[M+H]^+$ calcd. for $C_{31}H_{22}ClN_2O_3$: 505.13; found: 505.21.

2-(4-bromophenyl)-3-(4-methoxybenzoyl)-12'*H*-spiro[cyclopropane-1,6'-indolo[2,1-*b*] quinazolin]-12'-one (4f)

White solid. mp: 250-252 °C. IR (KBr, cm^{-1}): 3004, 2965, 1687, 1654, 1625, 1594, 1466. ^1H NMR (400 MHz, DMSO-d_6) δ: 8.49 (d, *J* = 8.0 Hz, 1H), 8.22 (d, *J* = 7.2 Hz, 1H), 7.78 (d, *J* = 8.8 Hz, 3H), 7.62 (d, *J* = 8.8 Hz, 2H), 7.50 (t, *J* = 7.6 Hz, 1H), 7.46 – 7.39 (m, 4H), 7.28 (t, *J* = 7.6 Hz, 1H), 7.24 (d, *J* = 7.2 Hz, 1H), 6.81 (d, *J* = 8.4 Hz, 2H), 4.71 (d, *J* = 8.8 Hz, 1H), 4.20 (d, *J* = 8.8 Hz, 1H), 3.67 (s, 3H). ^{13}C NMR (100 MHz, DMSO-d_6) δ: 190.83, 164.19, 159.71, 146.98, 139.85, 135.05, 132.87, 132.47, 131.91, 131.77, 131.20, 130.84, 129.81, 128.80, 128.46, 127.65, 127.10, 126.79, 126.60, 121.80, 120.96, 116.66, 116.11, 114.70, 114.16, 56.00, 42.89, 40.90, 40.71. ESI-MS (m/z): $[M+H]^+$ calcd. for $C_{31}H_{22}BrN_2O_3$: 549.08; found: 549.15.

2-(4-chlorobenzoyl)-3-phenyl-12'*H*-spiro[cyclopropane-1,6'-indolo[2,1-*b*]quinazolin]-12'-one (4g)

White solid. mp: 216-218 °C. IR (KBr, cm^{-1}): 3053, 2924, 1680, 1636, 1600, 1466. ^1H NMR (400 MHz, DMSO-d_6) δ: 8.53 (d, *J* = 8.0 Hz, 1H), 8.25 (dd, *J* = 8.0, 1.2 Hz, 1H), 7.90 (d, *J* = 8.4 Hz, 2H), 7.81 – 7.75 (m, 1H), 7.51 (d, *J* = 8.8 Hz, 5H), 7.48 – 7.43 (m, 1H), 7.40 (d, *J* = 8.0 Hz, 1H), 7.33 (dd, *J* = 8.0, 0.8 Hz, 1H), 7.29 (d, *J* = 7.6 Hz, 2H), 7.27 –

7.21 (m, 2H), 4.77 (d, *J* = 8.8 Hz, 1H), 4.29 (d, *J* = 8.8 Hz, 1H). ^{13}C NMR (100 MHz, DMSO-d_6) δ: 192.13, 159.72, 155.33, 147.00, 139.90, 139.30, 135.55, 134.91, 132.78, 130.66, 130.57, 129.57, 128.81, 128.50, 128.04, 127.83, 127.64, 127.01, 126.75, 126.59, 121.74, 121.01, 116.70, 42.98, 41.82, 41.14. ESI-MS (m/z): $[M+H]^+$ calcd. for $C_{30}H_{20}ClN_2O_2$: 475.12; found: 475.19.

2-(4-chlorobenzoyl)-3-(*p*-tolyl)-12'*H*-spiro[cyclopropane-1,6'-indolo[2,1-*b*]quinazolin]-12'-one (4h)

White solid. mp: 218-220 °C. IR (KBr, cm^{-1}): 3051, 2922, 1680, 1641, 1601, 1465. ^{1}H NMR (400 MHz, DMSO-d_6) δ: 8.52 (d, *J* = 8.0 Hz, 1H), 8.25 (dd, *J* = 8.0, 1.2 Hz, 1H), 7.90 (d, *J* = 8.8 Hz, 2H), 7.80 (td, *J* = 8.4, 1.6 Hz, 1H), 7.54 (dd, *J* = 8.0, 0.8 Hz, 1H), 7.51 (d, *J* = 8.8 Hz, 2H), 7.46 (d, *J* = 8.4 Hz, 2H), 7.41 (d, *J* = 8.0 Hz, 2H), 7.34 – 7.27 (m, 2H), 7.09 (d, *J* = 8.0 Hz, 2H), 4.76 (d, *J* = 8.8 Hz, 1H), 4.24 (d, *J* = 8.8 Hz, 1H), 2.25 (s, 3H). ^{13}C NMR (100 MHz, DMSO-d_6) δ: 192.37, 159.69, 155.43, 147.00, 144.98, 139.82, 134.93, 134.47, 132.88, 130.56, 129.97, 128.99, 128.87, 128.40, 128.04, 127.80, 127.63, 126.99, 126.75, 126.59, 121.77, 120.95, 116.66, 42.96, 41.90, 40.98, 21.64. ESI-MS (m/z): $[M+H]^+$ calcd. for $C_{31}H_{22}ClN_2O_2$: 489.13; found: 489.20.

2-(4-chlorobenzoyl)-3-(3-methoxyphenyl)-12'*H*-spiro[cyclopropane-1,6'-indolo[2,1-*b*]quinazolin]-12'-one (4i)

White solid. mp: 193-195 °C. IR (KBr, cm^{-1}): 3049, 2934, 1680, 1635, 1585, 1465. ^{1}H NMR (400 MHz, DMSO-d_6) δ: 8.52 (d, *J* = 8.0 Hz, 1H), 8.25 (d, *J* = 7.6 Hz, 1H), 7.90 (d, *J* = 8.0 Hz, 2H), 7.80 (t, *J* = 7.6 Hz, 1H), 7.55 – 7.49 (m, 3H), 7.45 (t, *J* = 7.6 Hz, 2H), 7.33 – 7.26 (m, 2H), 7.17 (s, 2H), 7.06 (d, *J* = 6.8 Hz, 1H), 6.80 (d, *J* = 7.6 Hz, 1H), 4.80 (d, *J* = 8.8 Hz, 1H), 4.27 (d, *J* = 8.4 Hz, 1H), 3.73 (s, 3H). ^{13}C NMR (100 MHz, DMSO-d_6) δ: 192.11, 159.74, 159.22, 155.37, 147.01, 139.89, 139.29, 135.54, 134.97, 134.29, 130.67, 129.56, 129.01, 128.82, 128.50, 127.64, 127.04, 126.79, 126.58, 122.96, 121.70, 121.05, 116.70, 115.84, 113.87, 55.62, 43.07, 41.83, 41.23. ESI-MS (m/z): $[M+H]^+$ calcd. for $C_{31}H_{22}ClN_2O_3$: 505.13; found: 505.21.

2-(4-chlorobenzoyl)-3-(4-fluorophenyl)-12'*H*-spiro[cyclopropane-1,6'-indolo[2,1-*b*]quinazolin]-12'-one (4j)

White solid. mp: 220-222 °C. IR (KBr, cm^{-1}): 3054, 2924, 1680, 1637, 1601, 1466. ^{1}H NMR (400 MHz, DMSO-d_6) δ: 8.52 (d, *J* = 7.6 Hz, 1H), 8.25 (d, *J* = 7.6 Hz, 1H), 7.90 (d, *J* = 8.4 Hz, 2H), 7.80 (t, *J* = 7.2 Hz, 1H), 7.60 – 7.55 (m, 2H), 7.54 – 7.47 (m, 3H), 7.46 –

7.40 (m, 2H), 7.34 – 7.27 (m, 2H), 7.10 (t, *J* = 8.4 Hz, 2H), 4.74 (d, *J* = 8.4 Hz, 1H), 4.30 (d, *J* = 8.4 Hz, 1H). ^{13}C NMR (100 MHz, DMSO-d_6) δ: 192.02, 163.17 (d, *J* = 242 Hz), 159.72, 155.35, 146.99, 139.96, 139.29, 135.53, 134.96, 132.70 (d, *J* = 8 Hz), 130.68, 129.56, 129.09 (d, *J* = 3.0 Hz), 128.67, 128.52, 127.62, 127.04, 126.76, 126.55, 121.74, 121.05, 116.70, 114.87 (d, *J* = 21.0 Hz), 43.23, 40.95, 40.63. ESI-MS (m/z): $[M+H]^+$ calcd. for $C_{30}H_{19}ClFN_2O_2$: 493.11; found: 493.17.

2-(4-chlorobenzoyl)-3-(4-chlorophenyl)-12'*H*-spiro[cyclopropane-1,6'-indolo[2,1-*b*]quinazolin]-12'-one (4k)

White solid. mp: 215-217 °C. IR (KBr, cm^{-1}): 3084, 3060, 1677, 1642, 1603, 1466. ^{1}H NMR (400 MHz, DMSO-d_6) δ: 8.52 (d, *J* = 8.0 Hz, 1H), 8.24 (d, *J* = 7.6 Hz, 1H), 7.89 (d, *J* = 8.4 Hz, 2H), 7.80 (t, *J* = 7.2 Hz, 1H), 7.57 (d, *J* = 8.0 Hz, 2H), 7.53 (bs, 1H), 7.50 (d, *J* = 8.4 Hz, 2H), 7.46 – 7.44 (m, 2H), 7.33 (d, *J* = 8.4 Hz, 2H), 7.29 (d, *J* = 8.0 Hz, 2H), 4.76 (d, *J* = 8.4 Hz, 1H), 4.31 (d, *J* = 8.8 Hz, 1H). ^{13}C NMR (100 MHz, DMSO-d_6) δ: 191.93, 159.71, 155.31, 146.97, 139.99, 139.31, 135.51, 134.98, 132.55, 132.42, 131.93, 130.69, 129.56, 128.57, 127.92, 127.64, 127.07, 126.77, 126.55, 121.81, 121.08, 116.70, 43.06, 41.03, 40.69. ESI-MS (m/z): $[M+H]^+$ calcd. for $C_{30}H_{19}Cl_2N_2O_2$: 509.08; found: 509.14.

2-(4-chlorobenzoyl)-3-(2-chlorophenyl)-12'*H*-spiro[cyclopropane-1,6'-indolo[2,1-*b*]quinazolin]-12'-one (4l)

White solid. mp: 220-222 °C. IR (KBr, cm^{-1}): 3067, 3021, 1672, 1644, 1605, 1467. ^{1}H NMR (400 MHz, DMSO-d_6) δ: 8.54 (d, *J* = 8.0 Hz, 1H), 8.26 (dd, *J* = 8.0, 1.2 Hz, 1H), 7.92 (d, *J* = 8.8 Hz, 2H), 7.88 (d, *J* = 7.6 Hz, 1H), 7.74 (td, *J* = 8.0, 1.6 Hz, 1H), 7.54 – 7.50 (m, 3H), 7.47 (td, *J* = 8.0, 1.6 Hz, 1H), 7.43 (td, *J* = 7.6, 1.2 Hz, 1H), 7.35 – 7.29(m, 3H), 7.26 (td, *J* = 6.0, 1.2 Hz, 1H), 7.18 (dd, *J* = 8.0, 0.8 Hz, 1H), 4.68 (d, *J* = 8.8 Hz, 1H), 4.11 (d, *J* = 8.4 Hz, 1H). ^{13}C NMR (100 MHz, DMSO-d_6) δ: 191.94, 159.71, 155.31, 146.97, 139.98, 139.31, 135.51, 134.99, 132.55, 132.41, 131.94, 130.69, 129.56, 128.57, 127.92, 127.64, 127.08, 126.78, 126.56, 121.81, 121.08, 116.70, 43.06, 41.02, 40.64. ESI-MS (m/z): $[M+H]^+$ calcd. for $C_{30}H_{19}Cl_2N_2O_2$: 509.08; found: 509.14.

2-(4-bromophenyl)-3-(4-chlorobenzoyl)-12'*H*-spiro[cyclopropane-1,6'-indolo[2,1-*b*]quinazolin]-12'-one (4m)

White solid. mp: 224-226 °C. IR (KBr, cm^{-1}): 3086, 3059, 1676, 1643, 1604, 1466. ^{1}H NMR (400 MHz, DMSO-d_6) δ: 8.52 (d, *J* = 8.0 Hz, 1H), 8.25 (dd, *J* = 8.0, 1.2 Hz, 1H), 7.89 (d, *J* = 8.8 Hz, 2H), 7.83 – 7.78 (m, 1H), 7.55 (dd, *J* = 8.4, 1.2 Hz, 2H), 7.51 (d, *J* =

2.0 Hz, 2H), 7.49 (d, *J* = 4.8 Hz, 2H), 7.48 – 7.43 (m, 3H), 7.34 – 7.30 (m, 1H), 7.28 (dd, *J* = 8.0, 1.6 Hz, 1H), 4.76 (d, *J* = 8.8 Hz, 1H), 4.29 (d, *J* = 8.8 Hz, 1H). ^{13}C NMR (100 MHz, DMSO-d_6) δ: 191.92, 159.71, 155.31, 146.97, 139.99, 139.31, 135.51, 134.99, 132.90, 132.35, 130.83, 130.69, 129.56, 128.57, 128.56, 127.65, 127.08, 126.78, 126.55, 121.82, 121.09, 121.01, 116.70, 43.01, 41.00, 40.77. ESI-MS (m/z): $[M+H]^+$ calcd. for $C_{30}H_{19}BrClN_2O_2$: 553.03; found: 553.10.

4-(2-(4-chlorobenzoyl)-12'-oxo-12'*H*-spiro[cyclopropane-1,6'-indolo[2,1-*b*]quinazolin]-3-yl)benzonitrile (4n)

White solid. mp: 220-222 °C. IR (KBr, cm^{-1}): 3033, 2924, 2232, 1682, 1645, 1602, 1465. ^{1}H NMR (400 MHz, DMSO-d_6) δ: 8.52 (d, *J* = 8.0 Hz, 1H), 8.25 (d, *J* = 7.2 Hz, 1H), 7.90 (d, *J* = 8.4 Hz, 2H), 7.80 (td, *J* = 8.0, 1.2 Hz, 1H), 7.77 – 7.74 (m, 4H), 7.55 (d, *J* = 7.2 Hz, 1H), 7.51 (d, *J* = 8.8 Hz, 2H), 7.49 – 7.44 (m, 1H), 7.40 (d, *J* = 8.0 Hz, 1H), 7.31 (q, *J* = 7.6 Hz, 2H), 4.80 (d, *J* = 8.8 Hz, 1H), 4.42 (d, *J* = 8.4 Hz, 1H). ^{13}C NMR (100 MHz, DMSO-d_6) δ: 191.74, 159.69, 155.25, 146.88, 140.10, 139.35, 138.96, 135.46, 135.00, 131.87, 131.82, 130.74, 129.56, 128.75, 128.26, 127.58, 127.14, 126.78, 126.56, 121.94, 121.12, 119.36, 116.72, 110.38, 42.98, 41.03, 40.61. ESI-MS (m/z): $[M+Na]^+$ calcd. for $C_{31}H_{18}ClN_3O_2Na$: 521.09; found: 521.27.

2-(4-bromobenzoyl)-3-phenyl-12'*H*-spiro[cyclopropane-1,6'-indolo[2,1-*b*]quinazolin]-12'-one (4o)

White solid. mp: 218-220 °C. IR (KBr, cm^{-1}): 3085, 3053, 1682, 1637, 1600, 1466. ^{1}H NMR (400 MHz, DMSO-d_6) δ: 8.53 (d, *J* = 8.0 Hz, 1H), 8.25 (dd, *J* = 8.0, 1.2 Hz, 1H), 7.82 (d, *J* = 8.4 Hz, 2H), 7.80 - 7.76 (m, 1H), 7.66 (d, *J* = 8.8 Hz, 2H), 7.55 - 7.50 (m, 3H), 7.48 – 7.44 (m, 1H), 7.40 (d, *J* = 8.0 Hz, 1H), 7.34 (d, *J* = 7.2 Hz, 1H), 7.29 (d, *J* = 6.8 Hz, 2H), 7.27 – 7.22 (m, 2H), 4.76 (d, *J* = 8.8 Hz, 1H), 4.30 (d, *J* = 8.8 Hz, 1H). ^{13}C NMR (100 MHz, DMSO-d_6) δ: 192.36, 159.72, 155.33, 147.00, 139.91, 135.85, 134.92, 132.79, 132.54, 130.74, 130.59, 128.81, 128.57, 128.51, 128.04, 127.83, 127.64, 127.02, 126.75, 126.59, 121.73, 121.02, 116.71, 42.96, 41.76, 41.10. ESI-MS (m/z): $[M+H]^+$ calcd. for $C_{30}H_{20}BrN_2O_2$: 519.07; found: 519.18.

2-(4-bromobenzoyl)-3-(*p*-tolyl)-12'*H*-spiro[cyclopropane-1,6'-indolo[2,1-*b*]quinazolin]-12'-one (4p)

White solid. mp: 216-218 °C. IR (KBr, cm^{-1}): 1679, 1640, 1600, 1584, 1464. ^{1}H NMR (400 MHz, DMSO-d_6) δ: 8.52 (d, *J* = 8.0 Hz, 1H), 8.25 (d, *J* = 7.2 Hz, 1H), 7.80 (d, *J* = 8.4 Hz,

3H), 7.65 (d, *J* = 8.4 Hz, 2H), 7.53 (t, *J* = 7.6 Hz, 1H), 7.46 (d, *J* = 8.4 Hz, 2H), 7.41 (d, *J* = 8.0 Hz, 2H), 7.35 – 7.30 (m, 1H), 7.29 – 7.26 (m, 1H), 7.09 (d, *J* = 7.6 Hz, 2H), 4.76 (d, *J* = 9.2 Hz, 1H), 4.24 (d, *J* = 8.8 Hz, 1H), 2.25 (s, 3H). ^{13}C NMR (100 MHz, DMSO-d_6) δ: 192.41, 159.72, 155.32, 147.03, 139.85, 136.97, 135.86, 134.95, 132.54, 130.72, 130.43, 129.55, 128.91, 128.62, 128.57, 128.44, 127.71, 127.01, 126.77, 126.59, 121.68, 121.02, 116.69, 42.95, 41.98, 41.29, 21.22. ESI-MS (m/z): $[M+H]^+$ calcd. for $C_{31}H_{22}BrN_2O_2$: 533.09; found: 533.23.

2-(4-bromobenzoyl)-3-(4-methoxyphenyl)-12'*H*-spiro[cyclopropane-1,6'-indolo[2,1-*b*]quinazolin]-12'-one (4q)

White solid. mp: 224-226 °C. IR (KBr, cm^{-1}): 3081, 2926, 1672, 1642, 1602, 1466. ^{1}H NMR (400 MHz, DMSO-d_6) δ: 8.52 (d, *J* = 8.0 Hz, 1H), 8.25 (d, *J* = 7.2 Hz, 1H), 7.80 (t, *J* = 8.4 Hz, 3H), 7.65 (d, *J* = 8.8 Hz, 2H), 7.53 (t, *J* = 7.6 Hz, 1H), 7.49 – 7.42 (m, 4H), 7.34 – 7.26 (m, 2H), 6.84 (d, *J* = 8.4 Hz, 2H), 4.74 (d, *J* = 8.8 Hz, 1H), 4.23 (d, *J* = 8.8 Hz, 1H), 3.70 (s, 3H). ^{13}C NMR (100 MHz, DMSO-d_6) δ: 192.43, 159.73, 159.05, 155.33, 147.06, 139.82, 135.88, 134.94, 132.53, 131.72, 130.70, 128.94, 128.54, 128.36, 127.71, 126.98, 126.75, 126.57, 124.48, 121.61, 121.00, 116.69, 113.42, 55.48, 43.12, 41.75, 41.28. ESI-MS (m/z): $[M+H]^+$ calcd. for $C_{31}H_{22}BrN_2O_3$: 549.08; found: 549.13.

2-(4-bromobenzoyl)-3-(3-methoxyphenyl)-12'*H*-spiro[cyclopropane-1,6'-indolo[2,1-*b*]quinazolin]-12'-one (4r)

White solid. mp: 164-166 °C. IR (KBr, cm^{-1}): 2925, 2853, 1680, 1637, 1600, 1466. ^{1}H NMR (400 MHz, DMSO-d_6) δ: 8.52 (d, *J* = 8.0 Hz, 1H), 8.25 (dd, *J* = 8.0, 1.2 Hz, 1H), 7.83 – 7.78 (m, 3H), 7.65 (d, *J* = 8.8 Hz, 2H), 7.54 (td, *J* = 8.0, 0.8 Hz, 1H), 7.47 – 7.42 (m, 2H), 7.34 – 7.26 (m, 2H), 7.19 – 7.15 (m, 2H), 7.06 (d, *J* = 7.6 Hz, 1H), 6.80 (dd, *J* = 8.0, 2.4 Hz, 1H), 4.79 (d, *J* = 8.8 Hz, 1H), 4.27 (d, *J* = 8.8 Hz, 1H), 3.74 (s, 3H). ^{13}C NMR (100 MHz, DMSO-d_6) δ: 192.33, 159.74, 159.22, 155.36, 147.01, 139.88, 135.84, 134.97, 134.28, 132.52, 130.73, 129.01, 128.81, 128.55, 128.51, 127.63, 127.05, 126.79, 126.58, 122.96, 121.68, 121.04, 116.71, 115.83, 113.87, 55.62, 43.05, 41.81, 41.22. ESI-MS (m/z): $[M+H]^+$ calcd. for $C_{31}H_{22}BrN_2O_3$: 549.08; found: 549.17.

2-(4-bromobenzoyl)-3-(4-fluorophenyl)-12'*H*-spiro[cyclopropane-1,6'-indolo[2,1-*b*]quinazolin]-12'-one (4s)

White solid. mp: 216-218 °C. IR (KBr, cm^{-1}): 1680, 1637, 1600, 1583, 1566, 1465. ^{1}H NMR (400 MHz, DMSO-d_6) δ: 8.52 (d, *J* = 8.0 Hz, 1H), 8.25 (dd, *J* = 8.0, 1.2 Hz, 1H),

7.81 (d, *J* = 8.4 Hz, 2H), 7.78 (d, *J* = 8.0 Hz, 1H), 7.65 (d, *J* = 8.4 Hz, 2H), 7.57 (dd, *J* = 8.4, 2.0 Hz, 2H), 7.53 (t, *J* = 7.2 Hz, 1H), 7.48 – 7.41 (m, 2H), 7.32 (t, *J* = 8.0 Hz, 1H), 7.27 (t, *J* = 6.4 Hz, 1H), 7.10 (t, *J* = 8.8 Hz, 2H), 4.74 (d, *J* = 8.8 Hz, 1H), 4.30 (d, *J* = 8.8 Hz, 1H). ^{13}C NMR (100 MHz, DMSO-d_6) δ: 192.23, 163.16 (d, *J* = 241.8 Hz), 159.72, 155.34, 146.99, 139.95, 135.83, 134.95, 132.70 (d, *J* = 8.2 Hz), 132.52, 130.75, 129.09 (d, *J* = 2.8 Hz), 128.66, 128.57, 128.52, 127.62, 127.03, 126.76, 126.55, 121.73, 121.05, 116.70, 114.87 (d, *J* = 21.2 Hz), 43.21, 40.94, 40.63. ESI-MS (m/z): $[M+H]^+$ calcd. for $C_{30}H_{19}BrFN_2O_2$: 537.06; found: 537.16.

2-(4-bromobenzoyl)-3-(4-chlorophenyl)-12'*H*-spiro[cyclopropane-1,6'-indolo[2,1-*b*]quinazolin]-12'-one (4t)

White solid. mp: 210-212 °C. IR (KBr, cm^{-1}): 3080, 3057, 1674, 1642, 1604, 1466. ^{1}H NMR (400 MHz, DMSO-d_6) δ: 8.52 (d, *J* = 8.0 Hz, 1H), 8.25 (dd, *J* = 8.0, 1.2 Hz, 1H), 7.81 (d, *J* = 8.4 Hz, 3H), 7.65 (d, *J* = 8.8 Hz, 2H), 7.58 (d, *J* = 8.4 Hz, 2H), 7.56 – 7.52 (m, 1H), 7.47 – 7.43 (m, 2H), 7.35 – 7.30 (m, 3H), 7.28 (t, *J* = 7.2 Hz, 1H), 4.76 (d, *J* = 8.8 Hz, 1H), 4.31 (d, *J* = 8.8 Hz, 1H). ^{13}C NMR (100 MHz, DMSO-d_6) δ: 192.16, 159.71, 155.31, 146.96, 139.98, 135.79, 134.99, 132.56, 132.52, 132.40, 131.93, 130.77, 128.58, 127.92, 127.64, 127.07, 126.78, 126.56, 121.79, 121.08, 116.71, 43.03, 40.99, 40.61 ESI-MS (m/z): $[M+H]^+$ calcd. for $C_{30}H_{19}BrClN_2O_2$: 553.03; found: 553.10.

2-(4-bromobenzoyl)-3-(2-chlorophenyl)-12'*H*-spiro[cyclopropane-1,6'-indolo[2,1-*b*] quinazolin]-12'-one (4u)

White solid. mp: 213-215 °C. IR (KBr, cm^{-1}): 3057, 2924, 1680, 1640, 1601, 1466. ^{1}H NMR (400 MHz, DMSO-d_6) δ: 8.55 (d, *J* = 8.0 Hz, 1H), 8.26 (dd, *J* = 8.0, 1.2 Hz, 1H), 7.88 (d, *J* = 7.6 Hz, 1H), 7.84 (d, *J* = 8.4 Hz, 2H), 7.77 – 7.71 (m, 1H), 7.66 (d, *J* = 8.4 Hz, 2H), 7.55 – 7.51 (m, 1H), 7.49 – 7.45 (m, 1H), 7.43 (td, *J* = 6.8, 0.8 Hz, 1H), 7.36 – 7.28 (m, 3H), 7.25 (td, *J* = 8.0, 0.8 Hz, 1H), 7.18 (d, *J* = 7.6 Hz, 1H), 4.68 (d, *J* = 8.4 Hz, 1H), 4.12 (d, *J* = 8.4 Hz, 1H). ^{13}C NMR (100 MHz, DMSO-d_6) δ: 192.15, 159.63, 155.40, 146.96, 140.05, 135.79, 135.12, 134.99, 132.91, 132.53, 131.96, 130.82, 129.79, 128.90, 128.73, 128.62, 128.54, 127.47, 127.19, 127.12, 126.79, 126.74, 121.59, 120.92, 116.69, 43.14, 40.64. ESI-MS (m/z): $[M+H]^+$ calcd. for $C_{30}H_{19}BrClN_2O_2$: 553.03; found: 553.10.

2-(4-bromobenzoyl)-3-(4-bromophenyl)-12'*H*-spiro[cyclopropane-1,6'-indolo[2,1-*b*]quinazolin]-12'-one (4v)

White solid. mp: 232-234 °C. IR (KBr, cm^{-1}): 3056, 2924, 1673, 1642, 1604, 1466. ^1H NMR (400 MHz, DMSO-d_6) δ: 8.51 (d, J = 8.0 Hz, 1H), 8.24 (d, J = 7.6 Hz, 1H), 7.81 (d, J = 8.4 Hz, 3H), 7.64 (d, J = 8.8 Hz, 2H), 7.55 – 7.51 (m, 3H), 7.48 – 7.42 (m, 4H), 7.32 (d, J = 7.6 Hz, 1H), 7.28 (d, J = 7.2 Hz, 1H), 4.75 (d, J = 8.8 Hz, 1H), 4.29 (d, J = 8.8 Hz, 1H). ^{13}C NMR (100 MHz, DMSO-d_6) δ: 192.14, 159.71, 155.31, 146.96, 139.98, 135.80, 134.98, 132.90, 132.52, 132.35, 130.83, 130.76, 128.58, 128.55, 127.65, 127.08, 126.78, 126.55, 121.80, 121.09, 121.01, 116.71, 42.98, 40.99, 40.75. ESI-MS (m/z): $[M+H]^+$ calcd. for $C_{30}H_{19}Br_2N_2O_2$: 596.98; found: 597.02.

5B.8. References

[1] A. P. Sakla, P. Kansal, N. Shankaraiah, *Eur. J. Org. Chem.* **2021**, *2021*, 757–772.

[2] T. Lu, R. Hayashi, R. P. Hsung, K. A. Dekorver, A. G. Lohse, Z. Song, Y. Tang, *Org. Biomol. Chem.* **2009**, *7*, 3331–3337.

[3] D. Y. K. Chen, R. H. Pouwer, J. A. Richard, *Chem. Soc. Rev.* **2012**, *41*, 4631–4642.

[4] C. N. Reddy, V. L. Nayak, G. S. Mani, J. S. Kapure, P. R. Adiyala, R. A. Maurya, A. Kamal, *Bioorg. Med. Chem. Lett.* **2015**, *25*, 4580–4586.

[5] G. H. Shen, J. H. Hong, *Nucleosides, Nucleotides and Nucleic Acids* **2012**, *31*, 503–521.

[6] P. B. Sampson, Y. Liu, N. K. Patel, M. Feher, B. Forrest, S. Li, L. Edwards, R. Laufer, Y. Lang, F. Ban, D. E. Awrey, G. Mao, O. Plotnikova, G. Leung, R. Hodgson, J. Mason, X. Wei, R. Kiarash, E. Green, W. Qiu, N. Y. Chirgadze, T. W. Mak, G. Pan, H. W. Pauls, *J. Med. Chem.* **2015**, *58*, 130–146.

[7] L. Chen, M. Huang, L. Feng, Y. He, H. Yun, Novel cyclopropane indolinone derivatives, WO2011069298A1, **2011**.

[8] D. M. Potter, M. S. Baird, *Br. J. Cancer* **2000**, *83*, 914–920.

[9] T. Jiang, K. L. Kuhen, K. Wolff, H. Yin, K. Bieza, J. Caldwell, B. Bursulaya, T. Y. H. Wu, Y. He, *Bioorg. Med. Chem. Lett.* **2006**, *16*, 2105–2108.

[10] M. Tone, Y. Nakagawa, S. Chanthamath, I. Fujisawa, N. Nakayama, H. Goto, K.

Shibatomi, S. Iwasa, *RSC Adv.* **2018**, *8*, 39865–39869.

[11] H. Maruoka, N. Kashige, T. Eishima, F. Okabe, R. Tanaka, T. Fujioka, F. Miake, K. Yamagata, *J. Heterocycl. Chem.* **2008**, *45*, 1883–1887.

[12] J. R. Potoski, W. Nyack, Process for the preparation of indoln-2-one dervatives useful as pr modulators, US 2008/0051585 A1, **2008**.

[13] C. F. Hirsch, J. M. Sigmund, Hapalindolinone compounds as vassopressen antagonsts, 4803217, **1989**.

[14] B. Yu, Z. Yu, P. P. Qi, D. Q. Yu, H. M. Liu, *Eur. J. Med. Chem.* **2015**, *95*, 35–40.

[15] Z. Y. Cao, J. Zhou, *Org. Chem. Front.* **2015**, *2*, 849–858.

[16] H. Nambu, Y. Onuki, N. Ono, K. Tsuge, T. Yakura, *Chem. Commun.* **2019**, *55*, 6539–6542.

[17] C. Köllmann, S. M. Wiechert, P. G. Jones, T. Pietschmann, D. B. Werz, *Org. Lett.* **2019**, *21*, 6966–6971.

[18] H. Lu, H. X. Zhang, C. Y. Tan, J. Y. Liu, H. Wei, P. F. Xu, *J. Org. Chem.* **2019**, *84*, 10292–10305.

[19] S. Hajra, S. Roy, S. K. A. Saleh, *Org. Lett.* **2018**, *20*, 4540–4544.

[20] W. Dohle, F. L. Jourdan, G. Menchon, A. E. Prota, P. A. Foster, P. Mannion, E. Hamel, M. P. Thomas, P. G. Kasprzyk, E. Ferrandis, M. O. Steinmetz, M. P. Leese, B. V. L. Potter, *J. Med. Chem.* **2018**, *61*, 1031–1044.

[21] S. Gatadi, T. V. Lakshmi, S. Nanduri, *Eur. J. Med. Chem.* **2019**, *170*, 157–172.

[22] A. A. M. Abdel-Aziz, L. A. Abou-Zeid, K. E. H. ElTahir, M. A. Mohamed, M. A. Abu El-Enin, A. S. El-Azab, *Bioorg. Med. Chem.* **2016**, *24*, 3818–3828.

[23] A. Dutta, D. Sarma, *Tuberculosis* **2020**, *124*, 101986–102028.

[24] D. N. Huh, Y. Cheng, C. W. Frye, D. T. Egger, I. A. Tonks, *Chem. Sci.* **2021**, *12*, 9574–9590.

[25] P. S. G. Nunes, H. D. A. Vidal, A. G. 0. Correâ, *Org. Biomol. Chem.* **2020**, *18*, 7751–7773.

[26] Y. Liu, H. Wang, J. Wan, *Asian J. Org. Chem.* **2013**, *2*, 374–386.

[27] L. Chen, J. He, *J. Org. Chem.* **2020**, *85*, 5203–5219.

[28] H. Mei, G. Pan, X. Zhang, L. Lin, X. Liu, X. Feng, *Org. Lett.* **2018**, *20*, 7794–7797.

[29] L. Wang, W. Cao, H. Mei, L. Hu, X. Feng, *Adv. Synth. Catal.* **2018**, *360*, 4089–4093.

[30] Y. You, B. X. Quan, Z. H. Wang, J. Q. Zhao, W. C. Yuan, *Org. Biomol. Chem.* **2020**, *18*, 4560–4565.

[31] Y. Su, H. He, Y. Zhao, Q. Li, Y. Feng, G. Cao, D. Huang, K. H. Wang, C. Huo, Y. Hu, *Asian J. Org. Chem.* **2021**, *10*, 1778–1785.

[32] S. S. Li, Q. Qin, Z. Qi, L. M. Yang, Y. Kang, X. Z. Zhang, A. J. Ma, J. B. Peng, *Org. Chem. Front.* **2021**, *8*, 3069–3075.

[33] M. Liu, C. F. Liu, J. Zhang, Y. J. Xu, L. Dong, *Org. Chem. Front.* **2019**, *6*, 664–668.

[34] Q. Y. Fang, M. H. Yi, X. X. Wu, L. M. Zhao, *Org. Lett.* **2020**, *22*, 5266–5270.

[35] B.-L. Zhao, D.-M. Du, *Eur. J. Org. Chem.* **2015**, *2015*, 5350–5359.

[36] I. Yavari, S. Sheikhi, J. Sheykhahmadi, Z. Taheri, M. R. Halvagar, *Synth.* **2021**, *53*, 2057–2066.

[37] D. Kumar, G. Mariappan, A. Husain, J. Monga, S. Kumar, *Arab. J. Chem.* **2017**, *10*, 344–350.

[38] C. B. P. Kumar, M. S. Raghu, K. N. N. Prasad, S. Chandrasekhar, B. K. Jayanna, F. A. Alharthi, M. K. Prashanth, K. Y. Kumar, *New J. Chem.* **2021**, *45*, 403–414.

[39] A. Boobis, U. Gundert-Remy, P. Kremers, P. Macheras, O. Pelkonen, *Eur. J. Pharm. Sci.* **2002**, *17*, 183–193.

[40] G. M. Morris, R. Huey, W. Lindstrom, M. F. Sanner, R. K. Belew, D. S. Goodsell, A. J. Olson, *J. Comput. Chem.* **2009**, *30*, 2785–2791.

[41] M. Prajapat, P. Sarma, N. Shekhar, H. Kaur, S. Singh, S. Kumar, H. Kaur, S. Mahendiratta, A. R. Sharma, S. Kaur, V. M. Mahalmani, B. Medhi, *J. Adv. Pharm. Technol. Res.* **2020**, *11*, 194–201.

5B.9. Selected IR, NMR (^{1}H and ^{13}C) and Mass spectra

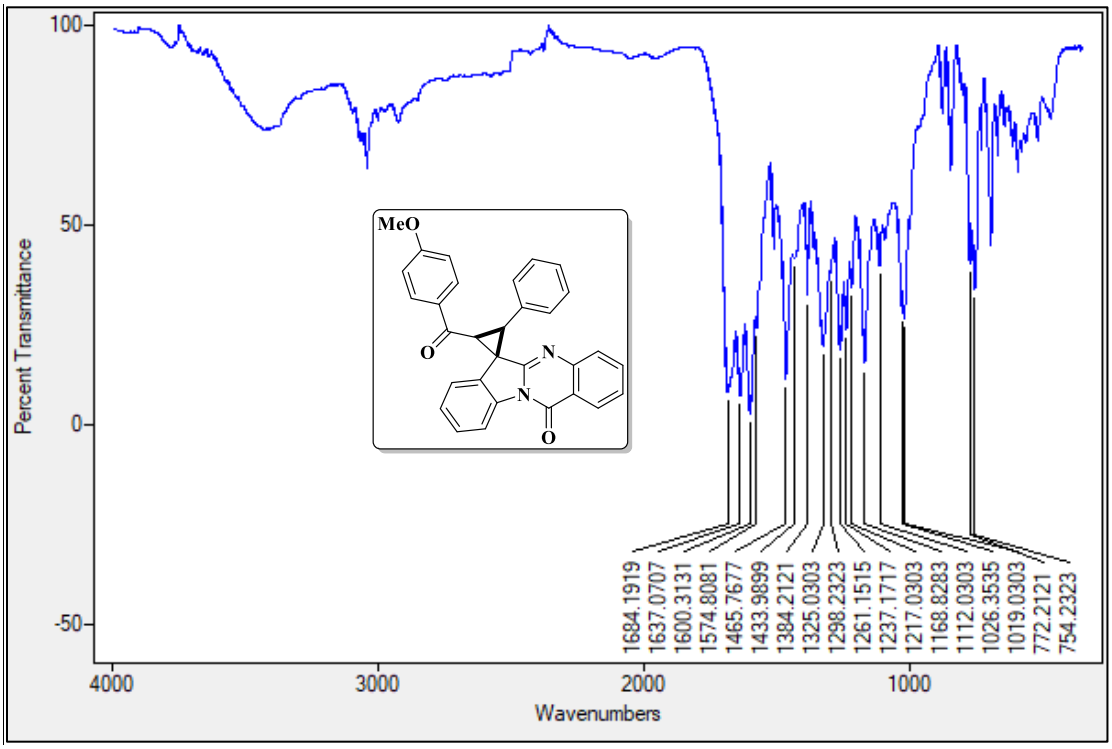

IR spectrum of the compound **4a**

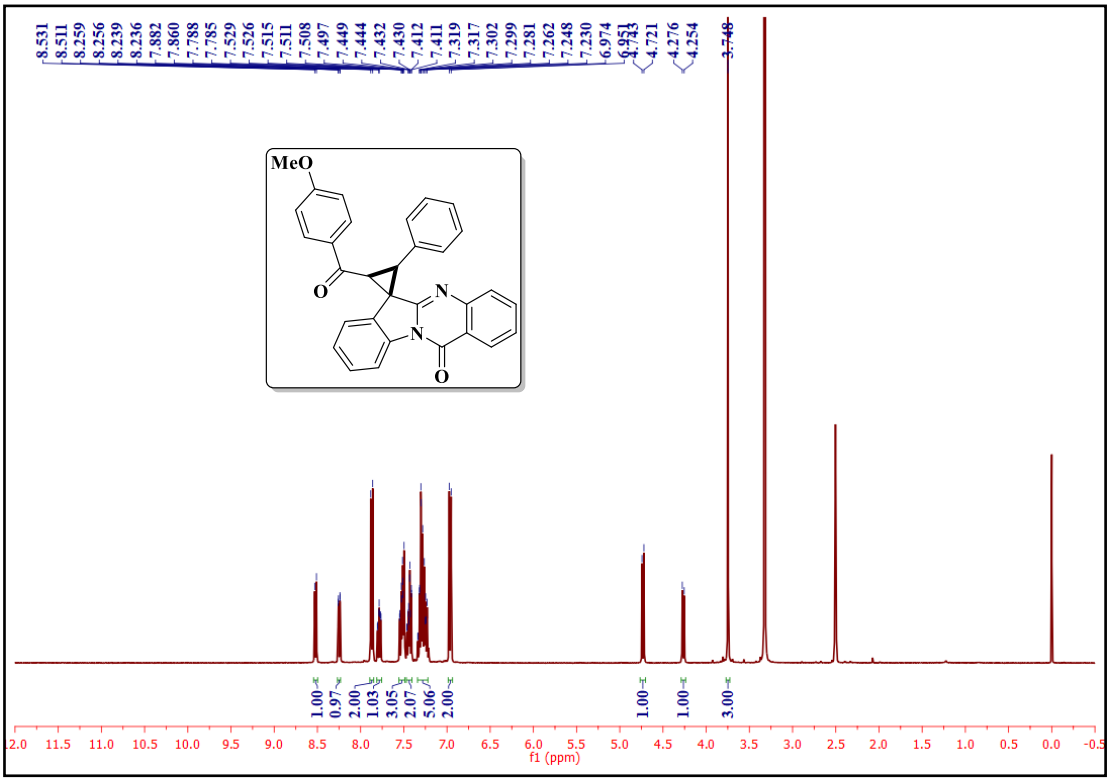

^{1}H NMR spectrum of the compound **4a**

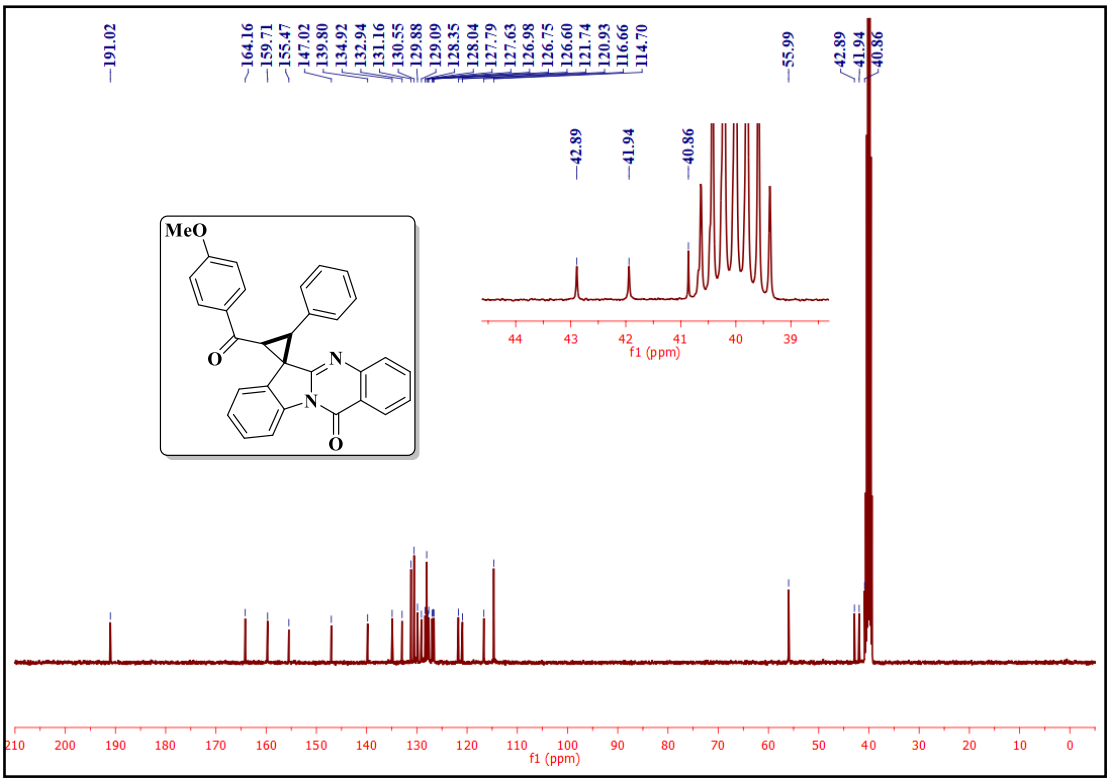

^{13}C NMR spectrum of the compound **4a**

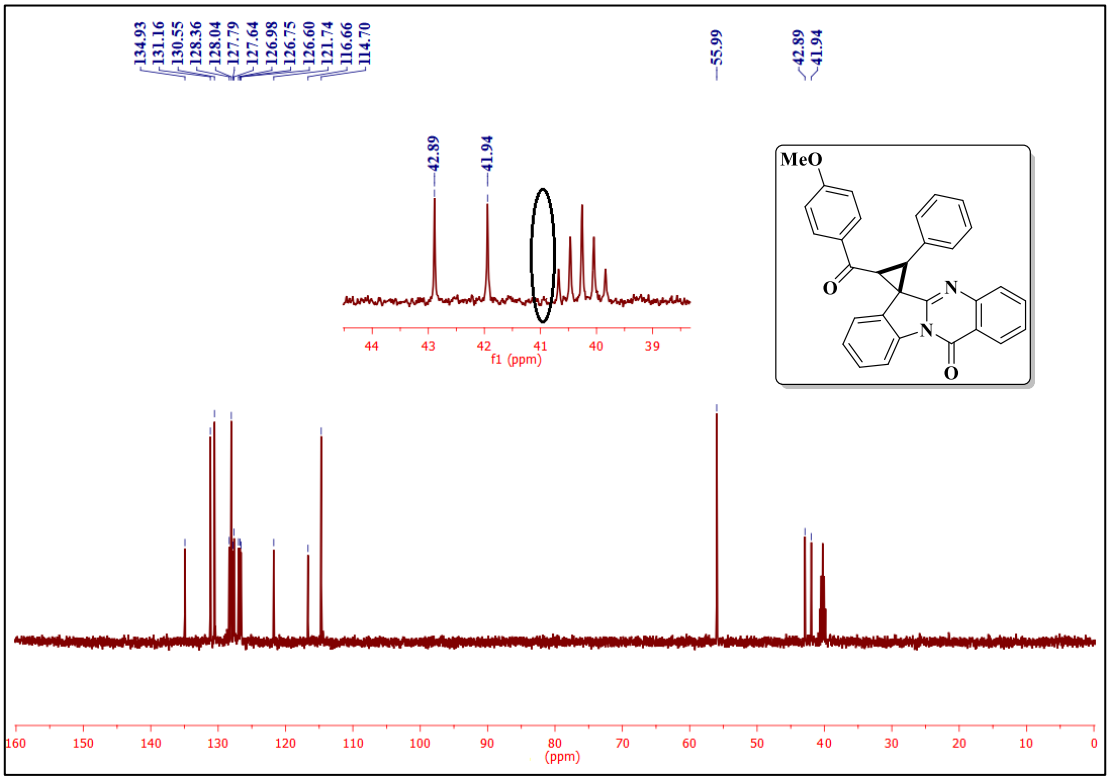

DEPT-135 NMR spectrum of the compound **4a**

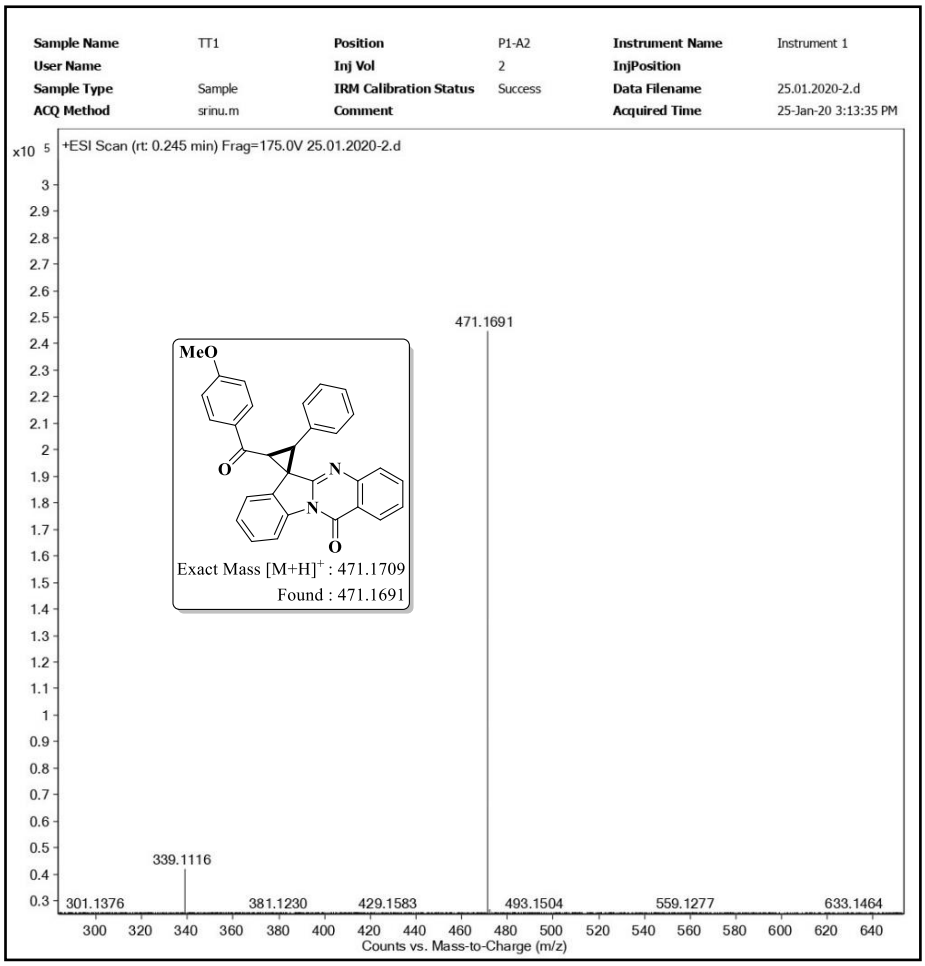

Mass spectrum of the compound **4a**

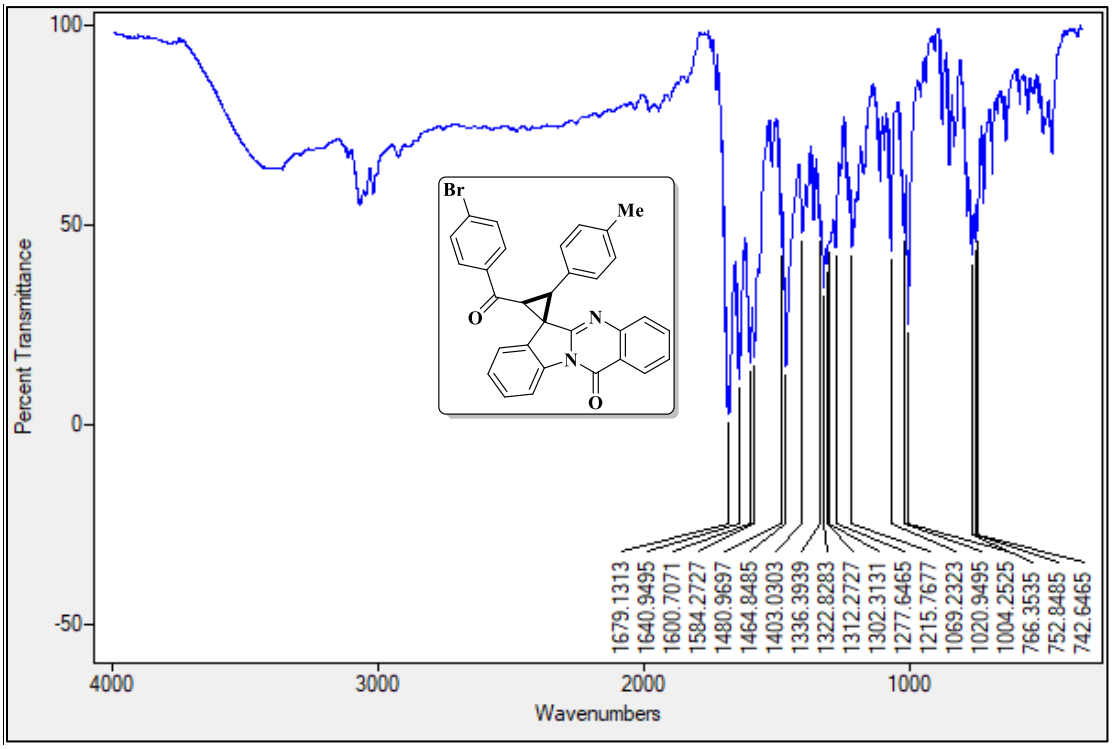

IR spectrum of the compound **4p**

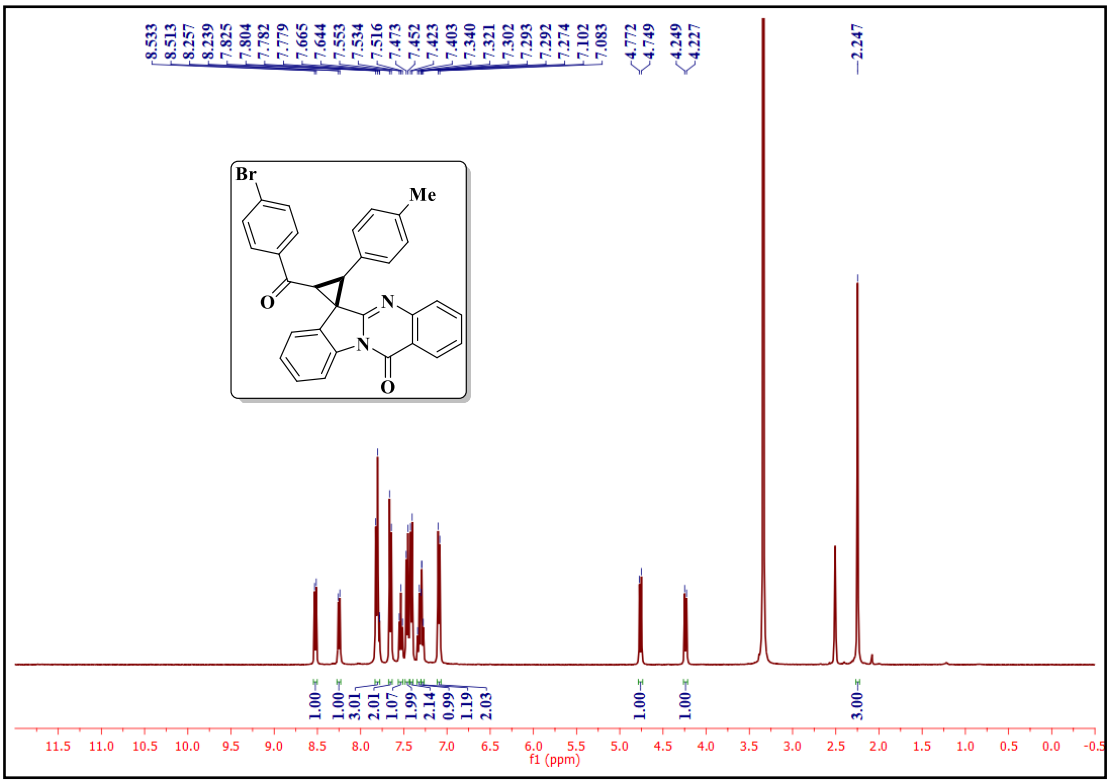

^{1}H NMR spectrum of the compound **4p**

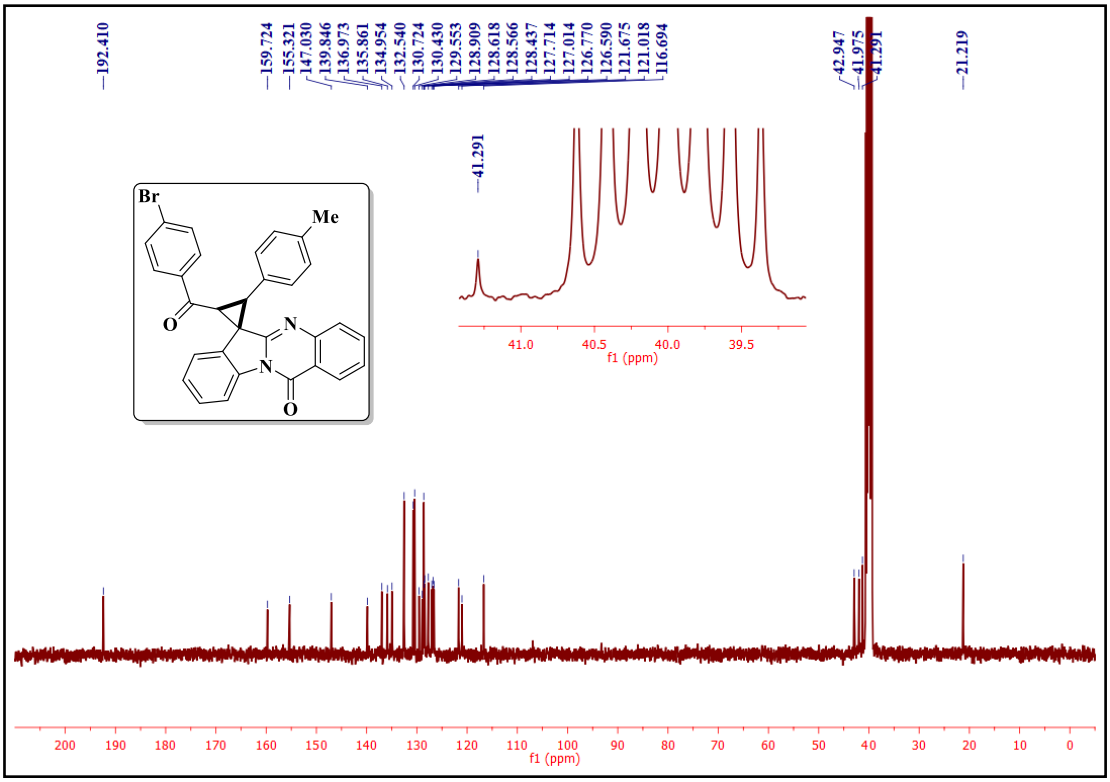

^{13}C NMR spectrum of the compound **4p**

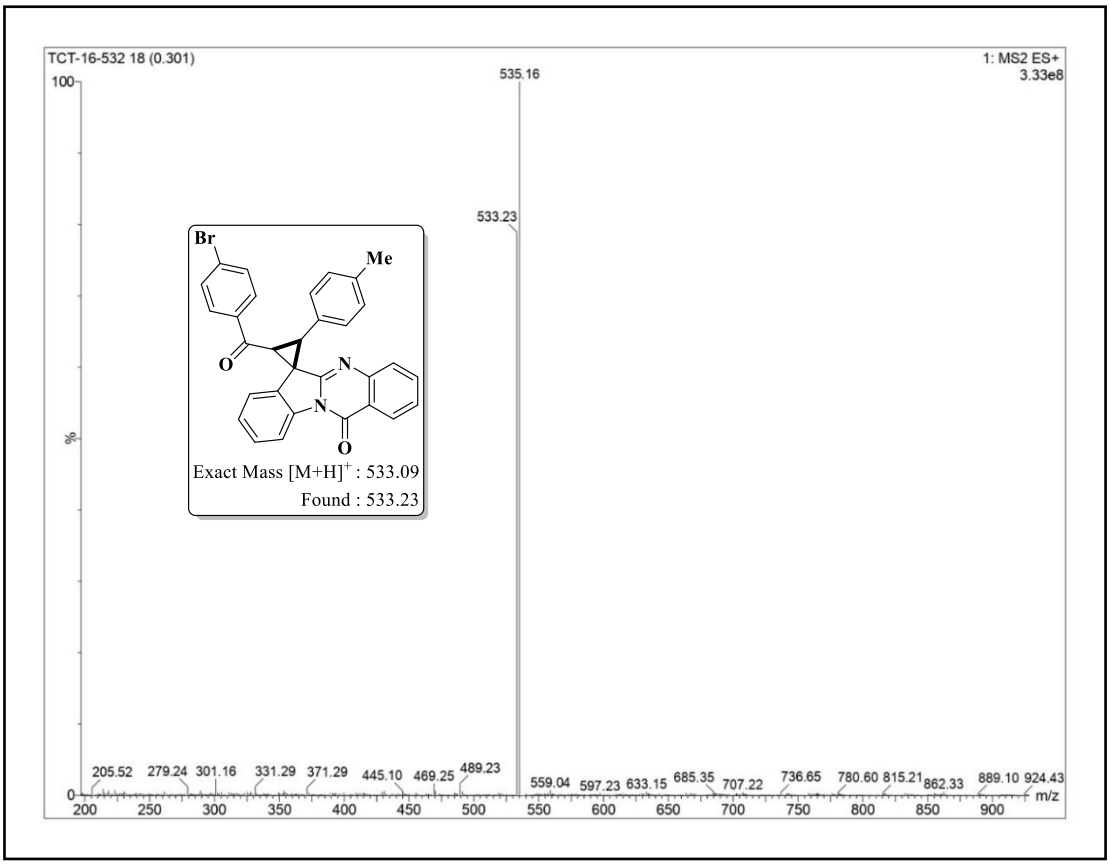

Mass spectrum of the compound **4p**

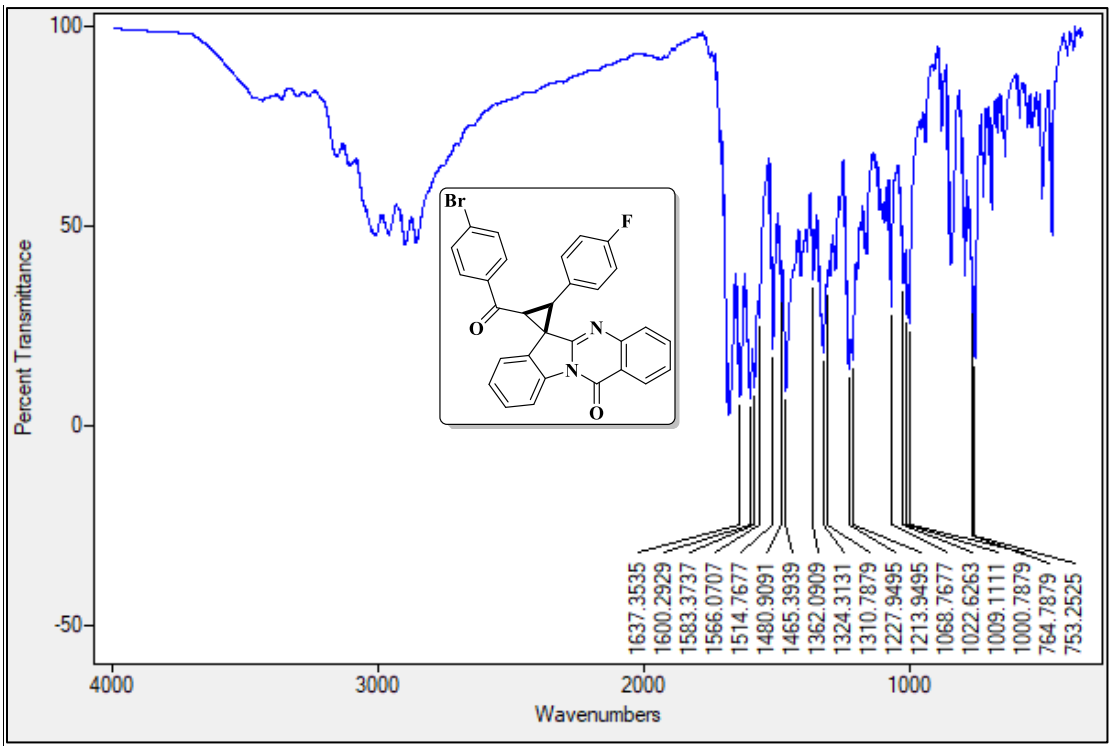

IR spectrum of the compound **4s**

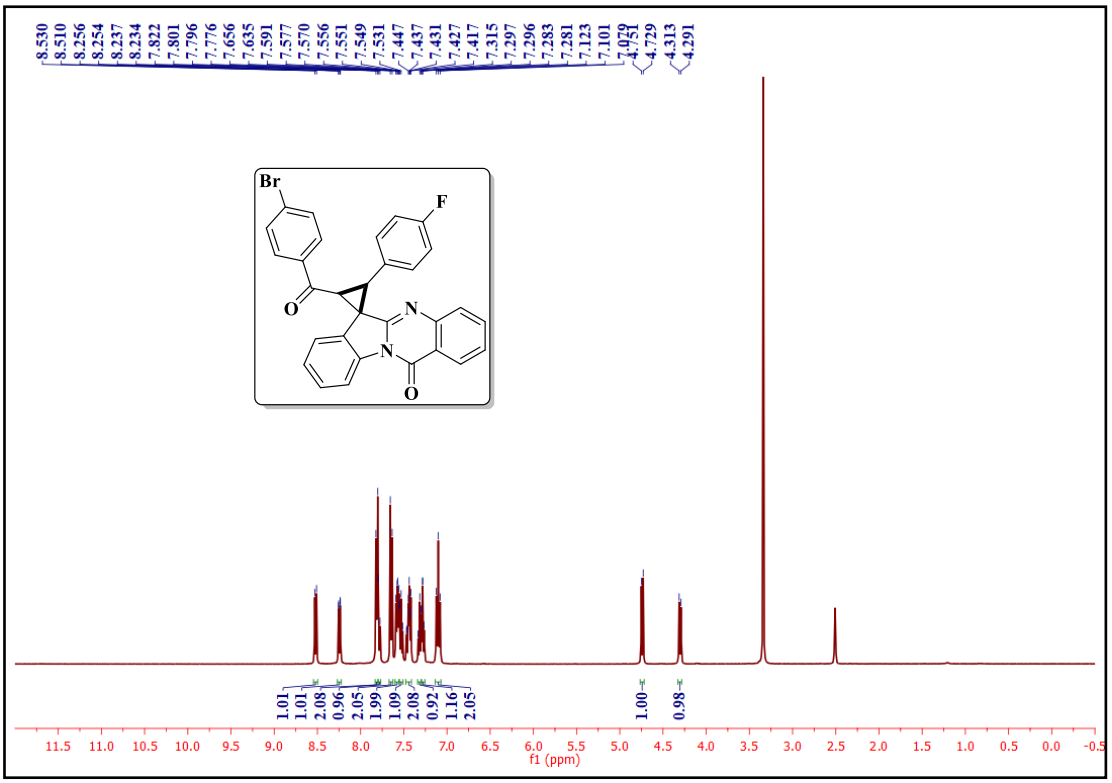

^{1}H NMR spectrum of the compound **4s**

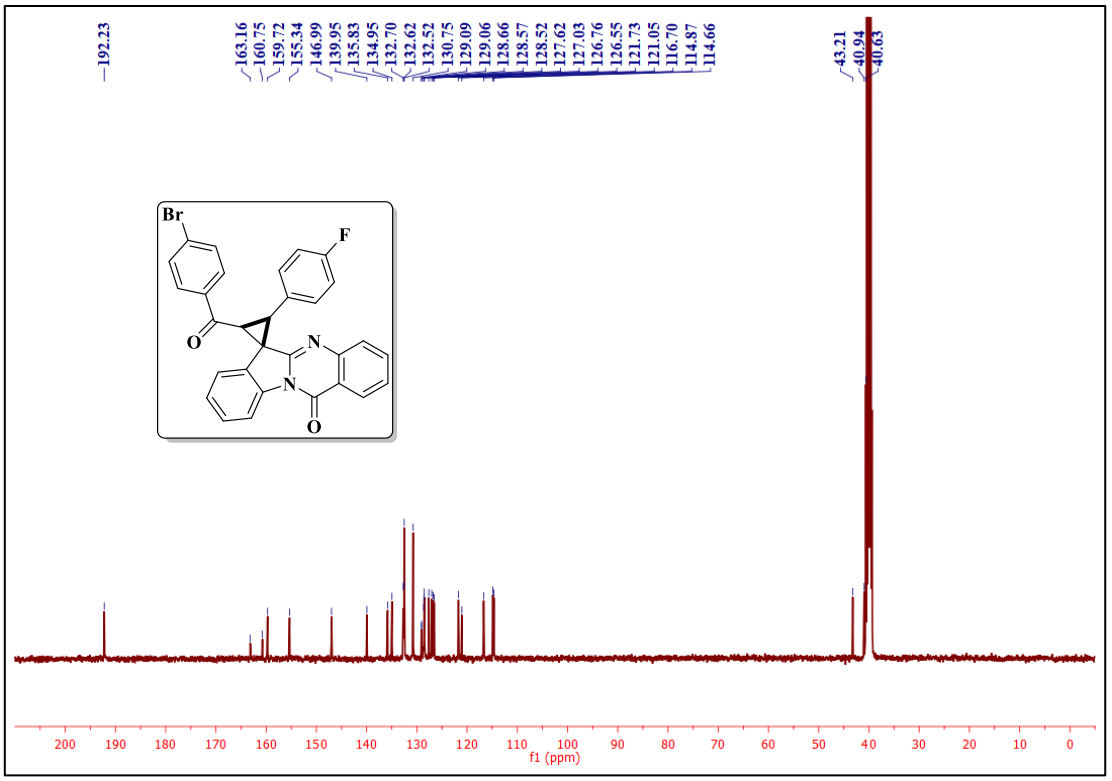

^{13}C NMR spectrum of the compound **4s**

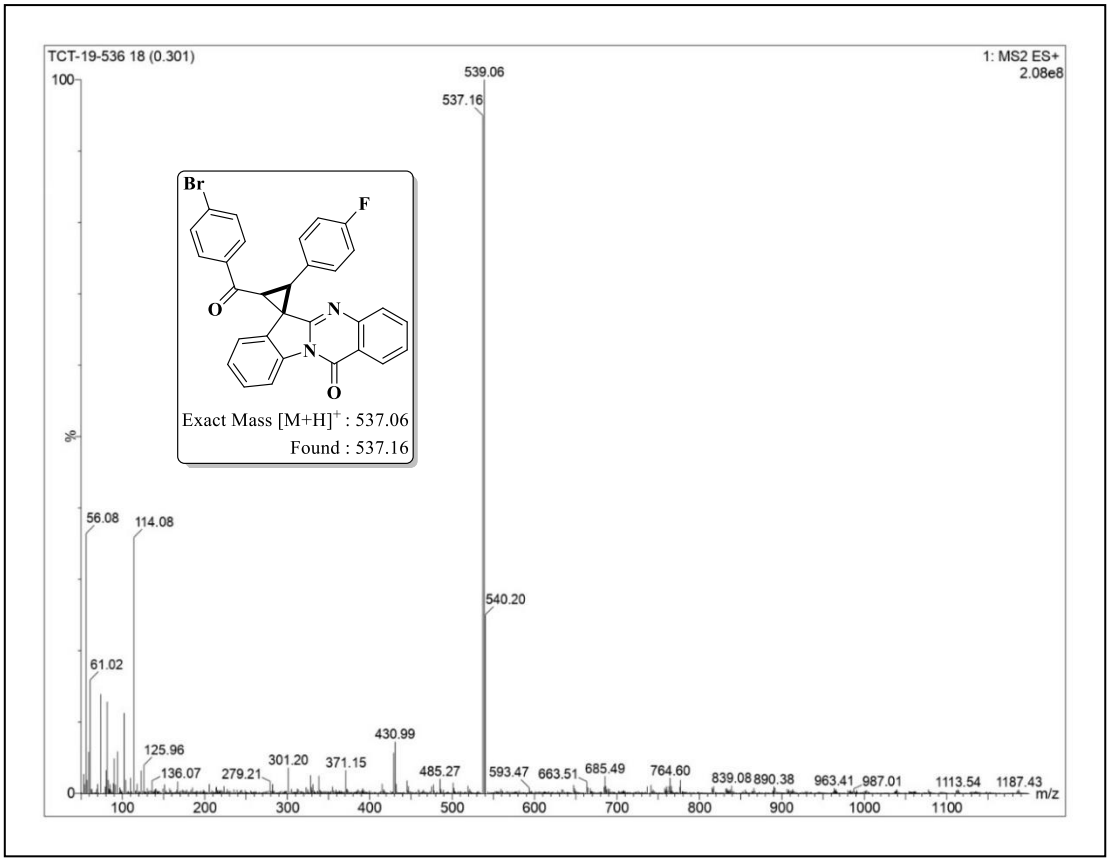

Mass spectrum of the compound **4s**

CHAPTER-VI
Section-A

Ultrasound promoted synthesis of novel quinazolinyl-bisspirooxindolo-pyrrolidines *via* [3+2] cycloaddition reaction

6A.1. Introduction

Green chemistry has become an emerging tool in synthetic chemistry and plays an important role in controlling the environmental pollution by utilizing eco-friendly solvents, catalysts and suitable reaction conditions [1]. In this view, ultrasonic irradiation is an extensively utilized green technique in organic synthesis according to its specific properties like shorter reaction time, higher yields, and waste minimization [2]. Ultrasonication cause acoustic cavitation which generate mechanical vibration between particles to produce mechanical and thermal energy for the utilization of chemical reaction without any significant change in reaction medium [3].

Owing to their unique structural features and interesting biological profiles, spirooxindoles are taken as privileged structural motifs for new drug discovery [4,5]. Synthetic and natural alkaloids having spirooxindole moiety shows wide range of biological activities such as anti-cancer [6], anti-malarial [7], anti-microbial [8], anti-oxidant [9], anti-viral [10] etc. In particular, bisspirooxindoles have emerged as attractive synthetic targets due to their versatile pharmacological properties [11,12].

6A.1.1. Reported methods for the synthesis and biological evaluation of bisspirooxindoles

Barakat and co-workers synthesized new bisspirooxindoles with pyrrolidines and thioxothiazolidinones *via* regioselective 1,3-dipolar cycloaddition reaction (Figure 6A.1). The synthesized compounds showed better anti-microbial and anti-fungal activity than the selected standard drugs [13].

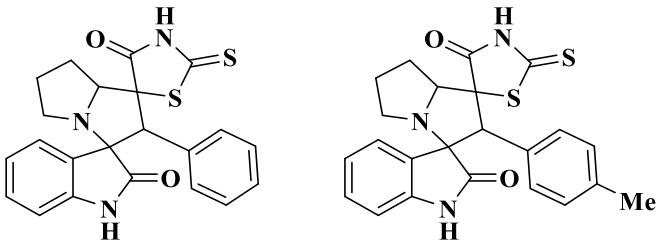

Figure 6A.1

Rouatbi et al. reported the synthesis of dispiro heterocyclic compounds through [3+2] cycloaddition reaction of azomethine ylides and bis(arylidene)indanones (Figure 6A.2). The synthesized compounds were screened against *Mycobacterium tuberculosis* using the agar dilution method and displayed good activities [14].

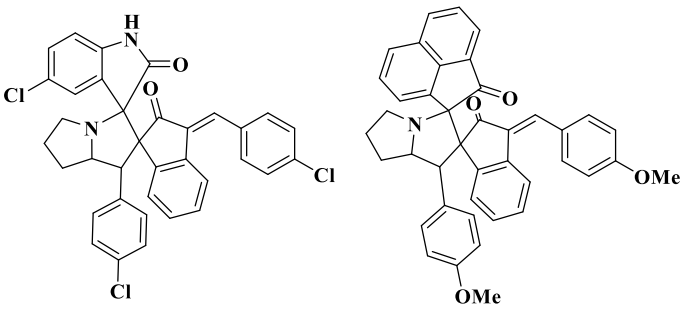

Figure 6A.2

Kia et al. disclosed one-pot three component reaction of 1-acryloyl-3,5-bisaryl methylidene-piperidinones with isatin and sarcosine to furnish bis-spiropyrrolidine heterocyclic compounds having functionalized piperidine, pyrrolidine and oxindole structural moieties (Figure 6A.3). These compounds displayed good inhibitory activity against acetylcholinesterase (AChE) and butyrylcholinesterase (BChE). Further, molecular docking studies were carried out and the obtained values were in good correlation with IC_{50} values of the synthesized compounds [15].

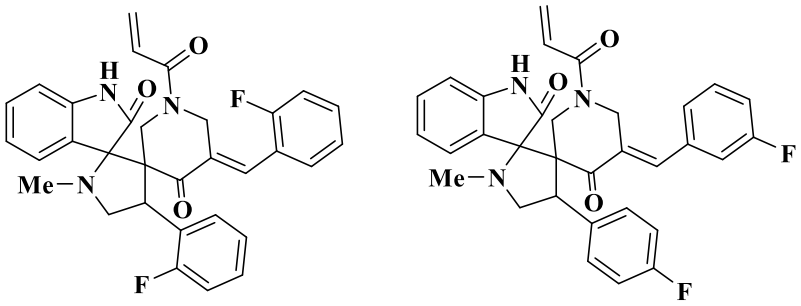

Figure 6A.3

Chakraborty et al. prepared dispirooxindolo andrographolide derivatives from isatin, *N*-benzyl glycine and andrographolide *via* azomethine ylide cycloaddition reaction (Figure 6A.4). The cytotoxic effect of the synthesized compounds was studied against MCF-7 breast cancer cell line [16].

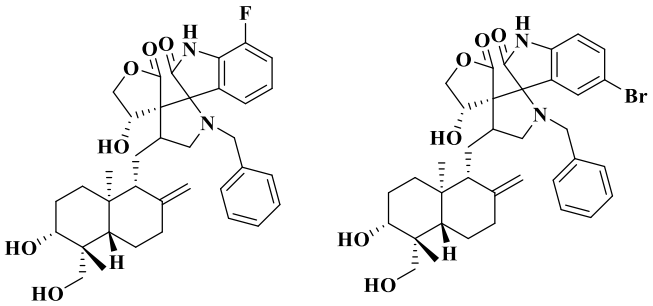

Figure 6A.4

Ramesh et al. produced a simple, efficient and regioselective synthesis of functionalized bisspirooxindolo-pyrrolidines using ceric ammonium nitrate as a catalyst in aqueous medium (Figure 6A.5). All the synthesized compounds were tested for *in vitro* anti-microbial activity and they have shown good anti-microbial activity against *bacillus subtilis* [17].

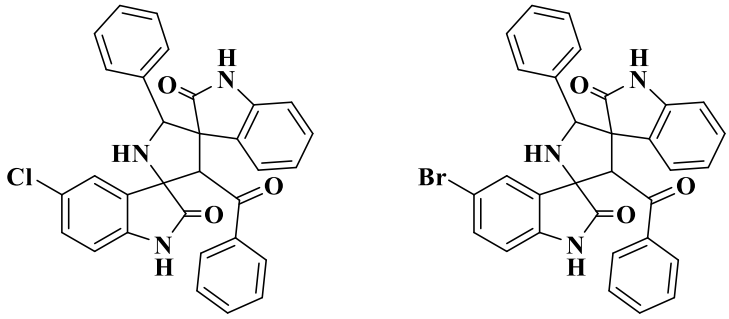

Figure 6A.5

Lotfy et al. demonstrated a regio- and stereo-selective synthesis of new bisspirooxindoles *via* 1,3-dipolar cycloaddition reaction (Figure 6A.6). Further, the compounds were evaluated for *in vitro* against two cancer cell lines, including MCF-7 breast cancer and K562-leukemia cell lines and they have exhibited good activity [18].

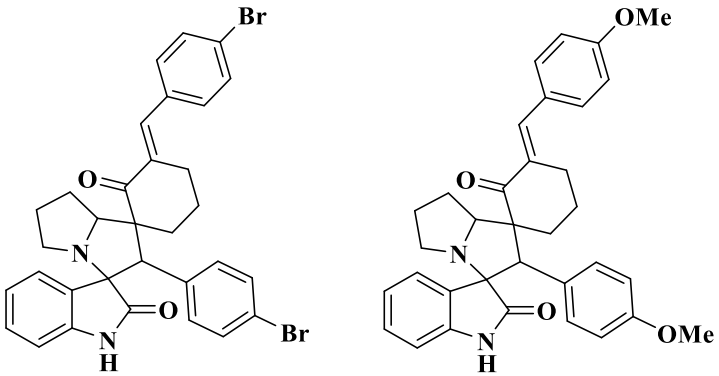

Figure 6A.6

Yuan and co-workers employed an organocatalytic asymmetric [3+2] cycloaddition reaction of trifluoroethylisatin ketimines with *β*-trifluoromethyl enones for the generation of bis(trifluoromethyl)-pyrrolidinyl spirooxindoles (Scheme 6A.1). The main significance of this protocol was its extremely high efficiency in the synthesis of structurally diverse spirocyclic oxindoles bearing four contiguous stereo-centers [19].

Scheme 6A.1

Zhang and co-workers described a facile synthesis of bisspirooxindoles through one-pot [3+2] cycloaddition reaction (Scheme 6A.2). The structures and relative configuration of the synthesized compounds were confirmed by single crystal X-ray diffraction analysis. High efficacy, mild reaction conditions and convenient operation were the main features of this protocol [20].

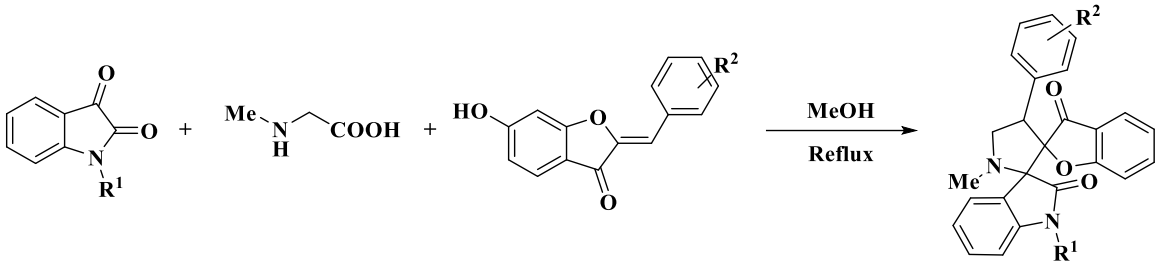

Scheme 6A.2

Bhandari et al. reported a facile approach for the synthesis of pyrrolidine fused bisspirooxindoles through microwave assisted one-pot three component [3+2] cycloaddition of azomethine ylides and 3-alkenyloxindoles (Scheme 6A.3). The additive free, high atom economy and wide substrate scope make this protocol attractive and useful for the synthesis of pharmacological heterocyclic compounds [21].

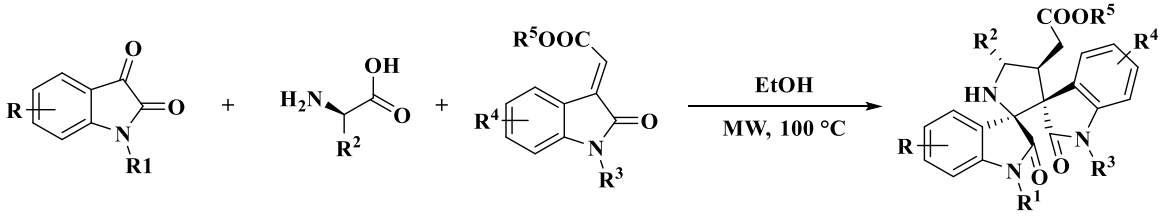

Scheme 6A.3

Shahrestani et al. demonstrated the synthesis of highly enantioenriched bisspirooxindole pyrrolidines *via* asymmetric [3+2] cycloaddition of isatin-derived azomethine ylides by 2-oxoindolin-3-ylidene acetyl sultam (Scheme 6A.4). These compounds can undergo retro-Mannich ring-opening cyclization and generated a new class of unusual diastereoisomers of bisspirooxindole pyrrolidines [22].

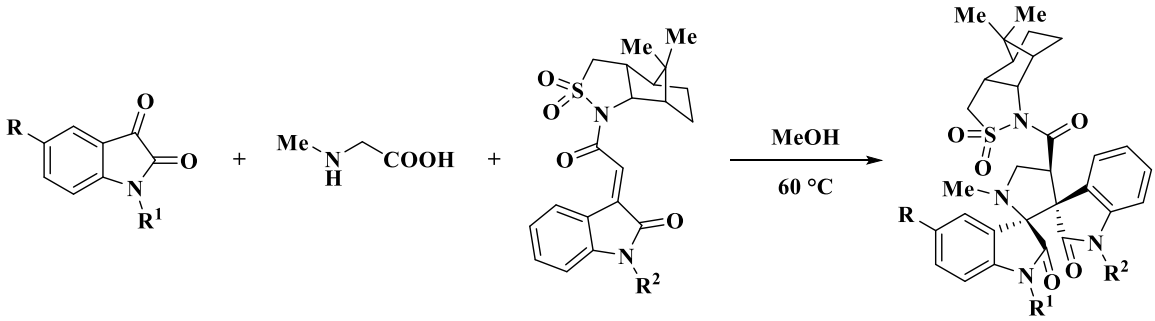

Scheme 6A.4

6A.2. Present work and design strategy

Spirooxindole bearing compound **A** (Figure 6A.7) exhibited potent anti-tubercular activity [23]. **Mhiri et al.** described dispirooxindolopyrrolizidines as potential anti-tubercular agents (Figure 6A.7, compound **B**) [24]. **Arumugam and co-workers** reported novel spirooxindolopyrrolidines as anti-mycobacterial (anti-TB) agents (Figure 6A.7, compound **C**) [25]. On the other hand, quinazolinones were also widely occur in pharmaceuticals [26], natural products [27] and shows broad spectrum of biological activities, including anti-cancer [28], anti-inflammatory [29] anti-viral [30] anti-microbial [31] anti-alzheimer [32] etc. **Kamal and co-workers** reported quinazolinones as anti-tubercular agents (Figure 6A.7, compound **D**) [33]. **Lu et al.** disclosed quinazolinone benzoates as novel anti-tuberculosis agents (Figure 6A.7, compound **E**) [34].

Encouraged by the above literature reports and considering the significance of bisspirooxindoles, we have designed and synthesized novel quinazolinone based pyrrolidino-bisspirooxindoles.

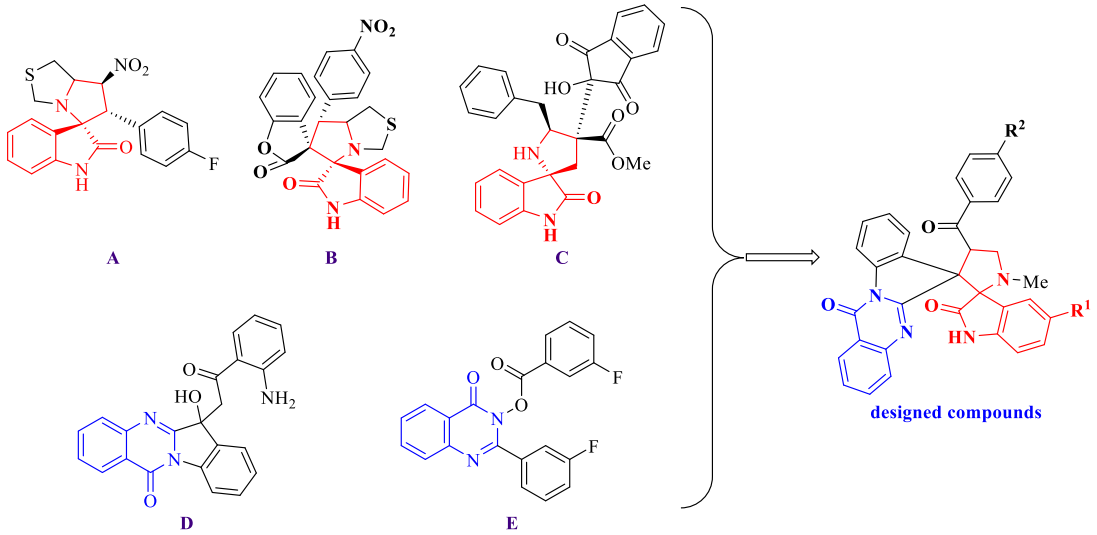

Figure 6A.7. Representative examples of anti-tubercular spirooxindoles, quinazolinones as well as the compounds designed in this study.

The title compounds **4a-o** were synthesized by taking isatins **1a-c**, quinazolinyl chalcones **2a-e** and sarcosine **3** as starting materials in CH_3CN under ultrasonication (Scheme 6A.5). Further, the title compounds were evaluated for *in vitro* anti-tubercular activity and *in silico* molecular docking studies.

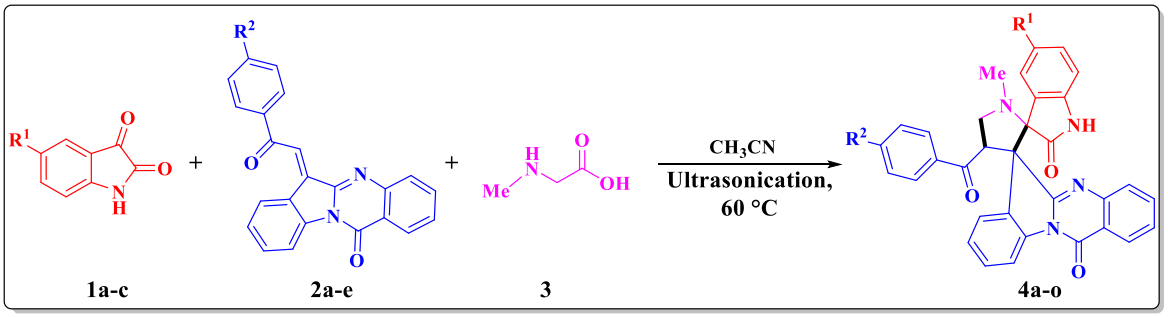

Scheme 6A.5. Synthesis of quinazolinyl-bisspirooxinolo-pyrrolidines **4a-o**.

6A.2.1. Results and discussion

We commenced our study by choosing isatin **1a**, 6-(2-oxo-2-phenyl-ethylidene)indolo[2,1-*b*]quinazolin-12(6*H*)-one **2a** and sarcosine **3** as the model reactants to get the optimized reaction parameters (Table 6A.1). Initially, the model reaction was carried in MeOH at room temperature resulting the desired product **4a** in 45% yield (Table 6A.1, entry 1). The product yield increased with the rising reaction temperatures (Table 6A.1, entries 2-6). Further, the reaction was conducted in different solvents such as EtOH, 1,4-dioxane, CH_3CN, toluene (Table 6A.1, entries 3-6). Among these, highest yield was obtained in CH_3CN (Table 6A.1, entry 5). To increase the product yield and environmental concerns an attempt was made under ultrasonication (RT and 60 °C), and to our surprise, the reaction was feasible (Table 6A.1, entry 7-9). The highest yield of product was obtained when the reaction was carried out in CH_3CN at 60 °C (Table 6A.1, entry 8). However, increasing reaction time has no significant impact on the yield (Table 6A.1, entry 9). Thus, 1.0 mmol of **1a**, 1.0 mmol of **2a** and 1.0 mmol of **3** in 3 mL of CH_3CN at 60 °C under ultrasonication (Table 6A.1, entry 8) is the best reaction condition for the generation of target compounds **4a-o**.

Table 6A.1. Optimization of the reaction conditions[a]

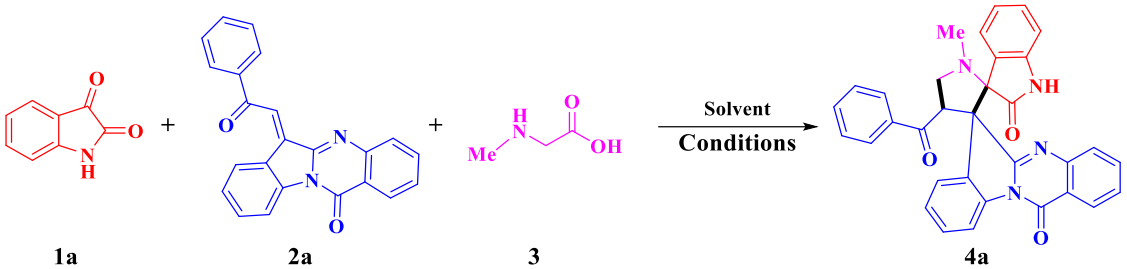

1a 2a 3 4a

Entry	Solvent	Method	Temp (°C)	Time	Yield (%)[b]
1	MeOH	Conventional	RT	20 h	45
2	MeOH	Conventional	Reflux	8 h	60
3	EtOH	Conventional	Reflux	8 h	65
4	1,4-Dioxane	Conventional	Reflux	9 h	47
5	CH_3CN	Conventional	Reflux	6 h	70
6	Toluene	Conventional	Reflux	10 h	48
7	CH_3CN	Ultrasonication	RT	120 min	75
8	**CH_3CN**	**Ultrasonication**	**60**	**35 min**	**83**
9	CH_3CN	Ultrasonication	60	90 min	84

[a]Reaction condition: isatin **1a** (1.0 mmol), compound **2a** (1.0 mmol), and sarcosine **3** (1.0 mmol), solvent (3 mL). [b]Isolated yields.

With the optimized reaction conditions in hand, we have explored the substrate scope by taking various isatins **1a-c**, quinazolinone chalcones **2a-e** and sarcosine **3** (Table 6A.2). Quinazolinone chalcones bearing electron donating (–Me, –OMe) and halogen (–Cl, –Br) substitutions have no substantial impact on the efficiency of the reaction. Nevertheless, we also found that halo (–Cl, –Br) substituted isatins could react smoothly to provide the desired products in good yields.

Table 6A.2. Synthesis of quinazolinyl-bisspirooxindolo-pyrrolidines **4**[a,b]

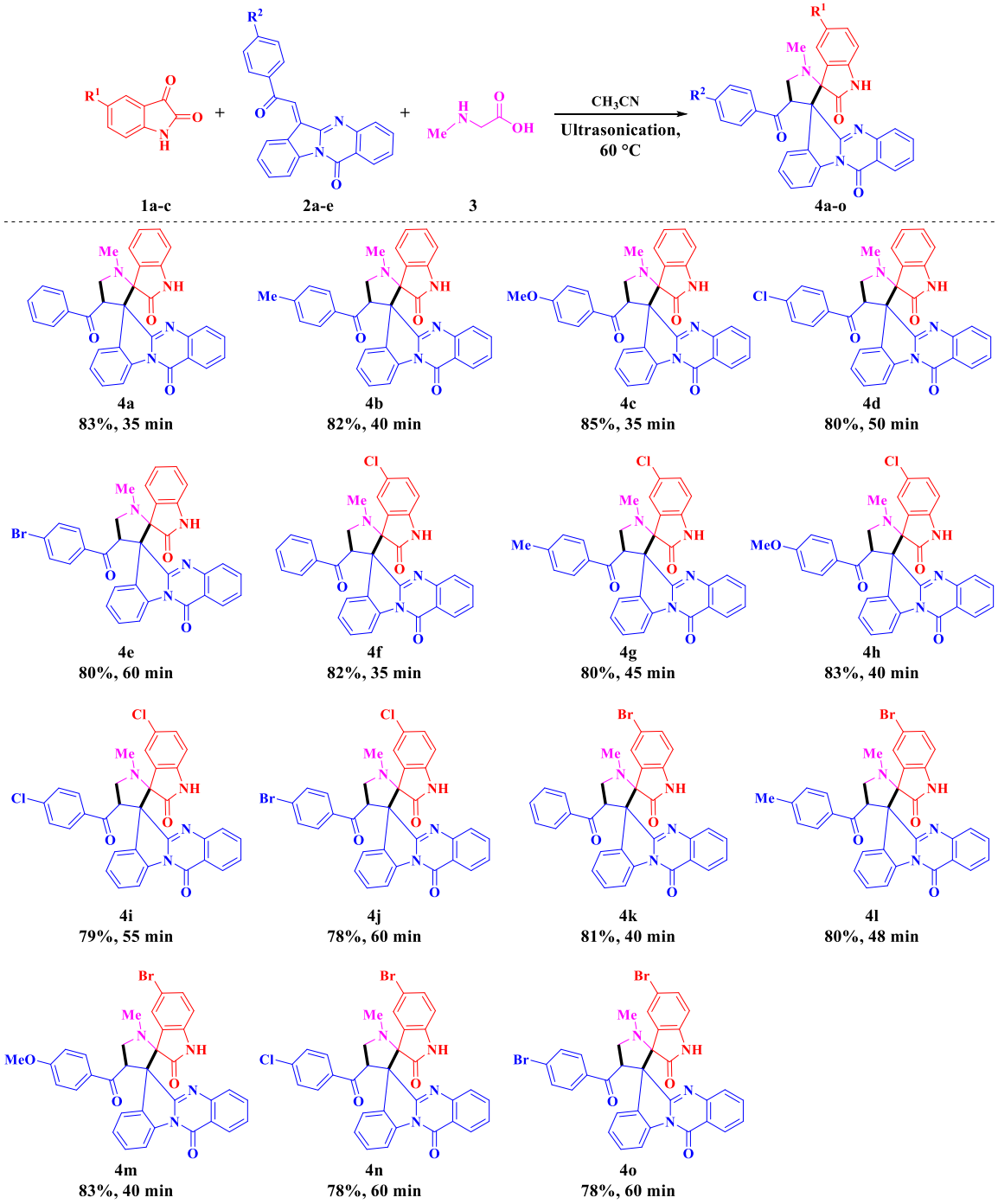

[a]Reaction condition: isatins **1a-c** (1.0 mmol), quinazolinone chalcones **2a-e** (1.0 mmol) and sarcosine **3** (1.0 mmol) in 3 mL of CH_3CN under ultrasonication at 60 °C. [b]Isolated yields.

The plausible reaction mechanism for the generation of target compounds **4** is illustrated in Scheme 6A.6. Initially, azomethine ylide **6** has generated *via* oxazolidinone **5** formation between isatin **1a** and sarcosine **3**, by the elimination of H_2O and CO_2. Later, it undergoes [3+2] cycloaddition reaction with quinazolinone chalcone **2a** delivers the target compound **4a**.

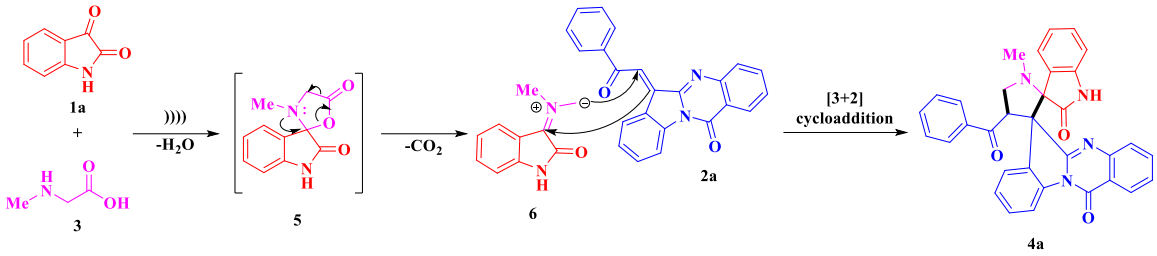

Scheme 6A.6. Plausible reaction mechanism for the generation of target compounds **4**.

The possible mode of approach of azomethine ylide (dipole **6**) is shown in Figure 6A.8. The regioselectivity of cycloaddition in the product formation can be demonstrated by considering secondary orbital interaction (SOI) of the nitrogen atom of the dipolarophile (chalcone **2a**) [35]. As a result of SOI, the observed regioisomer **4a** *via* path A is more favourable than path B, which was also evidenced by NMR and single crystal analysis.

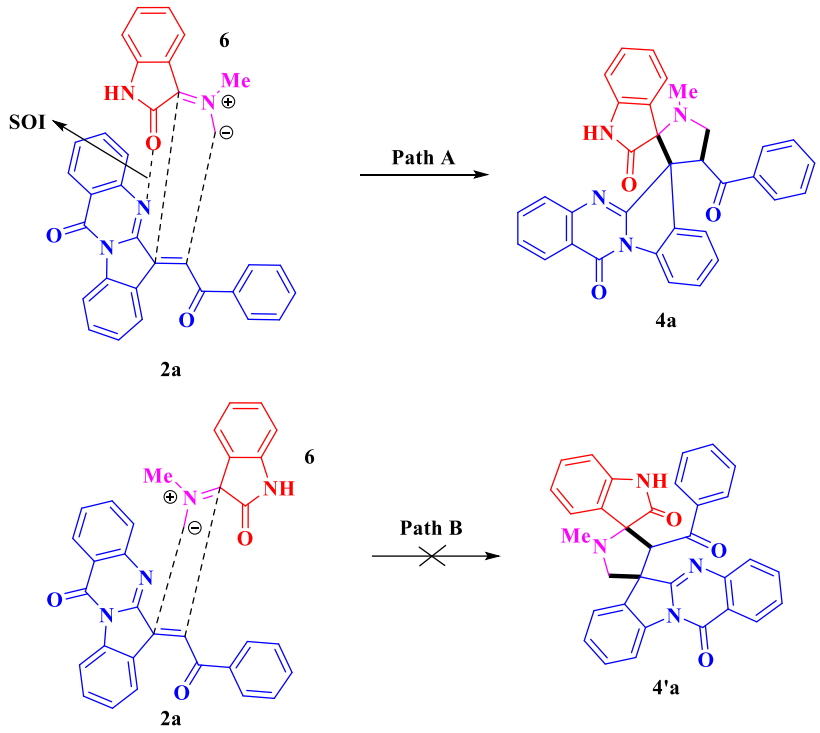

Figure 6A.8. mode of approach of azomethine ylide **6**.

The structures of all the target compounds **4a-o** were characterized by using spectroscopic (IR, ^{1}H, ^{13}C NMR and mass) methods, and finally authenticated by single crystal X-ray diffraction (SXRD) of **4a** (Figure 6A.9). In this context, IR spectrum of compound **4a** showed a band at 3186 cm^{-1} corresponds to –NH group and the bands at 1709 cm^{-1}, 1688 cm^{-1} and 1640 cm^{-1} represents benzoyl carbonyl group and the amide carbonyls of oxindole and quinazolinone moieties respectively [36]. In the ^{1}H NMR spectrum, peaks at δ 5.75 (dd, J = 10.0, 6.4 Hz, 1H), δ 4.22 (dd, J = 8.8, 6.8 Hz, 1H), and δ 3.89 (t, J = 10.0 Hz, 1H) *ppm* corresponds to the protons of pyrrolidine ring. In ^{13}C NMR the peaks at δ

79.07 and δ 62.03 represents the two spiro carbons of oxindole and quinazolinone moieties respectively, and the spiro carbons were further determined by absence of those peaks in DEPT-135 NMR spectrum (**4a**). The molecular ion peak at *m/z* 525.1853 $[M+H]^+$ in the mass spectrum determines the molecular weight of the compound **4a**. In addition, SXRD data of compound **4a** (*CCDC*: 2116963) demonstrates the regiochemistry of the generated compounds. The structure refinement parameters of the compound **4a** were represented in Table 6A.3.

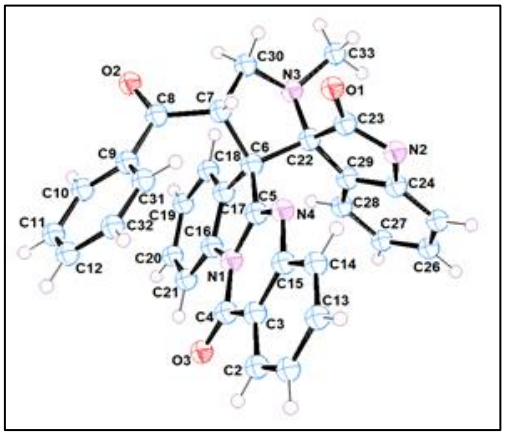

Figure 6A.9. ORTEP representation of the compound **4a** and the thermal ellipsoids were drawn at 50% probability level.

Table 6A.3. Salient features and crystallographic information of **4a**

Identification code	**4a**
Empirical formula	$C_{33}H_{24}N_4O_3$
Formula weight	524.5687
Crystal system	Triclinic
Space group	*P*-1
T (K)	100 K
a (Å)	9.5818 (3)
b (Å)	15.5984 (6)
c (Å)	17.7898 (6)
α (°)	74.743 (1)
β (°)	80.975 (1)
γ (°)	89.035 (1)
Z	2
V (Å^3)	2532.58 (15)
D_{calc} (g/cm^3)	1.375
F (000)	1094.0
μ (mm^{-1})	0.090
Θ (°)	28.719
Index ranges	$-12 \leq h \leq 12$ $-21 \leq k \leq 21$ $-24 \leq k \leq 24$

N-total	13104
Parameters	723
R_1 *[I > 2 σ (I)]*	0.0793
wR_2 (all data)	0.2346
GOF	1.439
CCDC	2116963

6A.2.2. Biological activity

6A.2.2.1. Anti-tubercular activity (anti-TB)

The *in vitro* anti-tubercular screening of the target compounds **4a-o** were evaluated against *Mycobacterium tuberculosis* H37Rv (ATCC27294) by the microplate alamar blue assay (MABA) method [37]. The minimum inhibitory concentration (MIC) values of **4a-o** along with standard drugs (Isoniazid, Rifampicin and Ethambutol) are provided in Table 6A.4. In comparison to the first line anti-TB drugs, compounds **4a-o** exhibited significant to moderate activity against Mtb with MIC values ranging from 3.125 µg/mL to 25 µg/mL. Among them, the compounds **4c**, **4f** and **4k** exhibit significant activity (MIC = 3.125 µg/mL) when compared to the standard drug ethambutol. Whereas the compounds **4a, 4h, 4i, 4m** and **4n** displayed good activity (MIC = 6.25 µg/mL). While the remaining compounds exhibit moderate to poor activity.

Table 6A.4. *In vitro* anti-tubercular activity of the target compounds **4a-o**

Entry	Compound	MIC (µg/mL)	% of Inhibition @25µM[a]
1	**4a**	**6.25**	**22.05**
2	4b	12.5	ND[b]
3	**4c**	**3.125**	**21.04**
4	4d	>25	ND
5	4e	12.5	ND
6	**4f**	**3.125**	**23.68**
7	4g	>25	ND
8	**4h**	**6.25**	**25.10**
9	**4i**	**6.25**	**18.92**
10	4j	12.5	ND
11	**4k**	**3.125**	**17.65**
12	4l	>25	ND
13	**4m**	**6.25**	**23.65**
14	**4n**	**6.25**	**21.14**
15	4o	12.5	ND
16	Isoniazid	0.05	ND
17	Rifampicin	0.1	ND
18	Ethambutol	1.56	ND

[a]% inhibition was examined using RAW 264.7 cell line, [b]ND = not determined.

6A.2.2.2. Cytotoxicity studies

The active analogues (**4a**, **4c**, **4f**, **4h**, **4i**, **4k**, **4m** and **4n**) were also evaluated for *in vitro* cytotoxicity effect against RAW 264.7 cells at 25μM concentration using MTT assay [38]. The percentage of inhibition data is presented in Table 6A.4. From this data, it has been concluded that the promising active compounds were less toxic to RAW 264.7 cells and were suitable for further mechanistic studies (Figure 6A.10).

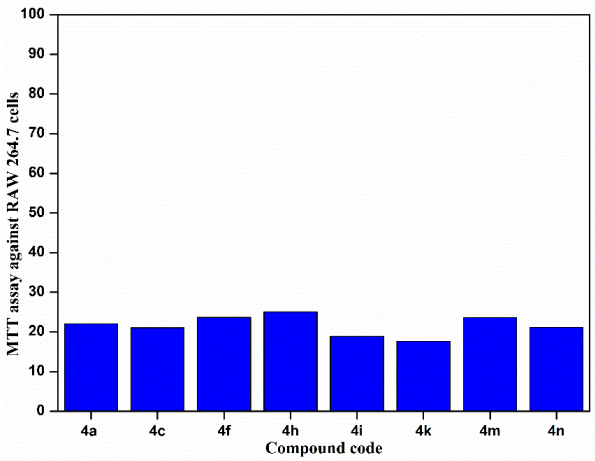

Figure 6A.10. % inhibition of potent anti-tubercular compounds on RAW 264.7 cell line at 25μM concentration.

6A.2.2.3. Structure activity relationship studies

The structure activity relationship (SAR) studies unveils that the diverse donor and acceptor abilities of substituted groups on the phenyl ring and structural changes are crucial in their anti-tubercular activity of the title compounds. The presence of methoxy (–OMe) substitution on the phenyl ring is significantly enhances the anti-tubercular activity when compared to other substitutions. Whereas, the compounds having halo (–Cl, –Br) substitution on isatin ring exhibited good activity than the unsubstituted isatin.

6A.3. Molecular docking studies

In order to investigate the binding sites and the protein-ligand interactions of target compounds **4a-o** the computational molecular docking studies were performed against dihydrofolate reductase of *Mycobacterium Tuberculosis* (PDB code: 1DF7) [39]. *In silico* molecular docking studies revealed that the active molecules showed good binding energy to the target protein, ranging from -7.94 to -10.06 kcal/mol. Among these, the most potent compounds **4c** and **4f** exhibited the lowest binding energies -10.03 kcal/mol and -10.06 kcal/mol respectively. The compound **4c** forms three H-bonds with the amino acid residues GLN28 (3.73 Å), LYS53 (2.64 Å), ILE94 (3.41 Å) and exhibited four hydrophobic interactons (π···π and π···alkyl) with the amino acid residues. Whereas, the compound **4f**

forms two H-bonds with the amino acid residues SER49 (2.95 Å), ILE94 (3.60 Å) and forms three hydrophobic (π···π and π···alkyl) interactions. The binding energies of active molecules and their H-bonding interactions found in the docking study were in good correlation with their anti-tuberculosis studies. The detailed H-bonding profile of the title compounds with the protein 1DF7 is given in Table 6A.5. The ligand interactions of the compounds **4c** and **4f** were presented in Figure 6A.11 and Figure 6A.12.

Table 6A.5 Docking results of the compounds **4a-o** against 1DF7

Ent-ry	Compound	Binding energy (kcal/mol)	No. of hydrogen bonds	Residues involved in the hydrogen bonding	Hydrogen bond length (Å)
1	**4a**	-9.03	5	ASP27, PHE31, LEU50, PRO51, ILE94	3.03, 3.29, 3.34, 3.42, 3.47
2	**4b**	-8.39	5	ALA7, ASP27, PHE31, TYR100	2.33, 2.77, 2.84, 2.84, 3.17
3	**4c**	**-10.03**	3	GLN28, LYS53, ILE94	3.73, 2.64, 3.41
4	**4d**	-8.49	5	ALA7, ASP27, PHE31, TYR100	2.20, 2.51, 2.77, 2.83, 3.17
5	**4e**	-8.69	2	ILE94	3.04, 3.57
6	**4f**	**-10.06**	2	SER49, ILE94	2.95, 3.60
7	**4g**	-8.46	1	ILE94	2.75
8	**4h**	-8.35	2	LYS53, ILE94	2.65, 2.77
9	**4i**	-8.56	1	ILE94	2.73
10	**4j**	-8.53	1	ILE94	2.70
11	**4k**	-9.69	3	PHE31, SER49, ILE94	2.59, 3.16, 3.65
12	**4l**	-8.09	1	ILE94	2.75
13	**4m**	-7.94	3	LYS53, ILE94	2.66, 2.78, 3.08
14	**4n**	-8.19	1	ILE94	2.99
15	**4o**	-8.20	1	ILE94	2.67

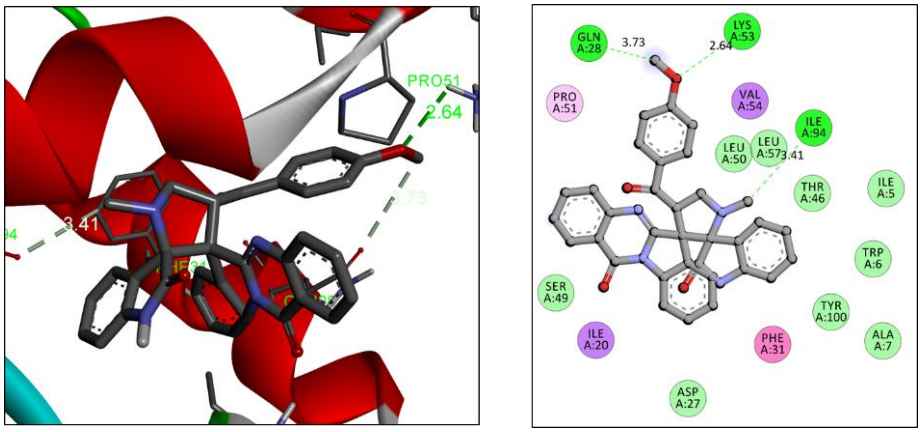

Figure 6A.11. Binding interactions between compound **4c** and active site of *Mycobacterium tuberculosis* protein (PDB ID: 1DF7).

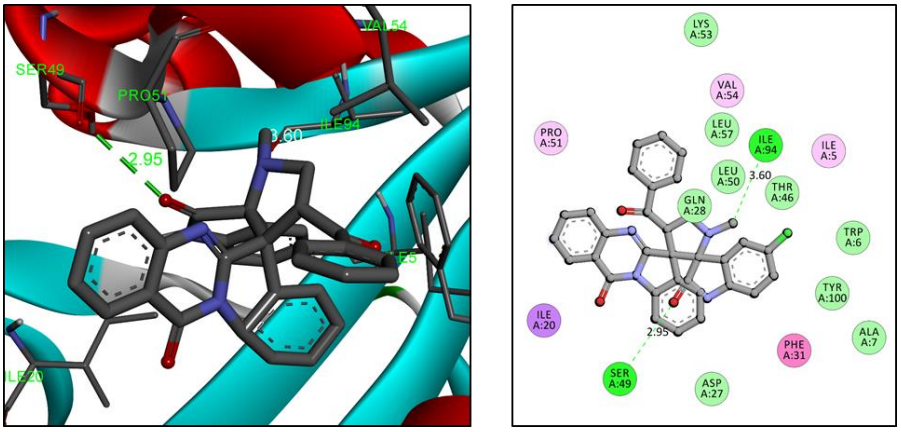

Figure 6A.12. Binding interactions between compound **4f** and active site of *Mycobacterium tuberculosis* protein (PDB ID: 1DF7).

6A.4. Conclusion

In this chapter a series of novel quinazolinone based pyrrolidino-bisspirooxindoles were designed and synthesized *via* [3+2] cycloaddition reaction under ultrasonication. The synthesized compounds were well characterized and determined by SXRD method (**4a**). *In vitro* anti-tubercular screening results revealed that, the compounds having methoxy (–OMe) substitution showed better anti-tubercular profile than other compounds against *M. tuberculosis* H37Rv. The active compounds were exhibited relatively low levels of cytotoxicity against RAW 264.7 cell line, which revealed their growth of therapeutic potential in the field of anti-tubercular agents. In addition, the molecular docking studies support that the potent compounds have better binding capacity towards the target enzyme. These results suggest that the synthesized pyrrolidino-bisspirooxindoles would be promising hits for the development of anti-TB leads.

6A.5. Experimental Section

6A.5.1. Typical procedure for the synthesis of quinazolinone based pyrrolidino-bisspirooxindoles 4a-o

A mixture of isatins **1** (1.0 mmol), quinazolinone chalcones **2** (1.0 mmol) and sarcosine **3** (1.0 mmol) in 3 mL of CH_3CN were heated at 60 °C under ultrasonication for 35-60 min. After the complete consumption of starting materials (monitored by TLC), the reaction mixture was cooled to room temperature. The resulting solid was filtered and recrystallized from methanol to furnish the desired products.

6A.5.2. Protocol for the anti-TB screening

The MIC of the synthesized compounds was tested using *in vitro* microplate alamar blue assay method [40]. The *Mycobacterium tuberculosis* H37Rv strain (ATCC27294) was

used for the screening. The inoculum was prepared from fresh LJ medium re-suspended in 7H9-S medium (7H9 broth, 0.1% casitone, 0.5% glycerol, supplemented oleic acid, albumin, dextrose, and catalase [OADC]), adjusted to a OD_{590} 1.0, and diluted 1:20; 100 µL was used as inoculum. Each drug stock solution was thawed and diluted in 7H9-S at four-fold the final highest concentration tested. Serial two-fold dilutions of each drug were prepared directly in a sterile 96-well microtiter plate using 100 µL 7H9-S. A growth control containing no antibiotic and a sterile control were also prepared on each plate. Sterile water was added to all perimeter wells to avoid evaporation during the incubation. The plate was covered, sealed in plastic bags and incubated at 37 ^{o}C in normal atmosphere. After 7 days incubation, 30 µL of alamar blue solution was added to each well, and the plate was re-incubated overnight. A change in colour from blue (oxidised state) to pink (reduced) indicated the growth of bacteria, and the MIC was defined as the lowest concentration of drug that prevented this change in colour.

6A.5.3. *In vitro* cytotoxicity screening

The *in vitro* cytotoxicity of the privileged anti-tubercular active analogues with lower MIC value were assessed by 3-(4,5-dimethylthiazol-2-yl)-2,5-diphenyltetrazolium bromide (MTT) assay against growth inhibition of RAW 264.7 cells at 25 µM concentration [41]. Cell lines were maintained at 37 °C in a humidified 5% CO_2 incubator (Thermo scientific). Detached the adhered cells and followed by centrifugation to get cell pellet. Fresh media was added to the pellet to make a cell count using haemocytometer and plate 100 µL of media with cells ranging from 5,000 - 6,000 per well in a 96-well plate. The plate was incubated overnight in CO_2 incubator for the cells to adhere and regain its shape. After 24 h cells were treated with the test compounds at 25 µg/mL diluted using the media to deduce the percentage inhibition on normal cells. The cells were incubated for 48 h to assay the effect of the test compounds on different cell lines. Zero hour reading was noted down with untreated cells and also control with 1% DMSO to subtract further from the 48 h reading. After 48 h incubation, cells were treated by MTT (4,5-dimethylthiazol-2-yl)-2,5-diphenyltetrazolium bromide) dissolved in PBS (5 mg/mL) and incubated for 3-4 h at 37 °C. The formazan crystals thus formed were dissolved in 100 µL of DMSO and the viability was measured at 540 nm on a multimode reader (Spectra max). The values were further calculated for percentage inhibition which in turn helps us to know the cytotoxicity of the test compounds.

6A.5.4. Molecular docking protocol

The docking studies are predominating tools for the assessment of the binding affinity to the ligand-protein receptor. All the synthesized compounds were subjected to *in silico* molecular docking studies by using the AutoDockTools (ADT) version 1.5.6 and AutoDock version 4.2.5.1 docking program [42]. The 3D-structures of all the synthesized compounds were prepared by using chem3D pro 12.0 software. The optimized 3D structures were saved in pdb format. The structure of the dihydrofolate reductase of *Mycobacterium tuberculosis* (PDB code: 1DF7) protein was extracted from the protein data bank (http://www.rcsb.org/pdb). The bound ligand and water molecules in protein were removed by using Discovery Studio Visualizer version 4.0 to prepare the protein. Non polar hydrogens were merged and gasteiger charges were added to the protein. The grid file was saved in gpf format. The three dimensional grid box having dimensions 60 x 60 x 60 $Å^3$ was created around the protein with spacing 0.3750 Å. The genetic algorithm was carried out with the population size and the maximum number of evaluations were 150 and 25,00,000 respectively. The docking output file was saved as Lamarckian Ga (4.2) in dpf format. The ligand-protein complex binding sites were visualized by Discovery Studio Visualizer version 4.0.

6A.6. Spectral data of synthesized compounds 4a-o

4'-benzoyl-1'-methyl-12''*H*-dispiro[indoline-3,2'-pyrrolidine-3',6''-indolo[2,1-*b*]quinazoline]-2,12''-dione (4a)

Off-white solid. mp: 239-241 °C. IR (KBr, cm^{-1}): 3186, 1709, 1688, 1640, 1470. ^{1}H NMR (400 MHz, DMSO-d_6) δ: 10.48 (s, 1H), 8.09-8.04 (m, 2H), 7.93 (t, J = 7.6 Hz, 1H), 7.833-7.784 (m, 2H), 7.60 (t, J = 7.6 Hz, 1H), 7.52 – 7.48 (m, 2H), 7.19 (t, J = 7.6 Hz, 1H), 7.04 (d, J = 7.6 Hz, 2H), 6.95 (t, J = 7.6 Hz, 1H), 6.84 (t, J = 7.6 Hz, 2H), 6.49 (d, J = 7.6 Hz, 1H), 6.42 (t, J = 7.6 Hz, 1H), 5.84 (d, J = 7.6 Hz, 1H), 5.75 (dd, J = 10.0, 6.4 Hz, 1H), 4.22 (dd, J = 8.8, 6.8 Hz, 1H), 3.89 (t, J = 10 Hz, 1H), 2.22 (s, 3H). ^{13}C NMR (100 MHz, DMSO-d_6) δ: 199.26, 175.74, 158.49, 156.21, 146.52, 143.69, 139.53, 137.46, 135.40, 132.59, 130.43, 129.98, 129.73, 128.37, 128.16, 127.92, 127.58, 126.60, 126.26, 125.40, 122.79, 121.16, 120.80, 115.69, 109.79, 79.07, 62.03, 53.54, 51.71, 35.30. ESI mass spectrum (m/z): calcd. for $C_{33}H_{25}N_4O_3$ $[M+H]^+$: 525.1927; obsd.: 525.1853.

1'-methyl-4'-(4-methylbenzoyl)-12''*H*-dispiro[indoline-3,2'-pyrrolidine-3',6''-indolo[2,1-*b*]quinazoline]-2,12''-dione (4b)

Pale brown solid. mp: 214-216 ℃. IR (KBr, cm^{-1}): 3193, 1714, 1670, 1638, 1463. ^{1}H NMR (400 MHz, DMSO-d_6) δ: 10.49 (s, 1H), 8.09 (t, J = 8.4 Hz, 2H), 7.93 (t, J = 7.6 Hz, 1H), 7.82 (d, J = 8.4 Hz, 1H), 7.78 (d, J = 8.0 Hz, 1H), 7.60 (t, J = 7.6 Hz, 1H), 7.54 – 7.44 (m, 2H), 6.96 (d, J = 8.0 Hz, 3H), 6.64 (d, J = 8.0 Hz, 2H), 6.50 (d, J = 7.6 Hz, 1H), 6.42 (t, J = 7.6 Hz, 1H), 5.86 (d, J = 7.2 Hz, 1H), 5.72 (q, J = 6.4 Hz, 1H), 4.18 (q, J = 7.2 Hz, 1H), 3.87 (t, J = 10.0 Hz, 1H), 2.22 (s, 3H), 2.03 (s, 3H). ^{13}C NMR (100 MHz, DMSO-d_6) δ: 198.82, 175.97, 158.56, 156.22, 146.50, 143.60, 143.01, 139.55, 135.42, 134.78, 130.44, 129.93, 129.69, 128.47, 128.34, 128.13, 127.94, 127.68, 126.41, 126.23, 125.43, 122.86, 121.21, 120.86, 115.75, 109.85, 78.90, 62.15, 53.60, 51.74, 35.27, 21.21. ESI mass spectrum (m/z): calcd. for $C_{34}H_{27}N_4O_3$ $[M+H]^+$: 539.2083; obsd.: 539.1985.

4'-(4-methoxybenzoyl)-1'-methyl-12''*H*-dispiro[indoline-3,2'-pyrrolidine-3',6''-indolo[2,1-*b*]quinazoline]-2,12''-dione (4c)

Off-white solid. mp: 200-202 ℃. IR (KBr, cm^{-1}): 3267, 1714, 1686, 1639, 1465. ^{1}H NMR (400 MHz, DMSO-d_6) δ: 10.47 (s, 1H), 8.11 – 8.08 (m, 2H), 7.95 – 7.91 (m, 1H), 7.84 – 7.81 (m, 1H), 7.79 (d, J = 7.6 Hz, 1H), 7.62 – 7.58 (m, 1H), 7.51 – 7.44 (m, 2H), 7.11 (d, J = 8.8 Hz, 2H), 6.94 (td, J = 8.0, 1.2 Hz, 1H), 6.49 (d, J = 7.6 Hz, 1H), 6.44 – 6.37 (m, 3H), 5.85 (d, J = 7.2 Hz, 1H), 5.72 (dd, J = 10.4, 6.4 Hz, 1H), 4.18 (dd, J = 9.2, 6.4 Hz, 1H), 3.87 (t, J = 9.6 Hz, 1H), 3.52 (s, 3H), 2.22 (s, 3H). ^{13}C NMR (100 MHz, DMSO-d_6) δ: 197.14, 175.83, 162.77, 158.60, 156.38, 146.59, 143.70, 139.51, 135.40, 130.38, 130.00, 129.90, 129.81, 128.41, 128.10, 127.98, 126.53, 126.16, 125.43, 122.91, 121.15, 120.89, 115.68, 113.33, 109.78, 78.92, 62.32, 55.68, 53.18, 52.01, 35.33. ESI mass spectrum (m/z): calcd. for $C_{34}H_{27}N_4O_4$ $[M+H]^+$: 555.2032; obsd.: 555.1954.

4'-(4-chlorobenzoyl)-1'-methyl-12''*H*-dispiro[indoline-3,2'-pyrrolidine-3',6''-indolo[2,1-*b*]quinazoline]-2,12''-dione (4d)

White solid. mp: 224-226 ℃. IR (KBr, cm^{-1}): 3195, 1717, 1681, 1637, 1462. ^{1}H NMR (400 MHz, DMSO-d_6) δ: 10.49 (s, 1H), 8.07 (t, 2H, J = 8.8 Hz), 7.93 (t, 1H, J = 8.0 Hz), 7.79 (t, 2H, J = 8.8 Hz), 7.60 (t, 1H, J = 7.6 Hz), 7.53 – 7.45 (m, 2H), 6.98 (d, 2H, J = 8.4 Hz), 6.93 (d, 1H, J = 7.6 Hz), 6.85 (d, 2H, J = 8.4 Hz), 6.50 (d, 1H, J = 7.6 Hz), 6.41 (t, 1H, J = 7.6 Hz), 5.84 (d, 1H, J = 7.6 Hz), 5.70 (dd, 1H, J = 10.0, 6.4 Hz), 4.17 (dd, 1H, J = 9.2, 6.4 Hz), 3.83 (t, 1H, J = 10.0 Hz), 2.19 (s, 3H).^{13}C NMR (100 MHz, DMSO-d_6) δ: 198.47,

175.93, 158.49, 155.97, 146.37, 143.54, 139.41, 137.55, 136.04, 135.56, 130.52, 130.17, 129.40, 128.40, 128.30, 127.99, 126.50, 126.39, 125.40, 122.72, 121.28, 120.66, 115.77, 109.91, 78.91, 62.01, 53.77, 51.46, 35.23. ESI mass spectrum (m/z): calcd. for $C_{33}H_{24}ClN_4O_3$ $[M+H]^+$: 559.1537; obsd.: 559.1464.

4'-(4-bromobenzoyl)-1'-methyl-12''*H*-dispiro[indoline-3,2'-pyrrolidine-3',6''-indolo[2,1-*b*]quinazoline]-2,12''-dione (4e)

Off-white solid. mp: 228-230 °C. IR (KBr, cm^{-1}): 3197, 1718, 1681, 1636, 1461. ^1H NMR (400 MHz, DMSO-d_6) δ: 10.50 (s, 1H), 8.10 (t, J = 8.0 Hz, 2H), 7.94 (t, J = 7.6 Hz, 1H), 7.83 (d, J = 7.2 Hz, 1H), 7.77 (d, J = 8.0 Hz, 1H), 7.62 (t, J = 7.6 Hz, 1H), 7.54-7.48 (m, 2H), 7.02 (d, J = 8.4 Hz, 2H), 6.97-6.91 (m, 3H), 6.50 (d, J = 8.0 Hz, 1H), 6.43 (t, J = 7.6 Hz, 1H), 5.86 (d, J = 7.6 Hz, 1H), 5.73 (dd, J = 10.0, 6.4 Hz, 1H), 4.19 (dd, J = 8.8, 6.7 Hz, 1H), 3.85 (t, J = 9.6 Hz, 1H), 2.22 (s, 3H). ^{13}C NMR (100 MHz, DMSO-d_6) δ: 198.62, 175.75, 158.44, 156.06, 146.42, 143.67, 139.50, 136.45, 135.49, 130.95, 130.48, 130.14, 129.52, 128.42, 128.22, 127.94, 126.56, 125.41, 122.76, 121.22, 120.78, 115.78, 109.86, 78.86, 62.03, 53.84, 51.50, 35.27. ESI mass spectrum (m/z): calcd. for $C_{33}H_{24}BrN_4O_3$ $(M+H)^+$: 605.1011; obsd.: 605.0904.

4'-benzoyl-5-chloro-1'-methyl-12''*H*-dispiro[indoline-3,2'-pyrrolidine-3',6''-indolo[2,1-*b*]quinazoline]-2,12''-dione (4f)

Off-white solid. mp: 212-214 °C. IR (KBr, cm^{-1}): 3363, 1680, 1662, 1646, 1464. ^1H NMR (400 MHz, DMSO-d_6) δ: 10.64 (s, 1H), 8.10 (d, J = 7.2 Hz, 2H), 7.94 (t, J = 7.2 Hz, 1H), 7.80 (d, J = 7.2 Hz, 2H), 7.61 (t, J = 7.6 Hz, 1H), 7.53 (bs, 2H), 7.21 (t, J = 7.2 Hz, 1H), 7.07 (d, J = 7.2 Hz, 2H), 7.02 (d, J = 7.6 Hz, 1H), 6.87 (t, J = 7.2 Hz, 2H), 6.50 (d, J = 8.0 Hz, 1H), 5.73 (d, J = 9.2 Hz, 2H), 4.22 (t, J = 7.6 Hz, 1H), 3.89 (t, J = 9.6 Hz, 1H), 2.24 (s, 3H). ^{13}C NMR (100 MHz, DMSO-d_6) δ: 199.04, 175.42, 158.49, 155.81, 146.44, 142.52, 139.56, 137.36, 135.46, 132.68, 130.30, 130.19, 129.42, 128.26, 127.98, 127.63, 126.65, 126.28, 125.50, 125.16, 124.80, 120.79, 115.79, 111.20, 79.16, 62.04, 53.38, 51.85, 35.38. ESI mass spectrum (m/z): calcd. for $C_{33}H_{24}ClN_4O_3$ $[M+H]^+$: 559.15; obsd.: 559.15.

5-chloro-1'-methyl-4'-(4-methylbenzoyl)-12''*H*-dispiro[indoline-3,2'-pyrrolidine-3',6''-indolo[2,1-*b*]quinazoline]-2,12''-dione (4g)

Pale brown solid. mp: 245-247 °C. IR (KBr, cm^{-1}): 3357, 1735, 1689, 1639, 1462. ^1H NMR (400 MHz, DMSO-d_6) δ: 10.64 (s, 1H), 8.12 (d, 2H, J = 7.6 Hz), 7.94 (t, 1H, J = 7.6 Hz), 7.79 (t, 2H, J = 9.2 Hz), 7.62 (t, 1H, J = 7.6 Hz), 7.56 – 7.48 (m, 2H), 7.03-6.97 (m, 3H),

6.67 (d, 2H, *J* = 7.6 Hz), 6.51 (d, 1H, *J* = 8.4 Hz), 5.75 (s, 1H), 5.69 (dd, 1H, *J* = 10.2, 6.4 Hz), 4.20 – 4.16 (m, 1H), 3.87 (t, 1H, *J* = 9.8 Hz), 2.24 (s, 3H), 2.05 (s, 3H). ^{13}C NMR (100 MHz, DMSO-d_6) δ: 198.51, 175.51, 158.53, 155.89, 146.45, 143.06, 142.51, 139.62, 135.45, 134.73, 130.28, 130.10, 129.46, 128.53, 128.22, 127.94, 127.77, 126.50, 126.23, 125.52, 125.17, 124.88, 120.91, 115.84, 111.20, 78.97, 62.17, 53.44, 51.93, 35.37, 21.25. ESI mass spectrum (m/z): calcd. for $C_{34}H_{26}ClN_4O_3$ $[M+H]^+$: 573.1693; obsd.: 573.1593.

5-chloro-4'-(4-methoxybenzoyl)-1'-methyl-12''*H*-dispiro[indoline-3,2'-pyrrolidine-3',6''-indolo[2,1-*b*]quinazoline]-2,12''-dione (4h)

Off-white solid. mp: 200-202 ℃. IR (KBr, cm^{-1}): 3353, 1659, 1643, 1464. ^{1}H NMR (400 MHz, DMSO-d_6) δ: 10.63 (s, 1H), 8.15 – 8.10 (m, 2H), 7.95 – 7.91 (m, 1H), 7.82 – 7.77 (m, 2H), 7.61 (td, *J* = 8.4, 1.2 Hz, 1H), 7.55 – 7.47 (m, 2H), 7.15 (d, *J* = 8.8 Hz, 2H), 7.01 (dd, *J* = 8.4, 2.4 Hz, 1H), 6.50 (d, *J* = 8.4 Hz, 1H), 6.42 (d, *J* = 8.8 Hz, 2H), 5.75 (d, *J* = 2.4 Hz, 1H), 5.70 (dd, *J* = 10.8, 6.8 Hz, 1H), 4.18 (dd, *J* = 9.2, 6.4 Hz, 1H), 3.87 (t, *J* = 10.0 Hz, 1H), 3.53 (s, 3H), 2.23 (s, 3H). ^{13}C NMR (100 MHz, DMSO-d_6) δ: 196.92, 175.52, 162.85, 158.61, 155.99, 146.52, 142.54, 139.56, 135.47, 130.26, 130.08, 130.02, 129.80, 129.64, 128.20, 127.99, 126.59, 126.19, 125.54, 125.17, 124.93, 120.90, 115.80, 113.40, 111.18, 79.02, 62.33, 55.70, 53.02, 52.16, 35.40. ESI mass spectrum (m/z): calcd. for $C_{34}H_{26}ClN_4O_4$ $[M+H]^+$: 589.1643; obsd.: 589.1662.

5-chloro-4'-(4-chlorobenzoyl)-1'-methyl-12''*H*-dispiro[indoline-3,2'-pyrrolidine-3',6''-indolo[2,1-*b*]quinazoline]-2,12''-dione (4i)

Pale green solid. mp: 229-231 ℃. IR (KBr, cm^{-1}): 3334, 1732, 1690, 1640, 1463. ^{1}H NMR (400 MHz, DMSO-d_6) δ: 10.65 (s, 1H), 8.12 (dd, *J* = 6.4, 5.2 Hz, 2H), 7.94 (t, *J* = 7.2 Hz, 1H), 7.80 (d, *J* = 6.4 Hz, 1H), 7.77 (d, *J* = 8.4 Hz, 1H), 7.62 (t, *J* = 7.2 Hz, 1H), 7.57 – 7.49 (m, 2H), 7.06 (s, 1H), 7.03 (s, 1H), 7.01 (dd, *J* = 8.4, 2.4 Hz, 1H), 6.91 (d, *J* = 8.4 Hz, 2H), 6.50 (d, *J* = 8.4 Hz, 1H), 5.74 (d, *J* = 2.0Hz, 1H), 5.73 – 5.69 (m, 1H), 4.19 (dd, *J* = 9.2, 6.4 Hz, 1H), 3.86 (t, *J* = 10.0 Hz, 1H), 2.23 (s, 3H). ^{13}C NMR (100 MHz, DMSO-d_6) δ: 198.14, 175.38, 158.46, 155.71, 146.37, 142.54, 139.55, 136.04, 135.52, 130.32, 129.52, 129.25, 128.31, 128.09, 127.96, 126.62, 126.35, 125.51, 125.19, 124.78, 120.80, 115.88, 111.23, 78.99, 62.06, 53.62, 51.72, 35.36. ESI mass spectrum (m/z): calcd. for $C_{33}H_{23}Cl_2N_4O_3$ $[M+H]^+$: 593.1147; obsd.: 593.1035.

4'-(4-bromobenzoyl)-5-chloro-1'-methyl-12''*H*-dispiro[indoline-3,2'-pyrrolidine-3',6''-indolo[2,1-*b*]quinazoline]-2,12''-dione (4j)

White solid. mp: 190-192 °C. IR (KBr, cm^{-1}): 3273, 1718, 1690, 1640, 1464. ^{1}H NMR (400 MHz, DMSO-d_6) δ: 10.66 (s, 1H), 8.14 (d, J = 7.6 Hz, 2H), 7.95 (t, J = 7.6 Hz, 1H), 7.82-76 (m, 2H), 7.63 (t, J = 7.6 Hz, 1H), 7.58-7.50 (m, 2H), 7.03 (t, J = 8.4 Hz, 3H), 6.96 (d, J = 8.0 Hz, 2H), 6.51 (d, J = 8.4 Hz, 1H), 5.75 (s, 1H), 5.71 (t, J = 6.8 Hz, 1H), 4.19 (t, J = 8.8 Hz, 1H), 3.86 (t, J = 10 Hz, 1H), 2.24 (s, 3H). ^{13}C NMR (100 MHz, DMSO-d_6) δ: 198.40, 175.41, 158.45, 155.69, 146.36, 142.53, 139.56, 136.37, 135.54, 131.03, 130.34, 129.59, 129.20, 128.31, 127.95, 126.66, 126.37, 125.51, 125.20, 124.79, 120.81, 115.90, 111.26, 78.95, 62.05, 53.68, 51.66, 35.36. ESI mass spectrum (m/z): calcd. for $C_{33}H_{23}BrClN_4O_3$ $[M+H]^+$: 639.0622; obsd.: 639.0509.

4'-benzoyl-5-bromo-1'-methyl-12''*H*-dispiro[indoline-3,2'-pyrrolidine-3',6''-indolo[2,1-*b*]quinazoline]-2,12''-dione (4k)

White solid. mp: 229-231 °C. IR (KBr, cm^{-1}): 3362, 1682, 1658, 1639, 1464. ^{1}H NMR (400 MHz, DMSO-d_6) δ: 10.64 (s, 1H), 8.10 (d, 2H, J = 7.6 Hz), 7.94 (t, 1H, J = 7.6 Hz), 7.79 (d, 2H, J = 8.0 Hz), 7.61 (t, 1H, J = 7.6 Hz), 7.56-7.49 (m, 2H), 7.21 (t, 1H, J = 7.6 Hz), 7.14 (d, 1H, J = 9.2 Hz), 7.07 (d, 2H, J = 7.6 Hz), 6.87 (t, 2H, J = 7.6 Hz), 6.45 (d,1H, J = 8.0 Hz), 5.86 (s, 1H), 5.73 (dd, 1H, J = 10.2, 6.4 Hz), 4.22 (dd, 1H, J = 8.8, 6.8 Hz), 3.89 (t,1H, J = 9.8 Hz), 2.24 (s, 3H). ^{13}C NMR (100 MHz, DMSO-d_6) δ: 199.06, 175.30, 158.51, 155.83, 146.45, 142.92, 139.59, 137.38, 135.47, 133.10, 132.69, 130.19, 129.46, 128.33, 128.27, 127.99, 127.65, 126.67, 126.26, 125.12, 120.81, 115.79, 112.86, 111.69, 79.19, 62.07, 53.35, 51.87, 35.40. ESI mass spectrum (m/z): calcd. for $C_{33}H_{24}BrN_4O_3$ $[M+H]^+$: 605.1011; obsd.: 605.0935.

5-bromo-1'-methyl-4'-(4-methylbenzoyl)-12''*H*-dispiro[indoline-3,2'-pyrrolidine-3',6''-indolo[2,1-*b*]quinazoline]-2,12''-dione (4l)

Pale brown solid. mp: 246-248 °C. IR (KBr, cm^{-1}): 3332, 1732, 1687, 1640, 1463. ^{1}H NMR (400 MHz, DMSO-d_6) δ: 10.63 (s, 1H), 8.11 (s, 2H), 7.92 (s, 1H), 7.78 (s, 2H), 7.60 (s, 1H), 7.52 (d, J = 6.0 Hz, 2H), 7.13 (s, 1H), 6.97 (s, 2H), 6.66 (s, 2H), 6.45 (s, 1H), 5.86 (s, 1H), 5.68 (s, 1H), 4.17 (s, 1H), 3.90 – 3.79 (m, 1H), 2.22 (s, 3H), 2.03 (s, 3H). ^{13}C NMR (100 MHz, DMSO-d_6) δ: 198.50, 175.34, 158.54, 155.91, 146.47, 143.04, 142.93, 139.65, 135.44, 134.76, 133.06, 130.09, 129.51, 128.54, 128.34, 128.21, 127.94, 127.78, 126.51,

126.18, 125.20, 120.94, 115.83, 112.84, 111.68, 79.01, 62.20, 53.40, 51.96, 35.39, 21.25. ESI mass spectrum (m/z): calcd. for $C_{34}H_{26}BrN_4O_3$ $[M+H]^+$: 619.1168; obsd.: 619.1099.

5-bromo-4'-(4-methoxybenzoyl)-1'-methyl-12''*H*-dispiro[indoline-3,2'-pyrrolidine-3',6''-indolo[2,1-*b*]quinazoline]-2,12''-dione (4m)

White solid. mp: 194-196 ℃. IR (KBr, cm^{-1}): 3353, 1730, 1687, 1642, 1464. ^{1}H NMR (400 MHz, DMSO- d_6) δ: 10.63 (s, 1H), 8.13 (t, J = 8.4 Hz, 2H), 7.93 (t, J = 7.6 Hz, 1H), 7.80 (t, J = 8.0 Hz, 2H), 7.61 (t, J = 7.6 Hz, 1H), 7.55 – 7.47 (m, 2H), 7.16 – 7.10 (m, 3H), 6.47 – 6.41 (m, 3H), 5.87 (s, 1H), 5.69 (dd, J = 10.0, 6.8 Hz, 1H), 4.17 (t, J = 8.4 Hz, 1H), 3.87 (t, J = 9.6 Hz, 1H), 3.54 (s, 3H), 2.23 (s, 3H). ^{13}C NMR (100 MHz, DMSO-d_6) δ: 196.92, 175.38, 162.85, 158.61, 155.99, 146.52, 142.93, 139.57, 135.47, 133.05, 130.09, 130.01, 129.81, 129.67, 128.35, 128.27, 128.20, 127.99, 126.59, 126.16, 125.24, 120.90, 115.78, 113.41, 112.85, 111.66, 79.05, 62.35, 55.71, 52.98, 52.18, 35.42. ESI mass spectrum (m/z): calcd. for $C_{34}H_{26}BrN_4O_4$ $[M+H]^+$: 633.1137; obsd.: 633.1046.

5-bromo-4'-(4-chlorobenzoyl)-1'-methyl-12''*H*-dispiro[indoline-3,2'-pyrrolidine-3',6''-indolo[2,1-*b*]quinazoline]-2,12''-dione (4n)

White solid. mp: 234-236 ℃. IR (KBr, cm^{-1}): 3317, 1730, 1693, 1643, 1463. ^{1}H NMR (400 MHz, DMSO-d_6) δ: 10.66 (s, 1H), 8.13 (t, 2H, J = 6.0 Hz), 7.95 (t, 1H, J = 7.2 Hz), 7.79 (dd, 2H, J = 11.6, 8.0 Hz), 7.63 (t, 1H, J = 7.6 Hz), 7.59 – 7.48 (m, 2H), 7.15 (d, 1H, J = 8.0 Hz), 7.06 (d, 2H, J = 8.0 Hz), 6.92 (d, 2H, J = 8.0 Hz), 6.47 (d, 1H, J = 8.4 Hz), 5.88 (s, 1H), 5.72 (dd, 1H, J = 9.2, 6.4 Hz), 4.19 (t, 1H, J = 7.6 Hz), 3.87 (t, 1H, J = 9.6 Hz), 2.24 (s, 3H). ^{13}C NMR (100 MHz, DMSO-d_6) δ: 198.17, 175.28, 158.48, 155.70, 146.37, 142.92, 139.56, 137.61, 136.15, 136.04, 135.55, 133.14, 130.32, 129.54, 128.33, 128.10, 126.63, 126.34, 125.09, 120.79, 115.87, 112.89, 111.74, 79.02, 62.07, 53.59, 51.73, 35.38. ESI mass spectrum (m/z): calcd. for $C_{33}H_{23}BrClN_4O_3$ $[M+H]^+$: 639.0622; obsd.: 639.0505.

5-bromo-4'-(4-bromobenzoyl)-1'-methyl-12''*H*-dispiro[indoline-3,2'-pyrrolidine-3',6''-indolo[2,1-*b*]quinazoline]-2,12''-dione (4o)

Pale green solid. mp: 239-241 ℃. IR (KBr, cm^{-1}): 3426, 1717, 1687, 1640, 1465. ^{1}H NMR (400 MHz, DMSO-d_6) δ: 10.67 (s, 1H), 8.15 (s, 2H), 7.96 (d, 1H, J = 2.0 Hz), 7.87 – 7.76 (m, 2H), 7.64-7.54 (m, 3H), 7.16 (d, 1H, J = 5.7 Hz), 7.02 (m, 4H), 6.47 (d, 1H, J = 6.0 Hz), 5.89 (s, 1H), 5.76 – 5.68 (m, 1H), 4.20 (d, 1H, J = 2.0 Hz), 3.88 (d, 1H, J = 9.2 Hz), 2.25 (s, 3H). ^{13}C NMR (100 MHz, DMSO-d_6) δ: 198.39, 175.26, 158.45, 155.70, 146.37, 142.93, 139.58, 136.38, 135.53, 133.13, 131.03, 130.33, 129.60, 129.24, 128.30, 127.95,

126.66, 126.33, 125.10, 120.82, 115.89, 112.88, 111.73, 78.98, 62.07, 53.65, 51.69, 35.38. ESI mass spectrum (m/z): calcd. for $C_{33}H_{23}Br_2N_4O_3$ $[M+H]^+$: 683.01; obsd.: 683.00.

6A.7. References

[1] P. S. V. Kumar, L. Suresh, T. Vinodkumar, B. M. Reddy, G. V. P. Chandramouli, *ACS Sustain. Chem. Eng.* **2016**, *4*, 2376–2386.

[2] I. V. Machado, J. R. N. dos Santos, M. A. P. Januario, A. G. Corrêa, *Ultrason. Sonochem.* **2021**, *78*, 105704–105751.

[3] R. Geetha Bai, K. Muthoosamy, F. N. Shipton, S. Manickam, *Ultrason. Sonochem.* **2017**, *36*, 129–138.

[4] L.-M. Zhou, R.-Y. Qu, G.-F. Yang, *Expert Opin. Drug Discov.* **2020**, *15*, 603–625.

[5] T. L. Pavlovska, R. G. Redkin, V. V. Lipson, D. V. Atamanuk, *Mol. Divers.* **2016**, *20*, 299–344.

[6] D. Bora, A. Kaushal, N. Shankaraiah, *Eur. J. Med. Chem.* **2021**, *215*, 113263–113301.

[7] S. Haddad, S. Boudriga, T. N. Akhaja, J. P. Raval, F. Porzio, A. Soldera, M. Askri, M. Knorr, Y. Rousselin, M. M. Kubicki, D. Rajani, *New J. Chem.* **2015**, *39*, 520–528.

[8] G. Bhaskar, Y. Arun, C. Balachandran, C. Saikumar, P. T. Perumal, *Eur. J. Med. Chem.* **2012**, *51*, 79–91.

[9] S. T. Al-Rashood, A. R. Hamed, G. S. Hassan, H. M. Alkahtani, A. A. Almehizia, A. Alharbi, M. M. Al-Sanea, W. M. Eldehna, *J. Enzyme Inhib. Med. Chem.* **2020**, *35*, 831–839.

[10] N. Ye, H. Chen, E. A. Wold, P. Y. Shi, J. Zhou, *ACS Infect. Dis.* **2016**, *2*, 382–392.

[11] W. Dai, X. L. Jiang, Q. Wu, F. Shi, S. J. Tu, *J. Org. Chem.* **2015**, *80*, 5737–5744.

[12] P. Brandão, C. S. Marques, E. P. Carreiro, M. Pineiro, A. J. Burke, *Chem. Rec.* **2021**, *21*, 924–1037.

[13] A. Barakat, S. M. Soliman, A. M. Al-Majid, M. Ali, M. S. Islam, Y. A. M. M. Elshaier, H. A. Ghabbour, *J. Mol. Struct.* **2018**, *1152*, 101–114.

[14] F. Rouatbi, M. Askri, F. Nana, G. Kirsch, D. Sriram, P. Yogeeswari, *Tetrahedron Lett.* **2016**, *57*, 163–167.

[15] Y. Kia, H. Osman, R. S. Kumar, A. Basiri, V. Murugaiyah, *Bioorg. Med. Chem.* **2014**, *22*, 1318–1328.

[16] D. Chakraborty, A. Maity, C. K. Jain, A. Hazra, Y. P. Bharitkar, T. Jha, H. K. Majumder, S. Roychoudhury, N. B. Mondal, *Medchemcomm* **2015**, *6*, 702–707.

[17] P. Ramesh, K. S. Rao, R. Trivedi, B. S. Kumar, R. S. Prakasham, B. Sridhar, *RSC Adv.* **2016**, *6*, 26546–26552.

[18] G. Lotfy, E. S. H. El Ashry, M. M. Said, E. S. El Tamany, Y. M. Abdel Aziz, A. Al-Dhfyan, A. M. Al-Majid, A. Barakat, *J. Photochem. Photobiol. B Biol.* **2018**, *180*, 98–108.

[19] Y. You, W. Y. Lu, Z. H. Wang, Y. Z. Chen, X. Y. Xu, X. M. Zhang, W. C. Yuan, *Org. Lett.* **2018**, *20*, 4453–4457.

[20] M. Zhang, W. Yang, K. Li, K. Sun, J. Ding, L. Yang, C. Zhu, *Synth.* **2019**, *51*, 3847–3858.

[21] S. Bhandari, S. Sana, B. Sridhar, N. Shankaraiah, *ChemistrySelect* **2019**, *4*, 1727–1730.

[22] N. Shahrestani, K. Tovfighmadar, M. Eskandari, K. Jadidi, B. Notash, P. Mirzaei, *Asian J. Org. Chem.* **2020**, *9*, 822–828.

[23] S. M. Rajesh, S. Perumal, J. C. Menéndez, P. Yogeeswari, D. Sriram, *Medchemcomm* **2011**, *2*, 626–630.

[24] C. Mhiri, S. Boudriga, M. Askri, M. Knorr, D. Sriram, P. Yogeeswari, F. Nana, C. Golz, C. Strohmann, *Bioorg. Med. Chem. Lett.* **2015**, *25*, 4308–4313.

[25] N. Arumugam, A. I. Almansour, R. S. Kumar, V. Siva Krishna, D. Sriram, N. Dege, *Bioorg. Chem.* **2021**, *110*, 104798–104804.

[26] P. R. Dongare, A. H. Gore, U. R. Kondekar, G. B. Kolekar, B. D. Ajalkar, *Inorg. Nano-Metal Chem.* **2018**, *48*, 49–56.

[27] L. Zheng, H. Wang, A. Fan, S. M. Li, *Nat. Commun.* **2020**, *11*, 1–10.

[28] C. J. Wang, X. Guo, R. Q. Zhai, C. Sun, G. Xiao, J. Chen, M. Y. Wei, C. L. Shao, Y. Gu, *Eur. J. Med. Chem.* **2021**, *224*, 113671–113685.

[29] S. E. Abbas, F. M. Awadallah, N. A. Ibrahin, E. G. Said, G. M. Kamel, *Eur. J. Med. Chem.* **2012**, *53*, 141–149.

[30] J. Qiu, W. Chen, Y. Zhang, Q. Zhou, J. Chen, L. Yang, J. Gao, X. Gu, D. Tang, *Eur. J. Med. Chem.* **2019**, *176*, 41–49.

[31] O. M. O. Habib, H. M. Hassan, A. El-Mekabaty, *Med. Chem. Res.* **2013**, *22*, 507–519.

[32] Z. Haghighijoo, O. Firuzi, B. Hemmateenejad, S. Emami, N. Edraki, R. Miri, *Bioorg. Chem.* **2017**, *74*, 126–133.

[33] A. Kamal, B. V. S. Reddy, B. Sridevi, A. Ravikumar, A. Venkateswarlu, G. Sravanthi, J. P. Sridevi, P. Yogeeswari, D. Sriram, *Bioorg. Med. Chem. Lett.* **2015**, *25*, 3867–3872.

[34] W. Lu, I. A. Baig, H. J. Sun, C. J. Cui, R. Guo, I. P. Jung, D. Wang, M. Dong, M. Y. Yoon, J. G. Wang, *Eur. J. Med. Chem.* **2015**, *94*, 298–305.

[35] P. Saravanan, S. Pushparaj, R. Raghunathan, *Tetrahedron Lett.* **2013**, *54*, 3449–3452.

[36] S. K. Ramadan, E. Z. Elrazaz, K. A. M. Abouzid, A. M. El-Naggar, *RSC Adv.* **2020**, *10*, 29475–29492.

[37] S. Ananthan, E. R. Faaleolea, R. C. Goldman, J. V. Hobrath, C. D. Kwong, B. E. Laughon, J. A. Maddry, A. Mehta, L. Rasmussen, R. C. Reynolds, J. A. Secrist, N. Shindo, D. N. Showe, M. I. Sosa, W. J. Suling, E. L. White, *Tuberculosis* **2009**, *89*, 334–353.

[38] E. J. Yang, J. G. Kim, J. Y. Kim, S. C. Kim, N. H. Lee, C. G. Hyun, *Cent. Eur. J. Biol.* **2010**, *5*, 95–102.

[39] P. Sittikornpaiboon, P. Toochinda, C. Thongpanchang, U. Leartsakulpanich, L. Lawtrakul, *Chiang Mai J. Sci.* **2016**, *43*, 931–945.

[40] S. Deng, Y. Wang, T. Inui, S.-N. Chen, N. R. Farnsworth, S. Cho, S. G. Franzblau, G. F. Pauli, *Phyther. Res.* **2008**, *22*, 878–882.

[41] Y. C. Chen, S. C. Shen, W. R. Lee, W. C. Hou, L. L. Yang, T. J. F. Lee, *J. Cell. Biochem.* **2001**, *82*, 537–548.

[42] N. El-Hachem, B. Haibe-Kains, A. Khalil, F. H. Kobeissy, G. Nemer, in *Neuroproteomics Methods Protoc.*, **2017**, pp. 391–403.

6A.8. Selected IR, NMR (^{1}H and ^{13}C) and Mass spectra

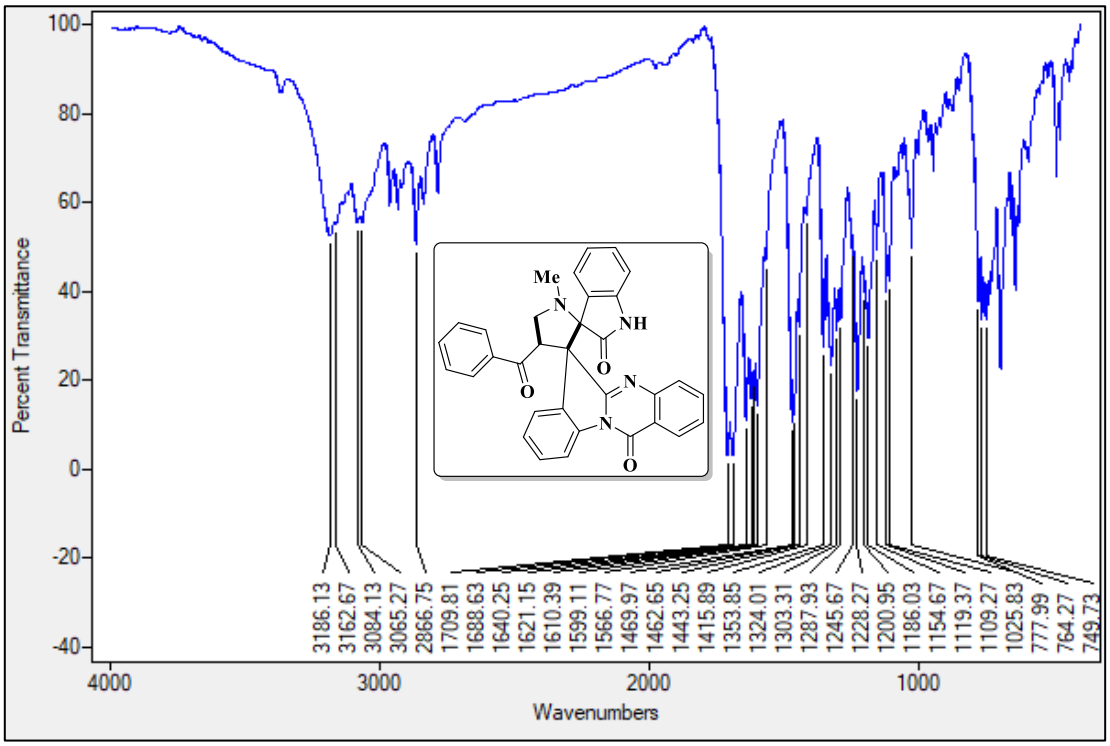

IR spectrum of the compound **4a**

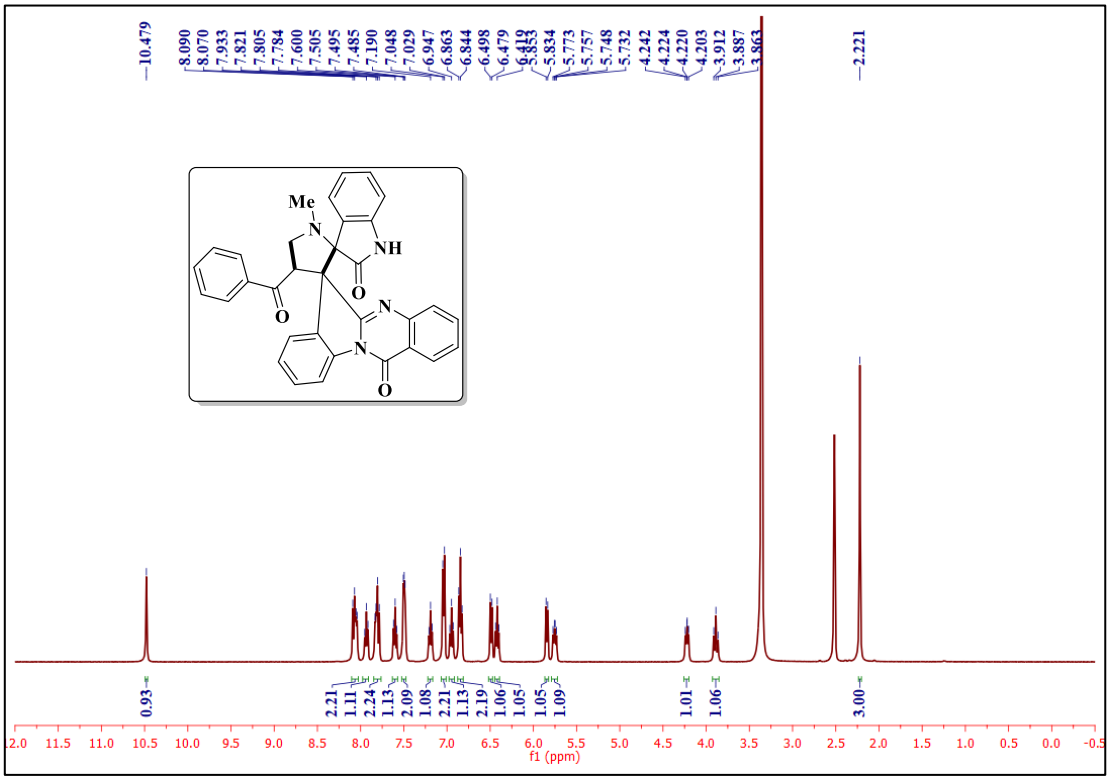

^{1}H NMR spectrum of the compound **4a**

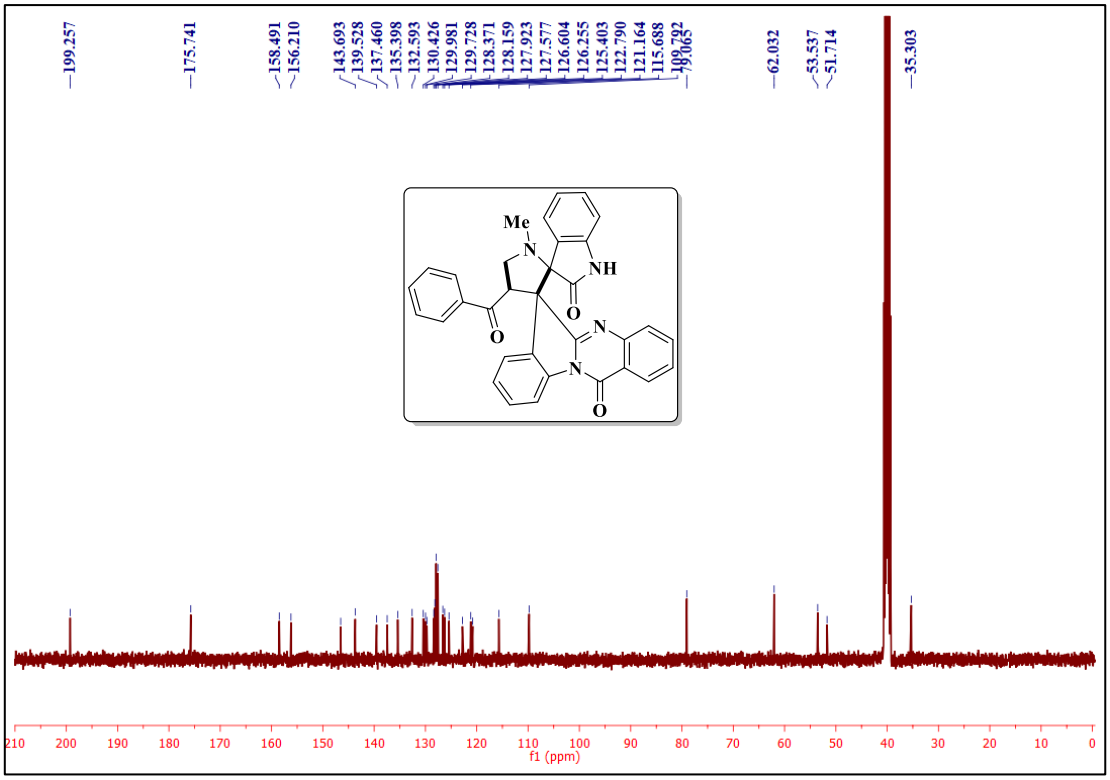

^{13}C NMR spectrum of the compound **4a**

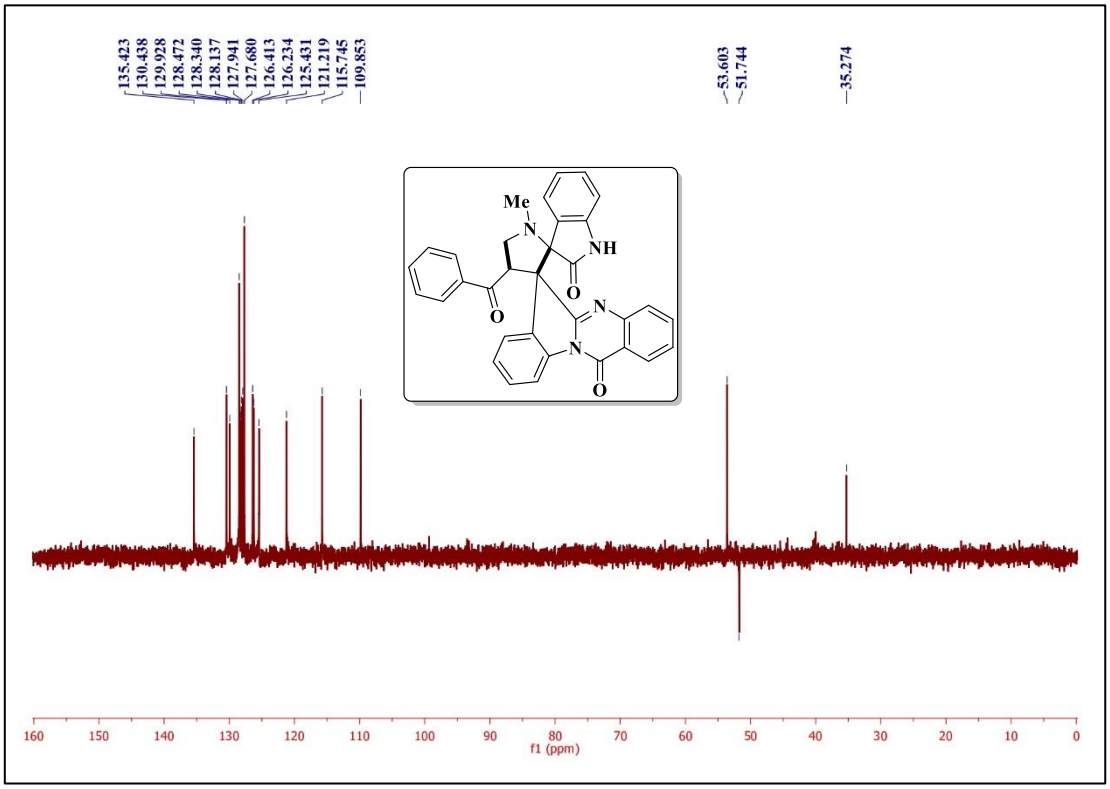

DEPT-135 NMR spectrum of the compound **4a**

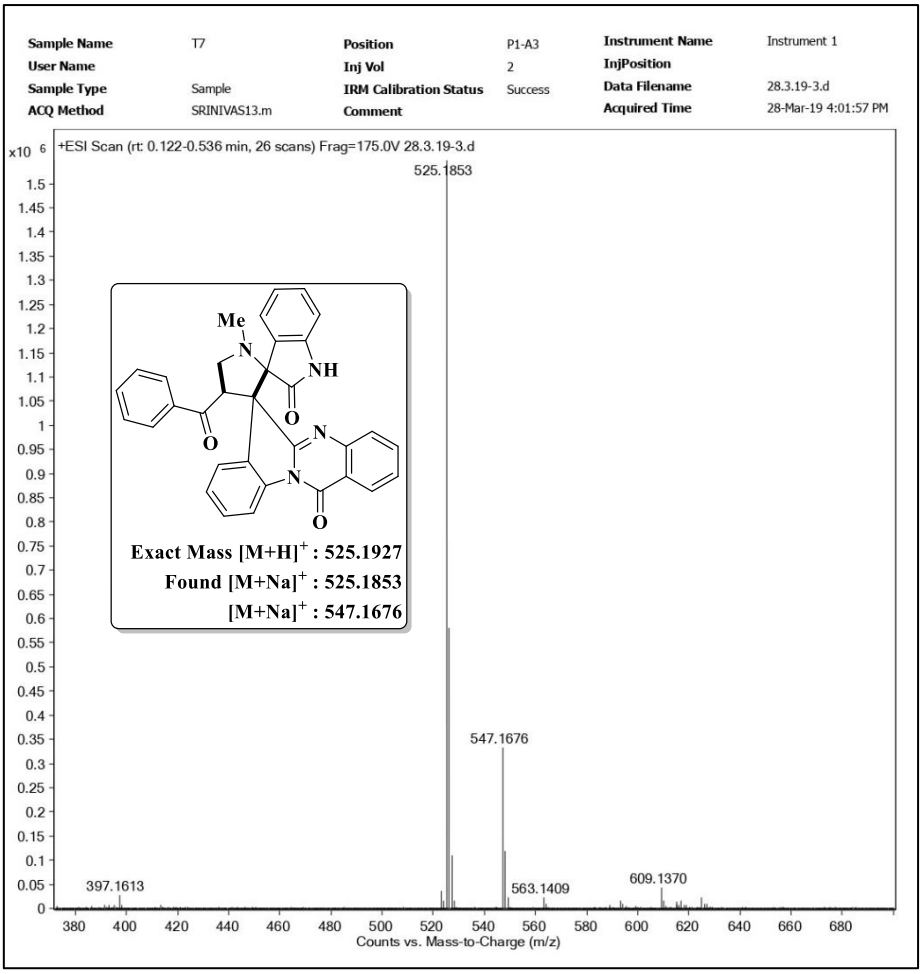

Mass spectrum of the compound **4a**

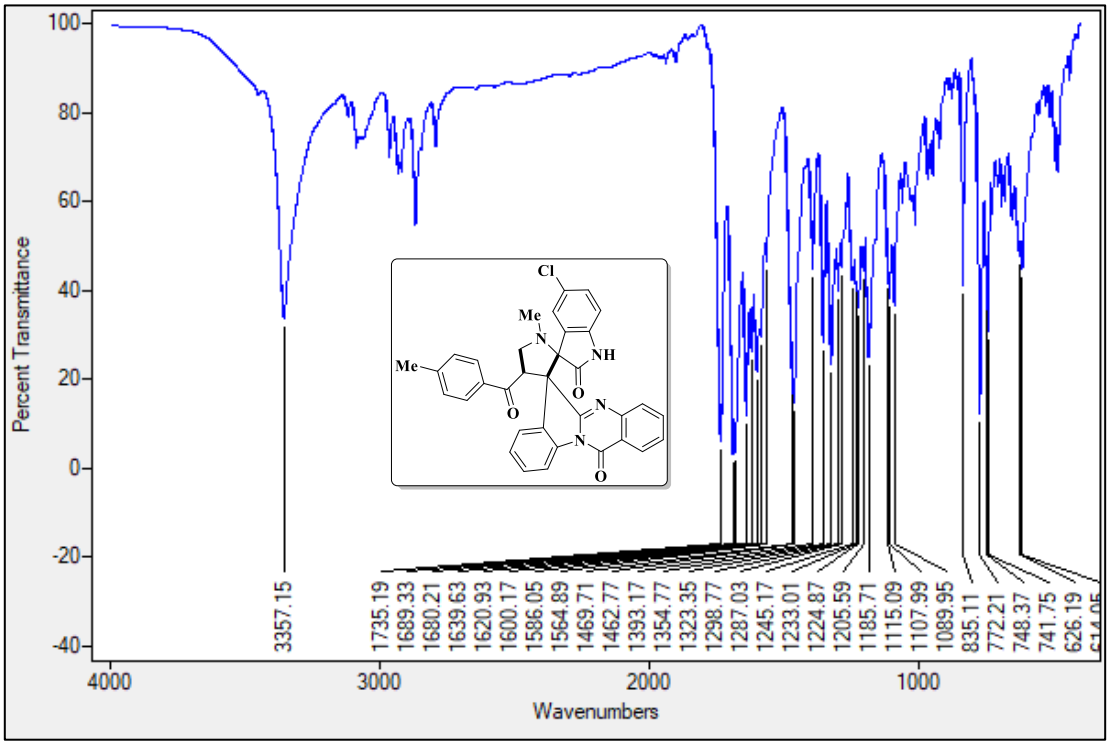

IR spectrum of the compound **4g**

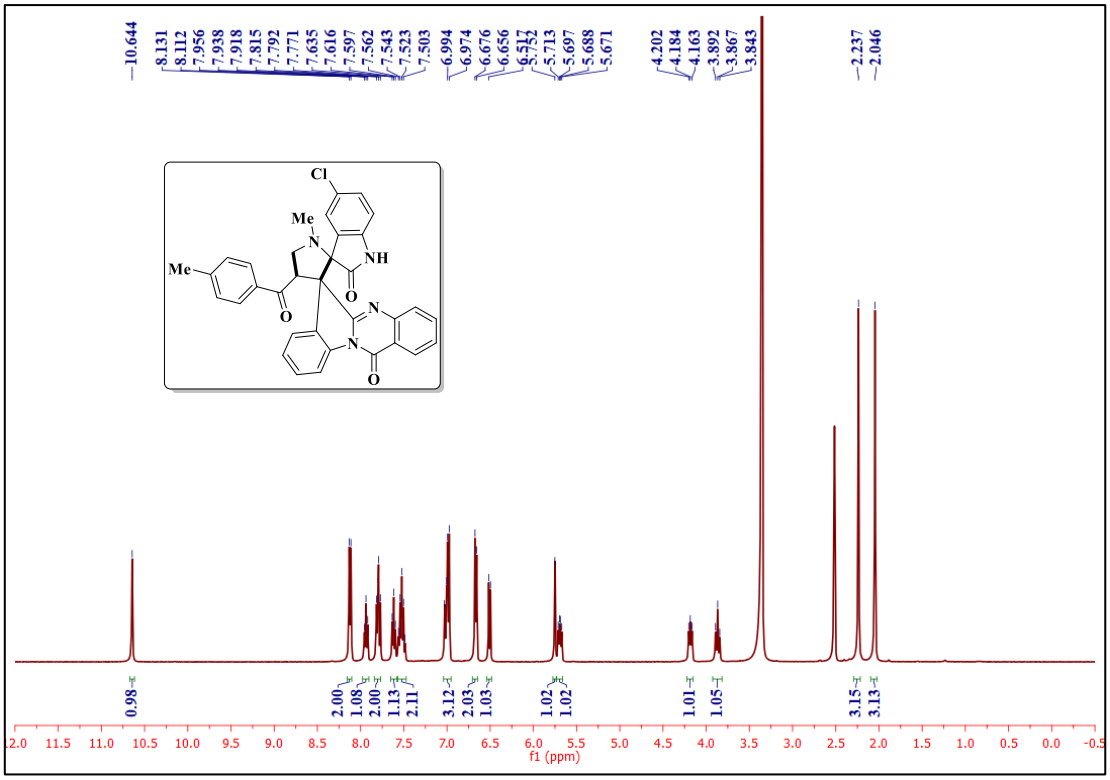

^{1}H NMR spectrum of the compound **4g**

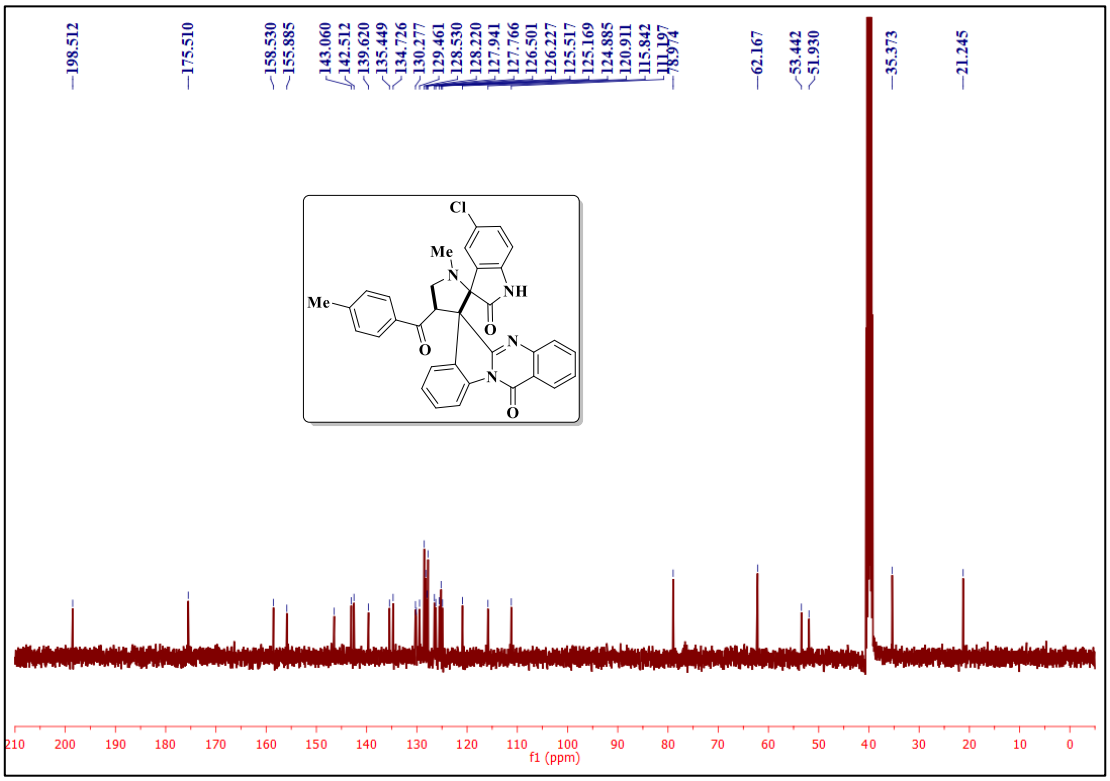

^{13}C NMR spectrum of the compound **4g**

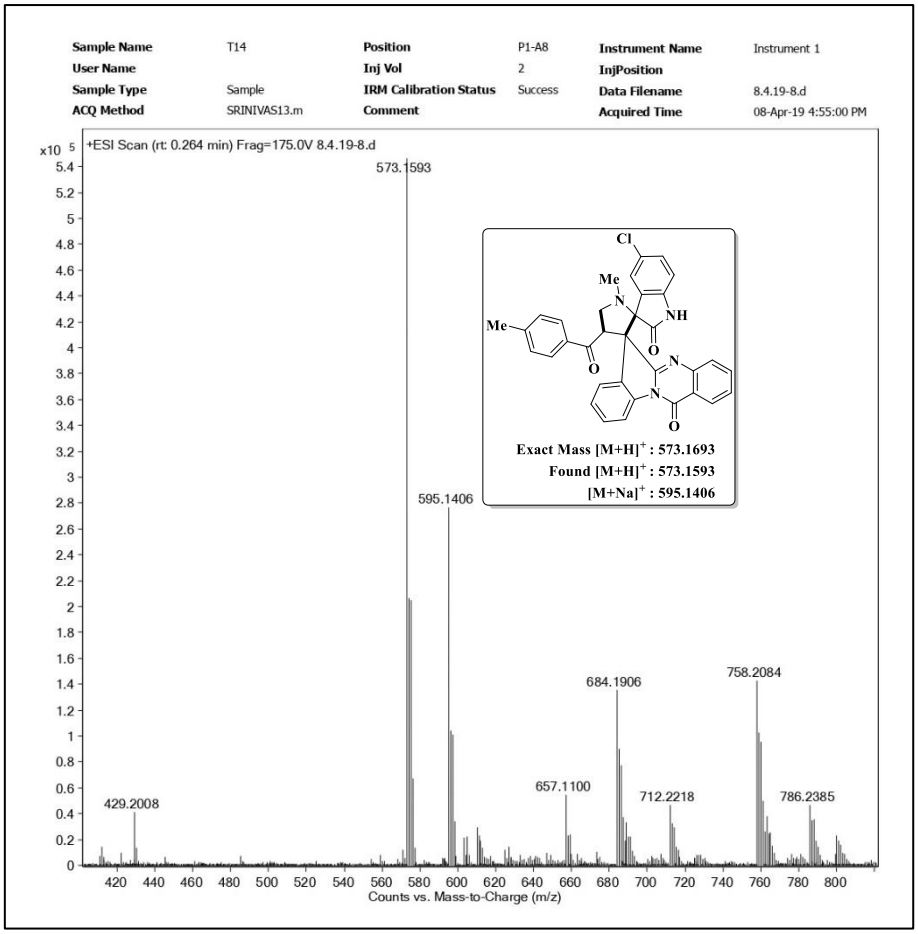

Mass spectrum of the compound **4g**

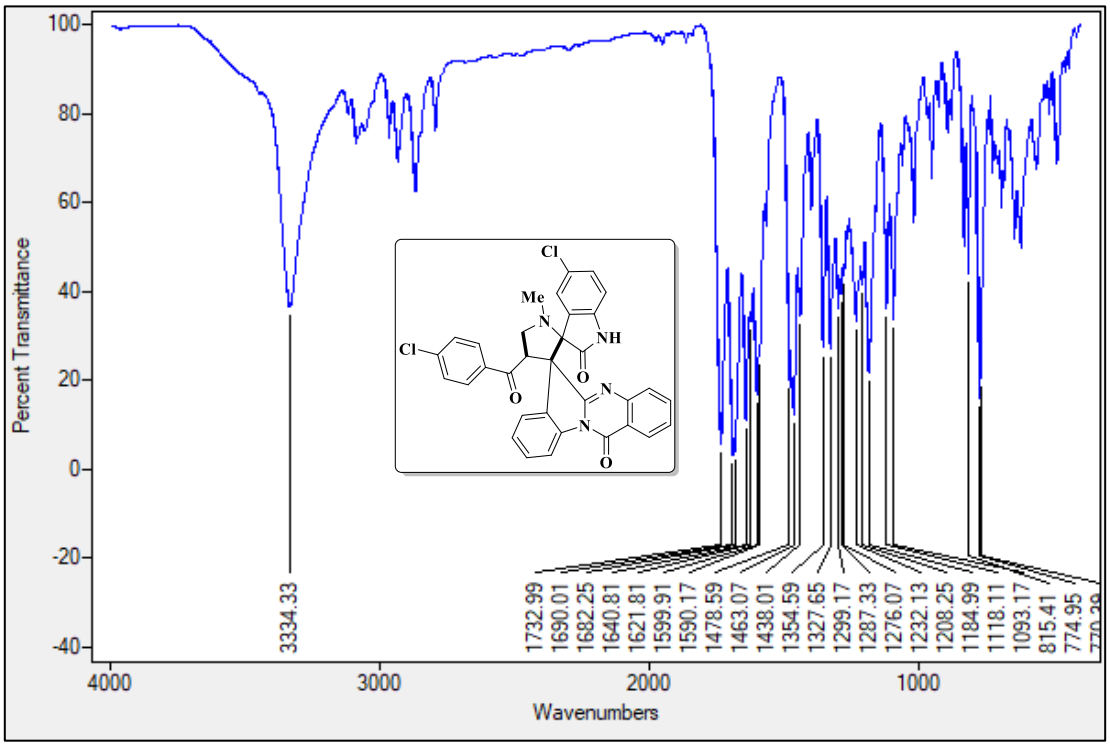

IR spectrum of the compound **4i**

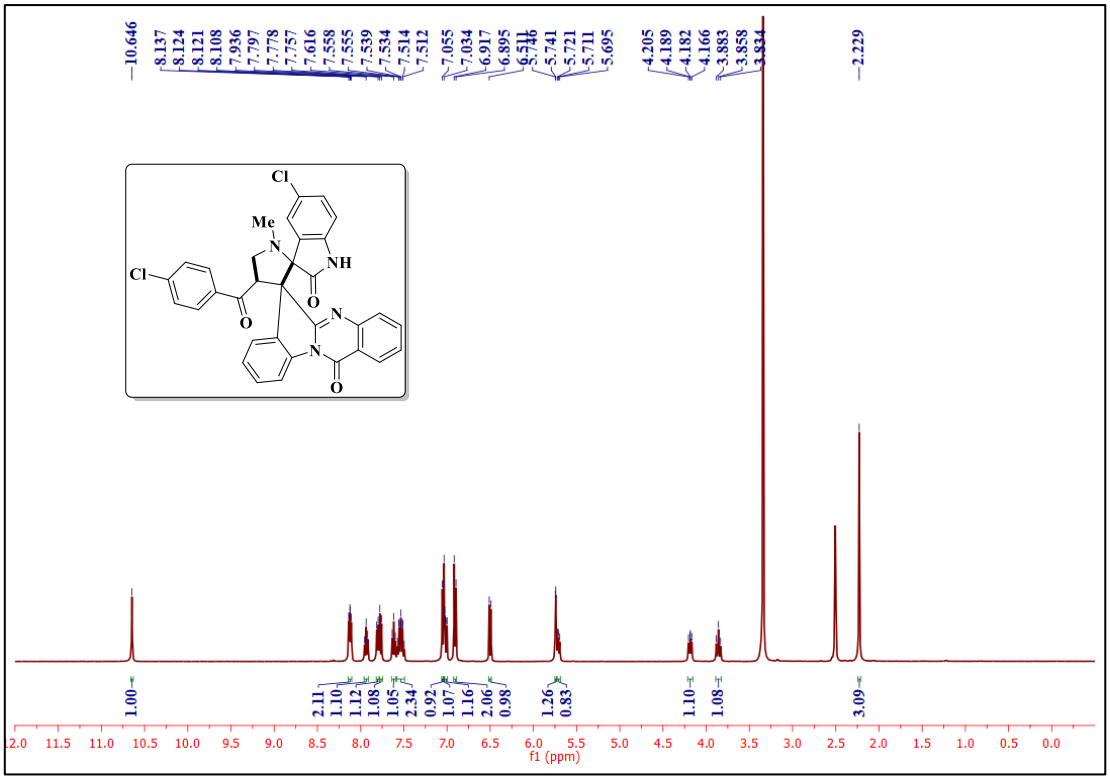

^{1}H NMR spectrum of the compound **4i**

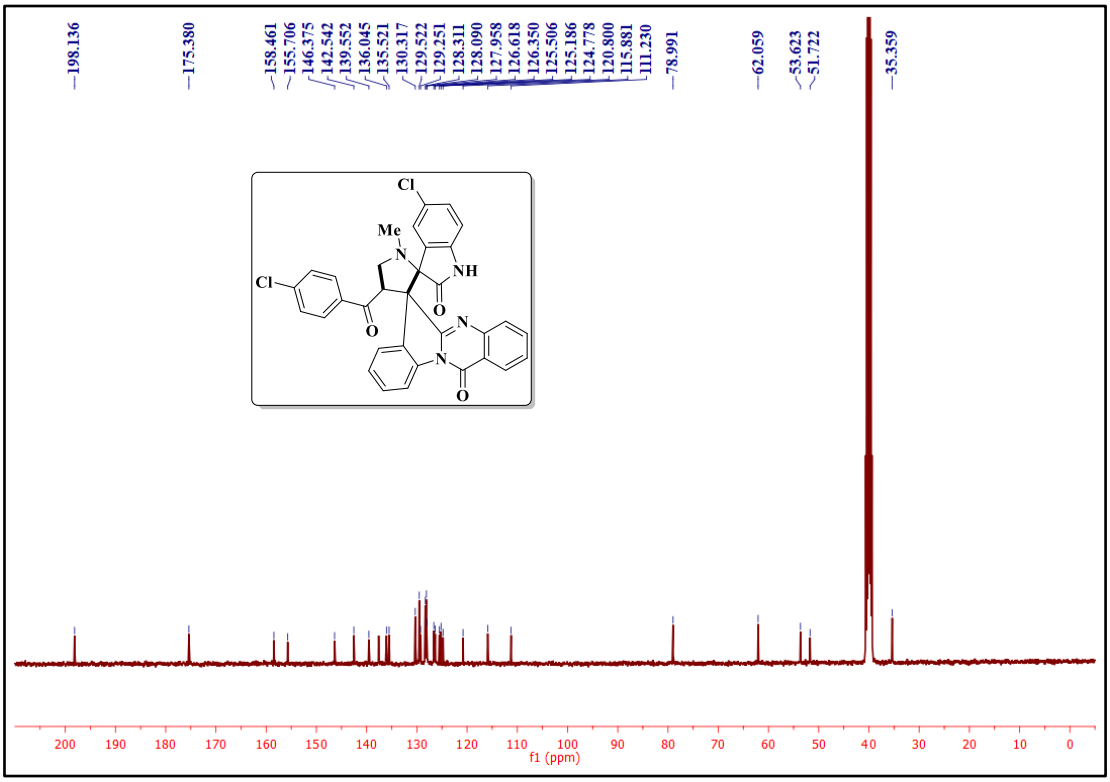

^{13}C NMR spectrum of the compound **4i**

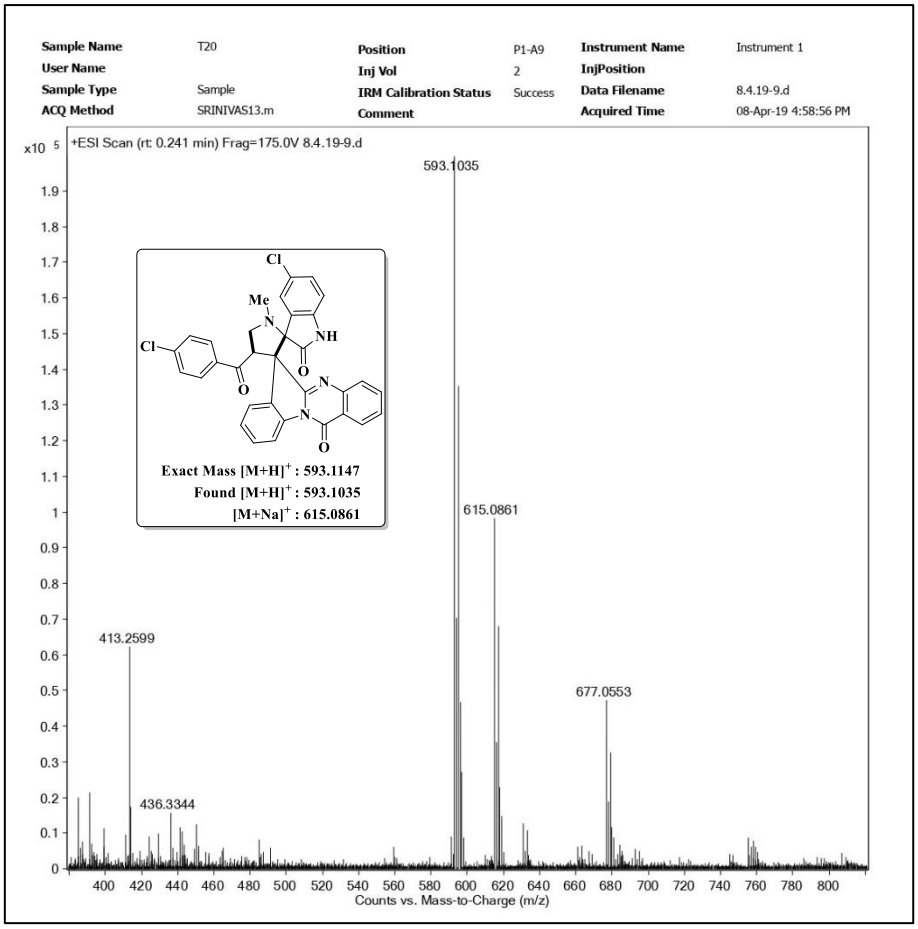

Mass spectrum of the compound **4i**

CHAPTER-VI
Section-B

A one-pot multicomponent [3+2] cycloaddition strategy for the synthesis of quinazolinyl-bisspirooxindolo-pyrrolizidines under ultrasonication

6B.1. Introduction

Ultrasound irradiation is a useful and ecofriendly technique that can be applied in various organic synthesis [1]. The chemical and mechanical effects that are permitted by acoustic cavitation enhance the application of this methodology to a broad scope of organic reactions [2]. The ability to achieve reaction selectivity that is not feasible with conventional heating, short reaction time, enhancing selectivity, improving reaction rates and yields are the main features of the ultrasound assisted synthesis [3]. Because of these advantages, the ultrasound irradiated organic reactions emerges new applications in industry [4].

On the other hand, spirooxindoles are important class of heterocyclic compounds in organic chemistry that are widely used in pharmaceutical [5] and natural products [6]. They exhibit wide range of biological activities such as anti-cancer [7], anti-bacterial [8], anti-microbial [9], anti-fungal [10], anti-tubercular [11] etc. Despite their therapeutic activities, spiro compounds are employed in various applications of science [12,13], industries [14,15] and agriculture [16,17]. Therefore, the generation of these kind of pharmaceutically and biologically active spirooxindoles is highly desirable in organic chemistry [18].

6B.1.1. Reported methods for the synthesis and biological evaluation of bisspirooxindoles

Dong et al. disclosed oxazolones grafted dispirooxindoles *via* three-component diversity oriented synthesis of benzylidene-2-phenyloxazolones with azomethine ylides (Figure 6B.1). All the synthesized compounds were displayed good *in vitro* anti-cancer activity against various cancer cell lines. Further, apoptosis studies and molecular docking studies were also evaluated for the active compounds [19].

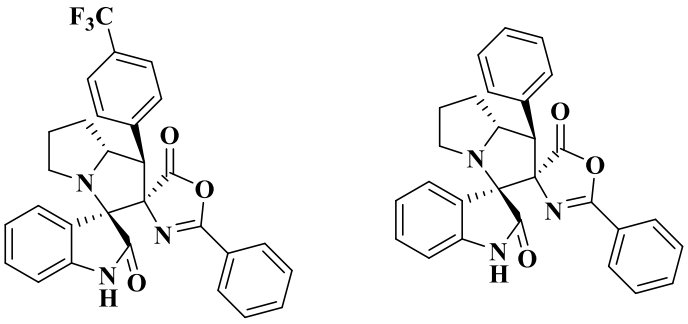

Figure 6B.1

Knorr and co-workers reported a diversity oriented synthesis of spiropyrrolo[1,2-*a*]isoquinolines *via* diastereoselective and regiodivergent multicomponent [3+2]

cycloaddition reaction (Figure 6B.2). Further, *in vitro* and *in vivo* anti-diabetic activity was evaluated for the synthesized compounds. In addition, *in silico* molecular docking and ADME prediction were studied for drug likeness properties of active compounds [20].

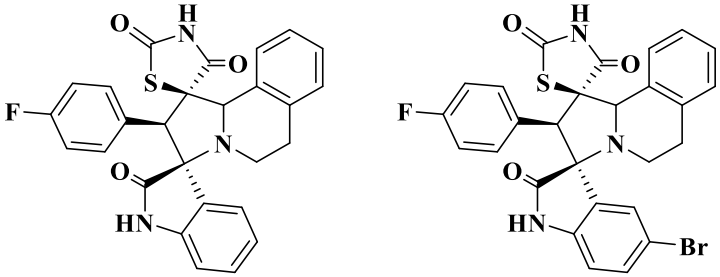

Figure 6B.2

Thangamani and coworkers synthesized dispirooxindole pyrrolothiazoles through multicomponent [3+2] cycloaddition reaction of azomethine ylide with 2,6-di (arylmethylidene)-4-methylcyclohexanones (Figure 6B.3). The synthesized compounds were subjected to cytotoxicity evaluation using K562-leukemia cell line. Further, green chemistry metrics and molecular docking studies were evaluated for the synthesized compounds [21].

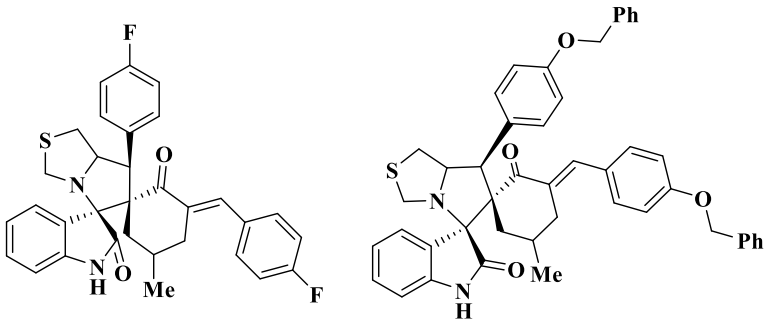

Figure 6B.3

Kumar and co-workers presented a stereoselective synthesis of novel dispiroheterocyclic hybrids including indolizine, oxindole and substituted piperidine moieties utilizing [bmim]Br as solvent and catalyst (Figure 6B.4). Further, they were tested for their anti-inflammatory activities against chronic inflammation in animal models and three compounds were exhibit significant activity [22].

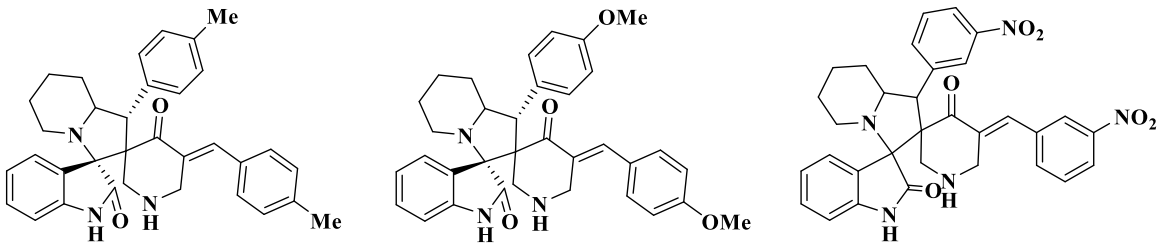

Figure 6B.4

Davis et al. explored the Diels-Alder [4+2] cycloaddition reaction of substituted oxindoles with cyclopentadiene to generate a series of spirocycles (Figure 6B.5). Further, these scaffolds were screened against cytochrome P450 enzyme CYP121 of *Mycobacterium tuberculosis* using UV–Vis spectrophotometric assay [23].

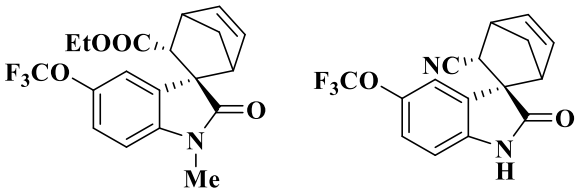

Figure 6B.5

Arumugam and co-workers employed a stereo and regioselective synthesis of β-lactam grafted spirooxindolopyrrolidine hybrids *via* ionic liquid mediated [3+2] cycloaddition reaction (Figure 6B.6). Further, *in vitro* anti-tubercular activity of the synthesized spiroheterocyclic compounds were assessed against *Mycobacterium tuberculosis* H37Rv, and some of the compounds showed potent activity [24].

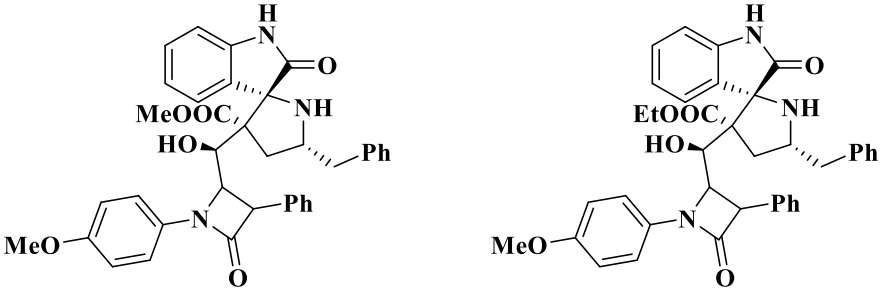

Figure 6B.6

Murali et al. prepared a series of dispiro compounds having oxindole-pyrrolo-carbazole hybrids *via* three component 1,3-dipolar cycloaddition reaction using azomethine ylide and 2-arylidenetetrahydrocarbazoleones (Figure 6B.7). The synthesized compounds were screened for *in vitro* cytotoxic activity by MTT assay on breast cancer cell line MCF-7 and lung cancer cell line A-549. In addition, morphological changes and apoptosis induction of the compounds were studied by fluorescent microscopic and by flow cytometry analyses [25].

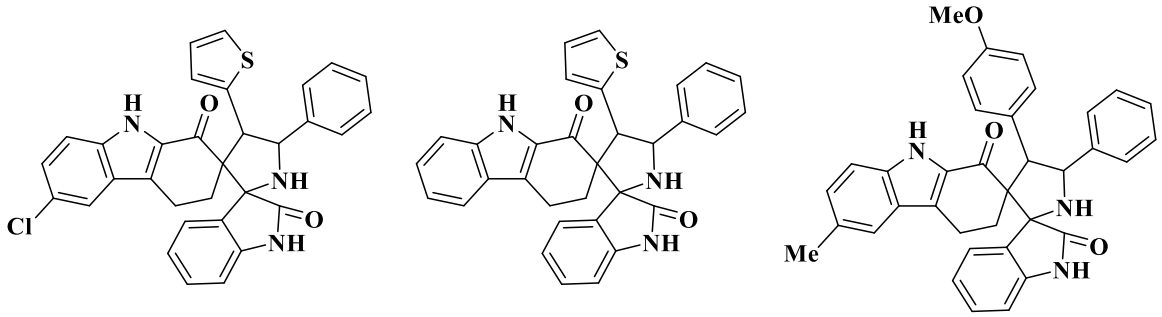

Figure 6B.7

Zhang and co-workers introduced a straightforward and highly efficient pseudo five-component reaction for the diastereoselective synthesis of bispirooxindolo-pyrrolidines with a butterfly shaped skeleton (Scheme 6B.1). Utilizing recyclable zeolite HY as catalyst, bioderived EtOH as a solvent and eliminating intermediate purification furnished this protocol as green synthesis [26].

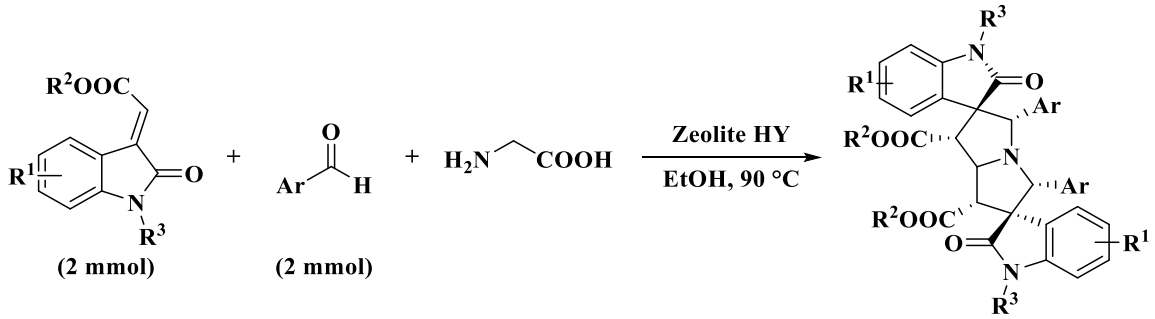

Scheme 6B.1

Lin et al. developed an efficient and practical organocatalytic asymmetric domino Michael/Mannich [3+2] cycloaddition of trifluoroethylisatin ketimines and arylidene azlactones for the generation of pyrrolidinyl dispirooxindoles (Scheme 6B.2). In this reaction, a broad range of dispirooxindoles having four contiguous stereogenic centers including two vicinal spiro quaternary chiral centers were obtained under mild reaction conditions [27].

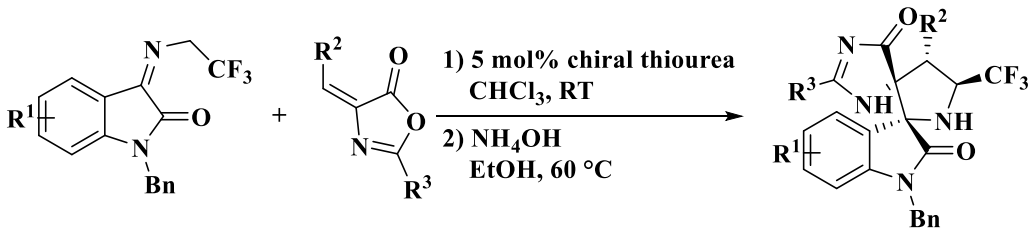

Scheme 6B.2

Chen et al. reported a highly regio and stereoselective asymmetric [3+2] cycloaddition reaction for the synthesis of cyclopentenyldispirooxindoles bearing two adjacent quaternary spirocenters (Scheme 6B.3). This straightforward annulation reaction generated the corresponding products with high stereoselectivities using chiral tertiary amine as catalyst [28].

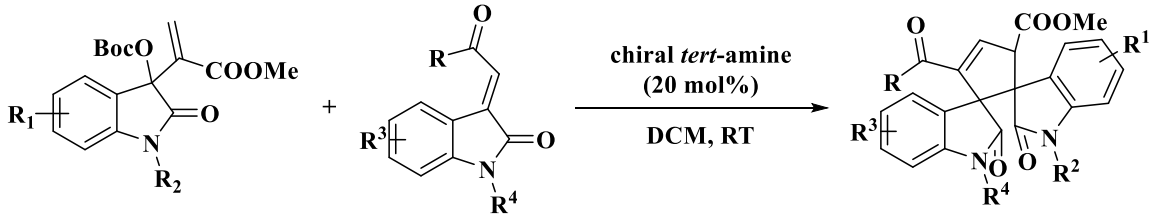

Scheme 6B.3

Xia et al. employed an efficient and diastereoselective oxa-1,3-dipolar cycloaddition reaction between oxindoles and amino acids for the generation of oxazolidine-dispirooxindoles having vicinal quaternary carbon centers (Scheme 6B.4). Operational simplicity, reliable scalability, broad substrate scope and chromatography-free purification rendered this protocol more efficient and environmentally benign [29].

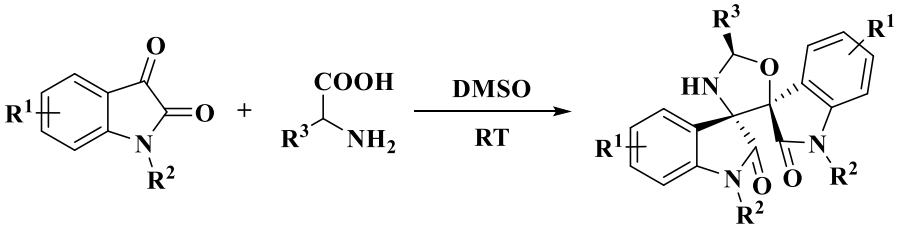

Scheme 6B.4

Yang and co-workers constructed a series of dispirooxindolo-piperazine ring systems through acid promoted self-1,3-dipolar [3+3] cycloaddition of azomethine ylides with various cyclic amino acids (Scheme 6B.5). In this reaction, a variety of unprecedented dispirooxindolo-piperazines were prepared with good diastereoselectivities [30].

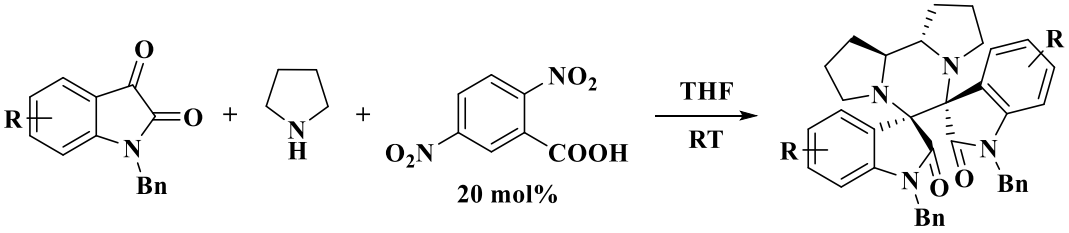

Scheme 6B.5

Reddy and co-workers explored a stereoselective synthesis of highly functionalized dispirooxindoles through [3+2] cycloaddition reaction of carbonyl ylides with

arylideneoxindoles using rhodium catalyst (Scheme 6B.6). This method accessed a wide range of substrates and paved a way to produce biologically relevant dispirooxindoles [31].

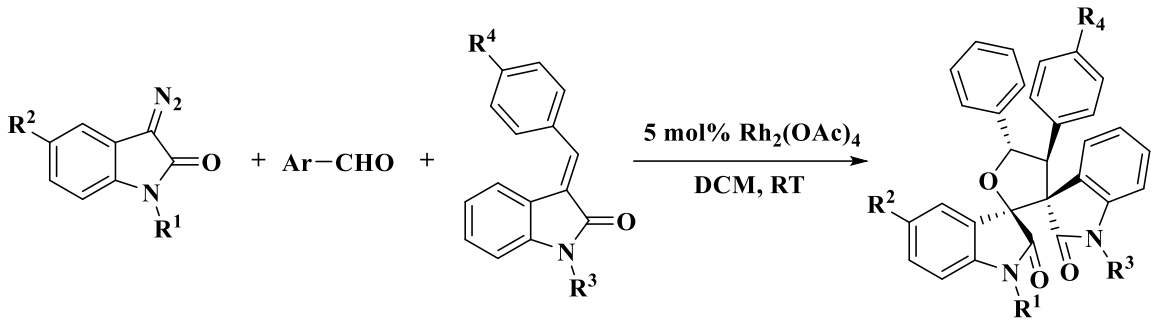

Scheme 6B.6

6B.2. Present work

Encouraged by the above literature reports and considering the significance of bisspirooxindoles, we have synthesized the novel quinazolinone based pyrrolizidino-bisspirooxindoles using quinazolinyl chalcones **1a-e**, isatins **2a-c**, and L-proline **3** as starting materials in CH_3CN under ultrasonication at 60 °C (Scheme 6B.7). Further, the title compounds were evaluated for *in vitro* anti-tubercular activity and *in silico* molecular docking studies.

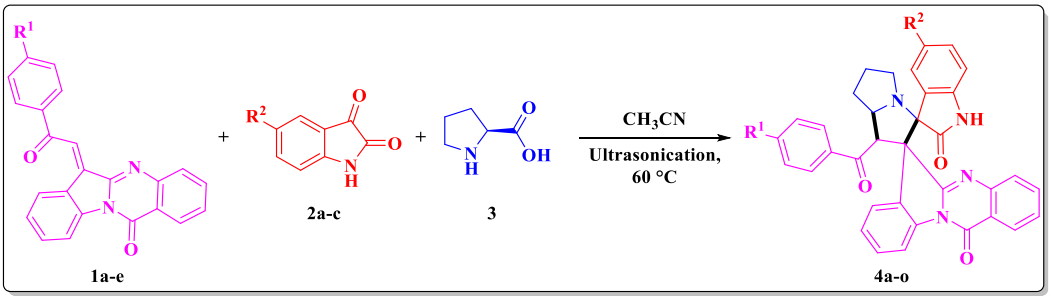

Scheme 6B.7. Synthesis of quinazolinyl-bisspirooxindolo-pyrrolizidines **4a-o**.

6B.2.1. Results and discussion

We commenced our study by choosing 6-(2-oxo-2-phenyl-ethylidene)indolo[2,1-*b*]quinazolin-12(6*H*)-one **1a**, isatin **2a** and L-proline **3** as the model reactants to get the optimized reaction parameters (Table 6B.1). Initially, the model reaction was carried in MeOH at room temperature resulting the desired product **4a** in 50% yield (Table 6B.1, entry 1). The product yield was increased with the rising reaction temperatures (Table 6B.1, entries 2-6). Further, the reaction was conducted in different solvents such as EtOH, 1,4-dioxane, CH_3CN, toluene (Table 6B.1, entries 3-6). Among these, highest yield was obtained in CH_3CN (Table 6B.1, entry 5). To increase the product yield and environmental concerns an attempt was made under ultrasonication (RT and 60 °C) and to our delight, the

reaction was feasible (Table 6B.1, entry 7-9). The highest yield of product was obtained when the reaction was carried out in CH_3CN at 60 °C (Table 6B.1, entry 8). However, increasing reaction time has no significant impact on the yield (Table 6B.1, entry 9). Thus, 1.0 mmol of **1a**, 1.0 mmol of **2a** and 1.0 mmol of **3** in 3 mL of CH_3CN under ultrasonication at 60 °C (Table 6B.1, entry 8) is the best reaction condition for the generation of target compounds **4a-o**.

Table 6B.1. Optimization of the reaction conditions[a]

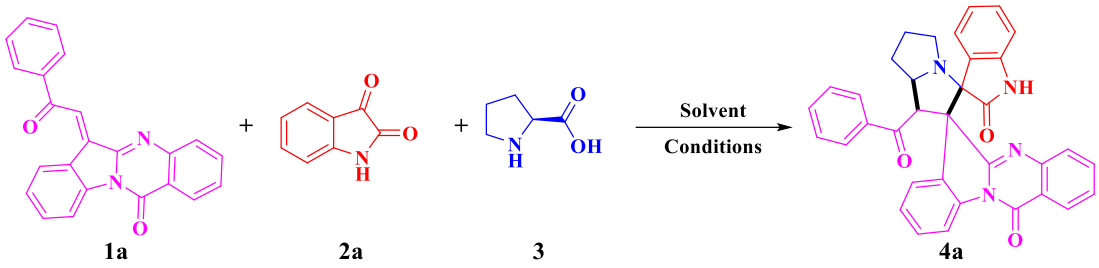

1a **2a** **3** **4a**

Entry	Solvent	Method	Temp (°C)	Time	Yield (%)[b]
1	MeOH	Conventional	RT	20 h	50
2	MeOH	Conventional	Reflux	6 h	65
3	EtOH	Conventional	Reflux	6 h	68
4	1,4-Dioxane	Conventional	Reflux	8 h	50
5	CH_3CN	Conventional	Reflux	6 h	75
6	Toluene	Conventional	Reflux	10 h	45
7	CH_3CN	Ultrasonication	RT	120 min	80
8	**CH_3CN**	**Ultrasonication**	**60**	**40 min**	**88**
9	CH_3CN	Ultrasonication	60	90 min	88

[a]Reaction condition: compound **1a** (1.0 mmol), isatin **2a** (1.0 mmol), and L-proline **3** (1.0 mmol), solvent (3 mL). [b]Isolated yields.

With the optimized reaction conditions in hand, we have explored the substrate scope by taking various quinazolinone chalcones **1a-e**, isatins **2a-c** and L-proline **3** (Table 6B.2). Quinazolinone chalcones bearing electron donating (–Me, –OMe) and halogen (–Cl, –Br) substitutions have no substantial impact on the efficiency of the reaction. Nevertheless, we also found that halo (–Cl, –Br) substituted isatins could react smoothly to provide the desired products in good yields.

Table 6B.2. Synthesis of quinazolinyl-bisspirooxindolo-pyrrolizidines **4**[a,b]

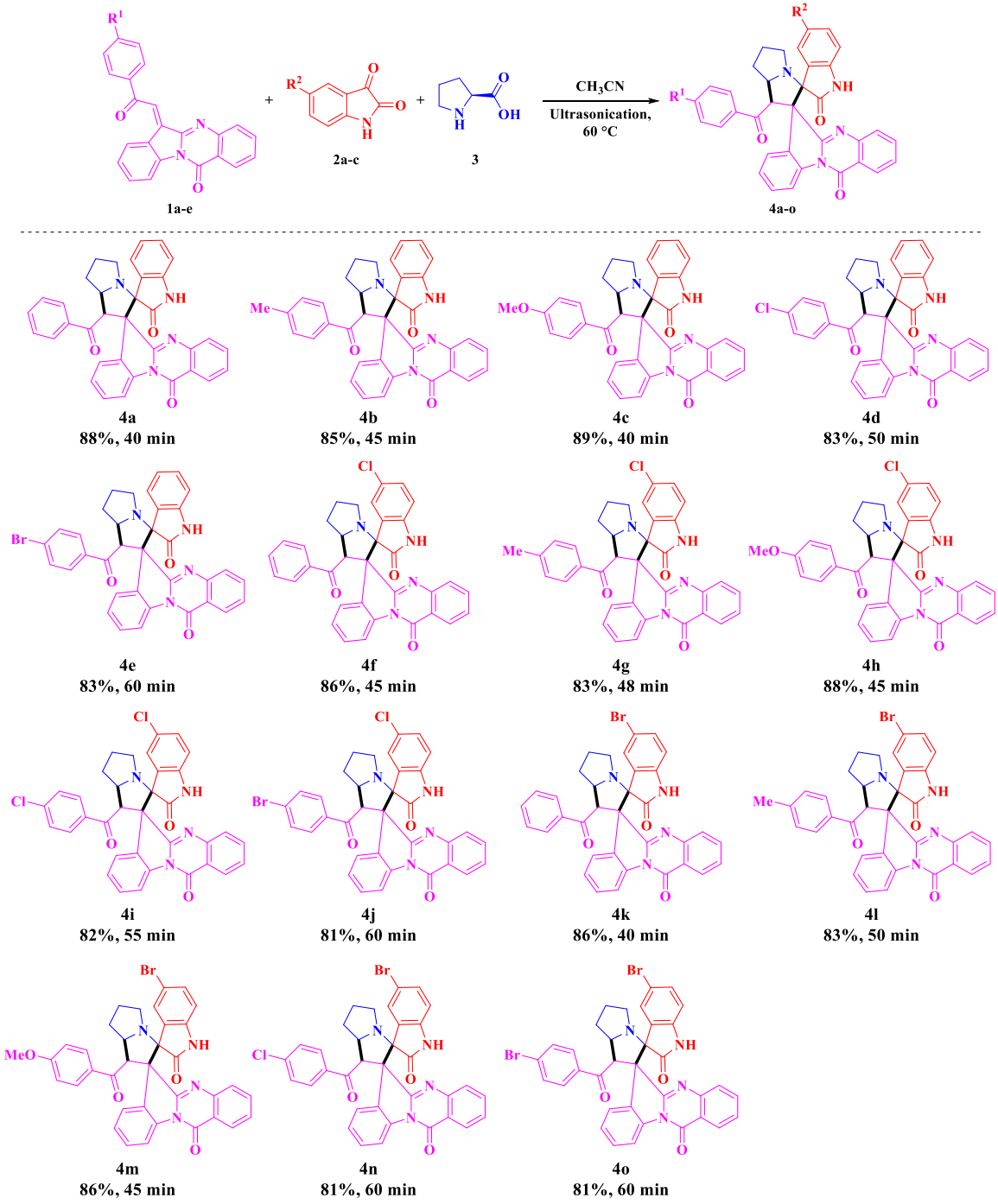

[a]Reaction condition: quinazolinone chalcones **1a-e** (1.0 mmol), isatins **2a-c** (1.0 mmol), and L-proline **3** (1.0 mmol) in 3 mL of CH_3CN under ultrasonication at 60 °C. [b]Isolated yields.

The plausible reaction mechanism for the generation of target compounds **4** is illustrated in Scheme 6B.8. Initially, azomethine ylide **6** has generated *via* oxazolidinone **5** formation between isatin **2a** and L-proline **3**, by the elimination of H_2O and CO_2. Later, it undergoes [3+2] cycloaddition reaction with quinazolinone chalcone **1a** delivers the target compound **4a**.

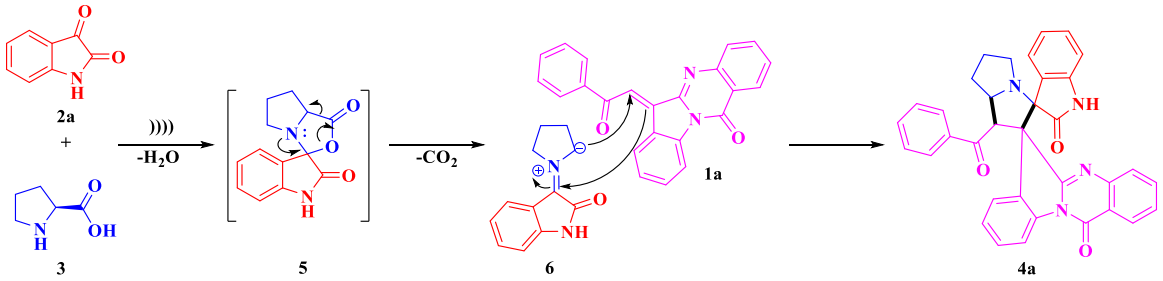

Scheme 6B.8. Plausible reaction mechanism for the generation of target compounds **4**.

The possible mode of approach of azomethine ylide (dipole **6**) is shown in Figure 6B.8. The regioselectivity of cycloaddition in the product formation can be demonstrated by considering secondary orbital interaction (SOI) of the nitrogen atom of the dipolarophile (chalcone **2a**) [32]. As a result of SOI, the observed regioisomer **4a** *via* path A is more favourable than path B, which was also evidenced by NMR analysis.

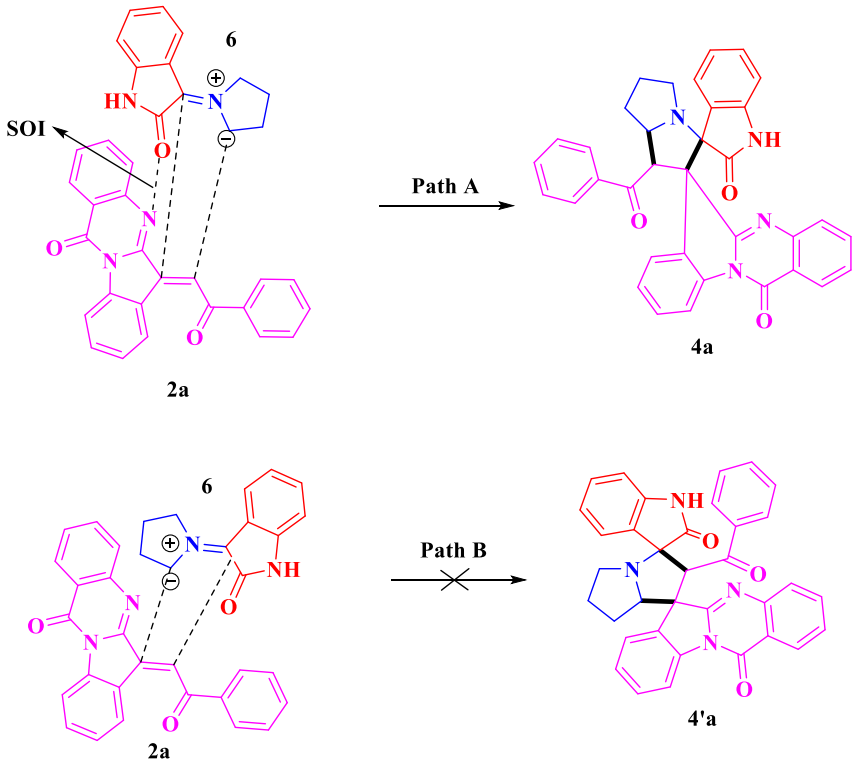

Figure 6B.8. mode of approach of azomethine ylide **6**.

The structures of the synthesized scaffolds **4a-o** were in well agreement with their spectral (IR, ^{1}H, ^{13}C NMR and mass) data. IR spectrum of the target compound **4a** showed a band at 3182 cm^{-1} represents the NH group, and the bands at 1743 cm^{-1}, 1686 cm^{-1} and 1639 cm^{-1} corresponds to benzoyl carbonyl group, amide carbonyls of oxindole and quinazolinone moieties respectively [33]. The ^{1}H NMR spectra showed the singlet signal corresponding to isatin NH proton at δ 10.50 *ppm*. Whereas, the multiplet in the range from

δ 4.70 to δ 2.00 *ppm* attributed to the protons of pyrrolizidine ring. ^{13}C NMR displayed signals at δ 78.40 and δ 67.38 *ppm* attributable for the two spiro carbons of oxindole and quinazolinone moiety respectively. The molecular ion peak at *m/z* 551.1983 $[M+H]^+$ in the mass spectrum determined the molecular weight of the compound **4a**.

6B.2.2. Biological activity

6B.2.2.1. Anti-tubercular activity (anti-TB)

The target compounds **4a-o** were subjected to *in vitro* anti-tubercular screening against *Mycobacterium tuberculosis* H37Rv (ATCC27294) by the microplate alamar blue assay (MABA) method [34]. Isoniazid, Rifampicin and Ethambutol were used as reference drugs. The minimum inhibitory concentration (MIC) values of **4a-o** were summarized in Table 6B.3. Among the tested compounds most of them showed good anti-tubercular activity with MIC values in the rage of 1.56 to 25 µg/mL. The compounds **4b** and **4i** exhibited potent activity (MIC = 1.56 µg/mL) than the reference drug ethambutol. Also, the compound **4e** displayed significant activity (MIC = 3.125 µg/mL) when compared to ethambutol. Whereas, the compounds **4d, 4g, 4h, 4j** and **4n** displayed good activity (MIC = 6.25 µg/mL). All the remaining compounds exhibited moderate to poor activity in the range of 12.5 to 25 µg/mL.

Table 6B.3. *In vitro* anti-tubercular activity of the target compounds **4a-o**

Entry	Compound	MIC (µg/mL)	% of Inhibition @25µM[a]
1	4a	12.5	ND[b]
2	**4b**	**1.56**	**17.12**
3	4c	25	ND
4	**4d**	**6.25**	**24.76**
5	**4e**	**3.125**	**16.79**
6	4f	12.5	ND
7	**4g**	**6.25**	**16.49**
8	**4h**	**6.25**	**24.16**
9	**4i**	**1.56**	**19.47**
10	**4j**	**6.25**	**17.82**
11	4k	12.5	ND
12	4l	12.5	ND
13	4m	12.5	ND
14	**4n**	**6.25**	**21.14**
15	4o	25	ND
16	Isoniazid	0.05	ND
17	Rifampicin	0.1	ND
18	Ethambutol	1.56	ND

[a]% inhibition was examined using RAW 264.7 cell line, [b]ND = not determined.

6B.2.2.2. Cytotoxicity studies

The active compounds (**4b**, **4d**, **4e**, **4g**, **4h**, **4i**, **4j** and **4n**) were tested for their cytotoxicity against RAW 264.7 cells at 25μM concentration using MTT assay [35]. As depicted in Table 6B.3, the promising active compounds exhibited poor cytotoxicity against normal cells RAW 264.7 cells and were suitable for further mechanistic studies (Figure 6B.9).

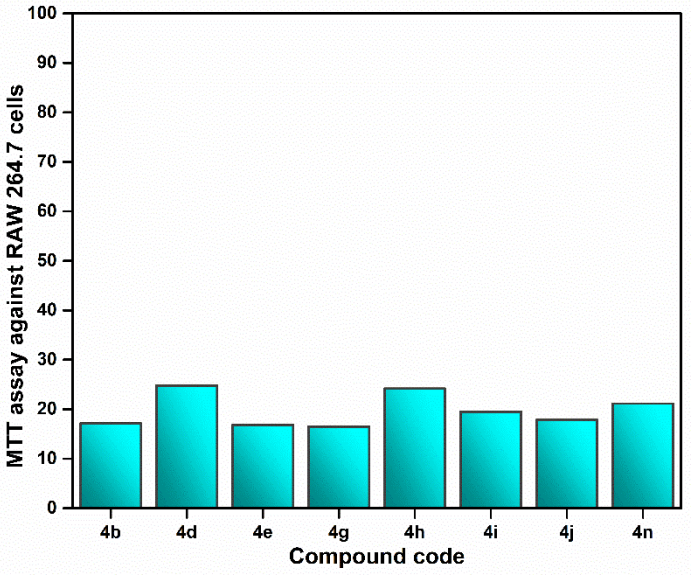

Figure 6B.9 % inhibition of potent anti-tubercular compounds on RAW 264.7 cell line at 25μM concentration.

6B.2.2.3. Structure activity relationship studies

Structure activity relationship (SAR) studies revealed that diverse donor and acceptor abilities of substituted groups on the phenyl ring are crucial in their anti-tubercular activity of the synthesized compounds. The presence of methyl (–Me) and chloro (–Cl) moieties on the phenyl ring is significantly enhances the anti-tubercular activity when compared with the other functional groups. Whereas the isatin moiety having chlorine (–Cl) substitution showed good activity than the other substituted or unsubstituted isatins.

6B.3. Molecular docking studies

In order to get a deeper insight into binding interactions of the spiropyrrolizidines, molecular docking studies were performed against dihydrofolate reductase of *Mycobacterium Tuberculosis* (PDB code: 1DF7) [36]. The observed binding energies were depicted in Table 6B.4. The docked compounds (**4a-o**) were well fitted in the binding site of the protein 1DF7 and gives different polar and non-polar interactions with amino acid residues. Among all, the compound **4i** exhibited more negative binding energy -9.26 kcal/mol, forms two hydrogen bonds with the amino acid residues PHE31 (3.02 Å), PRO51

(2.92 Å) and forms five hydrophobic interactions (π···π and π···alkyl) with the amino acid residues. Whereas, the compound **4b** showed binding energy -8.97 kcal/mol, forms three hydrogen bonds with amino acid residues GLN28 (1.70 Å), PHE31 (3.29 Å), ILE94 (2.17 Å) and forms two hydrophobic interactions (π···π) with the amino acids. In addition, the compounds **4f** and **4k** exhibited good binding energies -8.97 kcal/mol and -9.19 kcal/mol respectively. The ligand interaction diagrams of the compounds **4b** and **4i** were presented in Figure 6B.10 and Figure 6B.11.

Table 6B.4 Docking results of the compounds **4a-o** against 1DF7

Ent-ry	Compound	Binding energy (kcal/mol)	No. of hydrogen bonds	Residues invoved in the hydrogen bonding	Hydrogen bond length (Å)
1	**4a**	-8.69	2	ASP27	2.54, 2.60
2	**4b**	**-8.97**	3	GLN28, PHE31, ILE94	1.70, 3.29, 2.17
3	**4c**	-7.73	4	ILE20, GLN28, SER49, LEU50	2.18, 2.90, 3.36, 3.38
4	**4d**	-8.09	2	ILE20, LEU50	2.28, 3.05
5	**4e**	-6.97	2	PRO51, ILE94	2.10, 3.42
6	**4f**	**-8.97**	2	ASP27	2.46, 2.53
7	**4g**	-8.41	5	ASP27, GLN28, PHE31, LEU50, PRO51	2.14, 2.18, 2.44, 3.01, 3.20
8	**4h**	-8.15	4	ILE20, TRP22, GLN28, PHE31	2.15, 2.57, 2.96, 3.59
9	**4i**	**-9.26**	2	PHE31, PRO51	3.02, 2.92
10	**4j**	-8.30	4	PHE31, PRO51, ILE94	1.72, 3.02, 3.23, 4.14
11	**4k**	**-9.19**	2	ASP27	2.50, 2.61
12	**4l**	-8.54	5	ASP27, GLN28, PHE31, LEU50, PRO51	2.13, 2.19, 2.43, 3.01, 3.21
13	**4m**	-8.31	4	ILE20, TRP22, GLN28, PHE31	2.37, 2.52, 2.93, 3.70
14	**4n**	-8.40	6	ASP27, GLN28, PHE31, SER49, LEU50, PRO51	2.08, 2.20, 2.43, 3.00, 3.15, 3.24
15	**4o**	-8.20	5	GLN28, PHE31, SER49, LEU50, PRO51	1.77, 2.30, 3.05, 3.44, 3.68

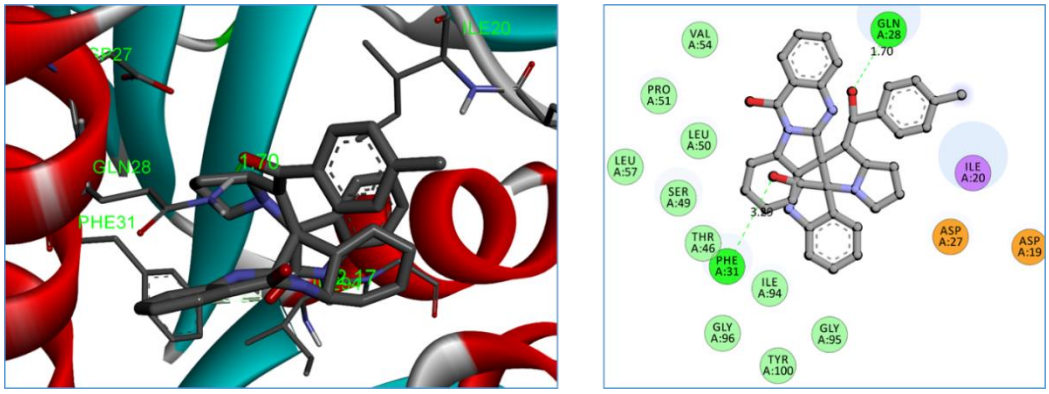

Figure 6B.10. Binding interactions between compound **4b** and active site of *Mycobacterium tuberculosis* protein (PDB ID: 1DF7).

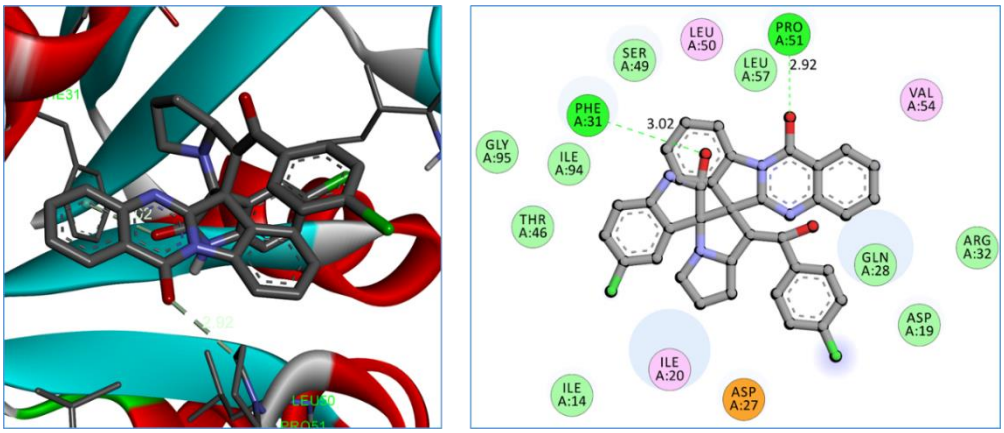

Figure 6B.11. Binding interactions between compound **4i** and active site of *Mycobacterium tuberculosis* protein (PDB ID: 1DF7).

6B.4. Conclusion

In this chapter a series of novel quinazolinone based pyrrolizidino-bisspirooxindoles were synthesized *via* [3+2] cycloaddition reaction under ultrasonication. *In vitro* anti-tubercular screening results revealed that, the compounds having methyl (–Me) and chloro (–Cl) substitutions on the phenyl ring showed better anti-tubercular profile than other compounds against *M. tuberculosis* H37Rv. The active compounds were exhibited relatively low levels of cytotoxicity against RAW 264.7 cell line, which revealed their growth of therapeutic potential in the field of anti-tubercular agents. In addition, the molecular docking studies support that the potent compounds have good binding capacity towards the target enzyme. These results revealed that the synthesized pyrrolizidino-bisspirooxindoles would be promising hits for the development of anti-TB leads.

6B.5. Experimental Section

6B.5.1. Typical procedure for the synthesis of quinazolinone based pyrrolizidino-bisspirooxindoles 4a-o

A mixture of quinazolinone chalcones **1** (1.0 mmol), isatins **2** (1.0 mmol) and L-proline **3** (1.0 mmol) in 3 mL of CH_3CN were heated at 60 °C under ultrasonication for 40-60 min. After the complete consumption of starting materials (monitored by TLC), the reaction mixture was cooled to room temperature. The resulting solid was filtered and recrystallized from methanol to furnish the desired products.

6B.5.2. Protocol for the anti-TB screening

The MIC of the synthesized compounds was tested using *in vitro* microplate alamar blue assay method [37]. The *Mycobacterium tuberculosis* H37Rv strain (ATCC27294) was used for the screening. The inoculum was prepared from fresh LJ medium re-suspended in 7H9-S medium (7H9 broth, 0.1% casitone, 0.5% glycerol, supplemented oleic acid, albumin, dextrose, and catalase [OADC]), adjusted to a OD_{590} 1.0, and diluted 1:20; 100 µL was used as inoculum. Each drug stock solution was thawed and diluted in 7H9-S at four-fold the final highest concentration tested. Serial two-fold dilutions of each drug were prepared directly in a sterile 96-well microtiter plate using 100 µL 7H9-S. A growth control containing no antibiotic and a sterile control were also prepared on each plate. Sterile water was added to all perimeter wells to avoid evaporation during the incubation. The plate was covered, sealed in plastic bags and incubated at 37 ^oC in normal atmosphere. After 7 days incubation, 30 µL of alamar blue solution was added to each well, and the plate was re-incubated overnight. A change in colour from blue (oxidised state) to pink (reduced) indicated the growth of bacteria, and the MIC was defined as the lowest concentration of drug that prevented this change in colour.

6B.5.3. *In vitro* cytotoxicity screening

The *in vitro* cytotoxicity of the privileged anti-tubercular active analogues with lower MIC value were assessed by 3-(4,5-dimethylthiazol-2-yl)-2,5-diphenyltetrazolium bromide (MTT) assay against growth inhibition of RAW 264.7 cells at 25 µM concentration [38]. Cell lines were maintained at 37 °C in a humidified 5% CO_2 incubator (Thermo scientific). Detached the adhered cells and followed by centrifugation to get cell pellet. Fresh media was added to the pellet to make a cell count using haemocytometer and plate 100 µL of media with cells ranging from 5,000 - 6,000 per well in a 96-well plate. The plate

was incubated overnight in CO_2 incubator for the cells to adhere and regain its shape. After 24 h cells were treated with the test compounds at 25 μg/mL diluted using the media to deduce the percentage inhibition on normal cells. The cells were incubated for 48 h to assay the effect of the test compounds on different cell lines. Zero hour reading was noted down with untreated cells and also control with 1% DMSO to subtract further from the 48 h reading. After 48 h incubation, cells were treated by MTT (4,5-dimethylthiazol-2-yl)-2,5-diphenyltetrazolium bromide) dissolved in PBS (5 mg/mL) and incubated for 3-4 h at 37 °C. The formazan crystals thus formed were dissolved in 100 μL of DMSO and the viability was measured at 540 nm on a multimode reader (Spectra max). The values were further calculated for percentage inhibition which in turn helps us to know the cytotoxicity of the test compounds.

6B.5.4. Molecular docking protocol

The docking studies are predominating tools for the assessment of the binding affinity to the ligand-protein receptor. All the synthesized compounds were subjected to *in silico* molecular docking studies by using the AutoDockTools (ADT) version 1.5.6 and AutoDock version 4.2.5.1 docking program [39]. The 3D-structures of all the synthesized compounds were prepared by using chem3D pro 12.0 software. The optimized 3D structures were saved in pdb format. The structure of the dihydrofolate reductase of *Mycobacterium tuberculosis* (PDB code: 1DF7) protein was extracted from the protein data bank (http://www.rcsb.org/pdb). The bound ligand and water molecules in protein were removed by using Discovery Studio Visualizer version 4.0 to prepare the protein. Non polar hydrogens were merged and gasteiger charges were added to the protein. The grid file was saved in gpf format. The three dimensional grid box having dimensions 60 x 60 x 60 $Å^3$ was created around the protein with spacing 0.3750 Å. The genetic algorithm was carried out with the population size and the maximum number of evaluations were 150 and 25,00,000 respectively. The docking output file was saved as Lamarckian Ga (4.2) in dpf format. The ligand-protein complex binding sites were visualized by Discovery Studio Visualizer version 4.0.

6B.6. Spectral data of synthesized compounds 4a-o

1'-benzoyl-5',6',7',7*a*'-tetrahydro-1'*H*,12''*H*-dispiro[indoline-3,3'-pyrrolizine-2',6''-indolo[2,1-*b*]quinazoline]-2,12''-dione (4a)

Off-white solid. mp: 200-202 °C. IR (KBr, cm^{-1}): 3182, 1743, 1686, 1639, 1469. ^{1}H NMR (400 MHz, DMSO-d_6) δ: 10.50 (s, 1H), 8.14 – 8.08 (m, 2H), 8.03 (d, J = 7.6 Hz, 1H), 7.92

(t, *J* = 7.2 Hz, 1H), 7.79 (d, *J* = 8.0 Hz, 1H), 7.60 – 7.52 (m, 3H), 7.16 (d, *J* = 7.2 Hz, 1H), 7.12 (d, *J* = 8.0 Hz, 2H), 6.93-6.85 (m, 3H), 6.47 (d, *J* = 7.6 Hz, 1H), 6.42 (t, *J* = 7.6 Hz, 1H), 6.18 (d, *J* = 7.6 Hz, 1H), 5.71 (d, *J* = 8.4 Hz, 1H), 4.70 (dd, *J* = 14.8, 9.6 Hz, 1H), 2.74 (t, *J* = 8.4 Hz, 1H), 2.62 (dd, *J* = 16.0, 9.2 Hz, 1H), 2.48 (d, *J* = 8.0 Hz, 1H), 2.34 – 2.25 (m, 1H), 2.18-2.08 (m, 1H), 2.05 – 2.00 (m, 1H). ^{13}C NMR (100 MHz, DMSO-d_6) δ: 199.58, 177.68, 158.40, 154.88, 146.38, 142.86, 139.25, 137.52, 135.30, 132.52, 130.12, 130.06, 128.90, 128.50, 128.17, 127.97, 127.88, 127.66, 126.48, 125.61, 125.03, 121.12, 120.84, 115.94, 109.71, 78.40, 67.38, 65.43, 56.78, 47.40, 31.33, 30.55. ESI mass spectrum (m/z): calcd. for $C_{35}H_{27}N_4O_3$ $[M+H]^+$: 551.2083; obsd.: 551.1983.

1'-(4-methylbenzoyl)-5',6',7',7*a*'-tetrahydro-1'*H*,12''*H*-dispiro[indoline-3,3'-pyrrolizine-2',6''-indolo[2,1-*b*]quinazoline]-2,12''-dione (4b)

Off-white solid. mp: 213-215 °C. IR (KBr, cm^{-1}): 3402, 1729, 1679, 1634, 1465. ^{1}H NMR (400 MHz, DMSO-d_6) δ: 10.58 (s, 1H), 8.35 (d, *J* = 7.2 Hz, 1H), 8.28 (d, *J* = 7.6 Hz, 1H), 8.08 (d, *J* = 8.0 Hz, 1H), 8.01 (t, *J* = 7.6 Hz, 2H), 7.75 (d, *J* = 7.6 Hz, 1H), 7.71 (d, *J* = 6.8 Hz, 1H), 7.32-7.21 (m, 3H), 7.04 (t, *J* = 7.6 Hz, 1H), 6.91 (d, *J* = 8.0 Hz, 1H), 6.72 (d, *J* = 8.4 Hz, 2H), 6.61 (d, *J* = 7.6 Hz, 2H), 5.55 (s, 1H), 4.85 (d, *J* = 8.4 Hz, 1H), 4.19 (q, *J* = 8.4 Hz, 1H), 2.69 (t, *J* = 7.6 Hz, 1H), 2.05 (s, 3H), 1.83 (dd, *J* = 12.4, 8.0 Hz, 2H), 1.73 – 1.66 (m, 1H), 1.40-1.32 (m, 1H). ^{13}C NMR (100 MHz, DMSO-d_6) δ: 198.59, 175.59, 158.61, 155.97, 146.53, 143.14, 142.59, 139.70, 135.53, 134.81, 130.36, 130.18, 129.54, 128.61, 128.30, 128.02, 127.85, 126.58, 126.31, 125.60, 125.25, 124.96, 120.99, 115.92, 111.28, 79.05, 66.71, 62.25, 53.52, 52.01, 35.45, 34.68, 21.33. ESI mass spectrum (m/z): calcd. for $C_{36}H_{29}N_4O_3$ $[M+H]^+$: 565.2240; obsd.: 565.2237.

1'-(4-methoxybenzoyl)-5',6',7',7a'-tetrahydro-1'*H*,12''*H*-dispiro[indoline-3,3'-pyrrolizine-2',6''-indolo[2,1-*b*]quinazoline]-2,12''-dione (4c)

Pale brown solid. mp: 189-191 °C. IR (KBr, cm^{-1}): 3330, 1734, 1671, 1640, 1464. ^{1}H NMR (400 MHz, DMSO-d_6) δ: 10.63 (s, 1H), 8.18 (d, *J* = 4.4 Hz, 1H), 8.07 (t, *J* = 8.0 Hz, 2H), 7.92 (t, *J* = 7.6 Hz, 1H), 7.79 (d, *J* = 7.2 Hz, 1H), 7.60 – 7.53 (m, 3H), 7.48 (t, *J* = 8.4 Hz, 1H), 7.22 (d, *J* = 8.0 Hz, 2H), 7.09 (d, *J* = 7.2 Hz, 1H), 6.43 (d, *J* = 7.6 Hz, 3H), 6.23 (s, 1H), 5.65 (d, *J* = 8.0 Hz, 1H), 4.67 (q, *J* = 8.0 Hz, 1H), 3.49 (s, 3H), 2.76 (t, *J* = 10.0 Hz, 1H), 2.62 - 2.57 (m, 1H), 2.44 – 2.37 (m, 1H), 2.30 -2.23 (m, 1H), 2.17 - 2.07 (m, 1H), 2.04 – 1.97 (m, 1H). ^{13}C NMR (100 MHz, DMSO-d_6) δ: 196.51, 175.11, 162.44, 158.20, 155.58, 146.11, 142.13, 139.16, 135.06, 129.85, 129.68, 129.61, 129.40, 129.24, 127.88, 127.79,

127.58, 126.18, 125.78, 125.13, 124.76, 124.52, 120.49, 115.39, 112.99, 110.77, 78.61, 66.92, 61.92, 55.29, 52.61, 51.75, 35.00, 34.04. ESI mass spectrum (m/z): calcd. for $C_{36}H_{29}N_4O_4$ $[M+H]^+$: 581.2189; obsd.: 581.2080.

1'-(4-chlorobenzoyl)-5',6',7',7*a*'-tetrahydro-1'*H*,12''*H*-dispiro[indoline-3,3'-pyrrolizine-2',6''-indolo[2,1-*b*]quinazoline]-2,12''-dione (4d)

White solid. mp: 209-211 ℃. IR (KBr, cm^{-1}):3363, 1696, 1680, 1646, 1464. ^{1}H NMR (400 MHz, DMSO-d_6) δ: 10.60 (s, 1H), 8.35 (d, J = 8.0 Hz, 1H), 8.31 – 8.27 (m, 1H), 8.05 (t, J = 7.6 Hz, 1H), 8.01 (d, J = 6.8 Hz, 1H), 7.77 (d, J = 7.2 Hz, 1H), 7.71 (t, J = 6.8 Hz, 1H), 7.32 (d, J = 7.6 Hz, 1H), 7.28 – 7.25 (m, 2H), 7.05 (t, J = 7.6 Hz, 1H), 6.90 (dd, J = 8.4, 6.6 Hz, 4H), 6.79 (d, J = 8.4 Hz, 2H), 5.55 (s, 1H), 4.84 (d, J = 7.6 Hz, 1H), 4.18 (q, J = 8.0 Hz, 1H), 2.69 (t, J = 8.0 Hz, 1H), 1.86-1.78 (m, 2H), 1.73-1.65 (m, 1H), 1.41 – 1.33 (m, 1H). ^{13}C NMR (100 MHz, DMSO-d_6) δ: 198.97, 177.34, 158.57, 154.67, 146.43, 142.32, 139.48, 136.67, 135.68, 132.99, 131.20, 130.70, 129.85, 128.73, 128.54, 128.18, 127.57, 126.87, 126.79, 123.76, 121.08, 116.36, 113.08, 111.89, 78.53, 67.61, 65.57, 57.14, 47.58, 31.53, 30.76. ESI mass spectrum (m/z): calcd. for $C_{35}H_{26}ClN_4O_3$ $[M+H]^+$: 585.1693; obsd.: 585.1616.

1'-(4-bromobenzoyl)-5',6',7',7*a*'-tetrahydro-1'*H*,12''*H*-dispiro[indoline-3,3'-pyrrolizine-2',6''-indolo[2,1-*b*]quinazoline]-2,12''-dione (4e)

Pale yellow solid. mp: 204-206 ℃. IR (KBr, cm^{-1}): 3344, 1731, 1692, 1639, 1466. ^{1}H NMR (400 MHz, DMSO-d_6) δ: 10.60 (s, 1H), 8.36 (d, J = 8.0 Hz, 1H), 8.29-8.27 (m, 1H), 8.07-8.00 (m, 3H), 7.76 (d, J = 7.6 Hz, 1H), 7.72 (t, J = 8.0 Hz, 1H), 7.32 (d, J = 8.0 Hz, 1H), 7.29 – 7.26 (m, 2H), 7.06 (d, J = 7.2 Hz, 1H), 7.02 (d, J = 8.4 Hz, 2H), 6.92 (d, J = 7.6 Hz, 1H), 6.71 (d, J = 8.4 Hz, 2H), 5.55 (s, 1H), 4.84 (d, J = 7.6 Hz, 1H), 4.21 – 4.14 (m, 1H), 2.68 (t, J = 7.6 Hz, 1H), 1.84 – 1.77 (m, 2H), 1.75-1.64 (m, 1H), 1.41 – 1.33 (m, 1H). ^{13}C NMR (100 MHz, DMSO-d_6) δ: 197.66, 176.03, 157.26, 153.36, 145.12, 141.01, 138.17, 135.36, 134.37, 131.69, 129.89, 129.39, 128.54, 127.42, 127.24, 126.87, 126.26, 125.56, 125.48, 125.44, 122.46, 119.77, 115.06, 111.77, 110.58, 77.22, 66.30, 64.26, 55.83, 46.27, 30.22, 29.45. ESI mass spectrum (m/z): calcd. for $C_{35}H_{26}BrN_4O_3$ $[M+H+2]^+$: 631.1188; obsd.: 631.1061.

1'-benzoyl-5-chloro-5',6',7',7*a*'-tetrahydro-1'*H*,12''*H*-dispiro[indoline-3,3'-pyrrolizine-2',6''-indolo[2,1-*b*]quinazoline]-2,12''-dione (4f)

Off-white solid. mp: 212-214 ℃. IR (KBr, cm^{-1}): 3309, 1738, 1670, 1639, 1466. ^{1}H NMR (400 MHz, DMSO-d_6) δ: 10.64 (s, 1H), 8.20 – 8.15 (m, 1H), 8.11 – 8.03 (m, 2H), 7.93 (t, *J* = 7.2 Hz, 1H), 7.79 (d, *J* = 7.2 Hz, 1H), 7.61 – 7.55 (m, 3H), 7.19-7.13 (m, 3H), 6.98 (dd, *J* = 8.4, 2.0 Hz, 1H), 6.90 (t, *J* = 7.6 Hz, 2H), 6.48 (d, *J* = 8.4 Hz, 1H), 6.09 (s, 1H), 5.67 (d, *J* = 8.0 Hz, 1H), 4.72-4.66 (m, 1H), 2.78 (t, *J* = 8.8 Hz, 1H), 2.61 (dd, *J* = 16.0, 7.6 Hz, 1H), 2.49 – 2.41 (m, 1H), 2.33 – 2.25 (m, 1H), 2.19 – 2.08 (m, 1H), 2.07 – 1.99 (m, 1H). ^{13}C NMR (100 MHz, DMSO-d_6) δ: 199.39, 177.33, 154.54, 146.31, 141.69, 139.30, 137.46, 135.39, 132.63, 130.35, 129.95, 128.63, 128.41, 127.99, 127.95, 127.73, 127.07, 126.80, 126.55, 126.51, 125.68, 125.15, 120.84, 116.07, 111.11, 78.52, 67.36, 63.76, 56.64, 54.10, 47.38, 31.42. ESI mass spectrum (m/z): calcd. for $C_{35}H_{26}ClN_4O_3$ $[M+H]^+$: 585.1693; obsd.: 585.1610.

5-chloro-1'-(4-methylbenzoyl)-5',6',7',7*a*'-tetrahydro-1'*H*,12''*H*-dispiro[indoline-3,3'-pyrrolizine-2',6''-indolo[2,1-*b*]quinazoline]-2,12''-dione (4g)

Pale brown solid. mp: 220-222 ℃. IR (KBr, cm^{-1}): 3344, 1734, 1673, 1639, 1465. ^{1}H NMR (400 MHz, DMSO-d_6) δ: 10.64 (s, 1H), 8.17 (t, *J* = 4.4 Hz, 1H), 8.07 (t, *J* = 7.6 Hz, 2H), 7.93 (t, *J* = 7.2 Hz, 1H), 7.77 (d, *J* = 8.4 Hz, 1H), 7.60 (d, *J* = 7.6 Hz, 1H), 7.58 – 7.53 (m, 2H), 7.02 (d, *J* = 8.0 Hz, 2H), 6.97 (d, *J* = 8.0 Hz, 1H), 6.66 (d, *J* = 7.6 Hz, 2H), 6.48 (d, *J* = 8.0 Hz, 1H), 6.12 (s, 1H), 5.62 (d, *J* = 8.0 Hz, 1H), 4.66 (dd, *J* = 14.4, 9.6 Hz, 1H), 2.77 (t, *J* = 8.4 Hz, 1H), 2.60 (dd, *J* = 16.8, 9.2 Hz, 1H), 2.44 (t, *J* = 9.6 Hz, 1H), 2.32 – 2.23 (m, 1H), 2.16 – 2.01 (m, 2H), 1.99 (s, 3H). ^{13}C NMR (100 MHz, DMSO-d_6) δ: 198.82, 175.97, 158.57, 156.22, 146.50, 143.60, 143.01, 139.55, 135.42, 134.78, 130.44, 129.93, 129.69, 128.47, 128.34, 127.94, 127.68, 126.41, 126.23, 125.43, 122.86, 121.22, 120.86, 115.75, 109.85, 78.90, 62.15, 53.61, 52.22, 51.75, 35.27, 31.95, 21.21. ESI mass spectrum (m/z): calcd. for $C_{36}H_{28}ClN_4O_3$ $[M+H]^+$: 599.1850; obsd.: 599.1843.

5-chloro-1'-(4-methoxybenzoyl)-5',6',7',7*a*'-tetrahydro-1'*H*,12''*H*-dispiro[indoline-3,3'-pyrrolizine-2',6''-indolo[2,1-*b*]quinazoline]-2,12''-dione (4h)

Off-white solid. mp: 190-192 ℃. IR (KBr, cm^{-1}):3333, 1729, 1667, 1639, 1462. ^{1}H NMR (400 MHz, DMSO-d_6) δ: 10.64 (s, 1H), 8.18 (t, *J* = 6.0 Hz, 1H), 8.09 (t, *J* = 5.6 Hz, 1H), 8.06 (d, *J* = 8.0 Hz, 1H), 7.93 (t, *J* = 7.2 Hz, 1H), 7.79 (d, *J* = 8.4 Hz, 1H), 7.60 (d, *J* = 7.6 Hz, 1H), 7.57 – 7.54 (m, 2H), 7.22 (d, *J* = 8.4 Hz, 2H), 6.98 (d, *J* = 10.0 Hz, 1H), 6.48 (d,

J = 8.0 Hz, 1H), 6.43 (d, *J* = 8.4 Hz, 2H), 6.12 (s, 1H), 5.66 (d, *J* = 8.4 Hz, 1H), 4.67 (dd, *J* = 14.4, 9.2 Hz, 1H), 3.49 (s, 3H), 2.77 (t, *J* = 8.4 Hz, 1H), 2.60 (dd, *J* = 16.0, 8.4 Hz, 1H), 2.45 – 2.37 (m, 1H), 2.31 – 2.24 (m, 1H), 2.16 – 2.07 (m, 1H), 2.05 – 2.01 (m, 1H). ^{13}C NMR (100 MHz, DMSO-d_6) δ: 196.97, 177.39, 162.84, 158.47, 154.64, 146.38, 141.69, 139.21, 135.40, 130.26, 130.21, 129.87, 129.12, 128.66, 128.22, 128.05, 127.18, 126.48, 126.39, 125.71, 125.16, 120.91, 116.05, 113.31, 111.11, 78.48, 67.75, 65.65, 55.95, 55.64, 47.35, 31.37, 30.53. ESI mass spectrum (m/z): calcd. for $C_{36}H_{28}ClN_4O_4$ $[M+H]^+$: 615.1799; obsd.: 615.1691.

5-chloro-1''-(4-chlorobenzoyl)-5',6',7',7*a*'-tetrahydro-1'*H*,12''*H*-dispiro[indoline-3,3'-pyrrolizine-2',6''-indolo[2,1-*b*]quinazoline]-2,12''-dione (4i)

Off-white solid. mp: 216-218 °C. IR (KBr, cm^{-1}): 3305, 1737, 1689, 1642, 1464. ^{1}H NMR (400 MHz, DMSO-d_6) δ: 10.64 (s, 1H), 8.21 – 8.16 (m, 1H), 8.09 – 8.06 (m, 2H), 7.96 – 7.91 (m, 1H), 7.77 (d, 1H, *J* = 8.0 Hz), 7.62-7.60 (m, 1H), 7.59 – 7.55 (m, 2H), 7.12 (d, 1H, *J* = 2.0 Hz), 7.10 (d, 1H, *J* = 2.0 Hz), 6.98 (dd,1H, *J* = 8.4, 2.4 Hz), 6.93 (d, 1H, *J* = 2.0 Hz), 6.91 (d, 1H, *J* = 2.0 Hz), 6.48 (d, 1H, *J* = 8.4 Hz), 6.12 (d, 1H, *J* = 2.4 Hz), 5.64 (d, 1H, *J* = 8.4 Hz), 4.71 – 4.63 (m, 1H), 2.76 (dd, 1H, *J* = 15.2, 7.2 Hz), 2.63-2.57 (m,1H), 2.47 – 2.39 (m, 1H), 2.31-2.25 (m, 1H), 2.18 – 2.08 (m, 1H), 2.05 – 2.00 (m, 1H). ^{13}C NMR (100 MHz, DMSO-d_6) δ: 198.48, 177.28, 158.36, 154.43, 146.22, 141.69, 139.24, 137.60, 136.10, 135.46, 130.47, 130.24, 129.97, 129.56, 129.16, 128.33, 128.04, 127.04, 126.56, 125.69, 125.19, 120.83, 116.15, 111.30, 111.16, 78.33, 67.39, 65.38, 56.87, 47.35, 31.31, 30.53. ESI mass spectrum (m/z): calcd. for $C_{35}H_{25}Cl_2N_4O_3$ $[M+H]^+$: 619.1304; obsd.: 619.20.

1''-(4-bromobenzoyl)-5-chloro-5',6',7',7*a*'-tetrahydro-1'*H*,12''*H*-dispiro[indoline-3,3'-pyrrolizine-2',6''-indolo[2,1-*b*]quinazoline]-2,12''-dione (4j)

White solid. mp: 212-214 °C. IR (KBr, cm^{-1}): 3303, 1737, 1669, 1640, 1465. ^{1}H NMR (400 MHz, DMSO-d_6) δ: 10.65 (s, 1H), 8.18 (dd, *J* = 5.6, 3.2 Hz, 1H), 8.08 (d, *J* = 6.4 Hz, 2H), 7.94 (t, *J* = 7.6 Hz, 1H), 7.76 (d, *J* = 8.0 Hz, 1H), 7.62 – 7.55 (m, 3H), 7.06 – 6.96 (m, 5H), 6.48 (d, *J* = 8.4 Hz, 1H), 6.11 (d, *J* = 1.6 Hz, 1H), 5.62 (d, *J* = 8.4 Hz, 1H), 4.66 (dd, *J* = 14.0, 9.0 Hz, 1H), 2.77 (t, *J* = 8.0 Hz, 1H), 2.63 – 2.56 (m, 1H), 2.46 - 2.39 (m, 1H), 2.31 – 2.24 (m, 1H), 2.17 – 2.08 (m, 1H), 2.05 – 2.01 (m, 1H). ^{13}C NMR (100 MHz, DMSO-d_6) δ: 198.26, 176.80, 157.87, 153.96, 145.74, 141.22, 138.77, 135.97, 134.98, 130.50, 130.01, 129.50, 129.13, 127.99, 127.82, 127.49, 126.57, 126.17, 126.09, 125.22, 124.71, 120.37,

115.68, 110.69, 77.82, 66.90, 64.85, 56.48, 46.87, 30.82, 30.06. ESI mass spectrum (m/z): calcd. for $C_{35}H_{25}BrClN_4O_3$ $[M+H]^+$: 665.0778; obsd.: 665.0664.

1'-benzoyl-5-bromo-5',6',7',7*a*'-tetrahydro-1'*H*,12''*H*-dispiro[indoline-3,3'-pyrrolizine-2',6''-indolo[2,1-*b*]quinazoline]-2,12''-dione (4k)

Pale green solid. mp: 215-217 ℃. IR (KBr, cm^{-1}): 3315, 1735, 1670, 1638, 1467. ^{1}H NMR (400 MHz, DMSO-d_6) δ: 10.63 (s, 1H), 8.16 (d, J = 0.8 Hz, 1H), 8.04 (d, J = 8.0 Hz, 2H), 7.91 (s, 1H), 7.78 (d, J = 6.8 Hz, 1H), 7.57 (s, 3H), 7.14 (d, J = 6.0 Hz, 3H), 7.10 (s, 1H), 6.89 (s, 2H), 6.42 (d, J = 6.8 Hz, 1H), 6.21 (s, 1H), 5.66 (d, J = 7.6 Hz, 1H), 4.68 (s, 1H), 2.76 (s, 1H), 2.59 (d, J = 8.0 Hz, 1H), 2.40 (s, 1H), 2.26 (d, J = 4.0 Hz, 1H), 2.15 – 2.08 (m, 1H), 2.03 (d, J = 3.6 Hz, 1H). ^{13}C NMR (100 MHz, DMSO-d_6) δ: 199.40, 177.21, 158.43, 154.53, 146.30, 142.06, 139.31, 137.46, 135.38, 132.74, 132.63, 130.33, 128.64, 128.49, 128.39, 128.29, 127.95, 127.72, 127.37, 126.53, 126.47, 120.83, 116.06, 112.85, 111.62, 78.55, 67.38, 65.61, 56.62, 47.39, 31.43, 30.51. ESI mass spectrum (m/z): calcd. for $C_{35}H_{26}BrN_4O_3$ $[M+H]^+$: 631.1168; obsd.: 631.1069.

5-bromo-1'-(4-methylbenzoyl)-5',6',7',7*a*'-tetrahydro-1'*H*,12''*H*-dispiro[indoline-3,3'-pyrrolizine-2',6''-indolo[2,1-*b*]quinazoline]-2,12''-dione (4l)

Off-white solid. mp: 225-227 ℃. IR (KBr, cm^{-1}):3344, 1735, 1673, 1639, 1465. ^{1}H NMR (400 MHz, DMSO-d_6) δ: 10.64 (s, 1H), 8.17 (s, 1H), 8.06 (d, J = 5.2 Hz, 2H), 7.93 (t, J = 8.4 Hz, 1H), 7.77 (d, J = 7.2 Hz, 1H), 7.61 – 7.56 (m, 3H), 7.09 (d, J = 7.2 Hz, 1H), 7.02 (d, J = 7.2 Hz, 2H), 6.66 (d, J = 7.2 Hz, 2H), 6.43 (d, J = 7.6 Hz, 1H), 6.24 (s, 1H), 5.61 (d, J = 8.4 Hz, 1H), 4.69-4.63 (m, 1H), 2.76 (t, J = 9.2 Hz, 1H), 2.59 (d, J = 10.0 Hz, 1H), 2.43 (t, J = 11.2 Hz, 1H), 2.30 – 2.24 (m, 1H), 2.16 – 2.03 (m, 1H), 1.99 (s, 3H). ^{13}C NMR (100 MHz, DMSO-d_6) δ: 198.87, 177.23, 158.42, 154.60, 146.32, 142.96, 142.08, 139.32, 135.37, 134.89, 132.71, 130.27, 128.58, 128.45, 128.20, 127.98, 127.81, 127.45, 126.39, 120.97, 116.08, 112.84, 111.62, 78.37, 67.53, 65.53, 56.69, 47.35, 31.39, 30.53, 21.21. ESI mass spectrum (m/z): calcd. for $C_{36}H_{28}BrN_4O_3$ $[M+H]^+$: 643.1345; obsd.: 643.1343.

5-bromo-1'-(4-methoxybenzoyl)-5',6',7',7*a*'-tetrahydro-1'*H*,12''*H*-dispiro[indoline-3,3'-pyrrolizine-2',6''-indolo[2,1-*b*]quinazoline]-2,12''-dione (4m)

White solid. mp: 210-212 ℃. IR (KBr, cm^{-1}):3295, 1737, 1673, 1643, 1464. ^{1}H NMR (400 MHz, DMSO-d_6) δ: 10.64 (s, 1H), 8.18 (d, J = 6.4 Hz, 1H), 8.11 – 8.05 (m, 2H), 7.92 (t, J = 7.2 Hz, 1H), 7.79 (d, J = 7.6 Hz, 1H), 7.60 (d, J = 7.2 Hz, 1H), 7.55 (d, J = 7.2 Hz, 2H), 7.22 (d, J = 8.0 Hz, 2H), 7.10 (d, J = 8.8 Hz, 1H), 6.43 (d, J = 8.4 Hz, 3H), 6.24 (s, 1H),

5.65 (d, *J* = 7.2 Hz, 1H), 4.68 (dd, *J* = 16.0, 10.0 Hz, 1H), 3.49 (s, 3H), 2.77 (t, *J* = 10.4 Hz, 1H), 2.60 (dd, *J* = 11.2, 6.8 Hz, 1H), 2.44 – 2.39 (m, 1H), 2.30 – 2.24 (m, 1H), 2.14 – 2.09 (m, 1H), 2.04 – 1.98 (m, 1H). ^{13}C NMR (100 MHz, DMSO-d_6) δ: 198.47, 175.93, 158.49, 155.97, 146.37, 143.54, 139.41, 137.55, 136.04, 135.55, 130.52, 130.17, 129.40, 128.40, 128.30, 127.99, 126.49, 126.39, 125.40, 122.72, 121.28, 120.66, 115.76, 109.91, 78.91, 65.72, 62.01, 57.18, 53.77, 51.46, 35.23, 32.62. ESI mass spectrum (m/z): calcd. for $C_{36}H_{28}BrN_4O_4$ $[M+H+2]^+$: 661.1273; obsd.: 661.1190.

5-bromo-1''-(4-chlorobenzoyl)-5',6',7',7*a*'-tetrahydro-1'*H*,12''*H*-dispiro[indoline-3,3'-pyrrolizine-2',6''-indolo[2,1-*b*]quinazoline]-2,12''-dione (4n)

White solid. mp: 221-223 °C. IR (KBr, cm^{-1}): 3306, 1730, 1666, 1642, 1464. ^{1}H NMR (400 MHz, DMSO-d_6) δ: 10.67 (s, 1H), 8.20 (d, *J* = 4.8 Hz, 1H), 8.09 (d, *J* = 3.2 Hz, 2H), 7.95 (s, 1H), 7.79 (s, 1H), 7.60 (s, 3H), 7.12 (d, *J* = 4.0 Hz, 3H), 6.94 (d, *J* = 5.2 Hz, 2H), 6.45 (d, *J* = 7.2 Hz, 1H), 6.25 (s, 1H), 5.64 (s, 1H), 4.68 (s, 1H), 2.83 – 2.75 (m, 1H), 2.61 (d, *J* = 7.2 Hz, 1H), 2.47 – 2.41 (m, 1H), 2.29 (s, 1H), 2.14 (d, *J* = 8.0 Hz, 1H), 2.07 – 2.00 (m, 1H). ^{13}C NMR (100 MHz, DMSO-d_6) δ: 198.49, 177.30, 158.37, 154.42, 146.21, 141.68, 139.23, 137.60, 136.09, 135.47, 130.47, 130.25, 129.97, 129.56, 129.15, 128.61, 128.33, 128.03, 126.51, 125.69, 125.20, 120.81, 116.14, 111.17, 78.33, 67.39, 65.37, 56.88, 47.35, 31.30, 30.52. ESI mass spectrum (m/z): calcd. for $C_{35}H_{25}BrClN_4O_3$ $[M+H]^+$: 665.0778; obsd.: 665.0690.

5-bromo-1''-(4-bromobenzoyl)-5',6',7',7*a*'-tetrahydro-1'*H*,12''*H*-dispiro[indoline-3,3'-pyrrolizine-2',6''-indolo[2,1-*b*]quinazoline]-2,12''-dione (4o)

Off-white solid. mp: 218-220 °C. IR (KBr, cm^{-1}): 3304, 1731, 1668, 1642, 1465. ^{1}H NMR (400 MHz, DMSO-d_6) δ: 10.67 (s, 1H), 8.20 (s, 1H), 8.09 (s, 2H), 7.99 – 7.92 (m, 1H), 7.78 (d, 1H, *J* = 7.6 Hz), 7.60 (d, 3H, *J* = 1.6 Hz), 7.11 (d, 1H, *J* = 8.0 Hz), 7.04 (d, 4H, *J* = 10.4 Hz), 6.45 (d, 1H, *J* = 8.0 Hz), 6.25 (s, 1H), 5.63 (d, 1H, *J* = 7.2 Hz), 4.69 (m, 1H), 2.83 – 2.73 (m, 1H), 2.61 (d, 1H, *J* = 8.4 Hz), 2.45 (dd, 1H, *J* = 10.8, 4.0 Hz), 2.33 – 2.25 (m, 1H), 2.15 – 2.00 (m, 2H). ^{13}C NMR (100 MHz, DMSO-d_6) δ: 198.75, 177.12, 158.35, 154.45, 146.21, 142.10, 139.26, 136.45, 135.46, 132.77, 130.98, 130.48, 129.63, 128.51, 128.32, 127.96, 127.35, 126.65, 126.57, 126.52, 123.54, 120.86, 116.14, 112.86, 111.67, 78.31, 67.39, 65.35, 56.92, 47.36, 31.31, 30.54. ESI mass spectrum (m/z): calcd. for $C_{35}H_{25}Br_2N_4O_3$ $[M+H]^+$: 709.0293; obsd.: 709.0149.

6B.7. References

[1] S. H. Banitaba, J. Safari, S. D. Khalili, *Ultrason. Sonochem.* **2013**, *20*, 401–407.

[2] A. Yildirim, D. Shi, S. Roy, N. T. Blum, R. Chattaraj, J. N. Cha, A. P. Goodwin, *ACS Appl. Mater. Interfaces* **2018**, *10*, 36786–36795.

[3] M. J. Lo Fiego, A. S. Lorenzetti, G. F. Silbestri, C. E. Domini, *Ultrason. Sonochem.* **2021**, *80*, 105834–105870.

[4] G. Cravotto, P. Cintas, *Chem. Soc. Rev.* **2006**, *35*, 180–196.

[5] R. Saeed, A. P. Sakla, N. Shankaraiah, *Org. Biomol. Chem.* **2021**, *19*, 7768–7791.

[6] C. V. Galliford, K. A. Scheidt, *Angew. Chemie Int. Ed.* **2007**, *46*, 8748–8758.

[7] B. Yu, D. Yu, H. Liu, *Eur. J. Med. Chem.* **2015**, *97*, 673–698.

[8] J. Zhang, J. Zhao, L. Wang, J. Liu, D. Ren, Y. Ma, *Tetrahedron* **2016**, *72*, 936–943.

[9] J. Wu, X. Zhang, Y. Zhang, J. Xie, *Org. Biomol. Chem.* **2015**, *13*, 4967–4975.

[10] K. Parthasarathy, Ch. Praveen, K. Saranraj, C. Balachandran, P. S. Kumar, *Med. Chem. Res.* **2016**, *25*, 2155–2170.

[11] V. V. Vintonyak, K. Warburg, H. Kruse, S. Grimme, K. Hübel, D. Rauh, H. Waldmann, *Angew. Chemie Int. Ed.* **2010**, *49*, 5902–5905.

[12] M. Palomba, E. Scarcella, L. Sancineto, L. Bagnoli, C. Santi, F. Marini, *Eur. J. Org. Chem.* **2019**, *2019*, 5396–5401.

[13] D. Du, Y. Jiang, Q. Xu, M. Shi, *Adv. Synth. Catal.* **2013**, *355*, 2249–2256.

[14] S. D. Lotesta, A. P. Marcus, Y. Zheng, K. Leftheris, P. B. Noto, S. Meng, G. Kandpal, G. Chen, J. Zhou, B. McKeever, Y. Bukhtiyarov, Y. Zhao, D. S. Lala, S. B. Singh, G. M. McGeehan, *Bioorg. Med. Chem.* **2016**, *24*, 1384–1391.

[15] S. Peiman, R. Baharfar, B. Maleki, *Mater. Today Commun.* **2021**, *26*, 101759–101771.

[16] L. Chen, J. Xie, H. Song, Y. Liu, Y. Gu, L. Wang, Q. Wang, *J. Agric. Food Chem.* **2016**, *64*, 6508–6516.

[17] L. Chen, Y. Hao, H. Song, Y. Liu, Y. Li, J. Zhang, Q. Wang, *J. Agric. Food Chem.*

2020, *68*, 10618–10625.

[18] D. Cheng, Y. Ishihara, B. Tan, C. F. Barbas, *ACS Catal.* **2014**, *4*, 743–762.

[19] H. Dong, S. Song, J. Li, C. Xu, H. Zhang, L. Ouyang, *Bioorg. Med. Chem. Lett.* **2015**, *25*, 3585–3591.

[20] A. Toumi, S. Boudriga, K. Hamden, I. Daoud, M. Askri, A. Soldera, J. Lohier, C. Strohmann, L. Brieger, M. Knorr, *J. Org. Chem.* **2021**, *86*, 13420–13445.

[21] N. Nivetha, A. Thangamani, *J. Mol. Struct.* **2021**, *1242*, 130716–130730.

[22] R. S. Kumar, P. Antonisamy, A. I. Almansour, N. Arumugam, G. Periyasami, M. Altaf, H. Kim, K.-B. Kwon, *Eur. J. Med. Chem.* **2018**, *152*, 417–423.

[23] H. J. Davis, M. E. Kavanagh, T. Balan, C. Abell, A. G. Coyne, *Bioorg. Med. Chem. Lett.* **2016**, *26*, 3735–3740.

[24] N. Arumugam, A. I. Almansour, R. S. Kumar, V. S. Krishna, D. Sriram, R. Padmanaban, *Arab. J. Chem.* **2021**, *14*, 102938–102947.

[25] K. Murali, H. A. Sparkes, K. J. Rajendra Prasad, *Eur. J. Med. Chem.* **2018**, *143*, 292–305.

[26] X. Zhang, W. Qiu, S. A. Murray, D. Zhan, J. Evans, J. P. Jasinski, X. Wang, W. Zhang, *J. Org. Chem.* **2021**, *86*, 17395–17403.

[27] Y. Lin, Y.-X. Song, D.-M. Du, *Adv. Synth. Catal.* **2019**, *361*, 1064–1070.

[28] Y. Chen, B.-D. Cui, Y. Wang, W.-Y. Han, N.-W. Wan, M. Bai, W. Yuan, Y. Chen, *J. Org. Chem.* **2018**, *83*, 10465–10475.

[29] P. Xia, J. Li, Y. Qian, Q. Zhao, H. Xiang, J. Xiao, X. Chen, H. Yang, *J. Org. Chem.* **2018**, *83*, 2948–2953.

[30] P. Xia, Y. Sun, J. Xiao, Z. Zhou, S. Wen, Y. Xiong, G. Ou, X. Chen, H. Yang, *J. Org. Chem.* **2015**, *80*, 11573–11579.

[31] B. V. S. Reddy, G. Karthik, T. Rajasekaran, B. Sridhar, *Eur. J. Org. Chem.* **2015**, *2015*, 2038–2041.

[32] N. V. Lakshmi, P. Thirumurugan, P. T. Perumal, *Tetrahedron Lett.* **2010**, *51*, 1064–1068.

[33] F. Azimi, H. Azizian, M. Najafi, F. Hassanzadeh, H. Sadeghi-aliabadi, J. B. Ghasemi, M. Ali Faramarzi, S. Mojtabavi, B. Larijani, L. Saghaei, M. Mahdavi, *Bioorg. Chem.* **2021**, *114*, 105127–105140.

[34] K. M. Gokhale, V. N. Telvekar, *Chem. Biol. Drug Des.* **2021**, *97*, 148–156.

[35] A. K. Awasthi, S. Gupta, K. R. Namdev, A. Banerjee, A. Srivastava, *Biomater. Sci.* **2021**, *9*, 3300–3305.

[36] S. J. Gawandi, V. G. Desai, S. Joshi, S. Shingade, R. R. Pissurlenkar, *Bioorg. Chem.* **2021**, *117*, 105331–10545.

[37] P. Sarojini, M. Jeyachandran, D. Sriram, P. Ranganathan, S. Gandhimathi, *J. Mol. Struct.* **2021**, *1233*, 130038–130044.

[38] R. Pradhan, A. Kalkal, S. Jindal, G. Packirisamy, S. Manhas, *RSC Adv.* **2021**, *11*, 798–806.

[39] A. K. Haleel, U. M. Rafi, M. A. Jayathuna, A. K. Rahiman, *J. Mol. Struct.* **2022**, *1250*, 131706–131716.

6B.8. Selected IR, NMR (^{1}H and ^{13}C) and Mass spectra

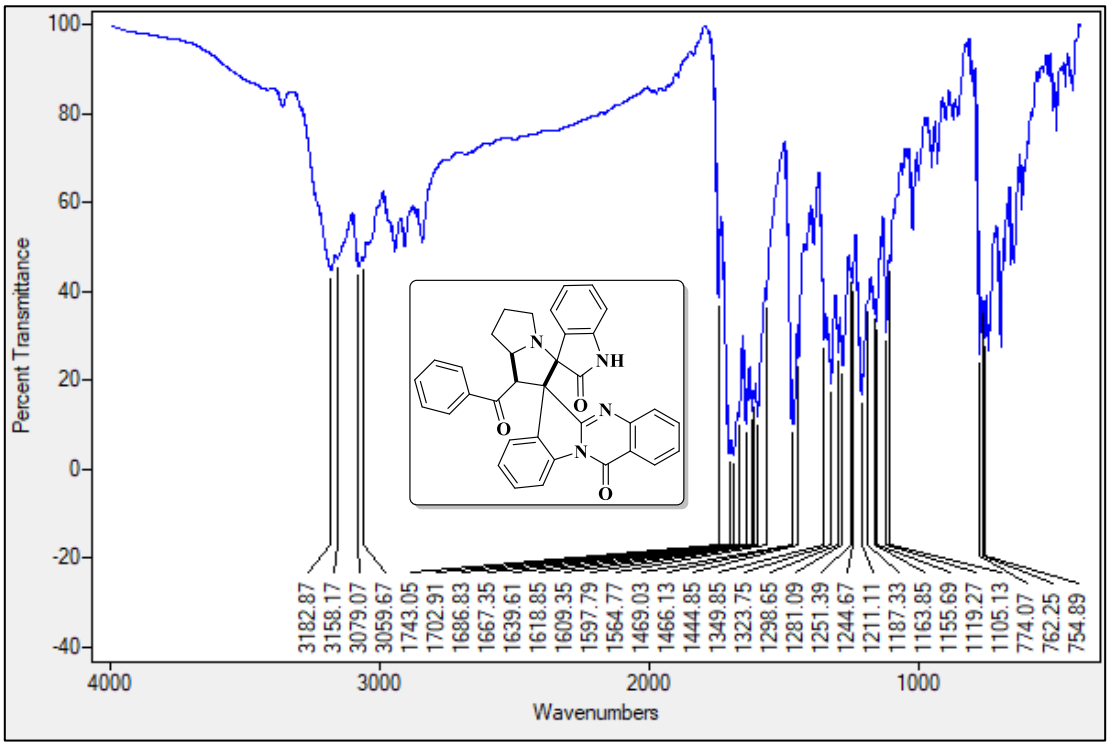

IR spectrum of the compound **4a**

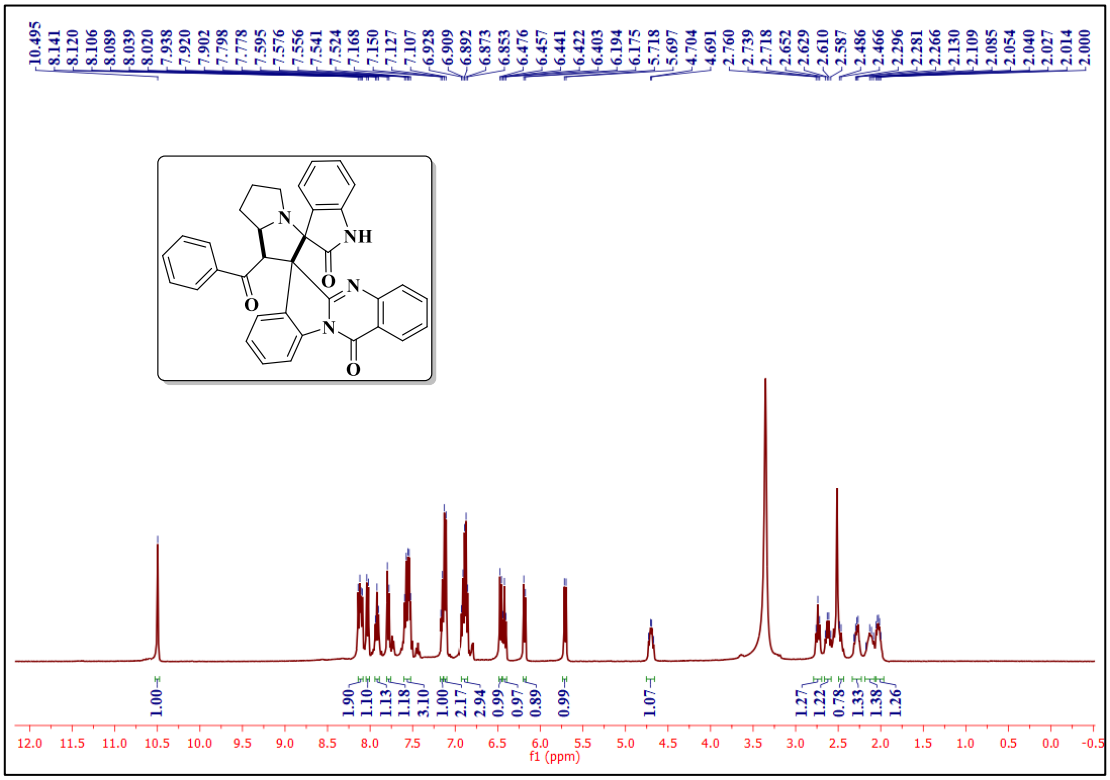

^{1}H NMR spectrum of the compound **4a**

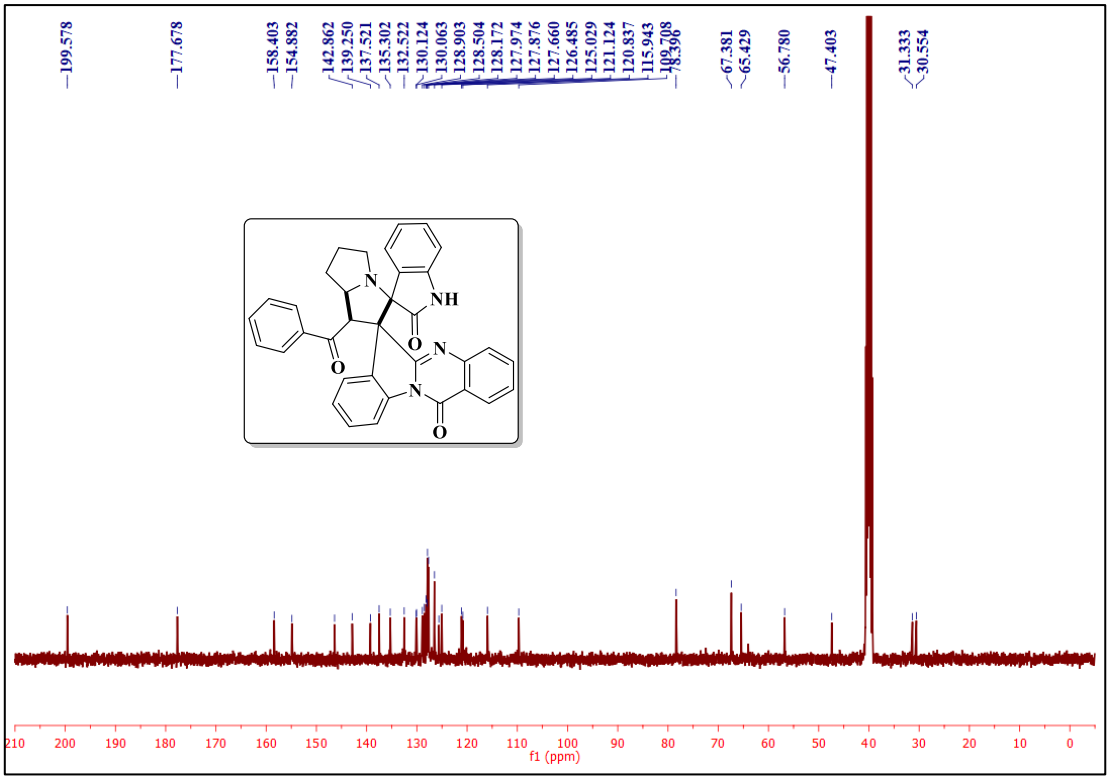

^{13}C NMR spectrum of the compound **4a**

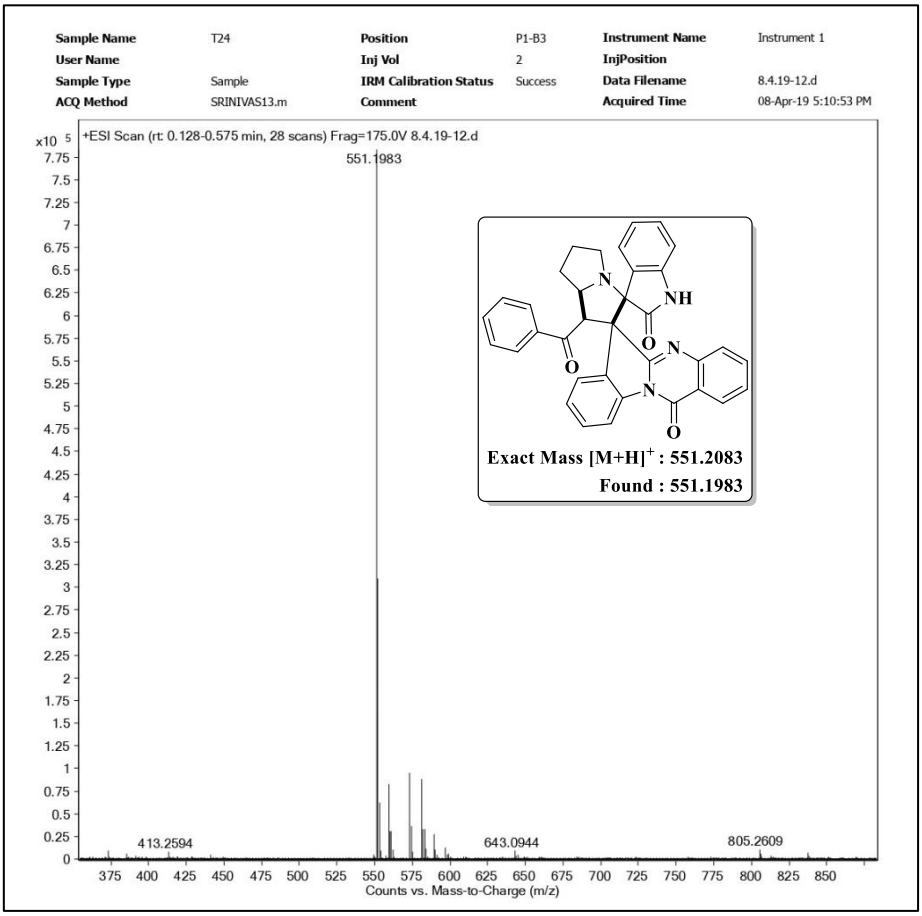

Mass spectrum of the compound **4a**

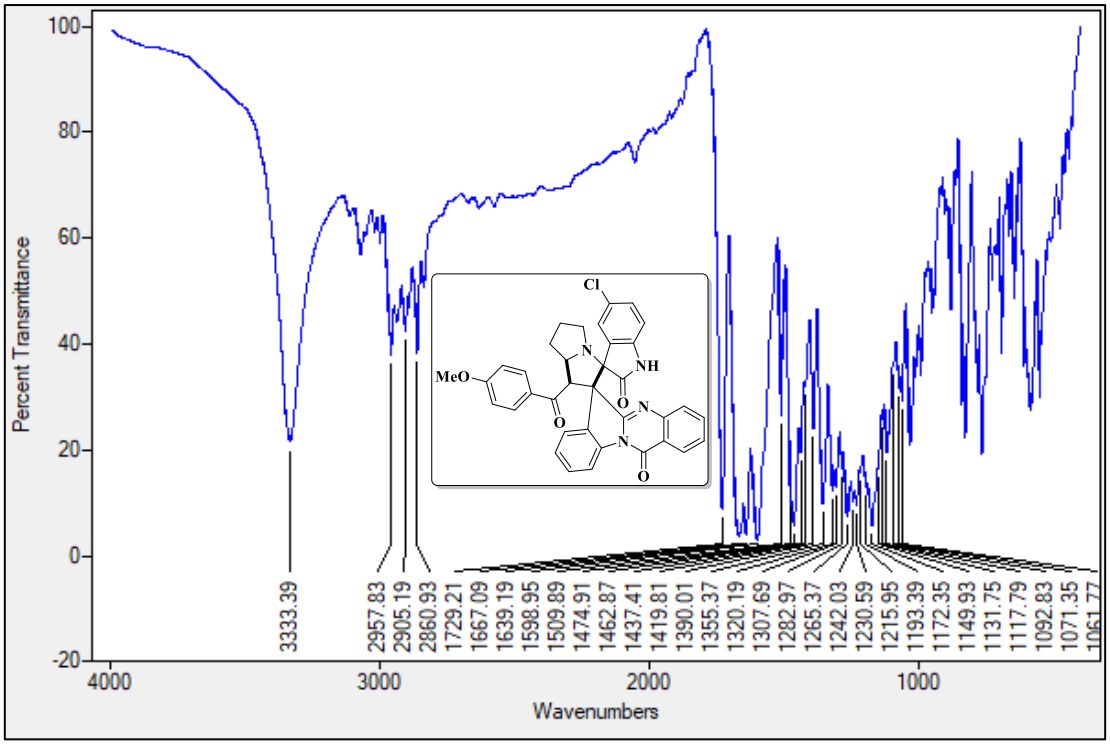

IR spectrum of the compound **4h**

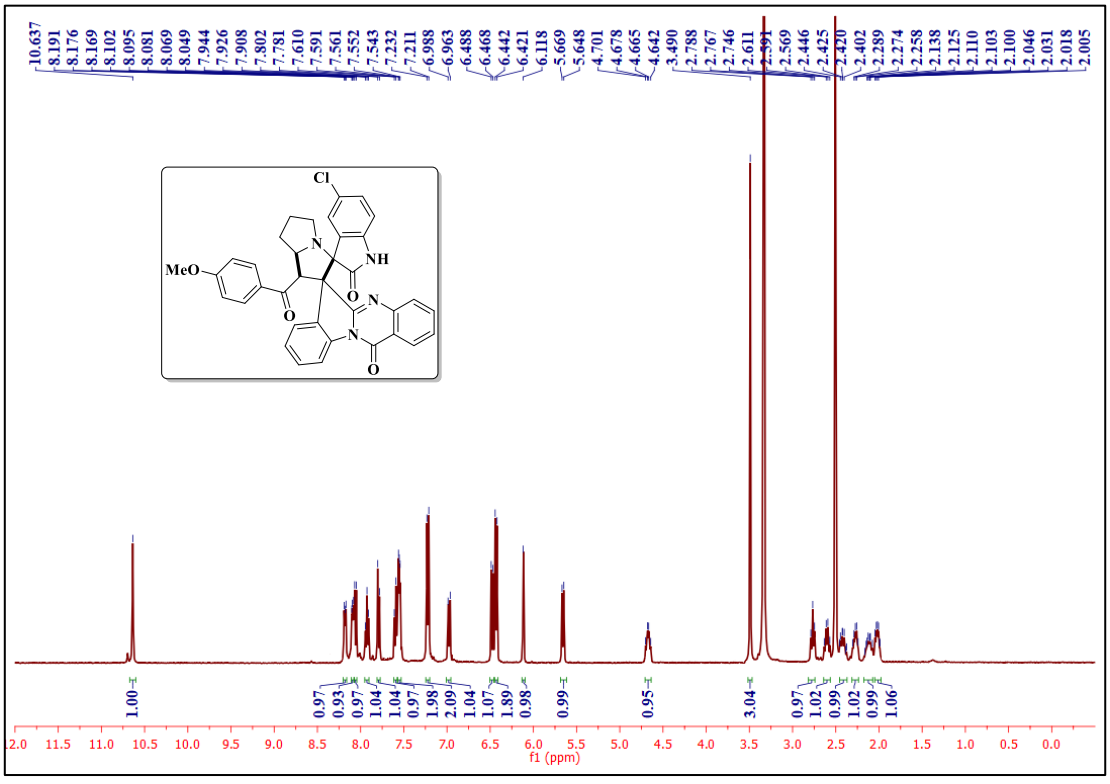

^{1}H NMR spectrum of the compound **4h**

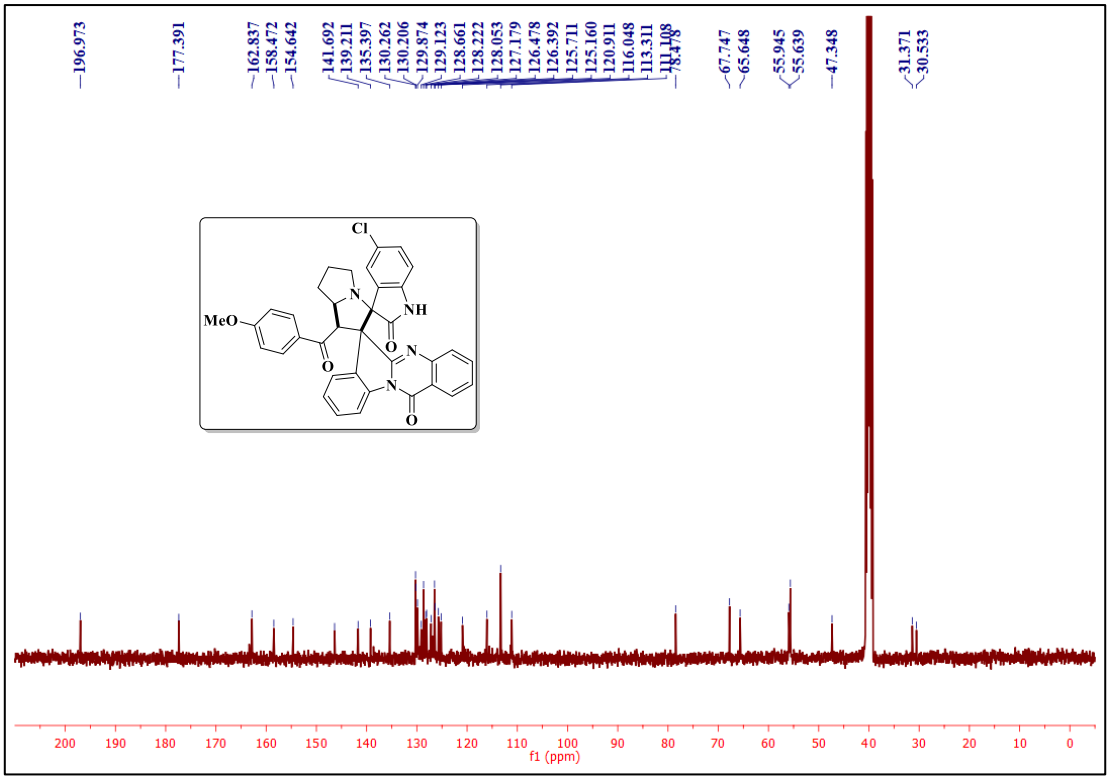

^{13}C NMR spectrum of the compound **4h**

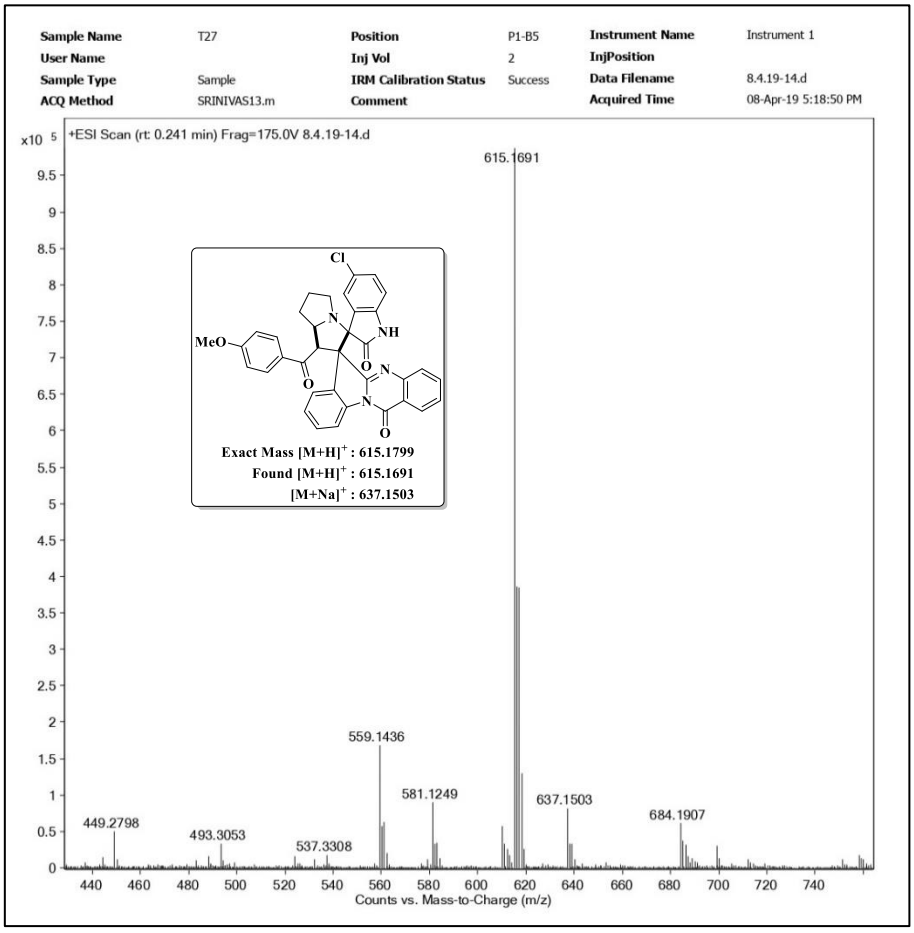

Mass spectrum of the compound **4h**

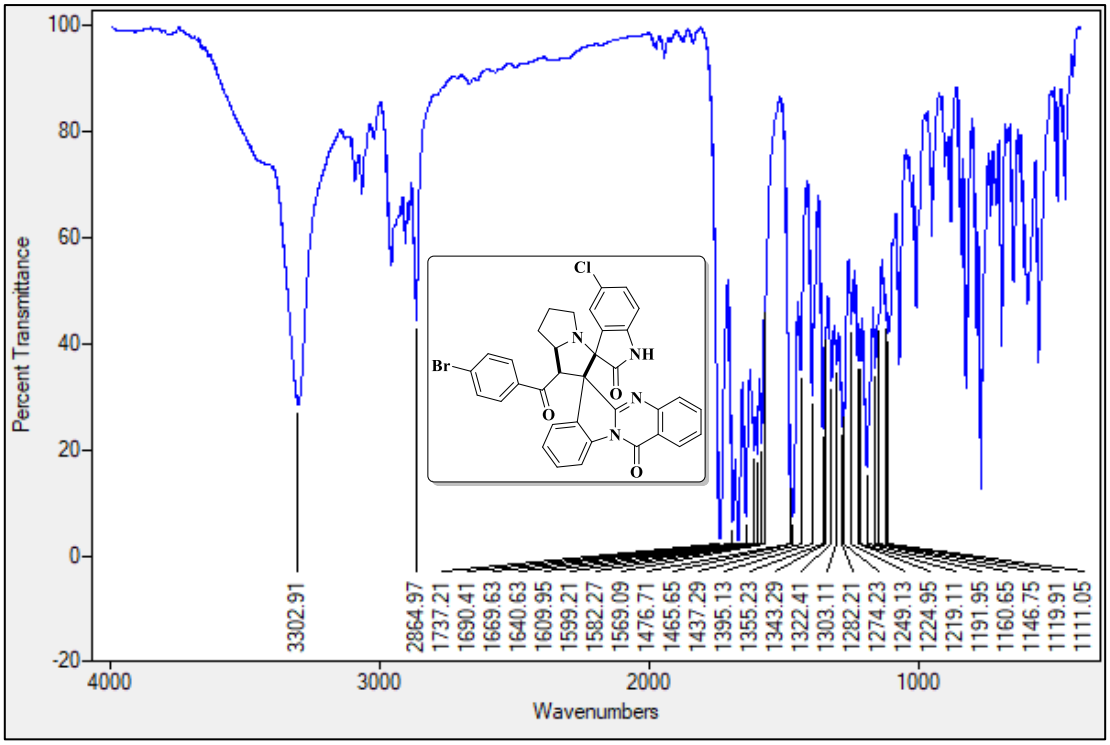

IR spectrum of the compound **4j**

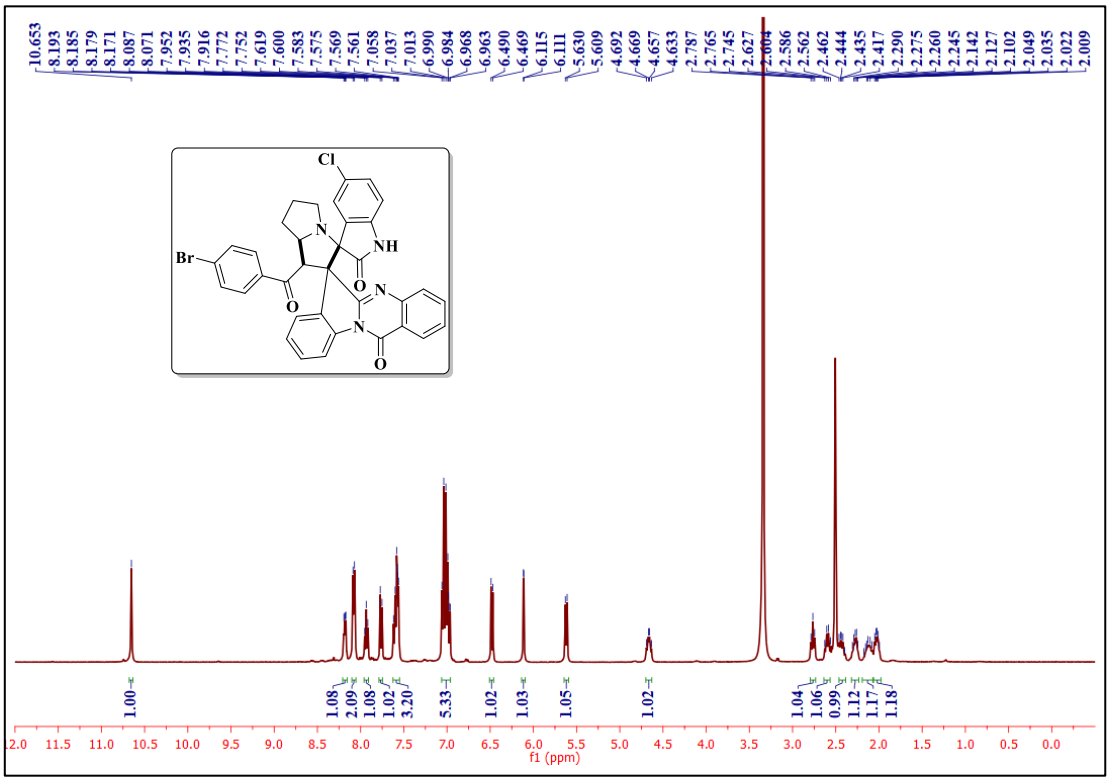

^{1}H NMR spectrum of the compound **4j**

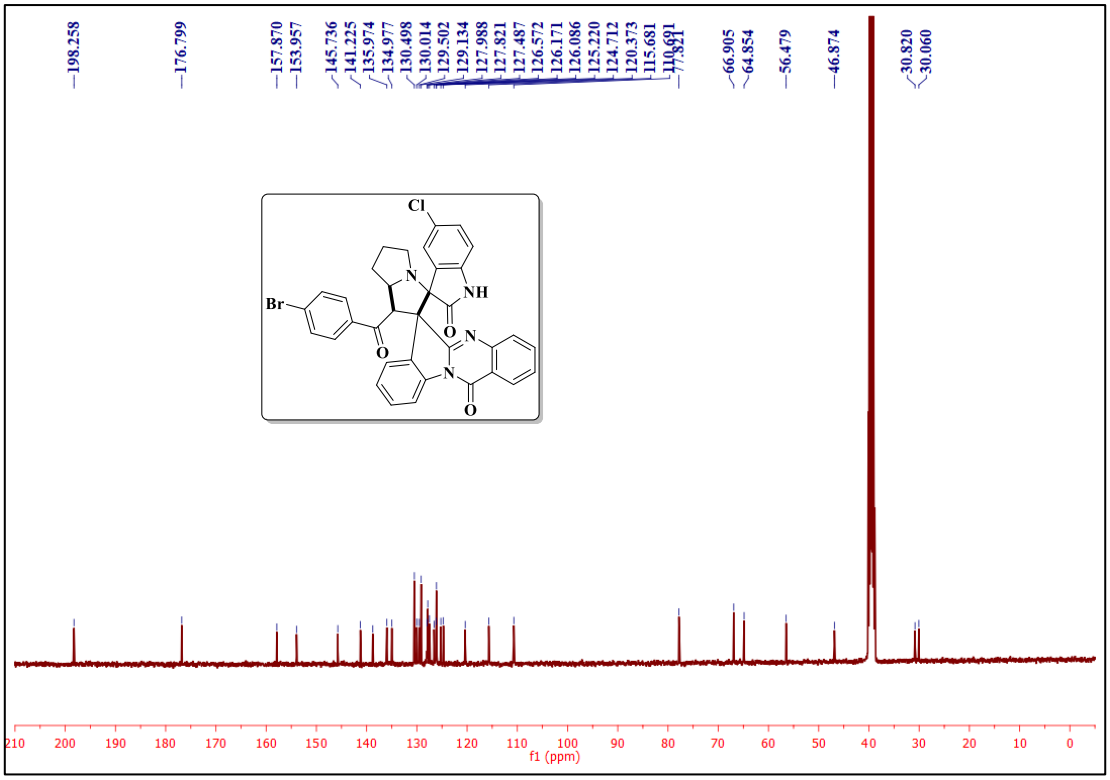

^{13}C NMR spectrum of the compound **4j**

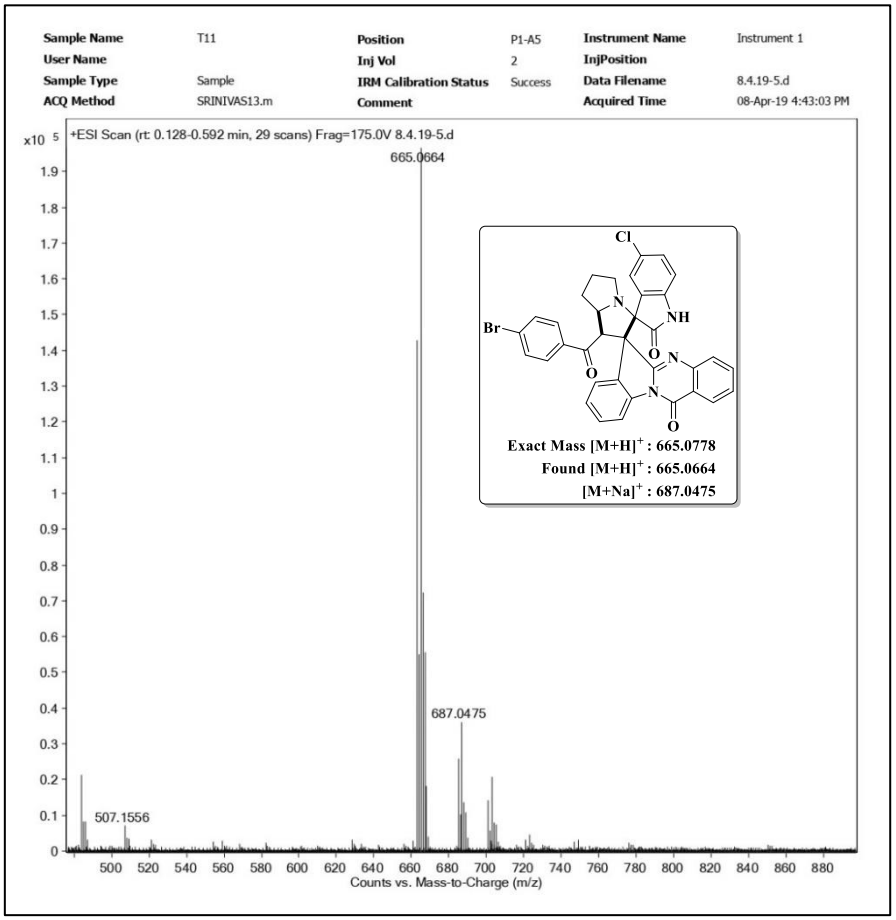

Mass spectrum of the compound **4j**

SUMMARY

Synthesis and anti-tubercular activity of heterocyclic and spiro compounds

CHAPTER-I

Introduction

This chapter describes literature survey, objectives and brief introduction about nitrogen, oxygen heterocycles and spiro heterocyclic compounds. Nitrogen or oxygen heterocycles such as pyrrole, pyrazole, triazole, furan and oxadiazole are the significant moieties for the discovery and development of many biologically potent molecules [1,2]. Development of new methodologies for the synthesis of nitrogen or oxygen containing heterocycles and spiro heterocyclics has become thrust area to the researchers across the world [3]. However, majority of the synthetic protocols involves use of toxic metals and harsh reaction conditions. For the past few decades green chemistry is playing a crucial role in minimizing the waste production and developing environment sustainable methodologies [4]. In this regard, green protocols such as one-pot approach, transition metal free and ultrasound assisted reactions are the emerging techniques for the synthesis of heterocyclic and spiro heterocyclic compounds under the green chemistry principles [5]. Based on the environmental concerns and biological applications of these heterocyclics, we have developed new methods for the generation of heterocyclic compounds.

All the compounds described in the thesis were characterized by FT-IR, NMR and Mass spectral data and the regiochemistry of the compounds were determined by single crystal X-ray diffraction method. The anti-tubercular (anti-TB) activity of the compounds were evaluated by Microplate Alamar Blue Assay method and ethambutol was used as the standard drug. The molecular docking studies were carried out by using AutoDock Tools (ADT) version 1.5.6, AutoDock version 4.2.5.1 docking program and the results were visualized by using Discovery tools software.

CHAPTER-II

Part A

A green catalyst $Fe(OTs)_3/SiO_2$ for the synthesis of 4-pyrrolo-12-oxoquinazolines

Iron based heterogeneous acid catalysts have been focused in the organic synthesis in view of their excellent catalytic performance including ease of separation, recyclability and reusability [6]. $Fe(OTs)_3/SiO_2$ is considered as one of the most important acid catalysts and has been utilized as an effective catalyst in organic transformations due to their high strength of

acidity, non-toxicity and high activity at low temperature [7]. On the other hand, utilization of solvent-free protocols remains as a straight forward process by simplifying the product recovery, avoiding the use of toxic solvents, lessening waste generation and reducing the operational costs without altering the physical properties of the starting materials and nature of the reactions [8]. Encouraged by these advantages, we depict an environmentally friendly green methodology for synthesizing 4-pyrrolo-12-oxoquinazolines by means of solvent-free grinding reaction.

The reaction of indolo[2,1-*b*]quinazoline-6,12-dione **A** (1 mmol) with acetophenone **B** (1 mmol) in methanol (3 mL) having 10% aq. NaOH at room temperature affords 6-hydroxy-6-(2-oxo-2-phenylethyl)indolo[2,1-*b*]quinazolin-12(6*H*)-one (**1'**). The obtained intermediate **1'** was treated with 20 mol% $BF_3.Et_2O$ in acetic acid at 60 °C generates the chalcone **1** in 88% yield (scheme 2A.1).

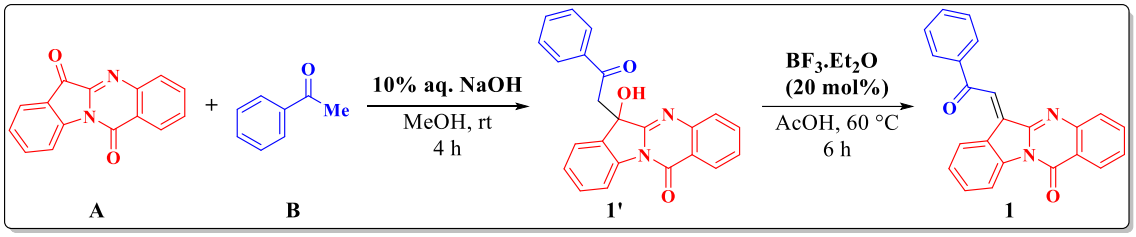

Scheme 2A.1. Synthesis of the chalcone **1**.

The optimal reaction conditions are, in an agate mortar a mixture of chalcones **1** (1 mmol), 1,3-diketone **2** (1 mmol), ammonium acetate **3** (2.5 mmol) and 100 mg of $Fe(OTs)_3/SiO_2$ were added and thoroughly grinded with a pestle manually until the completion of the reaction, after that ethyl acetate (5mL) was added. The catalyst was recovered by filtration, washed with ethanol. The filtrate was concentrated to furnish the desired products **4a-s** with 88-96% yields (Scheme2A.2).

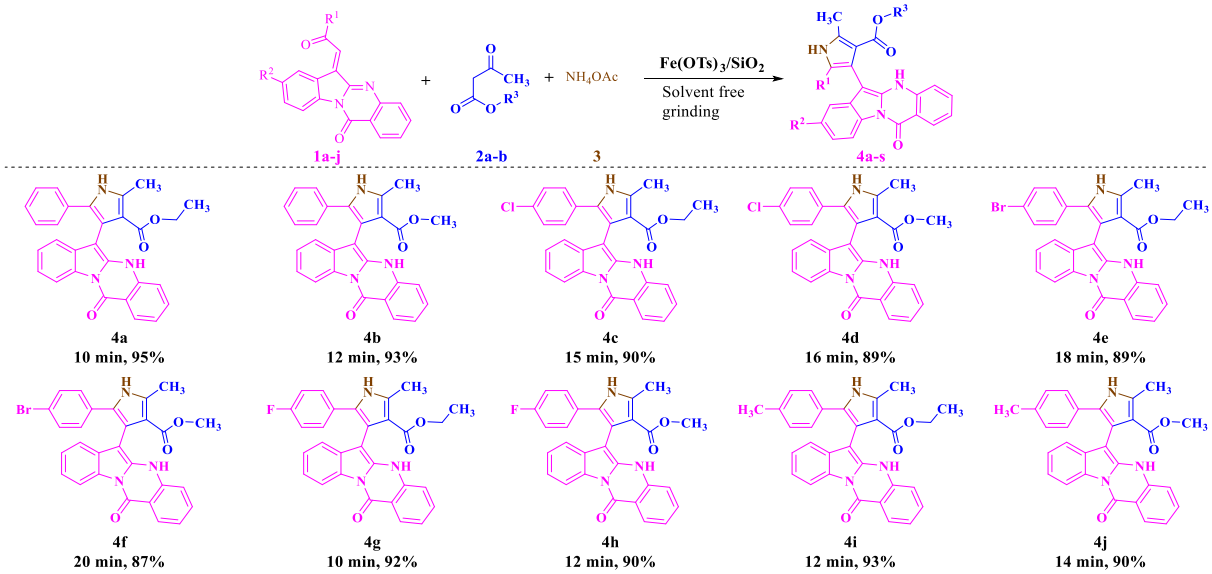

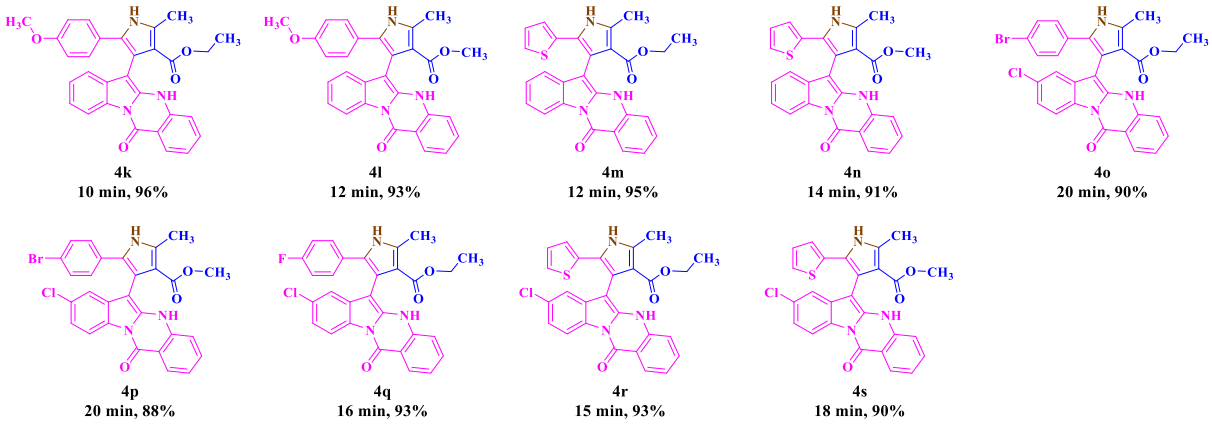

Scheme 2A.2. Synthesis of novel 4-pyrrolo-12-oxoquinazolines **4a-s**.

The *in vitro* anti-tubercular screening of the target compounds **4a-s** were evaluated against *Mycobacterium tuberculosis* H37Rv by the microplate alamar blue assay (MABA) method. Among them, two compounds (**4o** and **4r**) show moderate activity (MIC = 6.25 µg/mL) than the standard drug ethambutol (MIC = 1.56 µg/mL).

Molecular docking studies

The molecular docking studies were performed against *Mycobacterium tuberculosis* enzyme [PDB ID: 1DF7]. As observed from the docking, the compound **4o** displayed good inhibition activity with binding energy −11.59 kcal/mol and forms three hydrogen bonds with amino acid residues ILE5 (2.49 Å), SER49 (1.78 Å) and ILE94 (2.75 Å), nine hydrophobic interactions with TRP6, ALA7, ILE14, ILE20, PHE31 and LEU50 of the protein 1DF7 and its best docking poses were shown in figure 2A.1.

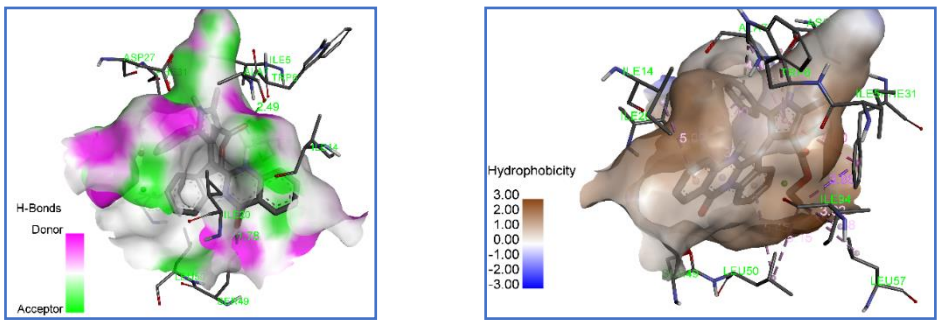

a) **b)**

Fig. 2A.1. The best docked pose of **4o** with the protein 1DF7. **a)** The hydrogen bonding interactions. **b)** The hydrophobic interactions.

CHAPTER-II

Part B

Transition metal- and oxidant-free regioselective synthesis of 3,4,5-trisubstituted pyrazoles *via* [3+2] cycloaddition reaction

Pyrazole moiety features a major role in heterocyclic compounds displaying wide range of biological activities such as anti-cancer, anti-mycobacterial, anti-microbial, anti-leukemic etc. They also act as ideal structural motifs in many pharmaceuticals and natural products [9]. The importance of pyrazoles and their derivatives has prompted the development of numerous routes to synthesize this kind of heterocycles [10]. However, these methods suffer from poor regioselectivity, use of transition metal sources and limited substrate scope. Therefore, transition metal free and high yielding protocol for poly substituted pyrazoles is highly desirable. By considering these, herein we report 3,4,5-trisubstituted pyrazoles under transition metal- and oxidant-free one-pot three component approach.

The optimized reaction conditions are as follows. In an oven dried round bottom flask, aldehyde **2** (1 mmol) and tosyl hydrazide **3** (1 mmol) were stirred in DMF for 10 min at room temperature, then the chalcones **1** (1 mmol) and cesium carbonate (3 eq) were added and the reaction mixture was allowed to stir at 100 °C to produce the targeted products **4a**-**y** in 75-88% yields (Scheme 2B.1). The regiochemistry of the compounds (**4a**) were determined by using single crystal X-ray diffraction method.

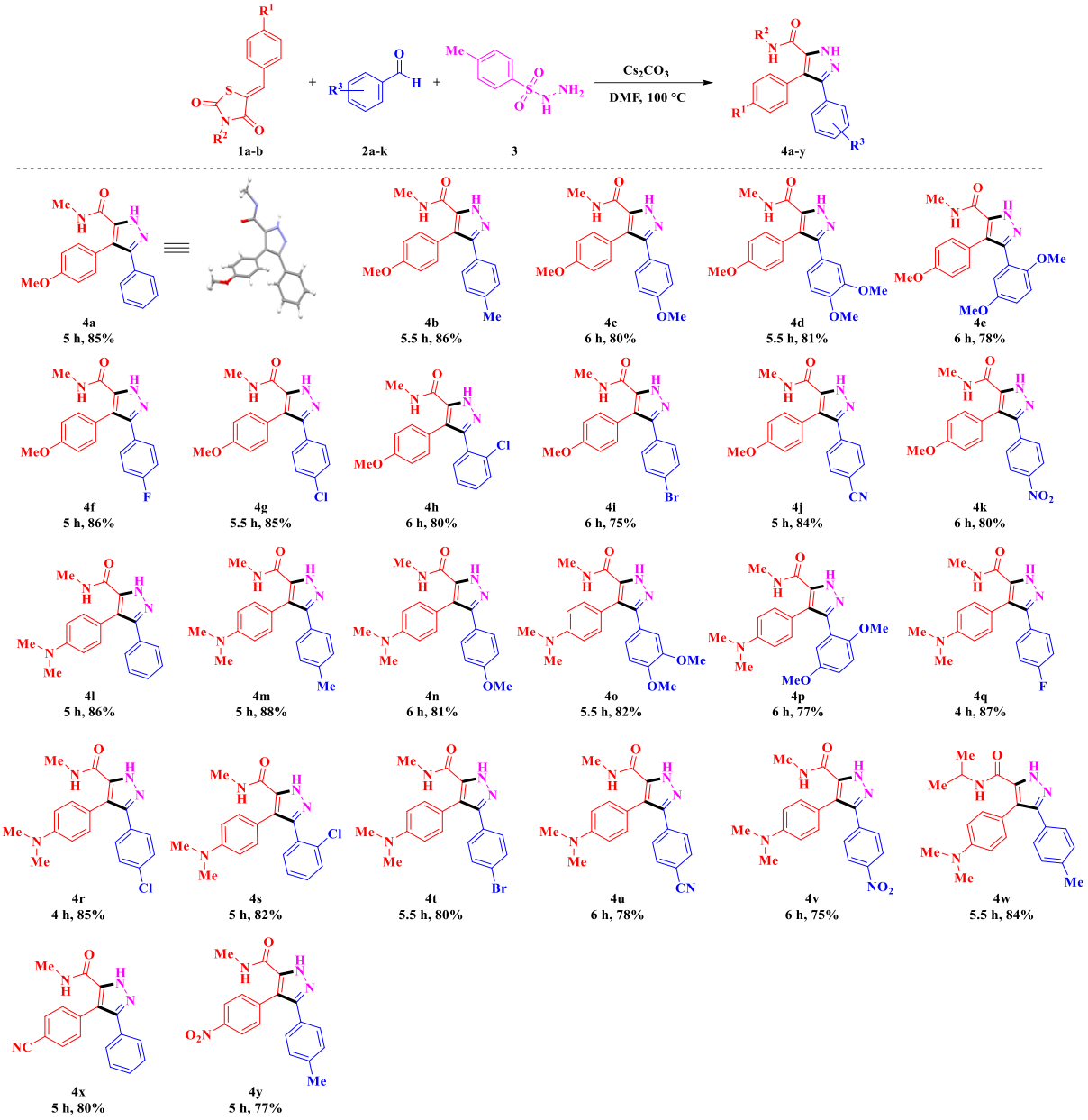

Scheme 2B.1. Synthesis of 3,4,5-trisubstituted pyrazoles **4a-y**.

The synthesized compounds **4a-y** were tested for their *in vitro* anti-tubercular activity against *Mycobacterium tuberculosis* H37Rv. Among all, two compounds (**4e** and **4o**) show good activity (MIC = 3.125 µg/mL) than the standard drug ethambutol (MIC = 1.56 µg/mL).

Molecular docking studies

The molecular docking studies were performed against *Mycobacterium tuberculosis* enzyme [PDB ID: 1DF7]. As observed from the docking, the compound **4o** displayed good inhibition activity with the more negative binding energy (−9.46 kcal/mol), forms two hydrogen bonds with amino acid residues ALA7 (2.24 Å), TYR100 (1.84 Å) and six hydrophobic

interactions with ILE5, ALA7, PHE31, and ILE94 of the protein 1DF7 and its best docking poses were shown in figure 2B.1.

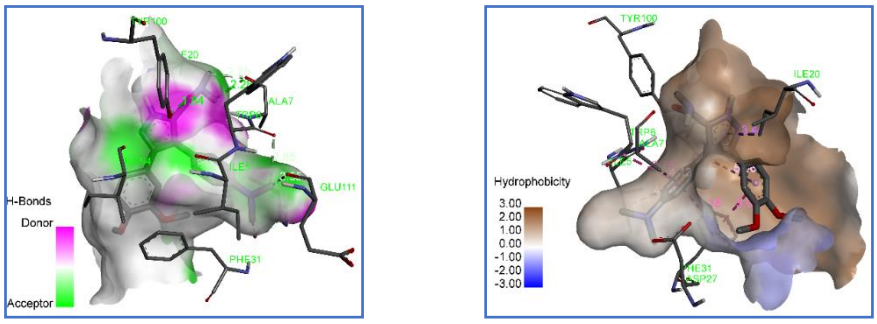

a) **b)**

Fig. 2B.1. The best docked pose of **4o** with the protein 1DF7. **a)** The hydrogen bonding interactions. **b)** The hydrophobic interactions.

CHAPTER-III

A photoinduced multicomponent regioselective synthesis of 1,4,5-trisubstituted-1,2,3-triazoles: Transition metal-, azide- and oxidant-free protocol

Triazoles constitute a major role in chemical community due to their wide range of applications in medicinal and in organic synthesis [11]. Because of their diverse applications in the field of medicinal and material sciences, several methodologies have been demonstrated to construct these interesting moieties [12]. However, most reactions reported so far depend on organic azides that are explosive and hard to handle on a large scale [13]. A noteworthy transition metal- and azide-free protocol for the synthesis of triazoles has been explored by multicomponent and oxidative coupling reactions. Therefore, more attention has been gained towards the design of transition metal- and azide-free routes for the synthesis of 1,2,3-triazoles from readily available and cheap starting materials [14]. In light of these, we report tosylhydrazone based transition metal-, azide- and oxidant-free route for the regioselective synthesis of 1,4,5-trisubstituted-1,2,3-triazoles.

The optimized reaction conditions are as follows, in an oven dried round bottom flask aldehyde **2** (1 mmol) and tosyl hydrazide **3** (1 mmol) were stirred in DMF for 10 min at room temperature, then isatin Schiff base **1** (1 mmol) and cesium carbonate (3 eq) were added and the mixture was allowed to stir at 100 °C under sunlight to produce the targeted products **4a-al** with 75-90% yields (Scheme 3.1). The regiochemistry of the compounds (**4g**) were determined by using single crystal X-ray diffraction method.

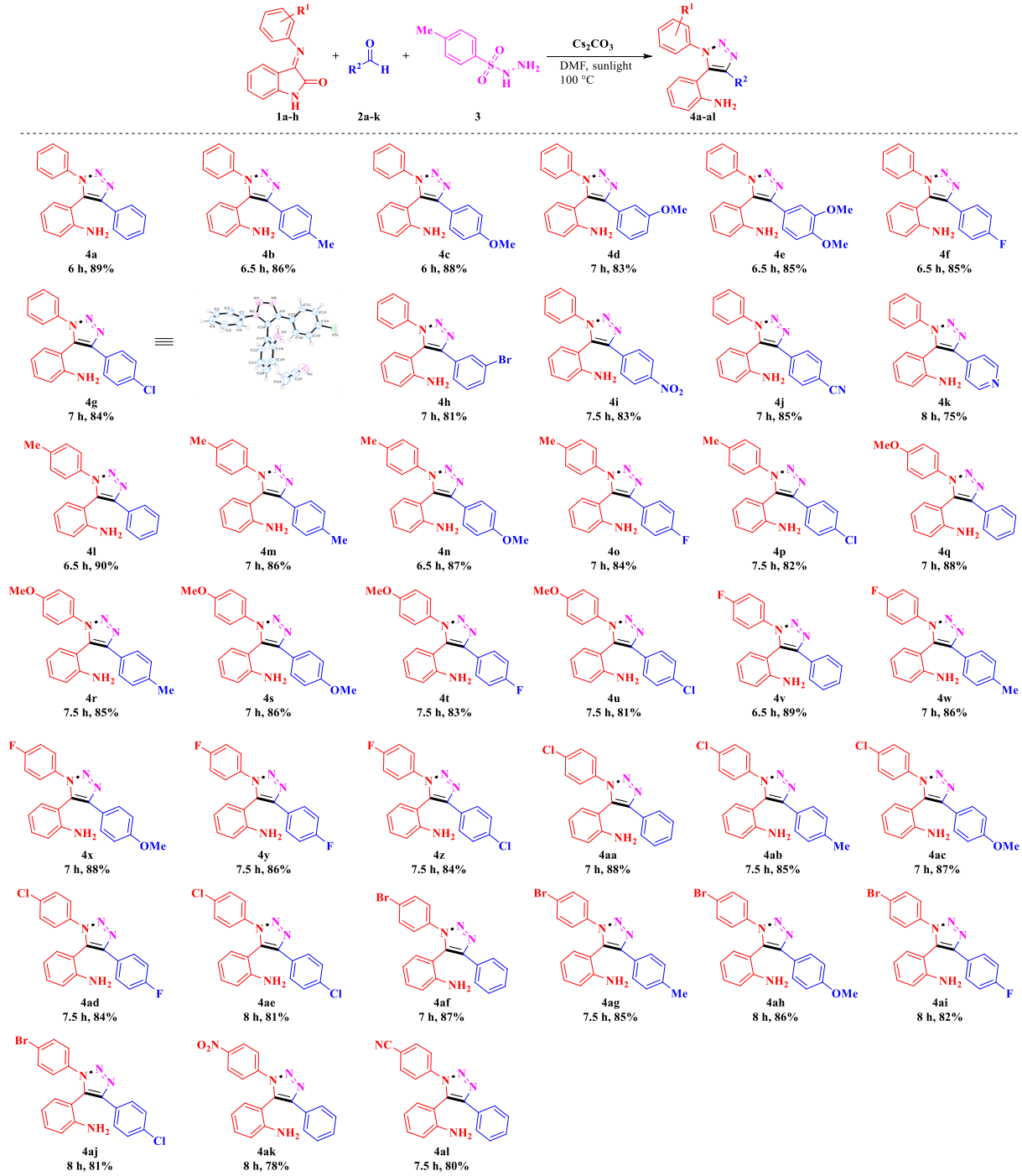

Scheme 3.1. Regioselective synthesis of 1,4,5-trisubstituted-1,2,3-triazoles **4a-al**.

The *in vitro* anti-tubercular screening of the target compounds **4a-al** were evaluated against *Mycobacterium tuberculosis* H37Rv. Among them, three compounds (**4a**, **4o** and **4z**) show moderate activity (MIC = 6.25 µg/mL), when compared with the standard drug ethambutol (MIC = 1.56 µg/mL).

Molecular docking studies

The molecular docking studies were performed against *Mycobacterium tuberculosis* enzyme [PDB ID: 1DF7]. As observed from the docking, the compound **4o** displayed good inhibition activity with the better binding energy −9.82 kcal/mol and forms two hydrogen bonds with amino acid residues ALA7 (2.21 Å) and TYR100 (2.26 Å), nine hydrophobic interactions with ILE5, ALA7, ILE14, ILE20, TYR100 and ALA126 of the protein 1DF7 and its best docking poses were shown in figure 3.1.

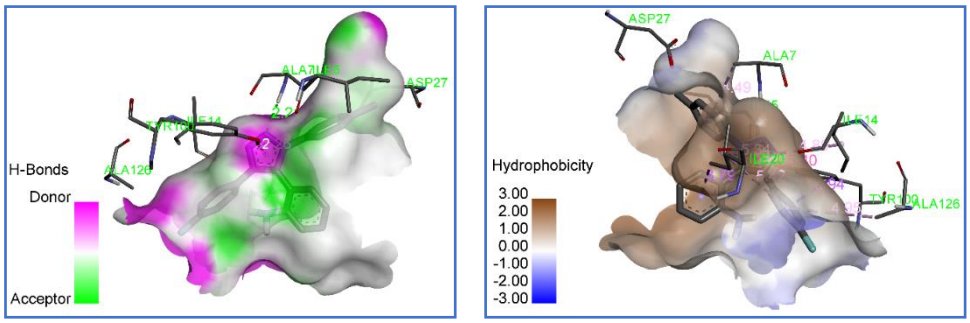

a) **b)**

Fig. 3.1. The best docked pose of **4o** with the protein 1DF7. **a)** The hydrogen bonding interactions. **b)** The hydrophobic interactions.

CHAPTER-IV

Part A

One-pot multicomponent reaction for the synthesis of functionalized 2'-oxo-spiro[furo-pyrrolo[2,1-*a*]isoquinolino-indolines

In the recent years of synthetic organic chemistry, spirooxindoles have gained much attention due to their diverse biological activities and pharmacological applications. Spirooxindole is a key structure of many naturally occurring substances and therapeutically important molecules [15]. On the other hand, isoquinoline and furan derivatives have attracted extensive research interest towards synthetic chemists due to their significant applications in medicinal chemistry [16,17]. Hence, the synthesis of molecular framework which contains spirooxindole and isoquinoline in a highly regioselective manner is challenging and have drawn much interest of researchers. Inspired by these, herein we report the regioselective synthesis of spiroisoquinolino-indolines by one-pot multicomponent approach.

The optimal reaction conditions are as follows. In an oven dried round bottom flask isatin **1** (1 mmol) and malononitrile **2** (1 mmol) were stirred in DCM for 5 min at room temperature, then the ylide **3** (1 mmol) and DABCO (1.2 mmol) were added and the mixture

was allowed to stir at room temperature for 4-6 hours to produce the desired products **4a-v** with 74-87% yields (Scheme 4A.1).

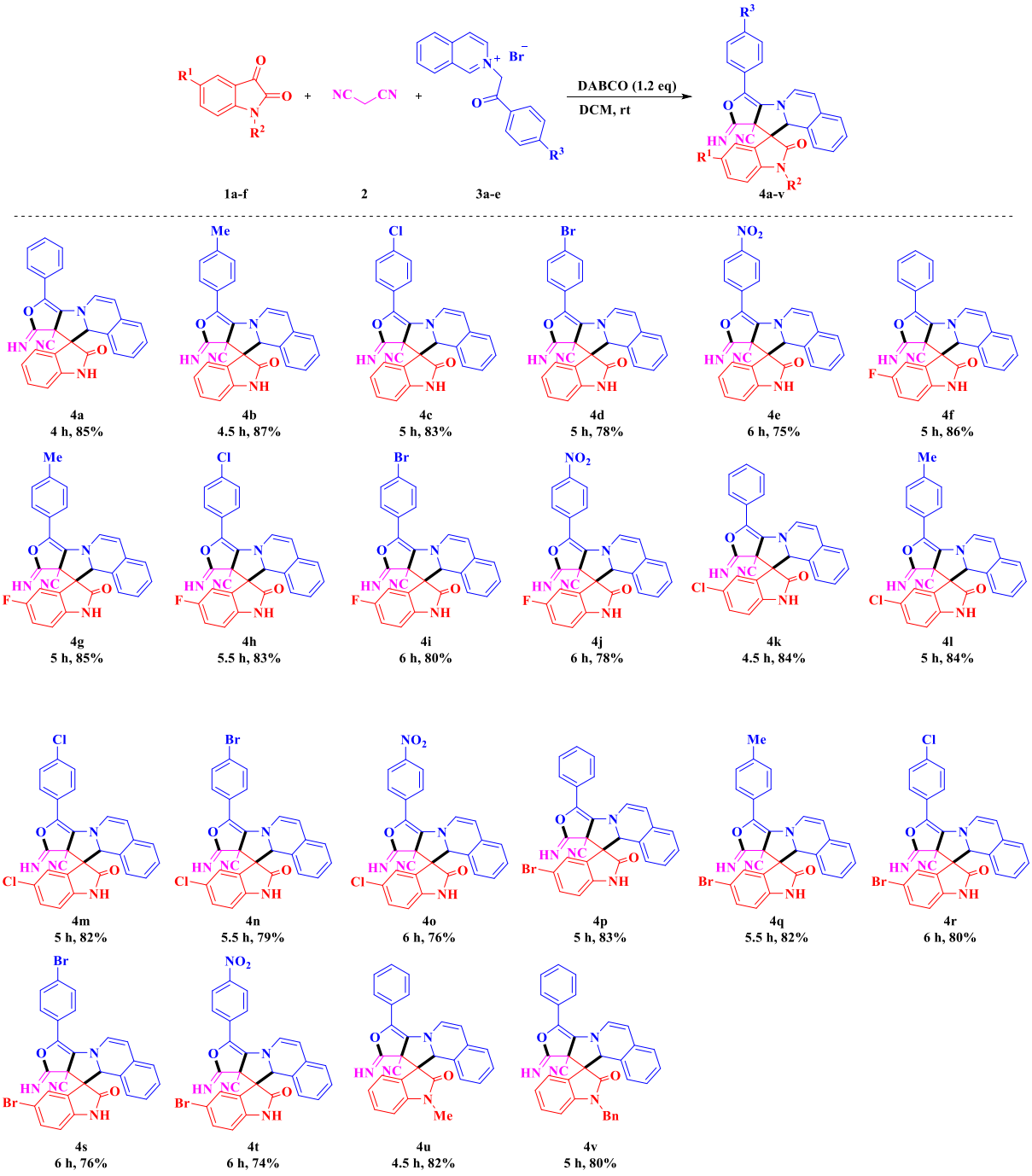

Scheme 4A.1. Synthesis of 2'-oxo-spiro[furo-pyrrolo[2,1-*a*]isoquinolino-indolines **4a-v**.

Molecular docking studies

The molecular docking studies were performed against *Mycobacterium tuberculosis* enzyme [PDB ID: 1DF7]. As observed from the docking, the compound **4n** displayed good inhibition activity with significant binding energy (−10.99 kcal/mol) and forms a hydrogen bond with amino acid residue SER49 (2.69 Å), seven hydrophobic interactions with ILE5,

ALA7, PHE31, ILE20, THR46 and PRO51 of the protein 1DF7 and its best docking poses were shown in figure 4A.1.

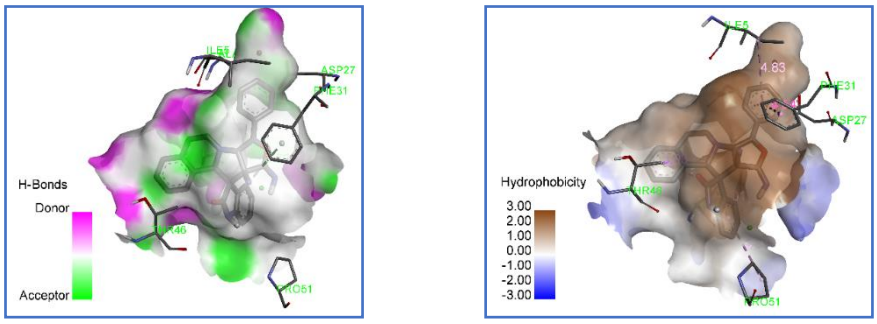

a) **b)**

Fig. 4A.1. The best docked pose of **4n** with the protein 1DF7. **a)** The hydrogen bonding interactions. **b)** The hydrophobic interactions.

CHAPTER-IV

Part B

A three component [3+2] cycloaddition reaction for the synthesis of spirooxindolo-pyrrolizidines

[3+2] cycloadditions are the fundamental reactions for the efficient synthesis of heterocycles, bioactive compounds and pharmaceutical agents [18]. In the recent years, construction of aza-spirooxindoles have attracted much attention due to their combination of two pharmacophores linked by a spiro core [19]. In this regard, we have demonstrated a highly regioselective synthesis of aza-spirooxindoles from one-pot three component reaction *via* [3+2] cycloaddition reaction between isatin-malononitrile adduct and azomethine ylides, generated *in situ* from cyclic α-amino acids and quinoline aldehydes.

The optimized reaction conditions for the target compounds **4a-t** are as follows, in 3 mL of THF, isatin-malononitrile adduct **1** (1 mmol), quinoline aldehydes **2** (1 mmol) and L-proline **3** (1 mmol) were added and the reaction mixture was kept at room temperature under ultrasonic bath for 40-60 minutes to produce the desired products **4a-t** with 78-88% yields (scheme 4B.1). The regiochemistry of the compounds (**4n**) were determined by using single crystal X-ray diffraction method.

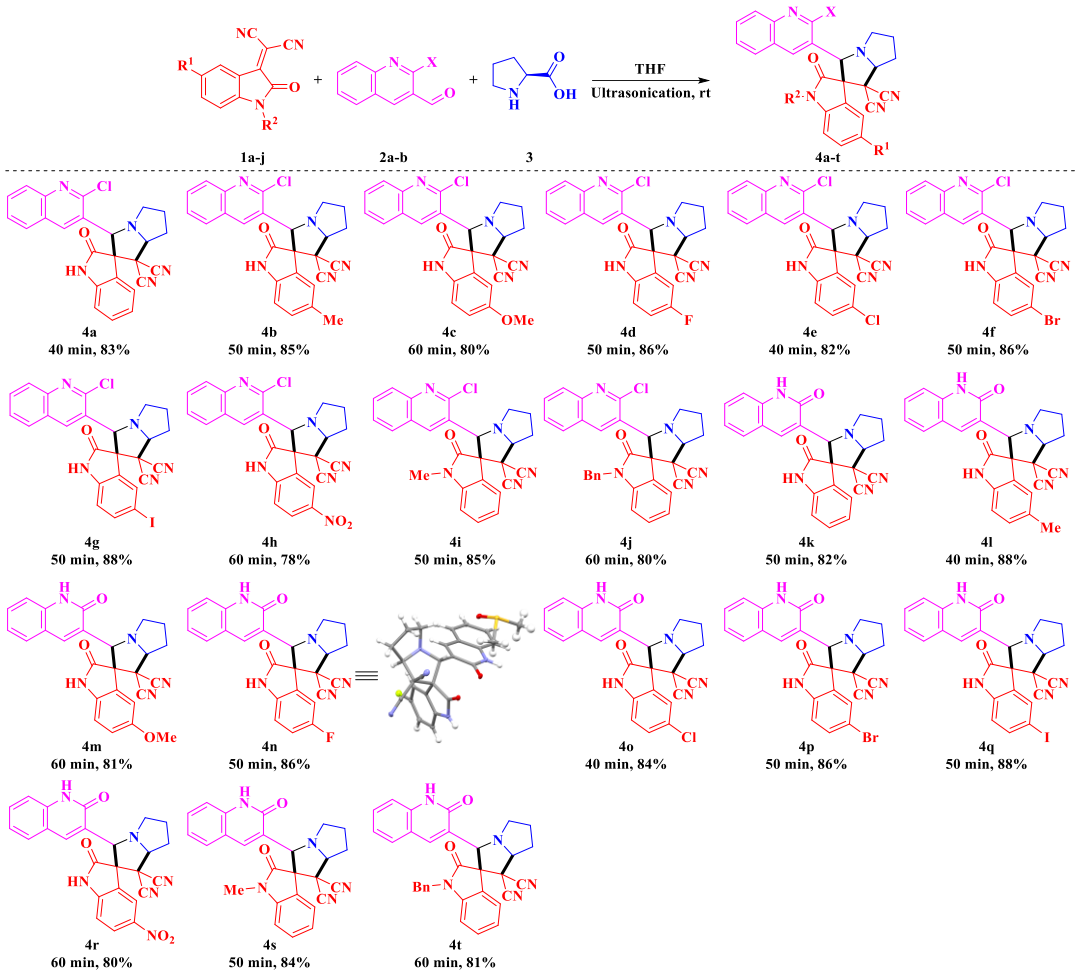

Scheme 4B.1. Synthesis of novel aza-spirooxindoles **4a-t**.

Molecular docking studies

The molecular docking studies were performed against *Mycobacterium tuberculosis* enzyme [PDB ID: 1DF7]. As observed from the docking, the compound **4j** displayed good inhibition activity with significant binding energy (−10.83 kcal/mol) and forms two hydrogen bonds with amino acid residue GLN28 (2.57 and 2.78 Å), eight hydrophobic interactions with ILE20, TRP22, PHE31, PRO51, VAL54 and LEU57 of the protein 1DF7 and its best docking poses were shown in figure 4B.1.

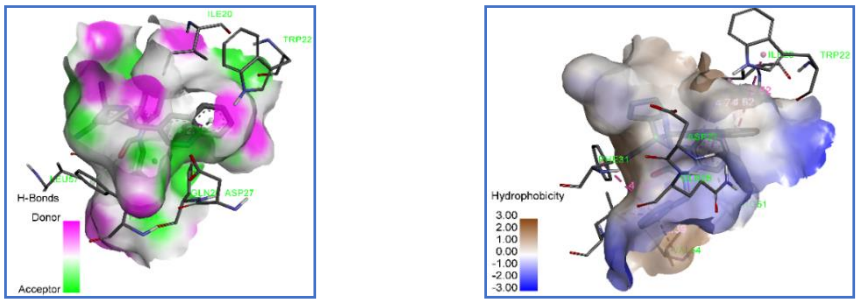

a) **b)**

Fig. 4B.1. The best docked pose of **4j** with the protein 1DF7. **a)** The hydrogen bonding interactions. **b)** The hydrophobic interactions.

CHAPTER-V

Part A

Quinazolinone based spirooxadiazole hybrids: Design, synthesis and anti-tubercular activity

Tuberculosis (TB) is the chronic infectious pulmonary disease induced by *Mycobacterium tuberculosis* (M. tuberculosis) and is one of the top ten causes of mortalities throughout the world [20]. 1,2,4-oxadiazole ring system acts as an essential part of the pharmacophore for several drugs, which exhibit various biological activities such as anti-cancer, anti-inflammation, anti-obesity [21] etc. Based on these, an attempt was commenced to design and synthesize the spiro heterocyclic system possessing quinazolinone-quinoline core connected by biologically prominent 1,2,4-oxadiazole moiety and further evaluated their *in vitro* anti-tubercular activity.

The optimized reaction conditions are as follows, to a solution of quinazolinone Schiff bases **1** (1 mmol) and *N*-hydroxycarbimidoyl chlorides **2** (1.1 mmol) in DCM (3 mL) was added Et_3N (2 eq) drop wise about 10 min. The reaction was allowed to stir at room temperature for 4-5.5 hours to afford the desired products **3a-o** in 78-86% yields (Scheme 5A.1).

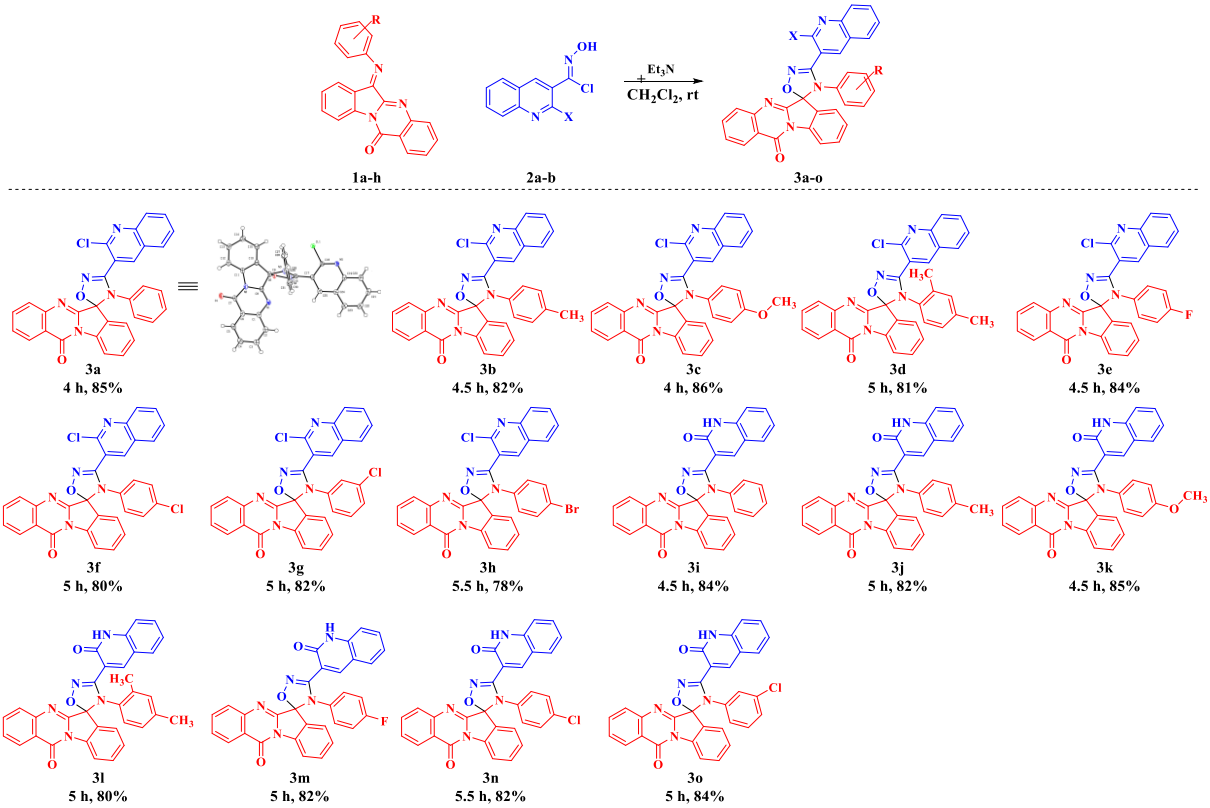

Scheme 5A.1. Synthesis of quinolinyl spiroquinazolinoneoxadiazoles **3a-o**.

The synthesized compounds **3a-o** were tested for their *in vitro* anti-tubercular activity against *Mycobacterium tuberculosis* H37Rv. Among all, five compounds (**3b**, **3e**, **3f**, **3h** and

3l) exhibit higher potency (MIC = 0.78 µg/mL) than the standard drug ethambutol (MIC = 1.56 µg/mL).

Molecular docking studies

The molecular docking studies were performed against *M. tuberculosis* enzyme [PDB ID: 1DF7]. As observed from the docking, the compound **3h** displayed good inhibition activity with the more negative binding energy (−12.92 kcal/mol) and forms three hydrogen bonds with amino acid residues GLN28 (2.76 Å), PRO51 (3.05 Å), and TYR100 (2.14 Å), nine hydrophobic interactions with ILE5, ALA7, ILE20, THR46, PRO51, and VAL54 of the protein 1DF7 and its best docking poses were shown in figure 5A.1.

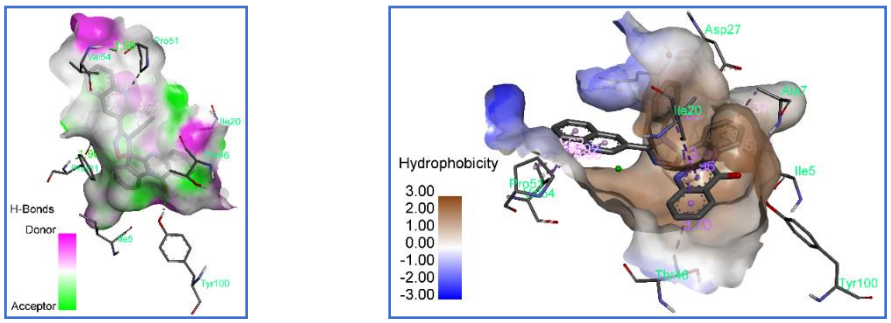

a) **b)**

Fig. 5A.1. The best docked pose of **3h** with the protein 1DF7. **a)** The hydrogen bonding interactions. **b)** The hydrophobic interactions.

CHAPTER-V

Part B

One-pot multicomponent synthesis of novel quinazolinone based spirocyclopropane hybrids and their *in silico* molecular docking studies

Quinazolinone is an important class of nitrogen heterocycles exhibits broad spectrum of biological applications including anti-cancer, anti-HIV, anti-inflammatory, and anti-mycobacterial activities [22]. Similarly, cyclopropane moiety is important building block for the researchers due to its wide pharmacological activities [23]. Based on biological significance of quinazolinone and cyclopropane derivatives, we have made an attempt to synthesize these moieties in a single frame *via* one-pot multicomponent approach.

The optimized reaction conditions for the target compounds **4a-v** are as follows. In a 3 mL of acetonitrile, aldehydes **2** (1 mmol) and tosyl hydrazide **3** (1 mmol) were added and stirred at room temperature for 10 min. To this, chalcones **1** (1 mmol) and cesium carbonate (20 mol%) were added and the reaction mixture was allowed to heat at 50 °C for 2-3 hours to

produce the desired products **4a-v** in 73-85% yields (scheme 5B.1). The synthesized compounds were well characterized by using IR, ^{1}H, ^{13}C NMR, mass spectral data and the structures of the compounds (**4j**) were confirmed by the single crystal X-ray diffraction method.

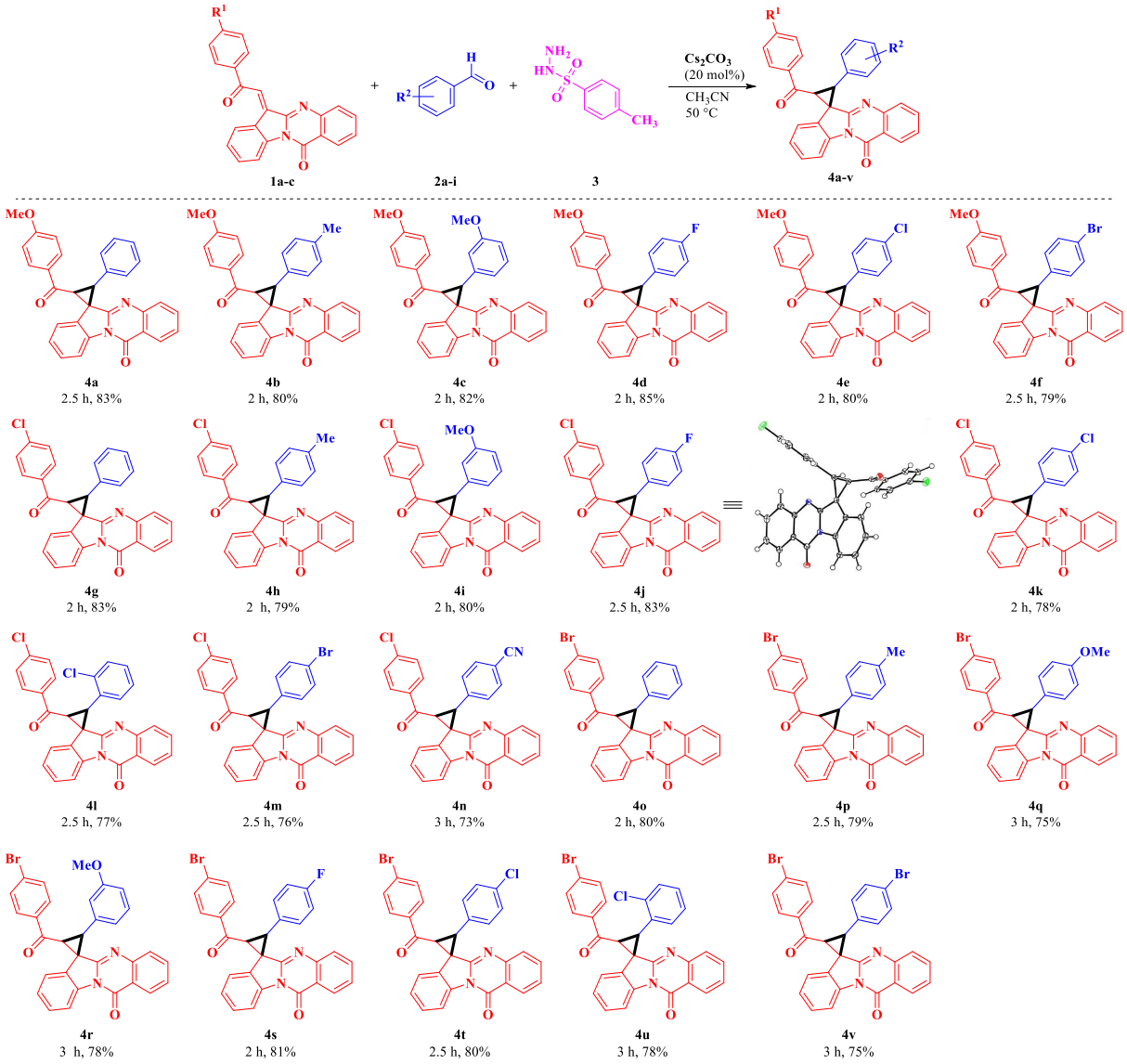

Scheme 5B.1. Synthesis of quinazolinone based spirocyclopropanes **4a-v**.

Molecular docking studies

The molecular docking studies were performed against *M. tuberculosis* enzyme [PDB ID: 1DF7]. As observed from the docking, the compound **4r** displayed good inhibition activity with more negative binding energy (−11.63 kcal/mol) and forms two hydrogen bonds with amino acid residues ALA7 (3.11 Å) and PHE31 (3.93 Å) and six hydrophobic interactions with ALA7, ILE20, PRO51 and VAL54 of the protein 1DF7 and its best docking poses were shown in figure 5B.1.

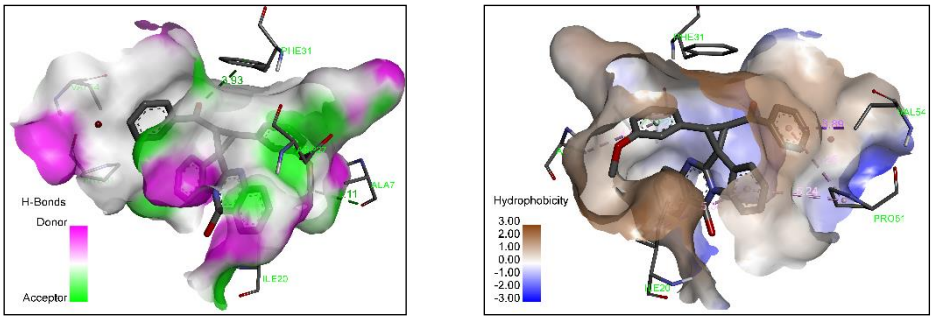

a) **b)**

Fig. 5B.1. The best docked pose of **4r** with the protein 1DF7. **a)** The hydrogen bonding interactions. **b)** The hydrophobic interactions.

CHAPTER-VI

Part A

Ultrasound promoted synthesis of novel quinazolinyl-bisspirooxindolo-pyrrolidines *via* [3+2] cycloaddition reaction

[3+2] cycloaddition reactions of azomethine ylides with olefinic dipolarophiles constitutes one of the major approaches for the regio- and stereo-selective synthesis of various pyrrolidine derivatives [24]. Owing to their unique structural features and interesting biological profiles, spirooxindoles are considered as privileged structural motifs for new drug discovery [25]. On the other hand quinazolinones are also widely occur in pharmaceuticals, natural products and shows broad spectrum of biological activities. In this context, we have demonstrated quinazolinyl bisspirooxindoles by incorporating the versatile motifs like spirooxindoles and quinazolinones in a single frame.

The optimized reaction conditions are as follows, in 3 mL of acetonitrile, isatins **1** (1 mmol), quinazolinone chalcones **2** (1 mmol) and sarcosine **3a** (1 mmol) were added and the reaction mixture was kept at 60 °C under ultrasonic bath for 35-60 minutes to produce the desired products **4a-o** with 78-85% yields (scheme 6A.1).

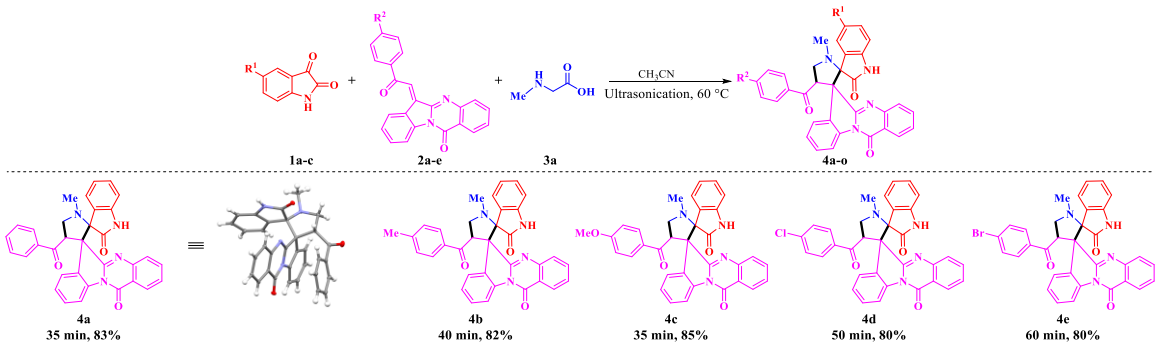

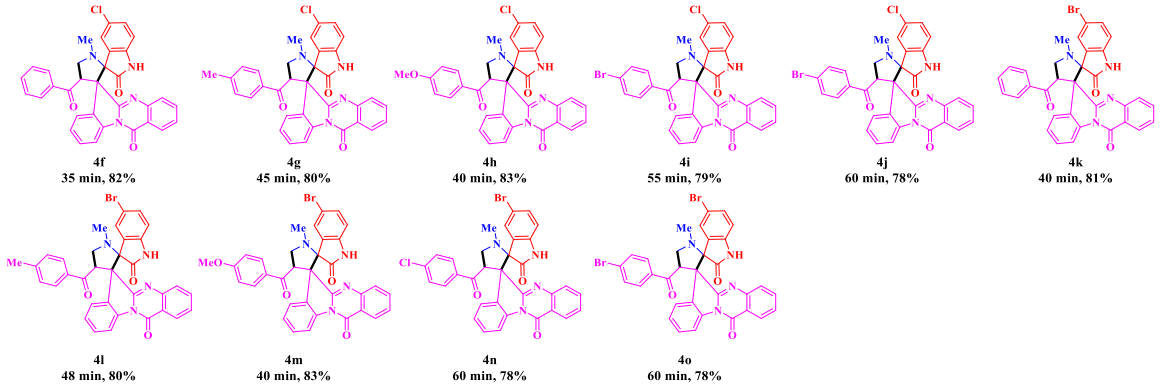

Scheme 6A.1. Synthesis of novel quinazolinyl-bisspirooxindolo pyrrolidines **4a-o**.

The *in vitro* anti-mycobacterial (anti-TB) screening of the target compounds **4a-o** were evaluated against *Mycobacterium tuberculosis* H37Rv. Among them, three compounds (**4c**, **4f** and **4k**) show good activity (MIC = 3.125 µg/mL), when compared with the standard drug ethambutol (MIC = 1.56 µg/mL).

Molecular docking studies

The molecular docking studies were performed against *Mycobacterium tuberculosis* enzyme [PDB ID: 1DF7]. As observed from the docking, the compound **4f** displayed good inhibition activity with better binding energy (−10.06 kcal/mol) and forms a hydrogen bond with amino acid residue SER49 (2.95 Å), five hydrophobic interactions with ILE20, PRO51, VAL54 and ILE94 of the protein 1DF7 and its best docking poses were shown in figure 6A.1.

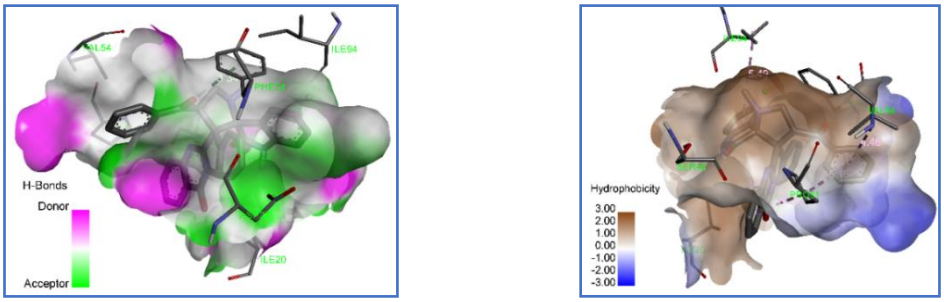

a) **b)**

Fig. 6A.1. The best docked pose of **4f** with the protein 1DF7. **a)** The hydrogen bonding interactions. **b)** The hydrophobic interactions.

CHAPTER-VI

Part B

A one-pot multicomponent [3+2] cycloaddition strategy for the synthesis of quinazolinyl-bisspirooxindolo-pyrrolizidines under ultrasonication

In the past few years the ultrasound assisted protocols became efficient methodology in synthetic organic chemistry as an alternative to traditional methods. In ultrasonication the chemical reactions are processed by cavitation made by ultra-sonic waves traveling in the liquid [26]. On the other hand, the 1,3-dipolar cycloaddition of isatin-derived azomethine ylides to dipolarophiles represents the most expedient route for the synthesis of spirooxindolo pyrrolizidines [27]. The foregoing biological applications of spirooxindole moieties encouraged us to construct the hybrid heterocycles having a bisspirooxindolo pyrrolizidine *via* ecofriendly ultrasound irradiation.

The optimized reaction conditions are as follows, in 3 mL of acetonitrile, isatins **1** (1 mmol), quinazolinone chalcones **2** (1 mmol) and L-proline **3** (1 mmol) were added and the reaction mixture was kept at 60 °C under ultrasonic bath for 40-60 minutes to produce the desired products **4a-o** with 81-89% yields (scheme 6B.1).

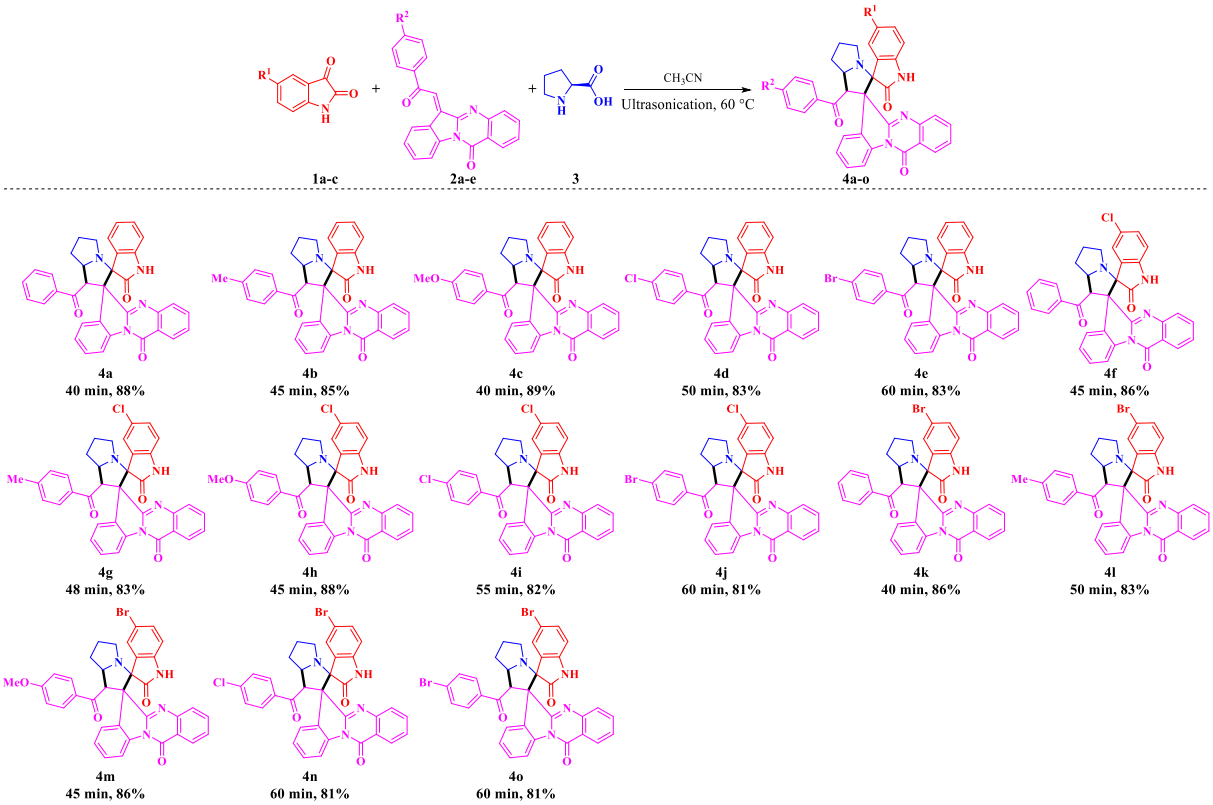

Scheme 6B.1. Synthesis of novel quinazolinyl-bisspirooxindolo pyrrolizidines **4a-o**.

The synthesized compounds **4a-o** were tested for their *in vitro* anti-tubercular activity against *Mycobacterium tuberculosis* H37Rv. Among all, two compounds (**4b** and **4i)** display significant activity (MIC = 1.56 µg/mL) to the standard drug ethambutol (MIC = 1.56 µg/mL).

Molecular docking studies

The molecular docking studies were performed against *Mycobacterium tuberculosis* enzyme [PDB ID: 1DF7]. As observed from the docking, the compound **4i** displayed good inhibition activity with a significant binding energy (−9.26 kcal/mol) and forms two hydrogen bonds with amino acid residues PHE31 (3.02 Å) and PRO51 (2.92 Å), five hydrophobic interactions with ILE20, LEU50, PRO51 and VAL54 of the protein 1DF7 and its best docking poses were shown in figure 6B.1.

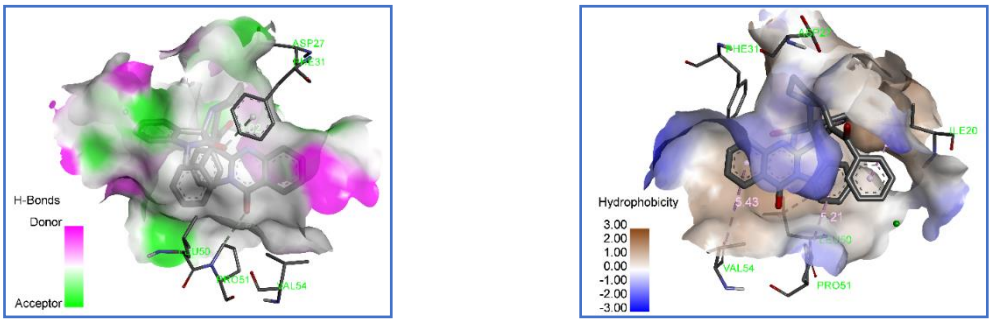

a) **b)**

Fig. 6B.1. The best docked pose of **4i** with the protein 1DF7. **a)** The hydrogen bonding interactions. **b)** The hydrophobic interactions.

References

[1] M. M. Heravi, V. Zadsirjan, *RSC Adv.* **2020**, *10*, 44247–44311.

[2] F. E. Bennani, L. Doudach, Y. Cherrah, Y. Ramli, K. Karrouchi, M. Ansar, M. E. A. Faouzi, *Bioorg. Chem.* **2020**, *97*, 103470–103532.

[3] C. Cabrele, O. Reiser, *J. Org. Chem.* **2016**, *81*, 10109–10125.

[4] I. T. Horváth, P. T. Anastas, *Chem. Rev.* **2007**, *107*, 2167–2168.

[5] E. P. Bacher, B. L. Ashfeld, *Tetrahedron* **2020**, *76*, 130692–130702.

[6] E. Bisz, M. Szostak, *Green Chem.* **2017**, *19*, 5361–5366.

[7] S. Tarannum, Z. N. Siddiqui, *RSC Adv.* **2015**, *5*, 74242–74250.

[8] G. Yashwantrao, V. P. Jejurkar, R. Kshatriya, S. Saha, *ACS Sustain. Chem. Eng.* **2019**, *7*, 13551–13558.

[9] A. Ansari, A. Ali, M. Asif, Shamsuzzaman, *New J. Chem.* **2016**, *41*, 16–41.

[10] A. Sapkal, S. Kamble, *ChemistrySelect* **2020**, *5*, 12971–13026.

[11] J. Huo, H. Hu, M. Zhang, X. Hu, M. Chen, D. Chen, J. Liu, G. Xiao, Y. Wang, Z. Wen,

RSC Adv. **2017**, *7*, 2281–2287.

[12] J. John, J. Thomas, W. Dehaen, *Chem. Commun.* **2015**, *51*, 10797–10806.

[13] M. Giel, C. J. Smedley, E. R. R. Mackie, T. Guo, J. Dong, T. P. Soares da Costa, J. E. Moses, *Angew. Chem., Int. Ed.* **2020**, *59*, 1181–1186.

[14] G. S. Mani, K. Donthiboina, S. P. Shaik, N. Shankaraiah, A. Kamal, *RSC Adv.* **2019**, *9*, 27021–27031.

[15] N. Ye, H. Chen, E. A. Wold, P. Y. Shi, J. Zhou, *ACS Infect. Dis.* **2016**, *2*, 382–392.

[16] X. F. Shang, C. J. Yang, S. L. Morris-Natschke, J. C. Li, X. D. Yin, Y. Q. Liu, X. Guo, J. W. Peng, M. Goto, J. Y. Zhang, K. H. Lee, *Med. Res. Rev.* **2020**, *40*, 2212–2289.

[17] P. Oliva, R. Romagnoli, S. Manfredini, A. Brancale, S. Ferla, E. Hamel, R. Ronca, F. Maccarinelli, A. Giacomini, F. Rruga, E. Mariotto, G. Viola, R. Bortolozzi, *Eur. J. Med. Chem.* **2020**, *200*, 112448–112465.

[18] U. Grošelj, J. Svete, H. H. Al Mamari, F. Požgan, B. Štefane, *Chem. Heterocycl. Compd.* **2018**, *54*, 214–240.

[19] Q. Ni, X. Wang, D. Zeng, Q. Wu, X. Song, *Org. Lett.* **2021**, *23*, 2273–2278.

[20] S. Tiberi, M. Muñoz-Torrico, R. Duarte, M. Dalcolmo, L. D'Ambrosio, G.-B. Migliori, *Pulmonology* **2018**, *24*, 86–98.

[21] S. C. Karad, V. B. Purohit, R. P. Thummar, B. K. Vaghasiya, R. D. kamani, P. Thakor, V. R. Thakkar, S. S. Thakkar, A. Ray, D. K. Raval, *Eur. J. Med. Chem.* **2017**, *126*, 894-909

[22] F. Plescia, B. Maggio, G. Daidone, D. Raffa, *Eur. J. Med. Chem.* **2021**, *213*, 113070–113094.

[23] C. N. Reddy, V. L. Nayak, G. S. Mani, J. S. Kapure, P. R. Adiyala, R. A. Maurya, A. Kamal, *Bioorg. Med. Chem. Lett.* **2015**, *25*, 4580–4586.

[24] M. Palomba, E. De Monte, A. Mambrini, L. Bagnoli, C. Santi, F. Marini, *Org. Biomol. Chem.* **2021**, *19*, 667–676.

[25] L. M. Zhou, R. Y. Qu, G. F. Yang, *Expert Opin. Drug Discov.* **2020**, *15*, 603–625.

[26] S. J. Tabatabaei Rezaei, M. R. Nabid, A. Yari, S. W. Ng, *Ultrason. Sonochem.* **2011**, *18*, 49–53.

[27] V. Pogaku, V. S. Krishna, C. Balachandran, K. Rangan, D. Sriram, S. Aoki, S. Basavoju, *New J. Chem.* **2019**, *43*, 17511–17520.

List of Publications

Published

1. Transition Metal- and Oxidant-Free Regioselective Synthesis of 3,4,5-Trisubstituted Pyrazoles by Means of [3+2] Cycloaddition Reactions
   Bhargava Sai Allaka, Srinivas Basavoju*, Gamidi Rama Krishna, ***Chemistry Select* 2022, *7*, 3-7.**

2. A photoinduced multicomponent regioselective synthesis of 1,4,5-trisubstituted-1,2,3-triazoles: transition metal-, azide- and oxidant-free protocol
   Bhargava Sai Allaka, Srinivas Basavoju*, Gamidi Rama Krishna, ***Advanced Synthesis & Catalysis* 2021, *363*, 3560-3565.**

3. A green catalyst $Fe(OTs)_3/SiO_2$ for the synthesis of 4-pyrrolo-12-oxoquinazolines
   Bhargava Sai Allaka, Srinivas Basavoju*, Gamidi Rama Krishna, ***Chemistry Select* 2020, *5*, 14721–14728.**

Manuscripts submitted

1. Quinazolinone based spirooxadiazole hybrids: design, synthesis and anti-tubercular evaluation
   Bhargava Sai Allaka, Srinivas Basavoju*, Estharla Madhu Rekha, Dharmarajan Sriram, Gamidi Rama Krishna.

2. Synthesis of quinazolinone based spirocyclopropanes *via* [3+2] cycloaddition reaction, *in silico* molecular docking analysis and ADME prediction
   Bhargava Sai Allaka, Srinivas Basavoju*, Gamidi Rama Krishna

3. Ultrasound promoted synthesis of novel quinazolinone based pyrrolidino-bisspirooxindoles as potent antitubercular agents
   Bhargava Sai Allaka, Srinivas Basavoju*, Estharla Madhu Rekha, Dharmarajan Sriram, Gamidi Rama Krishna

Manuscripts under preparation

1. A one-pot multicomponent [3+2] cycloaddition strategy for the synthesis of quinazolinyl-bisspirooxindolo-pyrrolizidines under ultrasonication
   Bhargava Sai Allaka and Srinivas Basavoju*

2. One-pot reaction for the synthesis of functionalized 2'-oxo-spiro[furo-pyrrolo[2,1-*a*]isoquinolino-indolines
   Bhargava Sai Allaka and Srinivas Basavoju*

3. A three component [3+2] cycloaddition reaction for the synthesis of spirooxindolo-pyrrolizidines
   Bhargava Sai Allaka and Srinivas Basavoju*

PAPERS PRESENTED IN INTERNATIONAL AND NATIONAL CONFERENCES

International

1. **Second Virtual International Conference on "Chemical Sciences in Sustainable Technology and Development (2nd IC^2S^2TD-2021)"** organized by the Department of Chemistry, Sardar Vallabhbhai National Institute of Technology, India in Association with the Department of Chemistry, Chung-Ang University, South Korea during 24th – 26th November 2021 (**oral presentation**).

2. **Online International Conference on "Conventional and Digital Methods in Chemical Education"** organized by Department of Chemistry, National Institute of Technology Warangal, during 29th – 31st July 2021.

3. **TEQIP – III Sponsored International Virtual Conference on "Frontiers in Chemical Sciences & Technologies"** organized by Department of Chemistry, Institute of Chemical Technology – IOC Bhubaneswar, during 26th – 27th September 2020.

4. **International conference on "Advances in Chemical Sciences and Technologies-2019 (ACST-2019)"** organized by Department of Chemistry, National Institute of Technology Warangal, during 23rd – 25th September 2019.

5. **International Conference on "Advanced Functional Materials (ICFAM-2017)**" organized by Department of Chemistry, RGUKT, Basar, during 18th – 20th December 2017.

National

1. **Online National Conference on "Organic Chemistry NITT Organic Chemistry Conference '21"** organized by Department of Chemistry, National Institute of Technology Tiruchirappalli, during 16th – 18th December 2021.

2. **Online Faculty Development Programme on "Teaching and Learning of NMR Spectroscopy for Structure Determination"** organized by Department of Chemistry in association with Teaching Learning Centre, National Institute of Technology Warangal, during 19th – 24th February 2021.

3. **Online National Workshop on "Spectral Analysis of Organic Molecules"** organized by National Institute of Pharmaceutical Education and Research (**NIPER**), Hyderabad on 16th – 17th July 2020.

4. **National Conference on "Medicinal Chemistry Conference (MEDCHEM-2017)"** organized by Indian Institute of Technology Madras, during 27th – 28th November 2017.

5. **National Conference on Recent Development in Chemical Sciences and Allied Technologies (RDCST-2017).** During 29-30th June, 2017. Organized by Department of chemistry, National Institute of Technology Warangal, Telangana.

ABOUT THE AUTHOR

Mr. Allaka Bhargava Sai was born in Payakaraopeta, Visakhapatnam district of Andhra Pradesh State, India. He has completed his secondary school education and Intermediate in Tuni. After completion of his B.Sc., and M.Sc., (Organic Chemistry) from Andhra University, he joined in the Department of Chemistry, National Institute of Technology Warangal for the Ph.D., programme on 12th December 2016 under the guidance of Dr. B. Srinivas (Assistant Professor) with the financial assistance from the UGC.